THE UNIVERSITY
of EDINBURGH

Use of Genetically Engineered Mouse Models in Preclinical Drug Development

Helen Creedon

PhD

University of Edinburgh

2014

Declaration

In accordance with university regulations, I declare that I have composed this thesis and that the work presented is my own, except where acknowledgement has been made in the text. No part of this work has been submitted for any other degree or qualification.

Helen Creedon

Acknowledgements

I wish to thank both Prof. David Cameron and Prof. Margaret Frame for allowing me the opportunity to undertake my PhD within the Edinburgh Cancer Centre and I am grateful to Cancer Research UK for funding my research. I am extremely grateful to my supervisor Prof. Val Brunton for her invaluable help, guidance and inspiration over the past 4 years and from whom I have learnt so much. I would also like to thank Dr. Larry Hayward for all his support and encouragment both during the course of this PhD and throughout my early clinical training. I would like to acknowledge Dr. Le Bihan for his assistance with the mass spectrometry experiment and its analysis and Dr. Teresa Klinowska at AstraZeneca for supplying the AZD8931. Thank you also to Professor Owen Sansom and Dr. Saadia Karim from the Beatson Institute for their collaboration on the role of dasatinib in the management of breast cancer. Thank you to all the past and present members of the Cancer Biology group, particularly to Morwenna Muir and Kenny Macleod for their eternal patience and technical support. Special thanks to Lucy Balderstone, whose friendship and encouragment have been invaluable.

Lastly, thank you to my family, particularly to my husband and my parents, for their unending patience and support.

Abstract

The paucity of well validated preclinical models is frequently cited as a contributing factor to the high attrition rates seen in clinical oncological trials. There remains a critical need to develop models which are accurately able to recapitulate the features of human disease. The aims of this study were to use genetically engineered mouse models (GEMMs) to explore the efficacy of novel treatment strategies in HER2 positive breast cancer and to further develop the model to facilitate the study of mechanisms underpinning drug resistance.

Using the BLG--HER2^{KI}-PTEN$^{+/-}$ model, we demonstrated that Src plays an important role in the early stages of tumour development. Chemopreventative treatment with dasatinib delayed tumour inititation (p= 0.046, Wilcoxon signed rank test) and prolonged overall survival (OS) (p=0.06, Wilcoxon signed rank test). Dasatinib treatment also induced squamous metaplasia in 66% of drug treated tumours. We used 2 cell lines derived from this model to further explore dasatinib's mechanism of action and demonstrated reduced proliferation, migration and invasion following *in vitro* treatment.

Due to the prolonged tumour latency and the low metastatic rate seen in this model, further studies were undertaken with the MMTV-NIC model. This model also allowed us to study the impact of PTEN loss on therapeutic response. We validated this model by treating a cohort of MMTV-NIC PTEN$^{+/-}$ mice with paclitaxel and demonstrated prolonged OS (p=0.035, Gehan Breslow Wilcoxon test). AZD8931 is an equipotent signalling inhibitor of HER2, HER3 and EGFR. We observed heterogeneity in tumour response but overall AZD8931 treatment prolonged OS in both MMTV-NIC PTEN $^{FL/+}$ and MMTV-NIC PTEN$^{+/-}$ models. PTEN loss was associated with reduced sensitivity to AZD8931 and failure to suppress Src activity, suggesting these may be suitable predictive biomarkers of AZD8931 response. To facilitate further studies exploring resistance, we transplanted MMTV-NIC PTEN$^{+/-}$ fragments into syngeneic mice and generated 3 tumours with acquired resistance to AZD8931. These tumours displayed differing resistance strategies; 1 tumour continued to express HER2 whilst the remaining 2 underwent EMT and lost HER2 expression reflecting to a very limited degree some of the heterogeneity of resistance strategies seen in human disease.

To further explore resistance to HER2 targeting tyrosine kinase inhibitors, we generated a panel of human cell lines with acquired resistance to AZD8931 and lapatinib. Western blotting demonstrated loss of HER2, HER3 and PTEN in all resistant lines. Acquisition of resistance was associated with a marked change in phenotype and western blotting confirmed all lines had undergone EMT. We used a combination of RPPA and mass spectrometry to further characterise the AZD8931 resistant lines and identified multiple potential novel proteins involved in the resistant phenotype, including several implicated in EMT.

In conclusion, when coupled with appropriate *in vitro* techniques, the MMTV-NIC model is a valuable tool for selection of emerging drugs to carry forward into clinical trials of HER2 positive breast cancer.

Abreviations

5-FU- 5-Fluorouracil

ABPI- Accelerated partial breast irradiation

ADCC- Antibody dependent cell cytotoxicity

AI- Aromatase inhibitor

ASCO- American Society of Clinical Oncology

BCS- Breast conserving surgery

BD- Twice daily

CAP- College of American Pathologists

CBR- Clinical benefit rate

CST- Cell signalling technology

CTCs- Circulating tumour cells

DMEM- Dulbecco's modified Eagle's Medium

DFS- Disease free survival

DLT- Dose limiting toxicity

EBC- Early breast cancer

EDTA- Ethylene Diamine Tetra Acetic Acid

EGFR- Epidermal growth factor receptor

ER- Oestrogen receptor

ESCs- Embryonic stem cells

FBS- Fetal bovine serum

FFPE- Formalin-fixed paraffin embedded

FGF3- Fibroblast growth factor

FISH- Fluorescent in situ hybridization

GDR- Glucose deprivation response

GEMM- Genetically engineered mouse models

GRB2- Growth Factor Receptor Bound 2

H_2O_2 –Hydrogen peroxide

HR- Hormone receptor

HER- Human Epidermal Growth Factor receptor

HER2- Human Epidermal Growth Factor receptor 2

HER3- Human Epidermal Growth Factor receptor 3

HFA- Hollow fibre assay

IAP- Inhibitor of apoptosis

ICH- International conference on harmonization

IHC- Immunohistochemistry

IP- Intra-peritoneal

LOH- Loss of heterozygosity

LVEF- Left ventricular ejection fraction

MBC- Metastatic breast cancer

MFP- Mammary fat pad

MMP- Matrix metalloproteinases

MMTV- Mouse mammary tumour virus

MTD- Maximum tolerated dose

mTOR- Mammalian target of rapamycin

NK – Natural killer

NSCLC- Non-small cell lung cancer

ORR- Overall response rate

OS- Overall survival

PBMC- Peripheral blood mononuclear cells

PBS- Phosphate buffered saline

PC-PLC- Phosphatidylcholine-specific phospholipase C

PCR- Pathological complete response

PD- Pharmacodynamic

PDGFR- Platelet derived growth factor

PDX- Patient derived xenograft

PFS- Progression free survival

PH- Pleckstrin homology

PI3K- PI3 kinase

PK- Pharmacokinetic

PPAR ɣ- Peroxisome proliferator-activated receptor ɣ

PR- Progesterone receptor

PTEN- Phosphatase and Tensin Homologue

RFI- Relative fluorescence intensity

RPPA-Reverse phase protein array

RT- Room temperature

RTK- Receptor tyrosine kinase

SEM- Standard error of the mean

SFKs – Src family kinases

Sos- Son-of-Sevenless

SRB- Sulphorhodamine B

T-DM1- Trastuzumab-DM1

TKI- Tyrosine kinase inhibitor

TTF- Time to treatment failure

TTP- Time to progression

TZDs-Thiazolidinediones

v:v- Volume:volume

WBI- Whole breast irradiation

W:v- Weight:volume

XIAP- X linked inhibitor of apoptosis.

List of Figures

List of Tables

Table of Contents

Chapter 1: Introduction

Traditionally, the systemic treatment of cancer has relied on the use of non-specific, highly toxic chemotherapeutics. However, significant progress in the field of molecular biology has led to a dramatic increase in our understanding of some of the complex processes underpinning the development of cancer. This in turn has led to the identification of multiple signalling molecules with altered expression or aberrant activity in cancer, which are potentially amenable to exploitation by modern anti-cancer therapies. The introduction of iconic drugs such as imatinib and trastuzumab has revolutionised the management of Chronic Myeloid Leukaemia (CML) [1] and HER2 positive breast cancer [2] respectively. However, after this initial success, numerous potential agents have been investigated in clinical trials yet relatively few have successfully been incorporated into mainstream clinical practice. Oncological drug development has historically been plagued by low success rates with less than 10%of drugs tested in phase 1 trials successfully making it to market [3] and studies suggest these rates have not improved in the last 2 decades [4], implying that recent biomedical innovations have not impacted on our ability to successfully identify active candidates. Most drugs fail late in the development process at a cost in excess of $400 million [5] placing a huge economic strain on the pharmaceutical industry and crucially resulting in exposure of potentially hundreds of patients to toxic, yet ineffective treatments. Traditional drug development programmes are not ideally suited to testing drug efficacy of more modern molecularly targeted agents, yet current programmes have largely failed to adapt to the vast numbers of these agents currently under investigation.

1.1 Conventional oncological drug development programmes

Drug development programmes consist of a preclinical and subsequent clinical phase. Generally, the mechanism of action of most conventional chemotherapeutics is unknown at the start of the drug development process and therefore potential compounds of interest are identified by empiric screening normally involving a panel of human cell lines aiming to encompass the major tumour types. Once *in vitro* efficacy has been established,

demonstration of activity using *in vivo* models remains a critical step providing the earliest evidence of drug efficacy within an animal as a whole and potentially allowing for the contribution of systemic factors, such as tumour-stromal cell interactions. *In vivo* studies also provide essential pharmacokinetic (PK) and pharmacodynamic (PD) data. PK data, including measurements of drug absorption, distribution and metabolism, are used to inform initial dosing levels in subsequent clinical trials whilst elimination data may be used to optimise the dosing schedule. The importance of the data generated during these studies has been highlighted by previous experiences where drugs have entered into late phase clinical trials despite the active murine dose being substantially above the human maximum tolerated dose (MTD) (see below) [6]. This has led to late stage and high profile, yet predictable, drug failures. A variety of different *in vivo* models are used in drug efficacy studies, including spontaneous murine models, hollow fibre assays and genetically engineered mouse models (GEMM) but xenografts remain the most commonly used. For further discussion on the different *in vivo* models in these studies see section 2.1.

On completion of preclinical testing, new agents must then pass through a series of clinical studies referred to as phase 1, 2 and 3 trials. Traditionally, phase 1 trials include a relatively small number of patients with advanced disease, often with mixed tumour types, for whom no standard treatment options exist. The main aims of phase 1 trials are to determine a novel drug's safety and tolerability either when given alone or in combination with the main outcome being determination of a recommended dose for further study [7]. It is assumed that for traditional chemotherapeutics, a common mechanism of action results in both tumour efficacy and drug induced side effects and therefore higher doses resulting in greater treatment toxicities will be more efficacious. The recommended dose for further study in these drugs generally equates to the MTD [8]. Phase 1 trials also frequently generate important PK and PD data and whilst preliminary evidence of efficacy may also be reported, these trials are generally not sufficiently powered to detect clinical activity [9].

Phase 2 trials may be designed as either single arm or randomized studies which aim to demonstrate either preliminary activity or to guide selection of specific tumour types for further study [10]. The main aim of most phase 3 trials is to compare the activity of a novel compound either alone or in combination with that of the gold-standard treatment within a well-defined disease population [11]. Both phase 2 and 3 clinical trials aim to give a measure of disease response and a range of endpoints are used including overall response rate (ORR), time to progression (TTP), progression free survival (PFS), overall survival (OS), time to treatment failure (TTF) and clinical benefit ratio (CBR).

Although drug development programmes can be described as a streamlined passage through from *in vitro* studies to *in vivo* and on through the various stages of clinical trial development, at present there is little in the way of consensus about key criteria that a drug must reach in order to successfully move from one phase into the next [4]. The decision to halt the progression of a drug after development of intolerable toxicity during a phase 1 trial at a lower dose than would be predicted to be efficacious is relatively straightforward. However, deciding whether there is sufficient evidence of drug activity to progress from pre-clinical to clinical studies or from phase 2 to phase 3 clinical trials may be much more complex and is likely to be influenced by a host of other non-scientific factors, including societal and economic pressures.

1.2 Developing appropriate drug development programmes for molecularly targeted agents

This schema for drug development is still generally applied to the development of molecularly targeted agents, despite several critical differences between these agents and traditional chemotherapeutics. The most fundamental of these differences is that, unlike during the process of generating a novel chemotherapeutic, the mechanism of action of molecularly-targeted agents is known at the start of the drug development process. Molecularly targeted therapies exploit differences in either the expression or activity of disease targets (primarily receptors or enzymes) between normal healthy cells and cancer cells. These targets therefore represent potential susceptibilities within the cancer cell, which when inhibited will negatively impact on the progression of the tumour [12]. Cancer is a highly heterogeneous condition with high levels of both intra- and inter-patient variability observed. Therefore, similarly to chemotherapeutics, molecularly targeted therapies are unlikely to be ubiquitously efficacious but instead activity is restricted to patient subgroups, defined on the basis of their genotype or proteomic phenotype. Extensive preclinical work up is required even prior to the generation of drug candidates to generate detailed information on both the potential positive and negative consequences of target inhibition and the level and timing (continuous versus intermittent) of target inhibition required to meaningfully moderate tumour behaviour. Following validation of the target, a variety of different approaches can be used to generate potential drugs, including high throughput screening of chemical libraries, screening of low molecular weight fragments, virtual screening or where the structure of the target is already known a custom-designed drug can be generated. Potential candidates are prioritised on the basis of their physiochemical, PK and toxicity profiles demonstrated using a range of *in silico* techniques. The most promising of these

candidates then undergo repeated cycles of production, testing and further modification to optimise their efficiency, physiochemical, PK and toxicity profiles during *in vitro* testing [13]. *In vivo* testing exploits the same range of models used during the testing of chemotherapeutics. In addition to demonstrating evidence of *in vivo* efficacy, these models ideally need to provide evidence of a direct relationship between the drug levels achieved, target inhibition and modulation of tumour behaviour [4].

Clinical trials using molecularly targeted agents also frequently follow the same programme as outlined above for chemotherapeutics. This includes the use of MTD as the main outcome for phase 1 trials. As many potential targets are differentially expressed or activated in cancer cells compared to healthy cells, it may be possible to inhibit cancer progression with minimal toxicity to healthy cells [4]. The mechanism of any observed treatment related toxicities may therefore be distinct from the drug's mechanism of action making the MTD an inappropriate end point. Determination of the *'biologically optimal dose'* may be a more relevant endpoint. In view of the vast range of drugs now available, Hunsberger proposed that identification of the *'biologically adequate dose',* which can be achieved with as little as 3 or 4 patients at each dose level, may be sufficient prior to commencing drug efficacy studies [14]. However, both these approaches require the development of appropriate biomarkers, which is an extremely complex and time-consuming process. The lack of such biomarkers may account, at least in part, for the results of a recent study which showed that toxicity was still used to define the dose recommended for phase 2 study in the majority of 60 phase 1 clinical trials involving targeted, non-cytotoxic drugs [15]. Incorporation of biomarkers into study end points would also likely require paired pre- and post-treatment biopsies. At present, there is still considerable reluctance to make repeat biopsies mandatory at the time of entry into clinical trials due to concerns that it might adversely impact on patient accrual and therefore the current feasibility of using biologically relevant doses as an endpoint in clinical trials is challenging. Alternative solutions that could avoid the need to perform repeat biopsies might include the use of a surrogate marker, such as target inhibition in peripheral blood mononuclear cells (PBMC) or the use of modern functional imaging techniques, such as digital contrast enhanced MRI, which has been used to measure tumour vascularity and permeability in dose finding studies of angiogenesis inhibitors. However, prior to adoption of these techniques, it would be essential to demonstrate that changes in the readout from such surrogates accurately reflect target inhibition within the tumour and modulation of tumour behaviour [4].

A further important difference between the design of clinical trials for chemotherapeutics and molecularly targeted agents is the use of therapeutic combinations. Before chemotherapeutics are trialled in combination, all individual agents must show evidence of disease activity. Considering the highly specific mechanism of action of targeted agents, this may not be appropriate and failure to account for this may result in rejection of a potentially active drug. For example, there is considerable preclinical evidence that Src activity moderates the behaviour of HER2 positive breast cancer [16]. However, a phase 2 trial of single agent dasatinib failed to show any single agent efficacy in HER2 positive breast cancer [17]. Arguably, the expectation that Src inhibitors alone would inhibit tumour growth might be considered optimistic whilst combining these drugs with HER2 directed therapies, such as trastuzumab, may have proved more fruitful.

When designing phase 2 and 3 trials for molecularly targeted agents, consideration needs to be given to appropriate patient recruitment. Traditionally trials have focussed on examining drug activity within a single condition assuming this represents a single entity, yet there is increasing recognition of the heterogeneity within given cancer subtypes and failure to account for this may lead to premature rejection of a potentially active drug. For example only 8% of patients with non-small cell lung cancer (NSCLC) possess a mutation in exons 19 and 21 of the epidermal growth factor receptor (EGFR), which predicts for response to the tyrosine kinase inhibitor (TKI) gefitinib [18]. As these mutations are relatively rare, the inclusion of all other NSCLC patients in these trials could easily mask the efficacy of this drug within this patient subgroup.

Selection of appropriate endpoints is a further important consideration when designing phase 2 and 3 trials with these agents. Whilst these agents may be cytotoxic, many are cytostatic in nature or have anti-metastatic properties and therefore slow tumour growth rather than causing tumour shrinkage. Traditional trial endpoints which rely on tumour shrinkage, such as ORR (defined as the proportion of patients with a tumour reduction of a predetermined amount within a specified time period), are therefore not suitable for use in these studies. OS unarguably remains the most meaningful end point in all clinical trials, irrespective of the nature of the drug being investigated. However, these trials are generally lengthy to conduct and the outcomes are susceptible to bias by cross over to other arms within the trial or by initiation of other treatments at the time of disease progression. Neither PFS nor TTF are dependent on tumour shrinkage and therefore represent meaningful endpoints for cytostatic drugs in phase 2 and 3 trials, although results can be influenced by the frequency of clinical and radiological follow up [4] [9].

In summary, there are numerous factors which contribute to the high attrition rates, which continue to be seen during oncological drug development. In the following experiments, we have elected to focus predominantly on the development of models, which might further improve selection of agents to take forward into clinical trials as appropriate selection of active agents and rejection of unsuitable agents at this stage of development would produce huge time and economic savings as well as minimising the numbers of patients exposed to ineffective treatments. There remains an urgent unmet need to develop *in vivo* models which are better able to recapitulate the key features of human cancer as highlighted by the finding that at present only 4% of patients participating in phase 1 clinical trials actually benefit from the treatment they receive [19].

1.3 Use of *in vivo* models in preclinical drug development

1.3.1 Hollow fibre assay (HFA)

The HFA consists of human tumour cells grown in bio-compatible hollow fibres and then transplanted into either subcutaneous or intraperitoneal sites of immune-deficient mice. The fibres contain narrow pores, enabling exposure of transplanted cells to anti-cancer drugs but preventing their escape into subcutaneous or intraperitonal locations. The NCI developed this technique to try and further refine selection of drugs with proven efficacy in the *in vitro* setting prior to commencing relatively costly and lengthy traditional *in vivo* studies [20]. Studies exploring the efficacy of this technique have shown that response in the HFA is predictive of response in subsequent xenograft studies and this predictive capability can be further enhanced by implantation of the fibres at intra-peritoneal locations. More recently, the HFA has been used to confirm drug-target interactions using a variety of PD end points, such as changes in protein/gene/mRNA expression or DNA damage [21].

1.3.2 Early *in vivo* models

The earliest animal studies used either chemical or radiation-induced murine leukaemias. However, activity in these models was not predictive of clinical activity [22] and they were superseded by mouse cell line allografts. The P388 and L1210 leukaemia cell lines were the earliest murine cell lines used to screen novel compounds for potential therapeutic activity [23]. These cell lines were used in the development process of several drugs which are still in use today for rapidly growing malignancies, such as haematological cancers. However, they were less suitable for use in predicting activity within solid tumours leading to the introduction of the B16 melanoma and Lewis lung carcinoma cell lines in the 1970s. These cell lines also benefited from the ability to generate lung metastases allowing novel compounds to be tested for efficacy against both the primary tumour and the development of metastases [24].

1.3.3 Xenograft based models

1.3.3.1 Subcutaneously implanted human tumour xenografts

Tumour xenografts remain the most frequently used *in vivo* models and have played a role in the development of most anti-cancer treatments in mainstream clinical practice today. However, the high attrition rates seen during the clinical phase of drug development suggest that these models are far from perfect and have a tendency to over-estimate the sensitivity of human tumours to novel therapeutic compounds. Indeed, when the efficacy of 39 drugs in a panel of xenografts was retrospectively compared to data from phase 2 clinical trials, it was found that drugs needed to be active in at least a third of tested xenografts to be predictive of efficacy in at least some clinical trials. Furthermore, the correlation between activity in tumour type specific xenografts and matched human tumours was low with only NSCLC xenografts correctly identifying drugs with activity in NSCLC clinical trials [25].

Traditionally, xenografts are established by subcutaneous inoculation of human tumour cells into the flanks of immunocompromised mice. This is technically straightforward and results in the timely generation of a single tumour; the growth of which can be followed using simple calliper measurements. The resulting tumour retains the histomorphology of the parental cell line from which it was derived, although after decades of *in vitro* culture this is unlikely to still

be representative of the tumour from which the cell line originated [26]. Furthermore, due to the limited treatment options at the time when many of these cell lines were generated, the resulting tumours are relatively treatment naive in comparison to the advanced disease states against which they will be tested in early phase clinical trials. Cancer is also a highly heterogeneous condition with high levels of variation observed both within and between individual tumours from the same cancer subtype. Use of well-established highly homogeneous immortalized cell lines to generate xenografts therefore fails to recapitulate the huge complexity seen in human disease. In addition, individual studies typically only use relatively few cell lines to generate xenografts and therefore these models represent only a very limited snap shot of the enormous diversity of genetic and epigenetic mutations that may be found within any given clinical tumour subtype. Some tumour types are also not amenable to current tissue culture techniques and therefore will inevitably be under-represented in xenograft studies.

Another critical limitation of xenografts is their dependency on immune compromised hosts, which prevents the exploration of any modulating effect the immune system might have on drug efficacy. The role of the immune system in moderating tumour behaviour is now well-established [27] and the inability of these models to explore this is likely to become an increasing issue due to the development of a growing number of immune modulatory drugs, including the CTLA4 inhibitor, ipilumumab, and the PD1 inhibitor, nivolumab, which have both recently been approved for use in malignant melanoma. The lack of a fully functioning immune system also doubtless contributes to the general frailty seen in host mice which may limit their ability to tolerate certain drugs. Furthermore, SCID mice possess significant DNA repair defects which may also affect response to drugs [5].

Whilst traditionally research has focused predominantly on the behaviour of epithelial cells within cancers, the importance of non-epithelial tumour components, such as stromal tissue, in moderating tumour behaviour is increasingly recognised [28]. Xenografts contain only limited amounts of stromal tissue and the epithelial-stromal cell interactions found in these tumours are unlikely to be reflective of those in human cancers as firstly the stromal tissue is host derived (i.e. mouse in origin) and secondly it originates from a non-native tumour site [29]. Studies comparing the response of xenografts to drugs have shown variable tumour responses depending on the xenograft location [30]. Undoubtedly, the development of tumours at non-native sites also contributes to the low rates of metastases seen with these models. Therefore, whilst these models can be used to explore drug efficacy in primary tumours, they are not suited to exploring the effect of drugs on processes such as local

invasion and the development of metastases. Given that the vast majority of patients with cancer die as a result of their metastatic disease rather than their primary tumours, this is clearly a fundamental issue and limits the degree to which drug testing in these models can accurately reflect clinical testing.

A final factor to consider when examining the differential activity of drugs during preclinical *in vivo* experiments and clinical studies is the use of dramatically differing trial endpoints [31]. Agents which slow the rate of tumour growth are generally considered active in xenograft studies, whilst more robust criteria must be met during clinical trials for a tumour to be classified responsive, including tumour shrinkage of at least 30% [32].

Despite these limitations, there are numerous examples of the successful use of xenografts in drug development, for example well characterised ovarian xenografts were initially used to demonstrate the activity of trabectedin in this tumour group [33]. This activity was later confirmed in phase 2 clinical trials [34] [35] and promising activity has also recently been identified in a phase 3 trial [36]. However, as already alluded to there are also numerous examples of xenograft studies which have supported the transition of drugs into early phase clinical trials only to result in disappointment. Worse still there have been cases where drugs, despite appearing efficacious in preclinical models, have subsequently been suggested to promote tumour progression in clinical trials. Thiazolidinediones (TZDs) are agonists of peroxisome proliferator-activated receptor ɣ (PPAR ɣ) and are widely used in the management of type 2 diabetes. They were shown to be active against colon cancer xenografts [37] but when troglitazone was trialled in a cohort of patients with colon cancer, all patients experienced disease progression within a matter of months of starting treatment [38]. This led some people to suggest that TZD treatment expedited disease progression, although subsequent epidemiological studies exploring the risk of cancer in diabetic patients treated with these drugs would not support this [39]. Xenograft studies alone are insufficient to accurately determine the *in vivo* efficacy of novel compounds. The tendency of these models to over-estimate tumour response to new drugs suggests they may be useful as initial screening tools as any drug which fails to display activity in xenografts is unlikely to be efficacious in later studies using more refined, potentially less sensitive and more specific models. However, as we begin to develop a greater understanding of the many complex factors acting together to influence a tumour's response to a drug, this assumption appears less robust and we must recognise the possibility that current models are equally capable of failing to identify active drugs. Xenografts are unlikely to disappear altogether from drug development programmes and it is increasingly clear in order to optimise the quality of the

data generated, efforts currently underway to genetically characterise the human cell lines used must continue. This will facilitate selection of appropriate models in which to test molecularly targeted agents but may also provide greater information on the potential mechanism of action of emerging chemotherapeutics [40].

1.3.3.2 Orthotopically implanted human tumour xenografts

Orthotopic transplantation involves the transplantation of donor tumour material into the appropriate anatomical location within the host, for example inoculation of the mouse mammary fat pad (MFP) with a human breast cancer cell line. This technique was developed to overcome 2 major limitations of subcutaneous xenografts; firstly that the subcutaneous location fails to accurately model the role of the local microenvironment in tumour development and secondly that the rate and sites of metastases seen in these more traditional models are not characteristic of those seen in human cancers. The earliest experiments using this approach involved syngeneic transplantation of a murine colon adenocarcinoma cell line into various sites within the gastrointestinal tract and resulted in high rates of mesenteric lymph node and hepatic metastases [41], consistent with the most common pattern of spread seen in human colorectal cancer [42]. Today, there are numerous reports describing the successful implantation of tumour material into most sites where human cancers commonly arise [30] although clearly certain tumour types are more amenable to this type of transplantation; for example implantation of human breast cancer cell lines into the mouse MFP is relatively straight forward, whilst transplantation of tumour material into the murine prostate gland or to deep sites within the brain is considerably more challenging.

In addition to the development of a metastatic pattern more in keeping with that observed in human disease, orthotopic transplantation is widely acknowledged as offering two other main advantages. Orthotopic transplantation allows the exploration of processes involved in local invasion at a clinically relevant site, for example angiogenesis. This is particularly relevant given that endothelial cells in different tissues have been shown to express different receptors [43]. Orthotopic models of colon cancer have been used to demonstrate the activity of the anti-angiogenic drug combretastatin A-4 phosphate both at primary and secondary tumour sites, although its activity in clinical disease has yet to be shown [30]. Several studies have suggested that orthotopic xenografts may also be more predictive of response to cytotoxics. For example, Kuo et al showed that an orthotopic SCLC xenograft

was sensitive to cisplatin, which constitutes the backbone of treatment for human SCLC, but when the same xenograft was transplanted subcutaneously, its sensitivity to the drug was lost [44]. However, the response of orthotopic xenografts is not universally predictive of human response; the matrix metalloprotease inhibitor baltimastat was found to be active in an orthotopic model of colon cancer yet unfortunately the results from a subsequent clinical trial were disappointing [30].

In addition to issues relating to the technical feasibility of transplanting tumour material into particular anatomical locations, other challenges associated with this approach include difficulty in monitoring tumour progression and response. Depending on the site of the transplant, costly, specialist imaging techniques may be required to facilitate this potentially limiting the widespread adoption of this technique. In addition, although these models result in more efficient development of metastases, most animals still die from their primary tumour. For example Bibby et al found that most mice with orthotopic colorectal implants died from their primary tumour whilst their metastatic burden was relatively low. However, resection of the primary tumour did permit the development of more extensive liver metastases thereby enhancing the ability of this model to reproduce the features of human disease [30]. Finally, orthotopic transplantation is still not able to overcome some major limitations associated with the use of traditional xenografts, such as the lack of a functioning immune system. Many studies continue to use established human cell lines to generate xenografts and therefore, similarly to traditional xenograft studies, are also limited by a lack of tumour heterogeneity. However, more recently this approach has been exploited in studies using GEMMs and patient derived xenografts (PDXs) in an attempt to overcome this (see below).

1.3.3.3 Patient derived xenografts (PDXs)

Recognising the issues relating to the generation of xenografts from homogeneous cell lines, many of which bear little resemblance to the original tumour from which they were derived, there has been a recent surge in the popularity of using fresh human material to generate xenografts. During these experiments, sections of fresh human tumour samples are transplanted either subcutaneously or orthotopically into immune-compromised mice. Once the xenograft is established, it can be propagated over successive generations (without any intervening period of *in vitro* culture) to generate a cohort of mice with tumours all derived from the same host material. Previous studies using comprehensive genome wide analysis

has shown retention of activity of the majority of key genes and signalling pathways in xenografts derived from a variety of tumour types, including small cell lung [45] [46] and pancreatic [47] cancers. Key benefits of PDXs include the preservation of molecular tumour heterogeneity and through co-transplantation of human stromal tissue along with tumour material the accurate recapitulation of the tumour microenvironment. One of the biggest collections of PDXs has been generated by Fiebig and colleagues, who subcutaneously transplanted material from 1600 tumours resulting in the successful generation of over 300 different xenografts representing all the major tumour types [48] [49]. Specifically, within the field of breast cancer, DeRose transplanted material from 49 primary or metastatic tumours following which 37% successfully engrafted and 24% resulted in the development of established xenografts which were successfully maintained over several passages. These xenografts resulted in the development of metastases in sites similar to those seen within the corresponding patient. The rate of tumour engraftment was not predicted by either hormone receptor or HER2 status although the rate of engraftment was predictive of patient survival [50].

Once generated the models can be used to explore a range of different scientific questions; for example transplantation into multiple different recipients could be used to facilitate the collection of tumour tissue at a variety of different time points and therefore enhance our understanding of molecular changes which accrue over time in evolving tumours and promote processes such as metastasis. This would be extremely valuable as at present tumour characterisation in humans is performed at a limited number of time points, for example at the time of diagnosis. However, it remains critical to compare the changes in molecular signature seen within the model with those observed in the corresponding human tumour to ensure that the model continues to reflect the original tumour from which it was derived. These xenografts have also been used in the successful development of biomarkers, for example studies in K-RAS mutant colorectal cancer PDXs and human colorectal cancer cell lines identified Wnt pathway activation as being predictive of resistance to the MEK1/2 inhibitor AZD6244 [51]. However, undoubtedly the most excitement surrounds their potential use in predicting therapeutic response in human disease. In one study, 15 colorectal PDXs were treated with 5-fluorouracil (5-FU) and oxaliplatin or irinotecan and when the response was compared to that of the corresponding human tumour a reasonable degree of concordance was observed [52]. This has led some to speculate that in the future PDXs may play a central role in determining an individuals' treatment through establishment of personalised, real-time clinical trials prior to initiation of any treatment. In reality the development of such trials is unlikely to be feasible on a mass basis (see below), however these models are valuable resources for identifying new therapeutic targets and for testing

the therapeutic response to novel agents within molecularly defined subtypes of cancer. For example, PDXs have been used to demonstrate the activity of a pan-aurora kinase inhibitor within triple negative breast cancer [53].

1.3.4 Genetically engineered mouse models (GEMMs)

Since the initial development of gene targeting technology, GEMMs have undergone numerous refinements to facilitate the more accurate modelling of human cancers. The earliest GEMMs were generated through manipulation of embryonic stem cells (ESCs) resulting in the ubiquitous over-expression of an oncogene or loss of a tumour suppressor gene at all stages of prenatal and postnatal development. Examples of models generated in this way include models with loss of p53 expression or expression of a mutant retinoblastoma (Rb) allele [5]. These models have improved our understanding of the role played by individual genes in tumourigenesis and have contributed to our greater understanding of the co-operation seen between different gene mutations during tumour evolution. However, the range of genes which can be studied using these models is restricted as where the gene has an essential, non-redundant function in prenatal development embryonic lethality is inevitable. In addition whilst these models accurately recapitulate the features of rare inheritable cancer susceptibility syndromes, they fail to model the sporadic onset of most human tumours. Furthermore, the ubiquitous expression or knockout of the gene of interest means these models frequently develop multiple tumours at different anatomical sites and have a high incidence of haematological malignancies. This results in a relatively short life-span, which largely prohibits their use in preclinical drug testing.

These limitations led to the development of the next generation of GEMMs, in which there is conditional expression of the gene of interest in a tissue-specific and/or time dependent manner. Several different approaches have been used to achieve this including the use of chemically induced transcription factors, such as the tetracycline-dependent system and somatic gene transfer. This later approach most commonly uses avian retroviruses and involves the manipulation of cells in the target tissue to express the retroviral receptor. The corresponding retroviral vector is then used to deliver the gene, which can only be taken up by cells expressing the receptor thereby restricting the expression/loss of expression of the gene in a tissue-specific manner [57]. However, the cre-lox P system is the most commonly used system to facilitate conditional expression/inactivation of an individual gene and relies

on the use of lox P recognition sites to guide cre-recombinase mediated recombination. In order to inactivate a gene, it must be flanked by lox P sites, which when placed in direct orientation, do not interfere with the gene's function in the absence of the enzyme cre-recombinase. Introduction of the enzyme, either by somatic delivery or by crossing with a cre-recombinase bearing mice results in recombination between the 2 recognition sites and deletion of the gene. This system can also be used to activate an oncogene; in the absence of cre-recombinase, a transcription terminator, flanked by 2 lox P sites, is used to separate the oncogene from its promoter. Introduction of cre recombinase triggers recombination and excision of the transcription terminator placing the oncogene under the control of its promoter resulting in gene transcription. An additional mechanism for regulating gene expression in a time-specific manner involves the CreERT2 transgene, which is created by fusing cre recombinase to the ligand binding domain of the oestrogen receptor (ER). When treated with the oestrogen analogue tamoxifen, ERT2 translocates to the nucleus allowing cre-mediated recombination to occur [58].

An alternative approach involves the stochastic activation of oncogenes and has recently been used to generate a KRAS2 model of spontaneous cancers. This is achieved by generating a silent mutant allele in which 2 exons of the gene (the second of which contains an activating mutation) are separated by a transcription terminator, such as a neomycin resistant gene. Genetic recombination is a low incidence, spontaneous event that occurs during mitosis and occasionally may occur in a random fashion to trigger excision of the transcription terminator resulting in concomitant expression of both the wild-type and mutant alleles. Whilst this is not the most efficient way to trigger oncogene activation and lacks the control seen with the previously described methods, it results in mosaic expression of the mutant allele under physiological conditions making this a potentially powerful method of modelling sporadically occurring cancers [59].

A further alternative approach is the use of chimeric models. Initial experiments involved the transplantation of ESCs, which had been manipulated *ex vivo* to ensure they contained all the required mutations, prior to transplantation into the mature tissue of the recipient animal. This allows the modified ESCs to proliferate in the context of a normally functioning organ and avoids the need for complex breeding schemes to generate the required genotype, although the initial manipulation of the ESCs is still time consuming. To try and overcome this, more recently techniques have been developed to extract progenitor cells from previously validated GEMMs for direct transplant into recipient animals, thereby avoiding the complex process of modifying the cells prior to transplantation [60].

Although potentially costly and time consuming to develop, once generated GEMMs are useful tools in a wide range of oncological experiments. To date, their major use has been in the fields of target validation and testing of novel and established therapeutic agents [5]. GEMMs are well characterised at the molecular level and allow us to explore the consequences of relevant gene mutations as well as providing a suitable model to test the efficacy of drugs which act against them. For example, combined treatment with the EGFR inhibitor erlotinib and gemcitabine resulted in a slight improvement in survival in Kras mutant model of pancreatic cancer compared to gemcitabine alone, reflecting the results of an earlier phase 3 clinical trial [61]. GEMMs also have a valuable role to play in determining the efficacy of more traditional cytotoxics. One of the earliest examples of the successful use of these models in the development of novel treatment strategies was in the management of acute promyelocytic leukaemia, which is caused by translocations involving chromosome 17. Using 2 different GEMMs, Pandolfi and colleagues demonstrated that the combination of arsenic trioxide with retinoic acid was an efficacious treatment for promyelocytic leukaemias caused by a PML-RARα translocation whilst an HDAC inhibitor and retinoic acid was suitable treatment for disease caused by a PLZF- RARα translocation. When these treatments were taken into the clinic they resulted in a high complete remission rate, reflecting the fact that the translocations used to drive tumorigenesis in the models recapitulated the driving mutations in human disease [56].

As already alluded to in the previous study, GEMMs have the potential to be powerful models in the development of biomarkers, both in facilitating early cancer diagnosis and in enabling prediction of therapeutic response. It is well established that early detection of cancer results in higher cure rates but at present this is largely dependent on the use of costly and specialist imaging techniques. Hung and colleagues used the Apcδ580 colorectal GEMM to demonstrate increased expression of the cysteine proteases cathepsin B and D in the plasma of tumour bearing mice [62]. Testing of human tumour colorectal cancers demonstrated up-regulation of cathepsin B expression in 82% of colorectal tumour samples and expression correlated with poor prognosis [63]. Should the increase in plasma concentration of cathepsin B and D be translated into the clinic, it may lead to development of the first blood test capable of diagnosing cancer at an early stage. GEMMs also have the potential to be valuable tools in the development of biomarkers which are able to identify patients who are likely to respond to specific therapeutic agents. For example, much controversy has surrounded the ability of PTEN status to predict response to trastuzumab. Although there is compelling *in vitro* preclinical evidence to support this, when tested in several large clinical trials the results have been mixed [64]. This is likely to be due at least in part due to the vast array of genetic and epigenetic permutations in human cancers, which

are also likely to impact on treatment response and may have obscured any predictive role of PTEN. Using a GEMM of HER2 positive breast cancer, Wang and colleagues demonstrated that loss of PTEN was associated with resistance to a HER2 targeting antibody [65].

A further important use of GEMMs is the identification of resistance mechanisms. Rottenberg and colleagues used the K14cre;Brca1$^{F/F}$;p53$^{F/F}$ model of BRCA1 deficient breast cancer to identify up-regulation of the efflux transporter P glycoprotein in tumours with acquired resistance to a poly(ADP-ribose) polymerase 1 (PARP1) inhibitor [66], although to date, there is no evidence that this mechanism of resistance is clinically relevant. The only mechanism of resistance which has been identified in clinical populations is genetic reversion of the original BRCA1 mutation through the acquisition of secondary mutations, which either correct or bypass the original mutation [67]. However, more global analysis of resistant tumours in the future is likely to provide further data on clinically relevant resistance mechanisms and potential resistance biomarkers.

GEMMS offer a number of advantages over more traditional xenograft based models. One of the major advantages is that spontaneous tumours develop within the appropriate organ and in the context of a fully functioning immune system. Furthermore, these models are highly molecularly characterised and the initiating genetic lesion underpinning tumour development is known making these models well suited to testing the efficacy of molecularly targeted agents. Importantly, models can be developed to ensure the driving genetic mutation has a correlate within human disease. In addition, the rate of metastases seen with these models tends to be more reflective of those observed in clinical disease and therefore they provide us with a greater opportunity to study some of the molecular processes underpinning this process. For example studies using the Rip1Tag2 model of pancreatic cancer showed that reduced neural cell adhesion molecules promoted the metastatic dissemination of pancreatic beta tumour cells [68]. However, most animals with metastatic disease still succumb as a result of the rapid growth of their primary tumour whilst their metastatic burden is relatively low, which is not reflective of the course of human disease. Where feasible, resection of the primary tumour prolongs animal survival allowing the development of more substantial secondary deposits [69], which could be exploited in the future to test the efficacy of novel agents in the metastatic setting. Finally, GEMMs, through the random acquisition of secondary mutations, are more able to recapitulate the heterogeneity of human cancer than xenografts and how this impacts on drug efficacy. In a Kras mutant model of pancreatic cancer, the combination of gemcitabine with an anti-VEGF monoclonal antibody improved OS in 50% of animals compared to gemcitabine alone but in the remaining 50% resulted in no survival advantage [61]. This difference in survival was seen despite the fact that

laboratory mouse strains are relatively inbred and cancer development occurs on a relatively homogeneous background.

GEMMs also have a number of limitations. Firstly, although significant overlap exists in the genes and pathways activated in human and murine cancers [70], some important differences have been identified. Inter-species variation in the distribution of genes between different chromosomes is seen, for example p53 and BRCA1 are found on the same chromosome in mice so co-deletion is more common than in human tumours [5]. Furthermore, fewer mutations are required to transform murine cells than human cells [71] and unlike tumours which develop in humans, those which develop in mice are generally chromosomally stable and contain fewer somatic structural rearrangements [72]. Additionally whilst telomerase dysfunction is frequently seen in human tumours, it is rare in cancers which develop in mice [73]. Secondly, despite the use of tissue-specific promoters, there may be some limited Cre expression in other tissues resulting in tumour development in non-target tissues. Thirdly, depending on the model used, lengthy and complex breeding programmes may be required to generate animals with the required genotype. Tumour penetrance rates can also be unpredictable and coupled with potentially lengthy tumour latency intervals (defined as the age of the mouse at the onset of tumour development), these experiments can be very protracted. Attempts to streamline these experiments have led to some groups performing othotopic transplants with either fragments from mature tumours or cell lines derived from the parental model. Whilst this may reduce the length of experiments, it also prevents the study of the stepwise development of tumour progression making it inappropriate for some experiments. Fourthly, similarly to orthotopic xenografts, depending on the model used, monitoring disease progression may be more complicated than when using subcutaneous xenografts and may require the use of specialist, complex imaging techniques. Fifthly, the development of new GEMMs is extremely time consuming and the number of models in existence is still relatively low. To try and develop sufficient models to reflect even a proportion of the diverse range of tumour initiating lesions seen in clinical practice would require an immense effort.

In summary, a range of different *in vivo* models are now available. All of these different models have their own relative strengths and weaknesses and in reality they are all likely to have a role to play in future oncological studies.

1.4 Breast cancer and its classification

It is a sobering thought that 1 in 8 women in the UK will develop breast cancer during their life time making it the most prevalent form of invasive cancer (excluding non-melanoma skin cancer) in the UK. Despite dramatic improvements in disease outcomes, 12 000 women and 80 men die each year from breast cancer (http://www.breastcancercampaign.org).

Breast cancer is no longer considered to be a single disease entity but is recognised to consist of several different pathological subtypes, which have distinctive histomorphologies and different clinical pictures [74]. Until recently, breast cancer was primarily classified according to the presence or absence of oestrogen receptor (ER), progesterone receptor (PR) and the HER2 receptor. Although, this is still the dominant mechanism of disease classification used clinically, gene expression studies using DNA micro-arrays have allowed breast cancers to be further classified into 5 groups on the basis of gene-expression pathways; luminal A and B, HER2 positive, normal-type and basal-like. Luminal tumours display similar features as those of luminal epithelial cells and tend to be hormone receptor (HR) positive whilst HER2 positive tumours are identified by the over-expression of the HER2 receptor. Normal-type tumours are characterised by high expression of basal epithelial-cell genes and low expression of luminal epithelial-cell genes. Basal-like tumours are identified by the absence of ER, PR and HER2 expression [75]. Several studies have shown that HER2 positive and basal-like tumours have worse outcomes than either luminal or normal-like tumours [76].

1.5 HER2

The human epidermal receptor (HER) family, comprising HER1 (EGFR), HER2, HER3 and HER4 is a family of structurally related transmembrane tyrosine kinase receptors, which are implicated in normal cell growth and development [77]. The receptors comprise an extracellular binding domain, an α helical transmembrane domain and an intracellular tyrosine kinase domain [78].

1.5.1 The role of HER2 in normal development

The HER family of receptors are expressed in a wide range of tissues. HER2 in particular plays an important role in the development of both cardiac myocytes and the peripheral nervous system [79]. Ubiquitous loss of HER2 expression in the developing embryo results in embryonic lethality at 10.5 days of gestation, most likely due to defective cardiac function as a result of absent trabeculae [79]. However, animals with a ventricular-restricted absence of HER2 expression were viable but develop cardiomyopathy, suggesting that HER2 plays an essential role in the prevention of this condition [80] [81].

HER2 is also expressed in the developing nervous system [82]. When mice with germline loss of HER2 were genetically rescued by myocardial expression of a HER2 transgene, the resulting animals died at birth due to severe defects affecting both motor nerves and Schwann cells.

1.5.2 The role of HER2 in breast cancer

HER2 gene amplification or protein over-expression is found in approximately 15 to 20% of all breast cancer cases [83]. Tumours are classified as HER2 positive if on immunohistochemistry (IHC) they demonstrate uniform, intense membranous staining of at least 30% of invasive cells (scored as 3+) or if using fluorescent in situ hybridization (FISH) they have at least 6 copies of the HER2 gene per nucleus or a FISH ratio (defined as HER2 gene signal to chromosome 17 signal) of more than 2.2 [83]. In breast cancer, HER2 status is positively correlated with tumour size, grade, proliferation index, lymph node status, DNA aneuploidy, p53 mutations and high urokinase-type plasminogen activator expression [84] [85]. Despite this, HER2 gene amplification is an independent predictor of poor clinical outcomes [86].

1.5.3 HER family signaling

1.5.3.1 HER receptor activation

Under normal physiological conditions, HER receptor signaling is regulated by the expression of their ligands. There are 6 HER receptor ligands, or EGF-related growth factors [87]; EGF, transforming growth factor α, amphiregulin, heparin-binding EGF, betacellulin, epiregulin and heregulin [78]. These ligands are initially produced as transmembrane proteins and are subsequently cleaved by cell surface proteases to release the mature ligand ready for signaling [87] [78].

Receptor homo- or hetero-dimerization is essential for HER receptor signaling. With the exception of HER2 (which has no known ligand and relies on cross-activation by other HER family receptors), HER receptors normally exist as inactive monomers. Binding of the respective ligands to the receptor induces conformational change leading to receptor dimerization [88]. Following receptor dimerization, there is asymmetric dimerization of the kinase domains resulting in sequential allosteric activation of one kinase domain by the other [89]. Activation of the kinase domains, results in phosphorylation of specific residues within the receptor's cytoplasmic tail, which then act as docking sites for a number of proteins leading to activation of downstream intracellular signaling pathways [78]. EGFR and HER4 both have recognized ligands and active kinase domains [78] and are therefore capable of forming both hetero- and homodimers. Heterodimers are more potent activators of downstream signaling pathways than homodimers and HER2-HER3 is widely acknowledged as being the most potent HER dimer in terms of strength of receptor interaction, ligand induced tyrosine phosphorylation and signaling pathway activation [90] [91]. HER3 is able to bind several ligands (including neuregulin 1 and 2 [77]) but is generally considered not to have an active kinase domain and is therefore considered incapable of binding ATP [92]. Therefore, it is dependent upon forming heterodimers with other receptors to activate intracellular signaling pathways. More recent experiments have shown that HER3 is locked in an inactive conformation and although it is able to bind ATP it remains catalytically inactive suggesting that it may function as a specialized allosteric activator of other HER receptors [93]. Conversely, whilst HER2 has no known ligand, it has an active catalytic domain and has the strongest kinase activity of all the HER receptors [94]. The ligand binding site of HER2 also differs from that of other receptors as it is in a conformationally active conformation making it the preferred heterodimerization partner for other HER family

receptors [95]. HER2-containing dimers are also slower to dissociate but undergo endocytosis and receptor recycling to the cell surface more frequently resulting in prolonged activation of intracellular signaling pathways [96]. When over-expressed, HER2 is able to signal in a ligand-independent fashion forming homo- and/or heterodimers resulting in uncontrolled cell growth, division and avoidance of apoptosis [77].

1.5.3.2 Intracellular signaling pathway activation

Phosphatidylinositol 3-kinase (PI3K)/Akt and mitogen-activated protein kinase (MAPK) signalling are the major biological readouts of ligand-dependent and -independent HER receptor activation (Figure 1.1).

1.5.3.2.1 MAPK signalling

Src homology 2-containing proto-oncogene (Shc) docking sites are found in numerous proteins and the cytoplasmic tails of all HER receptors contain at least 1 Shc docking site. This includes HER2 which contains 5 such docking sites making Shc the most common HER2 interacting protein [97]. Following phosphorylation, Shc associates with Growth Factor Receptor Bound 2 (Grb2), although Grb2 can also bind directly to HER2 at tyrosine residue 1139 [98]. In the cytosol, Grb2 is bound to the guanine nucleotide exchange factor Son-of Sevenless (Sos) and this complex binds to the membrane bound protein Ras catalysing the conversion of GDP to GTP with subsequent Ras activation [99]. Ras activates several effector proteins, including B-Raf, which in turn phosphorylates and activates MAPK (or MEK1). In turn, MAPK activates p44/42 MAPK (also referred to as ERK-1 and ERK-2) resulting in activation of members of the activator protein 1 (AP-1) family, including jun and fos. Following activation, jun and fos translocate to the nucleus, form a complex and bind to the AP-1 domain of DNA resulting in the transcription of genes involved in a range of different cellular processes, including proliferation, differentiation and cell survival.

1.5.3.2.2 PI3 Kinase (PI3K)/Akt signalling

PI3Ks are a family of lipid kinases characterised by their ability to phosphorylate inositol ring 3’ groups within inositol phospholipids [100]. Three distinct classes of PI3Ks exist with class I being the most heavily implicated in the pathogenesis of cancer [101]. PI3K gene mutations

are frequently identified in human cancers and are observed in between 20 and 25% of breast cancers [102]. Class 1 PI3Ks are heterodimers containing a catalytic subunit (p110) and an adaptor/regulatory subunit (p85). They can be further subdivided into class IA, which are activated by RTKs, and class Ib, which are activated by G protein coupled receptors [100].

There are 3 main mechanisms of PI3K activation. Firstly, binding of PI3K's adaptor subunit to a phospho-YXXM motif (where X represents any amino acid) on a RTK triggers the activation of PI3K's catalytic subunit (HER2 does not contain a PI3K docking site, although 6 such sites are found in the intracellular domain of HER3 [97]). Secondly, indirect binding of PI3K can occur to the RTK via GRB2 and its scaffold protein GAB, which in turn is capable of binding to the PI3Ks adaptor subunit triggering activation of the catalytic subunit. Finally, the GRB2-Sos complex can activate RAS, which can activate the catalytic subunit of PI3K independently of its adaptor subunit [103].

Once activated, the p110 subunit of PI3K binds to phosphatidylinositol-4,5-biphosphate (PIP_2) in the lipid bilayer of the cell membrane and phosphorylates it to form phosphatidylinositol-3,4,5-trisphosphate (PIP_3). PIP_3 activates a number of intracellular signalling pathways implicated in numerous cell functions including those involved in tumour initiation and progression. The tumour suppressor gene phosphatase and tensin homologue (PTEN) dephosphorylates PIP_3 back to PIP_2 thereby terminating PI3K signalling. Loss of PTEN is seen in approximately 50% of human tumours [104] resulting in hyperactivation of this signalling pathway. PIP_3 contains a pleckstrin homology (PH) binding site to which both the protein serine/threonine kinases 3'-phosphoinositide-dependent kinase-1 (PDK1) and Akt/PKB are able to bind [103]. When brought into close proximity, PDK1 activates Akt by phosphorylation at its threonine 308 residue [105]. For full activation, Akt must also be phosphorylated at its serine 473 residue. Initial studies identified multiple potential candidates capable of performing this second phosphorylation but more recent studies have suggested that mammalian target of rapamycin complex 2 (mTORC2) is the only kinase capable of phosphorylating Akt at its serine 473 residue [106].

1.5.3.2.3 Effects of activated Akt on cell behaviour

1.5.3.2.3.1 Inhibition of apoptosis

Activated Akt inhibits apoptosis through a number of different mechanisms. Firstly, it inhibits the activity of the pro-apoptotic proteins BAD and BAX [107]. It also negatively regulates the activity of the pro-apoptotic protein p53 through phosphorylation and activation of mouse double minute 2 homolog (Mdm2). Furthermore, activated Akt negatively regulates the transcription factor NFKβ resulting in an increase in the transcription of pro-survival and anti-apoptotic genes. It also negatively regulates the transcription of forkhead transcription factors, which reduces the production of cell-death promoting proteins such as Fas-ligand [108].

1.5.3.2.3.2 Cell cycle progression and proliferation

Akt inhibits glycogen synthase kinase 3 (GSK3) mediated phosphorylation of β catenin thereby increasing β catenin's stability. Unphosphorylated β catenin translocates to the nucleus, where it induces the expression of cyclin D and cell cycle progression [109]. Furthermore, Akt phosphorylates and enhances the stability of p21, a positive regulator of cell cycle progression [110]. Finally, it phosphorylates p27 preventing its translocation to the nucleus and inhibition of cyclin E/CDK2 [111].

1.5.3.2.3.3 Protein synthesis

Akt plays a critical role in protein synthesis through activation of the mammalian target of rapamycin (mTOR) pathway. mTOR forms 2 complexes; mTORC1 and mTORC2. Activated mTORC1 phosphorylates and activates p70 S6 kinase and eukaryotic initiation factor 4E binding protein 1, which increase mRNA translation [112]. mTORC2 is responsible for phosphorylation of Akt on serine residue 473, which is essential for full Akt activation [106]. In addition, mTORC is involved in regulation of cell morphology and the cytoskeleton [113].

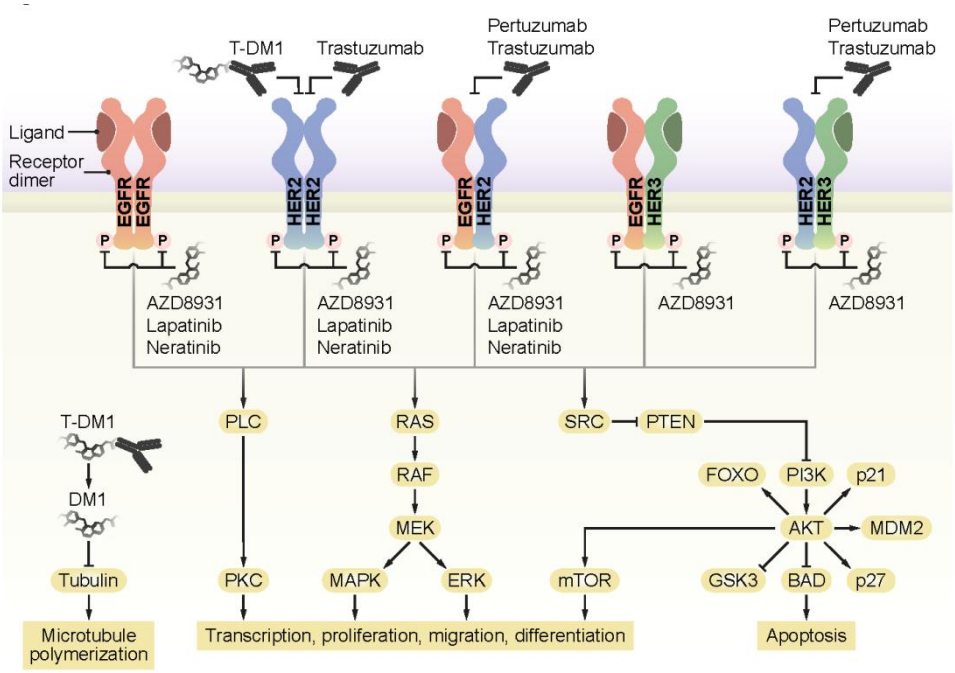

Figure 1.1: HER family signalling and site of action of targeted therapies in HER2 positive breast cancer (see section 1.5). HER family receptors are capable of forming either homo- or hetero-dimers at the cell surface in a ligand-dependent or independent fashion. Dimerization triggers transphosphorylation of tyrosine residues (P) and downstream signalling. Trastuzumab and pertuzumab are anti-HER2 monoclonal antibodies which target the extracellular domain of the HER2 receptor and inhibit receptor dimerization. T-DM1 is an antibody dependent conjugate of trastuzumab and maytansine. Binding of trastuzumab to the HER2 receptor results in internalization of the conjugate where subsequent lysosomal degredation results in intracellular release of DM-1 enabling it to bind to tubulin and inhibit microtubule polymerization. Lapatinib, neratinib and AZD8931 are TKIs with *in vitro* activity against EGFR and HER2. ERK, extracellular-signal-regulated kinase; FOXO, forkhead box O; GSK3, glycogen synthase kinase 3; MDM2, murine double minute 2; MEK, MAPK/ERK kinase; mTOR, mammalian target of rapamycin; PKC, protein kinase C. Taken from [114].

1.6 Treatment of HER2 positive breast cancer

The management of HER2 positive breast cancer is multi-modal. Surgery is currently the mainstay of treatment for early breast cancer and where appropriate is supplemented with radiotherapy, chemotherapy and targeted agents. The current guidelines used to guide management are discussed below, although in practice all treatment decisions must be made on an individual case by case basis taking into account individual patient factors.

1.6.1 Surgery

Mastectomy is the traditional management of early breast cancer although more recently breast conserving surgery (BCS) has become increasingly popular. This involves removal of the breast tumour without the need to remove the entire breast. Randomised trials comparing treatment outcomes following mastectomy and BCS have shown comparable survival rates but an increase in local recurrence rates following BCS, which can be abrogated by use of breast radiotherapy [115]. The more widespread use of neoadjuvant systemic therapy (see section 1.5.3), which involves the upfront administration of systemic treatment prior to surgical management, has led to greater use of BCS as tumours requiring mastectomy at diagnosis can often be down-staged to permit a more conservative surgical approach. In fact, in some cases neoadjuvant systemic therapy has been so successful that no viable tumour cells are found at the time of surgery (defined as a pathological complete response (PCR)) and this has led some to question whether surgery is still warranted. However, at present no data exists to support the omission of surgery in this context. A further area of contention is the role of surgery in the management of primary metastatic disease (defined as patients with metastatic disease at the time of presentation). Again, there is a lack of data from prospective randomized trials and what data is available has been drawn from retrospective studies which provide conflicting results [116] [117].

Appropriate management of the axillary lymph nodes is a further important surgical consideration. Treatment of the lymph nodes serves 2 main purposes; firstly it reduces the risk of local recurrence in the axilla and secondly as lymph node metastases are an important negative prognostic marker, it facilitates rationale decision making regarding further treatment. Axillary lymph node clearance remains the gold standard treatment for patients with evidence of lymph node involvement on ultrasound or ultrasound guided needle biopsy. In patients with no pre-operative evidence of axillary lymph node metastases at the

time of surgery, sentinel lymph node biopsy (which involves the identification of the lymph node most likely to be positive in the presence of axillary metastases) is now the standard of care. Only those with pathological evidence of lymph node metastases following biopsy are offered axillary clearance or radiotherapy [118]. In cases in which patients will receive adjuvant chemotherapy, endocrine therapy or targeted therapy some have questioned whether further treatment for a positive lymph node biopsy is still necessary.

1.6.2 Radiotherapy

Radiotherapy is aimed at further improving local control rates and is routinely used following BCS and in selected cases following mastectomy. Traditional treatment following BCS has involved whole breast irradiation (WBI) coupled with a boost in patients under the age of 50. A boost increases the delivery of radiotherapy to the tumour bed and the surrounding breast parenchyma (the areas at highest risk of harbouring residual microscopic disease) and reduces the risk of local recurrence. The lengthy duration of traditional WBI schedules and the potential for longstanding cosmetic changes has a detrimental effect on patients' quality of life. In efforts to overcome this, accelerated partial breast irradiation (ABPI) is becoming increasingly popular. ABPI involves delivering larger doses per radiotherapy fraction than standard regimes and focusing treatment on the tumour bed alone, giving an improved cosmetic outcome. It is currently considered in patients under the age of 50, with node negative tumours which are under 3cm in diameter. Ideally these patients should be treated within the context of a clinical trial as long term follow up data for ABPI versus WBI is still lacking.

Post mastectomy and axillary nodal surgery, the decision whether to proceed with chest wall radiotherapy or radiotherapy to the un-dissected regions of the axilla (upper axilla, internal mammary nodes and infra-clavicular and supra-clavicular nodes) is based on the risk of loco-regional recurrence. Features indicative of a high risk of recurrence and therefore mandating the use of radiotherapy include a substantial metastatic lymph node burden and a locally advanced tumour. Where neoadjuvant systemic therapy has been delivered, this decision is based on the disease stage prior to the delivery of any treatment, although in light of increasingly efficacious systemic options, there is a risk that patients are being over-treated. Reviewed in [119].

1.6.3 Chemotherapy

Unlike surgery and radiotherapy, chemotherapy aims to improve distant disease control (i.e control within organs other than the breast). It is used in the management of both early and metastatic breast cancer (MBC).

1.6.3.1 Use of chemotherapy in early breast cancer

In early breast cancer, the primary aim of chemotherapy is to eradicate micrometastatic disease thereby reducing recurrence rates and improving long-term OS. It can be delivered either post-operatively (adjuvant treatment) or pre-operatively (neo-adjuvantly). Neoadjuvant and adjuvant chemotherapy offer equivalent treatment outcomes [120] but neo-adjuvant therapy offers further advantages in terms of increasing BCS rates and providing an *in vivo* assay of chemotherapy efficacy within an individual tumour. The more wide-spread use of chemotherapy in early breast cancer has undoubtedly contributed to the reduction in disease-specific mortality observed in developed countries [121]. Current recommendations for adjuvant chemotherapy are based on evidence drawn from numerous clinical trials conducted over the past 30 years.

Combinational chemotherapy regimes, which contain an anthracycline (e.g. epirubicin and adriamycin), now form the cornerstone of adjuvant chemotherapy. Frequently used combinations include 5-FU and cyclophosphamide given either with epirubicin (FEC) or adriamycin (FAC). Comparison of anthracycline and non-anthracycline regimes demonstrated a 4% survival advantage at 10 years in favour of anthracyclines [122]. Anthracycline use is associated with significant acute treatment-related toxicities (e.g. alopecia, nausea, vomiting and mucositis). However, as treatment outcomes have improved, what has become increasingly evident is the significant longer-term complications associated with these drugs, including cardiotoxicity and the excess risk of secondary haematological malignancies [123].

Taxanes are used in addition to anthracyclines in patients with high risk early breast cancer. A systematic review comparing outcomes of taxane containing and non-containing regimes demonstrated an increase in the PCR rate following taxane treatment in 4 out of 5 neo-

adjuvant studies, although this failed to reach statistical significance. Furthermore, all 5 adjuvant studies included in the review demonstrated an increase in disease free survival (DFS) and 2 studies, which contained only patients with node positive disease, showed an improvement in OS following taxanes [124].

1.6.3.2 Use of chemotherapy in metastatic breast cancer

Although secondary breast cancer is incurable, a high proportion of metastatic tumours continue to respond to chemotherapy. When given in the metastatic setting, chemotherapy aims to palliate symptoms and improve OS, although the duration of treatment response is frequently disappointingly short.

Anthracyclines remain an important therapeutic option in patients who have not received adjuvant treatment or who were treated more than 1 year prior to the onset of metastatic disease. This latter group of patients who have received prior anthracyline treatment may require a dose reduction due to the greater risk of toxicity, particularly bone marrow suppression and cardiotoxicity. ORRs of approximately 30% have been observed following anthracycline treatment in patients with anthracycline naive disease [125].

Taxanes also remain an important option and are considered first line treatment for patients who have received adjuvant anthracyclines or progressed following anthracycline treatment in the metastatic setting. When used in metastatic disease ORRs of up to 50% have been seen [126].

Other treatment options include capecitabine and vinorelbine. Capecitabine (an oral fluoropyridimine prodrug) is widely used in metastatic disease. Major advantages of this treatment include its oral route of administration and that due to its well tolerated side-effect profile if disease responds, it can often be given long term as a maintenance treatment. ORRs of 20% have been seen with median survival in excess of 1 year even in patients with anthracycline and taxane resistant disease [127]. Vinorelbine is a vinka alkaloid which results in ORRs of up to 50% [128] although it is frequently poorly tolerated.

1.6.4 Endocrine therapy

Approximately 50% of HER2 positive breast cancers are also HR positive [129]. In the adjuvant setting, pre-menopausal patients with HR positive breast cancer receive between 5 and 10 years of tamoxifen treatment. In high risk cancers, anti-oestrogen therapy can be enhanced by the addition of GnRH analogues, or depending on patient preference, oophorectomy. Post-menopausal women with HR positive early breast cancer are either treated upfront with an aromatase inhibitor (AI) or with tamoxifen for 2 to 3 years before switching to an AI. These drugs are also active in the metastatic setting.

In the context of HER2 positive disease, preclinical data suggests that HER2 positivity confers intrinsic resistance to hormonal therapy [130] and that HER2 directed therapy may re-sensitize HER2 and HR positive cells to hormonal therapy [131]. This has been explored as part of two prospective, randomized clinical trials. Patients with newly diagnosed metastatic HER2 positive cancer were randomized to treatment with either the AI anastrozole or anastrozole plus trastuzumab as part of the Trastuzumab and Anastrozole Directed against Estrogen and HER2 Positive Carcinoma (TAnDEM) trial [132]. The EGF30008 trial also randomized patients with HR receptor positive breast cancer to treatment with the AI letrozole or letrozole and lapatinib [133]. In both TAnDEM and the HER2 positive subgroup of the EGF30008 trial, combinational therapy led to statistically significant increases in PFS, ORR and CBR. Neither trial demonstrated a statistically significant increase in OS, although survival was increased in TAnDEM despite a 70% cross-over from the single to the combined treatment arms. Together these trials support the combined use of hormonal and HER2 directed therapy, which is particularly relevant to patients with less aggressive metastatic disease or those who are too frail to receive chemotherapy.

1.6.5 Targeted therapy

The introduction of HER2 targeting agents has revolutionized the management of HER2 positive breast cancer. Chemotherapy demonstrates a lack of cell specificity and kills both healthy and cancerous cells. These agents, however, exploit the increased reliance of HER2 positive cancer cells on the HER2 signaling pathway and therefore exhibit more selective cytotoxicity and a reduced side-effect profile. Currently licensed therapies include monoclonal antibodies, tyrosine kinase inhibitors and most recently antibody dependent conjugates (Figure 1.1).

1.6.5.1 Currently licensed targeted therapies

1.6.5.1.1 Monoclonal antibodies

1.6.5.1.1.1 Trastuzumab

Trastuzumab was the first of the HER2 targeted agents to enter mainstream clinical practice and is approved for use in both early and metastatic HER2 positive breast cancer. It binds to subdomain IV of HER2's extracellular domain but despite its widespread use, its mechanism of action remains to be fully elucidated. Its mechanism of action is likely multimodal and thought to involve inhibition of ligand-independent receptor dimerization and downstream signalling, induction of cell-cycle arrest and apoptosis, interference with DNA repair, inhibition of angiogenesis, antibody-dependent cell-mediated cytotoxicity (ADCC) and inhibition of the cleavage of the HER2 extracellular domain preventing generation of the truncated constitutively active p95HER2 [2]. Although the efficacy of single agent trastuzumab is low, when given in combination with standard adjuvant chemotherapy it further reduces the risk of death by 33% [134]. The addition of trastuzumab to neoadjuvant chemotherapy also results in a significant increase in the PCR rate [135]. When given in combination with chemotherapy in metastatic disease, trastuzumab increases the rate and duration of responses and results in an approximate 4 month increase in OS [136]. This additional efficacy comes at the cost of little in terms of toxicity. The most common treatment related adverse event is asymptomatic reduction in left ventricular ejection fraction (LVEF), which is both generally treatable and reversible.

1.6.5.1.1.2 Pertuzumab

Pertuzumab binds to subdomain II of HER2's extracellular domain thereby inhibiting ligand-induced heterodimerization. Preclinical studies have suggested that when combined, trastuzumab and pertuzumab provided a more complete blockade of HER signalling than either drug alone (91). This is currently being tested in several ongoing clinical trials but following promising results in the NEOSPHERE trial [135] the combination of pertuzumab plus trastuzumab and docetaxel has already been granted accelerated approval by the FDA and European Medicines Agency for use in the neoadjuvant setting. Preliminary data from the CLEOPATRA study in which this same combination was tested in metastatic disease suggest that these findings from NEOSPHERE may be validated in larger, more definitive trials.

1.6.5.1.2 Tyrosine kinase inhibitors: Lapatinib

TKIs differ from monoclonal antibodies in several important ways. Firstly, they can be administered orally rather than intravenously, which is required for monoclonal antibodies. Secondly, as monoclonal antibodies bind irreversibly to the protein of interest whilst TKIs frequently bind reversibly, monoclonal antibodies tend to have a longer half-life. Thirdly, TKIs are generally considered to be less specific than monoclonal antibodies as they often target more than 1 kinase [137]. Lapatinib is currently the only TKI approved for use in trastuzumab refractory, metastatic HER2 positive breast cancer and it is given in combination with capecitabine [138]. Although classified as an ATP-dependent reversible TKI of HER2 and EGFR, it is a much more potent inhibitor of HER2 and it is questionable whether it inhibits EGFR signalling to any significant degree *in vivo*. It is active against ligand-dependent and independent signalling as well as p95HER2 receptors and thereby effectively inhibits downstream signalling [2].

Data from the Neo-ALLTO trial suggests that lapatinib given in combination with trastuzumab and chemotherapy is more effective than the combination of either drug alone with chemotherapy [139]. Lapatinib is also postulated to have better central nervous system penetration than trastuzumab and may therefore reduce the risk of brain metastases [140], although the results of a head to head comparison is awaited.

1.6.5.1.3 Antibody dependent conjugates: Trastuzumab-DM1

The most recent drug to gain approval for use in metastatic HER2 breast cancer is the antibody dependent conjugate Trastuzumab-DM1 (T-DM1). This is a conjugate of trastuzumab and the microtubule polymerization inhibitor DM1 (a derivative of mytansine). When used in heavily pre-treated trastuzumab and lapatinib resistant HER2 positive MBC RR of approximately 40% have been seen [141]. Furthermore, when compared with docetaxel and trastuzumab in the management of previously untreated metastatic disease, T-DM1 resulted in higher RR and an improved toxicity profile [2].

1.6.5.2 Targeted therapies currently in clinical trials

A number of therapies which specifically target HER family signalling are currently in clinical development and in addition to the drugs discussed below many others are in preclinical development. Furthermore, several drugs which target signalling pathways downstream of the HER receptors (e.g. PI3K, mTOR, IGF1R and heat shock protein 90 inhibitors) have been developed.

1.6.5.2.1 Monoclonal antibodies-MM-111

Multiple HER3 targeting antibodies have been developed. The most advanced of these is MM-111, a bispecific monoclonal antibody which is believed to inhibit HER3 ligand binding and thereby HER3 heterodimerization [142]. The activity of MM-111 is currently being explored in HER2 positive, heregulin-positive metastatic cancer (including patients with trastuzumab and lapatinib resistant disease). A further study is focussing on its efficacy in HER2 positive, heregulin-positive refractory breast cancer when given in combination with trastuzumab [143].

1.6.5.2.2 Broad spectrum TKIs

1.6.5.2.2.1 Neratinib

Irreversible TKIs result in longer target inhibition than their reversible counterparts. Neratinib is an irreversible inhibitor of HER2 and EGFR. When tested in HER2 positive metastatic disease, RR of 24% were seen in trastuzumab resistant disease and 56% in trastuzumab naive disease. A subsequent phase 1/2 trial of trastuzumab plus neratinib in trastuzumab resistant metastatic disease demonstrated a RR of 27% and a median PFS of 19 weeks. However, when tested head to head with lapatinib and capecitabine, neratinib and capecitabine offered equivocal OS. Phase 3 evaluation of neratinib in trastuzumab pre-treated early breast cancer is currently underway [143].

1.6.5.2.2.2 Afatinib

Afatinib is a further irreversible inhibitor of HER2 and wild type and mutant EGFR. During a phase 2 trial of afatinib in patients with trastuzumab refractory disease, 4 partial responses were identified in a cohort of 35 patients. Its activity is currently being explored in phase 2 and 3 trials [143].

1.6.5.2.2.3 AZD8931

AZD8931 is a reversible inhibitor of EGFR, HER2 and HER3 signalling that is believed to be preferentially active in ligand-dependent signalling. However, its efficacy in combination with either paclitaxel [144] or anastrozole [145] was disappointing.

1.6.5.2.3 HER2 vaccination

Several studies have shown that some patients develop spontaneous anti-HER2 specific immunity triggering efforts to develop anti-HER2 vaccinations. Amongst vaccines currently in development, peptide-based vaccines, particularly E75 (derived from the extracellular

domain of HER2), are the best studied. A recent retrospective analysis of patients with MBC treated with E75 demonstrated that 40% were still alive at a median follow up of 112 months and 75% exhibited persistent T cell immunity. Furthermore, the combined analysis of 2 phase 2 trials, which collectively contained 195 patients with either node positive or node negative early breast cancer, reported a recurrence rate of 5.6% in patients receiving the vaccine following standard treatment compared to 14.2% in the observation arm at a median follow up of 18 months. However, this difference was no longer significant at 24 months. Major draw backs of peptide-based vaccines include the requirement for HLA restriction (i.e. a T cell is only able to recognise a peptide antigen when it is bound to the host body's own HLA molecule) which limits the number of patients that may be potentially treatable with such an approach as if the peptide is unable to bind to an HLA molecule no immune response will be generated. Secondly, as the immune response is triggered by a limited number of epitopes, the magnitude of immune response is limited. Finally, peptide vaccines predominantly stimulate a CD8+ T-cell response and are therefore not able to generate a strong, sustained immunological memory in the absence of repeated antigen exposure and stimulation by antigen-presenting cells. To try and overcome these shortcomings, several other approaches are being used to generate vaccines, including protein-based, DNA, whole tumour cell and dendritic cell vaccines (Reviewed in [146]).

1.7 Mechanisms of resistance to HER2 targeted therapies

The development of resistance to HER2 targeted therapies has been the focus of numerous pre-clinical studies, although far fewer of these have been clinically validated (Table 1.1). Mechanisms of resistance can be broadly classified as involving: structural alterations in the HER2 receptor, development of HER2-independent strategies for activating intracellular signalling and defects in cell-cycle control or apoptosis [147]. More recently, several studies have identified changes in metabolic pathways, which are responsible for driving resistance to HER2 targeted agents. Patient specific factors, for example genetic polymorphisms have also been linked to inherent trastuzumab resistance. Several preclinical and clinical studies have demonstrated lapatinib efficacy in trastuzumab resistant cells suggesting in some circumstances discrete mechanisms of resistance exist. However, other studies have shown a degree of overlap in resistance mechanisms between the 2 drugs despite their different mechanisms of action, highlighting the multi-factorial nature of resistance to these drugs.

	Preclinical Data	Clinical Validation
Alterations in HER2 expression		
Loss of HER2 expression		Loss of HER2 during/after tx associated with reduced OS [148]
p95 HER2 expression	Stable transfection of HER2/p95 HER2 renders cells resistant to T but not L [149].	Conflicting data [64]
Bypass signalling/activation of alternative survival pathways		
Transactivation of HER2/HER3 by EGFR	T resistant cell lines show increased EGFR & pEGFR. EGFR TKIs inhibited HER2 activation. [147].	No consistent relationship between EGFR expression & outcome. No additional efficacy from combined tx with gefitinib & T [150]. Increased PCR rate observed with combined NAC+ T+L [139]
Increased heregulin expression &HER3 activity	Tx of HER2+ve lines with HER TKIs results HER3 re-activation & activation of PI3K pathway [147].	Inconsistent relationship between HER3 expression & tx outcomes [64]. Increased PCR rate with NAC+ T+ P tx [135]
Loss of PTEN	PTEN loss assoc with T resistance in HER2+ve cells [147] & GEMM [151]. PTEN knockdown in L tx cells has variable effect [152].	No consistent relationship between PTEN status & T sensitivity. PTEN loss not associated L resistance [153].
Activating p110α PI3K mutations	Over-expression of mutant PI3K confers T [147] & L [154] resistance.	Variable reports of impact of mutations on T sensitivity [64]. PI3 kinase mutations not associated L resistance [152].

Src hyperactivation	Increased Src activity in T& L resistant lines. Inhibition of Src restored sensitivity [155] [147].	High $pTyr^{416}$ Src expression associated reduced OS following T [155].
Increased Met/HGF expression	Knock down of MET increases T sensitivity [156]. HGF tx rescues L tx cells [157].	Increased MET and HGF expression in non-responders to T + chemotherapy [147].
HER2-IGF1R cross talk	Inhibition of IGF1R in T resistant cells inhibits HER2 phosphorylation & restores T sensitivity [147].	Conflicting reports on the impact of IGF1R expression on response to T [147] [150].
EphA2 expression	Overexpression of EphA2 by T resistant cells. EphA2 inhibition restored T sensitivity [158].	Elevated EphA2 gene expression associated with poor prognosis [158].
Increased TGFα expression	L sensitivity of HER2 +ve cells reduced by TGFα tx [159].	Low serum TGFα levels predictive of response to L + chemotherapy [159]. No correlation between tumour TGFα expression & response to T [64].
Elevated β(1) integrin expression	Transfection of β(1) integrin conferred T resistance [64].	High expression associated reduced TTP post T tx [64].
Erythropoetin receptor (EpoR) activation	Epo tx reduces sensitivity of HER2 +ve cells to T [147].	Concomitant tx with T & Epo associated with reduced OS [147].
p70 S6 kinase hyperphosphorylation	Increased p70 S6 kinase phosphorylation seen in L resistant HER2 transfected cells. Tx with rapamycin restored L sensitivity [160].	Elevated p70 S6 kinase expression associated with clinical response [161].

Up-regulation of ER signalling	Increased FOXO3A expression & ER & PR signalling in L resistant cells [162] [163].	Concomitant treatment with L & aromatase inhibitors associated with increased PFS in HER2 +ve/ER +ve tumours [132] [133].
Defects in cell-cycle control/ apoptosis		
Cyclin E gene amplification	Increased cyclin E & CDK2 activity observed in T resistant cell lines. CDK2 inhibition reduced growth of T resistant xenografts [147].	Gene amplification/protein over-expression associated with reduced CBR & PFS [147].
Elevated survivin expression	Increased expression seen in T & L resistant cell lines. Survivin knock down restored drug sensitivity [164] [165].	High pre-tx survivin RNA levels associated poor response to T + chemotherapy [164].
Elevated RelA activity	L resistant cell lines expressed increased RelA. Knockdown of RelA restored L sensitivity [153].	Trend towards reduced RelA expression in L responders [153].
Alterations in metabolic pathways		
Enhanced glucose deprivation response (GDR)	Network analysis showed increased expression of genes involved in GDR in L resistant cell line [166].	Over-expression of genes associated GDR associated with high relapse rate in HER2 +ve breast cancer [166].

Table 1.1-Clinically validated mechanisms of acquired to resistance to trastuzumab (T) and lapatinib (L). Tx, treatment. Adapted from [114]

1.7.1 Resistance due to alterations in HER2 expression and structure

The majority of published studies which have developed models of resistance to either trastuzumab or lapatinib have shown persistent HER2 expression. However, Lesniack described spontaneous loss of HER2 expression in SKBR3 cells associated with induction of an epithelial-to-mesenchymal transition (EMT) programme [167]**.** Whilst EMT has not been linked to clinical resistance, loss of HER2 expression has been identified in up to a third of metastatic tumours previously treated with trastuzumab ± lapatinib [168]. This suggests that loss of HER2 is a clinically relevant mechanism of resistance.

Mutations in the HER2 receptor itself are rare. In his seminal paper, Bose identified 25 mutations within the HER2 gene from a total population of 1499 patients. These mutations were all detected in tumours without HER2 gene amplification and as 50% of them were capable of driving tumourigenesis, these mutations identify a small additional subset of patients with the potential to benefit from trastuzumab treatment [169]. The majority of gene sequencing studies have focussed on tumours without HER2 gene amplification. However, in a small study of HER2 positive MBC (n=14) all 3 patients who developed metastases after more than a year of trastuzumab treatment had acquired a point mutation in exon 21 of the HER2 gene at the new metastatic site. These findings require further validation [64].

Increased expression of p95, a naturally occurring truncated form of HER2 which lacks the antibody binding domain, has been linked in preclinical studies to trastuzumab resistance [149] but not lapatinib resistance. Initial phase 2 clinical studies supported p95 as a potential biomarker of trastuzumab resistance. However, analysis of samples collected as part of 2 major neoadjuvant phase 3 trials failed to identify any association between p95 expression and PCR rate. Furthermore, in the GeparQuattro trial p95 positivity was actually predictive for a statistically significant increase in PCR rate [64]. Preclinical studies have identified a second naturally occurring HER2 receptor splice variant (HER2Δ16), which eliminates exon 16 in the receptor's extracellular domain, and represents approximately 9% of total HER2 expression. This does not prevent antibody binding but promotes the formation of intra-molecular disulphide bonds stabilizing HER2 homodimers and preventing their disruption by antibody binding [170]. The clinical significance of this variant remains to be determined.

Finally, whilst not an intrinsic alteration in the structure or expression of HER2, production of proteins which are capable of binding to HER2, such as mucin-4 (MUC-4), are able to abrogate trastuzumab-HER2 interaction. MUC-4 is a membrane associated glycoprotein, which when over-expressed can co-localize with HER2 and mask the antibody binding domain [171]. MUC-1 has also been reported to co-localize with the HER2 receptor in this /manner but other studies have shown that it can also homodimerize and initiate intracellular signalling independently of HER2 [147].

1.7.2 Resistance associated with strategies for enhancing PI3K and p44/42 MAPK signaling

Studies have identified several different strategies for enhancing PI3K/Akt and/or p44/42 MAPK pathway activity. These include up-regulation of HER family ligands or activation of other HER family receptors, acquisition of PI3K mutations/PTEN loss and activation by HER family independent signalling pathways.

1.7.2.1 Activation of PI3K/Akt signalling via HER family/PI3K/PTEN activity

1.7.2.1.1 The role of increased HER family ligands or alternate HER receptor activation in resistance

The disintegrin and metalloproteinase-17 (ADAM17) is involved in the proteolytic shedding of the membrane bound HER family ligands resulting in increased bioavailability of active, soluble HER family ligands and subsequently increased downstream HER family signalling. Studies have implicated 2 methods of ADAM17 activation in trastuzumab resistance; firstly enhanced TGFβ signalling [139] and secondly a trastuzumab induced reduction in Akt activity, which initiates a negative feedback loop enhancing ADAM17 activity and the availability of HER family ligands [172]. Increased expression of the ligand TGFα has also been linked to resistance to lapatinib. Time to progression was shorter in patients treated with lapatinib and capecitabine with elevated levels of TGFα than in those with lower concentrations of the ligand [159]. Finally, other studies have shown increased heregulin expression is predictive of poor treatment outcomes in patients with HER2 positive breast

cancer [173] although combining pertuzumab (which is most active in the presence of heregulin) with trastuzumab (which is most active in the absence if heregulin) appears to overcome this [174] [135].

Activation of other HER family receptors has also been linked to resistance. Ritter and colleagues generated trastuzumab resistant BT474 xenografts, which in addition to increased HER ligands, expressed elevated levels of EGFR and increased numbers of EGFR/HER2 heterodimers. Treatment with the EGFR TKI gefitinib, reduced HER2 phosphorylation and disrupted the interaction between HER3-PI3K suggesting that in this model, ligand mediated induction of EGFR led to transactivation of HER2 and HER3 and continued downstream signalling [175]. More recently, Xia postulated an alternative mechanism by which autocrine induction of heregulin in lapatinib resistant cells activated HER3. Activated HER3 dimerized with EGFR which had not been completely inactivated by lapatinib treatment, resulting in persistent PI3K/AKT signalling[173]. The clinical significance of this remains uncertain as the addition of gefitinib to trastuzumab did not improve treatment outcomes. However, only low number of tumours that over-expressed EGFR were included in this study leading to it being underpowered [64]. As previously discussed, promising clinical data has been obtained with the combination of lapatinib and trastuzumab [139] although the extent of *in vivo* EGFR inhibition obtained with lapatinib is debatable.

1.7.2.1.2 The role of PI3K mutations and loss of PTEN in resistance

PI3K is a positive regulator of Akt activity and activating 'hotspot' mutations within its catalytic domain have been linked to both trastuzumab and lapatinib resistance in preclinical models [147]. PI3K activity is antagonised by PTEN and compelling preclinical data also supports the role of PTEN in moderating trastuzumab sensitivity [147] [65]. However, the impact of PTEN loss on lapatinib sensitivity is less well defined [154] [152]. The use of these biomarkers to predict trastuzumab sensitivity has been the focus of multiple clinical studies. Several retrospective studies demonstrated that individually the predictive power of PTEN and PI3K mutational status was limited, although combining biomarkers indicative of PI3K/PTEN/Akt pathway hyperactivation improved the predictive capability. However, data from prospective studies trials did not provide any conclusive evidence that trastuzumab efficacy was restricted to patients with PI3K/PTEN/Akt pathway hyperactivation [64]. Furthermore, data from the phase 3 EMILIA trial suggested that T-DM1 sensitivity was independent of PI3K mutational status [176]. Clinically, considerable controversy also

surrounds the impact of PI3K status on lapatinib sensitivity [176] [152]. One explanation for this lack of consistency may be the combined analysis of all PI3K mutations as a single group, when their individual impact on treatment outcomes may be very different. Prospective analysis of samples collected as part of the Neosphere trial showed that overall PI3K mutational status was not predictive of treatment outcomes. However, on an individual basis, certain mutations were predictive of poor outcomes [135]. Downstream of PI3K/Akt, mTOR 1 and 2 have both also been implicated in lapatinib resistance [177, 178].

1.7.2.2 The contribution of HER independent signalling pathways to resistance

1.7.2.2.1 Src

Src inhibition appears a promising approach to tackling drug resistance as elevated Src activity is a common downstream consequence in resistant cell lines generated using several different approaches, including PTEN loss and over-expression of either EGFR or IGF1R [155]. Clinical resistance is multi-factorial in nature and therefore targeting features common to multiple resistance strategies is likely to provide the greatest therapeutic benefit. However, although high Src activity was correlated with reduced survival following trastuzumab treatment in MBC [155], response rates to single agent dasatinib were disappointing [179].

1.7.2.2.2 EphA2

The receptor tyrosine kinase, EphA2, is over-expressed in 92% of breast cancers and in patients with HER2 positive breast cancer, elevated gene expression is associated with reduced survival [180]. *In vitro*, trastuzumab induced Src activation led to increased EphA2 activity culminating in persistent PI3K/Akt and MAPK signalling. Inhibition of EphA2 restored trastuzumab sensitivity, suggesting that elevated EphA2 activity was capable of driving the resistant phenotype and was not simply a downstream consequence of Src activation [158].

1.7.2.2.3 Erythropoetin receptor

The addition of erythropoietin to standard therapy in HER2 positive MBC had a detrimental impact on treatment outcomes. A significant percentage of cells co-express HER2 and the erythropoietin receptor. It is believed that whilst trastuzumab binds to the HER2 receptor and abrogates its signalling, erythropoetin binds to its own receptor and activates Jak. This

subsequently results in the activation of Src and PTEN inactivation, thereby amplifying any residual PI3K/Akt signal [181].

1.7.2.2.4 IGF1R

IGF1R is able to activate both Akt and p44/42 MAPK signalling by forming complexes with HER2 and/or HER3 and is therefore able to induce trastuzumab resistance in both a HER2-dependent and –independent manner [147]. Furthermore, compelling *in vitro* evidence exists supporting the role of IGF1R in mediating resistance to HER2 targeted therapies; the sensitivity of HER2 positive cell lines to trastuzumab was enhanced by the addition of an IGF1R monoclonal antibody or IGF1R targeting TKI and lapatinib has been shown to reverse IGF1R mediated resistance [147]. Despite this, IGF1R has not readily translated into the clinic as a biomarker of resistance. Several studies have failed to demonstrate an association between IGF1R expression and treatment outcomes in either the adjuvant or metastatic setting, although its use in the neoadjuvant setting appears more promising. In a small phase 2 trial, membranous IGF1R expression was associated with reduced response rates to pre-operative vinorelbine and trastuzumab, although this is not standard treatment. Genetic profiling of samples collected in the phase 3 NOAH trial, which compared neoadjuvant/adjuvant trastuzumab plus chemotherapy with chemotherapy alone, demonstrated a correlation between low IGF metagene expression (defined as insulin receptor plus IGF1R expression [182]) and increased PCR rates amongst ER negative tumours in the combined treatment arm. Furthermore, low IGF1R expression was predictive of increased PCR rates amongst patients with ER negative tumours who received docetaxel with trastuzumab and pertuzumab in the Neosphere trial, although this finding was not replicated in other treatment arms [64]. Together, these results suggest that IGF1R signalling may be a clinically relevant resistant mechanism within ER negative tumours. Given the importance of ER signalling pathways in driving alternative survival pathways in HER2 positive/ER positive tumours [183], it is possibly unsurprising that these effects are most apparent in ER negative disease. A randomised phase 2 trial comparing the efficacy of capecitabine and lapatinib with and without cixutumumab, an IGF1R targeted monoclonal antibody, has finished accrual but has yet to be reported.

1.7.2.2.5 MET

The proto-oncogene MET is also capable of activating PI3K/Akt signalling. It is frequently co-expressed with HER2 in breast cancer and promotes trastuzumab resistance through sustained Akt activity. *In vitro*, loss of MET function, either through siRNA mediated knockdown or through TKI mediated inhibition, increased cell line sensitivity to trastuzumab

whilst MET activation reduced drug sensitivity. Interestingly, in HER2 positive breast cancer cells, MET expression was rapidly up-regulated in response to trastuzumab treatment thereby promoting its own resistance [156]. MET amplification has also been implicated in resistance to the EGFR targeting TKI, gefitinib, where it dimerized with HER3 causing downstream activation of PI3K/Akt [184]. In a separate study, RON, which is another member of the MET family, has also been linked to persistent PI3K/Akt activity and lapatinib resistance [185].

1.7.2.2.6 Axl

Over-expression of the receptor tyrosine kinase Axl has been linked both directly and indirectly to lapatinib resistance. *In vitro*, Axl and HER3 associate with the p85 subunit of PI3K and inhibition of both Axl and HER family receptors is required to fully inhibit PI3K/Akt activity. Unopposed Axl activity has been demonstrated to lead to lapatinib resistance [186]. Axl is also a common downstream effector of the epithelial-to-mesenchymal transition (EMT) programme [187], which has recently been linked to lapatinib resistance [167]. Furthermore, a recent study has shown that EMT is able to rewire the signalling pathways leading to PI3K/Akt activation demonstrating the complexities associated with effectively inhibiting this pathway in the context of drug resistance [188].

1.7.2.2.7 β_1 integrin

β_1 integrin is able to activate both the PI3K/Akt and p44/42 MAPK pathways. Using IHC, β_1 integrin over-expression was found to be an independent negative prognostic marker for TTP in a cohort of women with HER2 positive MBC treated with trastuzumab [189].

1.7.2.2.8 FGFR2

The FGFR2 gene has been shown to be amplified in a model of lapatinib resistance in which both HER2 and EGFR expression were down-regulated. Activation of FGFR2 was demonstrated to contribute to persistent Akt and p44/42 MAPK activity culminating in lapatinib resistance [190].

1.7.3 Activation of PI3K and p44/42 independent cell survival signaling pathways

Two studies have implicated up-regulation of ER signaling in lapatinib resistance. In untreated HER2 positive breast cancer, increased Akt activity represses FOXO3A activity and ER expression. Therefore, HER2 signaling dominates in the control of cell survival. However, the reduction in Akt signaling associated with lapatinib treatment abrogates Akt's inhibitory effects on FOXO3A and increases expression of ER and caveolin 1 (which further enhances ER activity). Comparison of lapatinib sensitive and resistant cell lines revealed increased FOXO3A expression and induction of ER and PR signaling pathways in the resistant cell line. This increase in ER signaling switched the dominant control of cell survival from HER2 to ER regulated, although HER2 expression persisted and continued to be inhibited by lapatinib [183]. Similarly, Wang and colleagues reported increased ER signaling in cells with acquired resistance to lapatinib or lapatinib plus trastuzumab. However, in resistant cells prolonged culture with lapatinib (>6 months) resulted in a switch back from endocrine to HER2 driven signaling. Interestingly, trastuzumab resistance was not associated with enhanced ER signaling [191]. This mechanism of resistance may only be relevant in ER positive tumours and both these studies relied heavily on the ER positive BT474 cell line. However, at least within ER positive tumours, this resistance mechanism is likely to be more generalisable as comparison of pre- and post-lapatinib treatment biopsies in ER positive tumours demonstrated increased HR pathway signaling [183]. Furthermore, results from the phase 3 clinical trials TAnDEM and EGF30008 clearly illustrated the importance of dual HER2 and ER signaling pathway blockade in tumours co-expressing the 2 receptors [132] [133] .

1.7.4 Resistance associated with induction of apoptosis and defects in cell cycle control

Several studies have linked resistance to HER2 directed therapies to changes in the expression of proteins involved in apoptosis. Elevated basal expression of survivin (an inhibitor of apoptosis) has been linked to primary [165] [192] and acquired [192] [183] resistance to both trastuzumab and lapatinib. This was tested clinically using microarray data derived from patients treated with neoadjuvant trastuzumab and docetaxel and it was confirmed that higher baseline survivin expression was predictive of lack of response to systemic therapy [164].

In a separate series of experiments, elevated NIBP expression, which potentiates NFkappa-β activity, was found in 11.1% of HER2 positive breast cancers [193]. Furthermore, Xia et al demonstrated that increased expression of RelA, the pro-survival subunit of NFkappa-β, was associated with acquired lapatinib resistance *in vitro*. Changes in phosphoRelA expression beween pre- and post-lapatinib treatment biopsies were of borderline significance for predicting therapeutic response [153].

Expression of Notch 1 and its ligand, Jagged 1, are believed to contribute to the pathogenesis of breast tumours by inhibiting cell differentiation and promoting cell survival and/or proliferation. Notch 1 expression is associated with poor OS in breast cancer although interestingly its expression is suppressed by HER2. Treatment with trastuzumab and an EGFR/HER targeting TKI abrogated HER2's suppressive effects on Notch 1 expression thereby driving the resistant phenotype. [194].

Other studies have detected differences in apoptosis regulating proteins in resistant cell lines including increased expression of X-linked inhibitor of apoptosis (XIAP) [195], an increase in the ratio of Bcl:Bax [196], up-regulation of MCL1 and down regulation of BAX [197] [198], although these have not been clinically validated. Finally, baseline levels of the pro-apoptotic protein Bim have been found to be predictive of *in vitro* lapatinib sensitivity in treatment naive cells [199].

Changes in the expression of proteins involved in the G1/S cell cycle checkpoint have also been implicated in trastuzumab resistance. The cyclin E/CDK2 complex plays a critical role in the G1/S cell cycle check point by inducing phosphorylation of the CDK inhibitor p27 marking it for ubiquitin mediated degradation and enabling cells to transit from the G1 to the S phase [200]. Trastuzumab is believed to act at least in part by inhibiting cyclin E/CDK2 mediated phosphorylation of p27 thereby inducing a G1/S phase arrest [201]. Scaltiti found that cells rendered resistant to trastuzumab displayed amplification of the cyclin E gene [202]. Furthermore, cyclin E gene amplification in a cohort of patients treated with trastuzumab was associated with reduced response rates [147]. Consistent with these findings, Nahta observed an increase in CDK2 activity and reduced p27 expression in resistant SKBR3 cells, which was reversed by exogenous p27 expression [201].

1.7.5 Resistance associated with defects in metabolic pathways

Oncometabolics is a rapidly evolving field and further experiments are likely to demonstrate a huge range of changes in metabolic pathways associated with resistance. Using global gene expression from matched lapatinib sensitive and resistant SKBR3 cell lines, Komurov identified an enhanced glucose deprivation response (GDR) in the resistant cell line. In the drug sensitive cell line, treatment resulted in reduced glucose metabolism and impaired glycolysis culminating in glucose deprivation induced cytotoxicity. Resistant cells adapted to a chronic state of hypoglycaemia by increasing the rate of glycolysis, up-regulating the expression of glucose transporters, increasing amino acid and fatty acid break down and enhancing glycogen breakdown. Analysis of microarray data showed that markers of GDR correlated with a higher risk of relapse in HER2 positive breast cancer [166].

Consistent with the increased rate of fatty acid break down seen as part of the GDR in the previous report, lapatinib and trastuzumab resistant BT474 xenografts exhibited greater sensitivity to G28UCM, a fatty acid synthase inhibitor, than their sensitive counterparts [203]. Finally, Griner noted that incubation of BT474 cells in adipocyte conditioned media increased Akt phosphorylation. The adipocytokines leptin and growth differentiating factor 15 (GDF15) were isolated from the conditioned media and resulted in lapatinib and trastuzumab resistance respectively.

1.7.6 Patient specific factors associated with inherent trastuzumab resistance

Antibody dependent cell cytotoxicity (ADCC) is well established as a major determinant of trastuzumab efficacy and therefore patient factors which affect this immune response have the potential to contribute to inherent trastuzumab resistance. Genetic polymorphisms in the gene encoding the FcgRIII receptor have been linked to trastuzumab efficacy [204]. Furthermore, leucocytes derived from patients who responded to trastuzumab demonstrated a higher level of *in vitro* ADCC than those from patients who did not respond [205]. A

subsequent study confirmed that it was the quantity and lytic efficiency of the CD16 (+) lymphocytes that specifically governed the efficacy of the trastuzumab response [205].

1.8 Project aims

The high drug attrition rates seen in late phase oncological trials are partially attributable to the inability of traditional preclinical models to detect ineffective agents. Even if novel agents are successfully adopted into clinical practice, their efficacy is usually limited as when used in metastatic disease, resistance is almost universally inevitable. This thesis has focused on the use of preclinical models, particularly GEMMs, to predict response in HER2 positive breast cancer.

The aims of this study were:

1. To characterize the BLG-HER2^{KI}PTEN$^{+/-}$ model of HER2 positive breast cancer.
2. To use of the BLG-HER2^{KI}PTEN$^{+/-}$ model to explore the potential role of dasatinib in the management of HER2 positive breast cancer.
3. To characterize the MMTV-NIC model of HER2 positive breast cancer.
4. To use the MMTV-NIC model to explore the role of PTEN in tumour growth, intracellular signaling and response to AZD8931.
5. To further develop the MMTV-NIC model for use in studies exploring mechanisms of acquired drug resistance.
6. To generate MMTV-NIC tumours with acquired resistance to AZD8931.
7. To generate a panel of cell lines with acquired resistance to either AZD8391 or lapatinib to facilitate further study of the drug resistance mechanisms using a proteomic approach, incorporating western blotting, reverse phase protein array (RPPA) and mass spectrometry.

Chapter 2: Materials and Methods

2.1 Materials

2.1.1 Buffers and solutions

The composition of buffers and solutions used in this study are described in table 2.1.

NAME	COMPOSITION
PBS	1 PBS tablet, 100mL dH_20.
Trypsin	1mM EDTA, 0.25%(v:v) Trypsin (Gibco). Made up in PBS.
Freezing medium (for tissue culture)	90% (v:v) media containing 10% FBS, 10% (v:v) DMSO.
Cryopreservation medium (for tumour fragments)	50% DMEM, 50% freezing mix (90% FBS, 10% DMSO)
Wash buffer (for harvesting in vivo tumours)	7.5mL PBS, 2.5mL ammonium chloride solution (Stem Cell Technologies), 1 x Complete mini protease inhibitor tablet (Roche), 1 x Phos-stop inhibitor tablet (Roche).
Digestion buffer	4mg/mL collagenase, 4mg/mL dispase, 0.25mg/mL hyaluronidase made up in DMEM supplemented with 1% L-glutamine but no FBS.
0.4% SRB solution in 1% acetic acid	2g SRB, 500mL acetic acid.
10 mM Tris solution (pH 10.5)	1.21g Tris base, 1L dH_20. Adjust to pH 10.5.
RIPA buffer	50mM Tris pH8.0 with HCl (Melfords), 150mM NaCl, 1% (v/v) NP40 (Calbiochem), 0.5% (w:v) Sodium Deoxycholate, 0.1% (v/v) SDS. Made up in dH_20.
Lysis buffer (for western blots)	1 Complete ultra mini tablet (Roche), 1 Phos-stop tablet (Roche),10mL RIPA buffer.
Lysis buffer (RPPA)	1%Triton X-100, 50mM HEPES (pH 7.4), 150mM sodium chloride, 1.5mM magnesium chloride, 1mM EGTA, 100mM sodium fluoride, 10mM sodium pyrophosphate, 1mM sodium vanadate, 10% glycerol, 1x Complete ultra mini tablet (Roche), 1 x Phos-stop inhibitor tablet (Roche).
6x sample buffer	2.4mL 2-mercaptoethanol, 1.3 mL 1M Tris pH6.8 with HCl (Melfords), 2.5mL 20% SDS,1.8mL dH_20, 2mL Glycerol.
4x RPPA sample buffer	40% glycerol, 8% SDS, 0.25M Tris HCl, (pH 6.8), 2-mercaptoethanol (1:10, v:v), added just before use of buffer.
Running buffer	10x Tris-Glycine-SDS running buffer. Made in dH_2O.
TBST	6.05g Tris, 8.76g NaCl,1mL Tween 20. Make up to 1L dH_20 Adjust to pH 7.6.
TBST with 5% BSA	12.5g BSA, 250mL TBST.
Sodium citrate retrieval buffer pH6	82mL 0.1M Sodium citrate, 18mL 0.1M Citric acid. Made up in 900mL dH_20 and adjusted to pH 6.0.
EDTA retrieval buffer, PH8	0.372g EDTA. Made up in 1L dH_20. Adjusted to pH8.0.
Scott's tap water	3.5g Sodium Bicarbonate, 20g Magnesium sulphate. Made up in 1L dH_20.
Mass spectrometry buffer	2.5% (v/v) acetonitrile, 0.1% (v/v) formic acid made up in dH_20.

Table 2.1- Composition of buffers and solutions used in this study. All reagents from sigma unless otherwise stated.

2.1.2 Primary antibodies

A list of the antibodies used in this research together with their dilutions for each assay can be found in table 2.2.

ANTIBODY	COMPANY	CATALOGUE NUMBER	SOURCE	APPLICATION AND DILUTION
ER	Abcam	ab16660	Rabbit	IHC: 1:100,CB*
PR	Abcam	ab62621	Rabbit	IHC: 1:100,CB
Ki-67	Vector	VP-RM04	Rabbit	IHC:1:500, CB
pTyr 1248/1173 HER2/EGFR	Cell Signaling	2240	Rabbit	WB 1:1000 RPPA: 1:250
HER2/EGFR	DAKO	A0485	Rabbit	RPPA: 1: 500
pTyr 992 EGFR	Cell Signaling	2235	Rabbit	WB: 1:1000 IHC:1:50, EDTA**
pTyr 1173 EGRF	Cell Signaling	4407	Rabbit	RPPA:1:1000
EGFR	Cell Signaling	4405	Rabbit	WB: 1:1000 IHC: 1:50,EDTA
EGFR	Cell Signaling	2232	Rabbit	RPPA: 1:1000
pTyr 1221/1222 HER2	Cell Signaling	2243	Rabbit	WB: 1:1000 IHC: 1:400,CB
HER2	Cell Signaling	2248	Mouse	WB:1:1000
HER2	Invitrogen	AH01011	Mouse	IHC:1:1000,CB
pTyr 1289 HER3	Cell Signaling	4791	Rabbit	WB: 1:1000 IHC: 1:100,EDTA RPPA: 1:500
HER3	Cell Signaling	4754	Rabbit	WB:1:1000

				RPPA: 1:500
pSer380,Thr382,Thr383 PTEN	Cell Signaling	9554	Rabbit	RPPA: 1:250
PTEN	Cell Signaling	9188	Rabbit	WB:1:1000 IHC:1:200, CB
PTEN	Cell Signaling	9552	Rabbit	RPPA: 1:500
PI3K p110α	Cell Signaling		Rabbit	RPPA: 1:500
pSer 473 Akt	Cell Signaling	4060	Rabbit	WB: 1:1000 RPPA: 1:500
pThr 308 Akt	Cell Signaling	2965	Rabbit	RPPA: 1:500
Akt	Cell Signaling	9272	Rabbit	WB: 1:1000 RPPA: 1:500
pSer2448 mTOR	Cell Signaling	2971	Rabbit	RPPA:1:250
pSer2481 mTOR	Millipore	09-343SP	Rabbit	RPPA: 1:1000
p70 S6 kinase	Cell Signaling	9202	Rabbit	RPPA: 1:500
pThr 389 p70 S6 kinase	Epitomics	1175-1	Rabbit	RPPA: 1:500
pSer235,Ser236 S6 Ribosomal protein	Cell Signaling	2211	Rabbit	RPPA:1:1000
pSer240,Ser244 S6 Ribosomal protein	Cell Signaling	2215	Rabbit	RPPA:1:250
S6 ribosomal protein	Cell Signaling	2217	Rabbit	RPPA: 1:250
GSK-3β	Cell Signaling	9315	Rabbit	RPPA:1:500
pSer 21/9GSK-3 α/β	Cell Signaling	9331	Rabbit	RPPA: 1: 500
pSer 9GSK-3-β	Cell Signaling	9336	Rabbit	RPPA: 1: 500

Phospho-p44/42 MAPK (ERK1/2) (Thr202/Tyr 204)	Cell Signaling	4370	Rabbit	WB:1:1000 RPPA:1:500
P44/42 MAPK (ERK 1/2)	Cell Signaling	9102	Rabbit	WB:1:1000 RPPA:1:500
SAPK/JNK	Cell Signaling	9258	Rabbit	RPPA: 1:500
MEK1/2	Cell Signaling	9122	Rabbit	RPPA: 1:1000
pTyr 416 Src	Cell Signaling	2101	Rabbit	WB: 1:1000 IHC:1:500,CB RPPA:1:500
Src	Cell Signaling	36D10	Rabbit	WB:1:1000 IHC: 1:500,CB RPPA:1:500
FAK	Cell Signaling	3285	Rabbit	WB:1:1000
pTyr397 FAK	Life Technologies	446246	Rabbit	WB:1:1000
pTyr 1162/1163 IGF1R-β	Cell Signaling	44-804G	Rabbit	WB:1:10000 RPPA: 1:500
EphA2	Cell Signaling	6997	Rabbit	WB:10000
pSer 897 EphA2	Cell Signaling	6347	Rabbit	WB:10000
Ezrin	Abcam	Ab50433	Rabbit	WB:10000
Stat 3	Cell Signaling	9132	Rabbit	RPPA:1:500
pTyr 694 Stat 5	Cell Signaling	9351	Rabbit	RPPA: 1:500
Stat 5	Invitrogen	44-368G	Rabbit	RPPA:1:5000

c-jun, N-term	Epitomics	1254-1	Rabbit	RPPA: 1:250
pThr58,Ser62 c-myc	Epitomics	1203-1	Rabbit	RPPA:1:250
c-myc	Cell Signaling	5605	Rabbit	RPPA: 1:250
pSer 660 pan-PKC	Cell Signaling	9371	Rabbit	RPPA:1:1000
pTyr 783 PLC-gamma1	Cell Signaling	2821	Rabbit	RPPA:1:250
PLCɣ	Cell Signaling	2822	Rabbit	RPPA: 1:500
pTyr 207 Crkl	Cell Signaling	3181	Rabbit	RPPA:1:500
pSer465/Ser423,Ser467/Ser425 Smad 2/3	Cell Signaling	9501	Rabbit	RPPA:1:500
E Cadherin	Cell Signaling	3195	Rabbit	WB:1:1000 IHC: 1:5000,CB RPPA:1:250
Vimentin	Cell Signaling	5741	Rabbit	WB:1:1000 IHC: 1:100,CB
N Cadherin	BD Bioscience	610920	Mouse	WB: 1:1000
Vinculin	Sigma	4139	Rabbit	WB:1:1000
Fibronectin	Abcam	ab2413	Rabbit	WB: 1:1000
BAG3	Abcam	ab7124	Rabbit	WB:1:1000
Valosin containing protein	Cell Signaling	2648	Rabbit	WB:1:1000
Profilin	Cell Signaling	3237	Rabbit	WB:1:1000
CDK2	Epitomics	1134-1	Rabbit	RPPA: 1:250

pSer 216 cdc25c	Cell Signaling	4901	Rabbit	RPPA:1:250
Bim	Epitomics	1036	Rabbit	RPPA: 1:250
pSer69 Bim	Cell Signaling	4585	Rabbit	RPPA: 1:500
Survivin	Cell Signaling	2808	Rabbit	RPPA: 1:250
Cleaved caspase 3	Cell Signaling	9664	Rabbit	IHC:1:200,CB
CD31	Santa Cruz	sc 1506-R	Rabbit	IHC: 1:10000,CB
HIF-1α	Abcam	ab659791	Rabbit	IHC: 1:100,CB
GAPDH	Life Technologies	1209025	Rabbit	WB: 1: 2500
ɣ tubulin	Sigma	T-3559	Rabbit	WB: 1:3000
β tubulin	Abcam	ab6046	Rabbit	RPPA:1:5000
β actin	Cell Signaling	4970	Rabbit	RPPA: 1:1000

Table 2.2- Antibodies and their applications. List of antibodies and the conditions for performing western blotting (WB), immunohistochemistry (IHC) and reverse phase protein array (RPPA). *CB- citrate buffer, PH6, **EDTA- EDTA buffer, pH8 refers to buffer used for antigen retrieval.

2.1.3 Cell Lines

Fourteen different cell lines were used in this study. The HER2 positive breast cancer cell lines SKBR3 and BT474 were also used to generate a further 7 cell lines, with acquired resistance to either lapatinib or AZD8931. A further 5 mouse cell lines were used; BLG 5957 and BLG-6222 were generated from the BLG-HER2^{KI}-PTEN$^{+/-}$ model by Dr. S. Karim. MNP 129 RM, MNP 135 RM and MNP 145 LU were generated from the MMTV-NIC PTEN$^{+/-}$ model by L. Balderstone. The growth conditions for all cell lines are summarised in table 2.3. Cell lines were maintained in tissue culture flasks, dishes and plates in a humidified atmosphere at 37^0C and 5% CO_2. All cell lines were routinely tested for mycoplasma and were negative.

CELL LINE	SOURCE	CELL TYPE	MAINTENANCE MEDIA	ROUTINE SUBCULTURE
BLG-6222	S. Karim (Beatson Institute)	Murine mammary carcinoma	DMEM (Gibco),10% FCS (Gibco), 2mM L-glutamine (Gibco), pen/strep[1].	1:20 twice weekly
BLG-5957	S.Karim	Murine mammary carcinoma	DMEM (Gibco),10% FCS (Gibco), 2mM L-glutamine (Gibco), pen/strep.	1:20 twice weekly
WGH 145LU	L. Balderstone	Murine mammary carcinoma	DMEM (Gibco),10% FCS (Gibco), 2mM L-glutamine (Gibco), pen/strep.	1:20 twice weekly
WGH 135RM	L. Balderstone	Murine mammary carcinoma	DMEM (Gibco),10% FCS (Gibco), 2mM L-glutamine (Gibco), pen/strep.	1:20 twice weekly
WGH 129 RM	L. Balderstone	Murine mammary carcinoma	DMEM (Gibco),10% FCS (Gibco), 2mM L-glutamine (Gibco), pen/strep.	1:20 twice weekly

SKBR3	ATCC	Human breast carcinoma	DMEM (Gibco),10% FCS (Gibco), 2mM L-glutamine (Gibco), pen/strep.	1:5 twice weekly
BT474	ATCC	Human breast carcinoma	RPMI (Gibco), 10% FCS (Gibco), 2mM L-glutamine (Gibco), pen/strep.	1:3 once weekly
8931 R-SKBR3a	H. Creedon	Human breast carcinoma	DMEM (Gibco),10% FCS (Gibco), 2mM L-glutamine (Gibco), pen/strep, AZD8931[2].	1:20 twice weekly
8931 R-SKBR3b	H.Creedon	Human breast carcinoma	DMEM (Gibco),10% FCS (Gibco), 2mM L-glutamine (Gibco), pen/strep, AZD8931.	1:20 twice weekly
8931 R-SKBR3c	H.Creedon	Human breast carcinoma	DMEM (Gibco),10% FCS (Gibco), 2mM L-glutamine (Gibco), pen/strep, AZD8931.	1:20 twice weekly
Lap. R-SKBR3a	H. Creedon	Human breast carcinoma	DMEM (Gibco),10% FCS (Gibco), 2mM L-glutamine (Gibco) pen/strep, lapatinib[3].	1:20 twice weekly

Lap. R-SKBR3b	H. Creedon	Human breast carcinoma	DMEM (Gibco),10% FCS (Gibco), 2mM L-glutamine (Gibco), pen/strep, lapatinib.	1:20 twice weekly
Lap. R-BT474a	H. Creedon	Human breast carcinoma	RPMI (Gibco), 20% FCS (Gibco), 2mM L-glutamine (Gibco), pen/strep, lapatinib.	1:20 twice weekly
Lap. R- bt474b	H. Creedon	Human breast carcinoma	RPMI (Gibco), 20% FCS (Gibco), 2mM L-glutamine(Gibco), pen/strep, lapatinib.	1:20 twice weekly

[1]1% Penicillin-Streptomycin combined antibiotic [2]AZD8931 670nM [3]Lapatinib 5μM

Table 2.3- Details of cell lines used in this study and their culture conditions.

2.2 Methods

2.2.1 Cell culture

2.2.1.1 Cell harvesting and counting

Cells were harvested when they reached 80% confluency. Adherent cells were harvested by aspirating off the media before washing the plate with Phosphate buffered saline (PBS), pH 7.3. Each plate was incubated with 1mL of 0.25% trypsin in sterile 1mM EDTA for between 1 and 5 minutes. The disaggregated cells were re-suspended in the appropriate complete media to give a final volume of ≥ 10mL to ensure complete inactivation of the trypsin. The cell suspension was aspirated several times to ensure complete cell disaggregation and generation of a single cell suspension. A proportion of the resulting suspension was transferred to appropriate tissue culture plates and dishes (Greiner bio-one) and maintained in complete media in a humidified atmosphere at 37^0C and 5% CO_2.

Where experiments required a fixed number of cells, 10μL of the above cell suspension was transferred to a haemocytometer. The cell count was obtained by manually counting the number of cells and averaging the count obtained across 2 of the $1mm^2$ grids.

2.2.1.2 Cryopreservation and liquid nitrogen recovery

Cells to be stored in liquid nitrogen were harvested as described in section 2.2.1.1. The cell suspension was centrifuged at 1300rpm for 3 minutes to generate a cell pellet. The pellet was re-suspended in freezing medium and on average for every $75cm^2$ of monolayer cells harvested, 3 liquid nitrogen stocks were generated by re-suspension of the cells in 3mL of freezing medium. The resulting suspension was then transferred to cryovials (Thermo Scientific) and placed in the -80^0C freezer for 24 hours before being transferred to the liquid nitrogen tank for long term storage.

Cells to be recovered from liquid nitrogen were defrosted and re-suspended in 10mL of complete media. The resulting suspension was pelleted by centrifugation at 1300rpm for 3 minutes. The supernatant was aspirated off and the pellet re-suspended in complete media before being transferred to appropriate tissue culture plates and dishes.

2.2.1.3 Images of cell culture

The Leica DM IL LED microscope in conjunction with the Q Imaging Retiga Exi Fast 1394 camera was used to capture phase contrast images of cells.

2.2.2 Animal husbandry and *in vivo* assays

2.2.2.1 Breeding, genotyping and monitoring of transgenic mouse lines

Two transgenic models were used during this study. Animal husbandry including breeding for the BLG-HER2^{KI} PTEN$^{+/-}$ model was carried out by staff at the animal unit of the Beatson Institute. BLG-Cre, HER2^{KI} and PTEN floxed mice were interbred to generate progeny with a knocked in HER2 transgene and loss of a single PTEN allele. These mice were crossed with the *Z/EGFP* mouse allowing the use of fluorescent imaging to follow tumour development [233]. This model was bred on a mixed strain background.

For the MMTV-NIC model, animal husbandry, including breeding, was carried out by staff at the Biomedical Research Facility, University of Edinburgh. Mice harbouring a bicistronic transcript expressing a constitutively activated HER2 transgene followed by an internal ribosome entry sequence (IRES) element and Cre recombinase under the control of the MMTV promoter were a gift from Prof. W. Muller (Goodman Cancer Centre, McGill University). These mice were cross-bred with a strain in which PTEN was floxed or not with loxP recognition sequences (129/J The Jackson Laboratory) to generate either MMTV-NIC

PTEN $^{FL/+}$ or MMTV-NIC PTEN$^{+/-}$ progeny. This model was bred on an FVB background as this strain is associated with high penetrance of mammary tumours. Genotyping was performed by Transnetyx on ear notch material from at least 14 day old mice. Any mice with unwanted genotypes were sacrificed using cervical dislocation. All experiments were conducted in compliance with UK Home Office guidelines.

Nulliparous females were monitored twice weekly, using manual palpation, for tumour formation. The greatest tumour dimension and its perpendicular measurement were recorded. Once tumours had reached their maximum size (17mm in the earliest experiments and 15 mm in subsequent experiments as determined by Home Office regulations), mice were sacrificed using schedule 1 cervical dislocation. Mammary tumours and lungs were collected as detailed in section 2.2.2.3.

2.2.2.2 Establishment of orthotopic mammary tumours

Three different techniques were used to generate single mammary tumours; mammary fat pad (MFP) inoculation with an established murine cell line, inoculation of the MFP with freshly harvested disassociated mammary tumours and orthotopic transplantation of mature tumour fragments.

2.2.2.2.1 Orthotopic implantation with established MMTV-NIC cell line (WGH 145 LU)

WGH 145LU cells were grown in T150 culture flasks before being harvested and counted as described in section 2.2.1.1. The resulting cell suspension was centrifuged at 1300 rpm for 3 minutes to generate a cell pellet, which was washed twice in PBS before being re-suspended in Hank's balanced salt solution (HBSS, Gibco) to a final concentration of $20*10^6$ cells/mL.

Eight week old female athymic mice were injected in their left flank subcutaneously with 0.05mg/kg of the analgesic buprenorphine (Henry Schein Animal Health). Isofluorane (Henry Schein Animal Health) at a flow rate of 5% was used to induce anaesthetization, which was then maintained at a flow rate of 2% throughout the procedure. The surgical field was cleaned with 70% ethanol and a plastic steri-drape (Millpledge Veterinary) was used to maintain an aseptic field. Sterile forceps were used to separate the skin from the underlying musculature at the level of the pubis before sterile blunt ended scissors were used to make a 2cm longitudinal incision in the skin to the left of the midline. The resulting skin flap was peeled back and pinned to a cork support to expose the underlying fourth left MFP. The MFP was inoculated with 50μL of the cell containing HBSS suspension (containing a total of $1*10^6$ cells) causing the MFP to visibly engorge. Following this procedure, the skin was returned to its original position and secured in place using 4-5 clay adams clips applied with the EZ clip applier (VetTech Solutions Ltd).

Post-surgery, mice were fed a diet of SDS RM1 (E) (DBM Food Hygiene) soaked in water and 2.5mg/kg of the anti-inflammatory carprofen (Henry Schein Animal Health) was added to their drinking water for 48 hours. Animals were checked and weighed daily for the first 7 days following surgery. Tumours were subsequently measured twice weekly (section 2.2.2.1) and tumours and lungs collected as described below (section 2.2.2.3).

2.2.2.2.2 Orthotopic transplantation with freshly harvested disassociated MMTV-NIC tumours

Tumours for disassociation were washed in room temperature PBS and finely chopped using a mechanical tissue chopper (Mickle Laboratory Engineering). The minced tumour was suspended in digestion buffer (containing 4mg/mL collagenase, 4mg/mL dispase and 0.25mg/mL hyaluronidase) and incubated on a shaking platform at 37^0C for 1 hour. The suspension was centrifuged at 1300rpm for 3 minutes to generate a cell pellet. The supernatant was removed and the pellet re-suspended in 0.25% trypsin (made up in EDTA) and incubated at 37^0C for 4 minutes. The trypsin was inactivated by the addition of 2% FBS (made up in PBS) to which 4μL of DNAase was added and incubated at room temperature for 2 minutes. A cell pellet was formed by centrifuging the suspension at 1300rpm for 3 minutes. The resulting pellet was then re-suspended in and incubated with an ammonium

chloride containing solution (125mM ammonium chloride made up in a 1:1 PBS: FBS solution) for 2 minutes on ice to lyse any residual red blood cells. After this, the cells were pelleted by centrifuging at 1300rpm for 3 minutes, the supernatant aspirated off and the pellet re-suspended in a PBS: FBS (1:1) mixture. Finally, the suspension was passed through a single cell filter (Stem Cell Technologies) and a cell count performed as described in section 2.2.1.1. The appropriate number of cells were pelleted and re-suspended in HBSS at a final concentration of either $20*10^6$ or $40*10^6$ cells/mL.

Disassociated tumour cells were used to inoculate the fourth left MFP of 9 to 14 week old virgin FVB mice. The left flank of recipient mice was shaved and injected subcutaneously with 0.05 mg/kg of the analgesic buprenorphine. Induction and maintenance of anaesthesia and exposure of the MFP was performed as described in section 2.2.2.2.1. The MFP was inoculated with either $1*10^6$ or $2*10^6$ cells in 50μL HBSS before the skin flap was replaced and secured in place using 4-5 clay adams clips applied with the EZ clip applier. Post-operative care was provided as described in section 2.2.2.2.1.

2.2.2.2.3 Orthotopic transplantation with MMTV-NIC tumour fragments

Tumours used for the generation of fragments were washed in ice cold PBS and cut into $1mm^3$ fragments and any macroscopic necrotic areas removed. The fragments generated and the PBS they were suspended in were transferred to an eppendorf and centrifuged at 450g for 1 minute. The supernatant, containing fibrous and necrotic material, was removed and the remaining fragments suspended in ice cold DMEM. An equal volume of freezing medium was then added a drop at a time before the fragments and the cryopreservation buffer in which they were suspended were placed in cryovials and stored at -80^0C.

At the time of transplantation, fragments were defrosted at room temperature and washed in PBS. The fourth left MFP was prepared and exposed as described in section 2.2.2.2.2. A 17Fg trocar was used to insert the tumour fragment into the MFP before the surgical wound was closed as described above. Post-operative care was provided as described in section 2.2.2.2.1.

2.2.2.3 Collection of mouse tissue

Once tumours had reached their maximum permitted size, mice were culled by cervical dislocation. The mouse was then placed on a wooden board in a supine position with the limbs spread and fixed firmly in place at an angle of 45^0 to the body. A pair of forceps was used to separate the skin from the underlying musculature and a pair of blunt ended scissors then used to make a midline incision along the length of the pelvic, abdominal and thoracic cavities. The resulting skin flaps were then folded back on themselves and pinned in place to allow direct visualisation of the mammary tumours. Prior to collection, callipers were used to record the longest tumour dimension and its perpendicular measurement. Tumours were then excised by using the scissors to carefully separate them from the surrounding tissue. Following excision, the weight of all tumours was recorded.

Tumours for analysis by IHC were fixed in formalin (Fisher Scientific) and stained as described below (section 2.2.4.2). Tumours to be dissociated for generation of single mammary tumours were processed as described in section 2.2.2.2.2. Tumours to generate tumour fragments for orthotopic transplantation were processed as described in section 2.2.2.2.3. Tumours for analysis by western blotting and RPPA were cut into fragments approximately $5mm^3$ in size, which were rinsed twice in ice cold wash buffer before being incubated for 5 minutes in fresh wash buffer to lyse red blood cells. The wash buffer was removed and tumours washed a further 2 times in PBS before being patted dry with tissue and transferred to cryovials for storage in liquid nitrogen.

The lungs were harvested by cutting along the length of the sternum to open the thoracic cavity. A pair of forceps was used to separate the 2 halves of the rib cage and the heart and lungs liberated by dissecting the main vessels. After removal from the thoracic cavity, the lung tissue was separated from the heart and transferred immediately into formalin for fixation.

2.2.3 Cell culture assays

2.2.3.1 Cell counting experiments

The effect of various conditions on cell proliferation was measured by cell counting. At the start of the experiment, a single cell suspension was generated and using the haemocytometer, as described in section 2.2.1.1, a predetermined number of cells were seeded into duplicate wells of a 6 or 12 well dish (termed c1). After a specified time interval (termed h), cells were trypsinized, a single cell suspension generated, and a further cell count performed (termed c2).

When required, an online calculator (http://www.doubling-time.com) was used to calculate the cell doubling time using the formula: h*ln(2)/ln (c2/c1).

2.2.3.2 Sulphorhodamine B (SRB) assay

SRB assays were used to measure cell growth. Cells were seeded at a density of 1250-5000 cells/well in 96 well plates (Greiner bio-one) and allowed to attach for 24 hours, at which point day 0 plates were fixed. In the remaining plates, the media was replaced with 200μL fresh media containing escalating doses of dasatinib (provided by Bristol Myers Squib, Princeton), lapatinib (SelleckChem) or AZD8931 (provided by AstraZeneca, Alderley Park) prepared in DMSO. All plates contained a DMSO control comprising 6 wells to which DMSO alone was added at an equivalent concentration to that used in the maximum drug treated cells to ensure that any observed cytotoxic effects were as a result of drug treatment rather than the cytotoxic effect of DMSO. The maximum concentration of DMSO used in any experiment was 1:1000. The remaining plates were fixed at allotted time points. Cells were fixed by the addition of 50μL of 25% cold trichloracetic acid and incubated at 4^0C for 1 hour before being washed 10 times under running water and dried overnight at room temperature. Plates were then stained by the addition of 50μL SRB dye (0.4% w:v SRB in 1% v/v acetic acid) to each well and incubated at room temperature for 30 minutes. The plates were then washed four times in 1% acetic acid to remove any excess, non-protein bound SRB dye. The SRB stain was solubilised by the addition of 150μL 10mM Tris solution (pH 10.5) and

incubated at room temperature for 1 hour under agitation. The optical density was then measured at 540nm on a plate reader (Biohit). Cell numbers at each drug concentration were calculated as an average of 6 wells and normalized against the average value of the untreated control wells at the same time point.

2.2.3.3 Migration assays

2.2.3.3.1 Wound healing assay

BLG-6222 and BLG-5957 cells were grown to confluence in a 12 well dish (Greiner bio-one). The monolayer was wounded using 10μL pipette tip and any detached cells removed by washing the plate gently 3 times with media. Cells were treated with escalating doses of dasatinib (ranging from 0 to 200nM) and serial images recorded every 15 minutes for 18 hours using the automated Olympus ScanR-screening station. The cell velocity was calculated from the distance advanced into the wound over time using Cell R software.

2.2.3.3.2 Random migration assay

To determine the effects of AZD8931 resistance on random migration, parental SKBR3 and AZD8931 resistant cells were seeded in duplicate wells of a 12 well dish at a density of 3000 cells/well. Cells were cultured in complete media supplemented with 10mM HEPES buffer (Gibco) for 16 hours and serial images recorded every 15 minutes using the automated Olympus ScanR-screening station. Image J software was used to calculate both the total distance and vectorial distance travelled by representative cells in each well during this time interval. Persistence was calculated using the formula: vectorial distance/ cumulative distance travelled.

2.2.3.4 Matrigel inverse invasion assays

Transwell inserts (Corning, Fisher Scientific) containing matrigel (Becton Dickinson) were seeded with 400 cells in 100μL of media and incubated at 37^0C for 4 hours. The inserts were then placed in 1mL of serum-free medium. Media supplemented with 10% FBS (containing when appropriate escalating doses of drug) was placed on top of the matrix. Seventy-two hours after seeding, invading cells were stained with Calcein-AM (Invitrogen) and visualized by confocal microscopy (Olympus FV1000). Serial optical sections were captured and quantified using ImageJ software using the area analysis module.

2.2.3.5 Generation of AZD8931 and lapatinib resistant cell lines

For a detailed description of the methods used to generate lapatinib and AZD8931 resistant cell lines please refer to chapter 7 sections 7.3 and 7.6 respectively.

2.2.4 Methods for protein analysis

2.2.4.1 Western blotting

2.2.4.1.1 Sample preparation

2.2.4.1.1.1 Generation of lysate and protein quantification for samples derived from cultured cells

Cells to be analysed by western blotting were cultured in 150mm dishes. Where the effects of a short term drug treatment on protein expression were to be studied, the appropriate drug treatment was applied once the cells reached 80% confluency and cells continued to be cultured in the presence of the drug for a further 12 hours. Cells which had developed resistance to a drug were maintained in the presence of the drug until they reached a

confluency of 80%. The media containing the drug was aspirated off and replaced with fresh media containing no drug in which the cells continued to be cultured for a further 12 hours. For all samples, at the end of the culture period, the media was removed and the plate washed 3 times in ice cold PBS before being snap frozen using dry ice. Plates were stored at -80^{0}C until an appropriate time for lysate generation.

Prior to generation of lysate, the plates were defrosted on ice. The cells were lysed by the addition of 300μL of lysis buffer and adherent cells scraped from the surface of the dish into the lysis buffer and transferred into an eppendorf. The resulting cell suspension was incubated on ice for 15 minutes prior to centrifugation at 13200rpm for 15 minutes at 4^{0}C. The supernatant was transferred to a fresh eppendorf and stored at -20^{0}C whilst the cell pellet was discarded.

A Micro BCA^{TM} protein assay kit (Thermo Scientific) was used to determine the protein concentration of individual samples. BCA reagent solution was prepared according to the manufacturers' instructions (50% reagent A, 48% reagent B and 2% reagent C). To generate standard BSA samples, 800μL of BCA reagent solution was added to 1μL lysis buffer and escalating concentrations of BSA (ranging from 0 to 10μg/mL). To analyse the protein concentration of protein lysates, 1μL of an individual lysate was added to 800μL of BCA reagent solution. All samples were then incubated at 60^{0}C for 45 minutes.

To measure absorbance, 100μL of each of the above solutions was transferred to individual wells in a 96 well plate and absorbance read using a plate reader set at 570 nm. To generate a standard BSA curve, the absorbance value of each BSA standard was plotted against the BSA concentration. The absorbance of each protein lysate sample was then plotted on the standard curve and its protein concentration obtained.

For each western blot, aliquots of lysate containing the same amount of total protein were prepared for each sample. Samples contained either 20μg or 40μg of protein depending on the abundance of the protein of interest and the affinity of the primary antibody. Sample

volumes were equalized using lysis buffer and 6x sample buffer added. Samples were denatured at 95 ^{0}C for 5 minutes and then briefly centrifuged.

2.2.4.1.1.2 Generation of lysate and protein quantification for samples derived from tumours

At the time of lysate preparation, a piece of each tumour, approximately 8mm in length, was placed in a pre-cooled matrix A-tube (MP biomedicals). These tubes contained a garnet matrix and a ceramic sphere and using the FastPrep 24 system, the tumour sample was ground down to a fine powder. Following the addition of RPPA lysis buffer, the mixture was incubated for 30 minutes at room temperature on a shaking platform and then centrifuged for 10 minutes at 13200 rpm at 4 ^{0}C. The supernatant was collected into micro-centrifuge tubes and its protein content determined using a Bradford assay. Standard BSA samples were generated as part of the Bradford assay by adding 5μL of RPPA lysis buffer to PBS and escalating concentrations of BSA (ranging from 0 to 0.6mg/mL) to give a final combined total volume of 100μL. The samples were diluted 1:20 with PBS and 10μL transferred to duplicate wells in a 96 well plate. For each sample to be analysed, 10 μL of the lysate was transferred to duplicate wells of a 96 well plate. 240μL of Coomassie Plus Protein Assay (Thermo Scientific) was then added to each well and the plate incubated at room temperature for 10 minutes. Absorbance was read using the plate reader set at 570nm. A standard BSA curve was generated by plotting the absorbance value of each BSA standard against its BSA concentration. The absorbance of each protein lysate sample was then plotted on the standard curve and its protein concentration obtained.

The protein concentration of each sample was adjusted to 2mg/ml by the addition of extra lysate buffer. 4xSDS (RPPA) sample buffer was then added and samples boiled for 5 minutes at 80 ^{0}C.

2.2.4.1.2 Protein electrophoresis

Proteins were electrophoretically resolved using a precast 4-15% mini protean TGX precast gel (Biorad Life Science) and running buffer (Biorad Life Science). 5μL precision plus protein

dual colour standard marker (Biorad Life Science) was run on all gels to facilitate identification of the band of interest. Gels were run at 240V for 40 minutes.

2.2.4.1.3 Western blot transfer

Proteins were transferred to a nitrocellulose membrane using the trans-blot turbo transfer system (Biorad Life Science).

2.2.4.1.4 Immunostaining

After transfer, the membrane was blocked with TBST-BSA (5%) for 1 hour at room temperature whilst constantly being agitated. The primary antibody in TBST-BSA (5%) was then added and the membrane incubated overnight at 4^0C with constant agitation.

The membrane was then washed 4 times in TBST, each for a period of 5 minutes, and then incubated with horseradish peroxidase conjugated secondary antibodies (New England Biolabs) in TBST-5% BSA for 45 minutes. HRP anti-mouse antibody was used at a concentration of 1:5000 and HRP anti-rabbit antibody was used at a 1:3000 concentration. The membrane was then washed a further 4 times in TBST and ECL (Biorad Life Sciences) reagent added for 2 minutes. The proteins were visualized using the Biorad Chemi Doc MP imaging system.

2.2.4.1.5 Densitometry

Bands on western blots were quantified using Image J software. Briefly, the corrected intensity of the band of interest was calculated by subtracting the background intensity from the intensity of the band of interest. This process was repeated for the tubulin loading control band and used to calculate the normalized intensity of the band of interest by dividing the corrected intensity of the band of interest by the corrected intensity of the tubulin loading control.

2.2.4.2 Immunohistochemistry (IHC)

Formalin fixed specimens were paraffin embedded, cut at 4μm sections and stained with haematoxylin and eosin (University of Edinburgh Histology Services). Additional blank sections were requested for IHC.

Unstained sections were dewaxed by washing twice in xylene (Fisher Scientific) for 5 minutes each. They were then rehydrated by 2 minute washes in a series of reducing concentrations of ethanol (99%, 99%, 80% and 50%) and then washed briefly in tap water. Antigen retrieval was performed by microwaving sections under pressure for 5 minutes in either pH 6 citrate buffer or pH8 EDTA buffer (for a full list of antigen retrieval buffers used with individual antibodies see table 2.2). Once cool, sections were washed briefly in tap water and outlined using an ImmEdge Hydrophobic barrier pen (Vector Laboratories). Sections were then incubated with peroxidase block (DAKO) for 10 minutes to quench peroxidase activity. The peroxidase block was then removed and sections were incubated with serum free protein block (DAKO) for 30 minutes to eliminate non-specific background staining, except for when the primary antibody being used was PTEN. When PTEN was the primary antibody, 5% FBS (made up in PBS) was used as the secondary block. Sections were then incubated with the primary antibody overnight at 4^0C at concentrations optimized for each antibody and tumour type (see table 2.2). All experiments included a negative control section, comprising a tumour section incubated in the absence of primary antibody to confirm the specificity of any staining observed.

After incubation with the primary antibody, sections were washed twice in TBST, each for a period of 5 minutes, and incubated with mouse/rabbit Envision (DAKO) for 30 minutes at room temperature to amplify the signal. Sections were then washed a further 2 times in TBST before incubation with 3,3' diaminobenzidine solution (DAB, DAKO) to enable detection of positive staining. Slides were then washed in water and counterstained in haematoxylin (Sigma) and Scott's tap water. Finally, the sections were dehydrated with 2 minute washes in a series of increasingly concentrated ethanol solutions (50%, 80%, 99% and 99%) and washed twice for 5 minutes each in xylene before being mounted with coverslips (Thermo Scientific) using di-n-butyl phthalate in xylene (DPX) mounting medium (Fisher Scientific).

The slides were viewed by light microscopy using an Olympus BX51 microscope and pictures captured using a DP73 camera with cellware software (Olympus).

2.2.4.3 Reverse Phase Protein Array (RPPA)

2.2.4.3.1 Preparation of samples

2.2.4.3.1 .1 Preparation of cell lysate from frozen tumour samples for RPPA

See section 2.2.4.1.2.

2.2.4.3.1.2 Preparation of cell lysate from cultured cell lines for RPPA

Cells were cultured *in vitro* and at approximately 80% confluence, snap frozen. The plates were subsequently defrosted on ice and washed twice in PBS prior to incubation with ice cold RPPA lysis buffer for 20 minutes. Adherent cells were scraped off into lysis buffer and then transferred into microcentrifuge tubes (Greiner Bio-One). The lysate was centrifuged at 1400 rpm for 10 minutes at 4^0C. The resulting lysate was transferred to a fresh eppendorf and the cell pellet was discarded. The protein concentration of the lysate was determined using a Bradford assay (see section 2.2.3.2.1.2). The concentration of the lysate was then adjusted to 1mg/ml by the addition of additional lysate buffer as required. Aliquots of each sample containing a fixed amount of total protein were transferred to eppendorfs and 4x SDS (RPPA) sample buffer added to the lysate. The samples were boiled at 95^0C for 5 minutes to denature the proteins.

2.2.4.3.2 RPPA

Samples were analyzed by K. Macleod. To facilitate quantification, lysates were serially diluted to produce a dose curve comprising 4 2-fold dilutions of each sample (1.5, 0.75, 0.375 and 0.1875 mg/ml). The diluted concentration series of each sample was then spotted onto nitrocellulose slides (Grace bio) in triplicate under conditions of constant 70% humidity

using the Ausha 2470 array platform. The slides were hydrated in blocking buffer (Thermo Fisher Scientific) for 1 hour at room temperature and then incubated for 18-24 hours with primary antibodies, which had previously been validated for use in RPPA (for a full list of primary antibodies used see table 2.2).

Slides were subsequently incubated with anti-Rabbit Dy light-800 conjugated secondary antibody (New England Biolabs) for 1 hour and then washed 3 times in TBST. The slides were read on the Innopsys 7101R scanner and images acquired at the highest gain without saturation of the fluorescent signal.

Mapix software was used to analyse RPPA data and to calculate the Relative Fluorescent Intensity (RFI) each sample replicate and to calculate the linear fit through each sample's dose curve. Where possible, the ratio of the signal from phosphorylated to unphosphorylated antibodies was calculated to give a measure of the activation of a specific protein across all samples [206]. All other signal intensities were normalized using the global normalization technique [40].

2.2.4.4 Mass spectrometry

2.2.4.4.1 Sample preparation

Parental SKBR3 and AZ8931 R-SKBR3c cells were cultured (in the absence of drug) in triplicate in 150mm tissue culture plates. When cells reached confluence, the medium was removed, the plates washed 3 times in PBS and adherent cells scraped into 1mL of PBS. The cells were pelleted by centrifugation at 13200rpm for 15 minutes. The supernatant was removed and the cell pellet stored at -80^{0}C.

2.2.4.4.2 Sample digestion

Samples were processed and analyzed by Dr. T. Le Bihan. Cell pellets were reconstituted in 250µL of 8M urea, 25 µL of 1M ammonium chloride and 25 µL of 200mM dithiothreitol (DTT) to denature and reduce the samples. Samples were incubated at room temperature for 30 minutes before cysteine alkylation was performed by the addition of 25 µL of 500mM iodoacetamide for 1 hour. Samples were incubated overnight at room temperature in the presence of 10µg of trypsin to allow sample digestion. The resulting peptide extracts were then cleaned on an SPE reverse-phase Bond Elut LMS cartridge (Agilent) and an aliquot of 10 µg of digest was dried under low pressure (SpeedVac; Thermo Jouan) and stored at -20^{0}C. The aliquots were subsequently re-suspended in 5 µL of 2.5% (v/v) acetonitrile, 0.1% (v/v) formic acid in water to give a final concentration of 1 µg/µL. The samples were then filtered using a Millex filter (Millipore) before being subjected to high-performance liquid chromatography–mass spectrometry (HPLC-MS).

2.2.4.4.3 HPLC-MS

Nano-HPLC-MS was performed using an on-line system consisting of a nano-pump (Dionex Ultimate 3000; Thermo Fisher Scientific) coupled to a Q Exactive instrument (Thermo Fisher Scientific) with a 300µm x 5mm pre-column (5µm particle size, Acclaim PepMap; Thermo Fisher Scientific) connected to a 75 µm x 50cm column (3µm particle size, Acclaim PepMap; Thermo Fisher Scientific). Samples were analyzed on a 2-hour gradient using data-dependent analysis with one 70k-resolution survey scan followed by the top five MS/MS scans at 17.5k resolution.

2.2.4.4.4 Label-free quantification

Progenesis (version 4.1; Nonlinear Dynamics) was used for HPLC-MS label-free quantification. Only MS peaks with a charge of 2+, 3+ or 4+ were included in the total number of features (defined as the signal at a given retention time and mass:charge ratio) and only the 5 most intense spectra within each feature were included in the analysis. Normalization was performed based on the sum of the ion intensities of these sets of multi-charged ions (i.e. 2+, 3+ and 4+) and an abundance value for an individual protein was

subsequently calculated by addition of the unique peptide ion intensities for the given protein. As this method detects a substantial number of low-abundance peptides, which generate near-zero intensities, log transformation was unsuitable for this dataset. Therefore, abundance values were transformed using an ArcSinH function. Transformed abundance values were used to calculate mean values for the parental SKBR3 and AZD8931R-SKBR3c cell lines and from this the fold change for expression of individual proteins within the AZD8931R-SKBR3c cell line relative to the parental SKBR3 cell line was calculated. P values were calculated using one-way ANOVAs based on the transformed values. Proteins were defined as demonstrating significant differences in expression when the following conditions were met: i) the number of detected peptides which were used in quantification was ≥ 2, ii) absolute fold change was ≥ 2, iii) calculated pair-wise p value was < 0.05.

2.2.4.4.5 Protein identification

MS data were searched using MASCOT software (version 2.4; Matrix Science) against both the Homo sapiens and Mus musculus subsets of the NCBI protein database to identify the proteins from which the identified peptide sequences were most likely to be derived. Features included in all searches were: i) variable methionine oxidation, ii) fixed cysteine carbamidomethylation, iii) precursor ion mass tolerance of 10 ppm, iv) product ion mass tolerance of 0.05 amu, v) significance threshold (p) below 0.05 (MudPIT scoring), vi) final peptide score of at least 20, and vii) up to two uncleaved tryptic cleavage sites per peptide.

Chapter 3: The effect of dasatinib on tumour development in the BLG-HER2^{KI} PTEN$^{+/-}$ model

The data in this chapter has been previously been published in:

Karim S, Creedon H, Patel H, Carragher N, Morton JP,Muller WJ et al. Dasatinib inhibits mammary tumour development in a genetically engineered mouse model. J. Pathology. 2013; 230 (4):430-440.

The non-receptor tyrosine kinase Src has attracted considerable attention as a potential therapeutic target in the management of solid cancers. However, despite compelling evidence for its role in the regulation of several critical processes in tumour development and the availability of dasatinib, a Src family kinase (SFK) inhibitor with proven efficacy in haematological malignancies, the results of clinical trials in solid tumours to date have been disappointing.

Src is involved in integrating signals from growth factor receptors and integrins and has been implicated in several fundamental processes involved in the malignant phenotype, including cell proliferation, invasion, migration and angiogenesis [207] [208]. Increased Src expression and activity has been observed in numerous different tumour types [209], including breast cancer, where it has been linked to reduced OS [210] [211]and shown to play a central role in multiple intracellular signalling pathways associated with breast cancer development. For example, Src and ER reciprocally moderate each other's activity [212]and several preclinical studies have shown that combining Src inhibitors with anti-hormonal treatment resulted in greater inhibition of cell proliferation and delayed the onset of drug resistance [213] [214]. Src has also been implicated in signalling downstream of HER family receptors [215] and was recently identified as a common factor in a number of independent signalling pathways leading to trastuzumab resistance [155].

Dasatinib is a small molecule inhibitor, which in addition to inhibiting SFK, inhibits several other kinases including BCR-ABL, c-Kit and platelet-derived growth factor receptor (PDGFR) [217]. It is licensed for use in imatinib-resistant chronic myeloid leukaemia (CML) and Philapdelphia chromosome positive acute lymphoblastic leukaemia (ALL), and has transformed both the management and outlook of these conditions. Looking at dasatinib's activity in solid tumours, results from both *in vitro* [218], [219] [220] and *in vivo* studies [220], [88], [221] suggest that inhibition of invasion and migration is its dominant mechanism of action in most tumour types, whilst inhibition of proliferation was observed in a more restricted subset of tumours. However, clinical trials using any one of several SFKs in breast cancer have yielded disappointing results [222] [17]. Several studies did describe isolated cases of prolonged disease stabilization or partial responses suggesting that whilst there may well be a role for SFK inhibitors in the management of breast cancer, when and in which patients to use them remains to be determined.

One potential explanation for SFKs apparent lack of clinical activity may be that to date clinical trials have focussed exclusively on their use in metastatic cancer whilst preclinical data suggests they may be more efficacious in early disease. We therefore decided to explore dasatinib's activity in a GEMM of breast cancer, focussing predominantly on its use in early disease. We opted to use the BLG-HER2^{KI}PTEN$^{+/-}$ model for these experiments as not only is Src implicated in HER2 signalling but patients with early HER2 positive breast cancer remain at increased risk of local [223] and distant, particularly central nervous system [224], recurrences despite the introduction of adjuvant trastuzumab. There is therefore an urgent need to develop new therapies in this field.

Specific aims of this section of the project included:

1. Characterisation of the growth kinetics and histomorphology of BLG-HER2^{KI}PTEN$^{+/-}$ tumours.
2. Determining the impact of single agent dasatinib on mammary tumour development and progression in the BLG-HER2^{KI}-PTEN$^{+/-}$ model.
3. Exploring the mechanism of action of dasatinib on HER2 positive cancer cells both *in vitro* and *in vivo*.
4. Describing the effect of dasatinib on intracellular signalling pathways in HER2 positive breast cancer cells.

3.1 Model background

In this model, tumourigenesis is driven by a HER2 transgene (herein referred to as $HER2^{KI}$), which has been rendered constitutively active by a valine to glutamine substitution at position 664 in the transmembrane domain [225]. The exact details of how this substitution results in a persistently activated receptor is not yet fully understood, although it is thought to alter the relative orientation of HER2 monomers in a predimerized state favouring the development of an activated receptor homodimer complex [226]. When this transgene was coupled to the MMTV promoter and injected into 1 cell mouse embryos, the resulting progeny demonstrated mammary specific expression of the transgene with subsequent development of multiple synchronous mammary tumours [225]. HER2 transgene expression was critical for mammary transformation but concern that the use of the viral MMTV promoter might compromise the model's physiological relevance drove the development of an alternative model in which the trangenes expression remained under the control of the endogenous HER2 promoter. Analysis of the resulting tumours confirmed that this model recapitulated many of the molecular features seen in human HER2 positive disease with a strong correlation between genomic amplification of the HER2 transgene and HER2 expression and co-amplification of many of the same genes as is seen in human disease. However, the prolonged tumour latency and poorly-invasive nature of these tumours limited the utility of this model [227].

Loss of the tumour suppressor gene PTEN is a common event in all cancers and is observed in up to 50% of cases of breast cancer, where it is considered a marker of poor prognosis [104] [228]. Specifically within HER2 breast cancer, loss of PTEN expression is seen in between 25% [229] and 50% [104] of cases. Although preclinical studies have linked its loss to trastuzumab resistance [230] this has yet to be confirmed clinically [150]. PTEN acts as a negative regulator of the Akt pathway and therefore its loss affects a range of processes including cell proliferation, survival, motility and stem cell self-renewal [231]. When mice bearing the HER2 transgene under the control of the HER2 promoter were crossed with a strain containing a floxed PTEN allele, the resulting mammary specific PTEN loss resulted in accelerated tumour development and progression and higher incidence of metastases [231].

Our lab has experience of using the Cre-recombinase system under the control of the β-lactoglobulin enhancer (BLG-Cre) to trigger mammary specific Cre-mediated recombination

resulting in knock down of adenomatous polyposis coli (APC) [232]. We therefore elected to cross-breed transgenic mice harbouring the $HER2^{KI}$ transgene and Cre-recombinase under the control of the BLG-promoter with a strain containing a floxed PTEN allele. The progeny which had mammary specific expression of the HER2 transgene and a floxed PTEN allele, were crossed with the Z-EGFP model enabling mammary tumour development to be monitored with fluorescent imaging [233] (Figure 3.1), although this was not subsequently undertaken.

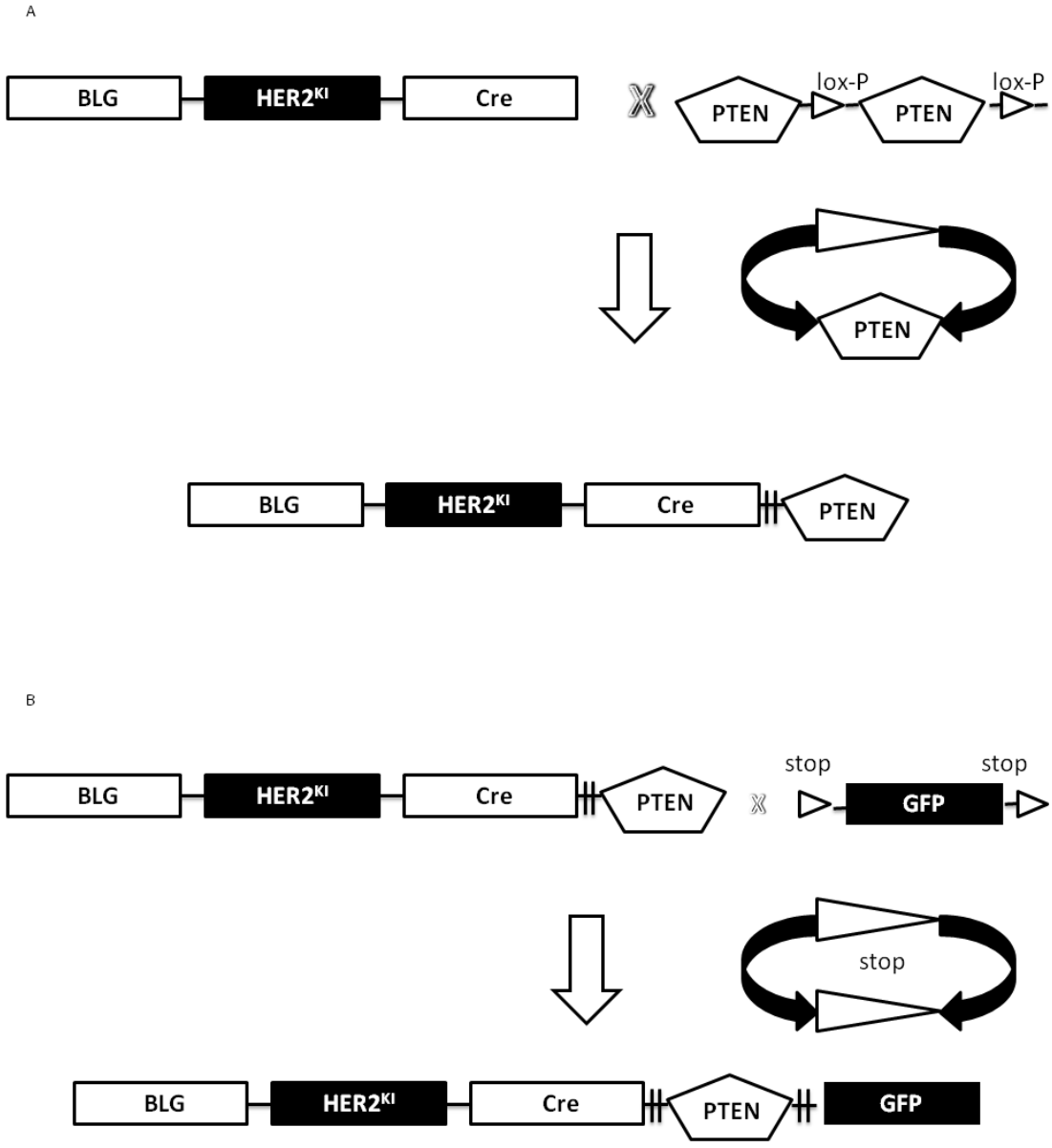

Figure 3.1- BLG-HER2^{KI} PTEN$^{+/-}$ genotype. A: Transgenic mice bearing the constitutively activated HER2 transgene (under the control of the HER2 promoter) and BLG-targeted Cre-recombinase were crossed with mice containing a floxed PTEN allele. B: The resulting progeny were crossed with the Z-EGFP model to enable tumour development to be followed by fluorescent imaging.

3.2 Model characterisation

3.2.1 Tumour development and growth in the BLG-HER2^{KI} PTEN$^{+/-}$ model

BLG- HER2^{KI} PTEN$^{+/-}$ mice were monitored twice weekly for tumour development and progression by palpation. Tumour onset was defined as the presence of a palpable tumour. Once tumours reached a diameter ≥ 1.7 cm in any direction, the animal was sacrificed.

All animals (n=24) developed unifocal mammary tumours with a median age of onset of 473 days (Figure 3.2A). Following tumour development, the median duration of survival was 42 days (Figure 3.2B) (**S. Karim**). We observed considerable variability in the timing of both tumour onset and survival following tumour development, which is reflective of the highly heterogeneous nature of human HER2 positive disease.

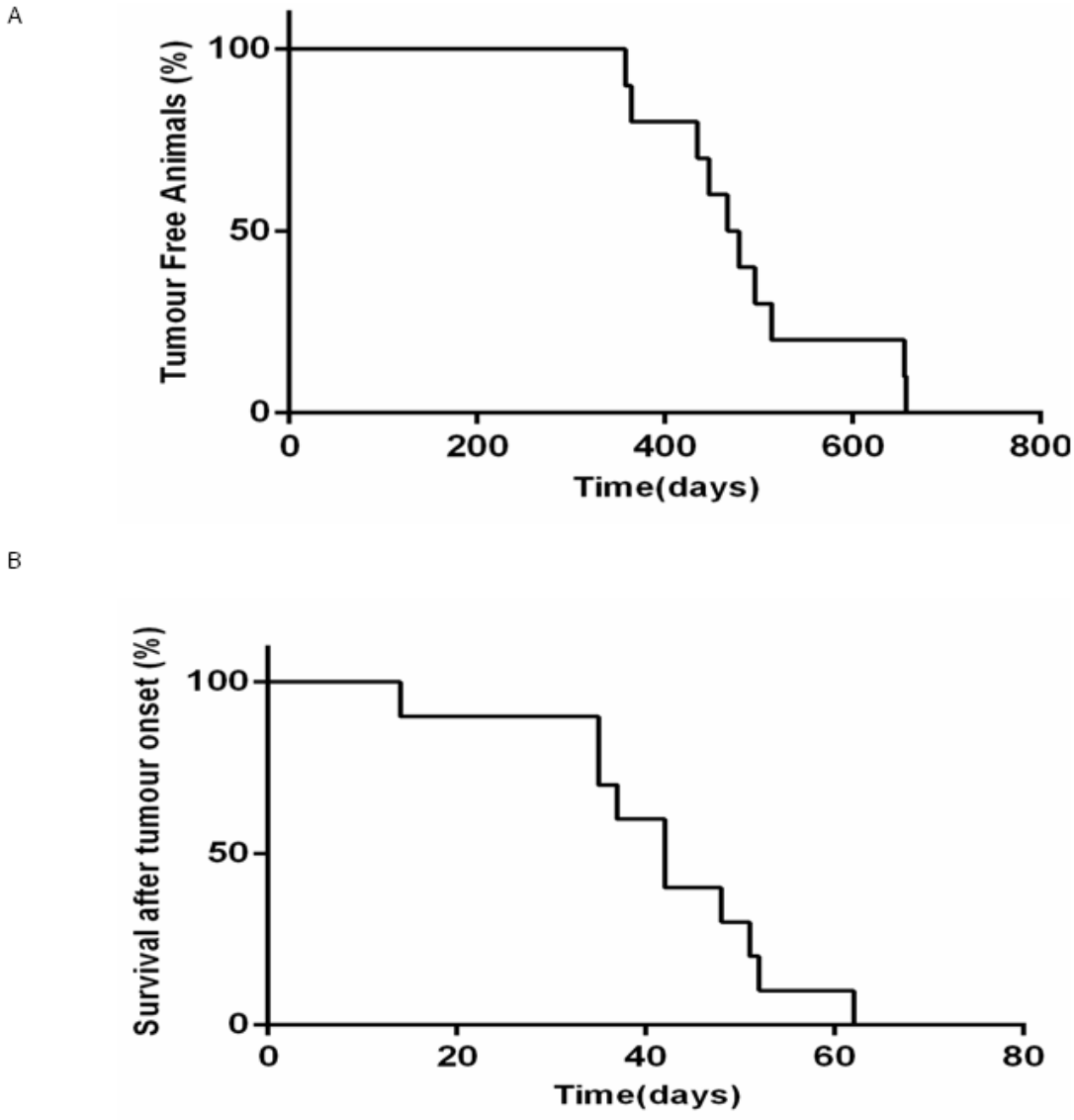

Figure 3.2- Universal development of mammary tumours in BLG- HER2^{KI} PTEN$^{+/-}$ mice. A cohort of BLG- HER2^{KI} PTEN$^{+/-}$ mice were monitored for tumour development and progression. A: Age at onset of palpable disease. B: Duration of survival following development of palpable disease.

3.2.2 Characterization of BLG-HER2^{KI} PTEN$^{+/-}$ tumours

3.2.2.1Histology of BLG-HER2^{KI} PTEN$^{+/-}$ tumours

Histological review of this tumour series (n=11) confirmed that they were comprised of moderately to poorly differentiated adenocarcinomas (**Prof. B. Gusterson, pathologist**). Lung metastases were identified in 18% (n=2) of animals when non-serial lung sections were examined. In both animals with evidence of metastatic disease, the metastases had the same histomorphology as the matched primary tumour (Figure 3.3) (**Prof B. Gusterson**).

3.2.2.2 IHC characterization of BLG-HER2^{KI} PTEN$^{+/-}$ tumours

We used IHC to further characterize these tumours. Using a HER2 antibody at a concentration of 1:100, we observed moderate staining for HER2 in BLG-HER2^{KI} PTEN$^{+/-}$ tumours. However, expression was substantially reduced compared to expression in the MMTV-NIC PTEN$^{+/-}$ model, an alternative model of HER2 positive breast cancer (see chapter 4), which showed strong staining at an antibody concentration of 1:1000 (Figure 3.4). Tumours were negative for both oestrogen receptor (ER) and progesterone receptor (PR).

We also performed IHC using a Ki67 antibody **(S. Karim)**, an established marker of cell proliferation [234]. When sections were manually scored for Ki67 expression, we observed considerable variation in the percentage of Ki 67 positive nuclei within individual tumours with actively proliferating cells found predominantly at the periphery of tumours and quiescent cells located more centrally (Figure 3.5). The mean percentage of Ki67 positive nuclei was 24.10%. The peripheral distribution of actively proliferating cells may reflect vascular insufficiency with more centrally located cells reliant on diffusion from peripherally located blood vessels and the resulting paucity of nutrients forcing cells into a quiescent state.

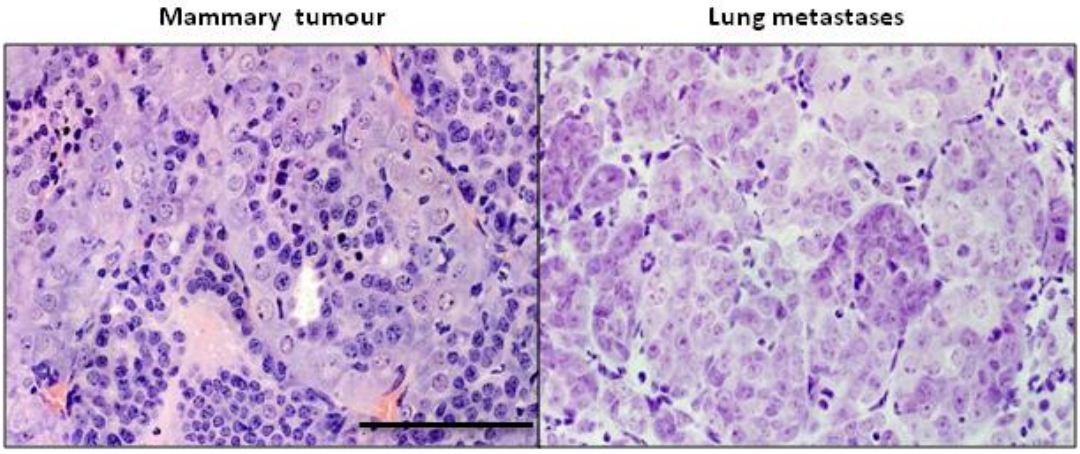

Figure 3.3- Matched mammary tumours and lung metastases displayed the same histomorphology. Representative H and E sections of a mammary tumour and its corresponding lung metastases. Mag x40, scale bar represents 100μM.

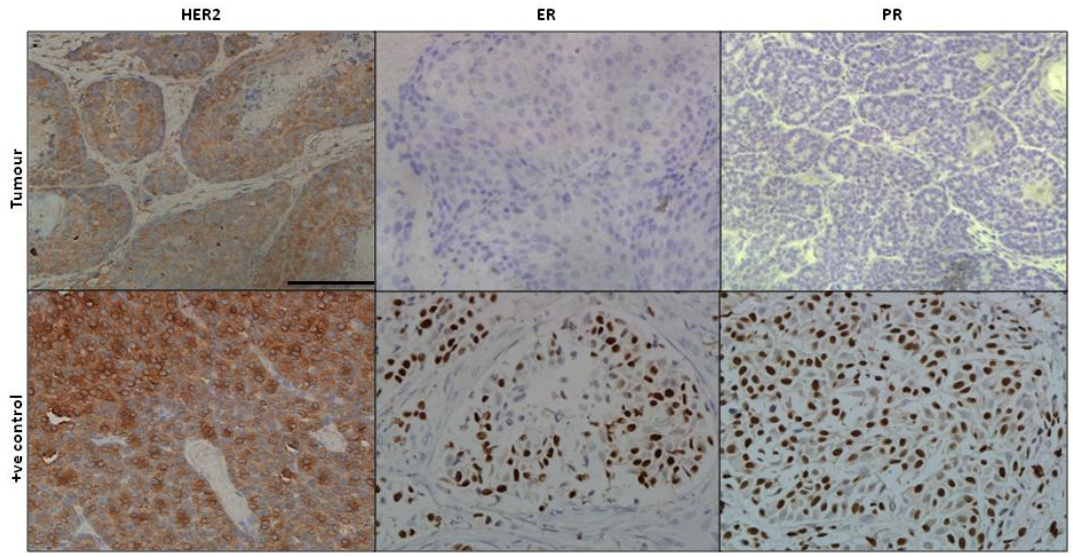

Figure 3.4-BLG- HER2^{KI} PTEN$^{+/-}$ tumours were HER2 positive but hormone receptor negative. IHC was performed with HER2, ER and PR antibodies on paraffin embedded sections of BLG- HER2^{KI} PTEN$^{+/-}$ tumours (n=3). Positive control for HER2 comprises section of MMTV-NIC PTEN$^{+/-}$ tumour incubated with HER2 antibody at concentration of 1:1000 (concentration 10-fold lower than used for BLG- HER2^{KI} PTEN$^{+/-}$ tumours). Positive controls for ER and PR comprise sections of human hormone receptor positive breast cancer stained with the appropriate antibody. Mag x40. Scale bar represents 100 µm.

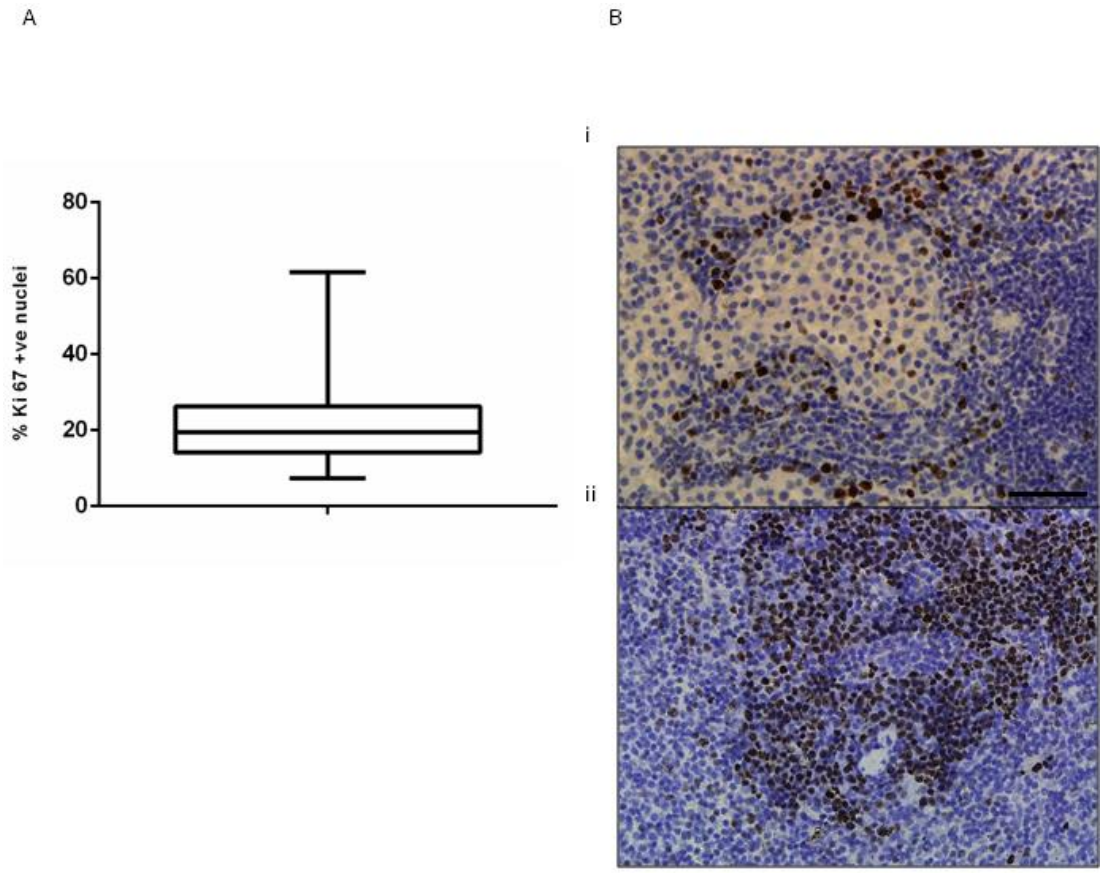

Figure 3.5- Variability in the proliferation of BLG- HER2^{KI} PTEN$^{+/-}$ tumours. IHC was performed on paraffin embedded sections of BLG- HER2^{KI} PTEN$^{+/-}$ tumours with a Ki67 antibody. Images were manually analysed to calculate the percentage of Ki67 positive nuclei in three low power fields (mag x20) per tumour. A: Box and whiskers plot of percentage Ki67 positive nuclei (n=4). B: Representative images of IHC staining for Ki67 showing regions of low (i) and higher (ii) proliferation. Mag x20. Scale bar represents 100 µm.

3.3 Effect of dasatinib treatment on tumour initiation and progression in the BLG-HER2^{KI} PTEN$^{+/-}$ model

We randomized cohorts of mice at the age of 8 weeks, prior to mammary tumour development, to either dasatinib (n=9) or vehicle (n=11) treatment. Mice received daily treatment with dasatinib (100mg/kg) suspended in citrate buffer or vehicle. Animals were monitored twice weekly for tumour development and progression and sacrificed once the maximum tumour diameter had reached 1.7cm, in accordance with the project license (**S. Karim)**.

We observed a statistically significant delay in tumour initiation in dasatinib treated animals (Figure 3.6A). The median age of tumour onset in drug treated mice was 585 days compared to 467 days in the vehicle treated cohort (p=0.046, Wilcoxon signed rank test). OS, measured from the date of birth until the date of death, was also increased in drug treated animals, although this did not reach statistical significance (Figure 3.6B). The median OS was 692 days in the dasatinib treated cohort and 624 days in the vehicle treated cohort (p=0.06, Wilcoxon signed rank test). This increase in OS was attributable to the delay in tumour onset as there was no difference in the survival following tumour development in the 2 cohorts (Figure 3.6c). Median survival following tumour development was 39 days in drug treated animals and 42 days in vehicle treated animals (p=0.284, Wilcoxon signed rank test). The majority of mice (85%) developed a single tumour whilst the remainder developed a small secondary tumour in a separate mammary fat pad (MFP).

Dasatinib did not appear to influence the incidence of lung metastases. In vehicle treated animals 18% (n=2) developed lung metastases compared to 22% (n=2) in the dasatinib treated arm. Although the low number of animals with metastatic deposits limited our ability to draw any conclusions from this experiment, the difference in the number of metastases found in the dasatinib and vehicle treated animals was striking. Vehicle treated animals with metastases had multiple lesions (23 and 35) whilst considerably fewer lesions were observed in the dasatinib treated animals (2 and 4). This could suggest that although dasatinib did not appear to influence tumour cell invasion and migration, it might influence the ability of cells to colonize secondary tumour sites.

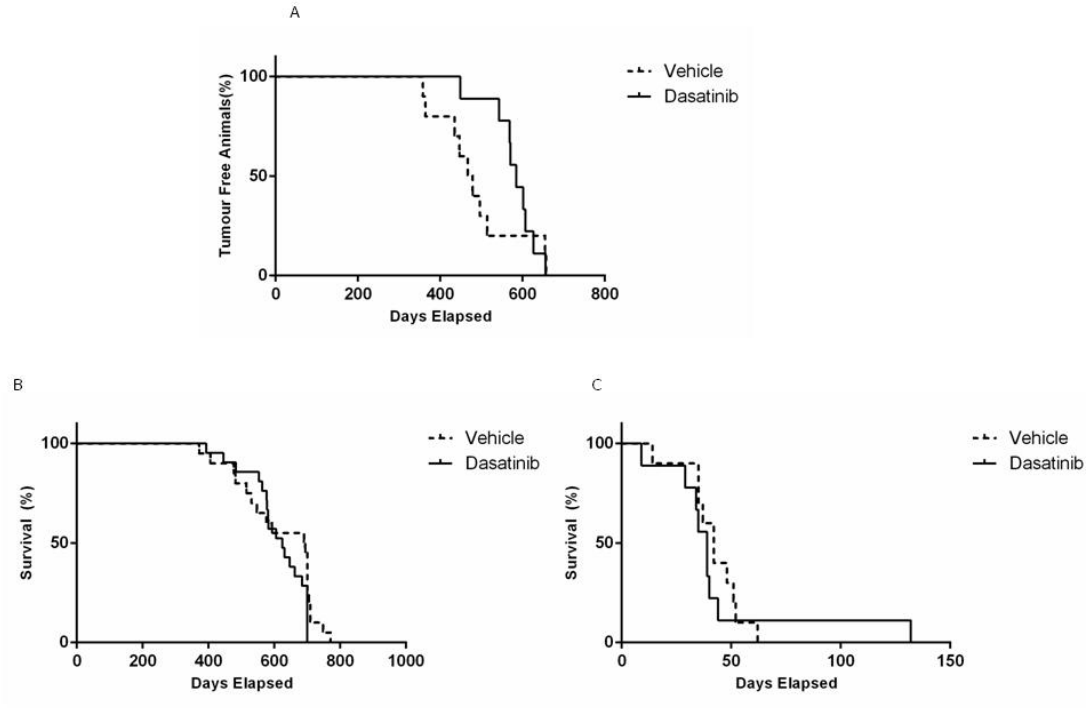

Figure 3.6- Dasatinib delayed tumour initiation in BLG- HER2^{KI} PTEN$^{+/-}$ mice but did not affect tumour progression. BLG- HER2^{KI} PTEN$^{+/-}$ mice were randomised to treatment with daily dasatinib or vehicle and tumour response monitored. A: Age of tumour onset in vehicle (n=11) and dasatinib (n=9) treated mice. p=0.046, Wilcoxon signed rank test. B: Overall survival in vehicle and dasatinib treated mice. p= 0.06, Wilcoxon signed rank test. C: Survival from time of tumour onset in vehicle and dasatinib treated mice. p=0.284, Wilcoxon signed rank test.

3.4 Effect of dasatinib on tumour differentiation

Histological examination of tumour sections revealed that dasatinib had a marked impact on tumour differentiation. In addition to the moderately to poorly differentiated adenocarcinoma found in vehicle treated tumours, 66% (n=6) of dasatinib treated tumours also contained prominent squamous metaplastic elements. In 5 of these tumours, squamous metaplasia occupied over 80% of the section and in one tumour both epidermal elements, consisting of keratin whorls and stratified squamous epithelium, and sebaceous elements were present (Figure 3.7). Again, examination of both matched primary tumours and their metastases revealed preserved tumour histomorphology, irrespective of the treatment group **(Prof. Gusterson)** (Figure 3.8).

To confirm the squamous nature of the metaplastic regions, we performed IHC with a CK5 antibody, a marker of stratified squamous epithelia [235]. Little or no CK5 expression was observed in vehicle treated tumours whilst dasatinib treated tumours exhibited prominent expression in the basal layer of the glandular tumour (**S.Karim)** (Figure 3.9). Squamous metaplasia has previously been linked to mammary-specific activation of Wnt, specifically β-catenin stabilization [236], [237]. Using IHC, we demonstrated low level β-catenin expression in vehicle treated tumours. Within the dasatinib-treated tumours, we observed increased expression in both the nuclei and at cell-cell junctions within regions of squamous metaplasia. In particular nuclear expression of β-catenin was observed in regions surrounding keratinized zones suggesting that increased β-catenin activity may have driven the squamous differentiation seen in dasatinib-treated tumours (**S.Karim)** (Figure 3.10).

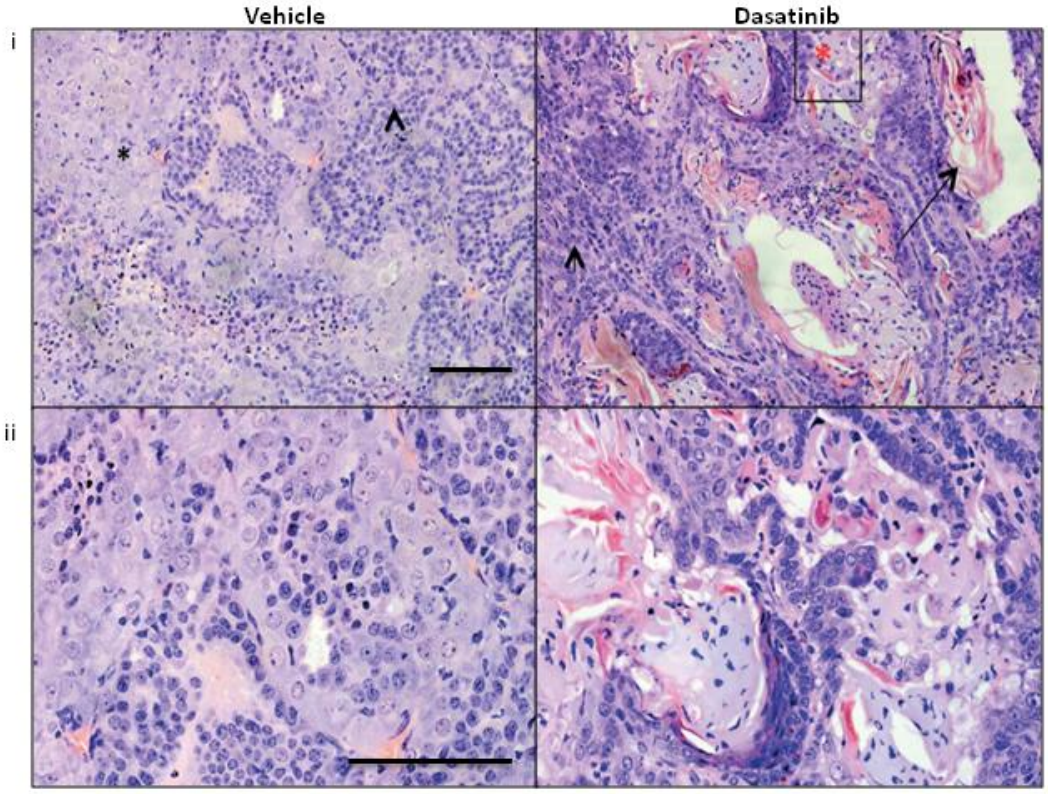

Figure 3.7- Representative H&E sections of vehicle and dasatinib treated tumours. i: low powered view of vehicle and dasatinib treated tumours (mag x20). The vehicle-treated tumour comprised poorly differentiated (asterix) and glandular (arrowhead) elements. The dasatinib-treated tumour contained glandular elements (arrowheads), sebaceous elements (red asterix) and keratin whorls (arrow). Scale bar represents 100 µm. ii: high powered view of vehicle and dasatinib treated tumours. Mag x40. Scale bar represents 100 µm (Prof. Gusterson).

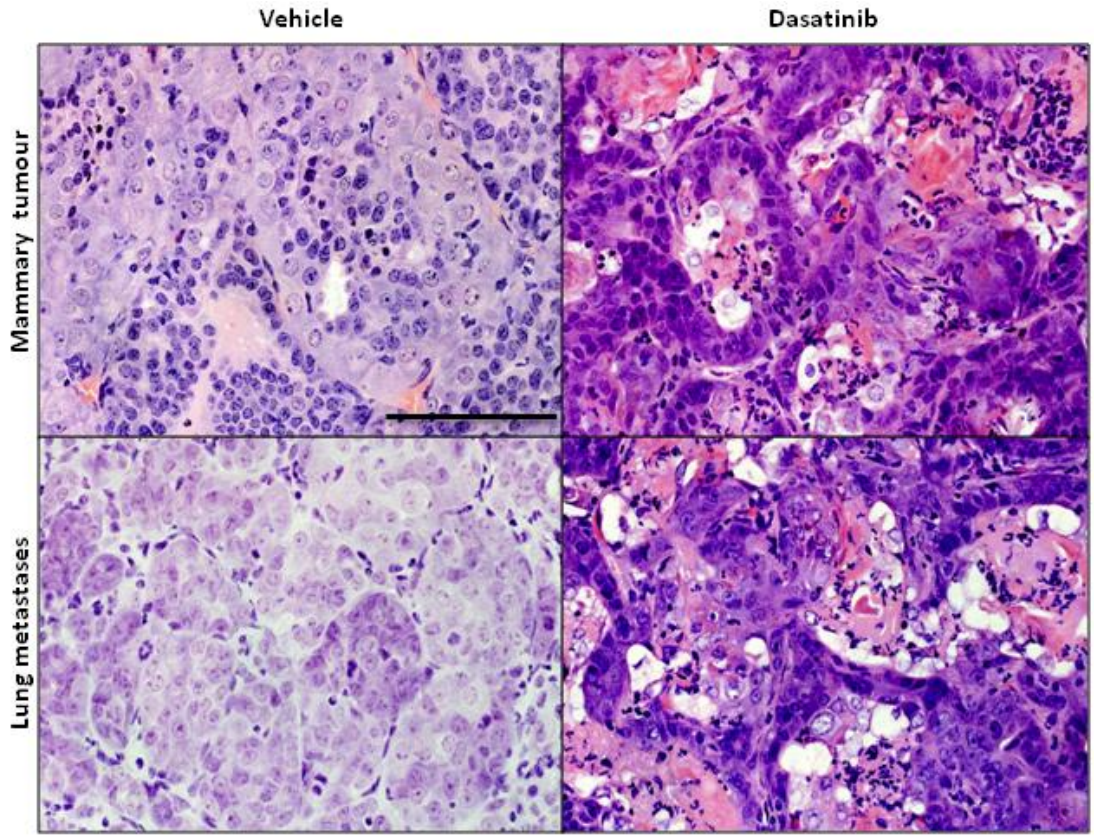

Figure 3.8- Representative H & E sections of matched primary and secondary tumours from vehicle and dasatinib-treated animals. Lung metastases demonstrated the same histomorphology as the corresponding primary tumour in both vehicle and dasatinib-treated animals. Mag x40. Scale bar represents 100 µm (Prof. Gusterson).

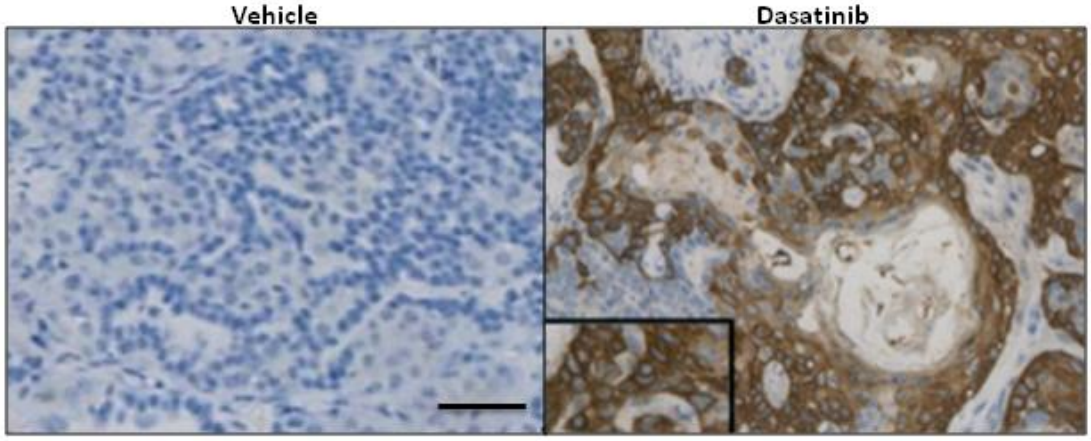

Figure 3.9- Representative images of IHC sections demonstrating increased CK5 expression in dasatinib treated tumours. IHC was performed on paraffin embedded sections of vehicle and dasatinib treated tumours with a CK5 antibody. Mag x40. Scale bar represents 100 µm (S. Karim).

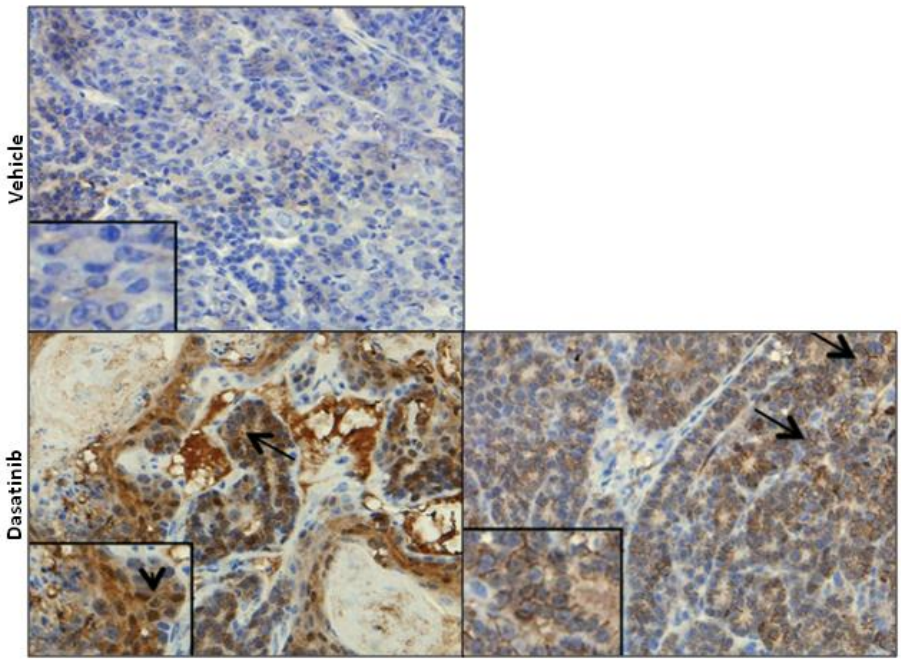

Figure 3.10-Representative images of IHC sections demonstrating increased β –catenin expression in dasatinib treated tumours. IHC was performed on paraffin embedded sections of vehicle and dasatinib treated tumours with a β –catenin antibody. β –catenin expression was expressed at cell-cell junctions (arrows) and in the nucleus (arrowhead) in dasatinib treated tumours. Mag x40. Scale bar represents 100 µm (S. Karim).

3.5 Effect of dasatinib on Src kinase activity

As well as inhibiting Src, dasatinib inhibits several other kinases, including BCR-ABL, c-Kit and PDGFR [217]. We therefore performed IHC with a pTyr416 Src antibody, a frequently used biomarker of Src activation, to confirm that the effects we observed *in vivo* reflected reduced Src activity. Quantification of pTyr416 Src expression was complicated by both considerable inter- and intra-tumoural variability in expression. However, we did observe a reduction in p Tyr 416 Src expression in dasatinib treated tumours although this did not reach statistical significance (Figure 3.11). The median p Tyr416 Src histoscore in dasatinib-treated tumours was 7.5 compared to 190 in vehicle-treated tumours (p= 0.103, Mann Whitney U test). Total Src expression was increased in dasatinib-treated tumours, although again this failed to reach statistical significance. The median Src histoscore in dasatinib-treated tumours was 285 and 140 in vehicle-treated tumours (p=0.110, Mann Whitney U test). Although we cannot be certain that the inhibition of other kinases did not contribute to dasatinib's effects on mammary tumour initiation, this data suggests that Src inhibition is at least likely to have contributed to it.

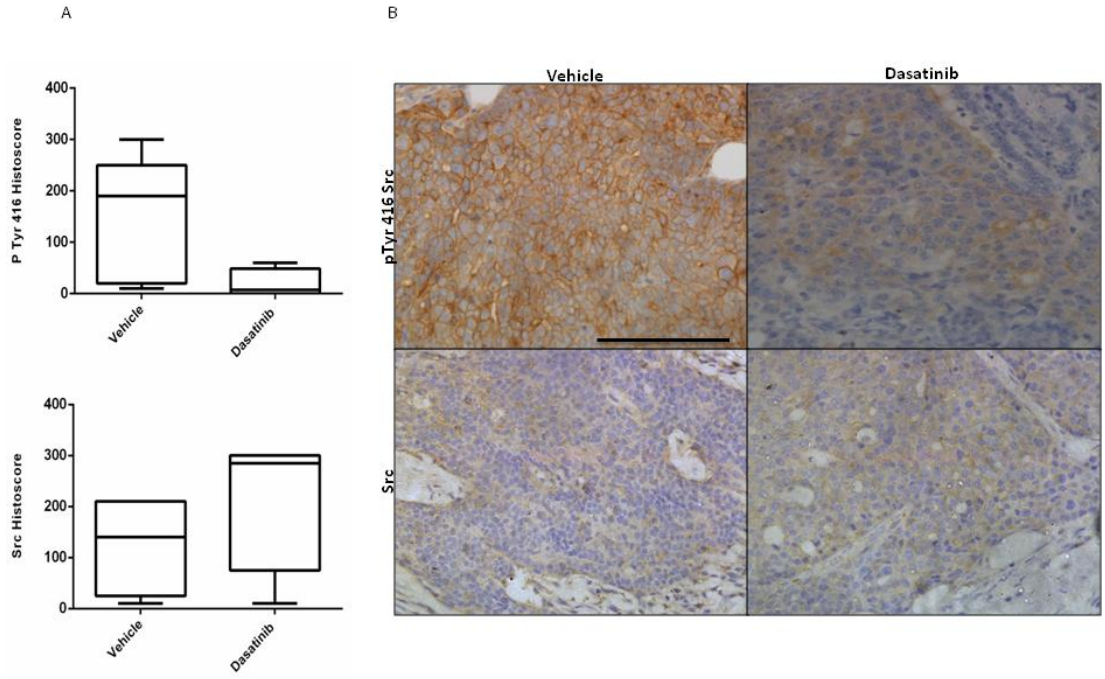

Figure3.11- Dasatinib treatment resulted in reduced Src activity. IHC was performed on paraffin embedded sections of dasatinib and vehicle treated tumours with p Tyr 416 Src (n=5 in each treatment group) and total Src antibodies (n=4 in each treatment group). The histoscore was calculated as the sum of the product of percentage cells stained by the intensity graded from 0-3, where 1=weak, 2=moderate and 3=strong staining (histoscore = (% *1) + (% *2) + (% *3)). A: IHC analysis of pTyr 416 Src (p=0.103, Mann Whitney U test) and Src (p=0.110, Mann Whitney U test) in dasatinib and vehicle treated tumours. B: Representative IHC images of vehicle and dasatinib treated tumours. Mag x40. Scale bar represents 100 µm.

3.6 Effect of dasatinib on tumour cell proliferation and apoptosis

Ki67 is a frequently used marker of cell proliferation [234] and has been validated as prognostic marker in breast cancer with high scores (>20%) associated with reduced disease free and overall survival [238]. To further explore dasatinib's mechanism of action, we performed IHC with a Ki67 antibody **(S. Karim)**. We found that the majority of cells with Ki67 positive nuclei were found at the periphery of both dasatinib and vehicle treated tumours, whilst few actively proliferating cells were seen more centrally. Comparison of the percentage of Ki67 positive nuclei found within 3 peripheral regions of both dasatinib and vehicle treated tumours showed no significant difference in the proliferative capacity of the 2 cohorts (Figure 3.12).The median percentage Ki67 positive nuclei was 20.8% in vehicle treated tumours and 20.05% in dasatinib treated tumours (p=0.736, Mann Whitney U test).

We also performed IHC with an antibody to cleaved caspase 3, a frequently used biomarker of apoptosis [239]. There was no evidence of significant apoptosis in either dasatinib or vehicle treated tumours (Figure 3.13).

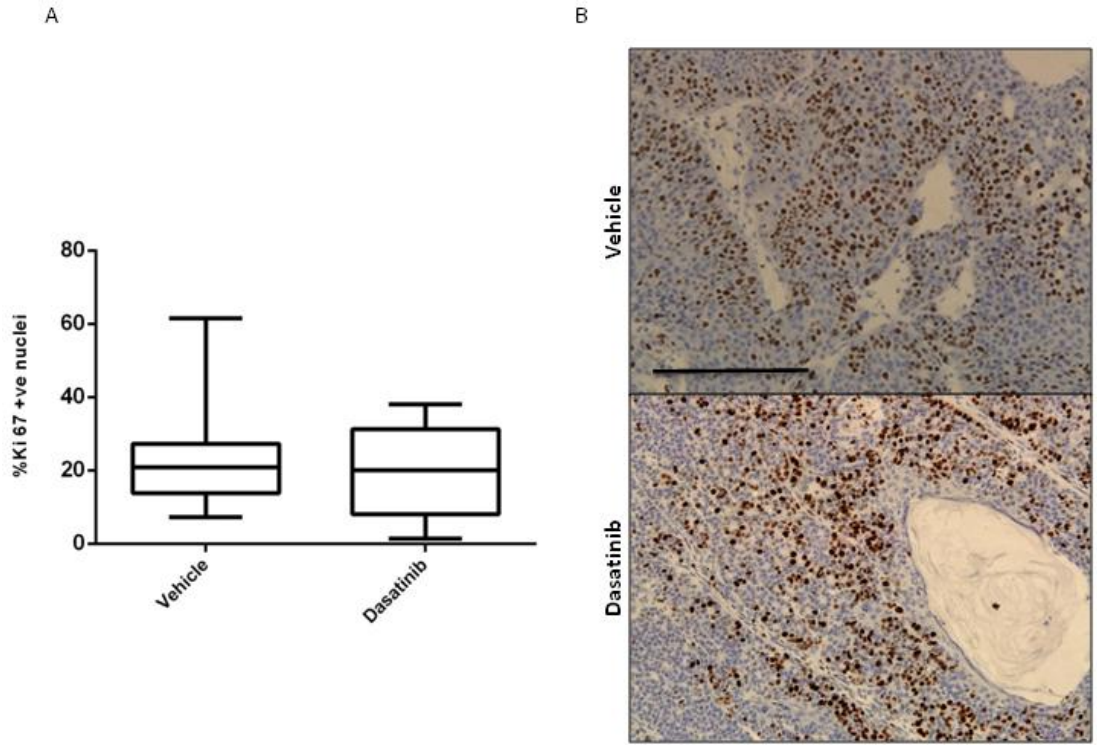

Figure 3.12- Dasatinib treatment did not inhibit tumour cell proliferation. IHC was performed on paraffin embedded sections of dasatinib (n=6) and vehicle treated (n=4) tumours with a Ki67 antibody. Images analysed manually to calculate percentage nuclei positive for Ki67 in 3 randomly selected low power fields (mag x20) per tumour. A: Box–whisker plot analysis of percentage of nuclei positive for Ki67 (p=0.736, Mann Whitney U test). B: Representative IHC images of vehicle and dasatinib treated tumours. Scale bar represents 100 µm. Mag x20.

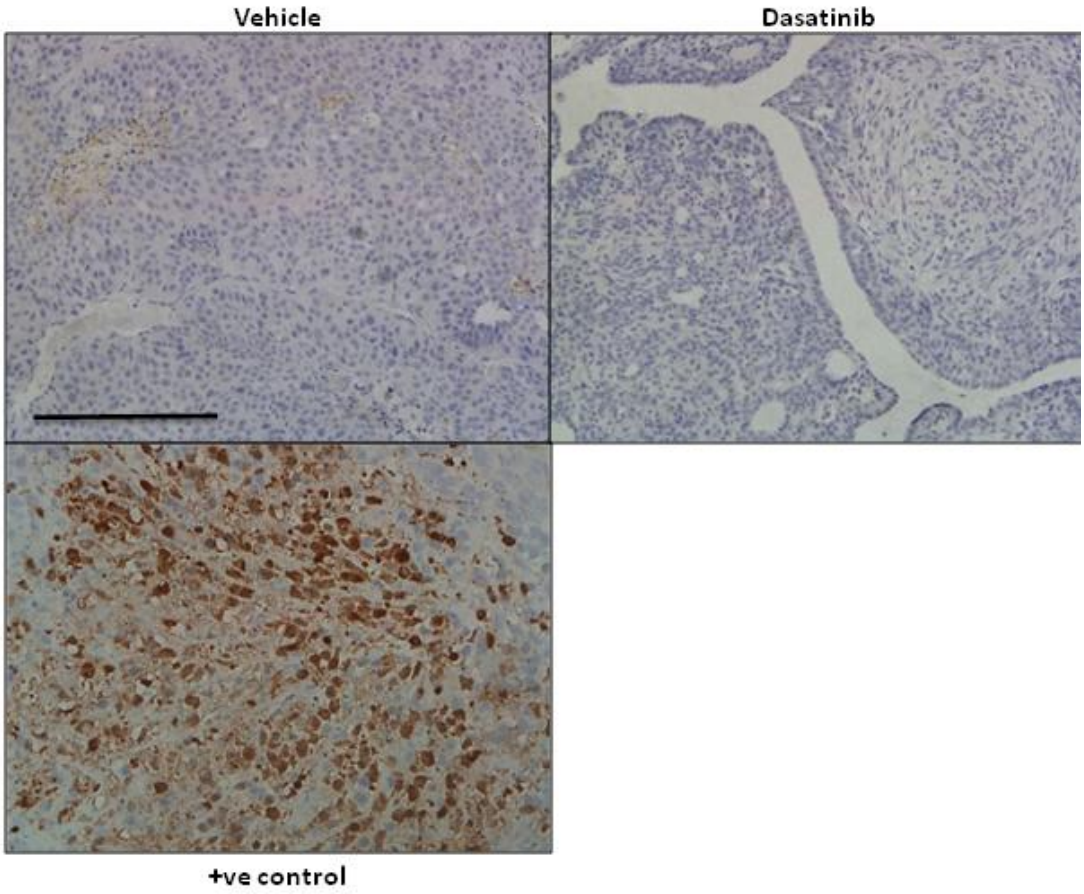

Figure 3.13- Dasatinib treatment did not result in apoptosis. IHC was performed on paraffin embedded sections of dasatinib (n=4) and vehicle (n=2) treated tumours. Positive control consists of 4T1 cells subcutaneously implanted in an FVB mouse and treated with doxorubicin. Mag x20. Scale bar represents 100μM.

3.7 Characterisation of BLG-HER2^{KI} PTEN$^{+/-}$ derived cell lines

In order to further explore dasatinib's mechanism of action, 2 cell lines were generated from vehicle treated BLG-HER2^{KI} PTEN$^{+/-}$ tumours **(S. Karim)**. Although both cell lines were derived from vehicle treated tumours, they exhibited heterogeneity in expression of some key receptors and signalling molecule (Figure 3.14). For example, expression of pTyr 416 Src expression was substantially increased in the first of these cell lines (BLG-6222) compared to expression in the second cell line (BLG-5957). We also observed greater Akt activity in the BLG-6222 cell line than in the BLG-5957 cell line. However, neither cell line expressed EGFR and unlike other mouse models of HER2 positive breast cancer (see chapter 4), both cell lines retained PTEN, which may have contributed to the long tumour latency observed during the *in vivo* study.

3.8 Effect of dasatinib on cell proliferation *in vitro*

As both cell lines continued to express Src, we decided to explore their sensitivity to dasatinib. Interestingly, in marked contrast to our observations *in vivo*, both BLG-6222 and BLG-5957 cell lines demonstrated dose-dependent inhibition of proliferation in response to dasatinib treatment with an IC_{50} of 85.9 nmol and 75.0 nmol respectively (Figure 3.15A). Using western blotting, we demonstrated a reduction in Src phosphorylation at concentrations which inhibited cell proliferation, despite an increase in total Src expression (Figure 3.15B).

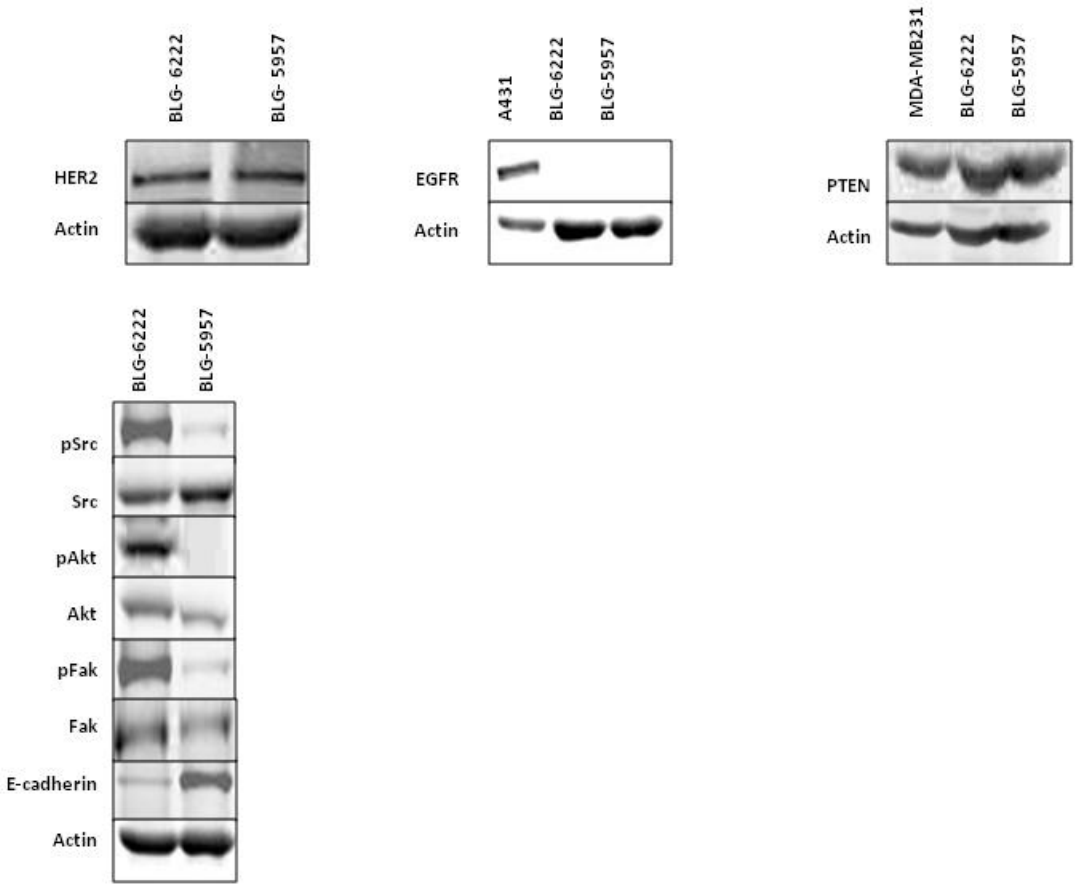

Figure 3.14- Characterisation of BLG-HER2^{KI} PTEN$^{+/-}$ derived cell lines by western blotting demonstrating heterogeneity in expression of key receptors and signalling molecules between the 2 cell lines derived from vehicle treated tumours. 20µg protein loaded in each lane. A431 used as positive control for EGFR. MDA-MB 231 used as a positive control for PTEN. Actin used as a loading control.

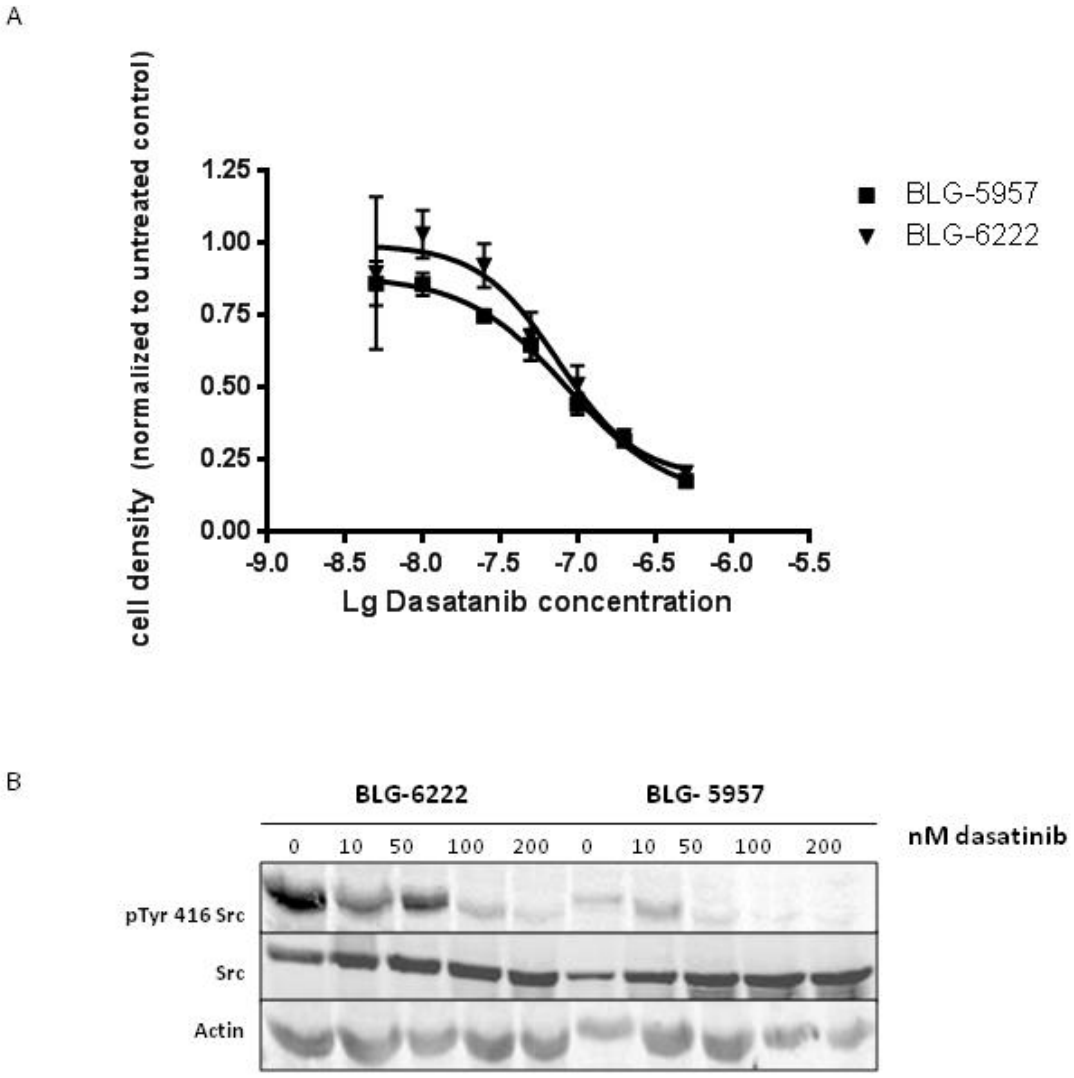

Figure 3.15- Dasatinib treatment of BLG-HER2^{KI} PTEN$^{+/-}$ cell lines resulted in dose dependent inhibition of proliferation and reduced Src activity. A. 2000 cells were plated out in each well of a 96 well plate and treated with escalating doses of dasatinib. After 72 hours an SRB assay was performed. Data was analysed using GraphPad Prism 6 software. Error bars represent SEM across 6 wells treated at the same drug dose within 1 experiment. IC_{50} 85.9 nmol in BLG-6222 and 75.0 nmol in BLG-5957. B: BLG-6222 and BLG-5957 cells were incubated overnight with escalating doses of dasatinib before being used to generate cell lysate for western blotting. 20µg protein loaded in each lane. Actin used as loading control.

3.9 Effect of dasatinib on *in vitro* cell migration

Previous studies have shown that dasatinib is capable of inhibiting cell migration in a number of different tumour types [219], [218]. Using wound healing assays, we demonstrated that dasatinib treatment resulted in a dose dependent inhibition of migration in both BLG-6222 and BLG-5957 cell lines with significant reductions in the velocity of migration (BLG-6222 $p<0.001$, one way ANOVA, BLG-5957 $p<0.001$, one way ANOVA, Figure 3.16). The IC_{50} for dasatinib's effect on migration was 0.12nM in BLG-6222 and 0.14nM in BLG-5957. To ensure that impaired wound closure was due to dasatinib's effects on migration and not as a result of reduced proliferation, 2500 cells were treated with escalating doses of dasatinib for 24 hours before being trypsinized and re-counted (Figure 3.17). No effect on proliferation was observed at any concentration of dasatinib in the BLG-6222 cell line ($p=0.105$, one way ANOVA). There was a statistically significant reduction in proliferation of the BLG-5957 cell line but only at dasatinib concentrations of 100nM and 200nM ($p=0.018$, one way ANOVA with Tukey's test), which is considerably greater than the concentrations required to inhibit migration. Taken together these results suggest that in both BLG-6222 and BLG-5957 lower concentrations of dasatinib were required to inhibit cell migration than were required to inhibit proliferation.

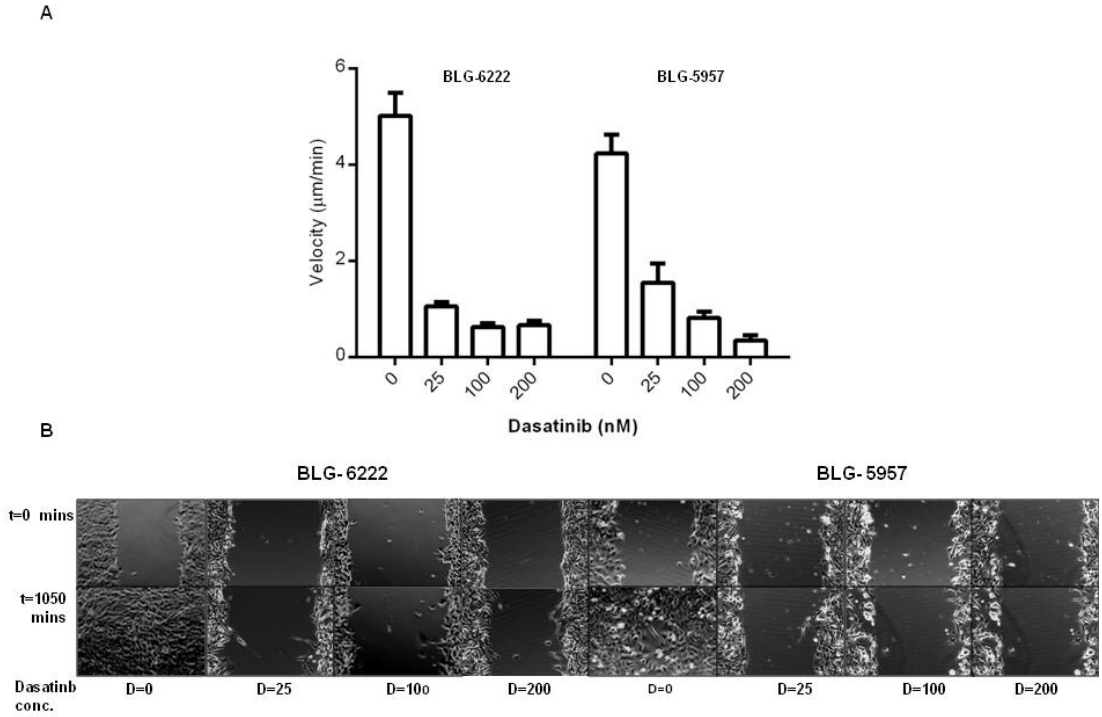

Figure 3.16- Dasatinib treatment resulted in dose dependent inhibition of cell migration. Cells were plated out in 12- well cell culture plate and grown to confluency. The monolayer was scratched with a pipette tip, washed with media to remove any floating cells and treated with either DMSO or escalating doses of dasatinib. The plate was placed in a microscope humidity chamber, which was maintained at 37^0C and supplemented with CO2. Wound closure was monitored overnight with an Olympus scan R microscope and sequential images recorded at 15 minute intervals. A: Effect of dasatinib on rate of migration. Mean value ± SEM (n= 3) displayed. B Representative images of cells migrating into the scratch.

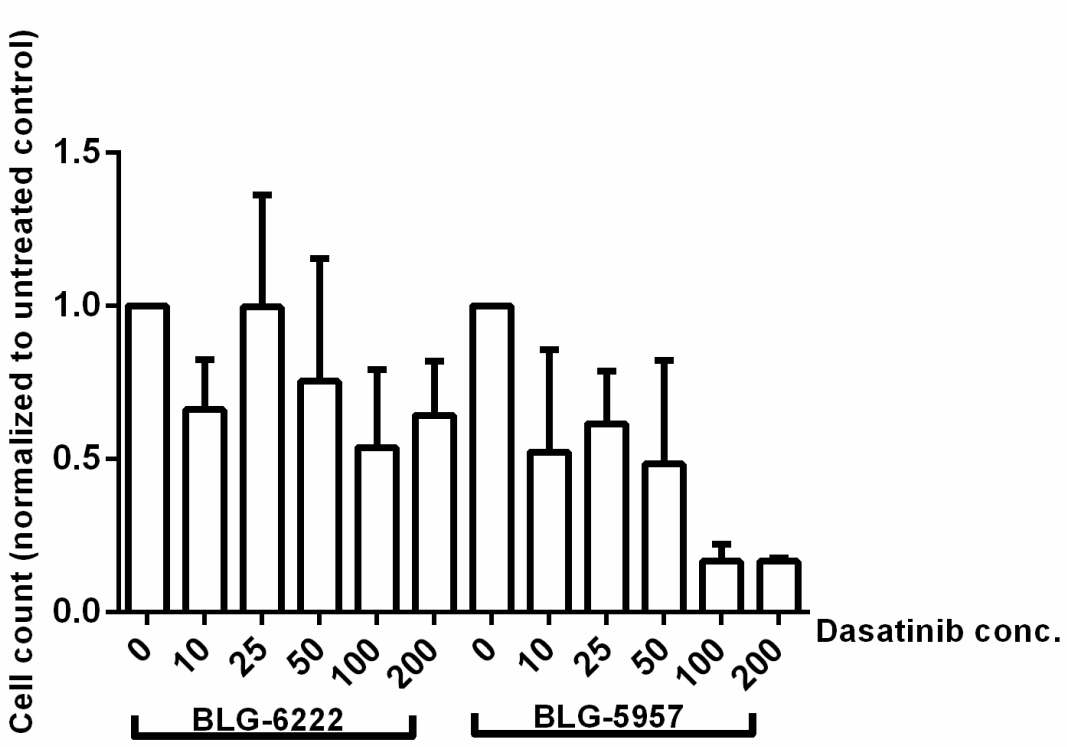

Figure 3.17- Dasatinib did not inhibit proliferation at concentrations required to inhibit migration. 2500 cells were seeded into a 12 well dish and treated with escalating doses of dasatinib. After 24 hours, cells were trypsinized and resuspended in media prior to being re-counted.

3.10 Effect of dasatinib on invasion

Previous studies have also established dasatinib's ability to inhibit invasion in several different cell lines [218] [219] [220]. When BLG-6222 cells were treated with dasatinib for 72 hours, we observed a dose dependent reduction in their invasion into Matrigel (Figure 3.18). Further cell counting experiments were performed to ensure that the observed effect was due to inhibition of invasion rather than impaired cell proliferation. After 72 hours of dasatinib treatment, proliferation was only significantly inhibited at a concentration of 10nM ($p=0.021$, one way ANOVA with Tukey's test, Figure 3.19), whilst invasion was significantly inhibited at dasatinib concentrations of 1nM onwards ($p \leq 0.001$, one way ANOVA with Tukey's test). BLG-5957 cells did not invade into Matrigel. Interestingly, on western blot this cell line was shown to express more E-cadherin than BLG-6222 and this may have accounted for its less invasive phenotype (Figure 3. 14).

Previous studies have shown that dasatinib inhibits tumour cell invasion by stabilization of E-cadherin –mediated cell-cell junctions. Using IHC, we demonstrated cytoplasmic and membranous E-cadherin expression in all tumours (Figure 3.20). However, whilst there was little membranous expression in the vehicle-treated cohort, both cytoplasmic and membranous expression was dramatically upregulated in dasatinib-treated tumours (**S.Karim**). This was subsequently confirmed on western blot **(S.Karim)**.

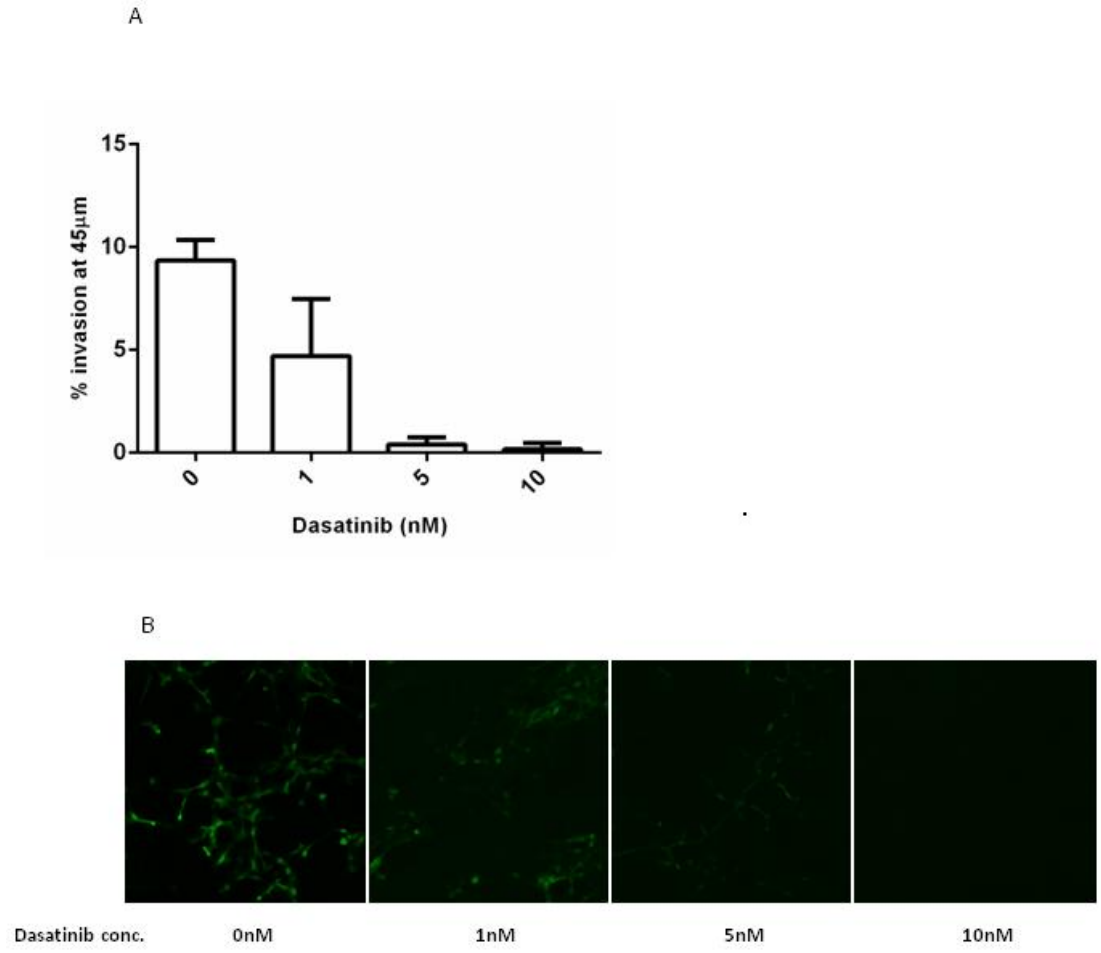

Figure 3.18- Dasatinib treatment resulted in dose dependent inhibition of invasion in BLG-6222. Cells were seeded on Transwell filters and allowed to invade into Matrigel. After 72 hours, cells were labelled with calcein AM and visualized in the Matrigel at 15µM increments (n=3). A: Percentage cell invasion into Matrigel at depth of 45µM. B: Representative composite images of invading cells at increasing doses of dasatinib.

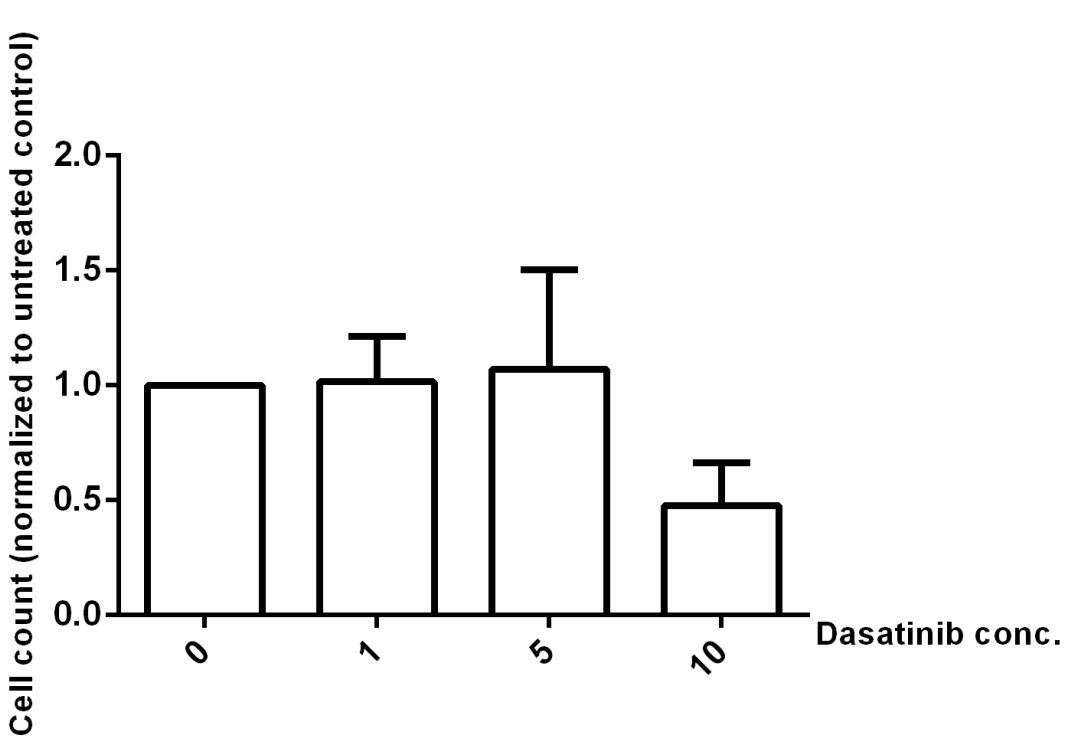

Figure 3.19- Dasatinib does not inhibit proliferation of BLG-6222 cells at concentrations required to inhibit invasion. 2500 cells were seeded into a 12 well dish and treated with escalating doses of dasatinib. After 72 hours, cells were trypsinized and resuspended in media prior to being re-counted.

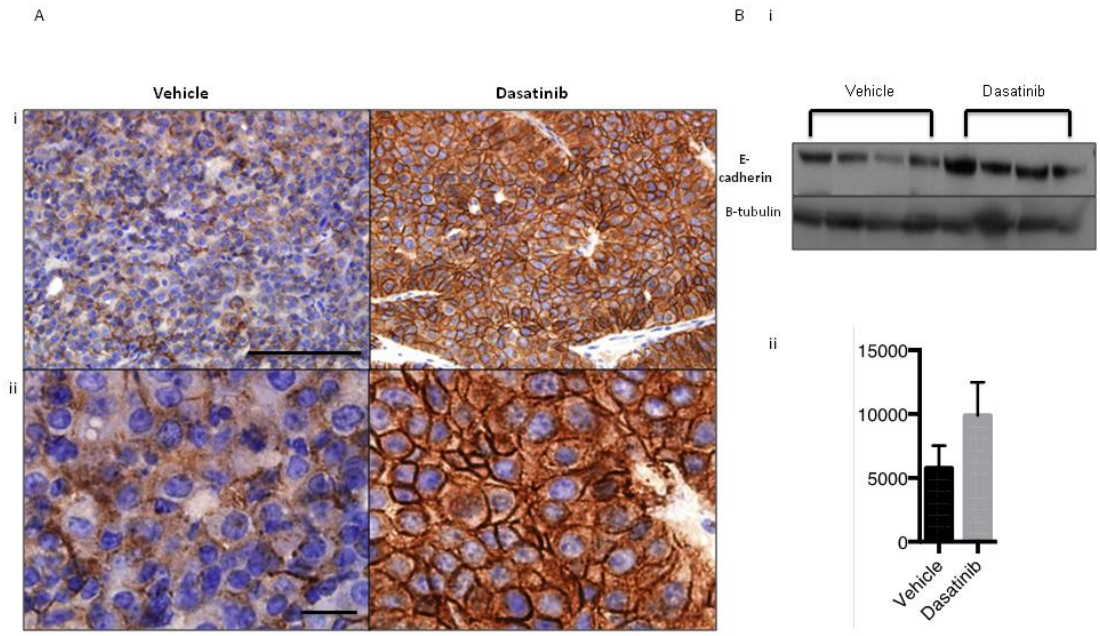

Figure 3.20- Dasatinib treatment resulted in increased cytoplasmic and membranous expression of E-cadherin. A. IHC was performed on paraffin embedded sections of dasatinib and vehicle treated tumours. i-Mag x20. ii- Mag x40. Scale bars represents 100μM. Bi: Western blot performed on tumour lysate confirmed increased expression of E-cadherin in dasatinib treated tumours. ii: Quantification of E cadherin expression normalized for β-tubulin expression.p=0.032, Mann Whitney U test (S.Karim).

3.11 The effect of dasatinib on downstream signalling

We next looked at the effect of dasatinib on HER2 expression and its downstream signalling activity. We used IHC to examine HER2 expression in both dasatinib and vehicle treated tumours. Whilst moderate HER2 expression was seen in vehicle treated tumours, HER2 was barely detectable in any of the dasatinib treated tumours (Figure 3.21) irrespective of the tumour's phenotype. Unfortunately, we were unable to detect HER2 expression by western blot on tumour lysates. We were also unable to detect HER2 activity using antibodies to key autophosphorylation residues, including pTyr 1221/1222 HER2 on IHC and pTyr 1248 HER2 on western blot. However, looking at signalling downstream of HER2, we observed reduced Akt activity following dasatinib treatment on western blot (Figure 3.22, **S.Karim)**. The tumour suppressor gene PTEN is a negative regulator of the Akt pathway and it was therefore intriguing to note that this reduction in Akt activity was seen despite a reduction in PTEN expression in the dasatinib treated tumours (**S.Karim).**

As the amount of tissue from the original GEMM tumours was limited, we used the BLG-6222 cell line to generate further tumours for analysis of downstream signalling pathways. We inoculated the fourth left mammary fat pad (MFP) of CD1 nude mice with $1*10^6$ BLG-6222 cells. All recipients subsequently developed a single mammary tumour and once these had reached a volume of $0.2cm^3$, animals were randomized to receive either a single dose of dasatinib (10mg/kg) or vehicle. Mice were sacrificed 2 hours later and the tumours used to generate further lysate for reverse phase protein microarray (RPPA) analysis. We did not observe any statistical differences in the activity of any of the signalling pathways examined during this experiment but this is most likely due to the low number of tumours used in each experimental arm. We did, however, observe a strong trend towards reduced Src activity on RPPA (Figure 3.23). We also observed a reduction in autophosphosphorylation of HER2 on Tyr 1248. Although the antibody used on this platform was also capable of detecting pTyr 1173 EGFR, no change in signal was observed when a pTyr 1173 EGFR specific antibody was used suggesting the change in signal associated with the combined antibody was a reflection of reduced HER2 activity alone. Hence, short-term dasatinib treatment was associated with both reduced HER2 and Src activity. Consistent with our previous findings, we also observed reduced Akt activity as demonstrated by reduced phosphorylation on both Thr 308 and Ser 473. For a full set of results see appendix 1.

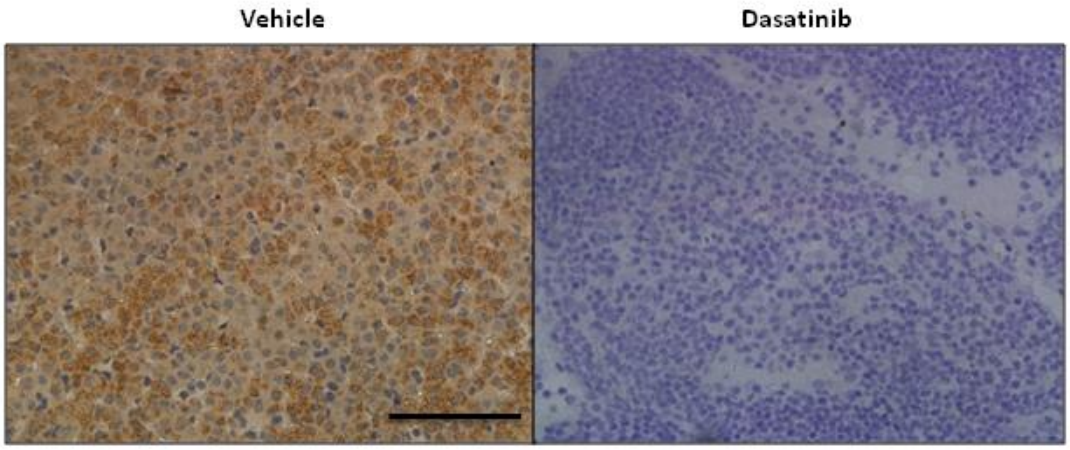

Figure 3.21- Dasatinib treatment inhibited HER2 expression. Representative images of IHC of HER 2 in vehicle (n=3) and dasatinib (n=3) treated tumours. Magnification x 40, scale bar represents 100µm.

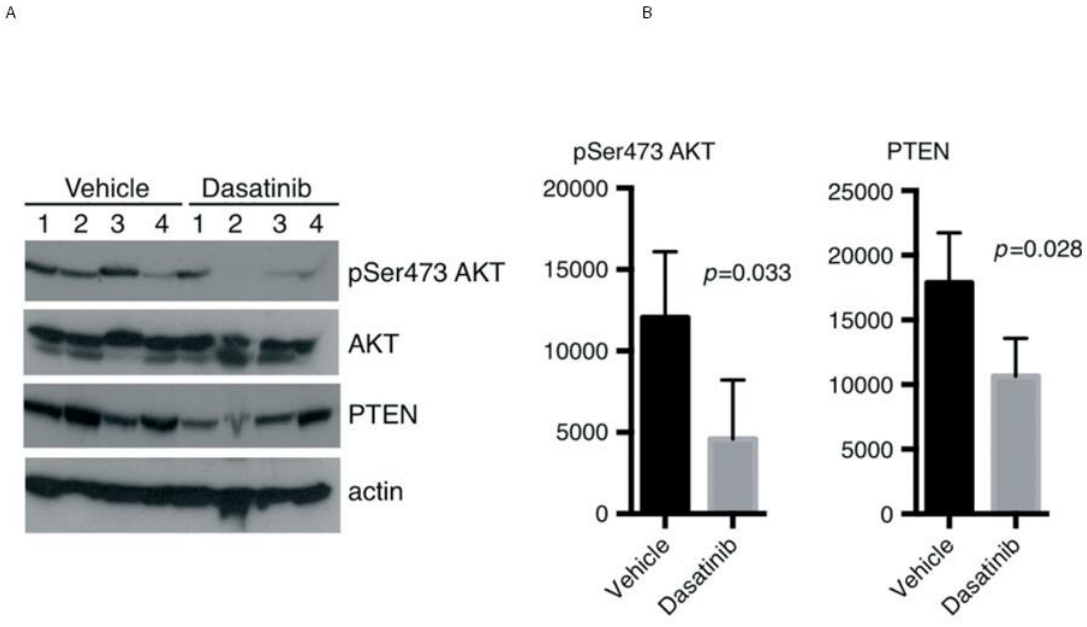

Figure 3.22- Dasatinib treatment led to reduced Akt activity and PTEN expression. Dasatinib (n=4) and vehicle (n=4) treated tumours were used to generate lysate for western blotting. A: Western blot demonstrating reduced Akt activity and PTEN expression. B: Quantification of western blots (S.Karim).

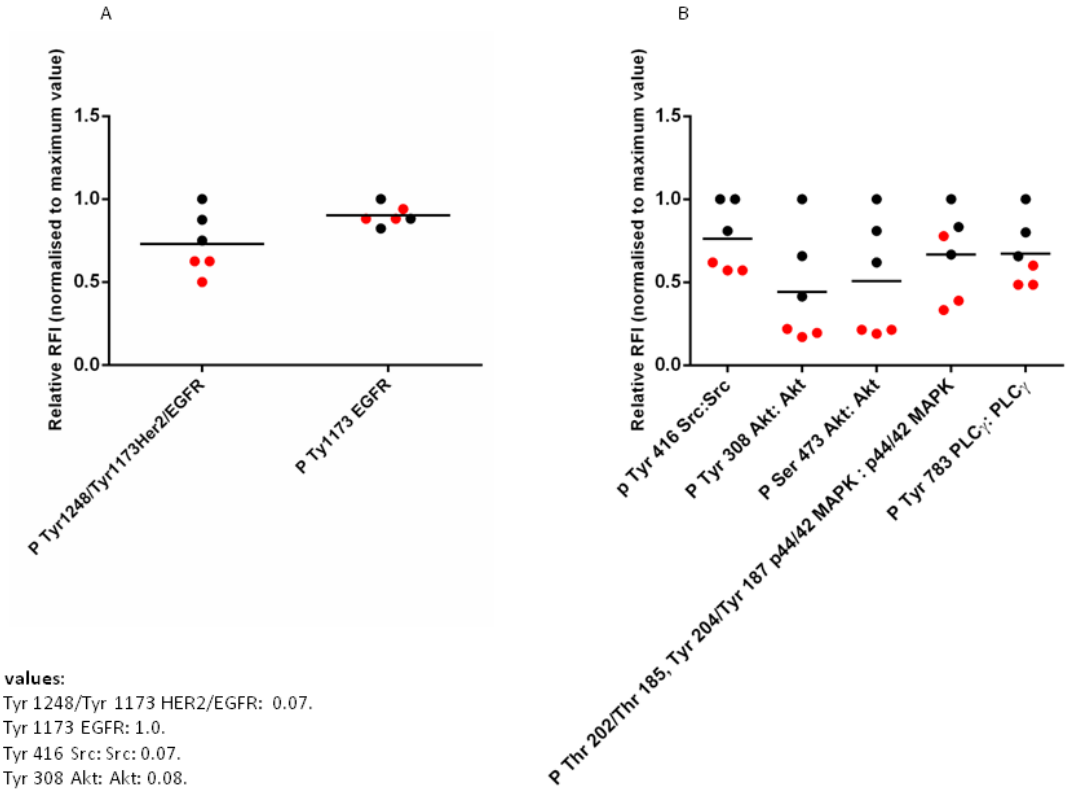

P values:
P Tyr 1248/Tyr 1173 HER2/EGFR: 0.07.
P Tyr 1173 EGFR: 1.0.
P Tyr 416 Src: Src: 0.07.
P Tyr 308 Akt: Akt: 0.08.
P Ser 473 Akt: Akt: 0.07.
P Thr202/Thr 185, Tyr 204/Tyr 187p44/42 MAPK: p44/42 MAPK: 0.19
P Tyr 783 PLCγ: PLCγ- 0.08

Figure 3.23- Dasatinib treatment led to reduced Src, HER2 and Akt activity. Animals bearing a BLG-6222 tumour were randomized to treatment with either a single dose of dasatinib (10mg/kg) or vehicle and sacrificed 2 hours later. Tumour lysate (n=3 in each arm) was analysed using reverse-phase protein array platform. Where ever possible ratio of phospho: total protein has been expressed to give a measure of signalling activity within specific pathways. All other values have been corrected using the global normalisation technique [40]. Red data points represent dasatinib treated tumours and black data points represent vehicle treated tumours. P values generated using Mann Whitney U test.

3.12 Discussion

Pre-clinical data demonstrating Src's fundamental role in a number of processes underpinning the malignant phenotype coupled with evidence of increased Src activity in numerous tumour types has generated much interest in the potential use of Src inhibitors as therapies in solid tumours. However, despite isolated responses, overall results of clinical trials have been disappointing suggesting that there is a need to better understand which patients and at what stage of their disease Src inhibitors are most likely to be efficacious. In this series of experiments, we aimed to describe tumorigenesis in the BLG- $HER2^{KI}$ $PTEN^{+/-}$ model, a GEMM of HER2 positive breast cancer, and to determine the response of the model to the Src inhibitor dasatinib.

3.12.1 Characterization of the BLG-$HER2^{KI}$ $PTEN^{+/-}$ model

Tumorigenesis in the BLG-$HER2^{KI}$ $PTEN^{+/-}$ model is driven by an activated HER2 transgene under the control of the BLG promoter which when combined with Cre-recombinase mediated loss of a PTEN allele results in the stochastic development of mammary tumours. Although tumorigenesis in all animals was driven by the same driver mutations, we observed considerable heterogeneity in both the age of tumour onset and duration of survival following tumour development. This most likely reflects the random accumulation of secondary mutations within the tumour and suggests that this model is better able to model the diverse range of tumour behaviours seen within human HER2 positive breast cancer than more traditional xenograft based models. Both the tumour microenvironment [28]and the immune system [27] are increasingly recognised to play pivitol roles in tumour development and therefore the development of these tumours within the appropriate organ in the context of a functioning immune system are further important benefits of this model over xenografts. However, the median age of tumour onset in vehicle treated animals was 467 days and this long interval is not fully reflective of the frequently aggressive nature of human HER2 positive disease. Previously published work using this HER2 transgene coupled with Cre-recombinase mediated PTEN loss under the control of the MMTV promoter enhancer described a much shorter tumour latency interval of 6.5 months [231]. There are several possible explanations for the vastly different latency intervals between these 2 models. Firstly, low levels of Cre mediated recombination have been described in cohorts of virgin

mice when under the control of the BLG promoter [240] whilst the MMTV promoter enhancer is well recognised as an efficient driver of cre mediated recombination [241]. Low rates of recombination in our model are likely to have resulted in retention of both PTEN alleles in many tumour cells and this is likely to have contributed to the prolonged tumour latency. Furthermore, loss of heterozygosity (LOH) for PTEN was described in 50% of tumours in the MMTV- driven model [231] whilst we observed continued PTEN expression in all BLG-HER2^{KI} PTEN$^{+/-}$ tumours and this is again likely to have contributed to the lengthy tumour latency interval. The efficiency of BLG-Cre mediated recombination is greatly enhanced in lactating mice [240] and therefore we could improve the efficiency of future experiments by allowing all mice to undergo 1 breeding cycle. We also noted that the level of HER2 expression in our model was substantially lower than in the MMTV-driven model and as HER2 has previously been shown to play a critical role in mammary epithelial cell transformation [225], this is also likely to have contributed to the longer tumour latency interval. Finally, these 2 models used different background mouse strains. The MMTV-driven model was bred on an FVB background whilst our model used a mixed background and it may be that these animals were not as susceptible to mammary tumour development.

In summary, despite the long tumour latency interval, this model is capable of recapitulating some of the key pathological features of human HER2 positive breast cancer and may therefore be a useful tool in the development of novel therapeutic strategies.

3.12.2 The effect of dasatinib on tumour initiation and progression

We found that tumour development was significantly delayed by dasatinib treatment. However, continued treatment following tumour initiation did not inhibit progression suggesting that whilst Src is important in the initial stages of tumour development, it may have a less significant role in the latter stages of disease. This is consistent with data from several other previously published studies; Webster et al reported that mammary-specific expression of activated Src resulted in the development of hyperplastic lesions but these rarely progressed to tumours [242]. Mammary-specific deletion of Src in the MMTV-polyoma middle T(PyMT) model reduced the proliferation of hyperplastic lesions and prevented the

development of tumours [243]. In addition, similar results were obtained following treatment with the Src inhibitor bosutinib in this model [244]. The importance of Src in early tumour development does not appear to be restricted to breast tumour development as Src inhibition in a model of skin carcinogenesis reduced the incidence of papillomas but did not prevent their conversion to squamous cell carcinomas [245]. In humans, increased Src activity has also been associated with the development of the pre-malignant hyper-proliferative skin lesions, human actinic keratoses [245].

Whilst dasatinib treatment delayed disease onset, all animals ultimately developed tumours due to the onset of acquired drug resistance. Using IHC we demonstrated that the onset of resistance was not associated with loss of Src inhibition. However, we did observe a significant reduction in the HER2 expression in dasatinib-treated tumours and this is likely to be a reflection of compensatory signaling changes associated with the development of resistance. Furthermore, although *in vitro* treatment of drug-naïve BLG-HER2^{KI} PTEN$^{+/-}$ tumour cell lines with dasatinib resulted in dose dependent inhibition of proliferation, no such effect was observed in our *in vivo* model. This was most likely due to the acquisition of other genetic changes which were responsible for the ongoing proliferation despite Src inhibition. Src's effects on cell proliferation appear to vary according to the model in which it is assessed. In previous studies using a HER2 driven mouse model of breast cancer, Src and HER2 were found to interact via their SH2 domains [246] [247] [248] resulting in enhanced Src activity and changes in breast cancer cell growth, survival and polarity [249] [250] [251]. In contrast, mammary-specific expression of CSK, a negative regulator of Src, did not alter the growth of HER2 positive mammary tumours in mice [252] and in studies using human HER2 positive breast cancer cell lines, no consistent relationship between HER2 activation and dasatinib was identified [253] [254] . Furthermore, in a GEMM of pancreatic cancer, dasatinib had no effect on proliferation in the primary tumour but did inhibit the development of metastases [220]. Src's variable impact on primary tumour cell proliferation highlights the critical need to develop biomarkers which are capable of predicting which patients are likely to benefit from dasatinib treatment.

It is also well established that dasatinib is capable of potently inhibiting tumour cell invasion and migration both *in vitro* and *in vivo* and in several models, including breast cancer derived cell lines, these are its dominant mechanisms of action [220] [88] [255] [256]. Whilst our *in vitro* data showed that dasatinib was capable of inhibiting both invasion and migration of BLG-HER2^{KI} PTEN$^{+/-}$ cells, we found that similar numbers of dasatinib and vehicle-treated

animals developed metastatic disease. Although the numbers of animals developing metastases were too low to permit statistical analysis, amongst animals with evidence of metastatic disease, we observed a striking reduction in the number of metastases in dasatinib-treated animals compared to vehicle-treated animals. These results are consistent with previously published data showing that dasatinib reduced the metastatic burden in both mouse models of pancreatic and prostate cancer [220] [88]. We also observed a substantial increase in E-cadherin expression in dasatinib treated tumours suggesting that dasatinib may inhibit E-cadherin endocytosis and enhance the protein's stability thereby preventing tumour dissemination [257] [258].

In summary, our data shows that in the BLG-HER2^{KI} PTEN$^{+/-}$ model dasatinib inhibited tumour initiation but had no effect on tumour cell proliferation or tumour progression. It also provides preliminary evidence that dasatinib was able to inhibit the development of metastases in this model.

3.12.3 Effect of dasatinib on tumour differentiation

The effect of dasatinib on tumour differentiation was one of our most striking observations with the presence of prominent squamous elements in dasatinib treated tumours. Squamous metaplasia has been linked to mammary-specific activation of the Wnt pathway in previous studies [236]. Consistent with these findings, we observed increased β-catenin expression in regions adjacent to the keratinized zones of dasatinib treated tumours suggesting that β catenin mediated signaling was responsible for driving the squamous differentiation. Our data is consistent with that of Hebbard et al who also observed squamous differentiation in the MMTV-PyMT mouse model following treatment with the Src inhibitor bosutinib [244] and taken together the data suggests that Src and Wnt are capable of co-operating to regulate mammary epithelial cell differentiation. Src and Wnt have also been shown to co-operate in regulating the differentiation of other cell types, including osteoblasts [162] [259].

3.12.4 Clinical relevance of these findings in the management of human HER2 positive breast cancer

Clinical trials to date have focused on the use of Src inhibitors in metastatic disease. However, increased Src activity is frequently observed in DCIS, where it is associated with factors predictive of high recurrence risk, including HER2 positivity [260]. Increased Src activity is frequently observed in invasive breast cancers but different studies have yielded conflicting results about the relationship between tumour stage and the level of Src activity [261] [262] [263]. Ito et al reported increased Src activity was more commonly observed in early rather than advanced disease [262] and taken together with the established anti-migratory roles of Src inhibitors this further supports the argument for their use in early or even pre-invasive disease. DCIS is not associated with mortality but current treatment strategies, which include mastectomy and breast conserving surgery (BCS) ± radiotherapy, result in significant morbidity. Recurrence rates after BCS in high risk subgroups, such as HER2 positive disease, can be as high as 40% [264] and as 50% of these patients will have developed invasive disease at the time of relapse [265], aggressive upfront surgical management of high risk DCIS is mandatory. Together with other previously published studies, our data support the use of Src inhibitors in facilitating BCS in patients with high risk DCIS.

3.13 Summary

In conclusion, our results provide further evidence that GEMMs can be useful tools in the development of novel therapeutic strategies for the management of solid tumours. We have also confirmed that Src plays important roles in the early stages of tumour development and in the development of metastases in our model providing a strong rationale for future clinical trials looking at the use of Src inhibitors in early and pre-invasive disease. However, the development of predictive biomarkers is essential if these drugs are to be successfully adopted into mainstream clinical practice.

Chapter 4: Validation and Characterisation of MMTV-NIC Model

Major advantages of using the BLG-HER2^{KI}-PTEN$^{+/-}$ model for use in preclinical drug studies include the development of primary tumours within the mammary fat pad, in the context of a functioning immune system and with a high penetrance rate. However, neither the long and varying latency period prior to the development of palpable disease or the low metastatic rate (8% of animals) is reflective of the frequently aggressive nature of HER2 positive disease in humans. Therefore an alternative model, the MMTV-Neu Internal Ribosome Entry Site (IRES)-Cre (NIC) model was selected for use in further experiments. From here on this model will be referred to as MMTV-NIC.

4.1 Model Background

Similarly to the BLG-HER2^{KI}-PTEN$^{+/-}$ model, tumourigenesis in the MMTV-NIC model is driven by a constitutively activated HER2 transgene. However, in this model the constitutive activity of the transgene is conferred by a 16 amino acid deletion in the extracellular domain of the HER2 receptor referred to as Neu in Frame Deletion (NDL) mutation. This promotes the formation of intermolecular disulphide bonds which results in persistently activated HER2 dimers. In comparison with wild type HER2, the NDL mutation has greater transforming capacity although its presence alone is insufficient to result in tumourigenesis. A 10 fold increase in activated HER3 is also observed in this model and it is likely the co-expression of both HER2 and HER3 together play a critical role in tumourigenesis [266]. A similar naturally occurring splice variant is observed in human breast cancers (HER2 Δ16), which also contains an extracellular domain deletion promoting the formation of stable disulphide bonds and enhanced transforming capacity. This alternative HER2 protein is found in approximately 50% of cases of human HER2 breast cancer and 90% of cases with lymph node involvement [267] making this model highly clinically relevant.

The MTMV-NIC model also differs from the BLG-HER2^{KI}-PTEN$^{+/-}$ model, in its use of th strong Mouse Mammary Tumour Virus (MMTV) promoter to regulate expression of the transgene. MMTV is a naturally occurring milk transmitted retrovirus that causes mammary tumour development by integration of the virus adjacent to proto-oncogenes such as Wnt-1, Fibroblast Growth Factor 3 (FGF3) and Notch [268]. Transgenic mouse models exploit a recombinant MMTV promoter, which is expressed from birth [241], and models in which this promoter is fused to oncogenes, such as c-myc, Wnt-1 and RET, have been widely used [268]. Previous studies using MMTV-driven activated HER2 expression have described development of multiple poorly differentiated mammary adenocarcinomas although discrepancy exists between whether these develop in a synchronous [225] or stochastic [269] manner. MMTV- driven expression of activated HER2 is largely confined to mammary tissue but limited expression is also observed in the adrenal glands, lung, pancreas, ovaries and salivary glands [270] [225] [269].

Unlike the BLG-HER2^{KI}-PTEN$^{+/-}$ model, the MMTV-NIC model employs a bicistronic transcript to co-express HER2^{NDL} with Cre-recombinase. Therefore, when crossed with a strain containing a floxed allele, the model can be used to explore the effect of conditional knockout of a tumour suppressor gene, such as PTEN (Figure 4.1). Whilst MMTV is an efficient promoter and is expressed in the majority of mammary epithelial cells, mosaicism has been observed with some cells 'escaping' from Cre-expression and subsequent genetic recombination [241]. The use of a bicistronic transcript couples HER2^{NDL} expression to the loss of a PTEN allele ensuring every HER2^{NDL} expressing cell has also lost a PTEN allele [270]. This alleviates problems associated with tumours containing mixed cell populations with combinations of HER2^{NDL} expressing and/or Cre positive PTEN$^{+/-}$ cells. As previously discussed, loss of PTEN is a common genetic event in breast cancer. It has been linked with resistance to trastuzumab but despite compelling *in vitro* evidence [271], analysis from various clinical trials have given conflicting results [150]. This model is therefore a useful tool to further explore this contentious area.

The MMTV-NIC model has several advantages over the BLG-HER2^{KI}-PTEN$^{+/-}$ model making it better suited to use in preclinical studies. Firstly, the greater efficiency of the MMTV promoter results in Cre-mediated recombination in the majority of luminal epithelial and myoepithelial cells [241] whilst only low level recombination is observed in the non-lactating gland when the BLG-promoter is used [240]. This results in a shorter latency period before

the onset of palpable disease and more rapid tumour progression (see below). Furthermore, loss of PTEN in the MMTV-NIC model has previously been demonstrated to accelerate tumourigenesis [272]. In this model, over 50% of mice with heterozygous loss of PTEN ($PTEN^{+/-}$) develop loss of heterozygosity (LOH) resulting in the loss of the second PTEN allele and further accelerating tumourigenesis [272]. Thirdly, as already described this model can be used to explore the role of PTEN in moderating drug sensitivity. Whilst the genetics of the BLG-$HER2^{KI}$-$PTEN^{+/-}$ model mean this is also technically possible, the long tumour latency and slow progression rate in this model means it is not logistically feasible to develop $HER2^{KI}$ expressing tumours with wild type PTEN ($PTEN^{FL/+}$) within the average life expectancy of a mouse. Finally, the considerably higher rates of lung metastases observed in the MMTV-NIC $PTEN^{+/-}$ model are more reflective of the virulent nature of human HER2 positive breast cancer.

Initial work focussed on characterising and validating the model as a preclinical tool for predicting response to drugs in human HER2 positive breast cancer. Subsequently, its response to AZD8931, a novel equipotent inhibitor of HER2 and EGFR was explored [273].

Specific aims of this section of the project included:

1. Determining the growth kinetics of MMTV-NIC $PTEN^{FL/+}$ and MMTV-$NIC^{+/-}$ tumours.
2. Comparing signalling pathway activity in MMTV-NIC $PTEN^{FL/+}$ and MMTV-NIC $PTEN^{+/-}$ tumours.
3. Describing MMTV-NIC $PTEN^{+/-}$ tumours in terms of histology, hormone receptor (HR) status, HER2 expression and Ki67 expression.
4. Exploring the response of MMTV-NIC $PTEN^{+/-}$ model to paclitaxel, an active drug in the management of human breast cancer.
5. Investigating the activity of AZD8931 in MMTV-NIC $PTEN^{FL/+}$ and MMTV-NIC $PTEN^{+/-}$ models.

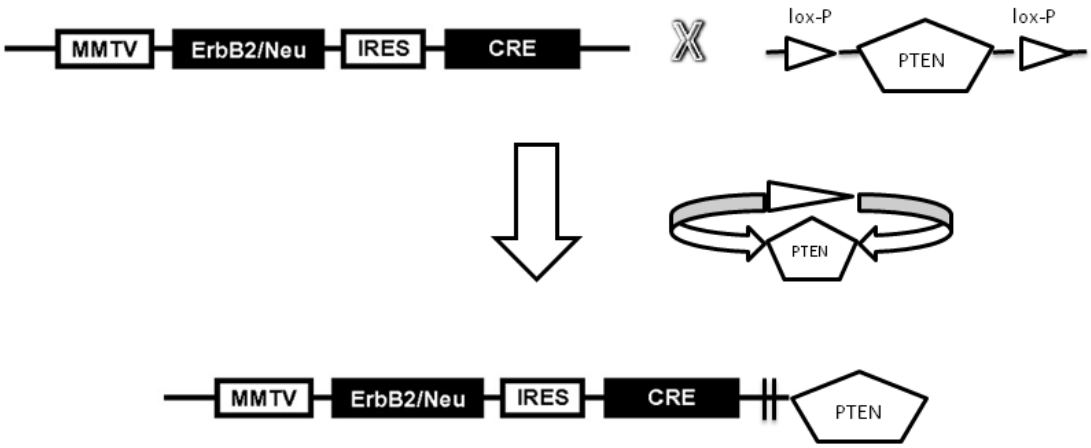

Figure 4.1- MMTV-NIC Genotype. Tumourigenesis in the MMTV-NIC model is driven by expression of a constitutively activated HER2 transgene under the control of the MMTV promoter. Use of a bicistronic transcript couples HER2 and Cre recombinase expression to facilitate study of HER2 over-expression in conjunction with loss of a tumour suppressor gene such as PTEN.

4.2 Model Characterisation and Validation

4.2.1 Growth of MMTV-NIC PTEN $^{FL/+}$ and MMTV-NIC PTEN$^{+/-}$ tumours

Both MMTV-NIC PTEN $^{FL/+}$ and MMTV-NIC PTEN$^{+/-}$ mice were monitored twice weekly for the development of tumour formation by palpation. Tumour onset was defined as the presence of a palpable tumour. Animals were sacrificed once their tumour burden reached ≥ 1.7 cm in any direction.

In both MMTV-NIC PTEN $^{FL/+}$ and MMTV-NIC PTEN$^{+/-}$ cohorts, 100% of mice developed multiple tumours in a stochastic manner. Loss of PTEN significantly accelerated tumour onset (Figure 4.2). The median age of tumour onset was 81 days in the MMTV-NIC PTEN$^{+/-}$ cohort compared to 138 days in the MMTV-NIC PTEN $^{FL/+}$ cohort (p=0.0001, Gehan-Breslow-Wilcoxon test). Following tumour onset, loss of PTEN also accelerated tumour progression. The median survival after tumour onset was 21 days in the MMTV-NIC PTEN$^{+/-}$ cohort compared to 38.5 days in the MMTV-NIC PTEN $^{FL/+}$ cohort (p=0.0005, Gehan-Breslow-Wilcoxon test) **(L. Balderstone)**.

A

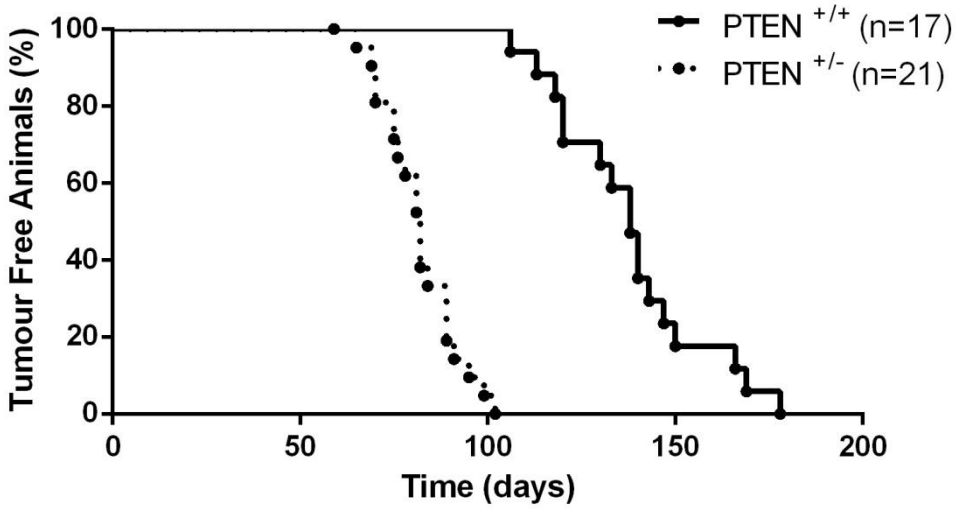

B

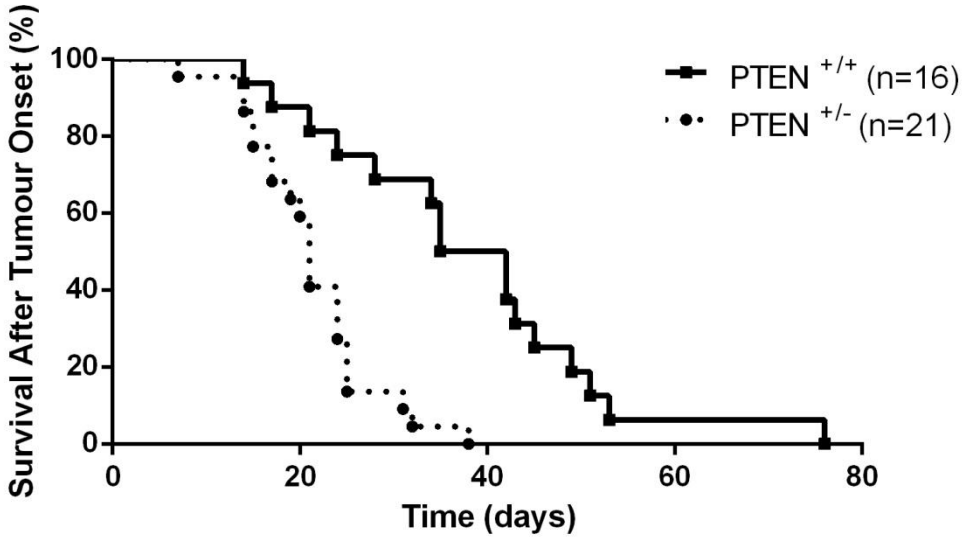

L. Balderstone

Figure 4.2- Loss of PTEN accelerated tumour onset and progression. Cohorts of MMTV-NIC PTEN $^{FL/+}$ and MMTV-NIC PTEN$^{+/-}$ mice were monitored for tumour development and progression. A: Age at onset of palpable disease. p=0.0001, Gehan-Breslow-Wilcoxon test. B: Duration of survival following onset of palpable disease. p= 0.0005, Gehan-Breslow-Wilcoxon test.

4.2.2 Comparison of signaling pathways between MMTV-NIC PTEN $^{FL/+}$ and MMTV-NIC PTEN$^{+/-}$ models

To explore the consequences of PTEN loss on downstream signaling pathways, we performed RPPA analysis on lysate from MMTV-NIC PTEN $^{FL/+}$ (n= 4) and MMTV-NIC PTEN$^{+/-}$ (n=3) tumours (**K. Macleod**). The full set of results is presented in Appendix 2.

We observed striking heterogeneity in the expression of both cell surface and downstream signaling molecules, even between tumours of the same genotype (Appendix 2). Overall, a significant difference in expression was detected in only 2 of the proteins assayed. Whilst the total PTEN antibody signal was too weak to accurately quantify, the pSer380, Thr382, Thr383 PTEN expression was reduced in MMTV-NIC PTEN$^{+/-}$ tumours. Phosphorylation of these carboxy-terminal residues results in increased enzyme stability [2] suggesting the amount of functional enzyme present at the cell membrane was reduced in MMTV-NIC PTEN$^{+/-}$ tumours (Figure 4.3). This was consistent with previous data from our group as using western blotting a non-statistically significant reduction in total PTEN expression had been demonstrated in an independent panel of MMTV-NIC PTEN$^{+/-}$ tumours compared to MMTV-NIC PTEN $^{FL/+}$ tumours (**L. Balderstone**, Figure 4.4).

Consistent with reduced PTEN expression, we observed increased Akt pathway activity in MMTV-NIC PTEN$^{+/-}$ tumours compared to MMTV-NIC PTEN $^{FL/+}$ tumours. A statistically significant increase in median pSer473 Akt: Akt ratio was observed on both RPPA analysis (p=0.01, Mann Whitney U test, Figure 4.3) and on western blot (p= 0.01, Mann Whitney U test, Figure 4.4). Median pThr308 Akt: Akt was also increased in MMTV-NIC PTEN$^{+/-}$ tumours on RPPA analysis although this did not reach statistical significance (p= 0.33, Mann Whitney U test). We also observed changes in the activity of several other signaling pathways using RPPA, including signaling molecules downstream of Akt, although none of these reached statistical significance.

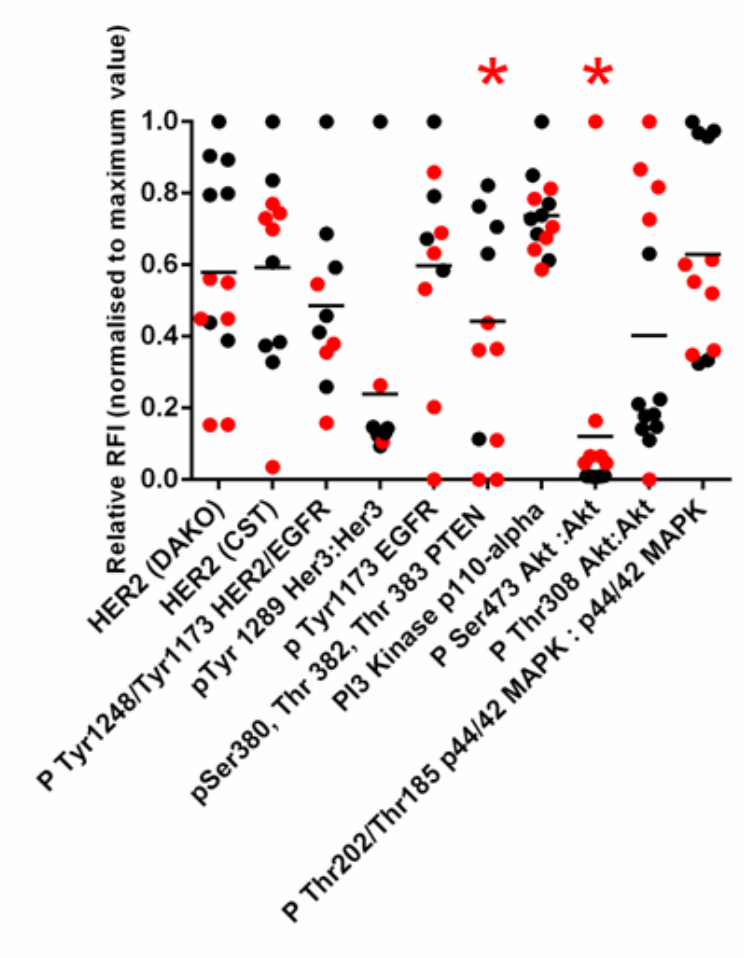

P Values:

HER2 (DAKO)-0.07
HER2 (CST)-0.93
P Tyr 1248/Tyr 1173 HER2/EGFR-0.22
pTyr 1289 HER3:HER3- 0.37
p Tyr 1173 EGFR- 0.24
P Ser 380, Thr 382, Thr 383 PTEN- 0.02
P13 Kinase p110-alpha- 0.35
P Ser 473 Akt: Akt-0.01
P Thr 308 Akt: Akt- 0.33
P Thr202/Thr 185p44/42 MAPK: p44/42 MAPK-0.38

Figure 4.2- RPPA analysis demonstrated reduced pSer 380, Thr 382, Thr 383 PTEN expression and increased Akt activity in MMTV-NIC PTEN$^{+/-}$ tumours. RPPA analysis was performed on lysate from MMTV-NIC PTEN$^{+/-}$ (red data points) and MMTV-NIC PTEN $^{FL/+}$ (black data points) tumours. Bar represents mean value for each data series. Asterix denotes statistically significant result. P values calculated using Mann Whitney U test.

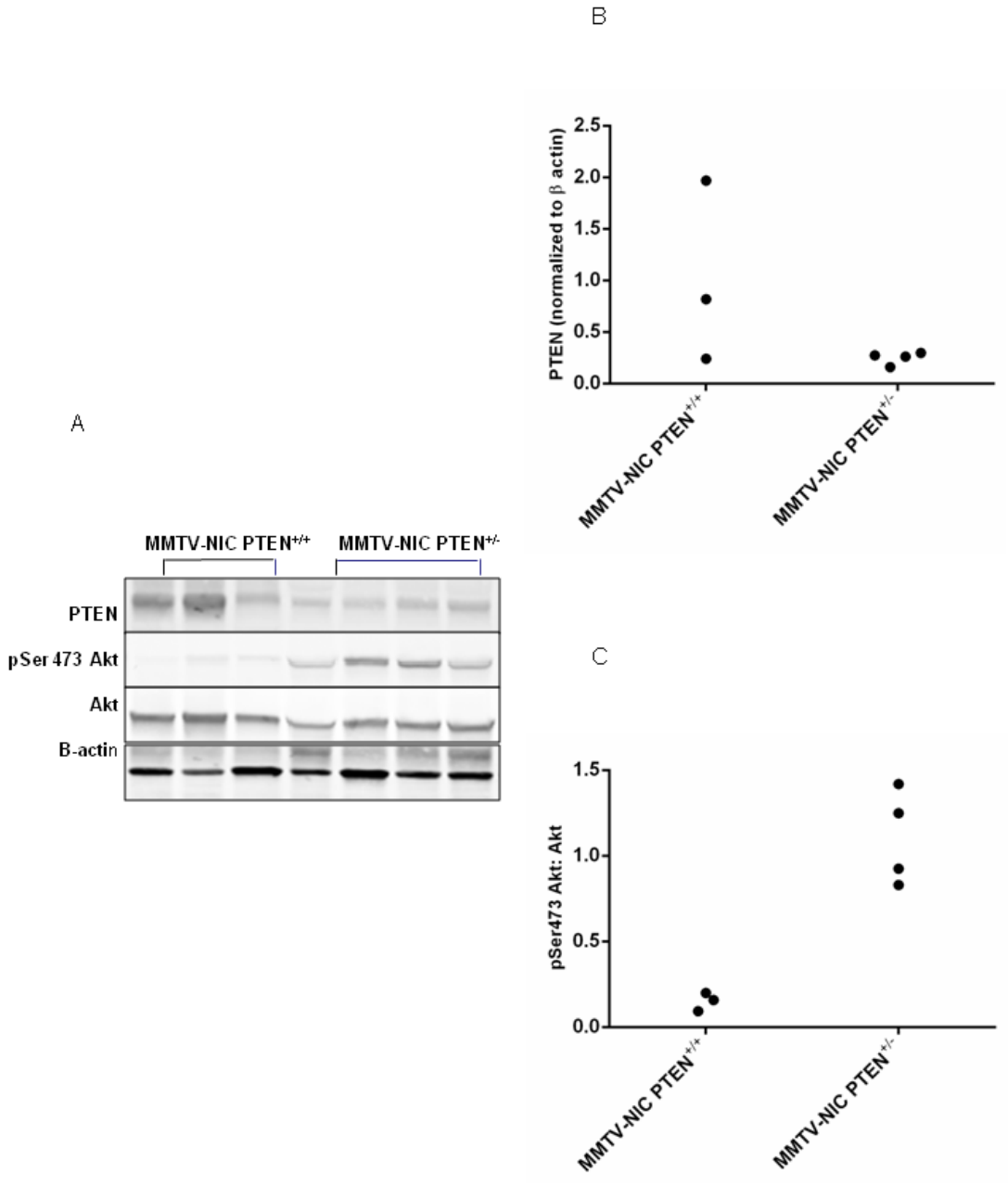

Figure 4.4- A. Western blot confirmed reduced PTEN expression and increased Akt activity in a panel of MMTV-NIC PTEN$^{+/-}$ tumours. 40 µg protein loaded in each lane. Actin used as loading control (L.Balderstone). B. Quantification of PTEN expression. Blots analysed using Image J. P=0.38, Mann Whitney U test. C. Quantification of Akt activity. Blots analysed using Image J. P=0.05, Mann Whitney U test.

4.2.3 Characterization of MMTV-NIC PTEN$^{+/-}$ tumours

4.2.3.1 Histology of MMTV-NIC PTEN$^{+/-}$ tumours

Histologically, these tumours were comprised of multiple highly cellular nodules (Figure 4.5A). Review of a series of mammary tumours by an experienced breast pathologist (**Dr. J. Loane, consultant pathologist**) confirmed the presence of highly mitotic (Figure 4.5B), grade 3 invasive carcinoma in all specimens (n=32). Extensive necrosis was observed in 71.8% (n=23) of samples and focal necrosis observed in a further 18.8% (n=6) (Figure 4.5C). There was no evidence of necrosis in 9.4% (n=3) of samples.

Using a single section of lung per mouse, we observed evidence of lung metastases in 25% (n=3) of 12 samples (Figure 4.5D). However, we only detected frank pulmonary metastases in one sample with disease being limited to micro-foci in the remaining two. The true rate of metastases is likely to be greater than that observed as we have inspected only one section per animal and it is likely that if the whole lungs were sectioned further metastases would be identified. Therefore, these findings suggest a significant proportion of tumour cells have the capacity to invade and metastasize even though the metastatic burden is low.

4.2.3.2 IHC characterization of MMTV-NIC PTEN$^{+/-}$ tumours

We used IHC to further characterize these tumours. Tumours were negative for both ER and PR (Figure 4.6). Using Ki67 to assess proliferation, we found that all tumours were highly proliferative (Figure 4.7). We also used IHC to assess HER2 expression in tumours (n=8) and found considerable variation in HER2 expression both within and between tumours (Figure 4.8B). According to the joint American Society of Clinical Oncology (ASCO) and College of American Pathologists (CAP) guidelines a human breast cancer must demonstrate uniform, intense (3+) membranous staining in over 30% of all tumour cells to be classified as HER2 over-expressing by IHC alone. According to these guidelines only 25% of tumours examined in this series were classifiable as HER2 over-expressing on the basis of their IHC result and a further 50% had an equivocal result (Figure 4.8). Despite this, the

majority of tumours still expressed high levels of HER2 and we therefore felt further characterization of this model in terms of response to cytotoxics and HER2 directed therapies was warranted.

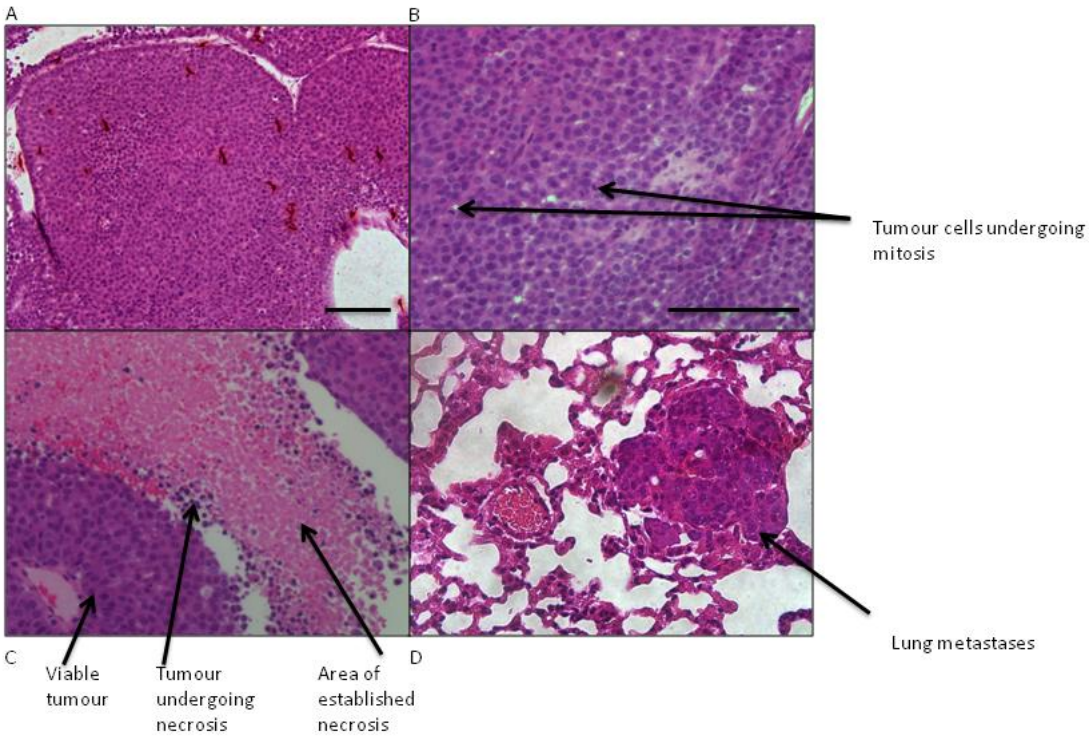

Figure 4.5- Representative H & E image of MMTV-NIC PTEN$^{+/-}$ mammary tumour and lung metastases. A: Mammary tumour (mag x20) showing the typical highly cellular nodules within the tumour. Scale bar represents 100 µm. B: Highly mitotic region of mammary tumour (mag x40). Scale bar represents 100 µm. C: Extensive necrosis within mammary tumour (mag x40). D: Section of lung demonstrating isolated lung metastases (mag x40).

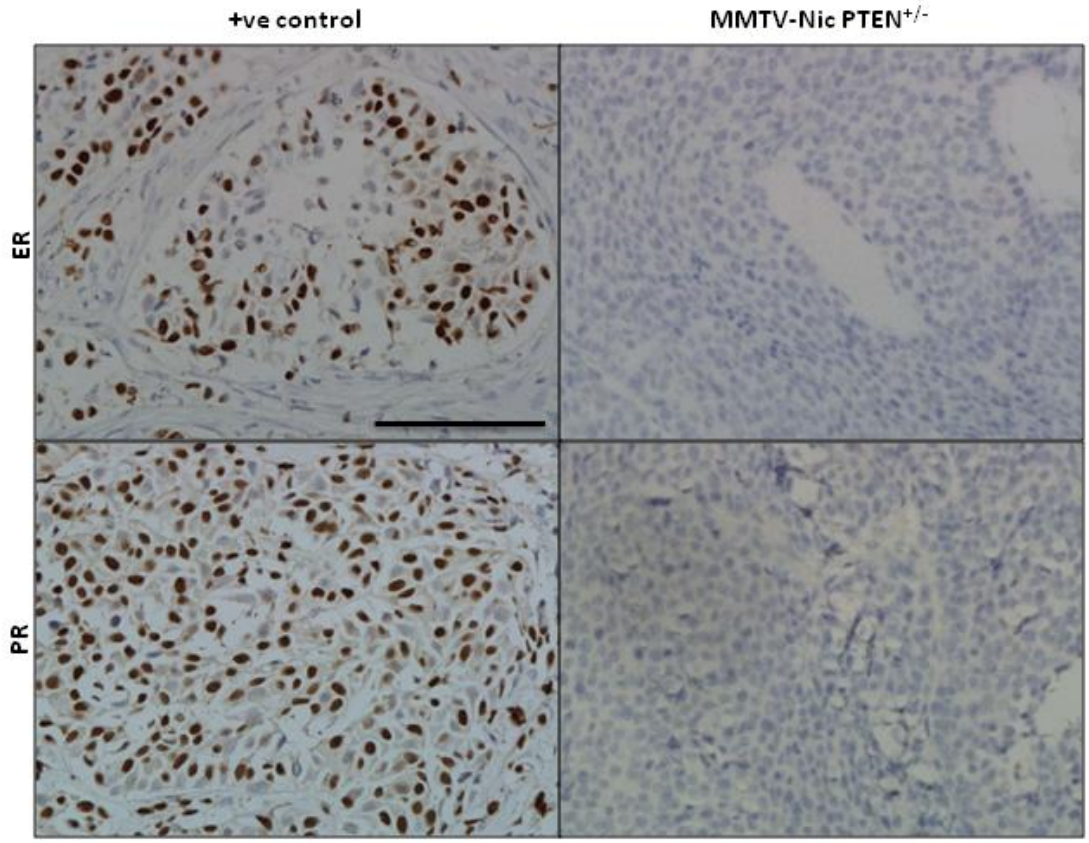

Figure 4.6- MMTV-NIC PTEN$^{+/-}$ tumours were hormone receptor negative. IHC was performed with ER and PR antibodies on paraffin embedded sections of MMTV-NIC PTEN$^{+/-}$ tumours (n=3). Positive controls comprise sections of human hormone receptor positive breast cancer stained with the appropriate antibody. Mag x40. Scale bar represents 100 µm.

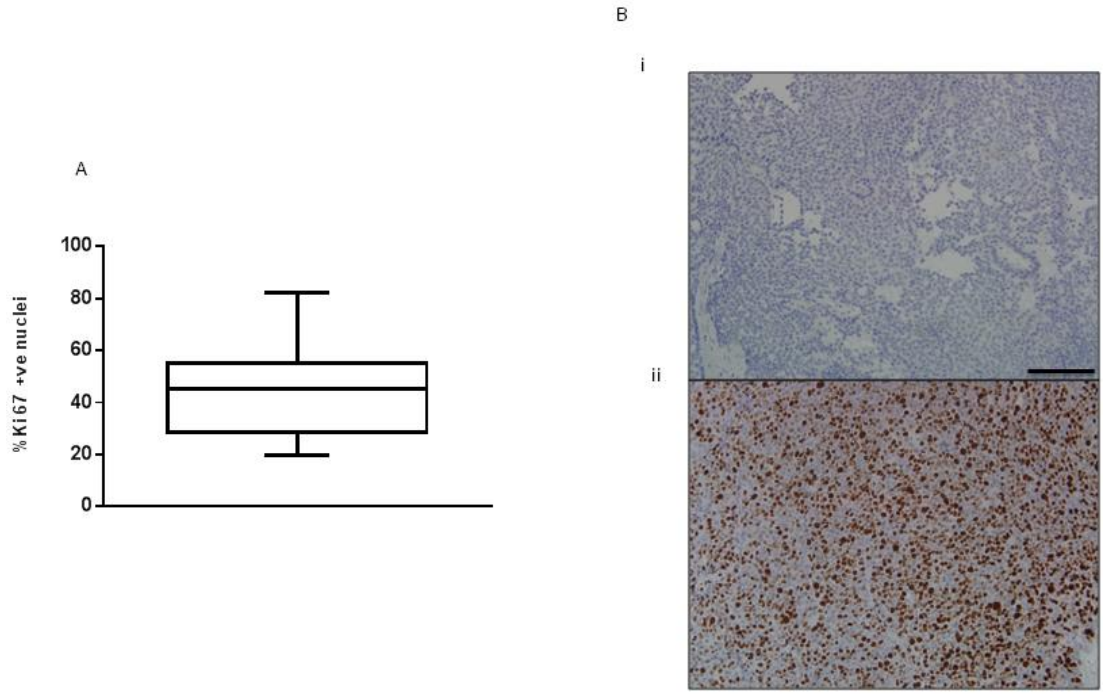

Figure 4.7- MMTV-NIC PTEN$^{+/-}$ tumours were highly proliferative. IHC was performed on paraffin embedded sections of MMTV-NIC PTEN$^{+/-}$ tumours with a Ki67 antibody. Images analysed using Immunoratio software to calculate percentage of Ki67 positive nuclei in six low power fields (mag x20) per tumour. A: Box and whiskers plot of percentage Ki67 positive nuclei (n=7). B: Representative images of IHC staining for Ki67 in negative control (i) and MMTV-NIC PTEN$^{+/-}$ tumour. Negative control consists of tumour section incubated in the absence of primary antibody. Mag x20. Scale bar represents 100 µm.

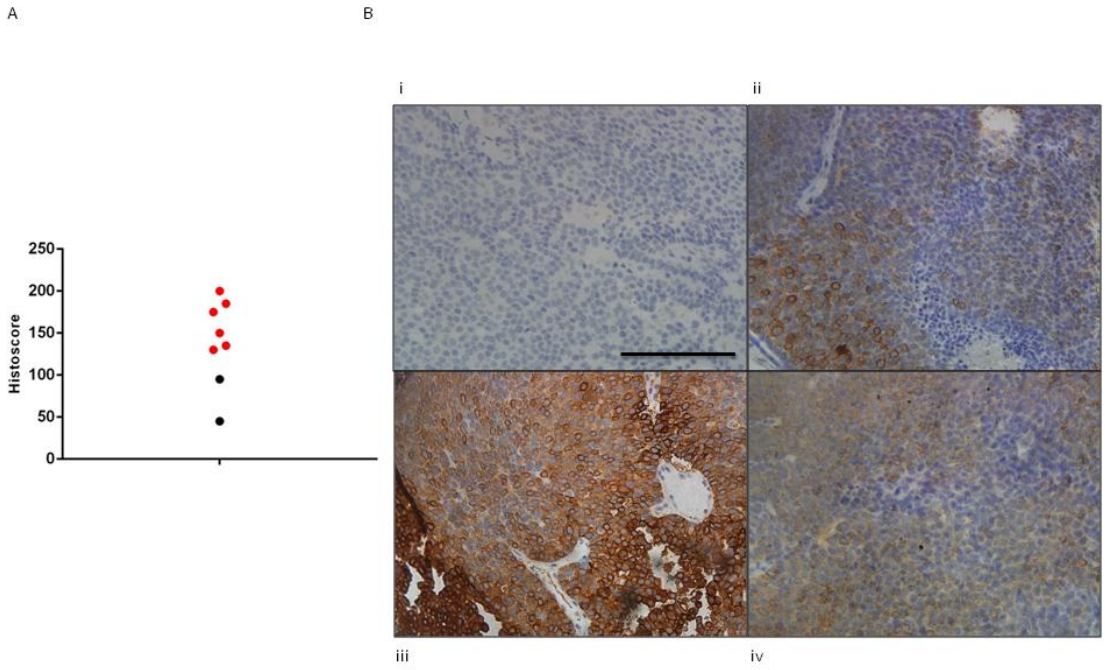

Figure 4.8- HER2 expression varied across a panel of MMTV-NIC PTEN$^{+/-}$ tumours. IHC was performed with a HER2 antibody on paraffin embedded sections of MMTV-NIC PTEN$^{+/-}$ tumours (n=8). Membranous histoscore determined using 6 representative high powered fields (x40 mag) and calculating the sum of the product of percentage cells stained by the intensity graded from 0-3, where 1=weak, 2=moderate and 3=strong staining (histoscore = (% *1) + (% *2) + (% *3)). A: Membranous HER2 histoscore in MMTV-NIC PTEN$^{+/-}$ tumours. Red data points represent tumours classified as over-expressing HER2 by IHC or with an equivocal result. Black data points represent tumours classified as not over-expressing HER2 by IHC. B: Representative images of HER2 IHC demonstrating negative control (i), limited membranous HER2 expression (ii), extensive membranous expression (iii) and cytoplasmic staining (iv). Negative control consists of tumour section incubated in the absence of primary antibody. Mag x40. Scale bar represents 100 µm.

4.2.4 Response of MMTV-NIC PTEN$^{+/-}$ tumours to Paclitaxel

The role of the taxanes in the management of both early [274] and metastatic breast cancer [275] is well established. In order to assess the response of the model to paclitaxel, we randomized animals with at least 1 tumour of a volume ≥ 0.15 cm^3 (defined as the index tumour) to treatment with paclitaxel (n=5) or vehicle (n=4) once weekly for a maximum of 4 doses. Animals were monitored twice weekly for tumour progression and sacrificed once any tumour had reached 1.5 cm (in any direction). All vehicle-treated animals were sacrificed before the final dose. However, 2 out 5 drug-treated animals completed the full treatment schedule and were sacrificed 72 hours after the final dose. In 1 of these animals the longest dimension of the index tumour was greater than 1.5 cm at the time of sacrifice. In the second animal, the longest dimension of all tumours was less than 1.5 cm at the time of sacrifice.

Despite small cohort sizes, paclitaxel treatment statistically significantly prolonged OS from a median of 13.5 days (range 7-18 days) in the control animals to 21 days (range 17-24 days) in drug treated animals (p=0.035, Gehan-Breslow-Wilcoxon test, Figure 4.9A). One third of animals (n=3) were sacrificed due to a non-index lesion and therefore to compare growth of vehicle and paclitaxel treated tumours, the growth rates of the largest tumours at the time of sacrifice were plotted (Figure 4.9B). This graph suggests that paclitaxel slowed tumour progression but did not cause tumour shrinkage. It is important to note that the timing of animal sacrifice was dictated by a single 2D measurement. Significant heterogeneity in tumour shape was observed and therefore variation in the tumour burden at the experiment's end point was considerable. Despite this, a non-statistically significant trend towards a reduction in total tumour mass (defined as sum of the mass of all individual tumours) at the time of sacrifice in the paclitaxel treated cohort was observed (p=0.17, Mann Whitney U test, Figure 4.9C).

Whilst paclitaxel delayed tumour progression, it did not prevent new tumour development. Paclitaxel-treated animals developed a median of 3 additional non-index tumours during the study compared to 2.5 in the vehicle-treated arm (p=0.60, Mann Whitney U test).

A

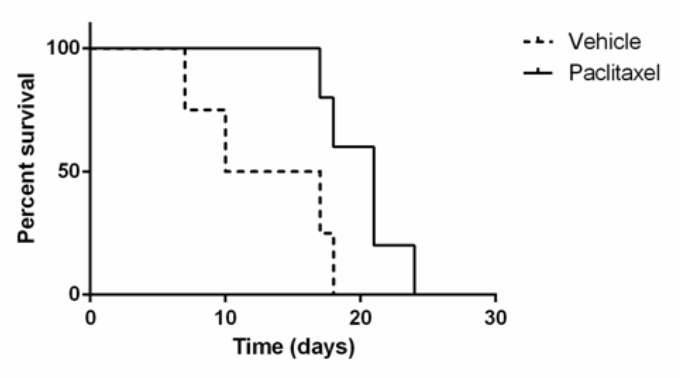

B

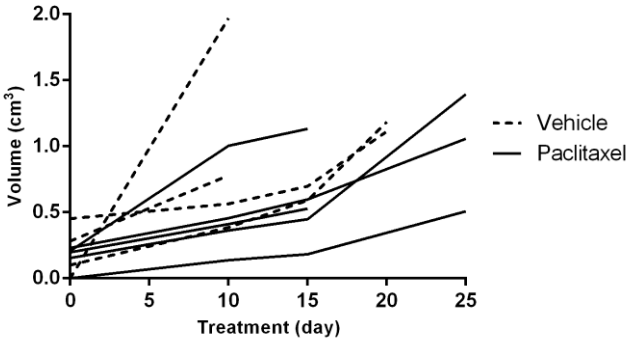

C

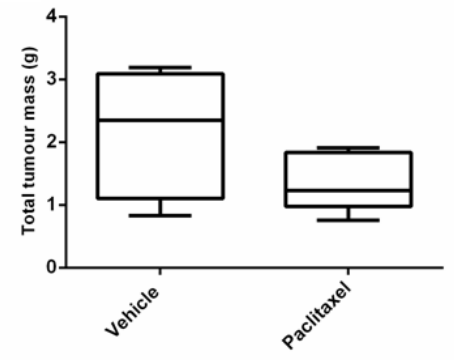

Figure 4.9- Paclitaxel slowed tumour growth and prolonged OS in MMTV-NIC PTEN$^{+/-}$ mice. A: Overall survival in vehicle (n=4) and paclitaxel (n=5) treated mice, p=0.035, Gehan-Breslow Wilcoxon test. B: Growth rate of largest (at the time of sacrifice) vehicle and paclitaxel treated tumours. C: Sum of all individual tumour weights at time of sacrifice in vehicle and paclitaxel treated animals, p=0.17, Mann Whitney U test.

Paclitaxel impairs microtubule depolymerisation and results in apoptosis [276]. Therefore, we performed IHC with an antibody to cleaved caspase 3, a frequently used biomarker of apoptosis [239], to try and confirm successful drug uptake by the tumours. Six representative low power fields (20x) were selected at random throughout each tumour and Image J was used to calculate the percentage of each field positively stained for cleaved caspase 3. Discrete foci of cells stained intensely for cleaved caspase 3 but the majority of tumours in both the drug and vehicle treated arms showed no staining (Figure 4.9). Despite this, paclitaxel treatment resulted in a significant increase in cleaved caspase 3 expression and apoptosis ($p= 0.02$, Mann Whitney U test).

In summary, this experiment provided limited evidence that the MMTV-NIC model responds to paclitaxel, one of the first line chemotherapeutic agents used in the management of breast cancer, suggesting the model may be a useful tool in predicting response to novel therapies for use in human HER2 positive breast cancer.

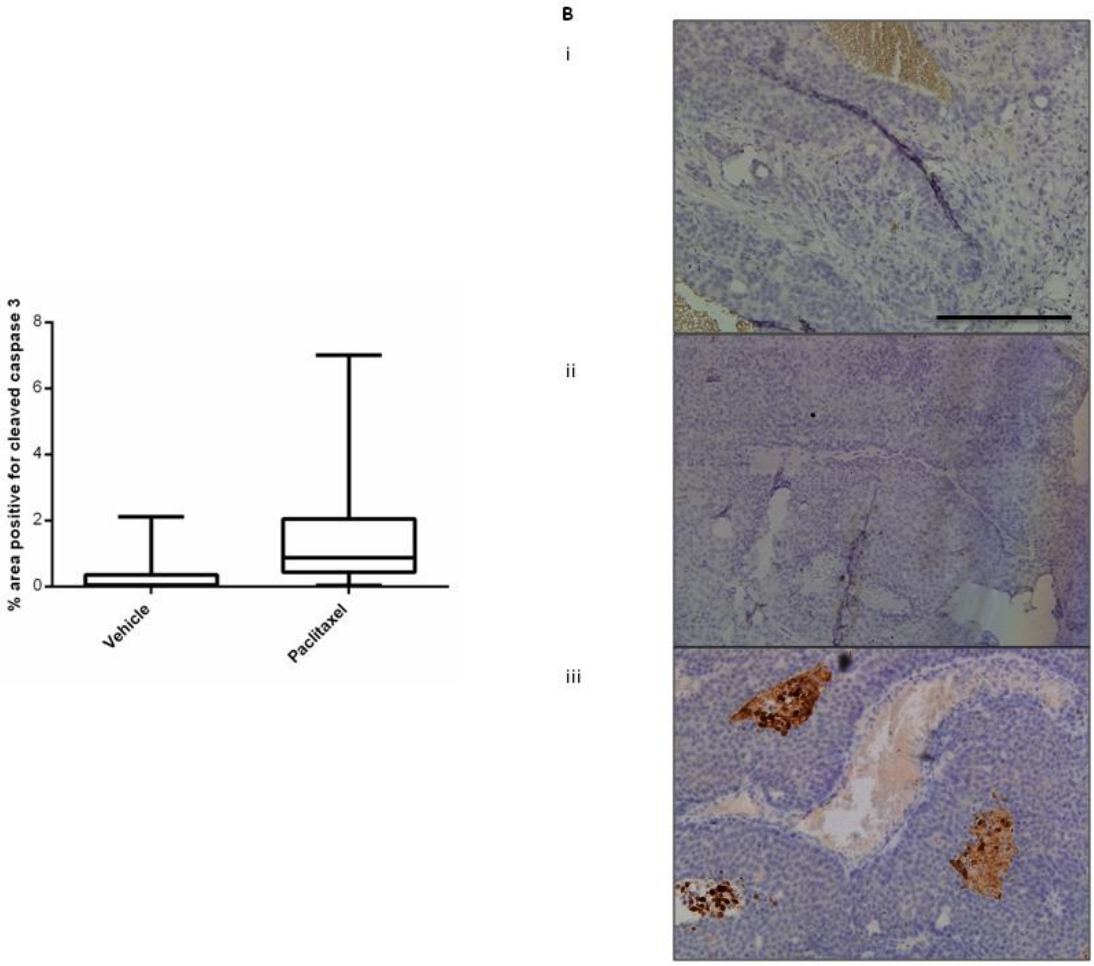

Figure 4.10- Paclitaxel resulted in apoptosis. IHC was performed on paraffin embedded sections of MMTV-NIC PTEN$^{+/-}$ paclitaxel and vehicle treated tumours with a cleaved caspase 3 antibody. Images analysed using Image J software to calculate percentage area staining positive for cleaved caspase 3 in six low power fields (mag x20) per tumour. A: Box–whisker plot analysis of percentage area positive for cleaved caspase 3 in vehicle (n=4) and paclitaxel (n=5) treated tumours. p=0.02, Mann Whitney U test. B: representative images of IHC; negative control (i), vehicle (ii) and paclitaxel (iii) treated tumours. Negative control consists of tumour section incubated in the absence of primary antibody. Scale bar 100 µm. Mag x20.

4.2.5 Response of MMTV-NIC PTEN $^{FL/+}$ and MMTV-NIC PTEN$^{+/-}$ tumours to AZD8931

The introduction of HER2 directed therapies has revolutionised the management of both early and advanced HER2 positive breast cancer. However, despite significant improvements in treatment outcomes, both inherent and acquired resistance are frequently encountered problems [277]. Emerging evidence from neo-adjuvant clinical trials suggests that use of different strategies to target multiple members of the HER family is more efficacious than single target inhibition alone. The Neo-ALTTO study reported that combined inhibition of EGFR and HER2 using lapatinib and trastuzumab was more efficacious than use of either single agent [139]. In the Neo-sphere trial, Gianni and colleagues reported that the combined use of pertuzumab and trastuzumab to inhibit HER2 and HER2/HER3 dimerization, was more active than either drug alone [2]. Currently there are no drugs in mainstream clinical practice which are able to directly target HER3 although HER3 expression has an independent negative impact on prognosis [141]. Furthermore, it has been postulated that following treatment with TKIs such as gefitinib and erlotinib, incomplete Akt inhibition triggers a shift in the steady-state phosphorylation equilibrium of HER3, favouring the active conformation, and enabling 'escape' from the growth-inhibitory effects of TKIs [279] [280]. Whilst lapatinib is classified as an reversible TKI of HER2 and HER3, the extent of EGFR inhibition *in* vivo is questionable. AZD8931 is a novel equipotent reversible tyrosine kinase inhibitor (TKI) of HER2 and EGFR, which through its robust inhibition of both these receptors is also capable of inhibiting HER3 signalling. Preclinical studies have previously shown it to be active in breast, head and neck and non-small cell lung cancer [273].

To assess the efficacy of AZD8931 in the MMTV-NIC model, we randomized cohorts of MMTV-NIC PTEN $^{FL/+}$ and MMTV-NIC PTEN$^{+/-}$ mice, to treatment with either AZD8931 (n=5 for each genotype) or vehicle (n=5 for each genotype). Treatment was commenced when mice had at least 1 tumour ≥ 0.1 cm^3 (index tumour) and continued until complete resolution of the index tumour or until the animal was sacrificed due to tumour size ≥ 1.5 cm (in any direction). Mice were dosed daily with AZD8931 (100 mg/kg) suspended in 1% Tween 80 (in PBS) by oral gavage.

AZD8931 treatment prolonged overall survival in both the MMTV-NIC PTEN $^{FL/+}$ (Figure 4.11A) and MMTV-NIC PTEN$^{+/-}$ mice (Figure 4.11B). Median overall survival in the vehicle arm of the MMTV-NIC PTEN $^{FL/+}$ cohort was 35 days (range 10- 39 days). AZD8931 treatment was stopped at day 40 in the MMTV-NIC PTEN $^{FL/+}$ drug-treated animals and the experiment terminated without further ageing of the mice. It is therefore not possible to define median OS in the AZD8931 treated arm more specifically than > 40 days (p=0.004, Gehan Breslow Wilcoxon test). In the AZD8931 group of the MMTV-NIC PTEN$^{+/-}$ cohort, 1 mouse was sacrificed after only 11 days of treatment due to respiratory compromise and on pathological review of a single section of lung, small foci of metastatic cells were identified (Dr. J. Loane). Despite this, median survival was prolonged to 45 days (range 11-124 days) in AZD8931 treated animals compared to 20 days (range 18-35 days) in vehicle treated mice, although this did not reach statistical significance (p= 0.1658, Gehan Breslow Wilcoxon test). The early loss of 1 animal in a study with a small sample size had a profound impact when calculating p values. If this experiment was repeated with a larger sample size, it is possible that AZD8931 treatment would have resulted in a statistically prolonged overall survival in the MMTV-NIC PTEN$^{+/-}$ cohort. Indeed, when this animal was excluded from analysis a highly significant difference in overall survival was observed (p=0.023, Gehan Breslow Wilcoxon test).

This experiment illustrates the significant heterogeneity in tumour behaviour and response to treatment seen with this model. When we looked at the growth of the individual tumours in the different cohorts we saw that all AZD8931 treated MMTV-NIC PTEN $^{FL/+}$ tumours initially responded to treatment and after 40 days of drug treatment 2 out of 5 tumours had fully resolved. A further 2 tumours displayed a downwards trend in volume and had achieved a reduction in volume of 29.8% and 76.4% compared to pre-treatment volumes. The final tumour initially responded but after 17 days of drug treatment became insensitive and began to increase in volume again. After 40 days of treatment, its volume had increased by 34.2% compared to its pre-treatment volume. Therefore the median reduction in tumour volume in the AZD8931 arm was 76.4% (range -34.2%-100%). In comparison, the tumours in the vehicle treated arm continued to grow throughout the experiment and when each animal was sacrificed due to tumour burden, the volume of all tumours had increased in volume by at least 60% (Figure 4.12 A). The difference in percentage change of tumour volume between drug and vehicle treated MMTV-NIC PTEN $^{FL/+}$ animals was highly statistically significant (p=0.012, Mann Whitney U test). In contrast, only 4 out of 5 AZD8931 treated MMTV-NIC PTEN$^{+/-}$ tumours initially responded to treatment with a median reduction in tumour volume

of 44.1% (range 6.9-74.3%). However, all 4 of these tumours rapidly became insensitive to AZD8931 and after a median of 12 days (range 7-17 days) of treatment, tumours had grown beyond their initial starting volume. Interestingly, the mammary tumour from the animal which was sacrificed due to symptoms of metastatic disease, did not respond to AZD8931 suggesting inherent resistance. As expected, all vehicle treated tumours continued to grow steadily throughout the experiment. All MMTV-NIC PTEN$^{+/-}$ mice were sacrificed due to tumour burden and at the time of sacrifice both drug and vehicle treated tumours had increased in volume by at least 60% (Figure 4.12B). The difference in percentage change of tumour volume between drug and vehicle treated MMTV-NIC PTEN$^{+/-}$ animals was not significant (p=0.531, Mann Whitney U test). In summary, AZD8931 resulted in tumour shrinkage in the majority of MMTV-NIC PTEN $^{FL/+}$ animals but whilst it slowed tumour growth in MMTV-NIC PTEN$^{+/-}$ animals it did not cause tumour resolution.

In addition to targeting established tumours, AZD8931 treatment also inhibited tumour initiation in both the MMTV-NIC PTEN $^{FL/+}$ and MMTV-NIC PTEN$^{+/-}$ models. In the MMTV-NIC PTEN $^{FL/+}$ model statistically fewer additional tumours developed during the study in the AZD8931 arm (median-0) compared to in the vehicle arm (median-3) (p=0.048, Mann Whitney U test). There was also a reduction in the median number of additional tumours which developed in the MMTV-NIC PTEN$^{+/-}$ cohort from 2 in the vehicle treated arm to 0 in the drug treated arm but this failed to reach statistical significance (p=0.087, Mann Whitney U test).

As there was little residual tissue from the AZD8931 treated MMTV-NIC PTEN $^{FL/+}$ tumours, histological examination was limited to the MMTV-NIC PTEN$^{+/-}$ tumours. Histological review of MMTV-NIC PTEN$^{+/-}$ tumours suggested that AZD8931 can cause a reduction in tumour grade (**Dr. J. Loane**). All vehicle treated index samples contained grade 3 carcinoma whilst only 60% (n=3) of AZD8931 index tumours were classified as grade 3. The remaining 40% (n=2) of AZD8931 index lesions consisted of grade 2 carcinoma. Interestingly, the rate of lung metastases was higher in the AZD8931 treated cohort (60%, n=3) than in the vehicle treated cohort (20%, n=1) and both animals with evidence of drug efficacy in the primary tumour, in terms of reduced tumour grade, had lung metastases at the time of sacrifice. Although the small size of cohorts in this study make it difficult to draw conclusions regarding the differential rate of lung metastases, it is feasible that the increased rate of metastases seen in the drug-treated cohort reflects their prolonged overall survival allowing sufficient

time for cells which had metastasised prior to the commencement of AZD8931 treatment to form established lesions detectable by light microscopy.

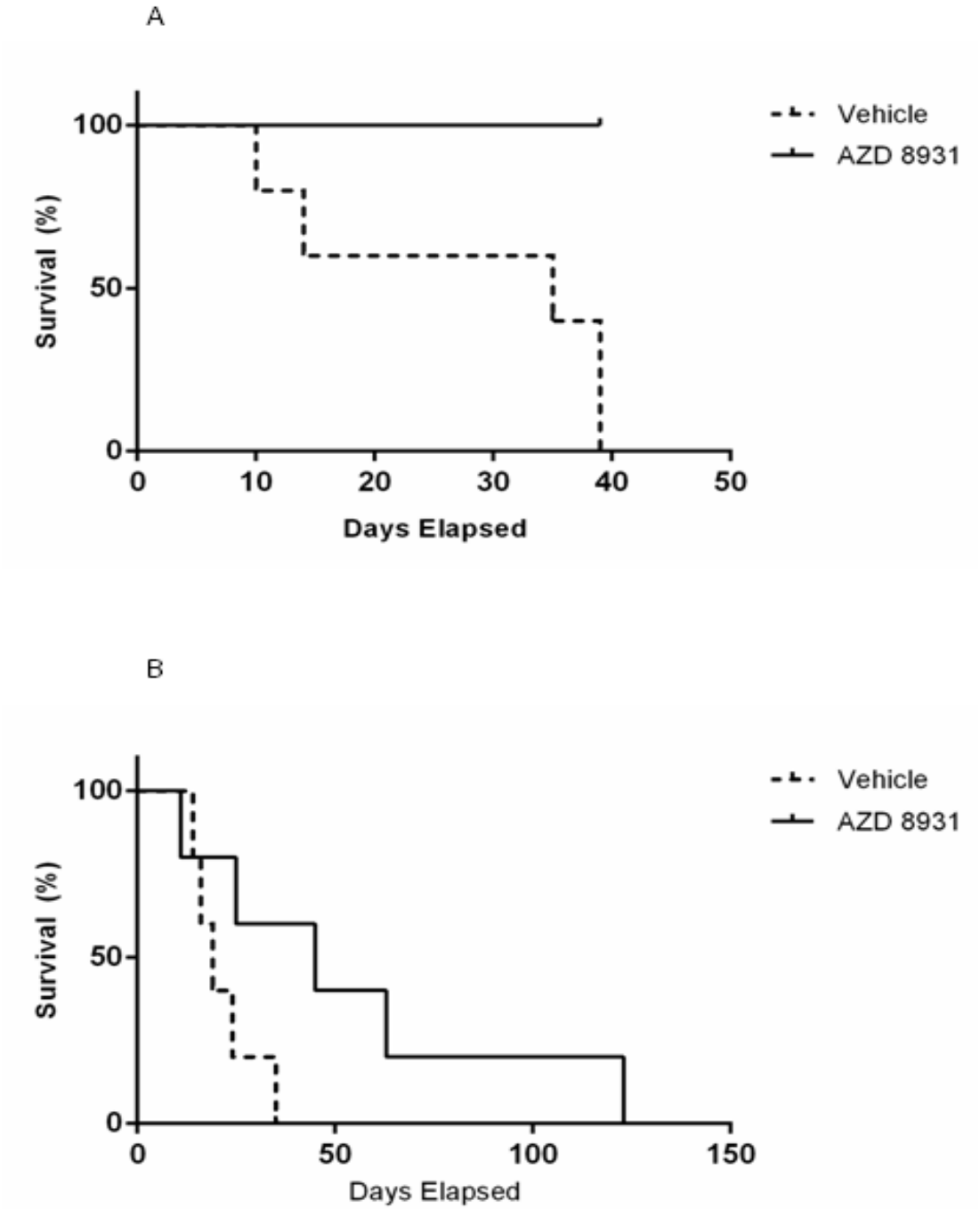

Figure 4.11- AZD8931 prolonged overall survival in MMTV-NIC PTEN $^{FL/+}$ and MMTV-NIC PTEN$^{+/-}$ mice. Cohorts of MMTV-NIC PTEN $^{FL/+}$ and MMTV-NIC PTEN$^{+/-}$ mice were randomized to treatment with daily AZD8931 or vehicle and tumour response monitored. A: Overall survival in vehicle (n=5) and AZD8931 (n=5) treated MMTV-NIC PTEN $^{FL/+}$ mice. p=0.004, Gehan-Breslow Wilcoxon test. B: Overall survival in vehicle (n=5) and AZD8931 (n=5) treated MMTV-NIC PTEN$^{+/-}$ mice. p=0.1658, Gehan-Breslow Wilcoxon test.

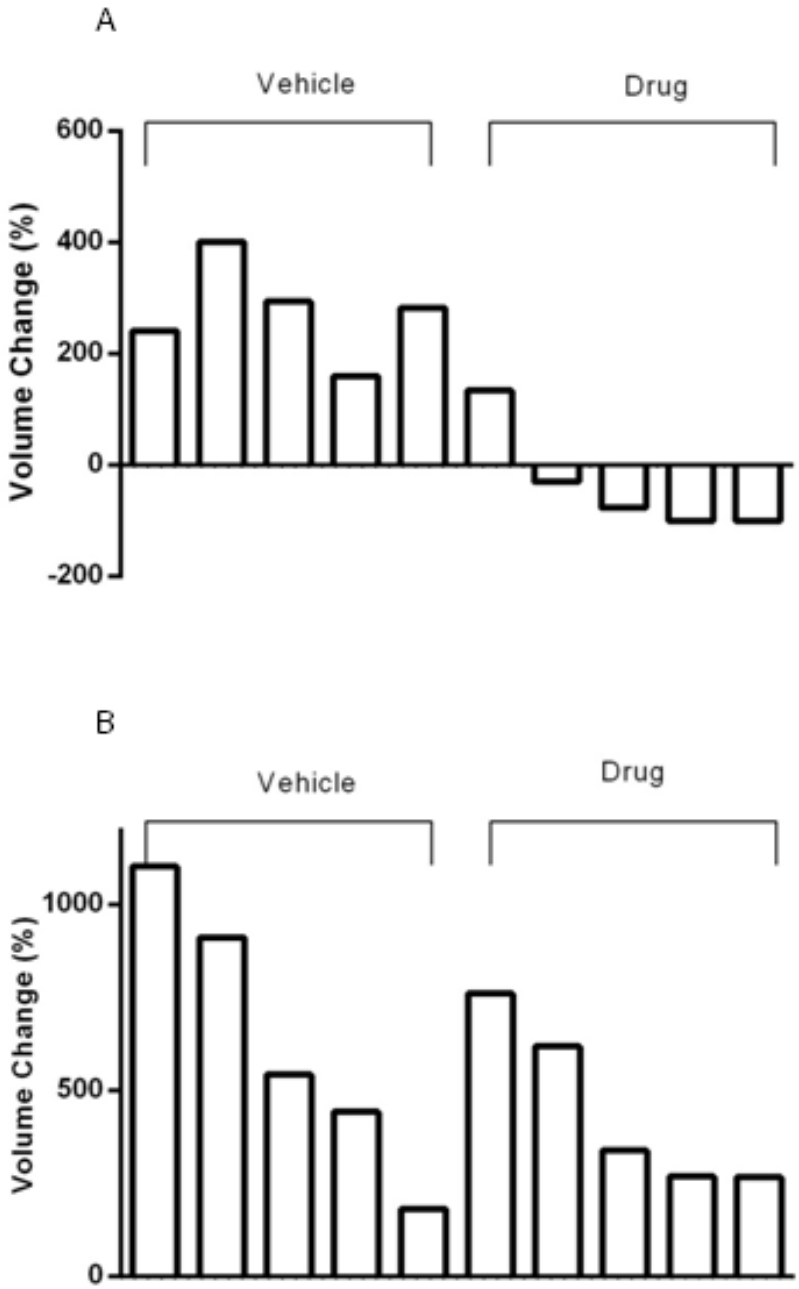

Figure 4.12- PTEN status determined sensitivity to AZD8931. A: Waterfall plot of percentage tumour volume change over duration of experiment in MMTV-NIC PTEN $^{FL/+}$ vehicle and AZD8931 treated animals. p=0.012, Mann Whitney U test. B: Waterfall plot of percentage tumour volume change over duration of experiment in MMTV-NIC PTEN$^{+/-}$ vehicle and AZD8931 treated animals. p=0.531, Mann Whitney U test.

4.3 Exploring the Mechanism of Action of AZD8931 *in vivo*

4.3.1 Inhibition of signaling via EFGR, HER2 and HER3

In order to investigate the effects of AZD8931 on signaling, we conducted a short term treatment study to ensure at completion of the experiment tumours were responsive to treatment and tissue was available for collection. MMTV-NIC PTEN $^{FL/+}$ and MMTV-NIC PTEN$^{+/-}$ mice were randomized to treatment with either AZD8931 (n=4 for each genotype) or vehicle (n=4 for each genotype) for 3 days. Treatment was commenced when animals had at least 1 tumour ≥ 0.3 cm^3. Mice were dosed daily with AZD8931 (100 mg/kg) suspended in 1% Tween 80 (in PBS) by oral gavage. Animals were sacrificed 2 hours after the final dose.

We used IHC to explore expression of HER family proteins in vehicle and drug treated tumours. Reduced expression of total HER2 was observed following AZD8931 treatment in MMTV-NIC PTEN $^{FL/+}$ tumours. The median HER2 histoscore was 120.0 in drug treated tumours compared to 225.0 in vehicle treated tumours (p= 0.05, Mann Whitney U test). Expression in MMTV-NIC PTEN$^{+/-}$ tumours was unaffected by AZD8931 treatment with a median histoscore of 90.0 in vehicle treated tumours compared to 80.0 in AZD8931 treated tumours (p=1.0, Mann Whitney U test) (Figure 4.13).

The activity of HER2 in tumours was assessed by measuring the phosphorylation of 2 key tyrosine autophosphorylation residues, Tyr 1221 and 1222 [97]. Expression of pTyr 1221/1222 HER2 was reduced in both AZD8931 treated MMTV-NIC PTEN $^{FL/+}$ and MMTV-NIC PTEN$^{+/-}$ tumours, although this reduction failed to reach statistical significance in either model (Figure 4.14). In the MMTV-NIC PTEN $^{FL/+}$ cohort median pTyr 1221/1222 HER2 histoscore was reduced from 225.0 in the vehicle arm to 135.0 in the drug treated arm (p=0.48, Mann Whitney U test). In the MMTV-NIC PTEN$^{+/-}$ cohort, median histoscores were 120.0 and 82.5 in vehicle and drug treated tumours respectively (p=1.0, Mann Whitney U test).

We also performed IHC using a pTyr 1289 HER3 antibody. This residue participates in PI3 kinase (PI3K) signaling [97] and therefore gives an accurate readout of HER3 activity. Again, in both the MMTV-NIC PTEN $^{FL/+}$ and MMTV-NIC PTEN$^{+/-}$ models, AZD8931 treatment resulted in a reduction in HER3 activity, although this also did not reach statistical significance (Figure 4.15). In the MMTV-NIC PTEN $^{FL/+}$ model, median pTyr 1289 HER3 histoscore was reduced from 57 in the vehicle treated cohort to 0 in the AZD8931 treated arm (p=0.2, Mann Whitney U test). In the MMTV-NIC PTEN$^{+/-}$ cohort, median pTyr 1289 HER3 histoscore was reduced from 80 in vehicle treated tumours to 31 in AZD8931 treated tumours (p= 0.07, Mann Whitney U test). IHC was used to explore the expression of total HER3 but we were not satisfied with the quality of the staining and therefore this data has not been included.

Expression of total EGFR (Figure 4.16) and p Tyr 992 EGFR, an autophosphorylation residue [281], (Figure 4.17) was determined. However, expression of both was too low to permit further quantification.

In summary, AZD8931 reduced activity of HER2 and HER3 in both the MMTV-NIC PTEN $^{FL/+}$ and MMTV-NIC PTEN$^{+/-}$ models, although this failed to reach statistical significance. Significant intra-tumoural heterogeneity was observed in terms of receptor expression, with staining predominantly focused at the periphery of the tumours. This coupled with the small sample sizes used in this study is likely to account for the lack of observed statistical reduction in HER2 and HER3 activity. AZD8931 treatment also reduced total HER2 expression in the MMTV-NIC PTEN $^{FL/+}$ cohort but not in the MMTV-NIC PTEN$^{+/-}$ cohort. Further experiments are currently underway to explore the impact of AZD8931 treatment on HER family signaling in a larger cohort of mice.

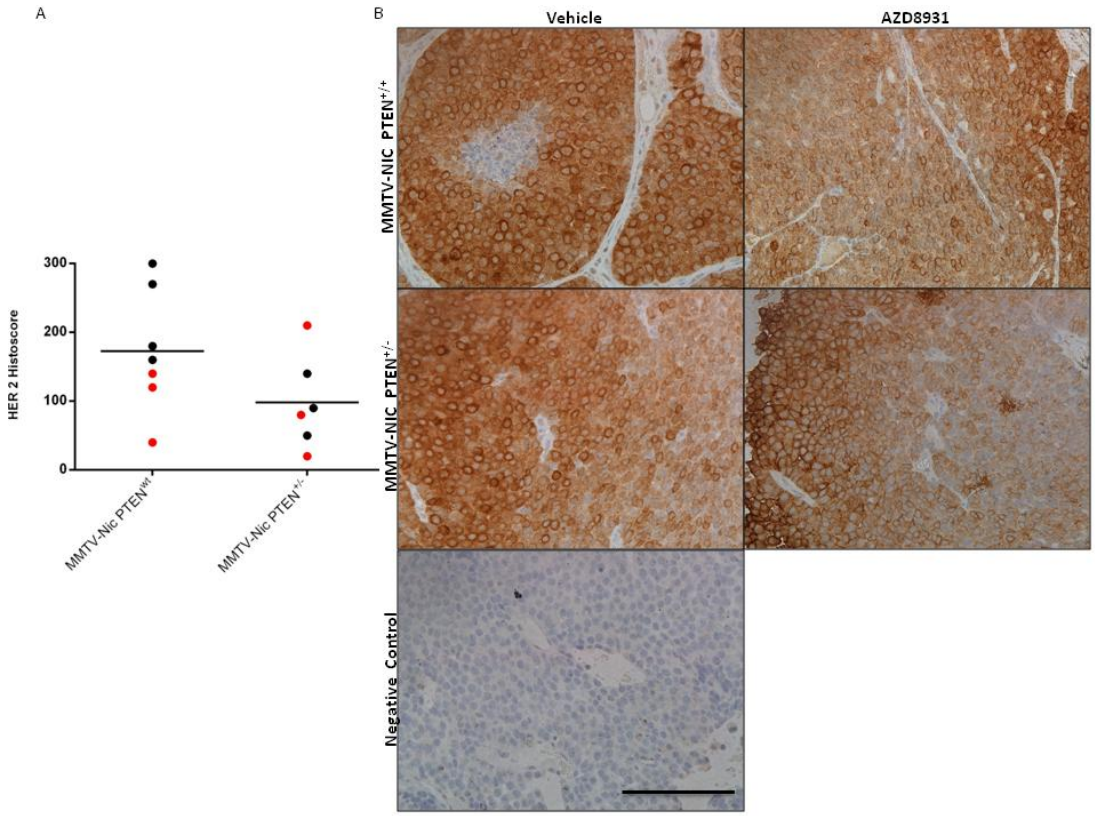

Figure 4.13- AZD8931 reduced HER2 expression in MMTV-NIC PTEN $^{FL/+}$ but not MMTV-NIC PTEN$^{+/-}$ tumours. IHC was performed on paraffin embedded sections of AZD8931 and vehicle treated tumours with a total HER2 antibody. Membranous histoscore calculated as the sum of the product of percentage cells stained by the intensity graded from 0-3, where 1=weak, 2=moderate and 3=strong staining (histoscore = (% *1) + (% *2) + (% *3)). A: IHC analysis of HER2 in AZD8931 and vehicle treated tumours. MMTV-NIC PTEN $^{FL/+}$: p=0.05, MMTV-NIC PTEN$^{+/-}$: p=1.0 (Mann-Whitney U test). Black data points represent vehicle treated tumours. Red data points represent AZD8931 treated tumours. Bar represent mean value for each genotype. B: Representative IHC images of vehicle and AZD8931 treated MMTV-NIC PTEN $^{FL/+}$ and MMTV-NIC PTEN$^{+/-}$ tumours. Negative control consists of tumour section incubated in the absence of primary antibody. Mag x40. Scale bar represents 100 µm.

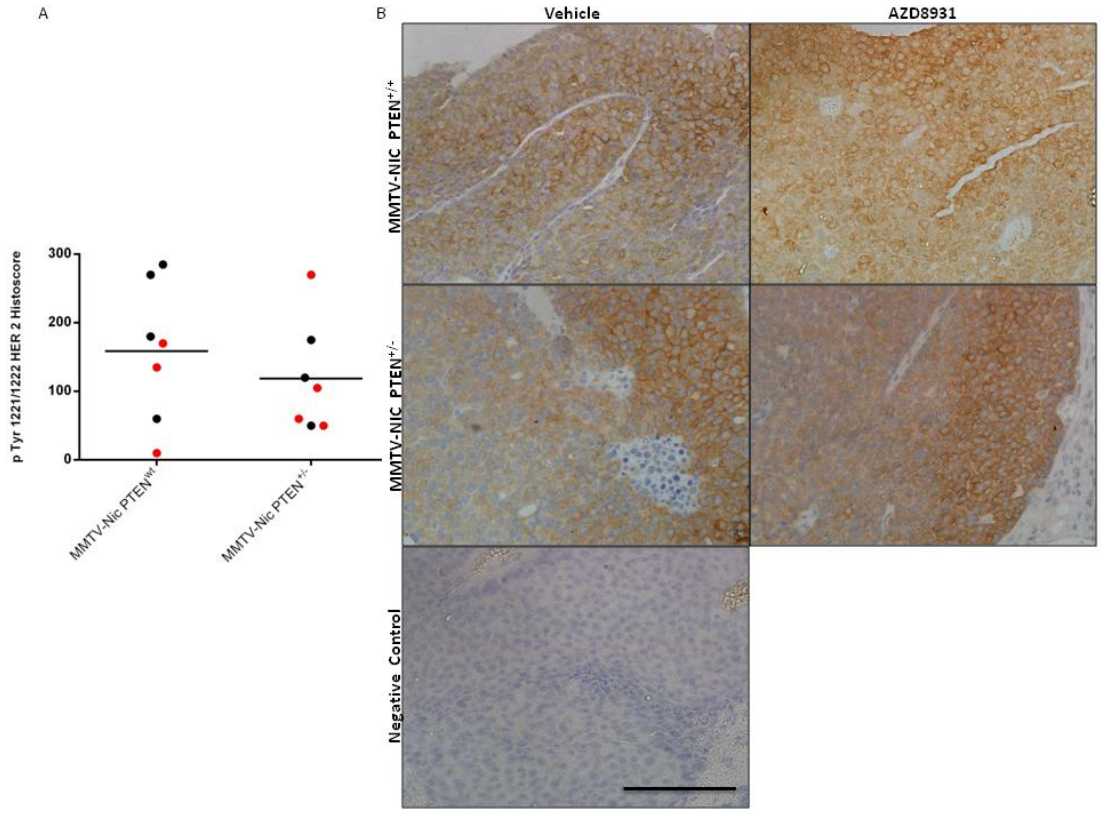

Figure 4.14- AZD8931 treatment reduced HER2 phosphorylation although this did not reach statistical significance. IHC was performed on paraffin embedded sections of AZD8931 and vehicle treated tumours with a pTyr 1221/1222 HER2 antibody. Membranous histoscore calculated as the sum of the product of percentage cells stained by the intensity graded from 0-3, where 1=weak, 2=moderate and 3=strong staining (histoscore = (% *1) + (% *2) + (% *3)). A: IHC analysis of pTyr 1221/1222 HER2 in AZD8931 and vehicle treated tumours. MMTV-NIC PTEN $^{FL/+}$: p=0.48, MMTV-NIC PTEN$^{+/-}$: p=1.0 (Mann-Whitney U test). Black data points represent vehicle treated tumours. Red data points represent AZD8931 treated tumours. Bar represent mean value for each genotype. B: Representative IHC images of vehicle and AZD8931 treated MMTV-NIC PTEN $^{FL/+}$ and MMTV-NIC PTEN$^{+/-}$ tumours. Negative control consists of tumour section incubated in the absence of primary antibody. Mag x40. Scale bar represents 100 µm.

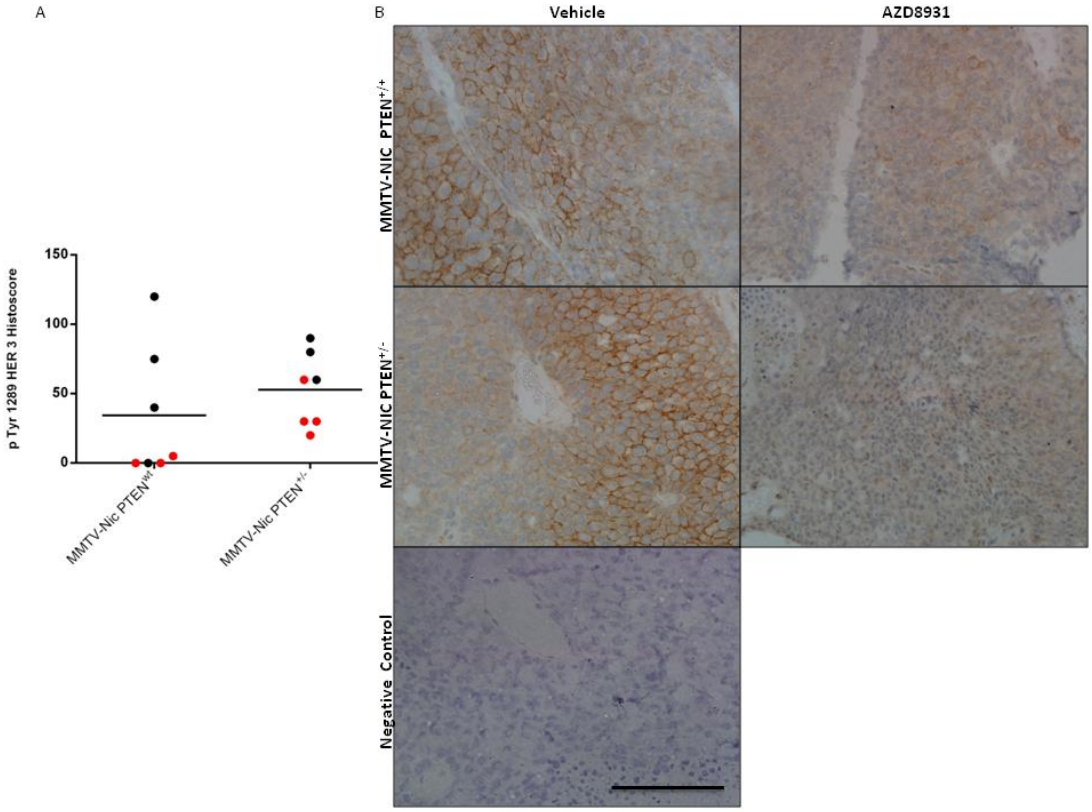

Figure 4.15- AZD8931 reduced HER3 activity, although this did not reach statistical significance. IHC was performed on paraffin embedded sections of AZD8931 and vehicle treated tumours with a pTyr 1289 HER3 antibody. Membranous histoscore calculated as the sum of the product of percentage cells stained by the intensity graded from 0-3,where 1=weak, 2=moderate and 3=strong staining (histoscore = (% *1) + (% *2) + (% *3)). A: IHC analysis of pTyr 1289 HER3 in AZD8931 and vehicle treated tumours. Black data points represent vehicle treated tumours. Red data points represent AZD8931 treated tumours. Bar represent mean value for each genotype. MMTV-NIC PTEN $^{FL/+}$: p=0.20, MMTV-NIC PTEN$^{+/-}$: p=0.07 (Mann-Whitney U test). B: Representative IHC images of vehicle and AZD8931 treated MMTV-NIC PTEN $^{FL/+}$ and MMTV-NIC PTEN$^{+/-}$ tumours. Negative control consists of tumour section incubated in the absence of primary antibody. Mag x40. Scale bar represents 100 µm.

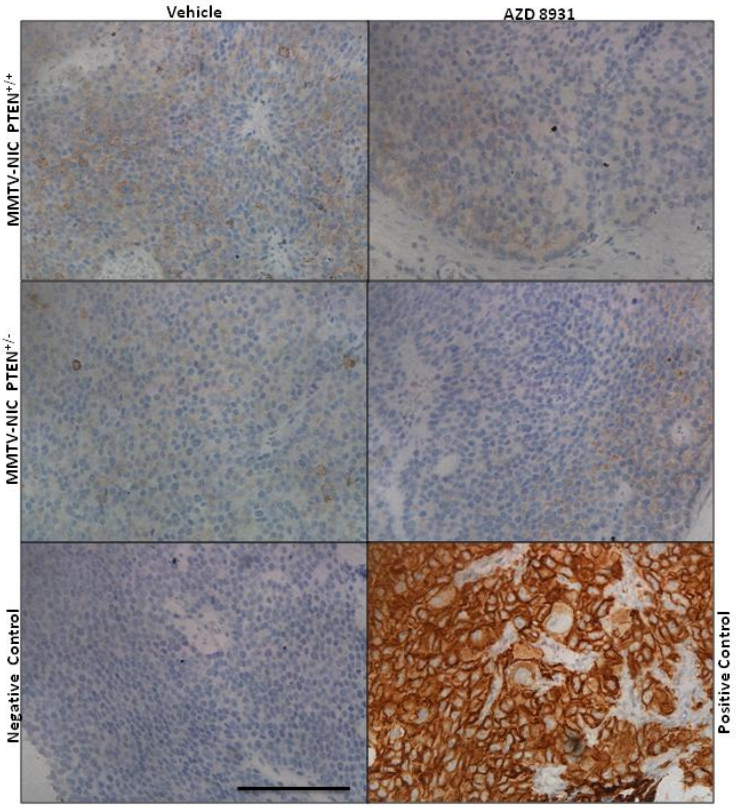

Figure 4.16- Limited expression of EGFR in MMTV-NIC PTEN $^{FL/+}$ and MMTV-NIC PTEN$^{+/-}$ tumours. IHC was performed on paraffin embedded sections of AZD8931 and vehicle treated tumours with an EGFR antibody. Representative IHC images of vehicle and AZD8931 treated MMTV-NIC PTEN $^{FL/+}$ and MMTV-NIC PTEN$^{+/-}$ tumours. Positive control consists of section of A431 derived xenograft stained with EGFR antibody. Negative control consists of tumour section incubated in the absence of primary antibody. Mag x40. Scale bar represents 100 µm.

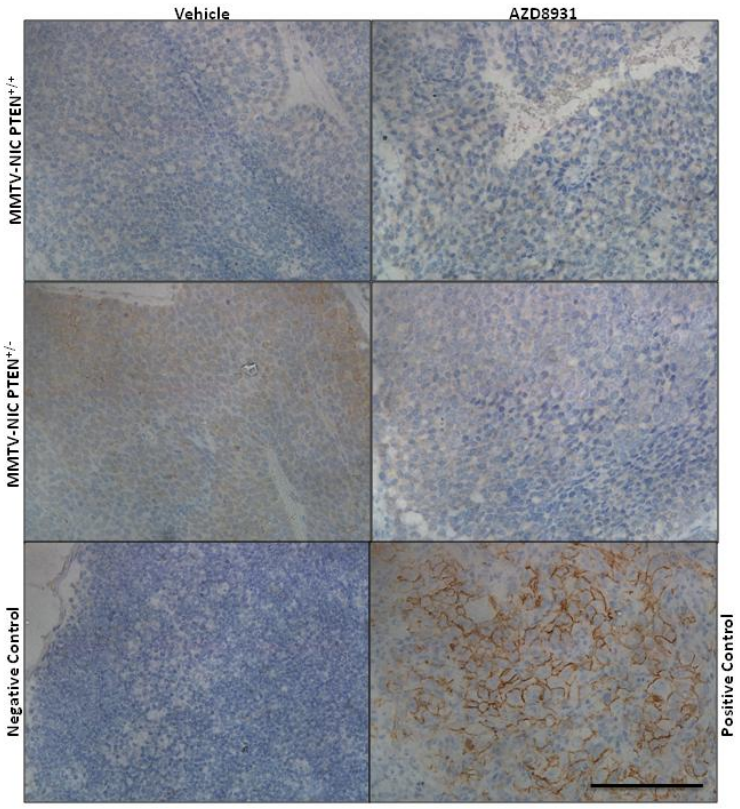

Figure 4.17- Limited pTyr 992 EGFR expression in both MMTV-NIC PTEN $^{FL/+}$ and MMTV-NIC PTEN$^{+/-}$ tumours. IHC was performed on paraffin embedded sections of AZD8931 and vehicle treated tumours with a pTyr 992 EGFR antibody. Representative IHC images of vehicle and AZD8931 treated MMTV-NIC PTEN $^{FL/+}$ and MMTV-NIC PTEN$^{+/-}$ tumours. Positive control comprises section of A431 xenograft stained with pTyr 992 EGFR antibody. Negative control consists of tumour section incubated in the absence of primary antibody. Mag x40. Scale bar represents 100 µm.

4.3.2 RPPA analysis of AZD8931 treatment in MMTV-NIC PTEN $^{FL/+}$ and MMTV-NIC PTEN$^{+/-}$ tumours.

In order to provide more definitive evidence of signaling changes, we carried out RPPA analysis on vehicle and drug treated tumours (**K. Macleod**), enabling us to look at changes in a range of signaling molecules (for full set of results see Appendix 3). Wherever possible the ratio of the phosphorylated protein to corresponding total protein was calculated to give a measure of the signaling pathway activity. Where this was not possible, data was corrected using the global normalization technique [282].

We wanted to use this platform to further assess changes in the activity of HER family proteins in response to AZD8931. Two antibodies were used to assess changes in total HER2 expression with differing results. One antibody from CST detected an increase in HER2 expression following AZD8931 treatment in both MMTV-NIC PTEN$^{+/-}$ (p=0.01, Mann Whitney U test) and MMTV-NIC PTEN $^{FL/+}$ (p=0.07, Mann Whitney U test) tumours (Appendix 3). However, the second antibody from DAKO did not detect any difference in HER2 expression between vehicle and AZD8931 treated tumours. When tested on western blot using a third total HER2 antibody and quantified using Image J, we observed a non-statistical increase in the median intensity of the HER2 band (corrected for loading using GAPDH) from 1.03 in vehicle treated tumours to 3.25 in drug treated MMTV-NIC PTEN $^{FL/+}$ tumours (p= 0.10, Mann Whitney test). Similarly, the HER2 band intensity was increased from 1.64 in vehicle treated tumours to 3.35 in drug treated MMTV-NIC PTEN$^{+/-}$ tumours (p= 0.11, Mann Whitney U test) (Figure 4.20).

Using RPPA, we initially explored HER2 activity using a pTyr 2243 HER2 antibody, which is validated for use on this platform. However, the antibody signal was too low in all samples to enable further quantification. The signal from an alternative HER2/EGFR pTyr1248/Tyr1173 antibody was more robust and as we have previously demonstrated, using IHC, that EGFR expression was low in these tumours, the signal from this antibody likely predominantly reflected HER2 activity alone. Our RPPA data identified a trend towards reduced pTyr1248/Tyr1173 HER2/EGFR expression in the MMTV-NIC PTEN$^{+/-}$ model, which did not reach statistical significance (p=0.30, Mann Whitney U test) (Figure 4.18B). Unexpectedly, RPPA did not demonstrate a reduction in HER2 activity in the MMTV-NIC PTEN $^{FL/+}$ model

(Figure 4.18A). However, when western blot was used to measure HER2 activity in these samples using a pTyr 1221/1222 HER2 antibody and quantified using Image J, a non-statistically significant reduction in HER2 activity was seen in both models. P Tyr1221/1222 HER2: HER2 (both corrected for variations in loading using GAPDH) was reduced from 0.94 in vehicle treated MMTV-NIC PTEN $^{FL/+}$ tumours to 0.34 in drug treated tumours (p=0.11, Mann Whitney U test, Figure 4.20A). Similarly, in MMTV-NIC PTEN$^{+/-}$ tumours, HER2 pTyr1221/1222: HER2 was reduced from 0.81 in vehicle treated tumours to 0.11 in drug treated tumours (p=0.11, Mann Whitney U test, figure 4.20B). The most likely explanation for the lack of concordance between our RPPA and western data is the heterogeneous nature of these tumours which were comprised of multiple different cell clones which were also likely to have varying sensitivity to AZD8931.

RPPA analysis also did not identify any convincing evidence of reduced HER3 or EGFR activity in either model although it is important to note that the antibody signal from all samples was extremely low. It is therefore impossible to confidently differentiate changes in signalling pathway activity from background 'noise'. We were unable to validate these changes using western blotting due to poor antibody signal.

Crucially, RPPA identified a statistically significant reduction in both Akt and MAPK activity in AZD8931 treated tumours in both models (Figure 4. 19). PTEN negatively regulates Akt activity. Consistent with this, Akt activity in vehicle treated MMTV-NIC PTEN $^{FL/+}$ tumours was lower than in MMTV-NIC PTEN$^{+/-}$ tumours (Appendix 3). However, AZD8931 treatment inhibited Akt activity (measured in terms of p Ser 473 Akt) in both models (Figure 4.19). MAPK activity was also suppressed to a similar extent in both models (Appendix 3). The reduction in Akt and MAPK activity in both models was corroborated using western blot (Figure 4.19). Furthermore, a statistically significant reduction in S6 ribosomal protein activity, which is downstream of Akt, was observed in both models on RPPA analysis (Figure 4.19). However, there was no reduction in other signalling pathways downstream of Akt, such as mTOR and GSK-3-beta (Appendix 3).

Our initial *in vivo* data demonstrated that the MMTV-NIC PTEN $^{FL/+}$ model was inherently more sensitive to AZD8931 than the MMTV-NIC PTEN$^{+/-}$ model. We therefore hoped that by

looking for differences in the AZD8931 triggered signalling response between the 2 models, we may be able to identify potential biomarkers capable of identifying patients with AZD8931 sensitive disease. In addition to the above changes, RPPA identified a statistically significant reduction in PI3K p110-alpha expression following AZD8931 treatment but only in the MMTV-NIC PTEN $^{FL/+}$ model (p=0.05, Mann Whitney U test). Although baseline Src expression was similar between both models, a significant reduction in Src activity (p=0.03, Mann Whitney U test) was seen in the MMTV-NIC PTEN $^{FL/+}$ model but not in the MMTV-NIC PTEN$^{+/-}$ model.

In conclusion, the reduced HER2 activity coupled with the profound inhibition of both Akt and MAPK activity provides compelling evidence that the drug response seen in these models is both real and due to on-target effects. Reduced PI3K p110-alpha expression and inhibition of Src activity following AZD8931 treatment may act as early positive predictive biomarkers for drug response.

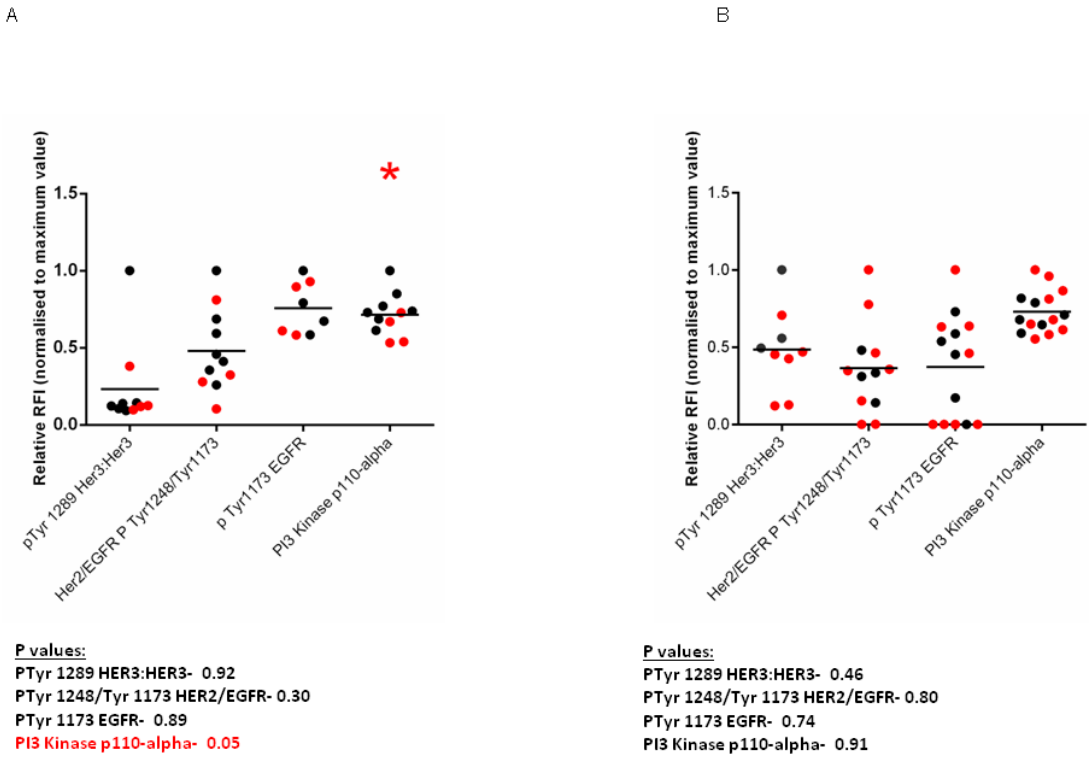

Figure 4.18- AZD8931 did not result in demonstrable target inhibition. RPPA analysis was performed on lysate from AZD8931 (red data points) and vehicle (black data points) treated MMTV-NIC PTEN $^{FL/+}$ (A) and MMTV-NIC PTEN$^{+/-}$ (B) tumours. The ratio of pTyr 1289 HER3 to total HER3 is presented. The RFI for all other antibodies are corrected using global normalization technique [40]. Each data series is normalised to its maximum value. Asterix denotes statistically significant result. P values calculated using Mann Whitney U test.

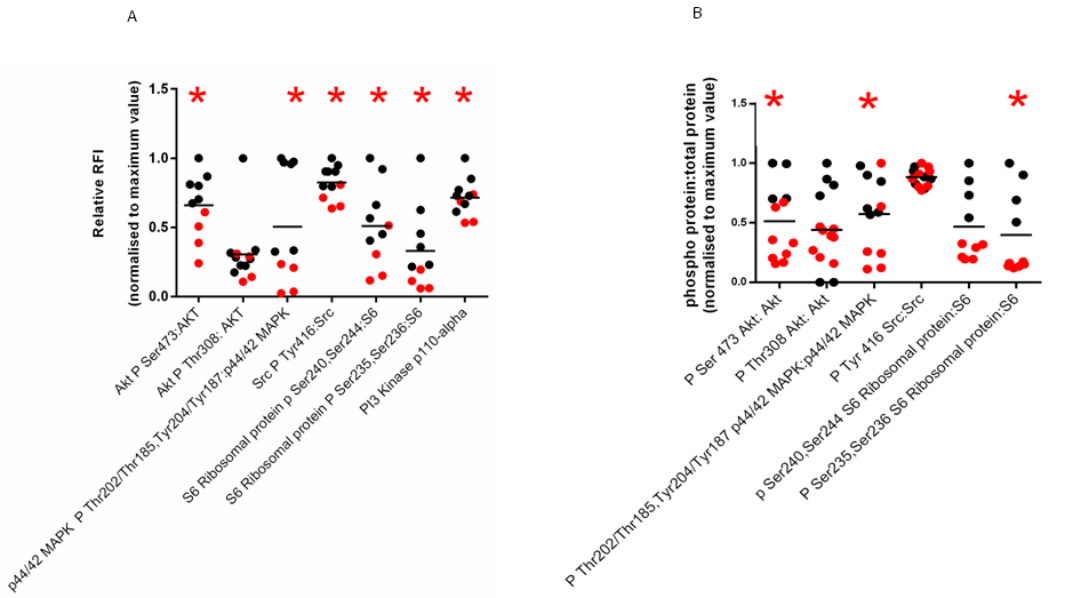

P value:

P Ser 473 Akt : Akt- 0.01
P Thr 308 Akt : Akt- 0.35
P Thr 202/Thr185, Tyr 204/Tyr 187p 44/42 MAPK: pp44/42 MAPK- 0.01
P Tyr 416 Src : Src- 0.03
P Ser 240, Ser 244 S6 Ribosomal protein : S6- 0.04
P Ser 235, Ser 236 S6 Ribosomal protein : S6- 0.01

P value:

P Ser 473 Akt : Akt- <0.01
P Thr 308 Akt : Akt- 0.33
P Thr 202/Thr185, Tyr 204/Tyr 187 p44/42 :MAPK pp44/42 MAPK - 0.03
P Tyr 416 Src : Src- 0.77
P Ser 240, Ser 244S6 Ribosomal protein : S6- 0.12
P Ser 235.Ser2 36 S6 Ribosomal protein : S6- 0.01

Figure 4.19- RPPA analysis demonstrated reduced Akt and p44/42 MAPK pathway activity. RPPA analysis was performed on lysate from AZD8931 (red data points) and vehicle (black data points) treated MMTV-NIC PTEN $^{FL/+}$ (A) and MMTV-NIC PTEN$^{+/-}$ (B) tumours. The ratio of phospho:corresponding total protein is presented [206], normalized to the maximum value in each data set. Asterix denotes statistically significant result. P values calculated using Mann Whitney U test.

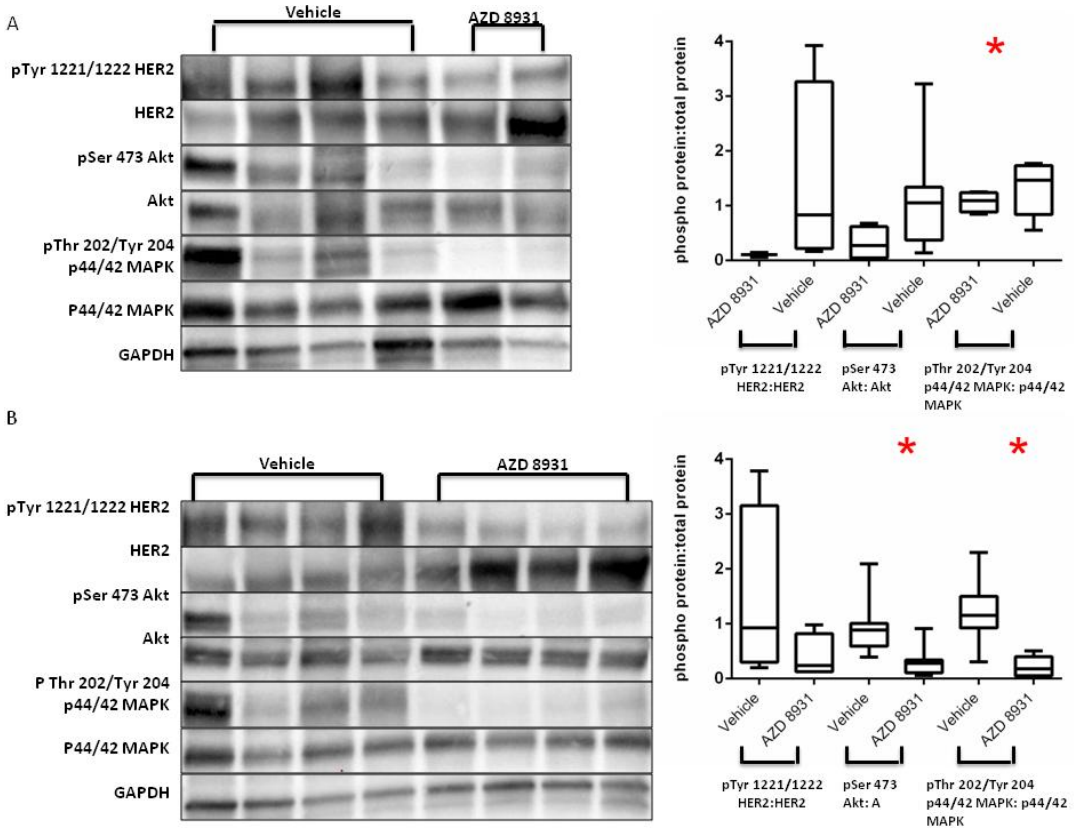

P values:

MMTV-Nic PTEN^{wt}:

pTyr 1221/1222 HER2: HER2- 0.35.
pSer 473 AKT: AKT- 0.07.
pThr 202/Tyr 204 P44/42 MAPK:MAPK- 0.03.

MMTV-Nic PTEN^{het}:

pTyr 1221/1222 HER2: HER2- 0.19.
pSer 473 AKT: AKT- < 0.01.
pThr 202/Tyr 204 P44/42 MAPK:MAPK- < 0.01.

Figure 4.20- Western blot confirmed RPPA findings that AZD8931 inhibited AKT and p44/42 MAPK (ERK1/2) activity in MMTV-NIC PTEN $^{FL/+}$ (A) and MMTV-NIC PTEN$^{+/-}$ (B) tumours. Representative blots shown from a series of 2. 40 µg protein loaded in each lane. GAPDH used as loading control. Image J used to quantify western blots and results shown in right panel. P values calculated according to Mann Whitney U test.

4.3.3 Effect of AZD8931 on tumour proliferation

We assessed proliferation of both MMTV-NIC PTEN $^{FL/+}$ and MMTV-NIC PTEN$^{+/-}$ tumours by performing IHC with a Ki67 antibody and used ImmunoRatio software to quantify the percentage of Ki67 positive nuclei [283]. MMTV-NIC PTEN$^{+/-}$ tumours grew more rapidly than MMTV-NIC PTEN $^{FL/+}$ tumours. It was therefore surprising that the median percentage Ki67 positive nuclei was higher in the vehicle treated MMTV-NIC PTEN $^{FL/+}$ tumours than in the vehicle treated MMTV-NIC PTEN$^{+/-}$ (p=0.004, Mann Whitney U test, Figure 4.21). However, AZD8931 reduced proliferation in both MMTV-NIC PTEN $^{FL/+}$ (n=3 for each treatment group) and MMTV-NIC PTEN$^{+/-}$ tumours (n=4 for each treatment group) (Figure 4.21). In the MMTV-NIC PTEN $^{FL/+}$ cohort median percentage Ki67 positive nuclei was reduced from 70.0% in vehicle to 32.2% in AZD8931 treated tumours (p=0.010, Mann Whitney U test). The median percentage Ki67positive nuclei was 54.6% in vehicle treated MMTV-NIC PTEN$^{+/-}$ tumours compared to 35.0% in AZD8931 treated tumours (p=0.005, Mann Whitney U test). There was no statistical difference in percentage of Ki67 positive nuclei in AZD8931 treated MMTV-NIC PTEN $^{FL/+}$ and MMTV-NIC PTEN$^{+/-}$ tumours (p= 0.766, Mann Whitney U test).

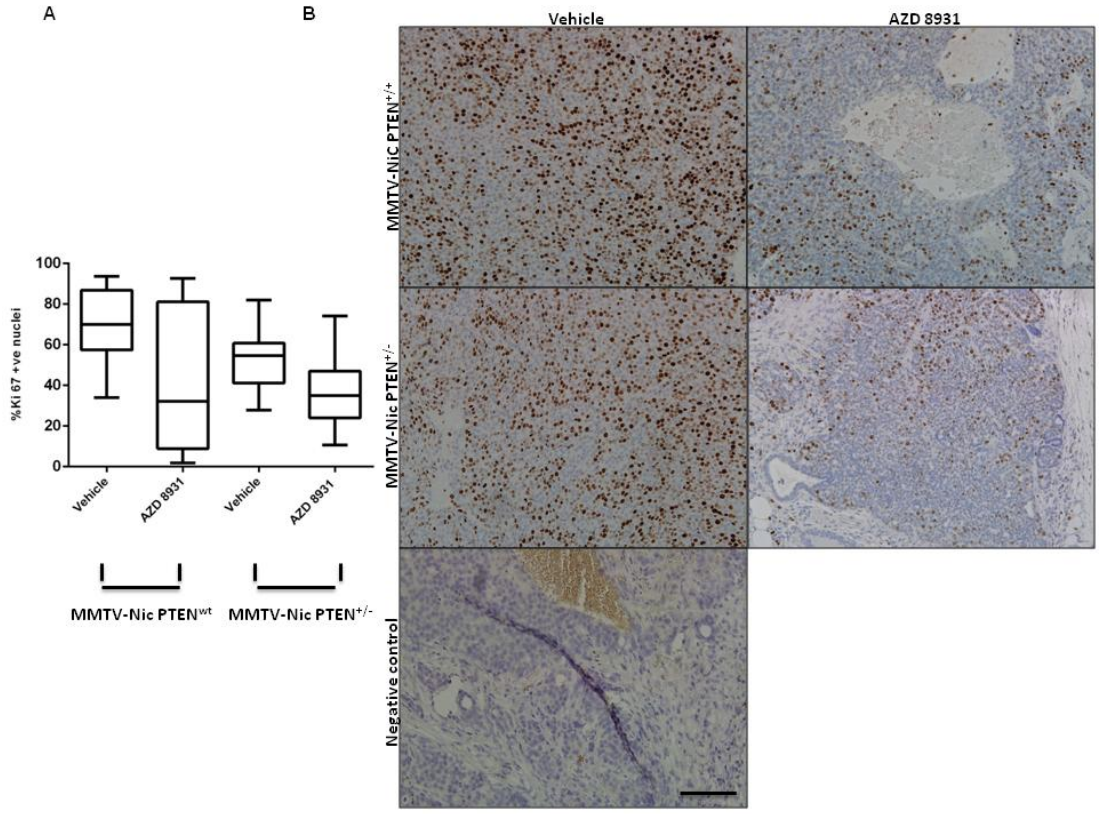

Figure 4.21- AZD8931 inhibited tumour proliferation. IHC was performed on paraffin embedded sections of AZD8931 and vehicle treated tumours with a Ki67 antibody. Images analysed using ImmunoRatio software to calculate percentage nuclei positive for Ki67 in six randomly selected low power fields (mag x20) per tumour. A: Box–whisker plot analysis of percentage of nuclei positive for Ki67. MMTV-NIC PTEN $^{FL/+}$ (n=3 in each treatment group, p= 0.010, Mann Whitney U test). MMTV-NIC PTEN$^{+/-}$ (n=4 in each treatment group, p=0.005). B: Representative IHC images of vehicle and AZD8931 treated MMTV-NIC PTEN $^{FL/+}$ and MMTV-NIC PTEN$^{+/-}$ tumours. Negative control consists of tumour section incubated in the absence of primary antibody. Scale bar represents 100 µm. Mag x20.

4.3.4 Effect of AZD8931 on apoptosis

AZD8931 treatment resulted in a minimal increase in apoptosis as evidenced by the presence of cleaved caspase 3 (Figure 4.22B). However, expression was low in all groups with 0.1% tumour area staining positively for cleaved caspase 3 in AZD8931 treated tumours in both MMTV-NIC PTEN $^{FL/+}$ ($p=0.05$) and MMTV-NIC PTEN$^{+/-}$ ($p=0.04$) cohorts (Figure 4.22A). Whilst this represents a statistically significant increase in expression compared to vehicle treated tumours, such low expression is likely to be of minimal biological relevance.

4.3.5 Effect of AZD8931 on tumour vascularization

Tumour progression is dependent on efficient tumour vascularization. Inhibition of angiogenesis is one of the proposed mechanisms of action of trastuzumab [284]. Therefore, we stained sections of vehicle and AZD8931 treated MMTV-NIC PTEN$^{+/-}$ tumours with a CD31 antibody, a marker of endothelial cells and vasculature [285]. To maximize the potential of identifying any impact on vascularization, only tumours from the long term treatment study were stained and analyzed. As long term AZD8931 treatment resulted in complete or near complete resolution of the majority of MMTV-NIC PTEN $^{FL/+}$ tumours, this analysis was restricted to MMTV-NIC PTEN$^{+/-}$ tumours. Vascularization was expressed in terms of the mean percentage area contained within a CD31 positive region in 6 representative low-powered fields (mag x20) per tumour. Prolonged AZD8931 treatment did not alter either vessel morphology or the extent of tumour vascularization ($p= 0.53$, Mann Whitney U test) (Figure 4.23).

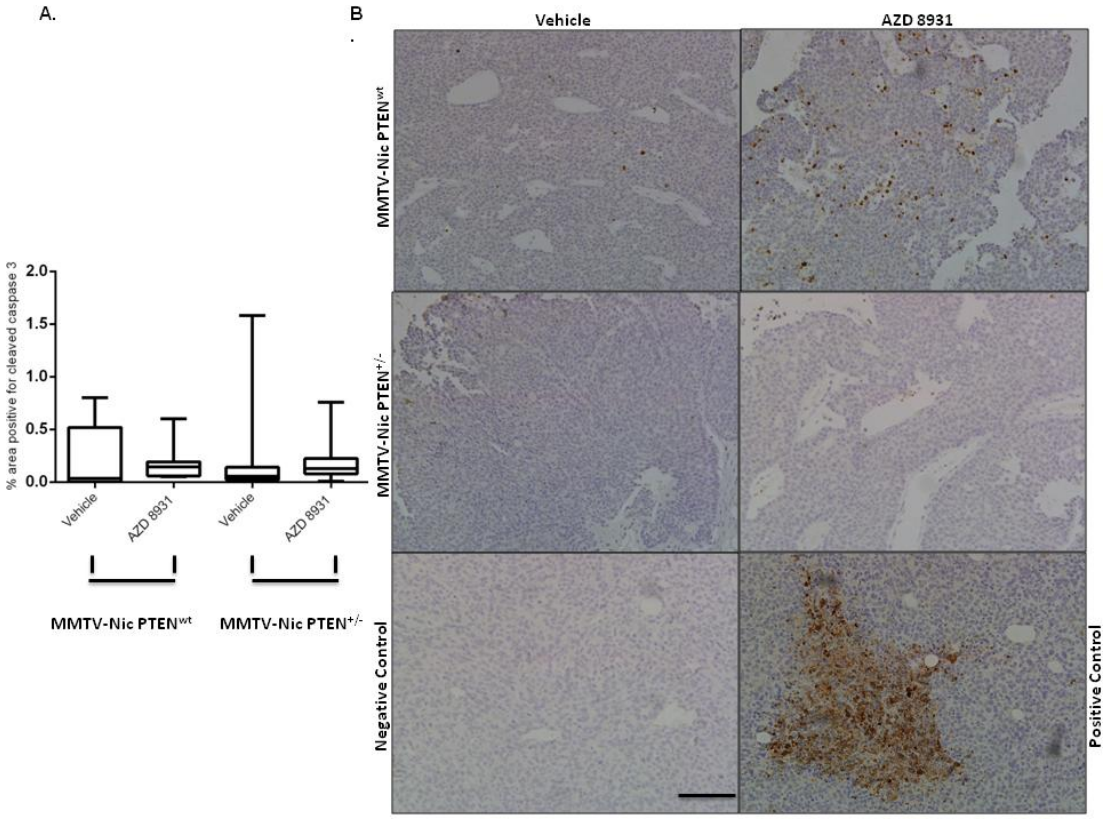

Figure 4.22- AZD8931 did not cause significant levels of apoptosis. IHC was performed on paraffin embedded sections of AZD8931 and vehicle treated tumours with a cleaved caspase 3 antibody. Images analysed using Image J software to calculate percentage area staining positive for cleaved caspase 3 in six randomly selected low power fields (mag x20) per tumour. A: Box-whisker plot analysis of percentage area positive for cleaved caspase 3 in MMTV-NIC PTEN $^{FL/+}$ (n=3 in each treatment group, p= 0.053, Mann Whitney U test) and MMTV-NIC PTEN$^{+/-}$ (n=4 in each treatment group, p=0.042). B: Representative IHC images of vehicle and AZD8931 treated MMTV-NIC PTEN $^{FL/+}$ and MMTV-NIC PTEN$^{+/-}$ tumours. Positive control consists of section of 4T1 tumour treated with doxorubicin. Scale bar represents 100 µm. Mag x20.

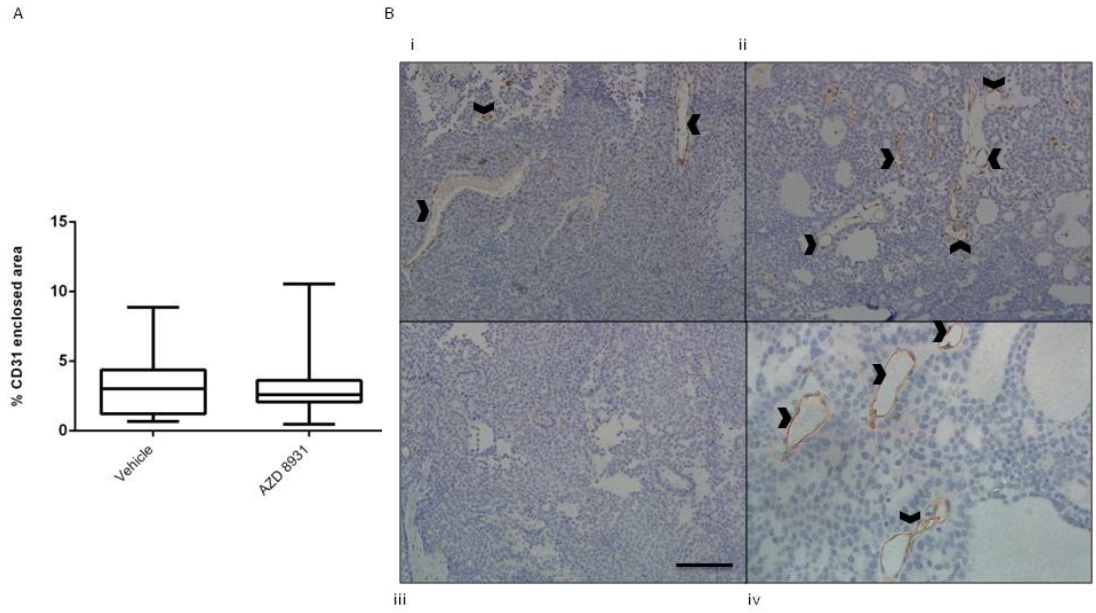

Figure 4.23- AZD8931 did not inhibit angiogenesis in MMTV-NIC PTEN$^{+/-}$ tumours. IHC was performed on paraffin embedded sections of AZD8931 (n=3) and vehicle (n=2) treated tumours with a CD31 antibody. Images analysed using Image J software to calculate percentage area within a CD31 positive region in six low power fields (mag x20) per tumour. A: Box–whisker plot analysis of extent of vascularization in vehicle and AZD8931 treated tumours (p=0.53, Mann Whitney U test). B: Representative IHC images of vehicle (i) and AZD8931 (ii) treated tumours. Arrowheads denote representative blood vessels. Negative control consists of tumour section incubated in the absence of primary antibody (iii). Scale bar represents 100 µm. Mag x20. High powered view of CD31 positive blood vessels (iv). Mag x40.

4.4 Discussion

In earlier experiments we used the BLG-HER2^{KI}-PTEN$^{+/-}$ model to assess response to dasatinib in HER2 positive breast cancer. However, due to concerns that the slow tumour growth in this model was not reflective of the aggressive course of human HER2 positive disease, we opted to use the MMTV-NIC model for further experiments. In this current series of experiments, we aimed to describe MMTV-NIC tumour development and to assess tumour response to drugs with known efficacy in HER2 positive breast cancer thereby determining whether this is an appropriate model of human disease. PTEN loss is a common genetic event occurring in between 25% [229] and 50% [104] of HER2 positive breast cancer cases. By crossing the model with a strain containing a floxed PTEN allele, we aimed to explore the role of PTEN status in determining sensitivity to HER2 directed therapies using AZD8931, a novel pan-HER inhibitor, as an example.

4.4.1 Characterisation of MMTV-NIC PTEN model

We used IHC to explore HER2 protein expression in MMTV-NIC PTEN$^{+/-}$ tumours. Although most tumours expressed large amounts of HER2, only 25% were classified as HER2 over-expressing on the basis of their IHC result alone according to the ASCO/CAP guidelines. A further 50% had an equivocal result (2+) and require further assessment using Fluorescent In Situ Hybridisation (FISH) to determine their HER2 status [83]. The ASCO/CAP guidelines were devised for use in human breast cancer and their relevance for determining thresholds of HER2 expression in transgenic mouse models is questionable. Tumourigenesis in human HER2 positive breast cancer is driven by genetic amplification and/or over-expression of wild-type HER2 [277]. Although spontaneous HER2 mutations have been identified, these have been in the context of tumours without HER2 gene amplification or protein over-expression [169]. In contrast, wild-type HER2 over-expression in mouse models only resulted in tumour development after the acquisition of secondary mutations [286] [287]. In the MMTV-NIC model, tumourigenesis is driven by a mutated and constitutively activated HER2 transgene, which shares similarities with the naturally occurring HER2Δ16 protein seen in human breast cancer. In this mutated transgene, a 16 amino acid deletion in the extracellular domain promotes the formation of inter-molecular disulphide bonds which stabilize HER2 homodimers and gives the transgene a 10-fold greater transforming capacity

than wild-type HER2 [266]. Given this enhanced transforming ability, lower expression of the mutant transgene may be required to generate the HER2 phenotype. This hypothesis is supported by previously published data showing that treatment with a HER2 directed antibody inhibited tumour growth in MMTV-NIC PTEN $^{FL/+}$ and MMTV-NIC PTEN$^{+/-}$ models [40]. Furthermore, in our own experiments we saw a marked response to treatment with single agent AZD8931. Despite the dependence of human HER2 positive breast cancer on the HER2/PI3K/Akt pathway, response rates to both single agent trastuzumab (15-26%) and lapatinib (24%) are modest [137]. Although there is no clinical data for AZD8931 efficacy in human HER2 positive disease, the response to drug in our experiments, particularly in the MMTV-NIC PTEN $^{FL/+}$ model, was more dramatic than anticipated. This may suggest that, despite reduced HER2 expression, the MMTV-NIC model is actually more dependent on HER2 signalling for growth than human disease and inhibition of this signalling pathway results in profound tumour responses.

The apparent discrepancy between lower than predicted HER2 expression and reliance on HER2 signalling may also be due to a variety of technical issues. Variations in tumour fixation and section storage have been reported to have a significant impact on HER2 staining in sections collected as part of large phase 3 clinical trials. The choice of primary antibody also impacts on the staining pattern and intensity [288] and in these experiments we did not use the FDA-approved Hercep Test (® DAKO), which is standard in clinical trials. Finally, histoscoring is a highly skilled technique and tumour sections in these experiments were scored by a single observer. Ideally tumours should be independently scored by at least 2 observers, although considerable inter-observer scoring variation is often seen. In fact, when a series of experienced scorers were assessed using the Hercep Test (® DAKO) only 57-65% demonstrated an acceptable standard of performance [288].

The localization of HER2 detected by IHC is also intriguing. As predicted, membranous staining predominated throughout most tumours. However, multiple tumours contained regions with extensive cytoplasmic staining but weak/little membranous staining. There are 2 main explanations for this. Firstly, it may be a result of the extracellular domain NDL deletion, which confers constitutive activity to the receptor but may also affect receptor targeting to the membrane. Secondly, following receptor activation and downstream signaling, the HER2 receptor complex is internalized and either degraded or recycled and returned to the receptor membrane [77]. Constitutive activation of HER2 may result in rapid receptor

signaling and subsequent internalization resulting in significant pools of the receptor within the cytoplasm.

Using IHC we also determined that MMTV-NIC PTEN$^{+/-}$ tumours did not express ER or PR. In a recent case series of over 3000 patients with HER2 positive breast cancer, 49% were classified as HR negative [129]. These patients tended to present with more advanced disease and had an increased risk of death in the 5 years following diagnosis [129]. This model is therefore not only clinically relevant but representative of a high risk patient group who require additional therapeutic options.

Using a single lung section, we identified evidence of metastatic spread in 25% of MMTV-NIC PTEN$^{+/-}$ mice and previously published data using a higher number of lung sections per mouse suggests this is likely to be an under-estimate [272]. The development of spontaneous metastases is frequently cited as a major advantage of GEMMs making them valuable tools for assessing drug efficacy in the metastatic setting. This is potentially a major advance as whilst many patients with early breast cancer are successfully treated, there are currently no curative treatments for metastatic disease and it is no longer possible to assume that drugs which are active in primary tumours will be active in metastases as subsets of genes have been shown to be differentially expressed between primary and metastatic tumours [168]. Furthermore, preclinical studies have shown that the normal tissue surrounding a tumour is also capable of influencing its response to treatment [289]. There therefore remains a major unmet need to develop preclinical models of metastatic disease. However, in this study the burden of metastatic disease was too low in all animals to permit further quantification. Although metastatic spread is now considered to be an early event in tumour progression [290], the rapid growth of mammary tumours in this model is likely to have resulted in the sacrifice of animals before the development of established metastatic deposits. Removal of multiple mammary tumours to enable to further growth of metastatic deposits in this model is not feasible and therefore in the following studies we have focused on drug efficacy in the primary tumours.

4.4.2 Predictive value of the MMTV-NIC PTEN$^{+/-}$ model for assessing drug response

We used paclitaxel, a drug with known efficacy in HER2 positive breast cancer, to determine the MMTV-NIC PTEN$^{+/-}$ model's appropriateness for predicting drug response in human HER2 positive disease. Four weekly doses of paclitaxel prolonged OS in MMTV-NIC$^{+/-}$ mice and resulted in a statistically significant increase in apoptosis, although the biological relevance of such a small increase is questionable. However, it did not cause tumour shrinkage instead resulting in slowed yet continual growth, which in the context of a clinical trial would be classified as progressive disease. This universal lack of tumour shrinkage stands in marked contrast to paclitaxel's activity in human disease, where response rates of between 22% and 78% have been described in metastatic disease [291]. This data precedes the introduction of routine HER2 testing and is therefore likely to reflect paclitaxel's efficacy in a mixed cohort of both HER2 positive and HER2 negative breast cancers. However, taxane sensitivity is generally believed to be independent of HER2 status [292] [293] and therefore similar response rates would be expected amongst an exclusively HER2 positive population. There is little available data for the use of single agent paclitaxel in the neoadjuvant setting in human HER2 positive breast cancer as it is generally given sequentially with an anthracycline and concomitantly with trastuzumab, which increases the pathological complete response rates (PCR) [294]. However, 25% of patients treated with neoadjuvant paclitaxel and 5-fluorouracil, epirubicin and cyclophosphamide (FEC) in the absence of trastuzumab achieved a PCR [294].

There are several possible explanations for the discrepancy between paclitaxel activity in humans and in the MMTV-NIC$^{+/-}$ model. Firstly, the polyclonal nature of these tumours coupled with their extremely rapid growth rate makes these tumours a greater therapeutic challenge than human breast cancer and the rapid development of resistant clones may be inevitable. Secondly, the limited efficacy of paclitaxel may be attributable to inefficient drug delivery as suggested by the focal nature of apoptosis within tumours. Extensive areas of necrosis are observed throughout many of these tumours, suggesting they outgrow their blood supply and therefore drug delivery to large regions of actively growing tumour may be compromised. Finally, in this study mice were treated at only 50% of the maximum tolerated dose (MTD) of paclitaxel. Interestingly, unlike in humans, the MTD in mice is dictated by the toxicity of the cremaphor vehicle rather than the active drug [295]. Therefore, the lack of

tumour shrinkage in response to paclitaxel may in part be related to the use of a suboptimal drug dose and future experiments should use the MTD of cremaphor.

We then went on to look at HER2 targeted therapies using AZD8931. In cohorts of MMTV-NIC PTEN $^{FL/+}$ and MMTV-NIC PTEN$^{+/-}$ mice, single agent AZD8931 increased OS, although the degree of tumour sensitivity was dependent on PTEN status (see section 4.7.2.4 for further discussion). Comparison of tumours with the same genotype demonstrated heterogeneity in the rate and extent of response to AZD8931, despite the use of predefined genetic mutations to drive tumour development. This variation in therapeutic response has been previously described in other GEMMs [296] and contrasts with the more uniform response seen in xenograft studies [26]. This is an important advance as it enables us to more accurately recapitulate the behaviour of human tumours and is most likely due to the random acquisition of secondary mutations during tumour development and progression. Consistent with this, human tumours have been shown to have more somatically acquired structural rearrangements than GEMM tumours [72] and display greater variation in therapeutic response than we have seen in our model.

As we have previously discussed, this model is not suitable to explore drug response in metastatic disease. However, the increased rate of metastases seen in the AZD8931 treated MMTV-NIC PTEN$^{+/-}$ cohort is an intriguing observation, although the use of small cohorts makes it impossible to draw any firm conclusions. The increased rate of detectable metastases is likely to reflect the increased OS of this cohort due to AZD8931's efficacy in reducing mammary tumour progression. However, this also suggests that AZD8931 is more efficacious in treating primary tumours than metastatic lesions, although further experiments are required to confirm this. If this is subsequently confirmed, it raises the possibility of using AZD8931 to control local disease facilitating the development of a greater metastatic burden, which could be therapeutically targeted with other novel agents.

The exact mechanism, by which AZD8931 inhibits mammary tumour progression remains to be fully determined. A robust reduction in the percentage of cells staining positively for Ki67 was seen in both the MMTV-NIC PTEN $^{FL/+}$ and MMTV-NIC PTEN$^{+/-}$ models following 3 days of treatment with AZD8931. Whilst this reduction in cell proliferation undoubtedly makes an

important contribution to AZD8931's efficacy *in vivo*, alone it is unable to account for the difference in sensitivity seen between the 2 models. Furthermore, given that MMTV-NIC PTEN$^{+/-}$ tumours grow more rapidly than MMTV-NIC PTEN $^{FL/+}$, the higher percentage of Ki67 positive nuclei seen in vehicle treated MMTV-NIC PTEN$^{+/-}$ tumours was also surprising. The choice of method used to quantify the percentage of Ki67 nuclei may account in part for these results. Currently, there are no standardized guidelines for quantification of Ki67 staining and we scored randomly selected tumour regions to give a measure of cell proliferation within the whole tumour. It may have been more appropriate to compare proliferation in the most mitotically active tumour regions, which are likely to contain most aggressive clones capable of dominating tumour behaviour [234].

A reduction in cell proliferation also does not explain the marked tumour shrinkage seen in the MMTV-NIC PTEN $^{FL/+}$ cohort. We therefore went on to look for changes in apoptosis following drug treatment. AZD8931 resulted in a minor yet statistically significant increase in apoptosis in both models. Whilst our GEMM tumours had a much more profound response to AZD8391 than predicted from the response of human tumours to trastuzumab or lapatinib, the percentage of cells undergoing apoptosis remained equally low [297]. The ability of IHC to quantify apoptosis is limited as it is only captures cells which are undergoing apoptosis at the time of sacrifice. Apoptosis is a transient event with a limited time between induction of apoptosis and removal of cell debris [298] and therefore in future experiments, use of modern intravital imaging techniques such as FRET-based probes may be give a more dynamic and informative estimate of drug-induced apoptosis [299]. Paclitaxel also results in necrotic cell death [300] and this may be the dominant mechanism of cell death in this model. We also used IHC to explore the impact of long term AZD8931 treatment on angiogenesis but did not detect any effect of treatment on either blood vessel structure or density in the MMTV-NIC PTEN$^{+/-}$ model.

Together, these experiments provide preliminary evidence that the MMTV-NIC model is a useful tool for predicting activity of therapeutic agents, particularly HER2 directed therapies, in human HER2 positive breast cancer. However, considerable inter-species variation in the magnitude of response may be observed due to the greater reliance of MMTV-NIC tumours on the HER2/PI3K/Akt pathway than their human counterparts. The heterogeneity of response to AZD8931 suggests that despite its limitations, this model is better suited for preclinical testing of targeted agents than traditional xenografts. Finally, although the exact

mechanism of AZD8931's actions remains to be determined, our data suggests that trials of AZD8931 in human HER2 positive breast cancer may be merited.

4.4.3 Analysing Target Pathway Inhibition in Response to AZD8931

One of the main problems with using the MMTV-NIC model to assess response to AZD8931 has been assessing target inhibition. RPPA and IHC analysis gave conflicting results regarding the effects of AZD8931 treatment on HER2 expression. With IHC, a borderline statistical reduction in HER2 expression was seen in AZD8931 treated MMTV-NIC PTEN $^{FL/+}$ tumours but not in MMTV-NIC PTEN$^{+/-}$ tumours. Two separate antibodies were used to assess HER2 expression on the RPPA platform, which again gave conflicting results. Data with the first antibody suggested that AZD8931 treatment had no effect on HER2 expression, whilst the second showed an increase in HER2 expression associated with drug treatment. This drug induced increase in HER2 expression was subsequently confirmed on western blot using a third independent HER2 antibody. Whilst an increase in total HER2 expression has been described following lapatinib treatment *in vitro* [301], the lack of consistency between antibodies on the RPPA platform and with our IHC result means this result must be interpreted with a degree of skepticism.

We then went on to examine the effects of AZD8931 on the activity of HER family receptors. Using a combination of IHC, RPPA and western blotting, we demonstrated a non-statistical reduction in HER2 activity following AZD8931 treatment. A non-statistical reduction in pTyr 1289 HER3 expression was also observed using IHC but this was not replicated using RPPA. The signal obtained on the RPPA platform with both the total HER3 and pTyr 1289 HER3 antibodies was weak and it is likely that the system lacked sufficient sensitivity to determine changes in this pathway's activity on these tumours. EGFR expression was too low for activity to be quantified using either RPPA or IHC.

Several factors are likely to have contributed to the difficulties in obtaining conclusive evidence of target receptor inhibition. Firstly, using both RPPA and IHC we found that expression of key signaling molecules was extremely heterogeneous, even amongst

tumours of the same genotype. This is likely due in part to the random acquisition of secondary mutations, which underpins the observed heterogeneity in tumour response to AZD8931. With such heterogeneity, further studies using larger cohorts are needed to fully explore the range of signaling responses to AZD8931 treatment and these experiments are currently underway. Furthermore, considerable heterogeneity in target receptor expression is observed even within individual tumours. This intra-tumoural variation is readily demonstrable using IHC, although scoring these samples is complex and ideally needs to be undertaken by skilled and experienced observers [288]. Whilst RPPA provides a quantitative readout, the small protein concentrations required make it particularly vulnerable to intra-tumoural sampling bias. Tumour lysate was prepared from whole tumours and therefore in addition to epithelial tumour cells is likely to include non-epithelial components, such as stromal tissue and macrophages, which are likely to add to the observed signaling pathway heterogeneity. As previously described, these tumours also contained large necrotic regions and whilst macroscopically necrotic areas were not used to prepare lysate, inclusion of microscopic regions may also have potentially obscured significant changes in signaling pathway activity. Use of H & E stained slides to guide selection of viable and tumour-rich regions for lysate preparation may help to overcome some of these issues in future experiments [302] as it has previously been shown that RPPA analysis of laser microdissected and non-microdissected samples from the same tumour show considerable differences in reported signaling pathway activity [303].

Despite lacking direct conclusive evidence of target receptor inhibition, we believe the robust reduction in both Akt and MAPK activity coupled with the marked *in vivo* response following AZD8931 treatment is compelling evidence that the drug's efficacy is due to on-target effects.

4.4.4 Understanding Mechanisms of Resistance to AZD8931

Whilst the introduction of HER2 targeted therapies such as trastuzumab and lapatinib has revolutionized the outlook for patients with HER2 positive breast cancer, inherent and acquired resistance are frequently encountered problems. Although, *in vitro* studies have identified numerous different mechanisms of resistance [147], to date none of these

resistance pathways or their associated biomarkers have transferred into standard clinical practice, reflecting the huge obstacles which need to be overcome during the transition from bench to bedside. The impact of PTEN loss on the sensitivity to HER2 targeted therapies is an example of a one such potential mechanism of resistance. Several preclinical studies have produced compelling evidence that PTEN loss is associated with trastuzumab resistance [271]. The effect of PTEN loss on lapatinib sensitivity has been explored in 2 preclinical studies with conflicting results [154] [254]. However, despite being the focus of several trials, no consensus has been reached on whether clinically PTEN expression determines sensitivity to either trastuzumab [150] or lapatinib [254] [304] [176]. The lack of concordance between preclinical and clinical data may be due to several factors. Firstly, the limited numbers of cell lines used in preclinical studies may fail to recapitulate the complex situation seen in a heterogenous disease population. Secondly, within clinical studies, analysis of specimens is complicated by the lack of a standardized, validated assay with variations in antibody and scoring techniques used. It may also reflect in part the restricted capabilities of the most widely used techniques to look at more than a limited range of resistance mechanisms. Several small retrospective studies suggested that combining markers suggestive of PTEN/PI3K/Akt hyperactivation may be more predictive of response to trastuzumab than PTEN alone, although prospective studies failed to conclusively demonstrate that benefit from trastuzumab was confined to patients with evidence of PTEN/PI3K/Akt pathway hyperactivation [150]. However, the major complication in interpreting data from clinical studies is the reliance on biopsies collected at the time of diagnosis although many of these trials are conducted in the metastatic setting. A 26% disconcordance rate for PTEN status between matched primary and secondary samples has been reported [182] and therefore it is likely that any impact PTEN loss has on trastuzumab resistance would be obscured by incorrect classification on the basis of PTEN status. As a more physiologically relevant preclinical model, the MTMV-NIC model therefore has the ability to provide a unique insight into this highly contentious issue. We found that single agent AZD8931 prolonged OS in both MMTV-NIC PTEN $^{FL/+}$ and MMTV-NIC PTEN$^{+/-}$ models. However, AZD8931 was more effective in the MMTV-NIC PTEN $^{FL/+}$ model, where it caused tumour eradication compared to slowed tumour progression in the MMTV-NIC PTEN$^{+/-}$ model. This is consistent with previously published data in this model showing that sensitivity to a HER2 targeted antibody was dependent on PTEN status [40]. Further studies to explore the activity of AZD8931 in MMTV-NIC PTEN$^{-/-}$ mice are currently underway.

Previous data from our laboratory showed a non-statistical reduction in PTEN expression in MMTV-NIC PTEN$^{+/-}$ tumours compared to MMTV-NIC PTEN $^{FL/+}$ tumours. However, whilst Schade et al reported that over 50% of MMTV-NIC PTEN$^{+/-}$ tumours had evidence of LOH with loss of the second PTEN allele [272], all 4 of the tumours in our panel retained low level PTEN expression. Whole tumours were used to prepare lysate for both western blotting and RPPA and therefore the most likely explanation for residual PTEN expression is the inclusion of non-epithelial tumour components in the lysate. In future experiments, macrodisection, to remove non-epithelial elements, could be used to overcome this issue [302]. Alternatively, IHC could be used to explore PTEN expression on an individual cell basis. There is also considerable heterogeneity in PTEN expression between the different tumours, especially amongst the MMTV-NIC PTEN $^{FL/+}$ tumours. Therefore, the use of a small tumour panel size may have failed to accurately capture the range of PTEN expression in the full cohorts and therefore repeating this experiment with a greater sample size may be beneficial.

Having identified PTEN loss as a key determinant of AZD8931 resistance, we sought to identify other, potentially drugable, downstream targets involved in the resistance pathway. PTEN is an important negative regulator of the PI3K/Akt pathway [305] and consistent with previously published data in this model [272] [40], we found baseline Akt activity was increased in MMTV-NIC PTEN$^{+/-}$ tumours compared to MMTV-NIC PTEN $^{FL/+}$ tumours. Both MMTV-NIC PTEN $^{FL/+}$ and MMTV-NIC PTEN$^{+/-}$ tumours displayed reduced Akt activity following treatment with AZD8931, although in both models there was still evidence of residual activity following AZD8931 treatment. Incomplete inhibition of Akt signaling is a well-established mechanism of resistance to HER2 targeted therapies [147] and is likely to contribute to the continued tumour progression in the MMTV-NIC PTEN$^{+/-}$ model. Consistent with this, Wang and colleagues found that combination therapy with a HER2 monoclonal antibody and an Akt inhibitor inhibited growth of MMTV-NIC PTEN$^{-/-}$ tumours, which were resistant to treatment with either drug alone [65].

By dephosphorylating PTEN, Src is able to amplify PI3K/Akt activity [216], [306]. AZD8931 treatment suppressed Src activity but only in the more sensitive MMTV-NIC PTEN $^{FL/+}$ model, suggesting that incomplete Src inhibition may also contribute to AZD8931 resistance. It is likely that in the MMTV-NIC PTEN $^{FL/+}$ model, AZD8931 prevents Src's inhibition of PTEN and therefore downregulates Akt signaling. Experiments are currently in progress to

try and determine whether combined treatment with AZD8931 and a Src inhibitor in the less sensitive MMTV-NIC PTEN$^{+/-}$ model will result in tumour shrinkage. Targeting Src as a means of overcoming resistance is a particularly promising approach as increased Src activity has been identified as a common event in cell lines rendered resistant to HER2 directed therapies using several approaches, such as PTEN loss and over-expression of the receptor tyrosine kinases EGFR and IGF1R [216]. As clinical resistance is multi-factorial, targeting features common to multiple different resistance pathways is likely to yield the greatest therapeutic benefits and high Src activity has been correlated with reduced OS following treatment with trastuzumab in metastatic breast cancer [216]. However, response rates to single agent dasatinib were disappointing in trastuzumab resistant HER2 positive breast cancer [50], although combined treatment with HER2 directed therapy and Src inhibitors may be more successful.

In conclusion, GEMMs are useful tools in ongoing efforts to validate putative biomarkers and potentially to identify and test therapeutic combinations aimed at overcoming resistance. The characteristics of GEMMs uniquely place them to overcome some of the issues seen with other preclinical and clinical approaches. They provide a more physiologically relevant model than *in vitro* cell line based assays and despite tumour progression occurring within the context of predefined genetic lesions, the stochastic accumulation of secondary mutations results in tumour heterogeneity so that results are more generalizable to the disease population. Although the degree of tumour heterogeneity seen between GEMMs is clearly less than that seen in the clinical HER2 positive population as a whole, the potential for GEMM tumours to develop different resistance strategies, which might mask the effect of the biomarker in question, is also less. Furthermore, the ability to genetically control expression of the biomarker under investigation overcomes the problem of defining high and low biomarker expression, which is encountered in clinical trials. Whilst the use of GEMMs alone is not sufficient for biomarker validation, they are clearly a useful addition to other existing strategies. At present, HER2 status is the only available predictive biomarker of response to both trastuzumab and lapatinib but it is unable to predict which patients with HER2 positive disease will benefit from treatment. There is a real need to develop better biomarkers for disease response and this is likely to become increasingly relevant with the advent of multi-agent HER2 directed therapy. Development of better biomarkers has the potential to spare patients with a good prognosis the additional toxicity and cost associated with these more complex treatment strategies.

In this series of experiments we have focussed on methods associated with inherent resistance. Studying acquired drug resistance involves generating a tumour which is initially sensitive to drug treatment but loses this sensitivity following prolonged drug exposure. Development of acquired resistance in these models is complicated by the generation of multiple tumours with differing inherent sensitivities as the presence of a tumour with *de novo* resistance will necessitate the premature termination of the experiment prior to sensitive tumours developing resistance. GEMMs have been used to explore acquired resistance [296], although this requires the use of techniques to generate a single tumour (see Chapter 5).

4.5 Summary

In conclusion, we have obtained preliminary evidence that the MMTV-NIC model is a useful tool for predicting response to drugs in human HER2 positive breast cancer, particularly HER2 targeted agents. However, the increased reliance of MMTV-NIC tumours on the HER2/PI3K/Akt pathway is likely to result in a greater response to HER2 targeted agents than may be expected in human disease. Finally, we have used the model to demonstrate that sensitivity to AZD8931 is dependent on PTEN status.

Chapter 5: Development of a model amenable to drug studies

Despite the improvements in outcomes seen since the introduction of trastuzumab and lapatinib to routine clinical care [307] approximately 5000 patients still die every year of HER2 positive metastatic breast cancer in the United States alone [2]. The development of acquired resistance to HER2 targeted agents is ultimately a universal phenomenon in advanced disease. Therefore, an improved understanding of clinically relevant mechanisms of acquired resistance and the development of more drugs which are active in metastatic disease remain 2 important unmet goals. Whilst the MMTV-NIC model is a useful tool for predicting the therapeutic response of primary tumours, the low metastatic burden makes it unsuitable for establishing drug activity in this setting. Furthermore, the development of multiple mammary tumours with differing drug sensitivities is a major obstacle in experiments investigating the development of acquired resistance. We therefore sought to develop methods of using the MMTV-NIC model to generate animals with a single mammary tumour, which could either be exposed to cyclical drug treatment to promote acquired resistance or resected to enable the development of established metastases.

Specific aims of this section of the project included:

1. Development and characterisation of tumours generated from mammary fat pad injection of established MMTV-NIC cell lines.
2. Development and characterisation of tumours generated from mammary fat pad injection of freshly harvested disassociated mammary tumours.
3. Use of MMTV-NIC tumour fragments to generate syngeneic orthotopic tumour transplants.
4. Exploration of factors which might affect outcomes of tumour fragment transplantation.

5.1 Use of established MMTV-NIC PTEN$^{+/-}$ cell lines to generate mammary tumours

The MMTV-NIC PTEN$^{+/-}$ model had previously been used to generate a panel of cell lines (**L.Balderstone**). A representative cell line (MNP 145 LU) was selected, which on western blot had been shown to express HER2 and both cytokeratins 8 and 14, suggesting it was derived from a mixed epithelial cell background containing both luminal and basal components (**L. Balderstone**). Recognising the influence of the tumour microenvironment on tumour progression [28] and response to therapy [289], we elected to perform orthotopic injections of the MNP 145LU cell line in an attempt to generate single mammary tumours. We injected $1*10^6$ cells into the four left mammary fat pad (MFP) of 8-week old athymic mice (n=6). Mice were monitored twice weekly and tumour size recorded. Tumours were permitted to grow to a maximal diameter of 1.5 cm (in any direction).

Tumourigenicity of the cell line was demonstrated with 100% of mice developing a tumour with a median onset 21.8 days (range 7.5 - 65.5 days) (Figure 5.1). However, 50% of animals (n=3) were sacrificed prematurely due to significant skin ulceration. The remaining 3 mice were sacrificed due to tumour burden at a median interval of 42 days (range 39-56 days) post tumour-onset.

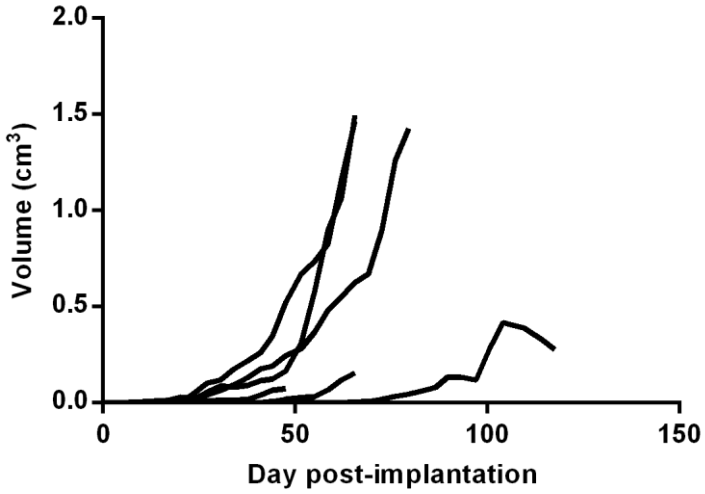

Figure 5.1- Growth curves of MNP 145 LU derived tumours. Mice were inoculated with $1*10^6$ MNP 145 LU cells and monitored twice weekly for tumour onset and progression. Mean volume calculated from 2 successive readings is plotted against time since fragment implantation. Median interval between MFP inoculation and tumour onset was 21.8 days (n=6). Median duration of survival post tumour development was 42 days (n=3).

Cell line derived tumours appeared phenotypically distinct compared to parental GEMM tumours with loss of the highly cellular nodules seen in the parental model (Figure 5.2). These tumours also exhibited an increased stromal content, within which irregular cellular palisades sat with loss of the normal cell-cell contact inhibition. We used IHC to further characterize tumours and to determine whether cell line derived tumours recapitulated the features of the parental GEMM. Using Ki67 as a marker of cell proliferation, we showed that cell line derived tumours were highly proliferative as we had previously demonstrated for the parental GEMM tumours (see chapter 4). However, unlike the parental GEMM tumours, we were unable to demonstrate any significant HER2 expression (Figure 5.2). We also found no evidence of metastatic spread when a single section of lung tissue per mouse was examined.

Although this technique allowed the rapid generation of mammary tumours, the striking loss of HER2 expression and the loss of tumour architecture in all tumours meant that this approach was not appropriate for further studies with AZD8391.

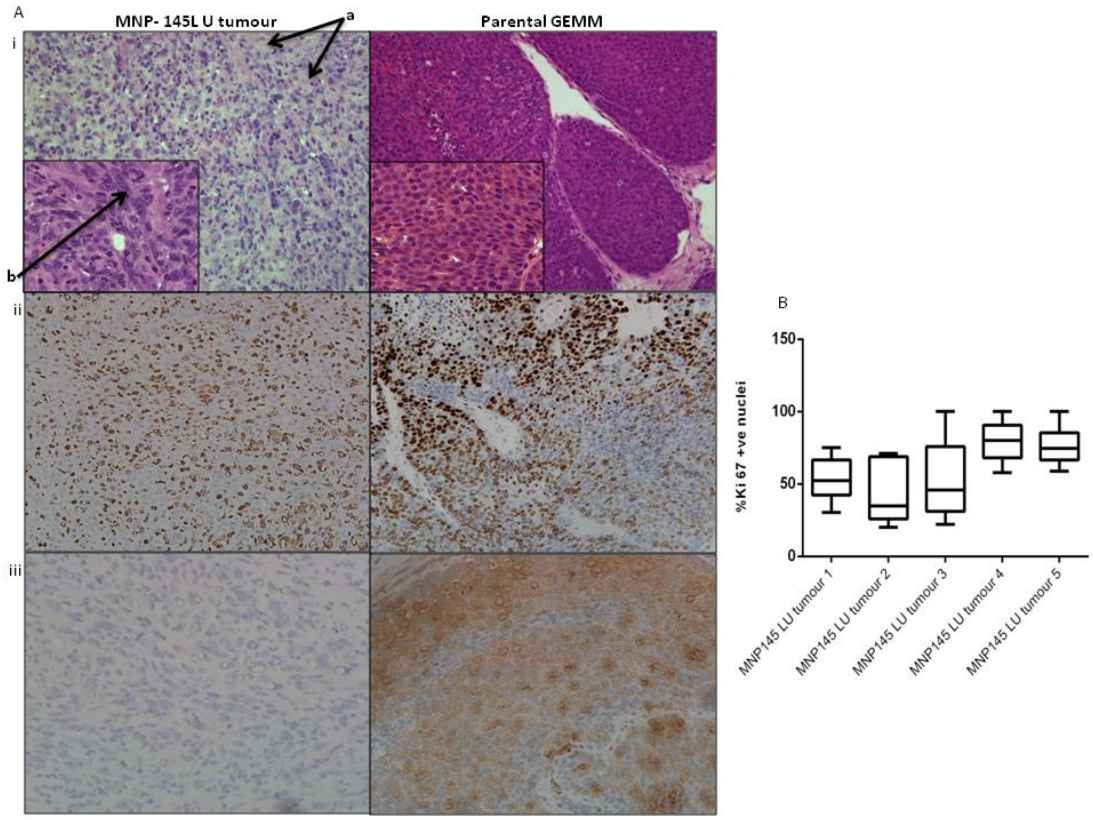

Figure 5.2- MNP 145 LU generated tumours were not representative of the parental GEMM from which they are derived. Ai: Representative H and E images demonstrating loss of cellular nodules in the cell line derived tumours. Cell line derived tumours contain increased stroma (a) within which sit palisades of cells with loss of contact inhibition (b). Main image mag x20, insert mag x40. Aii: Representative images of paraffin embedded sections stained with a Ki67 antibody demonstrating highly proliferative nature of tumours (n=5, mag x20). Aiii: Representative images of paraffin embedded sections stained with a HER2 antibody demonstrating loss of HER2 expression in cell line derived tumours (n=5) and preserved HER2 expression in GEMM tumour from which the cell line was derived (mag x40). B: Box whisker plot analysis of percentage of nuclei positive for Ki67 in MNP 145 LU derived tumours confirming the highly proliferative nature of these tumours, as previously demonstrated for the parental GEMM tumours (see chapter 4). Ki67 images analysed using ImmunoRatio software to calculate percentage nuclei positive for Ki67 in six low power fields (mag x20) per tumour.

5.2 Use of dissociated MMTV-NIC PTEN$^{+/-}$ tumours to generate mammary tumours

To try and overcome the issue of HER2 loss during *in vitro* culture, tumours from MMTV-NIC mice were harvested, dissociated using collagenase and $0.5*10^6$ cells injected into the fourth MFP of 3 9-week old FVB mice. As the immune system plays a critical role in tumour development [27], we decided to use immune-competent FVB mice as tumour recipients in this experiment to enhance the physiological relevance of the model. Mice were monitored twice weekly for tumour onset and growth.

Tumour penetrance was defined as the percentage of mice that developed a tumour which resulted in the animal being sacrificed due to tumour burden. Tumour penetrance was low with only 1 of 3 mice developing an established tumour. This tumour was not detected until 75 days after MFP inoculation, which is much later than the onset of tumours following injection of an established cell line. The animal was sacrificed 77 days after tumour onset. A second mouse developed an early tumour but this spontaneously regressed.

Due to the poor tumour penetrance rate, we repeated this experiment using a different parental tumour but in this experiment we used $2*10^6$ cells to inoculate the fourth MFP of 7 14-week old FVB mice. Again tumour penetrance rate was disappointing with only 1 of 7 (14%) mice developing an established tumour at 63 days post inoculation. The tumour experienced extremely rapid growth and the animal was sacrificed 7 days later due to tumour burden. A further 4 mice developed early tumours but these spontaneously regressed after a median of 15.5 days (range 7-42 days).

H and E sections of the resulting tumours demonstrated preservation of the parental tumour's nodular super-structure and stromal content, which was more reflective of that seen in the parental model (Figure 5.3). We used IHC with a Ki67 antibody to confirm these were highly proliferative tumours. However, unlike the MNP 145 LU tumours, we were able to demonstrate continued HER2 expression using IHC.

Histological examination of a single section of lung tissue revealed no evidence of lung metastases, although the small numbers of tumour bearing mice make it difficult to draw any firm conclusions about the potential of these tumours to metastasize.

In summary, inoculation of freshly dissociated MMTV-NIC PTEN$^{+/-}$ tumours generated tumours with similar histomorphological features to the parental GEMM. However, poor tumour penetrance was a major obstacle to using this approach.

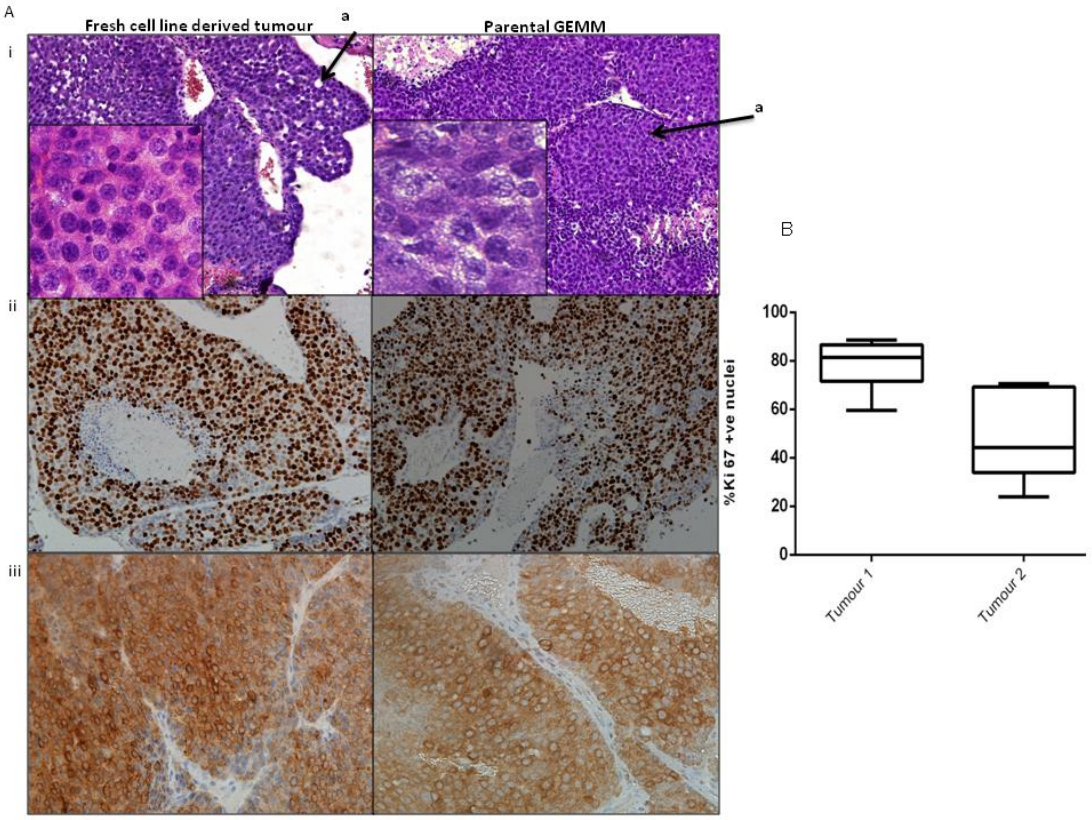

Figure 5.3- Inoculation of dissociated MMTV-NIC PTEN$^{+/-}$ tumours generated tumours with similar histomorphology to the parental GEMM tumours. Ai: Representative H and E images showing highly cellular nodules (a) in both GEMM and dissociated MMTV-NIC PTEN$^{+/-}$ tumours. Main image mag x20, insert mag x40. Aii: Representative images of paraffin embedded sections stained with a Ki67 antibody demonstrating highly proliferative nature of tumours (n=5, mag x20). Aiii: Representative images of paraffin embedded sections stained with a HER2 antibody confirming preserved HER2 expression in dissociated MMTV-NIC PTEN$^{+/-}$ tumours (n=5, mag x40). B: Box whisker plot analysis of percentage of nuclei positive for Ki67 in dissociated MMTV-NIC PTEN$^{+/-}$tumours.Ki67 images analysed using ImmunoRatio software to calculate percentage nuclei positive for Ki67 in six low power fields (mag x20) per tumour.

5.3 Use of MMTV-NIC PTEN$^{+/-}$ tumour fragments to generate mammary tumours

Although freshly harvested and dissociated MMTV-NIC PTEN$^{+/-}$ tumours remained tumourigenic when transplanted into syngeneic hosts, the high frequency of spontaneous tumour resolution made this approach unfeasible in further experiments. To try and preserve the structure of the mature tumour structure without the potentially damaging effects of the collagenase treatment, we decided to use fragments derived from mature MMTV-NIC PTEN$^{+/-}$ tumours to generate mammary tumours in syngeneic hosts. This approach has previously been successfully used with other GEMMs [308], [309] [69].

5.3.1 Optimization of fragment cryopreservation

In order to minimise the stock of recipient mice required, we opted to cryopreserve fragments following harvesting. Fragments were then defrosted and transplanted when a suitable cohort of recipient mice was available.

Two separate cryopreservation protocols have previously been used in the lab. To compare the two protocols, a single MMTV-NIC PTEN$^{+/-}$ tumour was harvested, washed in 70% ethanol and PBS and then cut into 2 mm fragments. Half the fragments (original protocol) were frozen at -80^{0}C in freezing mix (90% FBS, 10% DMSO). The remaining 50% of fragments (modified protocol) were re-suspended in PBS and centrifuged at 450 x *g* for 1 minute. The supernatant and any suspended material, comprising fat and fibrous tissue, were removed. The remaining fragments underwent step-rate freezing in 50:50 DMEM: freeze mix. At the time of surgery, both sets of fragments were defrosted and washed in PBS prior to transplantation into the fourth MFP of 6 15-week old FVB mice. Mice were monitored twice weekly for tumour onset and growth. Animals were sacrificed once tumours reached a maximum of 1.5 cm in any single direction. Tumour onset was defined as the development of a measurable tumour. OS was measured from the time of tumour onset to the time of sacrifice. Tumour penetrance rate was defined as the percentage of mice developing a tumour which resulted in the animal being sacrificed due to tumour burden.

We observed an increased tumour penetrance rate using the modified protocol. Of 6 mice which received fragments prepared using the modified protocol, 4 (66.6%) developed tumours with a median onset of 18 days following surgery. In comparison, only 1 mouse (16.6%) developed a tumour from a fragment prepared using the original protocol. This tumour did not become measurable until 153 days following surgery. The small number of tumours generated, particularly using the original protocol, makes it difficult to draw any firm conclusions regarding the impact of cryopreservation technique on subsequent tumour latency or growth rate. However, the results of this experiment suggest that, possibly unsurprisingly, once a tumour is established, further progression is not dependent on the method of cryopreservation (Figure 5.4). The median OS of mice bearing tumours derived from fragments prepared using the modified protocol was 117.5 days compared to 86 days for the single mouse with a fragment prepared using the original protocol.

The improved penetrance rate seen with the modified protocol was likely due at least in part to the slower freezing rate as it reduced the risk of intracellular ice crystal formation and subsequent cell trauma [310]. However, despite the random allocation of fragments between the 2 protocols, it was not possible to exclude variations in fragment composition as an explanation for the differing penetrance rates. This was a relatively small study, which we have not repeated, making it difficult to conclusively determine that the modified protocol was superior to the original protocol. However, our preliminary data does strongly suggest that the modified protocol is at least as efficacious as the original protocol and therefore we have continued to use this approach in all further experiments.

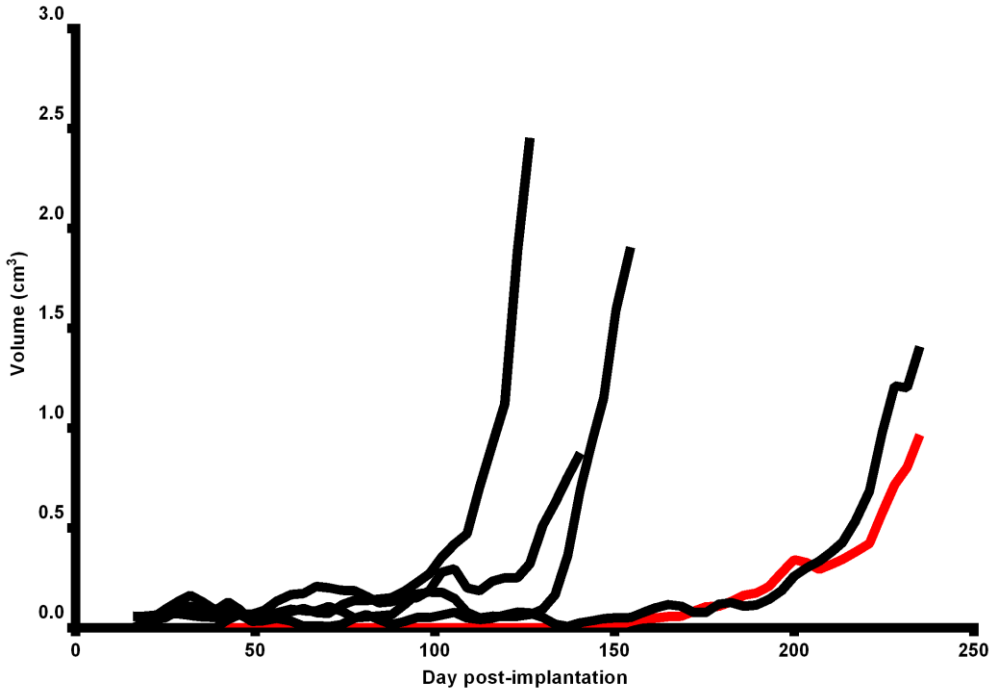

Figure 5.4- Growth curve of fragment derived tumours following original (red data line) and modified cryopreservation (black data lines) protocols. The efficacy of different cryopreservation protocols was compared using fragments derived from the same mature MMTV-NIC PTEN$^{+/-}$ tumour. Fragments from both protocols were transplanted into fourth MFP of 6 FVB mice. Mice were monitored twice weekly for tumour development and growth. Mean volume calculated from 2 successive readings is plotted against time since fragment implantation.

5.3.2 Determining reproducibility of MMTV-NIC PTEN$^{+/-}$ fragment transplantation

To determine the reproducibility of transplantation results, fragments from different parental tumours were transplanted into FVB recipients.

We observed considerable variations in tumour penetrance rates in the different experiments across this series (Table 5.1). The median tumour penetrance across all experiments was 40% (range 0-80%). Tumour latency was defined as the interval between fragment transplantation and the development of measurable disease. In transplanted fragments which successfully established a tumour, the median latency was 23.0 days (range 14-76 days) with no statistical difference between the latency interval of tumours generated within different experiments (p=0.38, single way ANOVA). Transplanted tumours recapitulated the variable growth rate seen in the parental model with individual tumours generated from the same parental tumour displaying marked differences in growth rates (Figure 5.5). However, there was no statistical difference in the OS of mice bearing tumours generated in different experiments (p=0.11, single way ANOVA) and this was most likely attributable to the wide variations in OS observed within individual experiments. Examination of a single H and E section per mouse revealed limited metastatic spread to the lungs in only 2 animals (4.1%) in the entire experimental series (**Dr. J. Loane, consultant pathologist**). In this limited data set there did not appear to be any relationship between the presence of metastases in the parental GEMM and fragment recipients although using a single lung section to characterize metastatic spread within the entire organ is likely to have resulted in a substantial under-estimation of the true incidence of lung metastases within both the parental GEMM and tumour fragment recipients. Whilst, further characterization using a greater number of lung sections per mouse would be informative, this initial data does suggest that, similarly to the parental GEMM, the growth rate of transplanted tumours was too rapid to permit the development of established metastatic disease prior to the time of sacrifice.

Experiment	N	% penetrance (n)	Median tumour latency in days (range)	Median OS in days (range)	% animals with lung mets (n)
1	6	66.4 (4)	14 (14-14)	38.5 (28-49)	14.3 (1)
2	6	0.0 (0)	-	-	-
3	6	66.4 (4)	20 (16-44)	114 .0(109-217)	14.3 (1)
4	6	14.3 (1)	61.0	101.0	0.0
5	5	40.0 (2)	28 (21-35)	87.5 (63-112)	0.0
6	4	25.0 (1)	35.0	49.0	0.0
7	8	50 (4)	33 (28-38)	75.0 (11-142)	0.0
8	5	80 (4)	23 (23-72)	40.0 (25-140)	0.0
9	3	0 (0)	-	-	-

Table 5.1- Outcomes of a series of MMTV-NIC PTEN$^{+/-}$ fragment transplant experiments. Fragments were harvested from different parental MMTV-NIC PTEN$^{+/-}$ tumours and transplanted into FVB mice. Mice were monitored twice weekly for tumour onset and growth for a minimum of 150 days. Tumour penetrance was defined as the percentage of mice which developed a tumour, which ultimately required the animal to be sacrificed. Tumour latency represents the interval between tumour transplantation and development of measurable tumour. Median OS was measured from the development of a palpable tumour to time of sacrifice.

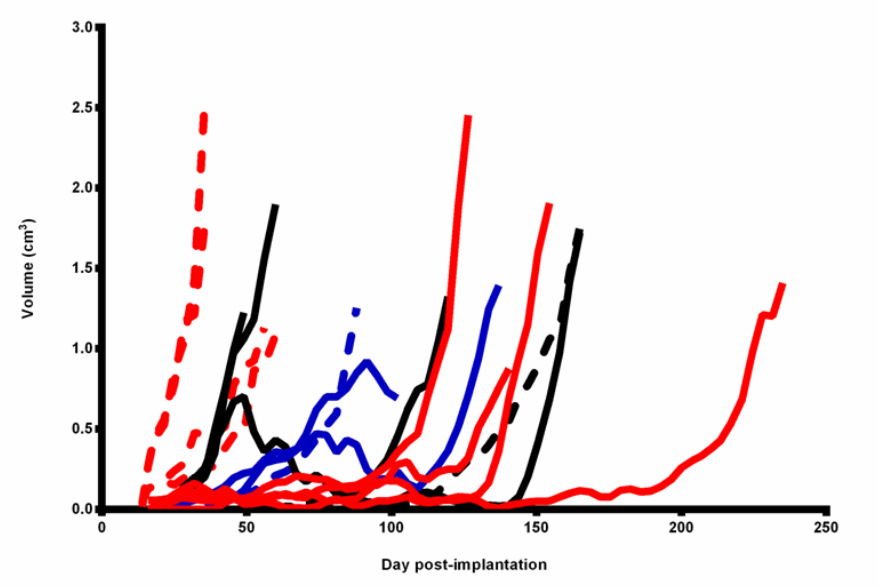

Figure 5.5- Comparison of growth curves of fragment derived tumours from different experiments. Fragments were harvested from different parental MMTV-NIC PTEN$^{+/-}$ tumours and transplanted into FVB mice. Mice were monitored twice weekly for tumour onset and growth. Mean volume calculated from 2 successive readings is plotted against time since fragment implantation. Tumours derived from the same parental tumour are denoted by curves of same colour and pattern.

5.3.3 Further characterization of fragment derived tumours

Examination of H and E sections from fragment derived tumours revealed that, similarly to the parental GEMM, they were comprised of highly cellular nodules (Figure 5.6). Examination by an experienced breast pathologist confirmed the presence of highly mitotic, grade 3 carcinomas with frequent areas of necrosis, which were indistinguishable from tumours developed in the parental GEMM (**Dr. J. Loane**). To ensure preservation of tumour histomorphology during transplantation, sections of fragment derived tumours and the parental tumour from which they were derived were stained for both HER2 and Ki67. Both parental and fragment derived tumours demonstrated inter- and intra-tumoural heterogeneity in HER2 expression. Consistent with the frequent observation of mitotic bodies on H and E sections, a high percentage of nuclei stained positively for Ki67 in both parental and fragment derived tumours.

Of the 3 methods used to generate single mammary tumours from the MMTV-NIC PTEN$^{+/-}$ model, fragment transplantation appeared the most promising and we therefore decided to use this approach in all further experiments.

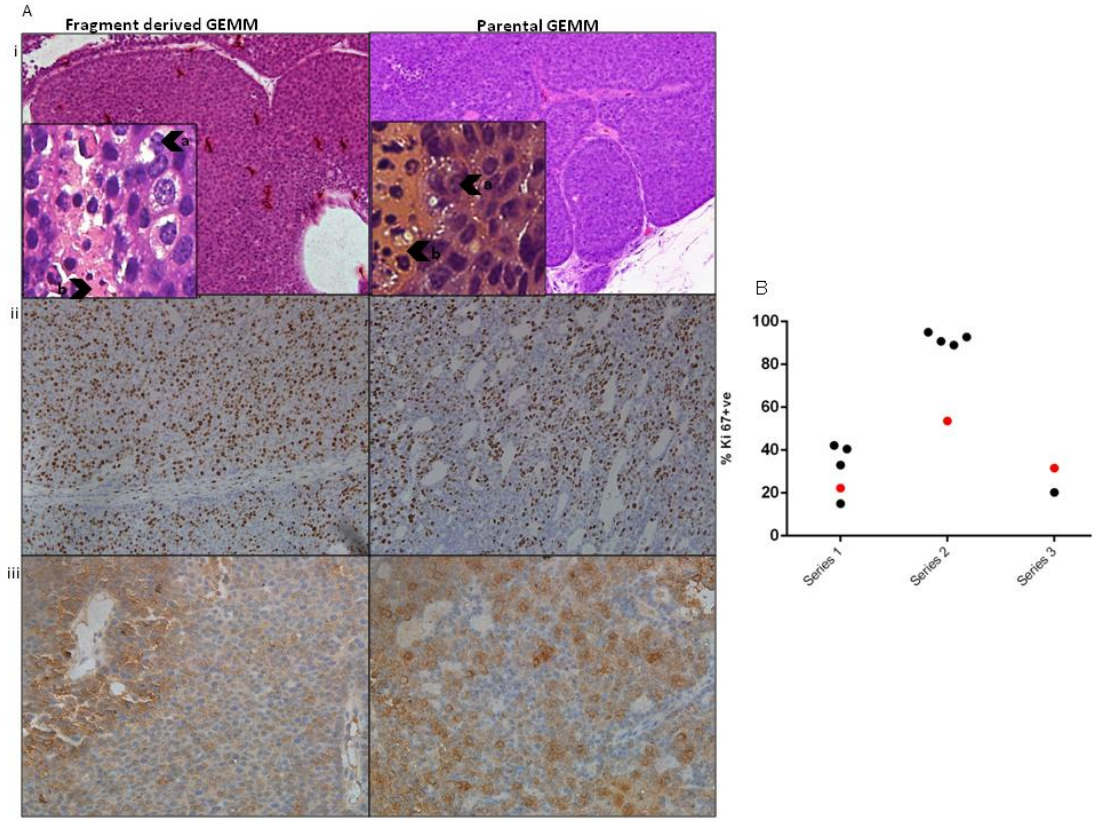

Figure 5.6- Transplantation of MMTV-NIC PTEN$^{+/-}$ fragments generated tumours which were indistinguishable from the parental GEMM tumours. Ai: Representative H and E images demonstrating that both GEMM and fragment derived tumours were comprised of highly cellular nodules. Tumours were highly proliferative and contained multiple cells undergoing mitosis (a). Both GEMM and fragment derived tumours contained frequent areas of necrosis (b). Main image mag x20, insert mag x40. Aii: Representative images of paraffin embedded sections stained with a Ki67 antibody demonstrating highly proliferative nature of tumours (n=12, mag x20). Aiii: Representative images of paraffin embedded sections stained with a HER2 antibody demonstrating heterogenous nature of HER2 expression in both GEMM and fragment derived tumours (n=5, mag x40). B: Graph of percentage nuclei positive for Ki67 in 3 sets of matched parental (red data point) and fragment derived tumours (black data points). Ki67 images analysed using ImmunoRatio software to calculate percentage nuclei positive for Ki67 in six low power fields (mag x20) per tumour. Series 1: p= 0.04, series 2: p=0.08, series 3: p=0.03 (Mann Whitney U test).

5.4 Exploring factors predictive of tumour penetrance

Tumour fragment transplantation allowed the generation of tumours, which recapitulated the features of the parental model. However, the variability in tumour penetrance rates was a major limitation. Identification of factors predictive of poor penetrance would help to reduce the number of recipient animals needed and expedite future experiments. We therefore sought to explore factors which might identify a parental tumour as being unsuitable for generating fragments.

5.4.1 Growth characteristics of parental tumour

Parental tumours were arbitrarily classified as highly penetrant if ≥ 40% of transplanted fragments generated a viable tumour. Tumours with a penetrance rate of <40% were classified as poorly/non-penetrant.

We initially examined the characteristics of the parental GEMM tumour from which the fragments were derived to determine if these influenced penetrance rates. Tumours arising in the first MFP were described as having a cervical origin whilst those originating in the second and third MFPs were described as axillary and those from the fourth and fifth MFP as inguinal. The site of origin of the parental tumour alone was not sufficient to predict tumour penetrance (Table 5.2). We then considered the latency period of the parental tumour to determine whether tumours which developed at a younger age conferred a more aggressive phenotype resulting in improved penetrance rates. We observed no difference in the latency interval between highly and poorly/non- penetrant tumours. The median age of tumour onset in highly penetrant tumours was 78 days compared to 66.5 days in poorly/non-penetrant tumours ($p=0.16$, Mann Whitney U test). Finally, we used OS from the time of parental tumour development as a surrogate for growth rate. All parental animals were sacrificed at a maximum of 28 days following tumour onset, irrespective of the size of the tumour. When the maximum tumour dimension <1.5 cm at the time of sacrifice, OS was defined as > 28 days. The median OS in highly penetrant tumours was 28 days compared to 26 days in poorly/non penetrant tumours.

To explore whether penetrance rates could be influenced by systemic factors in the donor animal, we generated fragments using cervical and axillary tumour from the same animal (experiments 6 and 7). Fragments from the cervical tumour were poorly penetrant whilst those from the axillary tumour were highly penetrant suggesting that systemic features of the donor-animal were not responsible for the variable penetrance rates observed. This is consistent with previously published data using the MMTV-PyMT driven GEMM, where axillary and inguinal tumours from the same animal demonstrated different growth rates and different genetic signatures [311].

To explore whether the recipient animal's characteristics could influence fragment transplant outcomes, we transplanted a second set of fragments generated during experiment 3 into a further cohort of FVB mice. Both experiments demonstrated similar penetrance rates (66.6% vs. 50%). There was also no statistical difference between the median latency interval of fragment derived tumours in the 2 experiments (20 vs. 33.5 days, p=0.16, Mann Whitney U test).

In summary, these experiments suggest that the fragment transplant outcomes are primarily dependent on, as of yet unidentified, parental tumour characteristics and are not influenced by systemic host or recipient-animal characteristics.

Experiment	Tumour penetrance	Origin of parental tumour	Parental tumour latency (days)	OS of parental tumours (days)
1	High	Inguinal	98	7
2	Poor	Inguinal	61	24
3	High	Inguinal	78	10
4	Poor	Inguinal	72	>28
5	High	Cervical	74	>28
6	Poor	Cervical	78	>28
7	High	Axillary	78	>28
8	High	Axillary	71	>28
9	Poor	Cervical	61	>28

Table 5.2- Parental tumour growth characteristics did not predict for tumour fragment penetrance rate. Parental tumours classified as highly or poorly/non- penetrant if ≥ 40% or <40% fragments generated a viable tumour respectively. Tumour latency represented the interval between tumour transplantation and development of measurable tumour. Median OS measured from the development of a palpable tumour to time of sacrifice.

5.4.2 Histomorphology of parental tumours

We used IHC to further explore parental factors which might influence the outcomes of tumour fragment transplantation. Using Ki67, we found all tumours were highly proliferative. There was no statistical difference in the percentage of nuclei which stained positively for Ki67 between poorly/non-penetrant and highly penetrant tumours ($p=0.60$, Mann Whitney U test, Figure 5.7). HER2 expression was also unchanged between highly and poorly/non-penetrant tumours. The use of non-transplanted tumour regions to predict fragment phenotype is clearly a limitation of these experiments, particularly as these are such heterogeneous tumours. Future experiments may be improved by selection of adjacent tumour tissue for assessing phenotype and generation of fragments to help minimise the effects of intra-tumoural heterogeneity.

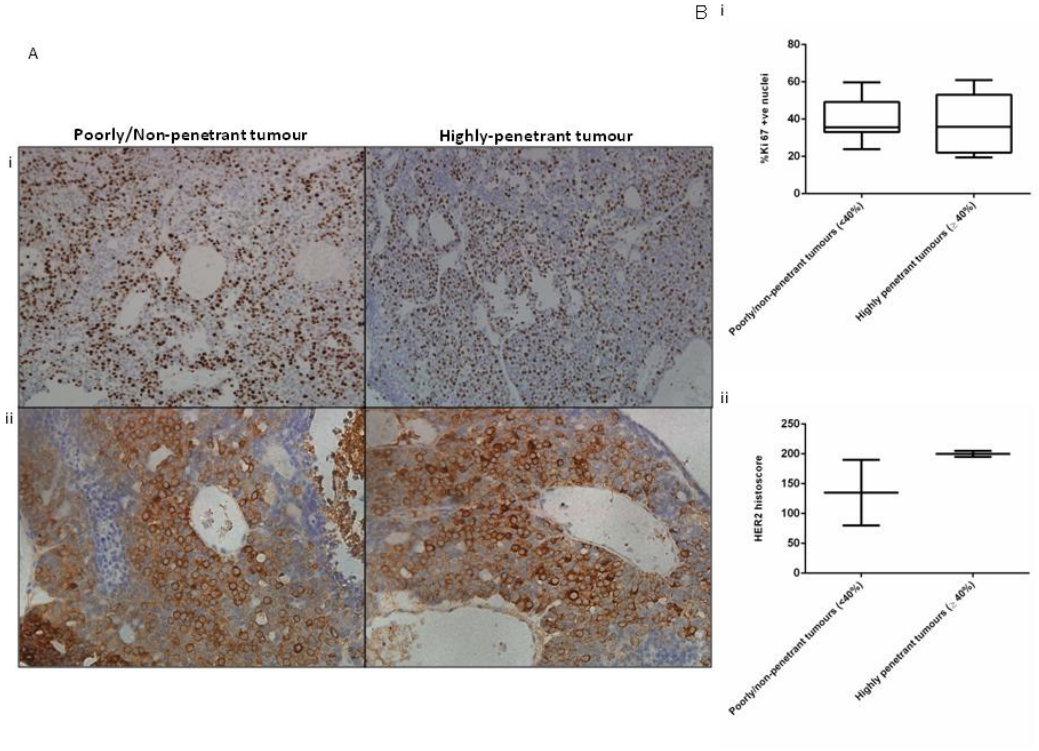

Figure 5.7- Ki67 and HER2 expression was unaltered between poorly/non-penetrant and highly-penetrant tumours. Ai: Representative images of paraffin embedded sections from both poorly/non-penetrant and highly-penetrant tumours stained with a Ki67 antibody (mag x20). Aii: Representative images of poorly/non-penetrant and highly-penetrant paraffin embedded sections stained with a HER2 antibody (mag x40). Bi: Quantification of percentage nuclei positive for Ki67 in both poorly/non-penetrant (n=2) and highly-penetrant tumours (n=2, p=0.60, Mann Whitney U test). Ki67 images analysed using ImmunoRatio software to calculate percentage nuclei positive for Ki67 in six low power fields (mag x20) per tumour. Bii: Membranous HER2 histoscore of poorly/non-penetrant (n=2) and highly penetrant (n=2) tumours. Histoscore determined by calculating the sum of the product of percentage cells stained by the intensity graded from 0-3, where 1 =weak, 2=moderate and 3=strong staining (histoscore = (% *1) + (% *2) + (% *3)).

5.4.3 Effect of vascularisation in the parental tumour on penetrance rate

Establishment of an independent vascular supply is a critical step in tumour progression. We frequently identified macroscopic areas of tumour necrosis within MMTV-NIC tumours, suggesting regions of these tumours were under-perfused. We performed IHC using a CD31 antibody, a marker of vasculature [285], to determine whether poor parental tumour vascularisation resulted in hypoxically stressed and non-viable tumour fragments. Due to the huge variation in the cross sectional area of individual blood vessels identified, we calculated the mean area occupied by blood vessels in 6 low-powered fields (mag x20). We observed non-statistically significant variations in the extent of vascularisation between individual tumours ($p=0.1$, one-way ANOVA) (Figure 5.8). However, no difference in the extent of vascularisation was identified between poorly/non-penetrant and highly penetrant tumours ($p= 0.37$, Mann Whitney U test).

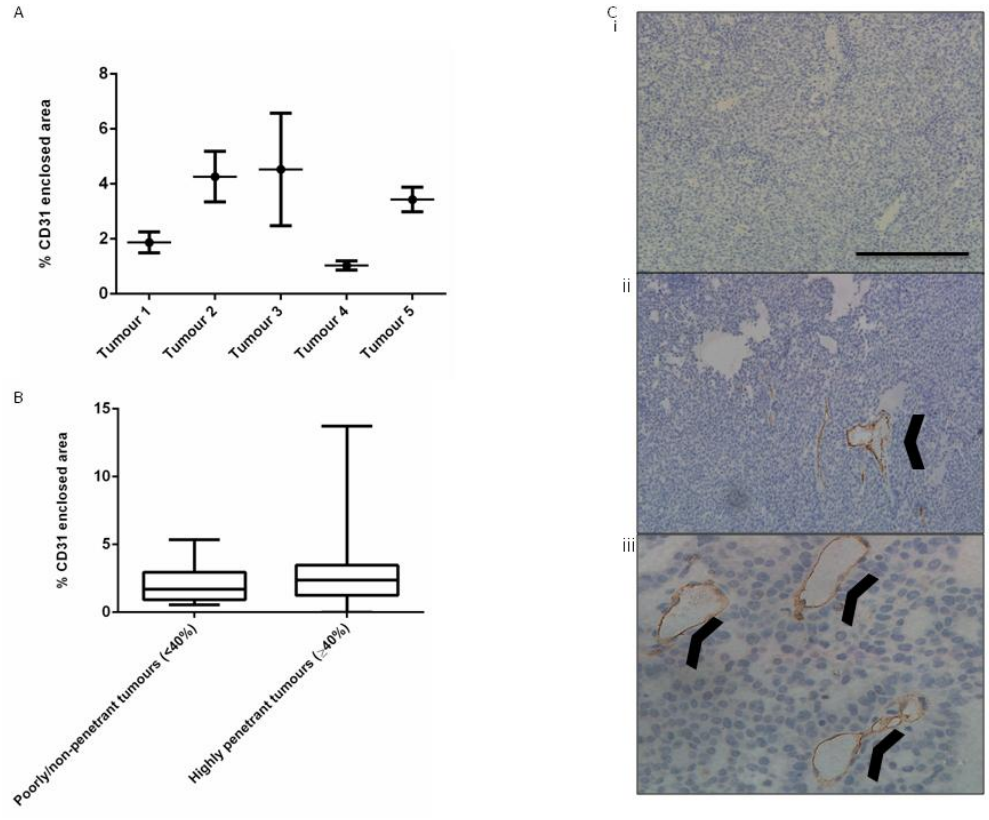

Figure 5.8- CD31 expression was unaltered between poorly/non-penetrant and highly-penetrant tumours. IHC was performed on formalin fixed paraffin embedded tumours with CD31 primary antibody. Images analysed using Image J software to calculate the sum of the area within blood vessel lumens as indicated by CD31 positive staining in 6 low powered fields per tumour. A: Variation in extent of vascularisation in panel of parental tumours. Mean value ± SEM depicted (p=0.10, one-way ANOVA). B: Box-whisker plot analysis of extent of vascularisation in poorly/non-penetrant (n=2) and highly penetrant (n=3) tumours (p=0.37, Mann Whitney U test). Ci: Negative control comprising of MMTV-NIC PTEN$^{+/-}$ tumour section incubated in the absence of CD31 antibody. Scale bar represents 100 µm. Cii: Representative image of IHC with CD31 antibody on MMTV-NIC PTEN$^{+/-}$ tumour (mag x20). Arrowhead denotes representative blood vessels. Ciii: High powered view of CD31 positive blood vessels (mag x40).

5.4.4 Effect of HIF1α on tumour penetrance

As the extent of vascularisation was unchanged between highly and poorly/non-penetrant tumours, we decided to explore whether differences in the ability to adapt to hypoxia were responsible for the variable penetrance rates observed. In human breast cancer, hypoxia, as measured by Hypoxia Inducible Factor 1α (HIF1α) expression, is associated with early relapse, development of widespread metastases and reduced OS [312]. In addition to hypoxia, HIF1α expression may be increased following loss of tumour suppressor genes, such as PTEN, increased expression of receptor tyrosine kinases, such as EGFR, and hyperactivation of intracellular signalling pathways, such as Akt and Src. Following its activation, HIF1α translocates to the nucleus and dimerizes with HIF1β to form HIF1. HIF1 regulates a range of pro-survival responses that select for an increasingly aggressive and invasive cancer phenotype [313].

Given the high expression of HER2 and hyper-activation of the Akt pathway, it was unsurprising that a panel of parental tumours all stained strongly for nuclear HIF1α when IHC was performed (Figure 5.9). However, there was no statistical difference in nuclear histoscore when highly and poorly/non-penetrant tumours were compared (p= 0.14, Mann Whitney U test).

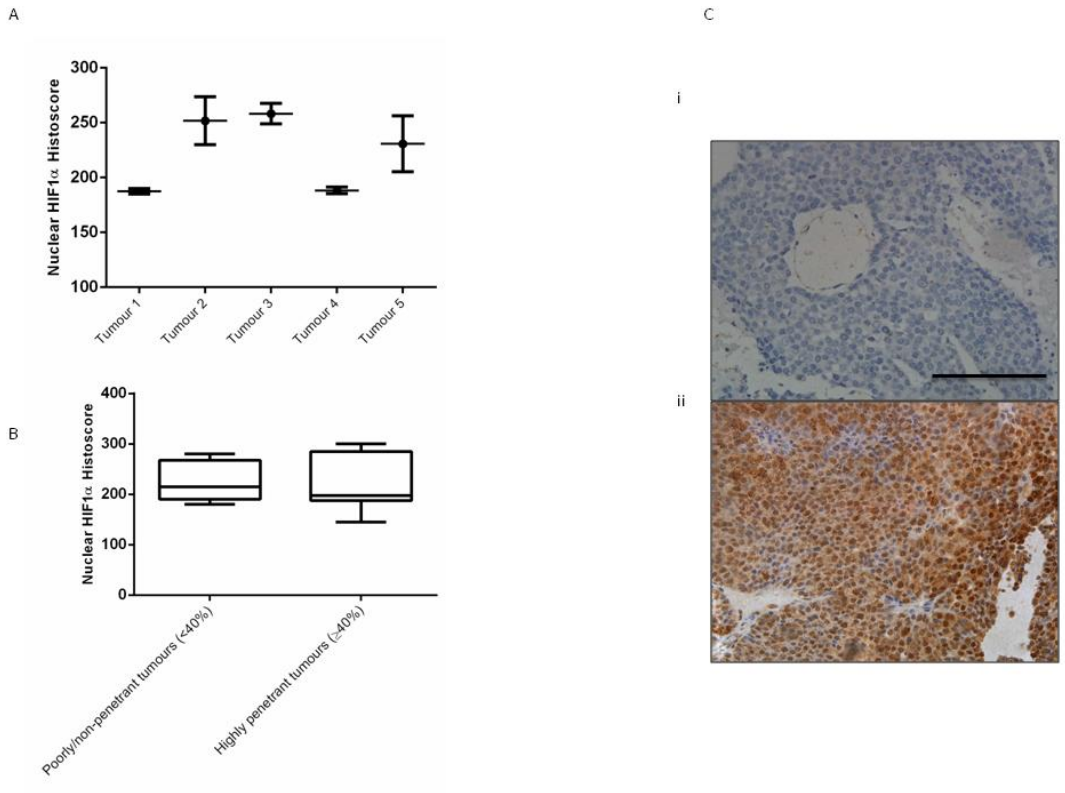

Figure 5.9- HIF1α expression was unaltered between penetrant and poorly/non-penetrant tumours. IHC was performed on formalin fixed paraffin embedded tumours with HIF1α primary antibody. Nuclear histoscore was determined using 6 representative high powered fields (x40 mag) and calculating the sum of the product of percentage cells stained by the intensity graded from 0-3 (histoscore = (% *1)+ (% *2) + (% *3)). A: Variation in expression of HIF1α in a panel of 5 parental tumours. Mean value ± SEM depicted (p=0.08, one way ANOVA). B: Box-whisker plot analysis of HIF-1α in poorly/non-penetrant (n=2) and highly penetrant (n=3) tumours (p=0.14, Mann Whitney U test). Ci: Negative control comprising of MMTV-NIC PTEN$^{+/-}$ tumour section incubated in the absence of HIF1α antibody. Scale bar represents 100 μm. Cii: Representative image of IHC staining with HIF1α antibody on MMTV-NIC PTEN$^{+/-}$ tumour. (Mag x40).

5.4.5 The effect of the immune system on tumour penetrance rate

In all the previously described experiments, we observed instances of spontaneous tumour resolution following initial growth. The MMTV-NIC model was generated on an FVB background and therefore fragment transplantation was classified as syngeneic. However, prior to transplantation, recipient animals had not been exposed to Cre-recombinase or the rat-derived HER2 transgene used in this model and therefore an immune response against epitopes on these proteins could be mounted. We hypothesised that increased immunogenicity might explain the low penetrance rates observed with some of these tumours.

To determine the effect of the immune system on tumour penetrance, fragments from a single MMTV-NIC PTEN$^{+/-}$ tumour were transplanted into the fourth MFP of either 6-week old immunocompetant FVB mice (n=5) or athymic nude mice (n=5). Tumour penetrance was high (80%) in both cohorts. However, the rate of tumour growth was slower in the athymic mice with a non-statistically significant delay in tumour onset (Figure 5.10). Median tumour onset was 33.5 days (range 27-44 days) in athymic mice compared to 23.0 days (range 23-72 days) in the FVB recipients (p=0.30, Mann Whitney U test). There was also a marked increase in OS from 42.5 days (range 25-139 days) in FVB recipients to 108.5 days (range 60-157 days) in athymic mice (p= 0.11, Mann Whitney U test). The lack of statistical significance was likely due to both the small cohort sizes used and the wide variation in OS seen within cohorts in this experiment.

To determine whether the reduced growth rate seen in the athymic cohort was due to the strain of the recipient animals or a consequence of impaired immunity, we transplanted fragments from a second parental tumour into either FVB mice (n=6) or age matched CD-1 nude mice (n=4). Animals were monitored twice weekly for tumour development and on development of established tumours FVB recipients were entered into drug-response studies (see section 6.1). Again tumour penetrance was high in both cohorts with 100% of the CD-1 nude mice and 66.7% of FVB mice developing established tumours. As in the previous experiment, we observed a delay in tumour development in CD-1 nude immunocompromised recipients compared to the FVB cohort. Median tumour onset in CD-1

nude mice was 32.0 days (range 20-48 days) compared to 21.5 days (range 16-37 days) in FVB mice (p=0.31, Mann Whitney U test, Figure 5.10B).

Coincidently, both parental tumours used in these experiments were highly penetrant in both immunocompetent and immunocompromised cohorts. It is therefore not possible to determine whether initiation of an early immune response against the growing tumour may have accounted for the low penetrance rates observed in some of our earlier experiments. However, the marked delay in tumour onset seen in both immunocompromised cohorts was striking and may suggest that an activated immune system plays an important role in tumour progression.

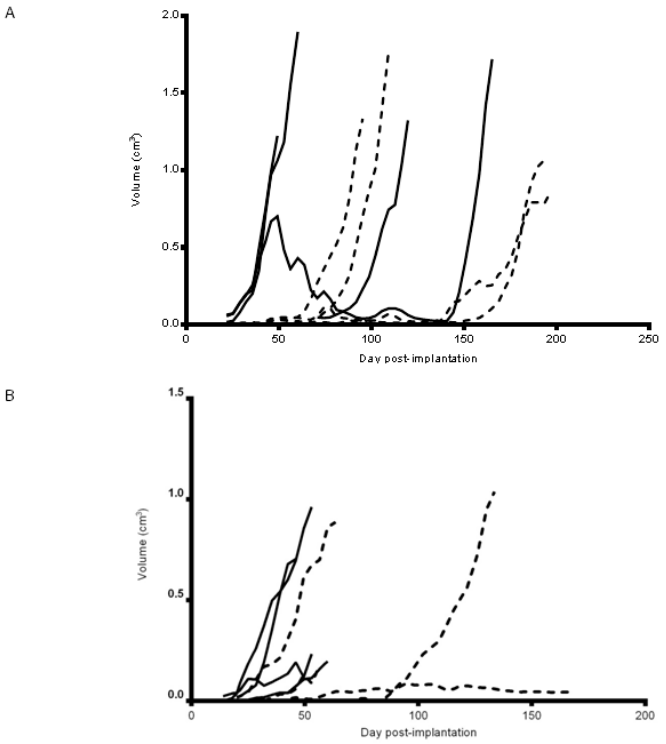

Figure 5.10- Tumour growth was delayed in athymic and CD-1 nude tumour-fragment recipients. Tumour fragments were transplanted into the fourth mammary fat pad of cohorts of FVB mice and immunodeficient mice. Mice were monitored twice weekly for tumour onset and progression. Mean volume calculated from 2 successive readings was plotted against time since fragment implantation. A: Growth curve of fragment derived tumours in FVB mice (solid data line) and athymic nude mice (dashed data line). B: Growth curve of fragment derived tumours in FVB mice (solid data line) and CD-1 nude mice (dashed data line).

5.4.6 The impact of PTEN status on fragment transplantation

5.4.6.1 Exploring the impact of PTEN genotype on tumour fragment transplantation

PTEN is an important tumour suppressor gene [314] and therefore its expression may impede successful generation of fragment-derived tumours. To explore this further, fragments harvested from mature MMTV-NIC PTEN $^{FL/+}$ tumours were transplanted into the fourth MFP of 7-week old FVB mice. This experiment was performed on 3 separate occasions using different parental tumours in each experiment. Mice were monitored twice weekly for tumour onset and growth for at least 180 days following fragment transplant. Overall, only 1 tumour was generated from 21 fragment transplants (Table 5.3). Generation of MMTV-NIC PTEN $^{FL/+}$ transplants was therefore not viable and all future experiments (see chapter 6) have focused on MMTV-NIC PTEN$^{+/-}$ transplants.

5.4.6.2 Determining the effect of PTEN protein expression on tumour penetrance rates

Previous studies have demonstrated that over 50% of MMTV-NIC PTEN$^{+/-}$ develop LOH for PTEN [272]. We therefore decided to explore whether MMTV-NIC PTEN$^{+/-}$ tumours which had lost the second PTEN allele were more readily transplantable than those which retained it. Using IHC, we demonstrated that PTEN expression was not detectable in the majority of both highly and poorly/non-penetrant tumours. All tumours contained small foci of cells which had retained PTEN expression but its expression was too restricted to permit further quantification (Figure 5.11). This data appears to suggest that PTEN expression was not a critical factor in determining tumour penetrance, although the use of non-transplanted material to determine the phenotype of the fragments means we cannot exclude residual PTEN expression within non-penetrant fragments.

Experiment	N	% penetrance (n)
1	9	0 (0.0)
2	6	1 (16.7)
3	6	0 (0.0)

Table 3.3- Transplantation of MMTV-NIC PTEN $^{FL/+}$ fragments failed to generate viable tumours. Fragments from 3 MMTV-NIC PTEN $^{FL/+}$ tumours were transplanted into the fourth MFP of FVB mice. Mice were monitored for tumour growth for at least 180 days.

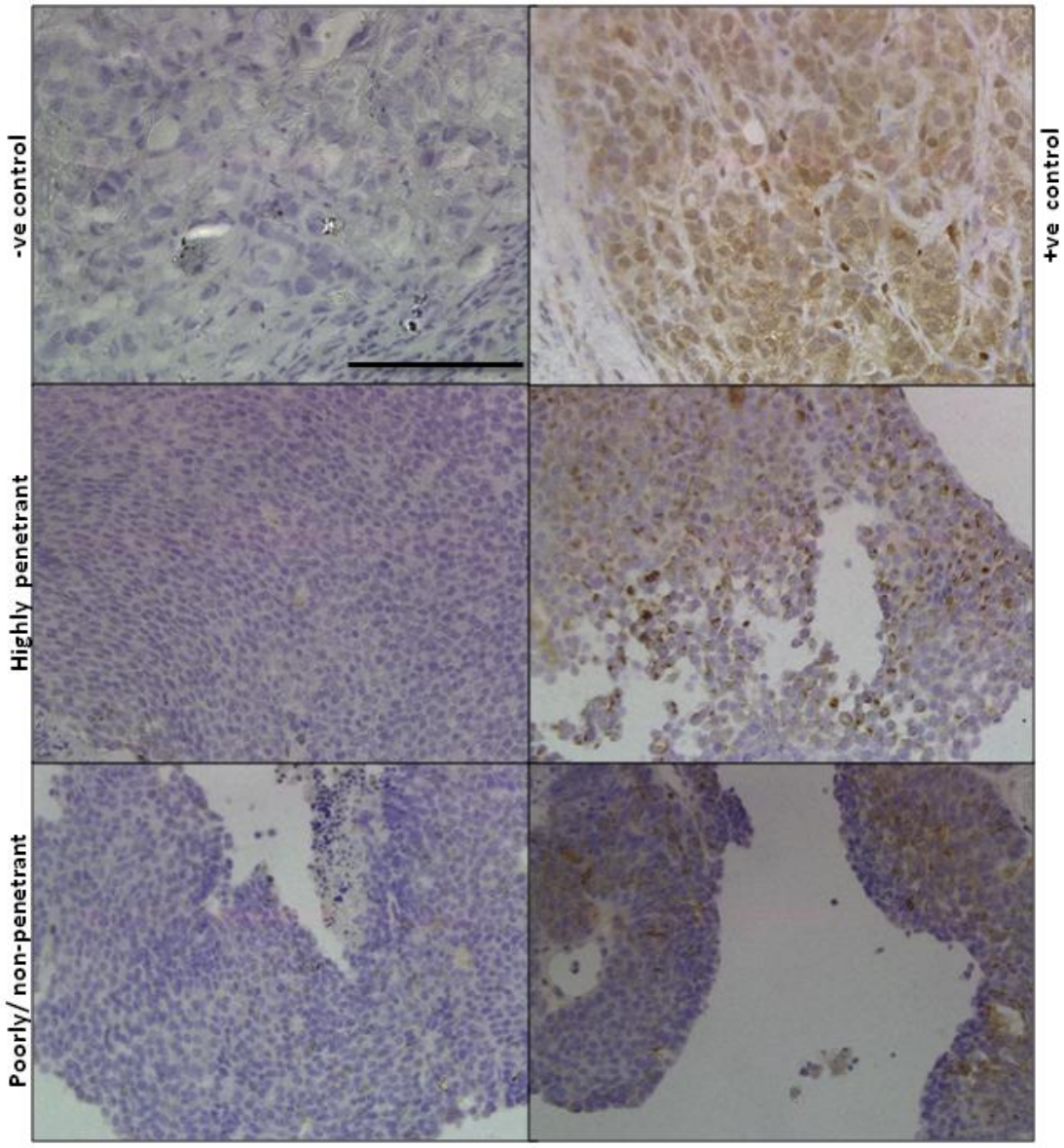

Figure 5.11- Representative images of PTEN expression in highly and poorly/non-penetrant tumours. IHC performed with a PTEN antibody on highly (n=3) and poorly/non-penetrant (n=3) tumours. Negative control consisting of MMTV-NIC PTEN$^{+/-}$ tumour section incubated in the absence of primary antibody. Positive control comprising section of BT474 xenograft stained with PTEN antibody. Mag x40. Scale bar represents 100 µm.

5.5 Serial transplantation of tumour fragments

As we had been unable to identify factors predictive of tumour penetrance, we decided to explore whether existing fragment-derived tumours could be used successfully to generate further fragments for transplantation. To determine the feasibility of serial transplantation, 3 fragment-derived tumours, each generated from a different, highly-penetrant parental tumour, were used to produce further fragments. Serial transplantation successfully recapitulated the features of first generation fragment transplantation with high penetrance and variable growth rates observed in all 3 experiments (Table 5.4). Furthermore, by comparing H and E sections and using IHC to stain for HER2 and Ki67 we demonstrated preservation of tumour histomorphology (Figure 5.12). Serial transplantation is therefore potentially a suitable option for increasing stocks of reliably transplantable tumour material thereby facilitating the efficient use of fragment transplantation in future experiments.

Experiment	N	% penetrance	Median latency in days (range)	P Value	Median OS in days (range)	P Value
1A	6	50.0	14.0 (14-14)	-	38.5 (28-46)	0.66
1B	6	66.7	75 .0 (28-117)		64.0 (10-66)	
2A	5	40.0	28.0 (21-35)	0.11	88.5 (65-112)	0.10
2B	5	80.0	62.0 (48-76)		29.5 (24-38)	
3A	8	50.0	33.0 (28-38)	0.10	70.0 (21-142)	0.64
3B	5	40.0	23.5 (20-27)		26 (24-28)	

Table 5.4- Serial transplantation of fragments resulted in cohorts of second generation fragment recipients with a high frequency of tumour development. Heterogeneity of growth characteristics was maintained following second generation transplantation. Fragment-derived tumours from highly penetrant parental tumour (experiments 1A, 2A and 3A) were selected at random and used to generate further fragments for transplant into further cohorts of FVB mice (experiments 1B, 2B and 3B). Animals were monitored twice weekly for tumour onset and development and were sacrificed when tumour burden ≥ 1.5 cm in any direction. Tumour latency was defined as interval between fragment transplantation and development of a measurable tumour. OS was defined from the development of measurable disease until time of sacrifice due to tumour burden. P values calculated using Mann Whitney U test.

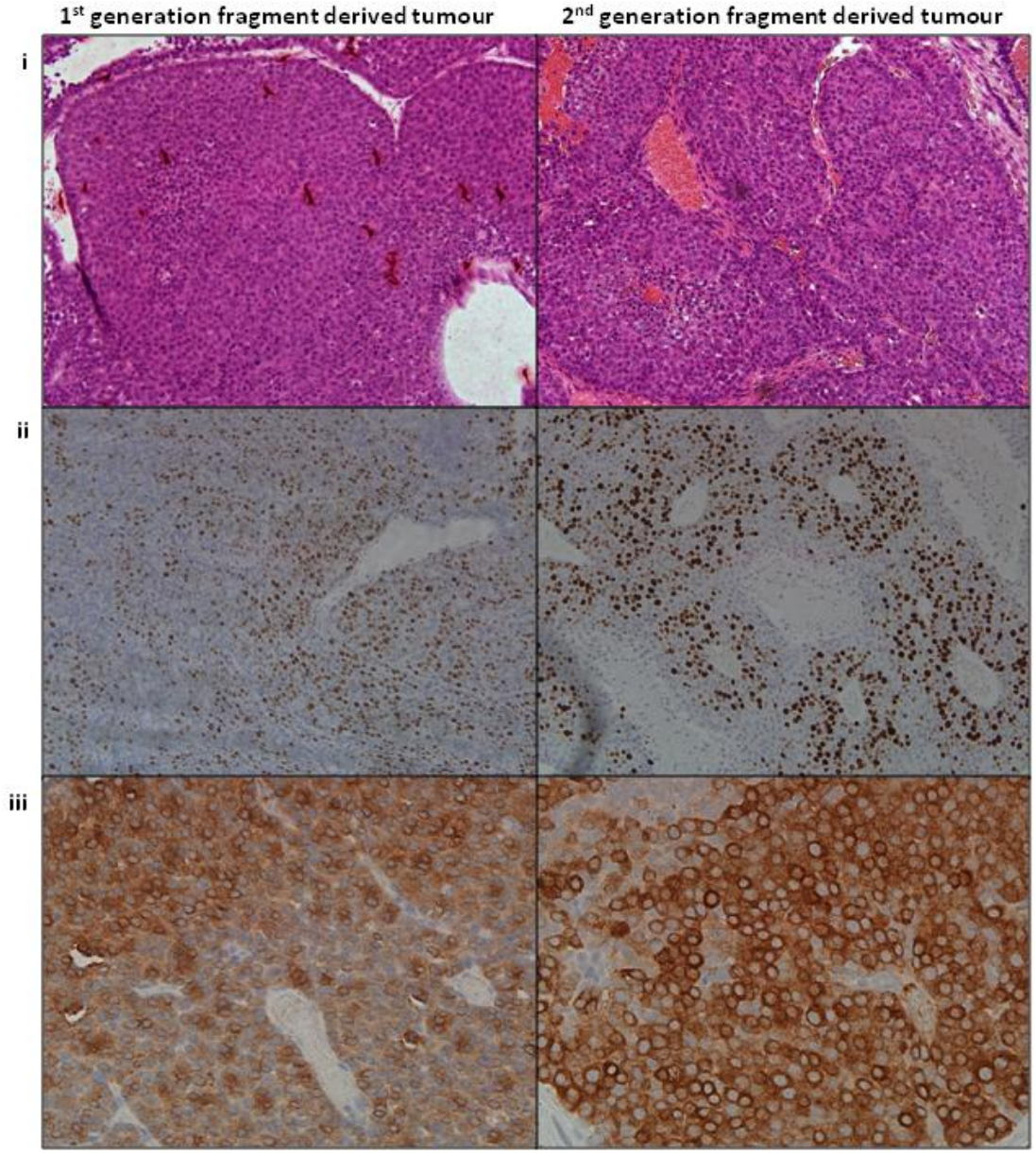

Figure 5.12- Transplantation of second generation MMTV-NIC PTEN$^{+/-}$ fragments generates tumours with preserved histomorphology of first generation transplant. i: Representative H and E images demonstrating preserved tumour morphology between first and second generation derived tumours (mag x20). ii: Representative images of paraffin embedded sections stained with a Ki67 antibody demonstrating highly proliferative nature of tumours (n=3,mag x20). iii: Representative images of paraffin embedded sections stained with a HER2 antibody demonstrating heterogenous nature of HER2 expression in both first and second generation fragment derived tumours (n=3, mag x40).

5.6 Discussion

Whilst the MMTV-NIC model is a useful tool for exploring drug efficacy in primary tumours, it is not suitable for use in studies looking to characterise drug efficacy in metastatic disease or for exploring mechanisms of acquired resistance. There is currently a major unmet need to develop models of metastatic breast cancer as it is not possible to assume that drugs which are active in early breast cancer will also be efficacious in advanced disease as subsets of genes can be differentially regulated between primary and secondary tumours [168]. In addition, preclinical studies have shown that the normal tissue surrounding a tumour is capable of influencing both the tumour's microenvironment and its response to therapy [289] suggesting that metastatic deposits within different organs may also respond differently to treatment. A second urgent priority is the development of physiologically relevant models suitable for studying mechanisms of acquired resistance. Acquired resistance to HER2 targeted therapies is ultimately inevitable in advanced breast cancer. Whilst many different resistance mechanisms have been identified using *in vitro* approaches, very few of these have been successfully corroborated in clinical studies. Studying drug activity in metastatic disease and the development of tumours with acquired resistance to HER2 targeted agents could be facilitated by use of a model with a single mammary tumour, which could be either resected to allow development of established metastases or exposed to cyclical drug treatment to generate resistant tumours. We therefore decided to explore 3 different methods of using the MMTV-NIC model to generate single mammary tumours.

5.6.1 Comparison of methods used for generating single mammary tumours

We initially used one of a panel of established MMTV-NIC PTEN$^{+/-}$ cell lines (MNP145 LU) to generate mammary tumours. We found that MFP injection of this cell line into a cohort of athymic mice resulted in the rapid generation of mammary tumours in all recipients. This was consistent with data previously obtained in the lab, which showed that both MFP and subcutaneous injections of MNP145LU into FVB recipients also resulted in the rapid development of tumours. However, although western blot had previously been used to demonstrate low HER2 expression in the cell line (**L. Balderstone**), we were unable to demonstrate any HER2 expression within the resulting tumours using IHC, precluding the

use of this approach in further experiments using AZD8931. Loss of HER2 expression during *in vitro* culture is common, although other groups have successfully managed to develop cell lines which retained HER2 expression and sensitivity to HER2 directed therapies [315]. The loss of HER2 expression may have been caused by a combination of several factors. Firstly, the lines were generated from whole tumours and therefore contained mixed cell populations. Developing tumours *in vivo* are subjected to continual selection pressure favouring the proliferation of HER2 expressing cells. The removal of this selection pressure during 2D *in vitro* growth results in the outgrowth of cell populations which are best adapted to tissue culture conditions but in this case it may be that these are not the populations which are most reflective of the parental tumour. Secondly, MMTV promoter expression is frequently lost during *in vitro* culture, which might also contribute to the loss of HER2 expression. This could be avoided in the future by supplementation of the media with either hydrocortisone or dexamethasone, which, by binding to the promoter's steroid response element, enhances MMTV transcription (H. Smith, personal communication). Finally, these cell lines are prone to undergoing EMT, which has previously been associated with loss of HER2 expression [167]. Use of 3D tissue culture techniques, which more accurately reproduce *in vivo* growth conditions [316], may help in the future to generate cell lines which more fully recapitulate the characteristics of the original tumour.

We used 2 further approaches to try and overcome the issue of HER2 loss during *in vitro* culture; firstly MMTV-NIC PTEN$^{+/-}$ tumours were harvested and dissociated with collagenase prior to the resulting cell suspension being used to inoculate the MFP of recipient mice and secondly we used mature MMTV-NIC PTEN$^{+/-}$ tumours to generate fragments for transplantation. Both methods resulted in the generation of tumours which continued to express HER2. A major benefit of both of these approaches over the use of established cell lines to generate further tumours was their ability to recapitulate the tumour microenvironment. Although breast cancer is classically considered to be a disease originating in epithelial cells, it is increasingly clear that other cell populations (including fibroblasts, myofibroblasts, endothelial cells and immune cells) within the tumour microenvironment are capable of influencing tumour progression. Comparison of normal and tumour associated stromal tissue has revealed multiple genetic and epigenetic changes affecting a wide variety of genes, including those implicated in invasion, angiogenesis and growth factor production. Many of these mutations develop early in tumour development and may predate the development of invasive disease. Furthermore, several studies have shown that the proliferation, survival, differentiation and invasive capacity of breast cancer cells can be influenced by both myoepithelial and stromal cell populations and that a healthy mammary microenvironment is able to induce a differentiated state in cancer cells

suggesting that cancer cells are dependent on the abnormal microenvironment in which they developed [28]. Therefore the ability of both of these approaches to recapitulate the tumour microenvironment is likely to result in the generation of tumours which more accurately reflect the behaviour and therapeutic response of the parental model.

Variable tumour penetrance rates remain an issue with both these techniques. Overall tumour fragment transplantation resulted in a 40% penetrance rate, which was higher than we observed in either experiment using dissociated tumour cells. This improvement in tumour penetrance may be due to preserved tumour architecture following fragment transplantation as although major cell populations may be represented following tumour disassociation the tumour's organisational structure is lost. However, the wide inter-experimental variations in penetrance rates observed following fragment transplantation means that in order to directly compare the 2 approaches we would need to use the same tumour to generate dissociated tumour cells and fragments for transplantation. However, based on our preliminary data, fragment transplantation appeared to be the most promising technique and therefore we opted to use this approach in all further experiments.

5.6.2 Use of fragment transplantation to generate tumours which recapitulate features of parental GEMM

Tumour fragment transplantation using the Brca $1^{-/-}$; $P53^{-/-}$ [66], [309] and K14Cre; Cdh1 $^{F/F}$; TP53 $^{F/F}$ [69] models has already successfully been used to test drug efficacy in metastatic breast cancer and to develop tumours with acquired resistance to cytotoxics. However, previous attempts to transplant MMTV-NIC fragments into immunocompetent hosts failed and it was postulated that this was due to an immune response against the rat derived HER2 transgene [311], which shares 94% homology with the equivalent murine gene [317]. In addition to the lack of prior exposure to the HER2 transgene, our MMTV-NIC model was bred on an FVB background and therefore prior to fragment transplantation, recipients had not been exposed to Cre-recombinase, which therefore also had the potential to act as an immune response trigger. To try and explore the contribution of the immune system to the variable penetrance rates observed, we transplanted fragments from the same parental tumour into cohorts of FVB and immunocompromised CD-1 or athymic mice. Coincidently, tumour penetrance was high in all cohorts in these experiments. Therefore although there was a small increase in penetrance when fragments were transplanted into the CD-1 nude cohort, it was not possible to fully determine any potential role the immune system might play

in determining the outcome of fragment transplantation. However, we observed a striking delay in tumour growth when fragments were transplanted into either of the immunocompromised strains. This delay may be a consequence of using unmatched immunocompetent and immunocompromised mouse strains, which at present is unavoidable. Immune-deficient FVB strains are not available and therefore to overcome this issue, the model would need to be re-derived on a different genetic background with a matched immune-deficient strain. However, the delayed growth may also be as a result of specific deficiencies within the immune system of the immune-deficient strains used. The immune system exists in a state of dynamic equilibrium and is capable of inducing both pro- and anti-tumorigenic states. Both the immune-compromised mouse models used in these experiments lacked any functioning T cells but retained B and natural killer (NK) cell activity [318]. Both B and NK cells have been implicated in the innate anti-tumour response whilst a variety of different subtypes of T cells exist, with differing effects on a growing tumour [27]. Loss of pro-tumourigenic T cells, specifically CD4+ Th2 cells, resulting in unopposed B and NK cell activity may have shifted the immune system balance in favour of tumour resolution. This could be further explored by fragment transplantation into the NOD-SCID IL2rɣ strain, which in addition to lacking functioning T cells also lacks B and NK cells. Alternatively, comparison of the immune-infiltrate of both highly and poorly/non-penetrant parental tumours may provide further evidence for the role of the immune system in moderating tumour development. Unfortunately, we were unable to optimise 2 antibodies to tumour associated macrophages on FFPE sections and would need to repeat these experiments collecting frozen sections for analysis.

Our fragment derived tumours demonstrated considerable inter- and intra-tumoural heterogeneity. We observed marked differences in the growth rate of fragment derived tumours even amongst tumours generated from the same parental tumour. Despite their development from only a small amount of parental tumour, we also observed marked intra-tumoural variation in HER2 expression. This is consistent with previously published data using the K14Cre; $Cdh1^{F/F}$; $TP53^{F/F}$ model, where fragment derived tumours contained discrete epithelial and mesenchymal regions suggesting that more than 1 cancer subclone in the initial fragment had successfully proliferated to generate a heterogeneous tumour [69]. This heterogeneity is essential in enabling fragment derived tumours to mimic the diverse clinical behaviours of human HER2 positive breast cancer and ensuring that fragment derived tumours are clinically relevant models. However, it also implies that continued selection pressure during *in vivo* growth could potentially result in the generation of tumours which do not necessarily reflect the parental tumour from which they were derived. Previously published studies have used comprehensive genetic analysis to confirm that

fragment derived tumours are genetically similar to the parental tumours from which they are derived [69], [309]. Use of either systematic genetic or proteomic approaches to ensure that our fragment derived tumours remain representative of the tumours from which they originated would be beneficial in the future.

One major limitation of this approach is the variability and unpredictability of tumour penetrance rates, potentially resulting in lengthy experiments using large numbers of recipient animals. Variation in tumour penetrance when using the MMTV-NIC PTEN$^{+/-}$ model to generate fragments appeared to be due to tumour-specific factors rather than generalised features within the donor as tumours from the same donor animal had different penetrance rates. Similarly, transplantation of fragments generated from the same tumour into 2 different cohorts of FVB mice resulted in similar penetrance rates suggesting that recipient characteristics were not the dominant factor in determining penetrance rates. The extremely low penetrance rates observed when MMTV-NIC PTEN $^{FL/+}$ tumours were used to generate fragments suggests that PTEN expression could be a crucial factor in determining fragment transplant outcomes. However, when we compared PTEN expression between highly and poorly/non-penetrant MMTV-NIC PTEN$^{+/-}$ tumours, we found it was unable to explain the differing penetrance rates. To date, we have not considered whether all or only a subset of tumour cells are capable of generating a further tumour and it would be interesting to explore specifically whether the percentage of cancer stem cells within the tumour might be predictive of tumour fragment penetrance. As well as helping to ensure that fragment derived tumours are representative of the parental model, a more comprehensive genetic or proteomic screening strategy may also be informative in determining the factors predictive of tumour penetrance. In the event we are unable to determine factors predictive of tumour penetrance, serial transplantation of highly-penetrant tumours would be an alternative option to increase our supply of reliably transplantable material.

A further limitation of using fragments to generate tumours is that fragment derived tumours are generated from mature, end-stage tumours and therefore cannot be used to explore events in early disease or evolving changes during disease progression. Whilst these events may be more readily studied in the original GEMM, issues surrounding the timing of metastatic seeding may be more problematic. Metastatic seeding is frequently an early event in spontaneous GEMMs and may predate the onset of classically defined invasive disease based on light microscopy findings [290]. Animals bearing fragment derived tumours will develop metastases from end-stage tumour cells, which have been subject to different selection pressures in the MFP than cells which metastasized at an early stage and

continued to evolve in the lung. Previous studies with the K14Cre; $Cdh1^{F/F}$;$TP53^{F/F}$ model showed that primary tumours and their metastases were genetically indistinguishable [69]. However, in human breast cancer, 15% of mutated genes show a differential mutational status between primary and recurrent tumours [319] suggesting that the site of metastases evolution may play a critical role in determining the phenotype of subsequent tumours and also potentially their response to therapy. If, in the future, we are able to use fragment derived tumours to generate established metastatic disease, it would be useful to compare the genetic and proteomic signatures of lung metastases from both spontaneous GEMM and fragment derived tumours.

5.7 Summary

The use of the MMTV-NIC model to produce animals bearing single mammary tumours will greatly facilitate our ability to explore both drug efficacy in metastatic disease and events involved in the development of acquired drug resistance. Of the 3 methods of developing isolated tumours we have explored, fragment transplantation was the most promising and resulted in the generation of strongly HER2 positive tumours. At present the major limitation of this approach appears to be the variable and unpredictable tumour penetrance rates, although more comprehensive genetic and/or proteomic screening is required to ensure that fragment derived tumours are truly representative of the parental GEMM. Serial transplantation of highly penetrant tumours is a viable option to overcome the unpredictability of tumour penetrance.

Chapter 6: Use of fragment derived tumours to measure therapeutic response

Using MMTV-NIC PTEN$^{+/-}$ fragment transplantation, we generated animals with a single mammary tumour, with the long-term goals of being able to study both mechanisms of acquired resistance and drug efficacy in metastatic disease. Previously published studies using K14cre; Brca 1$^{F/F}$; P53$^{F/F}$ [296] and the K14cre; cdh1$^{F/F}$; TP53$^{F/F}$ [69] models have shown that fragment transplantation resulted in a second generation of tumours which were genetically indistinguishable from the originating tumour. Furthermore, tumours derived from K14cre; Brca 1$^{F/F}$; P53$^{F/F}$ fragments displayed similar sensitivity to cytotoxic drugs as observed in the original GEMM. Encouragingly, fragment derived tumours displayed the same heterogeneity in response to cytotoxics as observed in the original model, suggesting that fragment derived tumours were capable of recapitulating the diverse range of tumour behaviour and responses seen in clinical practice.

In the following experiments, we sought to determine whether tumours generated as a result of MMTV-NIC PTEN$^{+/-}$ tumour fragment transplantation displayed the same response to drug treatment as the original model. Specific aims of this section of the project included:

1. Comparison of responses of MMTV-NIC PTEN$^{+/-}$ model and fragment derived tumours to paclitaxel.
2. Comparison of responses of MMTV-NIC PTEN$^{+/-}$ model and fragment derived tumours to HER2 directed therapies, using AZD8931 as an example.
3. Generation of fragment derived tumours with acquired resistance to AZD8931.

6.1 Determination of Therapeutic response of Fragment Derived Tumours to Paclitaxel

To explore the response of fragment-derived MMTV-NIC PTEN$^{+/-}$ tumours to paclitaxel, fragments were harvested from 2 separate MMTV-NIC PTEN$^{+/-}$ tumours and transplanted into FVB recipients. When tumours reached a volume ≥ 0.15 cm^3, mice were randomized to either treatment with weekly intraperitoneal (IP) paclitaxel (10 mg/kg) formulated in Cremaphor EL and ethanol (1:1, v:v) or vehicle for a maximum of 4 doses. Randomization was balanced to ensure that both drug (n=3) and vehicle (n=3) treated arms contained an equal number of tumours derived from the different parental tumours. Animals were monitored twice weekly for tumour progression and sacrificed once the tumour had reached 1.5 cm (in any direction) or at 72 hours following their final dose. OS was defined as the interval from commencing treatment to time of sacrifice.

As we had previously observed in the original MMTV-NIC PTEN$^{+/-}$ model (see chapter 4), paclitaxel treatment resulted in a statistically significant increase in OS of mice bearing fragment derived tumours (Figure 6.1A). Median OS was increased from only 14 days in vehicle treated animals (range 7-14 days) to 24 days (range 24-24 days) in drug treated animals (p=0.03, Gehan-Breslow Wilcoxon test). Looking at the response of individual tumours to treatment, we found that although paclitaxel slowed tumour growth, it did not result in tumour shrinkage (Figure 6.1B), again emulating our observations in the original model.

Using IHC with an antibody to cleaved caspase 3, we confirmed that paclitaxel treatment resulted in a small yet statistically significant increase in apoptosis. The median percentage area occupied by cells undergoing apoptosis was 0.98% in paclitaxel treated tumours compared to 0.36% in vehicle treated tumours (p=0.002, Mann Whitney U test, Figure 6.2). These results were consistent with the low levels of apoptosis observed in the original MMTV-NIC PTEN$^{+/-}$ model and are likely due at least in part to the very transient nature of apoptosis, which after completion becomes undetectable. Paclitaxel can also result in necrosis and again this may be the dominant mechanism of cell death in MMTV-NIC PTEN$^{+/-}$ tumours.

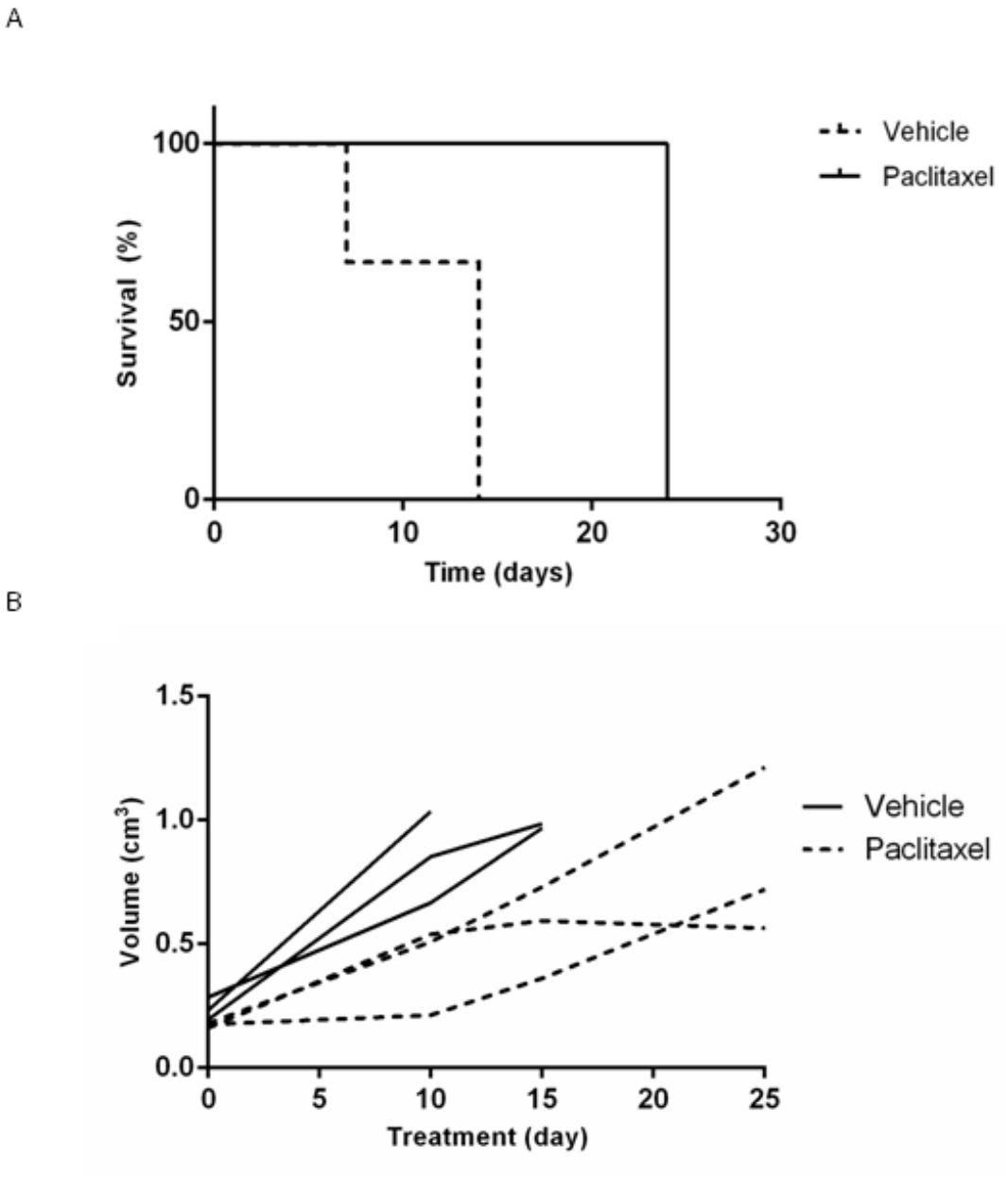

Figure 6.1: Paclitaxel treatment slowed tumour growth and prolonged OS in fragment derived MMTV-NIC PTEN$^{+/-}$ tumours mirroring the response seen in the original MMTV-NIC PTEN$^{+/-}$ model. A: Overall survival in vehicle (n=3) and paclitaxel (n=3) treated fragment derived tumours, p=0.003, Gehan-Breslow Wilcoxon test. B: Growth rate of vehicle and paclitaxel treated fragment derived tumours.

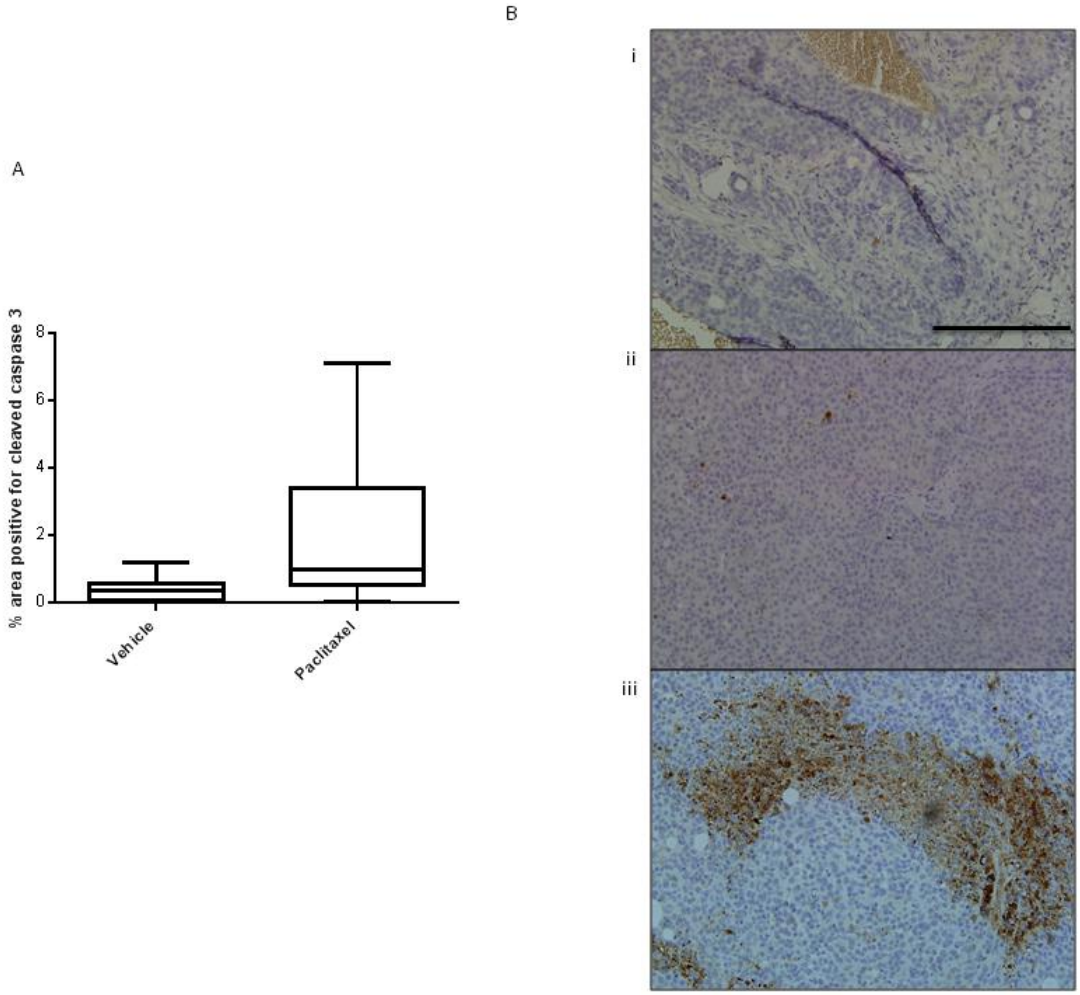

Figure 6.2: Paclitaxel resulted in apoptosis in fragment derived MMTV-NIC PTEN$^{+/-}$ tumours. A cleaved caspase 3 antibody was used to perform IHC on paraffin embedded sections of paclitaxel and vehicle treated fragment derived tumours. Images analysed using Image J software to calculate percentage area, which stained positive for cleaved caspase 3 in six low power fields (mag x20) per tumour. A: Box – whisker plot analysis of percentage area positive for cleaved caspase 3 in vehicle (n=3) and paclitaxel (n=3) treated tumours. p=0.0019, Mann Whitney U test. B: representative images of IHC; negative control (i), vehicle (ii) and paclitaxel (iii) treated tumour. Negative control consists of tumour section incubated in the absence of primary antibody. Scale bar 100 µm. Mag x20.

6.2 Determination of Therapeutic response of Fragment Derived Tumours to AZD8931

To determine the sensitivity of fragment derived tumours to AZD8931, fragments derived from 2 different parental tumours were transplanted into cohorts of FVB mice. Animals with an established tumour of ≥ 0.06 cm^3 were randomized to treatment with either vehicle (n=5) or AZD8931 (100 mg/kg, n=6) once daily by oral gavage. Treatment continued until complete tumour resolution, defined as an absence of measurable disease, or until the animal was sacrificed due to tumour burden (tumour ≥1.5 cm, in any direction). Tumours were randomized according to the parental tumour of origin, to ensure both vehicle and drug treated groups contained approximately equal numbers of tumours from each of the parental tumour.

Similarly to our earlier observations in the MMTV-NIC $PTEN^{+/-}$ model (see chapter 4), AZD8931 treatment prolonged OS in mice bearing fragment derived tumours (p=0.002, Gehan-Breslow Wilcoxon test, Figure 6.3). The median OS of vehicle treated animals was 53 days (range 14-102 days). In comparison, all 6 of the fragment bearing animals treated with AZD8931 survived for at least 102 days. It was not possible to further clarify OS in the AZD8931 treated cohort as drug treatment was withdrawn following complete tumour resolution and restarted when the primary tumour recurred in an effort to generate tumours with acquired resistance to AZD8931 (see section 6.4).

Comparison of the response of individual MMTV-NIC $PTEN^{+/-}$ model tumours and fragment-derived tumours to AZD8931 revealed a striking difference in drug sensitivity (Figure 6.4). As previously described, MMTV-NIC $PTEN^{+/-}$ model tumours initially responded to AZD8931 with 2 out of 5 tumours shrinking by at least 50% and the remaining 3 maintaining a stable volume (Figure 6.4A). However, they rapidly developed resistance and continued to grow through ongoing drug treatment (Figure 6.4B and Chapter 4 Figure 4. 11B). In contrast, fragment derived tumours were more sensitive to AZD8931 as all tumours fully resolved, albeit over varying treatment durations. The median duration of AZD8931 treatment required to cause tumour resolution was 25.5 days (range 10-98 days)(Figure 6.4 C and 4D). After AZD8931 withdrawal, 60% of tumours recurred after a median interval of 42 days (range 10-

88 days) off treatment. The remaining animals were observed for a minimum of 152 days off drug treatment but did not develop tumour recurrence during this period.

During our initial experiment using the MMTV-NIC model, AZD8931 treatment was commenced when tumours reached a volume ≥ 0.1 cm^3. In case the increased sensitivity of fragment derived tumours was caused by initiating treatment at a lower starting volume (0.06 cm^3), we repeated this experiment in a second cohort of fragment bearing mice but started treatment at a volume ≥ 0.1 cm^3. AZD8931 resulted in complete tumour eradication in drug treated animals (n=2).

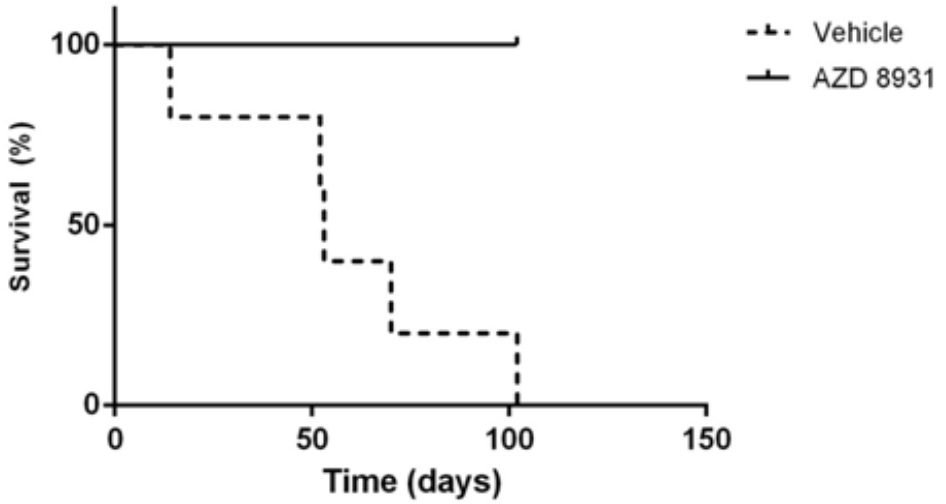

Figure 6.3: AZD8931 treatment prolonged OS in MMTV-NIC PTEN$^{+/-}$ fragment derived tumours. Animals with fragment derived tumours ≥ 0.06 cm^3 were randomized to treatment with vehicle (n=5) or AZD8931 (n=6). Mice were monitored twice weekly for tumour onset and development and sacrificed when tumour burden ≥ 1.5 cm in any direction. Survival was defined as interval from commencing treatment until time of sacrifice due to tumour burden. P=0.002, Gehan Breslow Wilcoxon test.

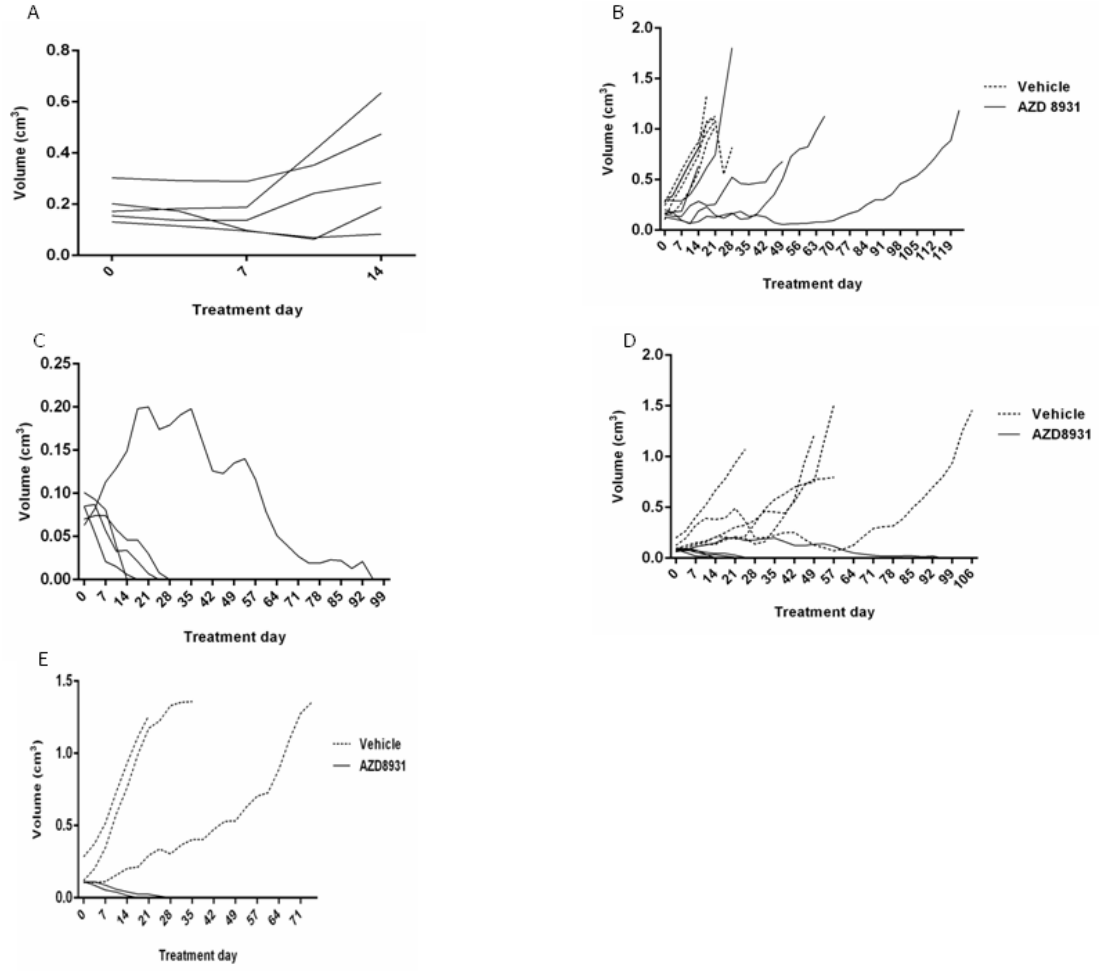

Figure 6.4: MMTV-NIC PTEN$^{+/-}$ fragment derived tumours were more sensitive to AZD8931 than the MMTV-NIC PTEN$^{+/-}$ model. A: Initial responses of MMTV-NIC PTEN$^{+/-}$ model tumours to AZD8931 before all tumours became resistant and grew through drug treatment. B: Response of MMTV-NIC PTEN$^{+/-}$ model to AZD8931 (n=5) and vehicle (n=5). C: MMTV-NIC PTEN$^{+/-}$ fragment derived tumours fully resolved in response to AZD8931 when commenced at volume ≥ 0.06 cm^3 but over varying time intervals. D: Response of MMTV-NIC PTEN$^{+/-}$ fragment derived tumours to AZD8931 (n=5) and vehicle (n=5). E: MMTV-NIC PTEN$^{+/-}$ fragment derived tumours fully resolved in response to AZD8931 when commenced at volume ≥ 0.1 cm^3.

6.3 Exploring factors contributing to enhanced sensitivity of fragment derived tumours to AZD8931

The increase in sensitivity of fragment derived tumours to AZD8931 compared to the original GEMM was surprising, particularly as we had already demonstrated that the response to paclitaxel was preserved following fragment transplantation. We considered 3 possible explanations for this; firstly changes in target receptor expression, secondly altered vascularisation and finally changes in the ability to adapt to hypoxia.

AZD8931 resulted in complete tumour eradication amongst the fragment derived tumours. Therefore, these analyses have been conducted on the matched untreated parental and fragment derived tumours generated during our earlier experiments.

6.3.1 Comparison of HER2 expression between parental and fragment derived tumours

We used IHC with a HER2 antibody to demonstrate that the significant intra-tumoural heterogeneity of expression observed in the parental tumours was also present in fragment derived tumours with all tumours containing regions of strong, moderate and absent HER2 expression (Figure 6. 5A). Comparing HER2 expression across 3 sets of matched parental and fragment derived tumours, we found a close agreement between each parental tumour and the corresponding fragment derived tumours (Figure 6.5B), suggesting that increased HER2 expression in fragment derived tumours was not responsible for the increased sensitivity to AZD8391.

We also used IHC to compare expression of pTyr 1221/1222 HER2 and pTyr 1289 HER3 in model and fragment derived tumours but the patchy nature of expression prevented us from drawing any conclusions.

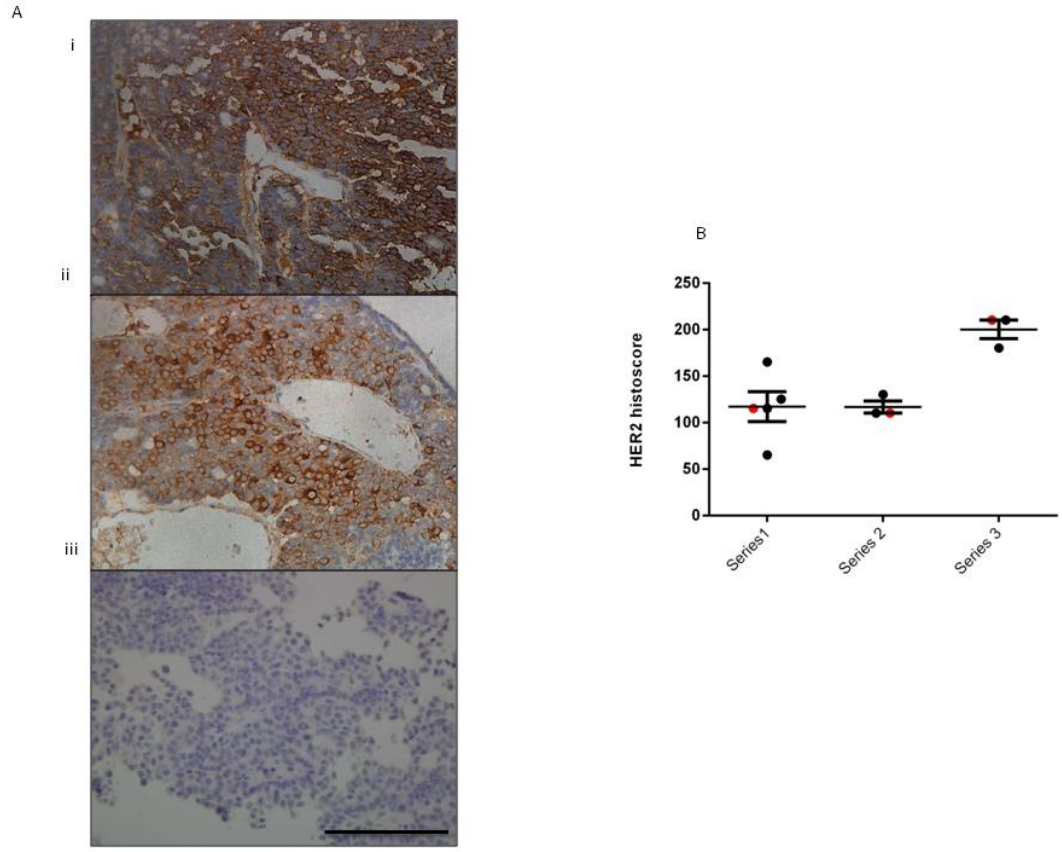

Figure 6.5: HER2 expression was consistent between matched parental and fragment derived MMTV-NIC PTEN$^{+/-}$ tumours. IHC was performed on paraffin embedded sections of parental and fragment derived tumours with a total HER2 antibody. A: Representative IHC images of parental (i) and fragment derived tumours (ii). Negative control (iii) consists of tumour section incubated in the absence of primary antibody. Mag x40. Scale bar represents 100 µm. B: Immunohistochemical analysis of membranous HER2 expression in matched parental and fragment derived tumours. Red data points represent parental tumours. Black data points represent fragment derived tumours. Bar represent mean value for each series.

6.3.2 Comparison of vascularisation between parental and fragment derived tumours

IHC with a CD31 antibody was performed to determine whether altered vascularisation resulting in enhanced drug delivery might contribute to the increased sensitivity of fragment derived tumours to AZD8931. In the 2 tumour series we examined, there was no consistent relationship between vascularisation in the parental and transplanted tumours (Figure 6.6). There was no difference in the extent of vascularisaion between parental and fragment derived tumours in the first tumour series we examined. However, in the second series we examined, the mean percentage area contained within a CD31 positive region was significantly higher in fragment derived tumours than the parental tumour ($p=0.01$, Mann Whitney U test).

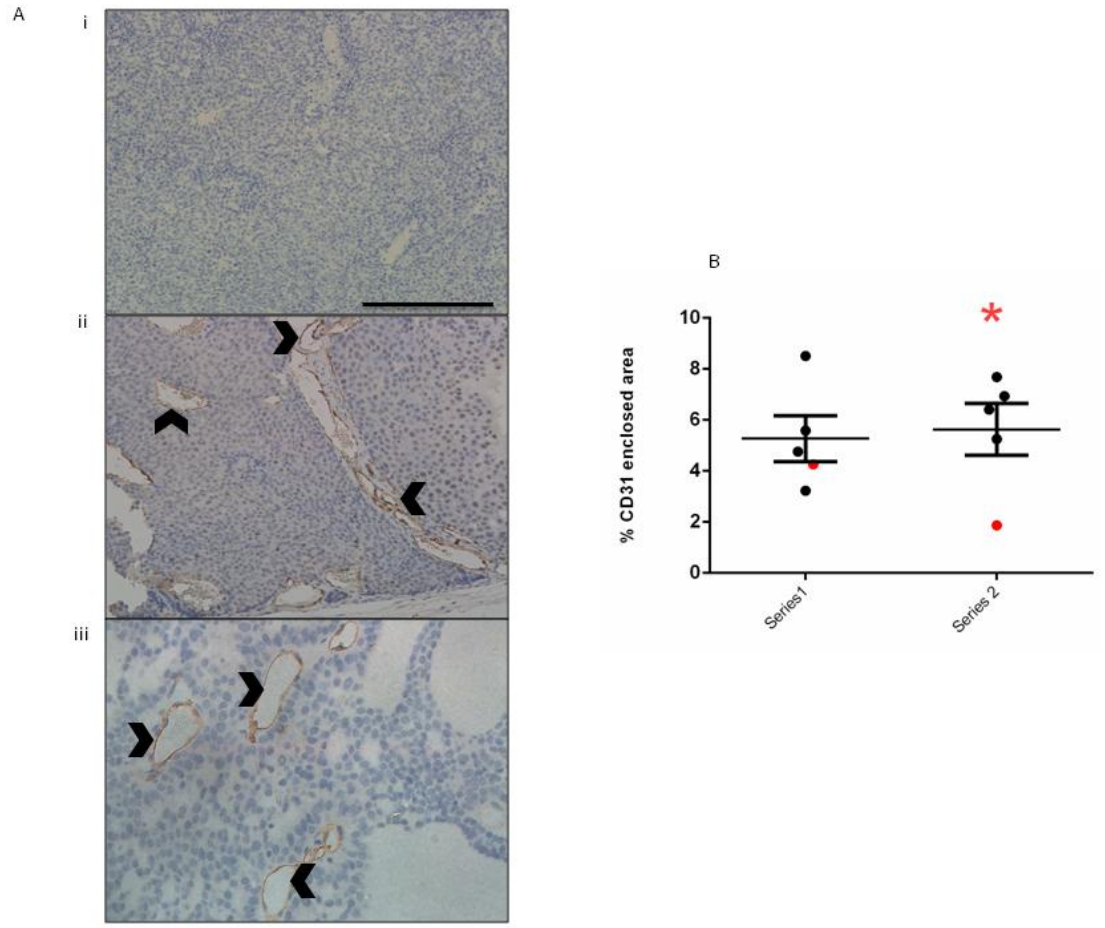

Figure 6.6: Comparison of vascularisation in parental and fragment derived MMTV-NIC PTEN$^{+/-}$ tumours. IHC was performed on matched sections of parental and fragment derived formalin fixed paraffin embedded tumours with CD31 primary antibody. Images analysed using Image J software to calculate area encompassed in a CD31 positive region in 6 low powered fields per tumour. Ai: Negative control comprising of fragment derived tumour section incubated in the absence of CD31 antibody. Scale bar represents 100 µm. Aii: Representative image of IHC with CD31 antibody on fragment derived tumour (mag x20). Arrowhead denotes representative blood vessels. Aiii: High powered view of CD31 positive blood vessels (mag x40). Arrowhead denotes representative blood vessels. B: Box-whisker plot analysis of extent of vascularisation in parental tumours (red data point) and matched fragment derived tumours (black data points). Horizontal line represents mean and error bar the SEM for each series. Asterix denotes statistically significant p value in second tumour series (p=0.01), calculated using Mann Whitney U test.

6.3.3 Comparison of HIF1α expression between parental and fragment derived tumours

As changes in the extent of vascularisation did not account for the differential sensitivity to AZD8931 observed between parental and fragment derived tumours, we explored whether alterations in HIF1α expression might explain it. In addition to hypoxia, HIF1α expression is upregulated in response to PTEN loss, changes in the expression of receptor tyrosine kinases, such as EGFR, and hyperactivation of intracellular signalling pathways, eg Akt and Src [313]. HIF1α expression therefore acts as a composite biomarker for multiple factors which individually confer a more aggressive tumour phenotype [313]. Furthermore, preclinical studies also support a role for these factors in the development of resistance to HER2 targeted agents [147].

Using IHC, we demonstrated variable HIF1α expression between different parental and to a lesser extent amongst different fragment derived tumours, although all specimens expressed moderate to high levels of the protein (Figure 6.7). Comparison of HIF1α expression revealed statistically significant differences between matched parental and fragment derived tumours in 2 out of 3 tumours series we examined. However, there was no consistency in the direction of change with increased expression in the parental tumour in series 2 and reduced expression in series 3 compared to the corresponding fragment derived tumours.

In summary, MMTV-NIC PTEN$^{+/-}$ fragment derived tumours were more sensitive to AZD8931 than the original GEMM, although the cause of this remains to be determined.

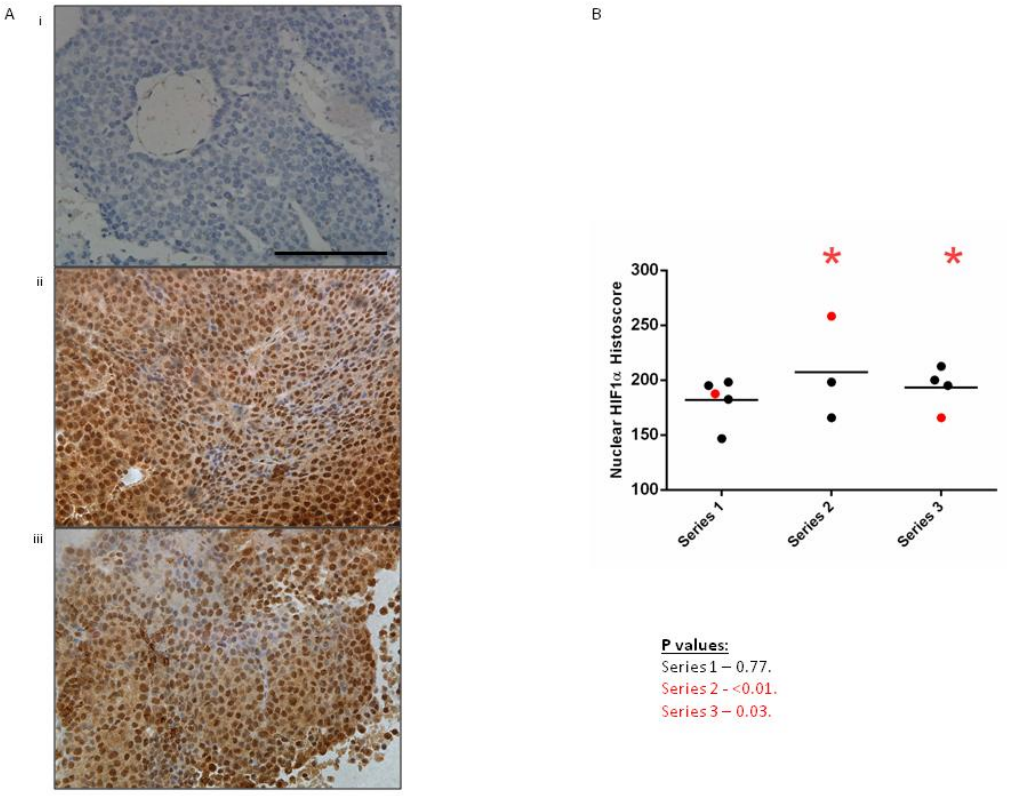

Figure 6.7: Both parental and fragment derived MMTV-NIC PTEN$^{+/-}$ tumours strongly expressed HIF1α. IHC was performed on formalin fixed paraffin embedded parental and corresponding fragment derived tumours with HIF1α primary antibody. Nuclear histoscore determined using 6 representative high powered fields (x40 mag) and calculating the sum of the product of percentage cells stained by the intensity graded from 0-3 (histoscore = (% *1) + (% *2) + (% *3)). A: Representative IHC images-i: Negative control consisting of tumour section incubated in the absence of primary antibody. Scale bar represents 100 μm. ii: parental MMTV-NIC PTEN$^{+/-}$ tumour section stained with HIF1α antibody. iii: fragment derived tumour section stained with CD31 antibody. Mag x40.

6.4 Generation of fragment derived tumours with acquired resistance to AZD8931

One of our major goals has been to use fragment derived tumours to study mechanisms of acquired resistance to HER2 targeted therapies. In order to begin exploring factors underpinning acquired resistance to AZD8931, we generated fragments from 3 separate MMTV-NIC PTEN$^{+/-}$ tumours and transplanted them in to cohorts of FVB mice. Following the development of established tumours, we randomised mice to treatment with either vehicle or AZD8931. In the initial 2 experiments, randomization was performed once the tumour had reached a volume ≥ 0.06 cm^3. Animals continued to receive daily vehicle treatment until they were sacrificed due to mammary tumour burden at a maximum dimension of 1.5 cm. AZD8931 was administered in a pulsatile manner with mice receiving daily treatment until the tumour was no longer measurable. Treatment was then withdrawn and the tumour allowed to re-grow to a sufficient size that it could be accurately measured at which point treatment was re-instituted. Tumours were classified as resistant when able to continue growing in the presence of ongoing AZD8931 treatment and were permitted to grow to a maximum dimension of 1.5 cm, although the animal bearing the resistant tumour in experiment 2 had to be culled prematurely due to the tumour's slow growth and the animal's advanced age. We observed a high rate of tumour loss within the first 2 treatment cycles in AZD8931 treated animals with only 1 out of 3 tumours becoming fully drug resistant in both experiments. To try and reduce the incidence of tumour loss in the third experiment, we decided to delay starting treatment until tumours had a volume of ≥ 0.3 cm^3 and to withdraw treatment when tumours had a volume ≤ 0.15 cm^3. Treatment was not restarted until the tumour had re-grown to at least 0.3 cm^3. Despite the adjustments to the treatment schedule, the rate of tumour loss remained high with only 1 out of 3 tumours developing resistance to AZD8931. All 3 of our resistant tumours required 4 cycles of AZD8931 treatment to become drug resistant, although the treatment duration required for individual tumours to become resistant varied considerably (Figure 6.8).

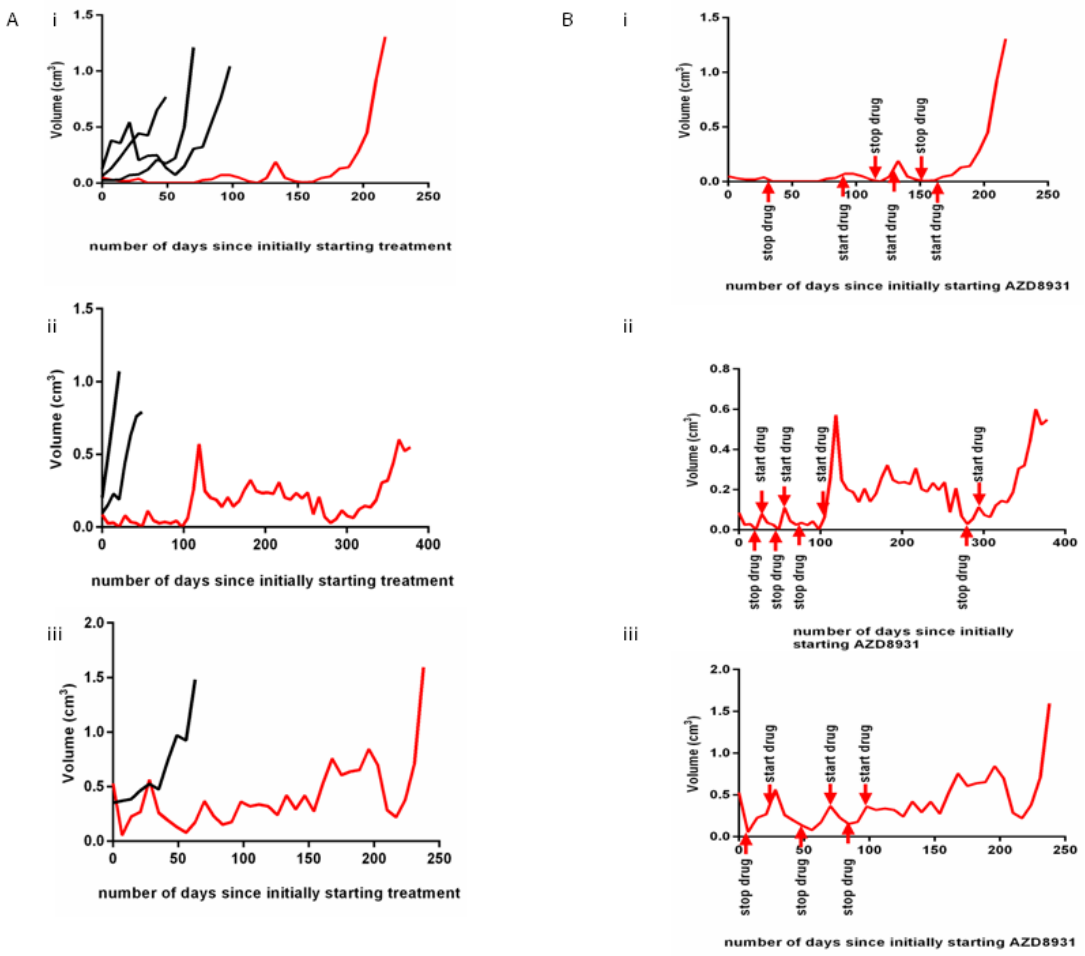

Figure 6.8: Generation of fragment derived tumours with acquired resistance to AZD8931. Tumour fragments, generated from 3 different parental tumours, were transplanted into cohorts of FVB mice and after developing tumours, mice were randomised to treatment with vehicle or AZD8931. Repeated cycles of AZD8931 were administered to facilitate the selection of tumour cell clones with acquired resistance to AZD8931. Ai-iii: growth curves of vehicle treated (black lines) and AZD8931 treated (red lines) tumours in 3 separate experiments. Bi-iii: Growth curves of AZD8931 resistant tumours showing timing and duration of AZD8931 treatment.

6.5 Initial characterisation of AZD8931 resistant tumours

6.5.1 Histological comparison of AZD8931 sensitive and resistant tumours

Examination of the matched AZD8931 naive and resistant tumours generated in the first experiment confirmed they were histologically indistinguishable from each other (Dr **J. Loane, consultant pathologist**). However, whilst the AZD8931 naive tumours generated in the later 2 experiments were similar in appearance, the 2 resistant tumours had a more pleomorphic appearance and were comprised of highly mitotic spindle cells (Figure 6.9) with similar histology to that seen in human metaplastic carcinoma.

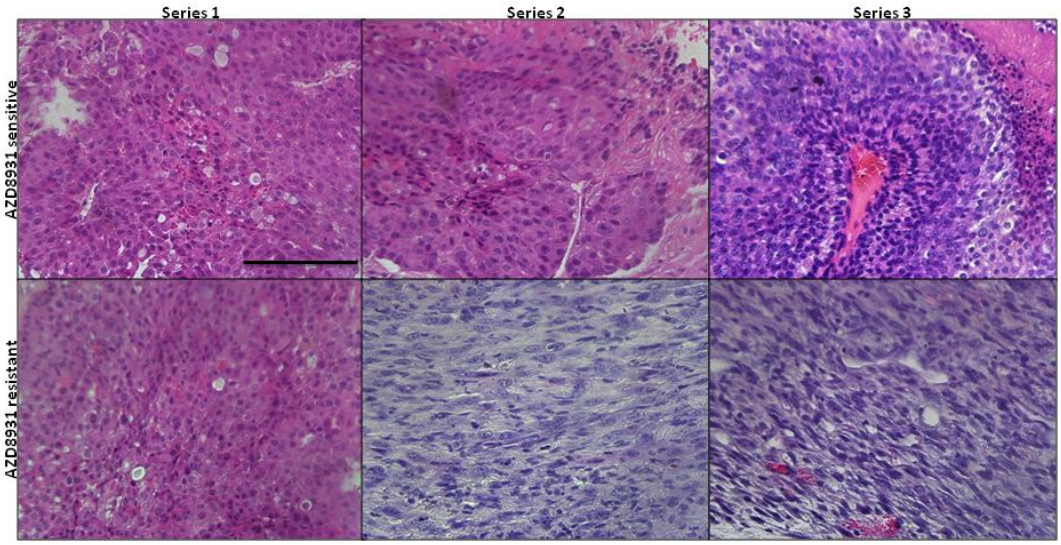

Figure 6.9: Representative H and E images of AZD8931 naive and resistant tumours showing heterogeneity in mechanisms used by tumours to develop resistance to AZD8931. Series 1: AZD8931 resistant tumour was phenotypically indistinguishable from AZD8931 sensitive tumour. Series 2 and 3: AZD8931 resistant tumours consisted of spindle shaped cells. Mag x40. Scale bar represents 100 µm.

6.5.2 Comparison of HER2 expression between AZD8391 naive and resistant tumours

Previous preclinical studies have linked changes in the expression of HER family receptors to resistance to HER2 targeted therapies [147]. Furthermore, loss of HER2 expression has been described in up to 30% of metastases originating from a HER2 positive breast cancer [64] and is highly likely to contribute to acquired drug resistance. We therefore decided to compare HER2 expression in AZD8931 naive and resistant tumours to determine whether changes in HER2 expression underpinned resistance in our model. Using IHC, we demonstrated preserved HER2 expression in the resistant tumour generated in the first experiment but total loss of membranous HER2 expression in both spindle cell tumours (Figure 6.10). Over 90% of metaplastic breast cancers are HER2 negative [320] and therefore this is consistent with the histological phenotype of these tumours.

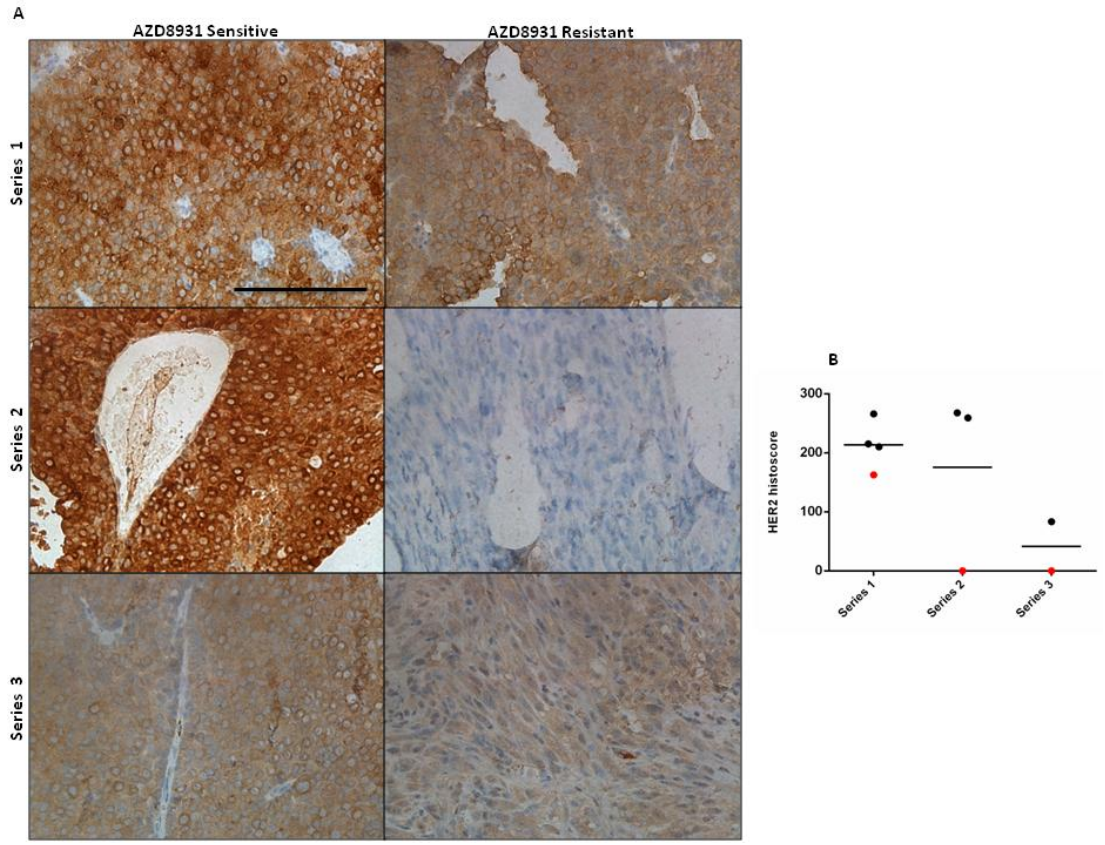

Figure 6.10- Acquisition of spindle cell morphology was associated with loss of membranous HER2 expression in AZD8931 resistant tumours. IHC was performed with a HER2 antibody on paraffin embedded sections of AZD8931 naive and resistant tumours. Membranous histoscore determined using 6 representative high powered fields (x40 mag) and calculating the sum of the product of percentage cells stained by the intensity graded from 0-3, where 1=weak, 2=moderate and 3=strong staining (histoscore = (% *1) + (% *2) + (% *3)). A: Representative images of tumours stained with HER2 antibody. Mag x40. Scale bar represents 100 µm. B: Membranous HER2 histoscore. Black data points represent AZD8931 sensitive tumours. Red data points represent AZD8931 resistant tumours.

6.5.3 Comparison of expression of markers of epithelial to mesenchymal transition (EMT) between spindle cell and epithelial tumours

Although the origin of metaplastic breast carcinoma remains to be determined, EMT has been postulated as a critical event in its pathogenesis. Furthermore, previously published studies have linked the induction of EMT to HER2 loss and resistance to HER2 targeted therapies [167] *in vitro*. We therefore used IHC to compare expression of E-cadherin and vimentin between our different tumours. All of the AZD8931 naïve tumours and the resistant tumour generated in our first experiment showed strong E-cadherin expression but did not express vimentin, consistent with an epithelial phenotype. However, E-cadherin expression had been lost in both spindle cell carcinomas (Figure 6.11) and there was ubiquitous expression of vimentin (Figure 6.12), consistent with a mesenchymal phenotype.

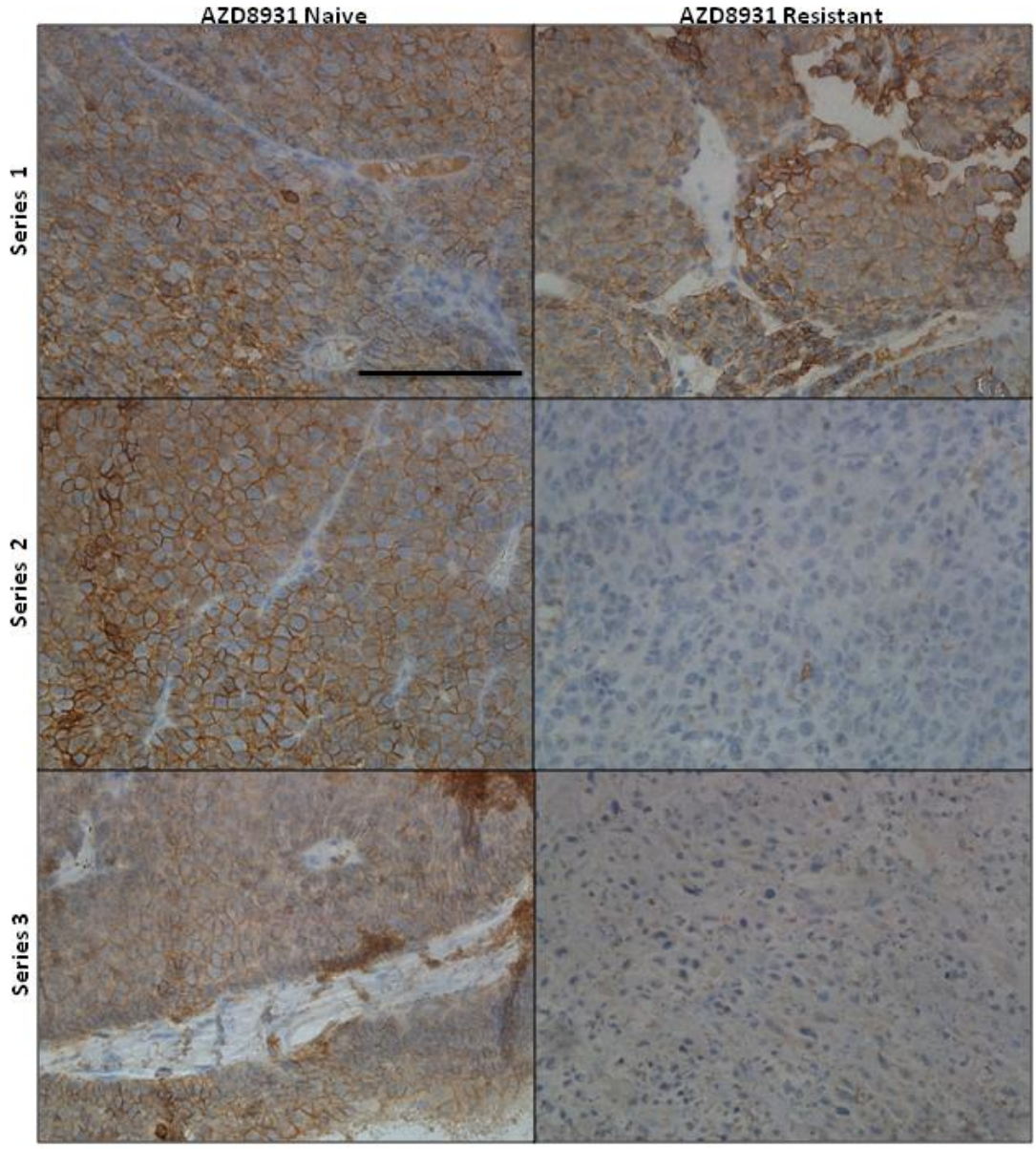

Figure 6.11: Acquisition of spindle cell morphology is associated with loss of E-cadherin in AZD8931 resistant tumours. IHC was performed with an E-cadherin antibody on paraffin embedded sections of AZD8931 naive and resistant tumours. Mag x40. Scale bar represents 100 µm.

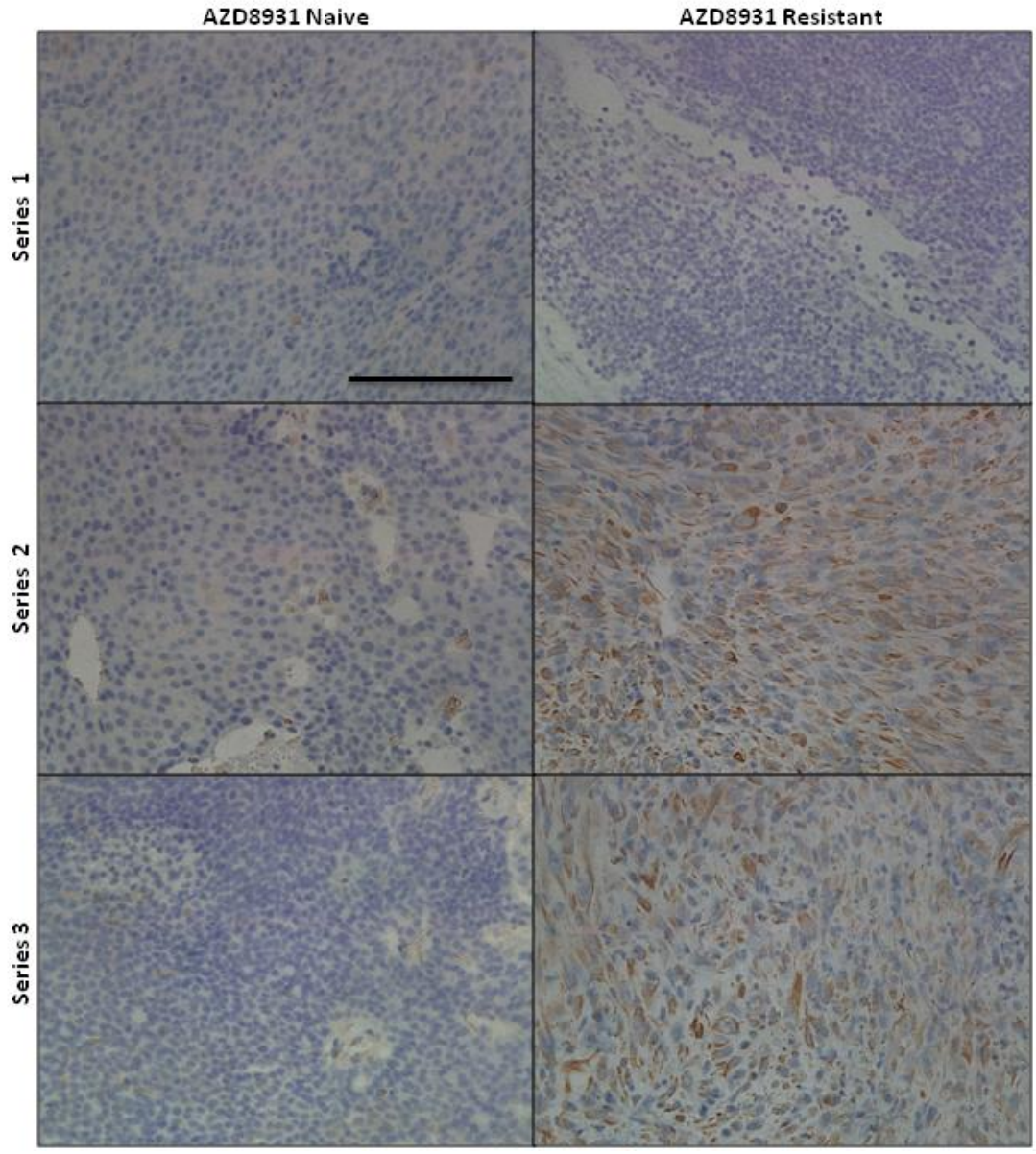

Figure 6.12: Acquisition of spindle cell morphology is associated with vimentin expression. IHC was performed with a vimentin antibody on paraffin embedded sections of AZD8931 naive and resistant tumours. Mag x40. Scale bar represents 100 µm.

6.5.4 Comparison of proliferation between AZD8931 naïve and resistant tumours

Alterations in cell cycle progression and apoptosis are well established strategies used by tumour cells to develop resistance to HER2 targeted agents *in vitro*. We used Ki67 to compare cell proliferation in our AZD8931 resistant and naive tumours. We found there was no statistical difference in the percentage of Ki67 positive nuclei between our AZD8931 naive and resistant tumour in experiment 1 ($p=0.27$, Mann Whitney U test). Interestingly, although the resistant tumours generated in experiments 2 and 3 had both undergone EMT, the impact on cell proliferation was very different. The percentage of Ki67 positive nuclei in the resistant tumour was significantly reduced compared to the 2 vehicle treated tumours in experiment 2 ($p<0.001$, Mann Whitney U test). Conversely, in experiment 3, the resistant tumour had a significantly increased percentage of Ki67 positive nuclei compared to its AZD8391 naive counterpart ($p=0.005$) (Figure 6.13).

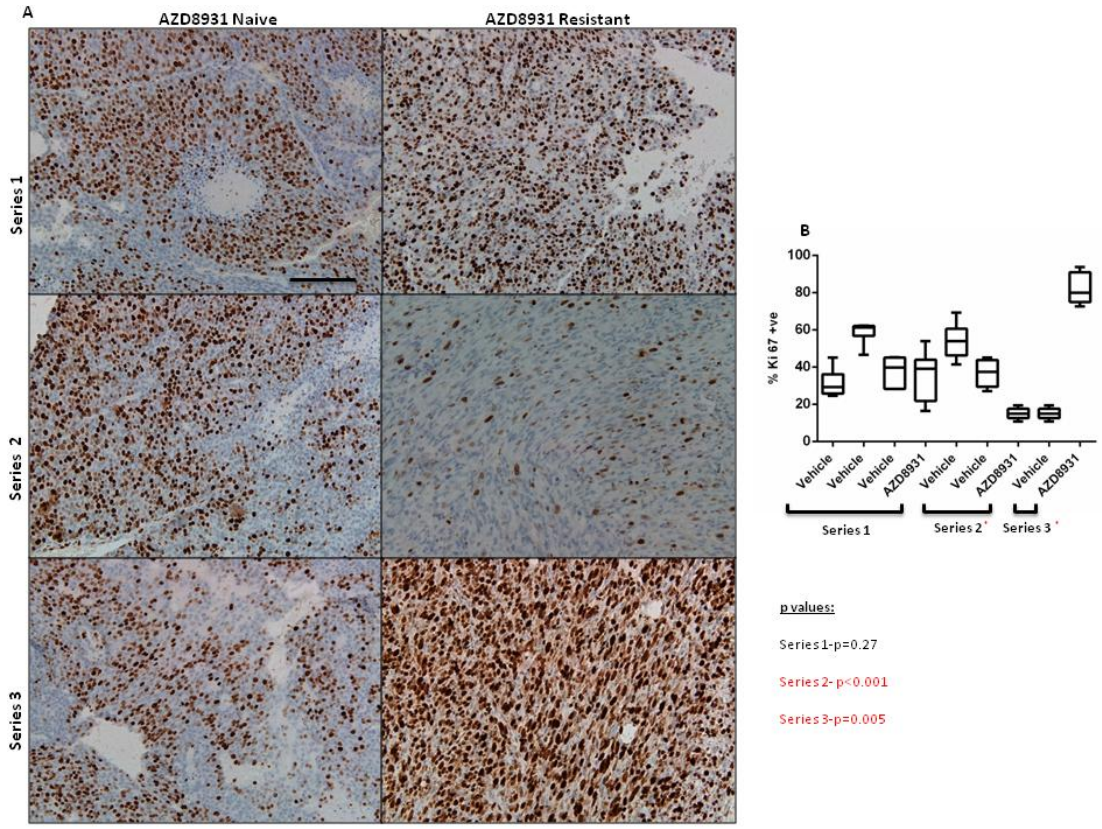

Figure 6.13: Different resistance strategies had differing effects on cell proliferation. IHC performed on paraffin embedded tumour sections with a Ki67 antibody. Images analysed using Immunoratio software to calculate percentage of Ki67 positive nuclei in six low power fields (mag x20) per tumour. A: Representative images of IHC staining for Ki67 in AZD8931 naive and resistant tumours. Mag x20. Scale bar represents 100 µm. B: Box and whiskers plot of percentage Ki67 positive nuclei in AZD8931 naive and resistant tumours. Asterix denotes statistically significant p value. P values calculated using Mann Whitney U test.

6.6 Discussion

6.6.1 Comparison of GEMM and fragment derived tumours to paclitaxel and AZD8931

To further characterise our fragment derived tumours, we decided to compare their response to both cytotoxics and HER2 directed agents, using paclitaxel and AZD8931 as examples. We found that both MMTV-NIC PTEN$^{+/-}$ mice and animals with fragment derived tumours responded similarly to paclitaxel. In both groups of animals, paclitaxel prolonged OS but failed to cause tumour shrinkage (see chapter 4 for further discussion). This preserved response to cytotoxics between the parental GEMM and fragment derived tumours was consistent with previously published data using the K14cre; Brca 1$^{F/F}$; P53$^{F/F}$ model, where a similar response to doxorubicin [308], docetaxel [296] and topotecan [309] has previously been reported.

We also found that AZD8931 increased OS in both MMTV-NIC PTEN$^{+/-}$ mice and recipients of fragment derived tumours. However, whilst tumours in the original GEMM rapidly became resistant to AZD8931, fragment derived tumours fully resolved whilst on treatment and 40% did not recur despite prolonged observation off treatment, suggesting the tumours had been completely eradicated. This difference in sensitivity remains to be explained but our preliminary data suggest that it is not attributable to changes in HER2 expression or HIF1α expression. We did observe a statistically significant increase in vascularisation in 1 series of fragment derived tumours, although in absolute terms this only corresponded to a 4.7% change, which is relatively small to account for such a profound difference in tumour behaviour. Our experiments did only quantify total vasculature and previous studies have demonstrated differences in the percentage of functional vasculature between parental and transplanted models of pancreatic adenocarcinoma, when the percentage total vasculature remained unchanged [321]. It could be in our model that differences in functional vasculature were more marked than changes in total vasculature although if increased vascularisation was responsible for the enhanced response of fragment derived tumours to AZD8931, we would anticipate a similar response to paclitaxel, which was not observed. An alternative explanation for the differential sensitivity of GEMM and fragment derived tumours to AZD8931 may relate to differences in the tumour microenvironment. Tumour fragments were

transplanted into healthy MFP whilst in the GEMM the peri-tumoural MFP was highly abnormal [272]. The abnormal MFP in the original GEMM may produce growth factors which, acting in either a paracrine or systemic fashion, promote continued tumour growth despite AZD8931 treatment. The absence of these growth factors might have rendered fragment derived tumours more susceptible to AZD8931. Although we have yet to explain the lack of concordance in the activity of AZD8931 between the original GEMM and fragment derived tumours, it is important to determine whether this is specific to AZD8931 or whether it is also observed with other molecularly targeted agents with either proven (e.g. lapatinib) or predicted (e.g Akt inhibitors) efficacy in HER2 positive breast cancer.

Encouragingly, the heterogeneity of response to AZD8931 seen in the original GEMM was also preserved following fragment transplantation. Whilst all fragment derived tumours did ultimately resolve on AZD8931 treatment, we observed considerable variation in the rate of response, even amongst tumours derived from the same parental tumour. This preservation of heterogeneity was consistent with previously published data in both the K14cre; Brca $1^{F/F}$; $P53^{F/}F$ [309], [308] and K14cre; $cdh1^{F/F}$; $TP53^{F/F}$ [69] models and most importantly was reflective of the diverse behaviours seen in HER2 breast cancer in the clinic.

6.6.2 Use of fragment transplantation to generate tumours with acquired resistance to AZD8931

We also used fragment transplantation to generate a small panel of tumours with acquired resistance to AZD8931. Despite limited numbers, preliminary analysis showed that different tumours utilised a variety of strategies for developing drug resistance, again modelling the broad range of therapeutic responses seen in clinic. Specifically, we observed evidence of EMT in 2 of our resistant tumours, which we have also identified as being linked to the development of HER2 targeted therapy resistance during our *in vitro* studies (see chapter 7 for further discussion). The ability to generate drug resistance *in vivo* is potentially a useful tool in preclinical drug resistance studies. To date, the majority of studies exploring resistance to HER2 directed therapies have used cell line based techniques and although numerous resistance mechanisms have been identified *in vitro*, clinical validation has proved challenging. The use of fragment-derived tumours to explore resistance mechanisms offers a more physiologically relevant model with tumours developing resistance whilst exposed to

ongoing *in vivo* selection pressures. Therefore any resistance strategies identified may be more predictive of clinically relevant resistance mechanisms and in this case helps to validate our *in vitro* findings. More comprehensive analysis of these tumours is required to further understand the drivers of resistance in this model. However, our preliminary data provides a strong rationale for basing therapeutic decisions on the biology of the individual resistant tumour, which may be very different from that of the primary tumour. The observation that 2 out of 3 of our resistant tumours no longer expressed HER2 further emphasises this point. To date, major advances in overcoming clinical resistance to trastuzumab have focussed on alternative strategies for targeting HER2 signalling, either through combining drugs which target different HER family receptors or through use of drug-antibody conjugates such as trastuzumab-emtansine (T-DM1). As it is rarely mandatory to re-biopsy tumours at the time of entry into clinical trials, patients whose tumours no longer express HER2 risk being exposed to the toxicity of treatments which might not be anticipated to be effective. Furthermore, failure to characterise resistant tumours could also result in novel agents being incorrectly labelled as ineffective if the trials in which their efficacy is determined unknowingly contain large numbers of patients in whom the treatment would not be expected to be efficacious.

Two major limitations of this approach are the low numbers of resistant tumours generated and the lengthy nature of these experiments. Further studies are required to generate a larger panel of resistant tumours. Although this will initially require transplantation of multiple fragments from different parental tumours to try and generate a tumour panel which includes a broad range of resistant mechanisms, we plan to streamline subsequent studies by using resistant tumours to generate further fragments for transplantation. Previously published data using the K14cre; Brca $1^{F/F}$; $P53^{F/F}$ model has shown that tumour resistance is preserved following transplantation of resistant material into new hosts [308]. Hopefully in the future this will enable the creation of cohorts of animals bearing resistant tumours, suitable for use in drug studies aiming to reverse resistance.

6.7 Summary

Transplantation of MMTV-NIC PTEN$^{+/-}$ fragments resulted in the generation of tumours with a preserved response to paclitaxel and enhanced sensitivity to AZD8931. Using fragment transplantation, we also demonstrated the heterogeneous nature of acquired resistance to AZD8931 highlighting the need for repeat tumour assessment prior to starting therapy in the context of relapsed or metastatic disease.

Chapter 7: Generation and characterisation of cell lines with acquired resistance to HER2 directed tyrosine kinase inhibitors (TKI)

The introduction of HER2 directed therapies has arguably been one of the greatest advances in the management of breast cancer in recent years. Trastuzumab in combination with chemotherapy has been hugely successful as first line therapy in both early and metastatic breast cancer. However, although 50% of patients with metastatic breast cancer initially respond to treatment [136], the development of resistance is ultimately universal. Until recently the only other licensed therapeutic option was lapatinib, a HER2 and EGFR targeting TKI. Yet despite high initial response rates in HER2 positive tumours [138], resistance is also inevitable. A greater understanding of the mechanisms underpinning the development of resistance therefore remains a key priority. Numerous potential mechanisms of resistance have been identified in preclinical studies yet few of these have been tested clinically. One mechanism of resistance which has been explored clinically is a compensatory increase in the signalling of other HER family receptors. Preclinical studies using trastuzumab have shown that forced over-expression of EGFR by HER2 positive SKBR3 cells rendered cells trastuzumab resistant [322]. However, clinical studies have failed to identify any consistent relationship between EGFR expression and trastuzumab sensitivity and the addition of gefitinib to trastuzumab failed to improve treatment efficacy [64]. Yet, combination therapy such as lapatinib with trastuzumab [139] [323] and pertuzumab, trastuzumab and docetaxel have successfully improved treatment outcomes [324] [325], suggesting that inhibition of multiple HER family receptors might be more efficacious than single target inhibition and as such may help to delay the onset of acquired resistance. However, despite the initial success of these complex, multi-agent regimes, resistance still remains ultimately inevitable.

Lapatinib is classified as dual inhibitor of EGFR and HER2, but in reality it is a more potent inhibitor of HER2 and the extent of EGFR inhibition *in vivo* remains uncertain. Preclinical studies have suggested that incomplete inhibition of EGFR in conjunction with increased heregulin expression drives continued PI3K/Akt signalling and lapatinib resistance [173] and cell line studies have shown an inverse correlation between expression of phospho-EGFR and HER3 and lapatinib sensitivity [271]. AZD8931 is a novel equipotent reversible TKI of EGFR and HER2, which through robust inhibition of both EGFR and HER2 also reduces

HER3 signalling. Preclinical data suggests that AZD8931 is predominantly active in ligand driven HER family signalling and therefore, following preliminary evidence of its efficacy in phase1 trials [326], further clinical studies have focussed on its role in populations with mixed or low HER2 expressing tumours [145], [145]. However, given its activity in the MMTV-NIC model (see chapters 4 and 6) and its potential to provide more global inhibition of HER family signalling, we decided to compare its activity and the mechanisms involved in acquired resistance in HER2 positive breast cancer cell lines with that of lapatinib. Initial experiments used cell lines derived from the MMTV-NIC PTEN$^{+/-}$ model. However, due to lack of sensitivity and poor reproducibility, we conducted further studies in established human HER2 positive breast cancer cell lines.

Specific aims of this section of the project included:

1. Determining the sensitivity of MMTV-NIC PTEN cell lines to lapatinib and AZD8931.
2. Determining the sensitivity of human HER2 positive cell lines to lapatinib and AZD8931.
3. Development of cell lines with acquired resistance to lapatinib and AZD8931.
4. Initial characterisation of resistant cell lines using western blotting.
5. Further analysis of AZD8931 resistant cell lines using RPPA and mass spectrometry.

7.1 Sensitivity of MMTV-NIC PTEN$^{+/-}$ cell lines to lapatinib and AZD8931

To determine the *in vitro* effects of lapatinib and AZD8931 on proliferation of the MMTV-NIC PTEN$^{+/-}$ cells, 2 cell lines (WGH 129RM and WGH 135RM) were selected from a panel previously generated in the lab (**L. Balderstone**). Both cell lines had already been shown to express HER2 and CK8, confirming that they were derived from a HER2 expressing epithelial cell clone within MMTV-NIC PTEN$^{+/-}$ tumours. These cell lines differed with respect to PTEN expression; WGH 135RM continued to express PTEN whilst WGH 129RM showed no residual expression by western blot (**L. Balderstone**). Therefore by using these 2 cell lines, we aimed to explore the role of PTEN expression in determining *in vitro* sensitivity to lapatinib and AZD8931.

We treated cells with escalating doses of either lapatinib or AZD8931 for 72 hours before performing an SRB assay. The mean IC_{50} for WGH 129RM and WGH 135RM cells treated with lapatinib was 3.12 µM and >5 µM (the drug's maximum aqueous solubility) respectively. Using AZD8931, we calculated mean IC_{50}s of 4.12 µM and 2.22 µM in WGH 129RM and WGH 135RM cells (Figure 7.1). All these calculated IC_{50}s were greater than the peak plasma concentrations recorded during phase1 clinical trials [327] [326] and therefore we considered both cell lines to be resistant to these drugs. The *in vitro* resistance of MMTV- NIC PTEN$^{+/-}$ cell lines to AZD8391 was in marked contrast to the drug's profound effects on proliferation *in vivo* (Chapter 4) and this loss of sensitivity was most likely due to reduced HER2 expression during *in vitro* culture, which we have previously observed with another cell line in this panel (Chapter 5), coupled with the tendency of these cell lines to undergo EMT (H. Smith, personal communication). We also encountered issues with reproducibility, particularly when using AZD8931, as we observed wide variations in IC_{50} across different experiments (Figure 7.1). Both these cell lines contain multiple phenotypically distinct subpopulations, which are likely to exhibit different drug sensitivities. Whilst this heterogeneity may be more reflective of the multiple clones found within a tumour during *in vivo* growth, it is also likely to have contributed to the wide variations in drug response seen in vitro. For these reasons, we decided to conduct all further experiments on established human HER2 positive cell lines.

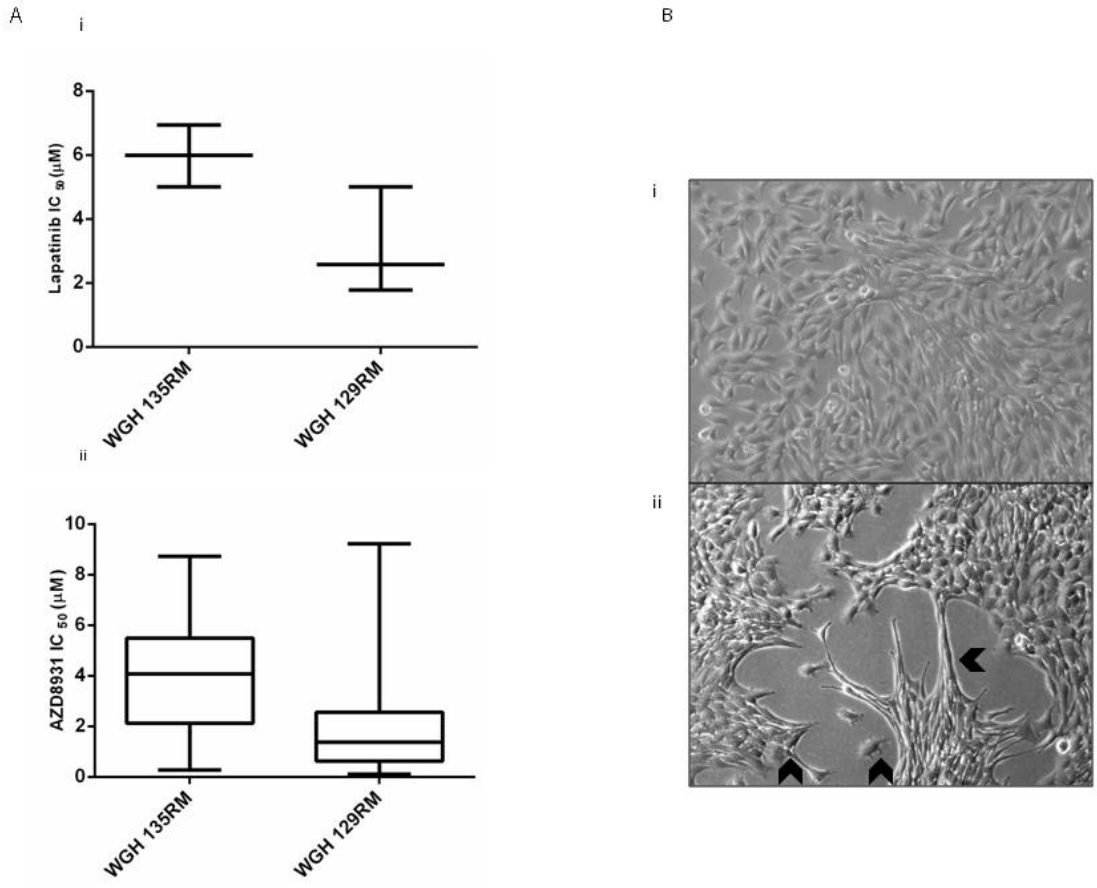

Figure 7.1- MMTV-NIC PTEN$^{+/-}$ derived cell lines were resistant to lapatinib and AZD8931. MMTV-NIC PTEN$^{+/-}$ WGH 135RM and WGH 129RM cell lines were treated with either lapatinib or AZD8931 for 72 hours and an SRB performed. Data was analysed using GraphPad Prism 6 software. Ai: Mean IC_{50} from series of SRB assays with lapatinib (n=3) and AZD8931 (n=15). Error bars represent SEM. Lapatinib mean IC_{50} ± SEM: WGH 135RM 5.98 ± 0.56 μM, WGH 129 RM- 3.12 ± 0.97 μM. AZD8931 mean IC_{50} ± SEM: WGH 135RM- 4.12 ± 0.80 μM, WGH 129 RM- 2.22 ± 0.79 μM. B: Representative phase images of WGH 135 RM (i) and WGH 129 (ii). Arrowheads on lower image demonstrating phenotypically distinct cell populations. Mag x20.

7.2 Determining sensitivity of SKBR3 and BT474 cell to lapatinib and AZD8931.

We chose to use SKBR3 and BT474 cell lines in all further experiments as whilst both cell lines strongly expressed HER2, they differed with respect to several other important characteristics. Neither cell lines expressed ER but whilst BT474 cells strongly expressed PR, SKBR3 cells were only weakly positive (Figure 7.2). SKBR3 has therefore been classified as belonging to the HER2 over-expressing molecular subgroup whilst BT474 belongs to the luminal B subgroup [328]. The cell lines are also reported to differ with regards to their PI3K mutational status; SKBR3 cells express wild type PI3K whilst BT474 cells contain an activating mutation in the catalytic domain [329]. Both cell lines, however, continued to express PTEN (Figure 7.2).

To determine the sensitivity of both cell lines to lapatinib and AZD8931, we cultured cells in the presence of escalating doses of either drug for 72 hours before performing an SRB assay. Each experiment was performed in triplicate and the mean IC_{50} and SEM calculated (Figure 7.3). Both drugs inhibited proliferation of SKBR3 and BT474 cells. For lapatinib the mean IC_{50} was 0.07 μM in SKBR3 cells and 0.06 μM in BT474 cells. For AZD8931, the mean IC_{50} was 0.46 μM in SKBR3 cells and 0.36 μM in BT474 cells.

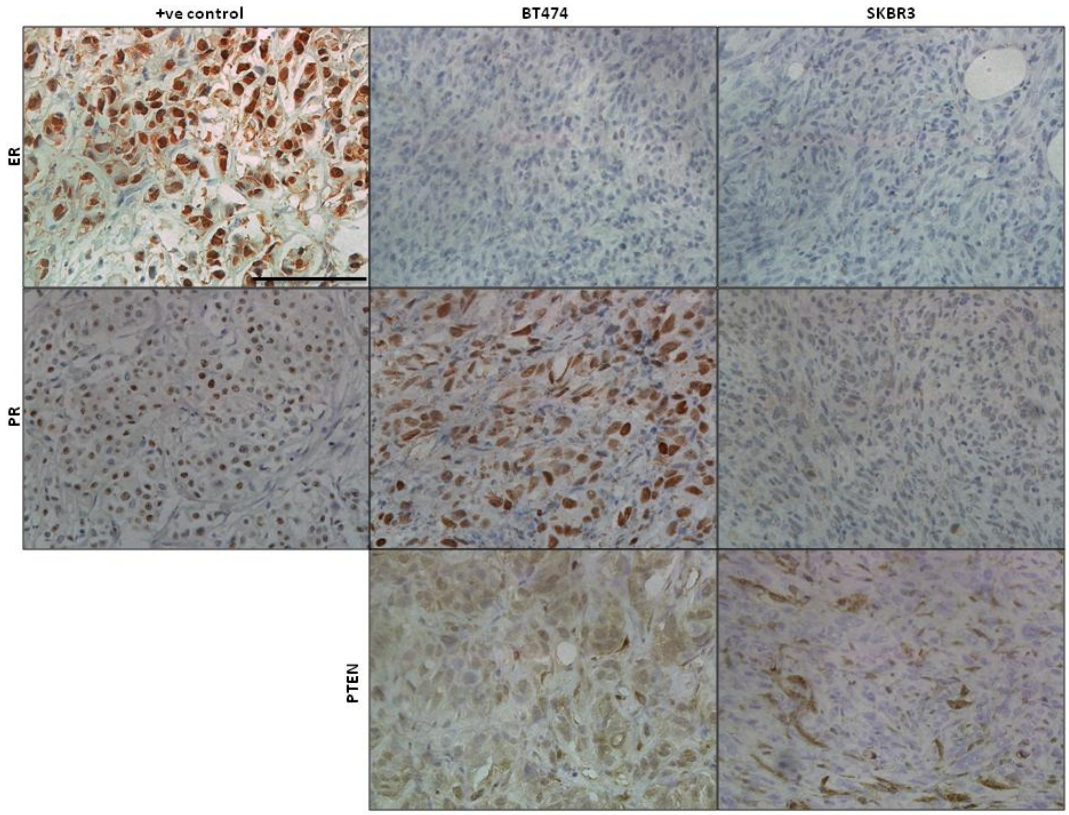

Figure 7.2- Characterisation of SKBR3 and BT474 cell lines in terms of HR status and PTEN expression. SKBR3 and BT474 xenografts were generated by inoculation of the MFP with $5*10^6$ cells suspended in matrigel. IHC was performed on paraffin embedded sections of the resulting tumours. Positive controls comprise sections of human hormone receptor positive breast cancer stained with the appropriate antibody. Mag x40. Scale bar represents 100 µm.

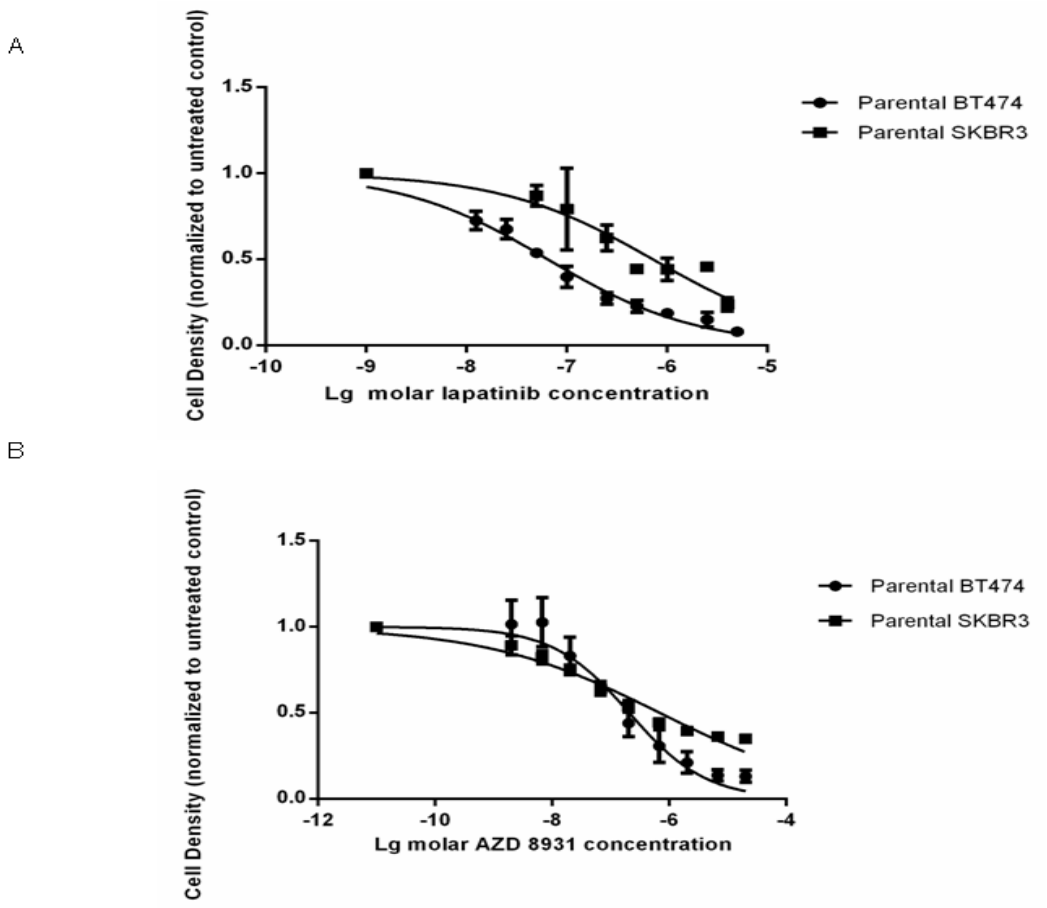

Figure 7.3- Both lapatinib and AZD8931 inhibited proliferation of SKBR3 and BT474 cell lines. 5000 cells were plated out into each well of a 96 well plate and 24 hours later treated with escalating doses of either lapatinib or AZD8931. After 72 hours an SRB assay was performed. Data was analysed using GraphPad Prism 6 software. Representative curves from a series of 3 experiments displayed. Error bars represent SEM across 6 wells treated at the same drug dose within 1 experiment. Lapatinib mean IC_{50} ± SEM: SKBR3- 0.07 ± 0.05 µM, BT 474- 0.06 ± 0.01 µM. AZD8931 mean IC_{50} ± SEM: SKBR3- 0.46 ± 0.05 µM, BT 474- 0.36 ± 0.18 µM.

7.3 Generation of lapatinib resistant cell lines

BT474 and SKBR3 cells were cultured in T25 flasks and when cells were approximately 80% confluent, treatment was commenced with lapatinib. We used 3 different starting concentrations of drug to try and encompass the active dose range observed in the previous proliferation assays thereby maximising the efficiency with which resistant lines were generated. The lowest concentration we started treatment at was 0.04 μM, which was in the range of the IC_{50} for both cell lines. In separate flasks we also commenced treatment at 0.1 μM and 5 μM, which was the highest drug concentration achievable due to the limited aqueous solubility of the drug. On reaching confluence, 50% of each flask was passaged on and the remainder frozen down so that the entire spectrum of resistant cells was available for use in future experiments if required (Figure 7.4). Cells were maintained at the same concentration of lapatinib for a minimum of 2 passages prior to dose escalation. All experiments were performed in duplicate.

No cells from either cell line survived culture with the maximum concentration of lapatinib. However, SKBR3 cells did survive in the presence of 0.1 μM lapatinib although they initially failed to proliferate. After 7 weeks, cells in 1 of the 2 flasks (Lap. R-SKBR3a) started to develop a more mesenchymal phenotype and proliferate rapidly (Figure 7.5). After a further 2 weeks, we observed similar changes in the second flask (Lap. R-SKBR3b). Cells continued to proliferate despite the rapid escalation of lapatinib concentration and were classified as resistant when able to proliferate in the presence of 5 μM lapatinib. Both Lap. R-SKBR3a and b became resistant after 11 weeks of culture in the presence of lapatinib. Cells in the flask which commenced treatment at 0.04 μM lapatinib were surplus to requirements and therefore frozen down early in the dose escalation process.

Despite the presence of an activating PI3K mutation, BT474 cells were less easily rendered resistant to lapatinib. No BT474 cells survived in the presence of lapatinib at either 5 μM or 0.1 μM. Cells survived in culture in the presence of 0.04 μM lapatinib for approximately 17 weeks but failed to proliferate. We therefore decided to increase the percentage of FBS which the cells were cultured in to 20%. After a further 2 weeks, the cells had become confluent and the dose was escalated. As the lapatinib dose was increased, the cells also developed an increasingly mesenchymal appearance with a spindle-shaped morphology and

instead of the close cell-cell contacts observed in the parental cell line, resistant cells only made contact with each other at focal points (Figure 7.5). Both Lap. R-BT474 a and b cell lines were classified as resistant after 27 weeks of culture in the presence of the drug, when they were able to survive in the presence of 5 μM lapatinib. Following the acquisition of resistance, all cell lines continued to be maintained in the presence of 5 μM lapatinib.

We performed cell counting experiments to further quantify the difference in growth rate observed between both sets of parental and resistant cell lines. SKBR3 and BT474 cells were counted and plated out at 3 different concentrations ($0.03*10^6$ cells/ml, $0.06*10^6$cells/ml and $0.12*10^6$ cells/ml). Cells were re-counted 96 hours later, when cells at the top concentration were approximately 80% confluent. All resistant cell lines grew extremely rapidly and therefore despite reducing the initial number of cells ($0.03*10^6$ cells/ml and $0.015*10^6$ cells/ml), we repeated our cell counts after only 48 hours, again when cells were approximately 80% confluent (Figure 7.6). All experiments were performed in triplicate. The doubling time of resistant SKBR3 and BT474 cells was significantly shorter than their parental counterparts ($p<0.001$. one way ANOVA) (Tables 7.1 and 7.2).

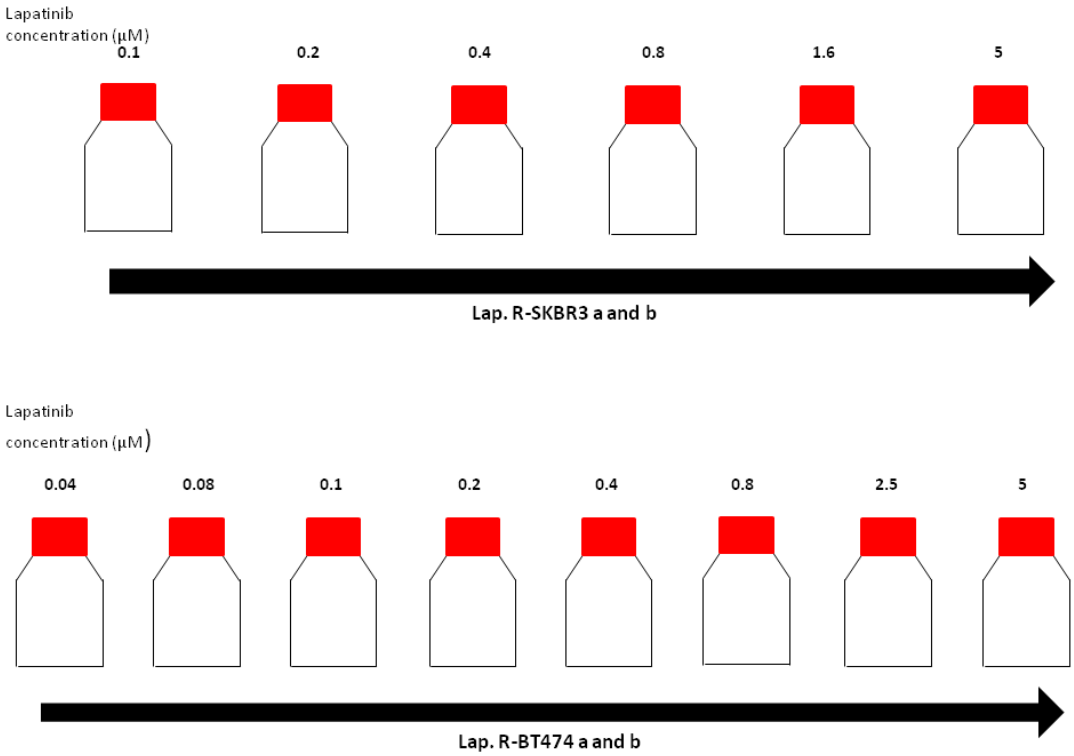

Figure 7.4- Incremental dose escalation of lapatinib to generate resistant cell lines. The concentration of lapatinib was kept constant for at least 2 passages prior to dose escalation. A flexible dose escalation strategy was used so that the magnitude of dose increase was adjusted according to the cells' ability to adapt to the previous dose escalation.

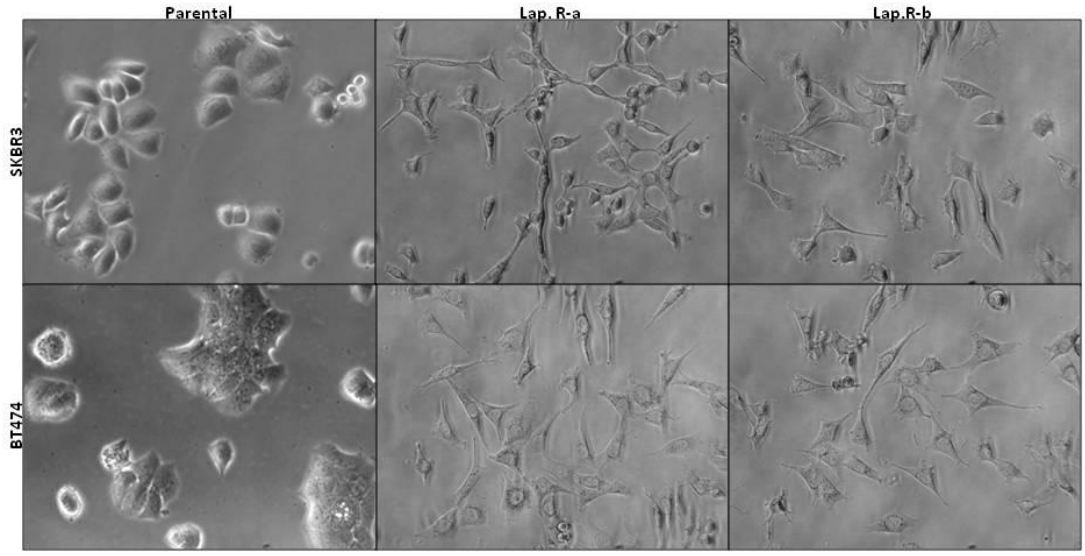

Figure 7.5- Acquisition of resistance to lapatinib coincides with development of mesenchymal phenotype in both SKBR3 and BT474 cell lines. Both parental cell lines have a classical rounded epithelial appearance and form attachments to neighbouring cells along the entire length of the cell. Lapatinib resistant cells appear spindle shaped and form cell-cell connections at focal points only. Mag x20.

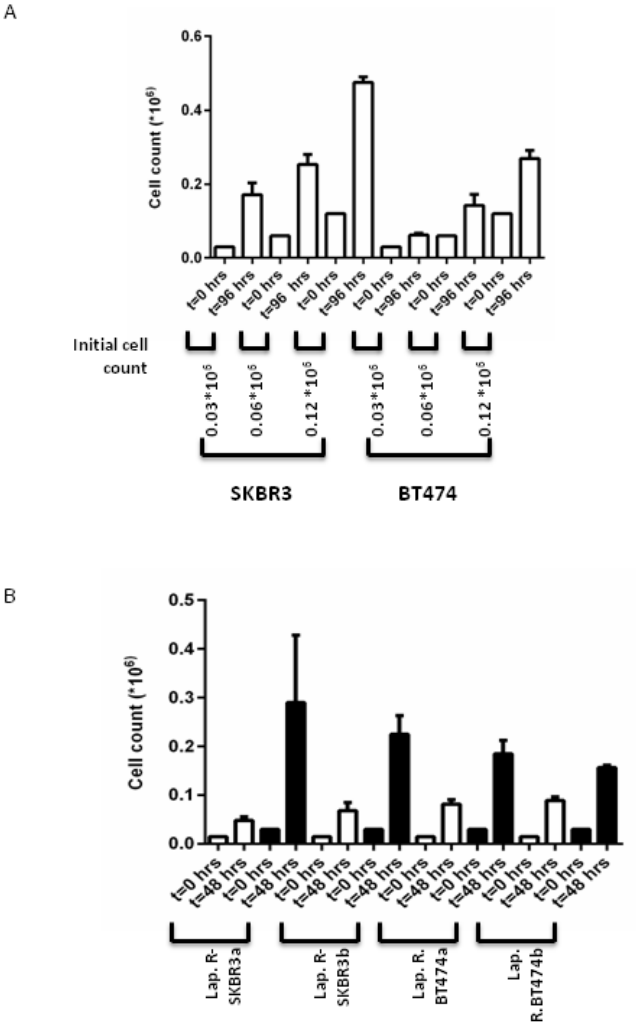

Figure 7.6- Proliferation of parental (A) and lapatinib resistant cell lines (B). Parental cells were seeded in a 12-well plate at 3 different concentrations. Each concentration was plated in duplicate. Proliferation was measured 96 hours later by cell counting. Resistant cell lines were seeded in duplicate at 2 different concentrations. White bars represent an initial cell count of $0.015*10^6$ and black bars represent a starting cell count of $0.03*10^6$ cells. To avoid cells becoming confluent, proliferation was assessed in all resistant cell lines after 48 hours. Mean values with SEM displayed from a series of 3 experiments.

Cell Line	Mean doubling time (± SEM) in hours
Parental SKBR3	59.39 ± 3.8
Lap. R-SKBR3a	14.90 ± 0.83 ∗
Lap. R-SKBR3b	19.02 ± 1.78 ∗

Table 7.1-Cell doubling time of parental SKBR3 cells was significantly prolonged compared to lapatinib resistant cell lines (p<0.001, one way ANOVA). ∗ denotes statistically similar means.

Cell Line	Doubling time (± SEM) in hours
Parental BT474	88.53 ± 6.99
Lap. R-BT474a	19.91 ± 0.97 ∗
Lap. R-BT474b	19.58 ± 0.76∗

Table 7.2- Cell doubling time of parental BT474 cells was significantly prolonged compared to lapatinib resistant cell lines (p<0.001, one way ANOVA). ∗ denotes statistically similar means.

7.4 Confirmation that lapatinib resistant cell lines were resistant to lapatinib

After cells had been maintained in 5 μM lapatinib for at least 2 passages, we rechecked their sensitivity to the drug. Both parental SKBR3 and BT474 cells and their resistant counterparts were treated with escalating doses of lapatinib for 72 hours and then an SRB assay was performed. All experiments were performed in triplicate. Despite treating cells up to a lapatinib concentration of 5 μM, which is the maximum achievable dose, the IC_{50} of resistant cell lines was not reached. We also found that following prolonged culture, the parental SKBR3 cell line became less sensitive to lapatinib and therefore we opted to compare percentage cell kill in the resistant cell lines at the equivalent concentration to the parental cell line's IC_{50} in each individual experiment. Even allowing for the loss of sensitivity of SKBR3 cells to the drug, we found that the percentage cell kill was significantly reduced in both Lap.R-SKBR3a and b cell lines with a mean percentage cell kill of 0.2% and 0% respectively ($p=0.002$, one way ANOVA). The percentage cell kill was also significantly reduced in Lap. R-BT474 a and b cells compared to their parental cell line with a mean percentage cell kill of only 8.13% and 7.47% respectively at the parental cell line's IC_{50} dose ($p=0.001$, one way ANOVA) (Figure 7.7).

To determine the long-term stability of the resistant phenotype, we seeded all resistant cell lines into 2 separate flasks. For each cell line, cells in the first flask continued to be cultured in the presence of 5 μM lapatinib whilst those in the second were grown in the absence of drug. After a minimum of 8 weeks, we re-checked the drug sensitivity of cells which had been grown in both the presence and absence of lapatinib. All experiments included a positive control comprising of the parental cell line treated with increasing doses of lapatinib to confirm continued potency of the drug. After 8 weeks of culture in the absence of drug, we observed a statistically significant increase in the percentage cell kill of lap. R-SKBR3a cells from 0.2% to 11.9%, although despite this the cell line must still be classified as lapatinib resistant. The percentage cell kill of lap. R-SKBR3b cells also increased from 0% to 5.13% but this did not reach statistical significance ($p=0.001$, one way ANOVA with Tukey's test). No difference in the percentage kill of either of the BT474 resistant cell lines was observed, irrespective of whether they were cultured in the presence or absence of lapatinib ($p=0.774$, one way ANOVA) (Figure 7.8).

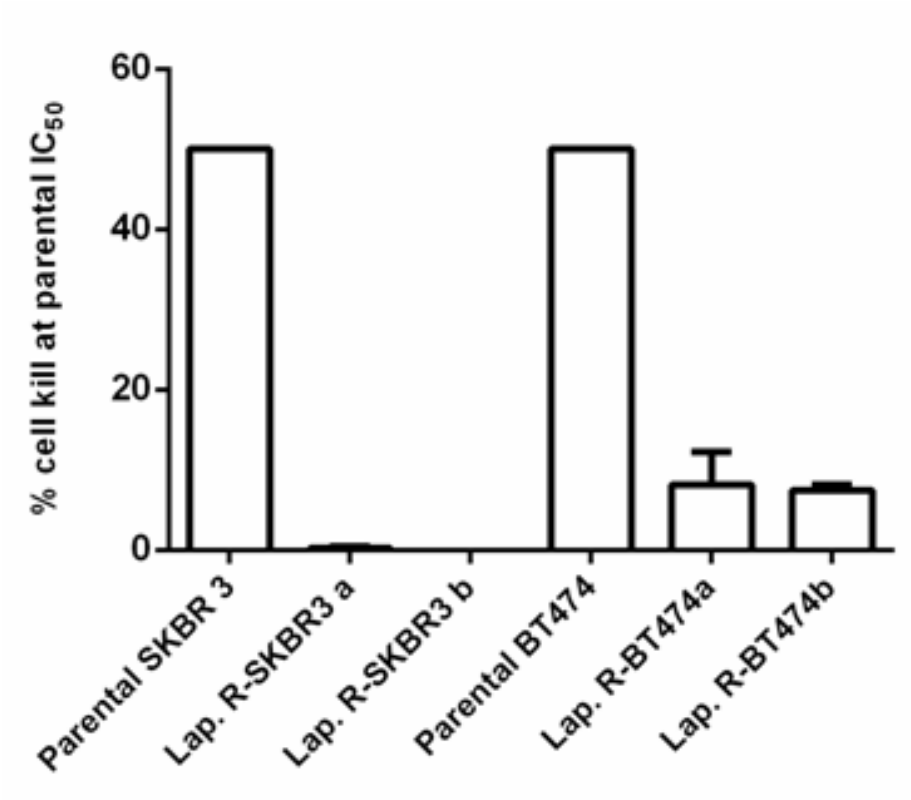

Figure 7.7- Proliferation of lapatinib resistant cell lines is not substantially inhibited by the parental cell line's IC_{50} dose. Parental SKBR3 and BT474 cells (5000 cells/well) and their resistant counterparts (1250 cells/well) were seeded into 96 well plates. After 24 hours, cells were treated with escalating doses of lapatinib for 72 hours before an SRB assay was performed. Data was analysed using GraphPad Prism 6 software. Mean percentage cell kill ± SEM for each cell line calculated from a series of 3 experiments is displayed.

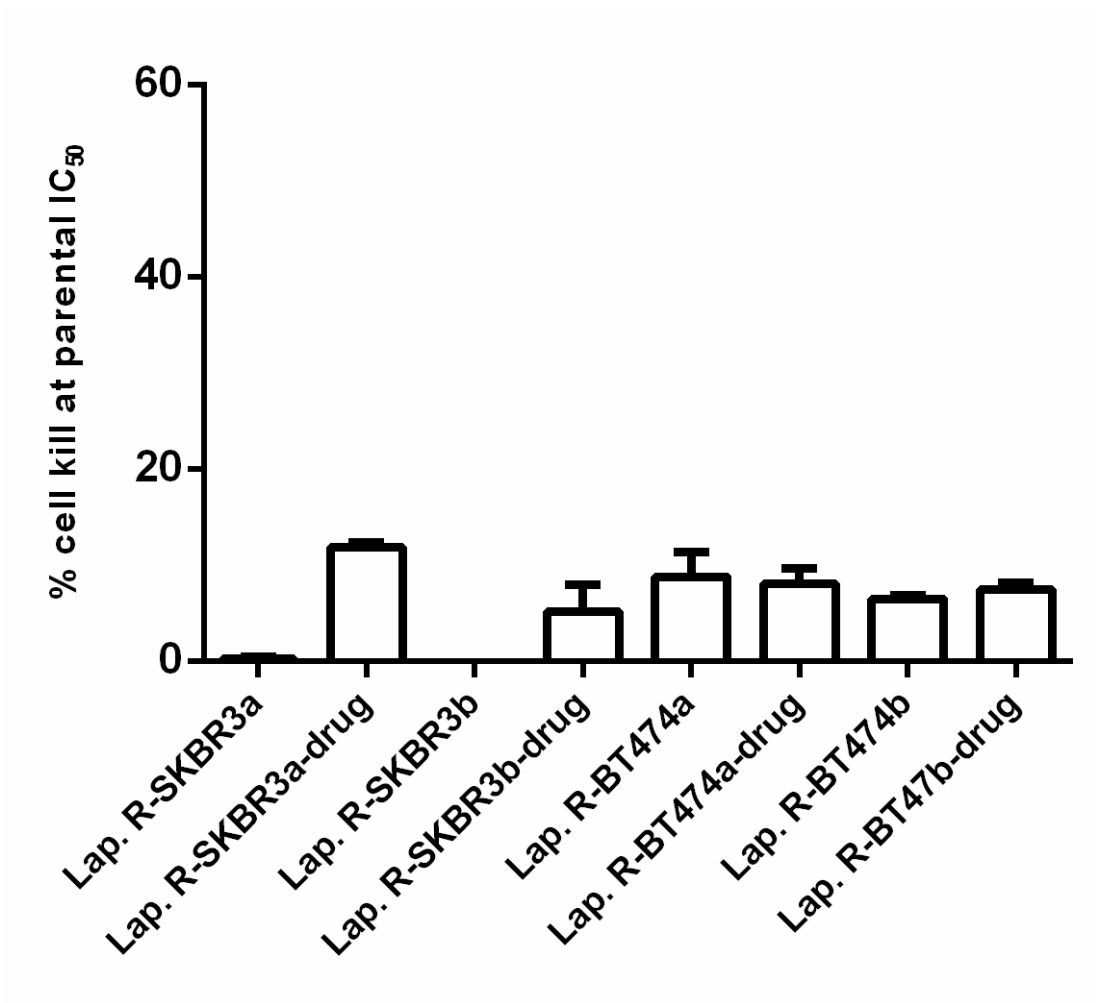

Figure 7.8- Lapatinib resistance was not reversible following drug withdrawal for 8 weeks. Two flasks were seeded with each resistant cell line. One flask per cell line continued to be cultured in the presence of 5 μM lapatinib, whilst the second flask was cultured in the absence of drug. After an interval of at least 8 weeks, drug sensitivity assays were repeated in cell lines cultured both in the presence and absence of drug. All experiments included a positive control comprising of the parental cell line treated with escalating doses of lapatinib to confirm the continued potency of the drug. Data was analysed using GraphPad Prism 6 software. Mean percentage cell kill ± SEM for each cell line calculated from a series of 3 experiments is displayed.

7.5 Demonstration that lapatinib resistant cell lines were cross resistant to AZD8931

To determine whether lapatinib resistant cells remained sensitive to AZD8931, we treated both lapatinib sensitive and resistant SKBR3 AND BT474 cells with escalating doses of AZD8391 for 72 hours prior to performing an SRB assay. All lapatinib resistant cell lines were significantly less sensitive to AZD8931 than the parental cell lines from which they were derived but there was no statistical difference in the percentage cell kill observed between the different resistant cell lines (Figure 7.9). At the parental SKBR3 cell line's IC_{50} dose, the mean percentage cell kill observed in lap. R-SKBR3a and lap. R-SKBR3b was 10.4% and 13.4% respectively ($p=0.002$, one way ANOVA with Tukey's test). At the parental BT474 cell line's IC_{50} dose, the mean percentage cell kill in lap. R-BT474a and lap. R-BT474b was 6.6% and 5.1% respectively ($p<0.001$,one way ANOVA with Tukey's test).

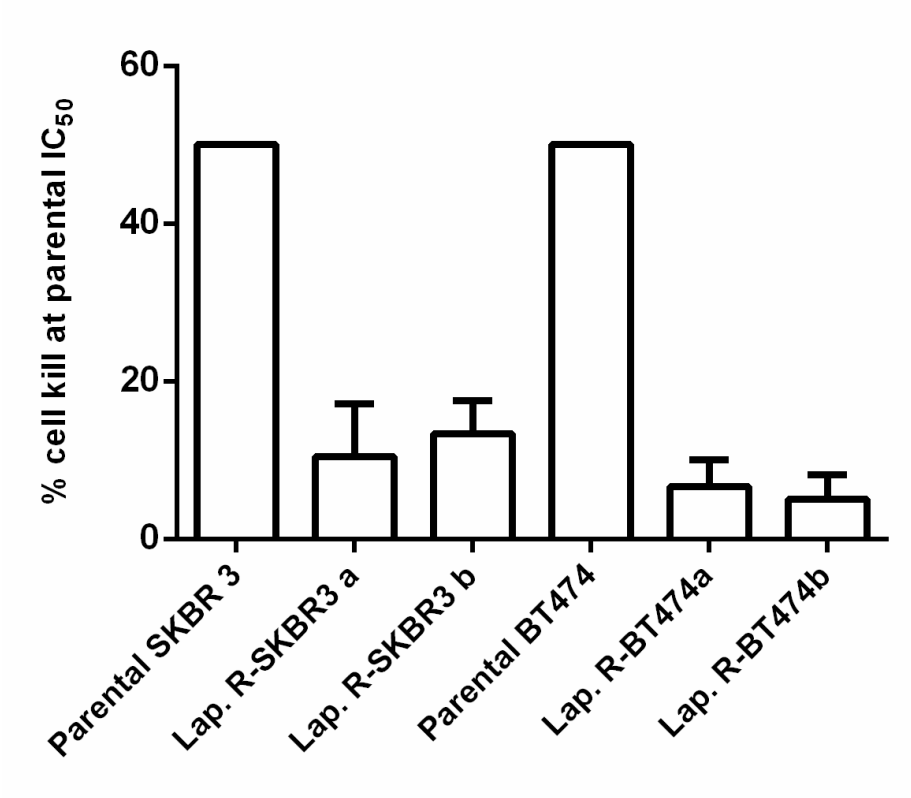

Figure 7.9- Lapatinib resistant SKBR3 and BT474 cells were less sensitive to AZD8931 than parental cell lines. Parental SKBR3 and BT474 cells (5000 cells/well) and their resistant counterparts (1250 cells/well) were seeded into 96 well plates. After 24 hours cells were treated with escalating doses of AZD8931 for 72 hours before an SRB assay was performed. Data was analysed using GraphPad Prism 6 software. Mean percentage cell kill ± SEM for each cell line calculated from a series of 3 experiments is displayed.

7.6 Generation of AZD8931 resistant cell lines

We adopted a similar dose escalation strategy to generate cell lines which were resistant to AZD8931. Again BT474 and SKBR3 cells were cultured in T25 flasks and commenced on AZD8931 when cells were approximately 80% confluent. Treatment was commenced at 1 of the following 3 concentrations; 0.0067 μM (the minimum concentration required to inhibit proliferation in previous experiments), 0.231 μM (approximates to the IC_{50} of both cell lines), or 0.670 μM, (the maximum concentration viable BT474 cells were observed at in above experiments). However, during our initial experiments prolonged treatment with 0.670 μM resulted in total cell death in both cell lines and in the BT474 cell line there were few viable cells at the lower 2 concentrations. Therefore, a further flask in which treatment was commenced at 0.0035 μM was set up. Media, containing fresh drug, was replaced twice weekly and on reaching confluence, 50% of each flask was passaged on and the remainder frozen down so that the entire spectrum of resistant cells was available for use in future experiments if required. Again, a constant concentration of AZD8931 was maintained for at least 2 passages prior to dose escalation and all experiments were performed in duplicate.

Attempts to generate AZD8931 resistant BT474 cell lines were unsuccessful. The maximum concentration of AZD8931 which BT474 cells could be maintained in was 0.077 μM and despite increasing the percentage of FBS to 20%, growth at this concentration was too slow to generate sufficient cells for use in further experiments. After continuous culture with AZD8931 for approximately 1 year, this cell line was rejected as being unable to adapt to AZD8931 exposure.

SKBR3 cells were able to adapt to culture with AZD8931. Both flasks treated at 0.0067 μM and 1 of the 2 flasks treated at 0.231μM AZD8931 retained viable cells after prolonged culture in the presence of the drug. Flasks containing cells incubated with 0.0035 μM of AZD8931 were therefore superfluous and frozen down early in the dose escalation process. Viable cells in all other flasks were incubated with incrementally increasing concentrations of AZD8931 (Figure 7.10). A flexible dose escalation scheme was employed so that the magnitude of dose escalation could be adjusted to reflect the ease with which cells had adapted to the previous dose level. Therefore, when the time interval spent at a dose level

was prolonged, the next dose escalation was more cautious than when cells rapidly grew through a particular AZD8931 concentration. Cells were considered resistant once they were able to actively proliferate in the presence of 0.670 μM AZD8931, which equates to a concentration of 317.5 ng/ml. This concentration is within the range of plasma concentrations detected at the MTD during the phase I trial [326] and therefore resistance mechanisms exhibited at this drug concentration were likely to be clinically relevant. Following the acquisition of resistance, cells continued to be constantly cultured in the presence of 0.670 μM AZD8931.

Three AZD8931 resistant SKBR3 derived cell lines were generated. Resistance was achieved in the first of these cell lines (8931 R-SKBR3c) after 11 weeks. Resistance was achieved in the final 2 cell lines in 24 weeks (8931 R-SKBR3a) and 25 weeks (8931 R-SKBR3b). Similarly to our lapatinib resistant cell lines, development of resistance in all 3 cell lines coincided with acquisition of a distinct mesenchymal phenotype (Figure 7.11), characterized by development of a spindle-shaped cell morphology. Again, the close intercellular connections seen in the parental cell line were replaced by focal point connections in all resistant cell lines. This phenotypic change was also accompanied by an increase in growth rate and cell counting experiments were performed to further quantify this change (Figure 7.12). The cell doubling time was significantly reduced in all 3 resistant cell lines compared to the parental SKBR3 cell line ($p<0.001$, One way ANOVA) (Table 7.3).

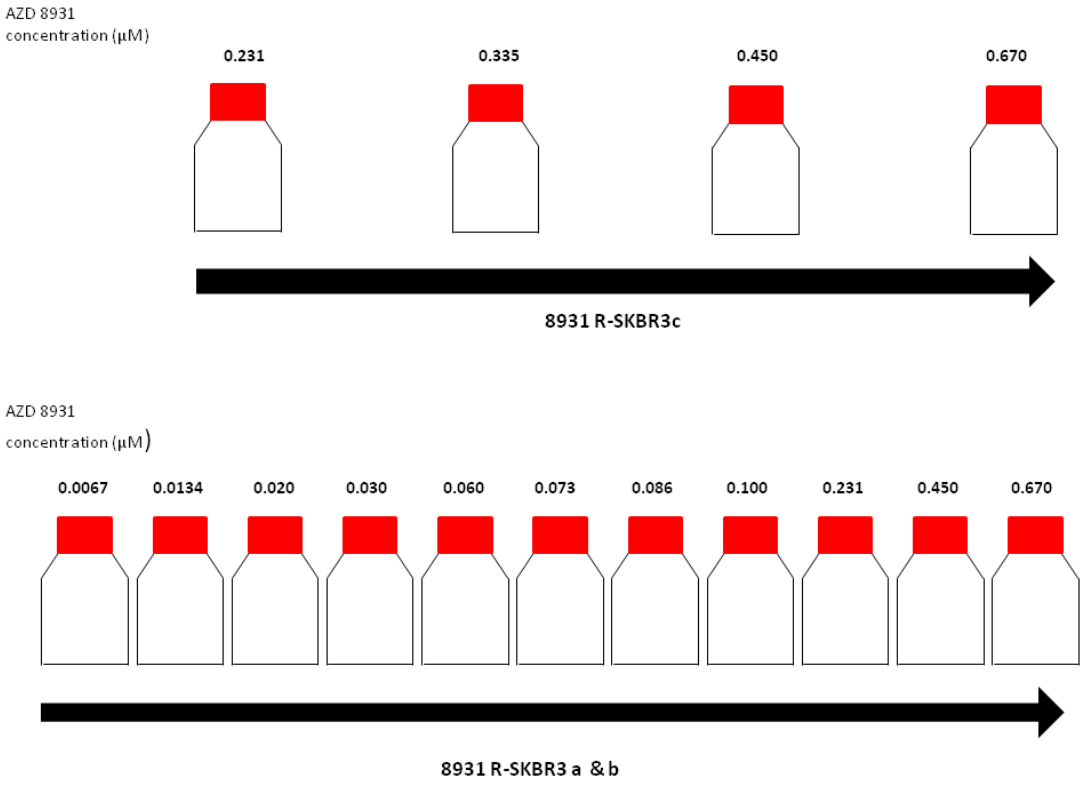

Figure 7.10- Incremental dose escalation of AZD8931 to generate AZD8931 resistant cell lines. The concentration of AZD8931 was maintained for at least 2 passages prior to dose escalation. A flexible dose escalation strategy was used so that the magnitude of dose increase was adjusted according to the cells' ability to adapt to the previous dose escalation.

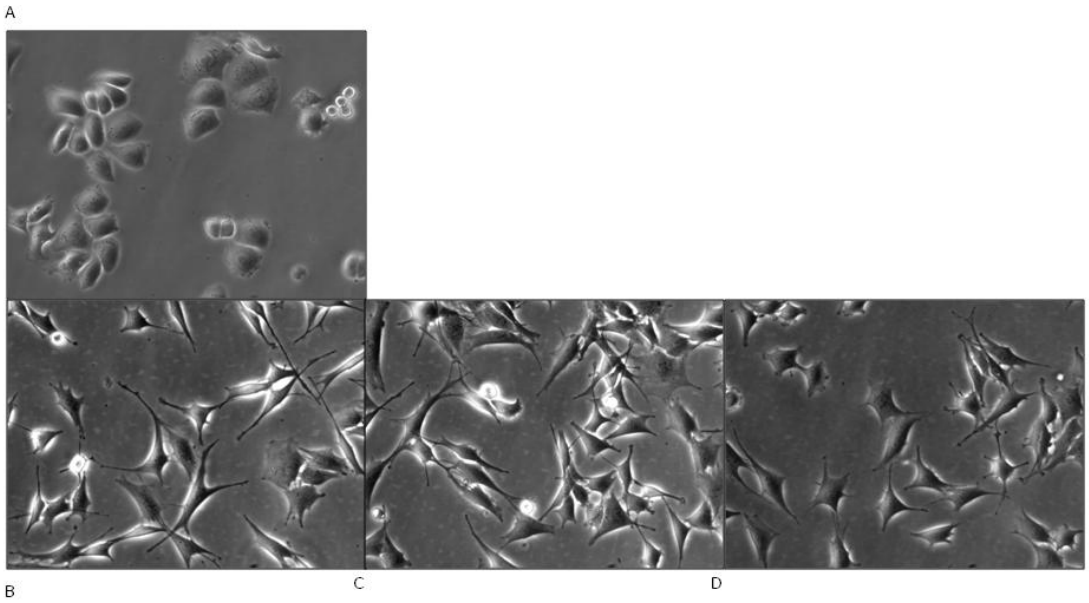

Figure 7.11- Development of resistance coincided with acquisition of a distinct mesenchymal phenotype. A: Parental cells have a rounded, epithelial appearance and form close cell-cell attachments along the cell's entire length. Resistant cell lines 8931 R-SKBR3a (B), 8931 R-SKBR3b (C) and 8931 R-SKBR3c (D) appeared spindle shaped and cell-cell interactions were focal in nature. Mag x20.

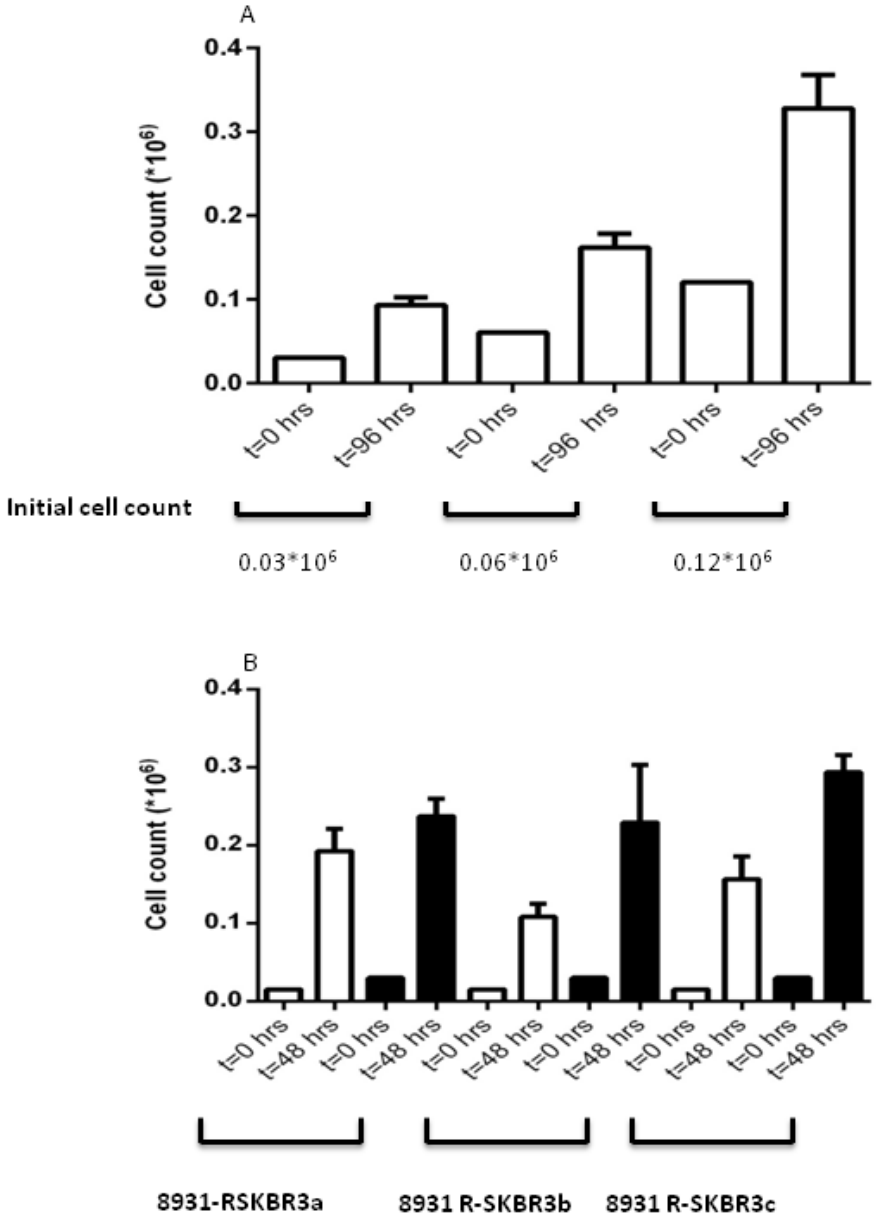

Figure 7.12- Parental cells were seeded in a 12-well plate at 3 different concentrations. Each concentration was plated in duplicate. Proliferation was measured 96 hours later by cell counting. Resistant cell lines were seeded in duplicate at 2 different concentrations. White bars represent an initial cell count of $0.015*10^6$ and black bars represent a starting cell count of $0.03*10^6$ cells. To avoid cells becoming confluent, proliferation was assessed in all resistant cell lines after 48 hours. Mean values with SEM displayed from a series of 3 experiments.

Cell Line	Mean doubling time (± SEM) in hours
Parental SKBR3	59.39 ± 3.8
8931 R-SKBR3a	14.90 ± 0.83 ∗
8931 R-SKBR3b	19.02 ± 1.78 ∗
8931 R-SKBR3c	13.87 ± 0.77 ∗

Table 7.3: Cell doubling time of parental SKBR3 cells was significantly prolonged compared to AZD8931 resistant cell lines ($p<0.001$, one way ANOVA). ∗ denotes statistically similar means.

7.7 Confirmation that 8931 R-SKBR3 a-c cell lines were resistant to AZD8931

Once cells had been maintained in AZD8931 0.670 μM for at least 2 passages, we re-checked their sensitivity to the drug. Both parental and resistant SKBR3 cell lines were cultured in the presence of escalating doses of AZD8931 for 72 hours before SRB assays were conducted. All experiments were performed in triplicate. Despite increasing the maximum concentration of AZD8931 to 20 μM, the IC_{50} of resistant cell lines was not reached. As previously noted when checking lapatinib sensitivity, we found that following prolonged culture parental SKBR3 cells also became less sensitive to AZD8931. Therefore, in the following analysis we have again compared percentage cell kill in the resistant cell lines at the parental cell line's IC_{50} concentration within each individual experiment. Even allowing for the loss of sensitivity in the parental cell line, we found that the percentage cell kill was significantly reduced in all 3 resistant cell lines. At the parental cell line's IC_{50}, the mean percentage cell kill was 0.1%, 0.0% and 1.1% in 8931 R-SKBR3a, 8931 R-SKBR3b and 8931 R-SKBR3c respectively (Figure 7.13). There was no significant difference in the percentage cell kill for any of the 3 resistant cell lines ($p<0.001$, one way ANOVA).

We determined the long-term stability of the resistant phenotype by seeding all 3 resistant cell lines into 2 flasks. For each cell line, 1 flask continued to be cultured in the presence of AZD8931 0.670 μM and the second flask was cultured in the absence of drug. Sensitivity to AZD8931 was re-checked after all cell lines had been cultured in the absence of drug for a period of at least 8 weeks. No difference in the percentage cell kill of any resistant cell line was observed, irrespective of whether they were cultured in the presence or absence of AZD8931 ($p=0.01$, one way ANOVA), suggesting that once established resistance was persistent despite drug withdrawal (Figure 7.14).

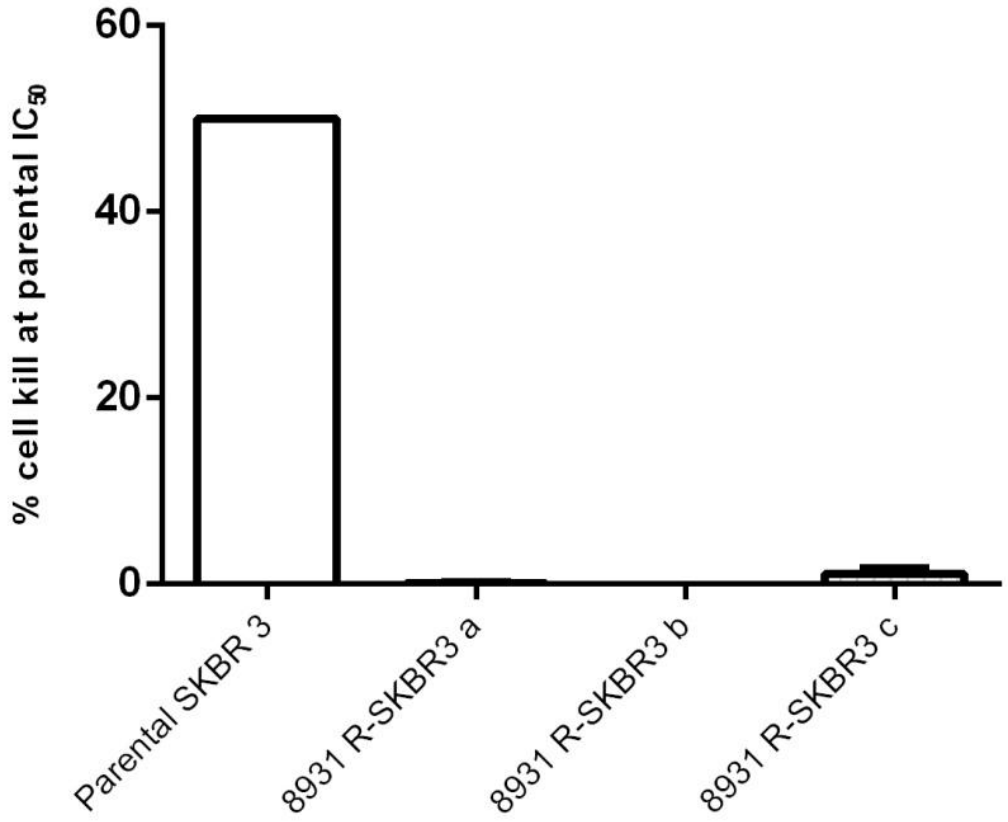

Figure 7.13- Proliferation of 8931-RSKBR3 a-c was not inhibited by the dose of AZD8931 which inhibited proliferation of the parental cell line by 50%. Parental SKBR3 cells (5000 cells/well) and 8931 R-SKBR3a-c cells (1250 cells/well) were seeded into 96 well plates. 24 hours later cells were treated with escalating doses of AZD8931 for 72 hours before SRB assays were performed. Data was analysed using GraphPad Prism 6 software. Mean percentage cell kill ± SEM for each cell line calculated from a series of 3 experiments is displayed.

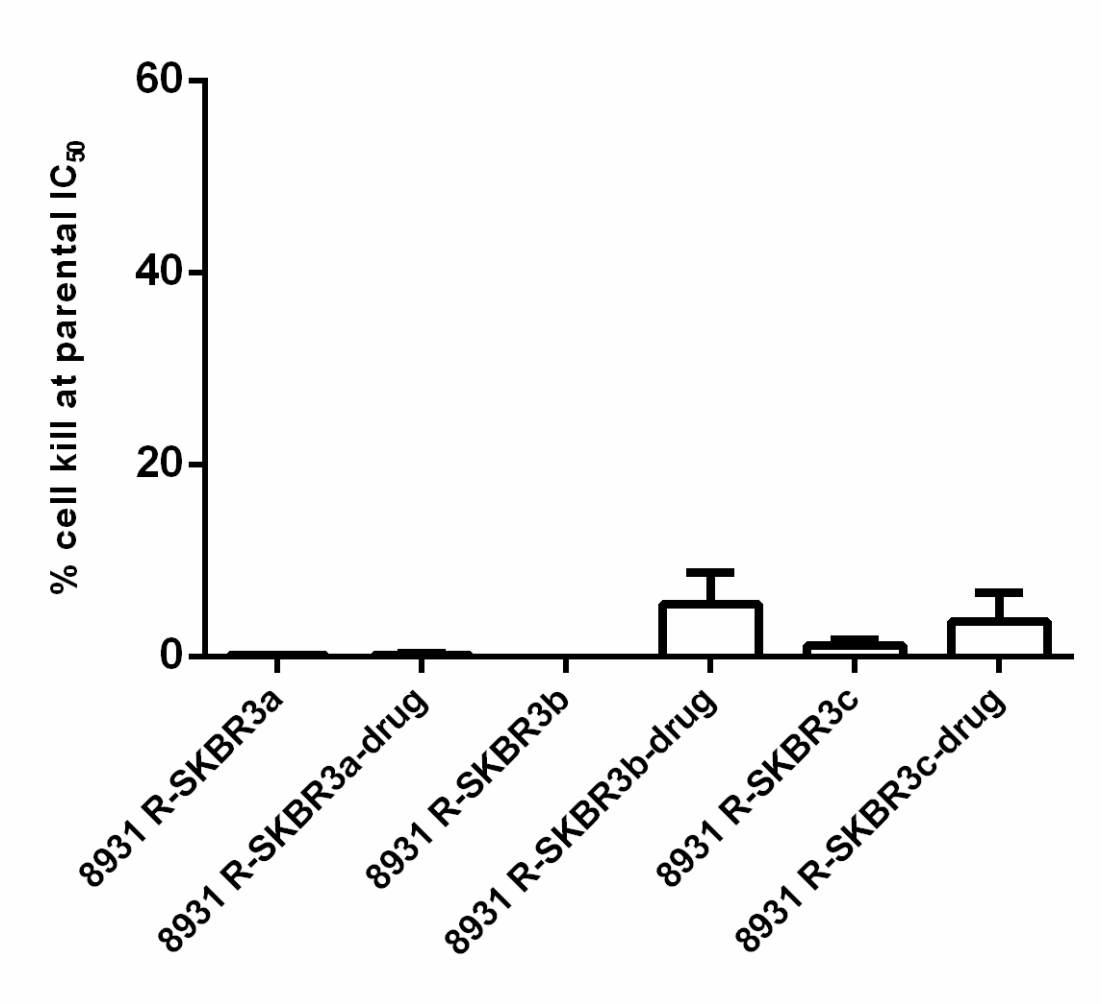

Figure 7.14- AZD8931 resistance was not reversible following drug withdrawal for 8 weeks. Two flasks were seeded with each resistant cell line. One flask per cell line continued to be cultured in the presence of 0.670 μM AZD8931, whilst the second flask was cultured in the absence of drug. After an interval of at least 8 weeks, drug sensitivity assays were repeated in cell lines cultured both in the presence and absence of AZD8931. All experiments included a positive control comprising of parental SKBR3 cells treated with escalating doses of AZD8931 to confirm the continued potency of the drug. Data was analysed using GraphPad Prism 6 software. Mean percentage cell kill ± SEM for each cell line calculated from a series of 3 experiments is displayed.

7.8 Demonstration that AZD8931 resistant cell lines were cross resistant to lapatinib

To explore whether AZD8931 resistant cells remained sensitive to lapatinib, we treated both parental and AZD8931 resistant cells with increasing doses of lapatinib for 72 hours and then performed SRB assays. All 3 AZD8931 resistant cell lines were also resistant to lapatinib (Figure 7.15). At the parental SKBR3 cell line's $IC_{50,}$ the mean percentage cell kill in the resistant cell lines was 0.27%,0.93% and 0.0% in 8931R-SKBR3a, 8931R-SKBR3b and 8931R-SKBR3c respectively ($p<0.001$, one way ANOVA).

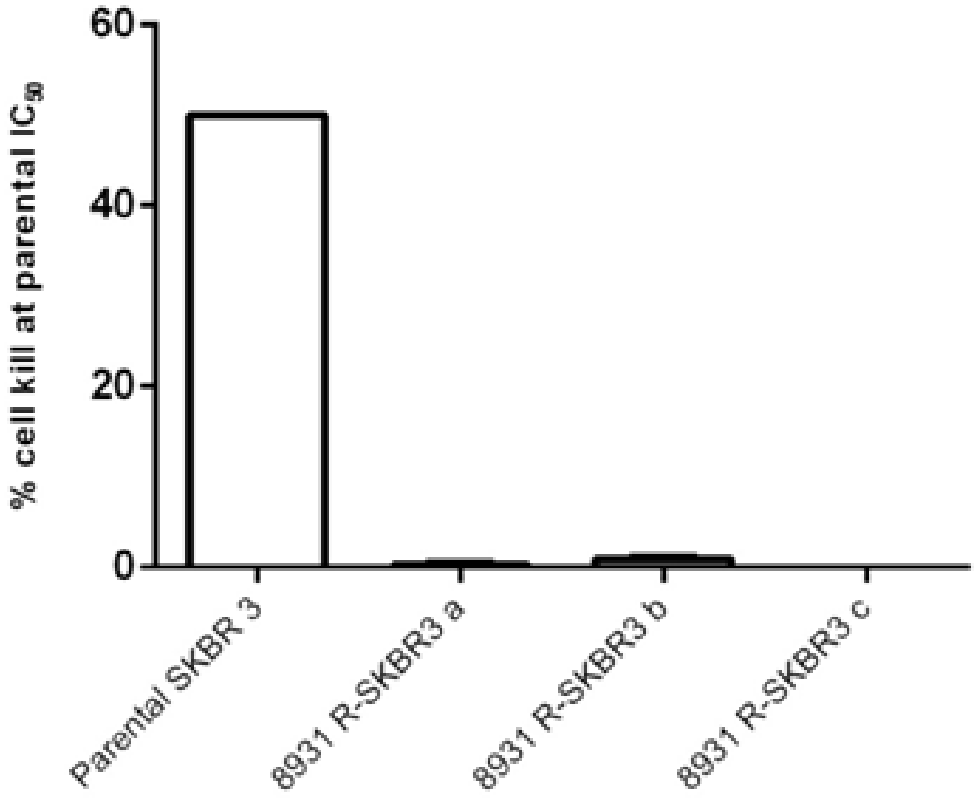

Figure 7.15- AZD8931 resistant cell lines were resistant to lapatinib. 96 well plates were seeded with parental SKBR3 (5000 cells/well) and AZD8931 resistant cell lines (1250 cells/well) and 24 hours later treated with increasing doses of lapatinib for 72 hours. SRB assays were then performed. Data was analysed using GraphPad Prism 6 software. Mean percentage cell kill ± SEM for each cell line calculated from a series of 3 experiments is displayed.

7.9 Confirmation of target inhibition at lapatinib and AZD8931 concentrations which inhibit proliferation

Many existing TKIs, such as dasatinib, are classified as promiscuous drugs as although they potently inhibit their targets, they lack specificity. Therefore, in addition to inhibition of their target tyrosine kinases, many have a range of off-target effects caused by inhibition of non-target kinases. To explore whether the effects of lapatinib and AZD8931 on proliferation were due to on-target effects, we performed western blots on cell lysate from parental BT474 cells which had been treated with escalating doses of lapatinib and parental SKBR3 cells which had been treated with either escalating doses of lapatinib or AZD8931 for 24 hours. We aimed to incorporate drug concentrations in these experiments which encompassed the IC_{50} of the cell lines as calculated in the above SRB experiments. However, we found that the sensitivity of the SKBR3 cell line to both lapatinib and AZD8931 was reduced following prolonged culture. We therefore recalculated the IC_{50} of the SKBR3 cell line to both drugs at the time of performing these western blots and selected appropriate doses to encompass the modified IC_{50}. The modified IC_{50} for the SKBR3 cells treated with lapatinib was 0.5 μM and for AZD8931 it was 1.5 μM. The IC_{50} for the parental BT474 cell line was unchanged following prolonged *in vitro* culture.

As predicted, we observed dose dependent reductions in both pTyr 1248/Tyr 1173 HER2/EGFR and pTyr 1221/1222 HER2 expression in both AZD8391 and lapatinib treated cells (Figure 7.16a). We also observed a reduction in pTyr 1289 HER3 expression in both lapatinib treated SKBR3 and BT474 cells and also in AZD8931 treated SKBR3 cells. A trend towards increased total HER2 expression was seen in all cell lines and HER3 expression also appeared to be increased, although this was most marked in lapatinib treated cells. Both the expression and activation of EGFR was too low in both BT474 and SKBR3 cells to enable us to draw any firm conclusions about the effect of these drugs on this signalling pathway. Akt and p44/42 MAPK are 2 important downstream readouts of HER family signalling. Consistent with reduced HER2 and HER3 activity, we observed dose dependent reductions in both Akt and p44/42 MAPK activity in both lapatinib and AZD8931 treated cells (Figure 7.16b).

In summary, this data shows that target inhibition is achieved at drug concentrations which inhibit cell proliferation.

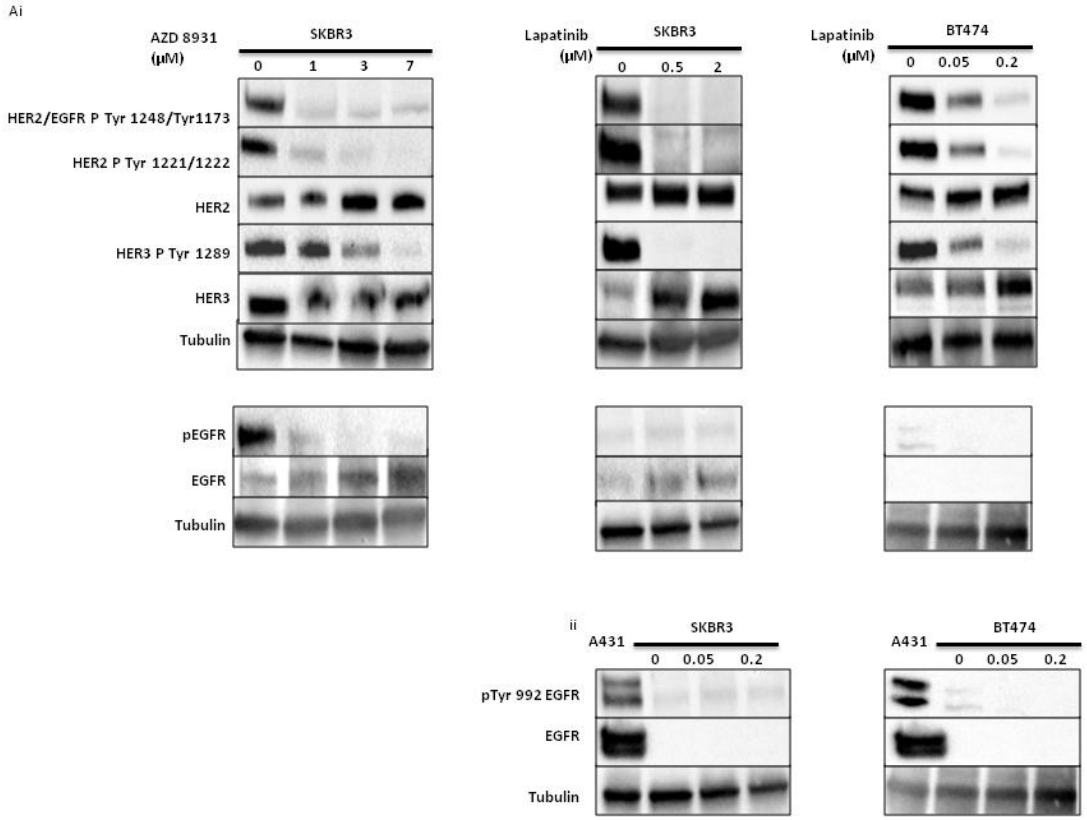
Ai
AZD 8931 (μM)
SKBR3
0 1 3 7
HER2/EGFR P Tyr 1248/Tyr1173
HER2 P Tyr 1221/1222
HER2
HER3 P Tyr 1289
HER3
Tubulin
Lapatinib (μM)
SKBR3
0 0.5 2
Lapatinib (μM)
BT474
0 0.05 0.2
pEGFR
EGFR
Tubulin
ii
A431
SKBR3
0 0.05 0.2
A431
BT474
0 0.05 0.2
pTyr 992 EGFR
EGFR
Tubulin

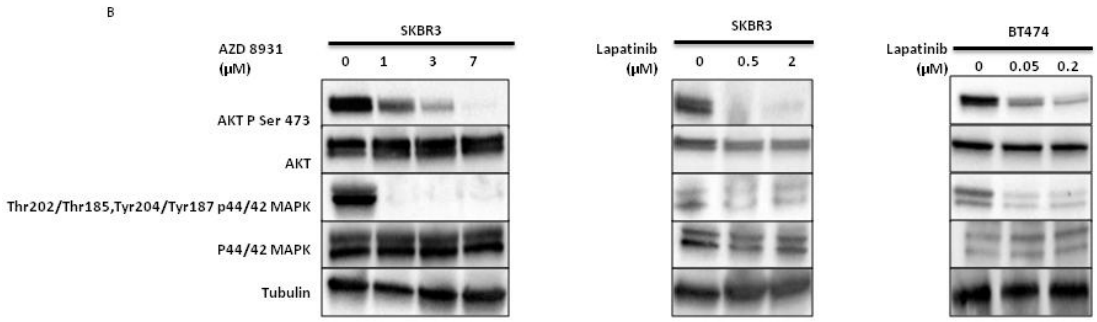

Figure 7.16- Lapatinib and AZD8931 inhibited HER family signalling (Ai, ii) resulting in inhibition of downstream signalling pathways (B). Parental BT474 and SKKBR3 cells were incubated overnight with increasing doses of lapatinib before being used to generate cell lysate for western blotting. Lysate was also generated from SKBR3 cells, which had been treated overnight with AZD8931. Aii: Lysate from untreated A431 cells included as a positive control for EGFR and pTyr 992 EGFR antibodies in lapatinib treated assays. 20 μg protein loaded in each lane, except on EGFR and pEGFR blots where 40 μg protein loaded. Tubulin used as loading control.

7.10 Comparison of parental and resistant cell lines

7.10.1 Comparison of target receptor expression and downstream pathway activation

Altered expression of HER family proteins has previously been described as underlying acquired resistance to both trastuzumab and lapatinib [147]. Therefore, we used western blotting to compare expression of target receptors in untreated parental SKBR3 cells and in our AZD8391 resistant cell lines (Figure 7.17A). We initially used tubulin as a loading control but despite replicating these blots, we noticed consistent variations in the signal obtained with this antibody across the different cell lines tested, particularly when comparing the parental SKBR3 cell line with AZD8931 resistant cell lines. These differences were not present in our initial blots comparing receptor expression within the different parental cell lines suggesting that these changes were related to the development of a mesenchymal phenotype during the development of resistance. We therefore elected to use GAPDH as an alternative loading control in western blots comparing expression of proteins in parental and resistant cell lines, which suggested loading was uniform across the tested cell lines. We used Image J to quantify densitometry changes in replicate blots (Tables 7.4). We found statistically significant reductions in expression of both total HER2 ($p<0.001$, one way ANOVA, Table 7.4) and HER3 ($p=0.002$, one way ANOVA) in our resistant lines. Expression of pTyr 1221/1222 HER2 and pTyr 1289 HER3 was also reduced in our resistant cell lines, where its expression was barely detectable. However, we found that expression of total EGFR was up-regulated in all resistant lines, although this did not reach statistical significance, most likely as a consequence of the low number of blots analysed. Despite this up-regulation, the receptor was largely inactive, with minimal pTyr 992 EGFR expression in either the parental or resistant lines. Looking downstream of the HER family receptors, we found a statistically significant increase in expression of both total Akt ($p=0.013$, one way ANOVA) and p44/42MAPK ($p<0.001$, one way ANOVA Figure 7.4). We also observed a corresponding increase in the expression of the phosphorylated and active fractions of these signalling molecules, suggesting that our resistant cell lines had managed to adapt to reduced HER family signalling through up regulation of both Akt and p44/42 MAPK to ensure continued signalling through these critical pathways. The functional consequences of these signalling changes have been addressed in further experiments (see section 7.11).

To determine whether these changes were specific to AZD8931 resistant cell lines or reflected changes found more widely in cell lines with acquired resistance to HER2 targeted TKIs, we compared HER family receptor expression in parental SKBR3 cells and in untreated lapatinib resistant SKBR3 cell lines. We observed reductions in expression of both total HER2 and HER3 of approximately 95% ($p = <0.001$, one way ANOVA, table 7.5) and 85% ($p<0.001$, one way ANOVA) respectively. Again, expression of both pTyr 1221/1222 HER2 and pTyr 1289 HER3 was barely detectable in either resistant cell line. Unlike our AZD8931 resistant cell lines, we did not observe an increase in total EGFR expression in our lapatinib resistant SKBR3 cell lines and expression of both total EGFR and pTyr 992 EGFR was too low in all cell lines to permit further analysis. As in our AZD8931 resistant cell lines, we observed an increase in total Akt expression in both lapatinib resistant SKBR3 cell lines (Table 7.5). However, pSer 473 Akt was undetectable in both resistant cell lines, suggesting that, unlike in our AZD8931 resistant cell lines, this increase in expression was not accompanied by increased activation. Unlike in our AZD8931 resistant cell lines, we observed no increase in p44/42 MAPK expression in lapatinib resistant cell lines. However, expression of pThr202/Thr185, Tyr 204/187 p44/42 MAPK was reduced in both resistant cell line consistent with reduced signalling p44/42 MAPK signalling activity. Together, this data suggests that survival in our lapatinib resistant SKBR3 cell lines was independent of both Akt and p44/42 MAPK signalling.

To explore whether these changes were specific to SKBR3 derived cell lines or whether they might be generalizable to other cell lines, we examined changes in HER receptor expression in our lapatinib resistant BT474 derived cell lines. Again, we observed significant reductions in expression of both total HER2 ($p<0.001$, one way ANOVA) and HER3 ($p=0.002$, one way ANOVA) in both lapatinib resistant BT474 cell lines. Again, expression of both pTyr 1221/1222 HER2 and pTyr 1289 HER3 was barely detectable in either resistant cell line. Expression of total EGFR was too low to permit quantification in any of the cell lines. However, pTyr 992 EGFR was readily detectable in the parental cell line but was undetectable in either resistant cell line. As in our lapatinib resistant SKBR3 cell lines, the BT474 resistant cell lines appeared to have developed Akt and p44/42 independent signalling mechanisms as we did not observe an increase in expression of these signalling molecules (Table 7.5). Furthermore, we observed marked reductions in the expression of both pSer 473 Akt and pThr202/Thr185, Tyr 204/187 p44/42 MAPK.

Taken together, these results suggest that reduced HER family receptor expression is a common mechanism employed by cells to develop resistance to HER2 targeting TKIs. However, the downstream consequences of this loss appears to be drug specific; our AZD8931 resistant SKBR3 cell lines adapted by up regulating Akt and p44/42 MAPK to support ongoing signalling through these critical pathways whilst both our lapatinib resistant SKBR3 and BT474 cell lines had developed independent, alternative signalling mechanisms in order to survive.

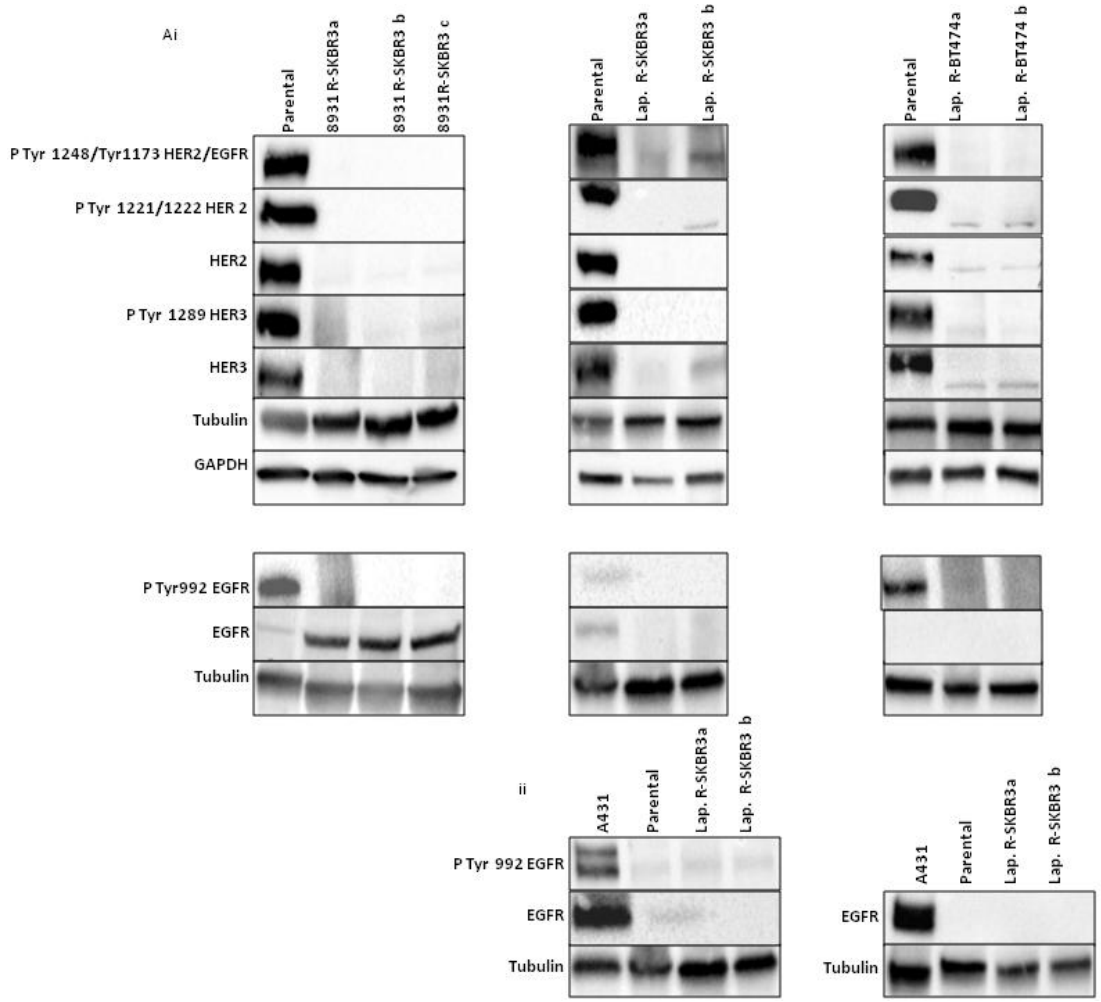
Ai
Parental
8931 R-SKBR3a
8931 R-SKBR3 b
8931R-SKBR3 c
P Tyr 1248/Tyr1173 HER2/EGFR
P Tyr 1221/1222 HER 2
HER2
P Tyr 1289 HER3
HER3
Tubulin
GAPDH
Parental
Lap. R-SKBR3a
Lap. R-SKBR3 b
Parental
Lap. R-BT474a
Lap. R-BT474 b
P Tyr992 EGFR
EGFR
Tubulin
ii
A431
Parental
Lap. R-SKBR3a
Lap. R-SKBR3 b
P Tyr 992 EGFR
EGFR
Tubulin
A431
Parental
Lap. R-SKBR3a
Lap. R-SKBR3 b
EGFR
Tubulin

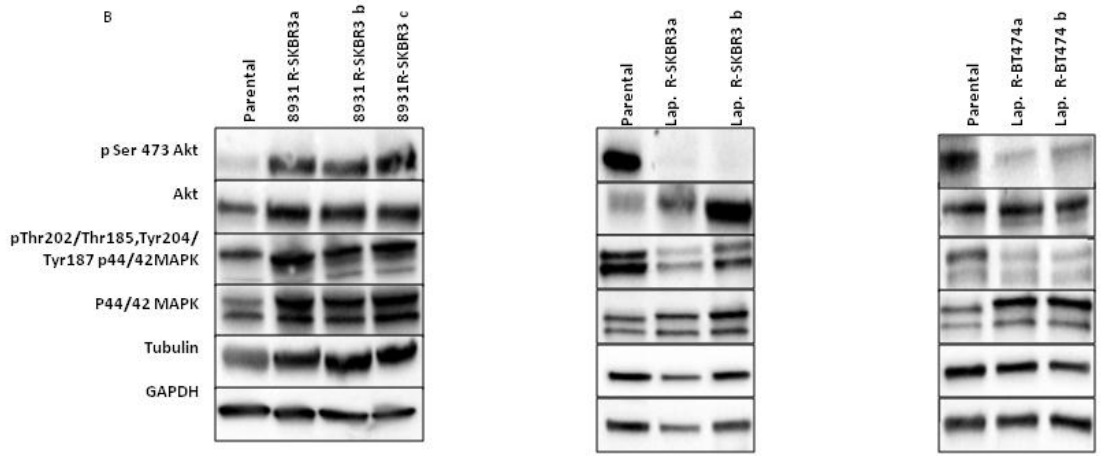

Figure 7.17- Representative western blots comparing expression of target receptors (A) and downstream pathway activation (B) in untreated parental and AZD8931 or lapatinib resistant cell lines. Aii: Lysate from untreated A431 cells included as a positive control for EGFR and pTyr 992 EGFR antibodies. 20 µg protein loaded in each lane, except on EGFR and pEGFR blots where 40 µg protein loaded. Tubulin and GAPDH used as loading control.

	Mean 8931-RSKBR3a expression (SD)	Mean 8931-RSKBR3b expression (SD)	Mean 8931-RSKBR3c expression (SD)	P value
HER2	0.06 (0.02)*	0.045 (0.01)*	0.06 (0.01)*	<0.001
HER3	0.15 (0.08)*	0.08 (0.05)*	0.13 (0.01)*	0.002
EGFR	7.15 (4.57)	13.48(12.25)	13.47 (12.54)	0.451
AKT	1.95 (0.09)*	1.90 (0.45)*	1.79 (0.37)*	0.013
P44/42 MAPK	1.63 (0.02)*	1.72 (0.07)*	1.81 (0.09)*	0.001

Table 7.4- Quantification of changes in total protein expression in AZD8931 resistant cell lines by western blot. Expression in resistant cell lines displayed relative to parental cell line expression (which always equalled 1). Image J software used to quantify changes in total protein expression in a series of 3 experiments. P values, comparing differences in protein expression between parental and resistant cell lines, calculated using one way ANOVA with Tukey's test. Statistically similar means denoted by *.

	Lap. R-SKBR3			Lap. R-BT474		
	Mean relative expression in a (SD)	**Mean relative expression in b (SD)**	**P value**	**Mean relative expression in a (SD)**	**Mean relative expression in b (SD)**	**P value**
HER2	0.05(0.03)*	0.04 (0.03)*	<0.001	0.10 (0.06)**	0.13 (0.07)**	0.001
HER3	0.12 (0.04)*	0.16(0.05)*	<0.001	0.20 (0.04)**	0.13 (0.01)**	<0.001
EGFR	1.05 (0.79)	0.76 (0.36)	0.829	1.35 (0.02)*	0.89 (0.04)**	0.001
AKT	1.30 (0.17)	1.77 (0.004)	0.010	1.01 (0.37)	0.66 (0.26)	0.315
P44/42 MAPK	1.12 (0.25)	1.61 (0.07)	0.055	0.91 (0.18)	0.86 (0.29)	0.788

Table 7.5- Quantification of changes in total protein expression in lapatinib resistant cell lines on western blot. Expression in resistant cell lines displayed relative to parental cell line expression (which always equalled 1). Image J software used to quantify changes in total protein expression in a series of 2 experiments. P values comparing differences in protein expression between parental and resistant cell lines calculated using one way ANOVA with Tukey's test. Statistically similar means denoted by *.

7.10.2 Comparison of signaling pathway changes in response to lapatinib and AZD8931 in parental and resistant SKBR3 cells.

To further explore the contribution of HER family receptor expression changes on the resistant phenotype, parental and resistant cell lines were incubated overnight with escalating doses of AZD8391 or lapatinib. As previously described, parental cell lines demonstrated dose-dependent reductions in phosphorylation and activation of HER2, HER3 and EGFR. Dose dependent reductions in both Akt and p44/42 MAPK activity were also observed. In all our resistant cell lines, we observed persistent Akt and p44/42 MAPK activity when treated with escalating doses of AZD8931 (Figure 7.18) or lapatinib (Figure 7.19, Figure 7.20) despite reduced HER receptor expression. Increasing the dose of lapatinib used to treat Lap. R-SKBR3b cells to 2 μM resulted in a substantial reduction in Akt activity. Resistant cell lines were maintained in the presence of 5 μM of lapatinib and this therefore suggests that persistent Akt activity alone was not sufficient to account for the resistant phenotype in this cell line.

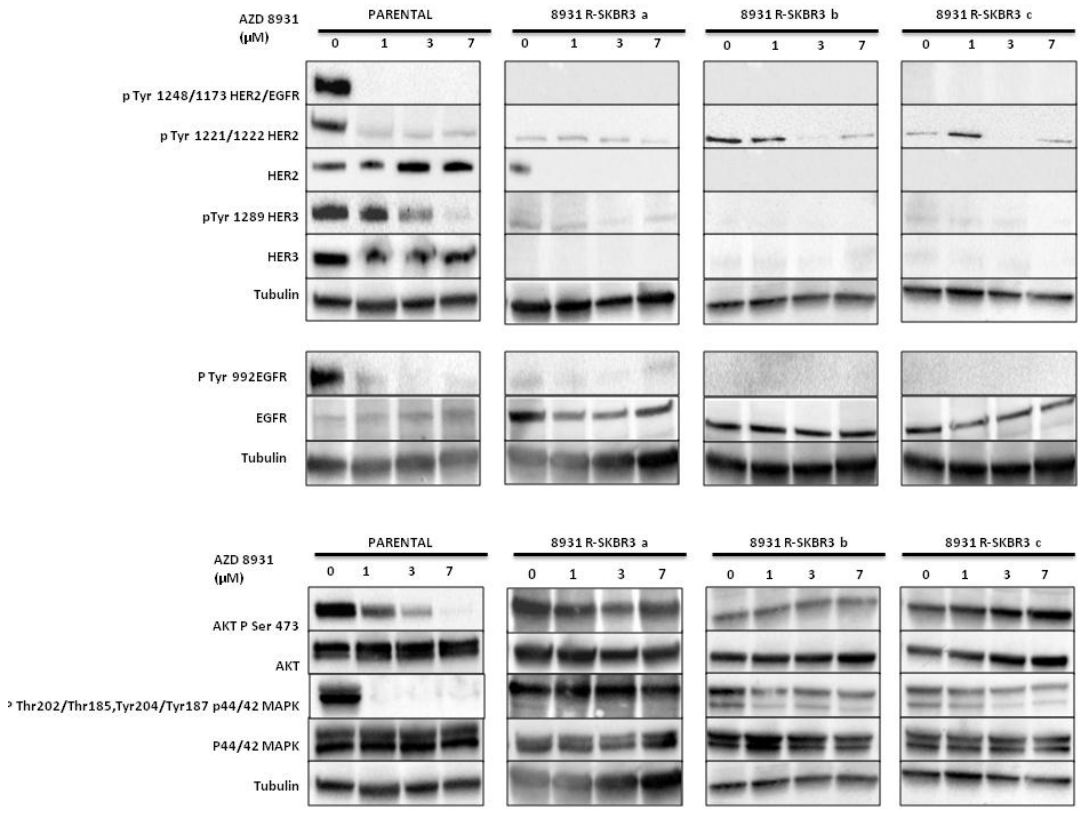

Figure 7.18: AZD8931 resistance was associated with persistent Akt and p44/42 MAPK activity in the presence of AZD8931. Parental and resistant cell lines were treated overnight with escalating doses of AZD8931 before lysate was generated for western blotting. Optimal exposures for each individual cell line displayed and therefore parental and resistant cell line images not necessarily contemporaneous. 20 μg protein loaded in each lane except for EGFR and pTyr 992EGFR where 40 μg protein loaded. Tubulin used as loading control.

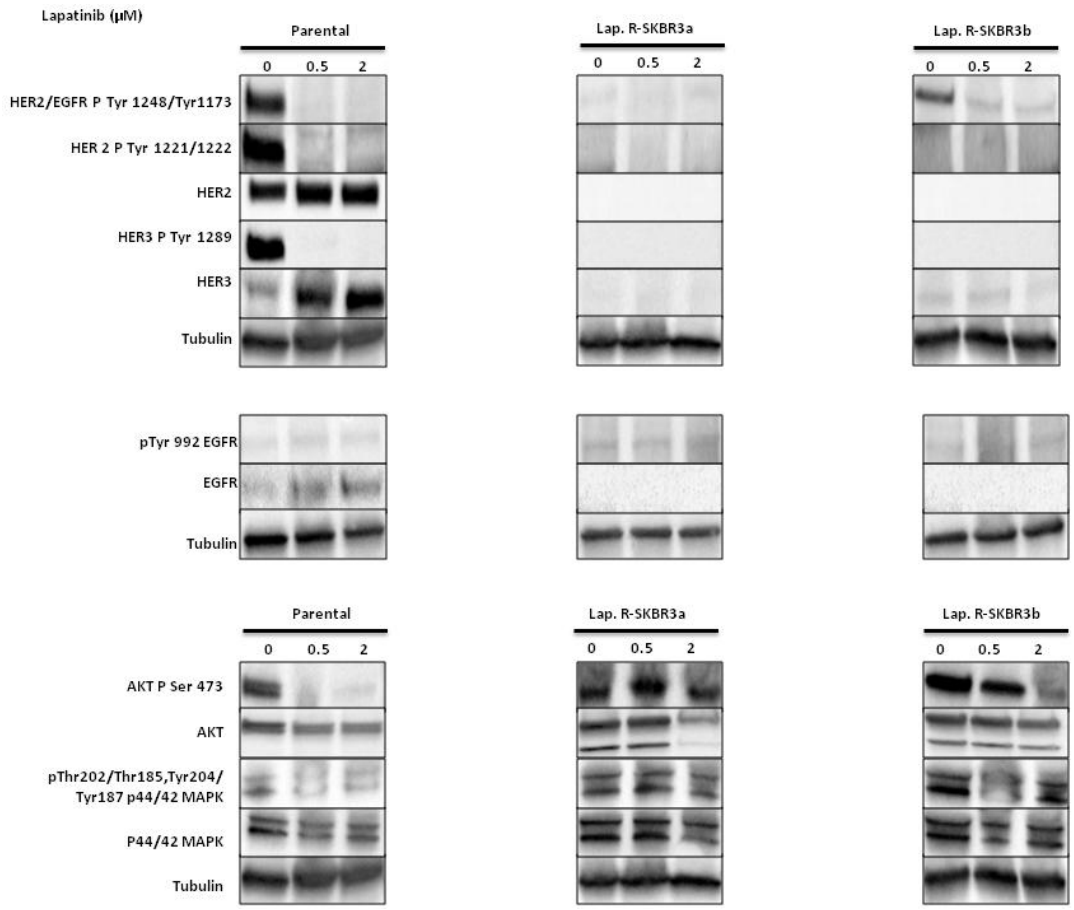

Figure 7.19: Lapatinib resistance in SKBR3 cells was associated with persistent Akt and p44/42 MAPK activity in the presence of lapatinib. Lysate was generated from parental and resistant cell lines treated with escalating doses of lapatinib. Optimal exposures for each individual cell line displayed and therefore parental and resistant cell line images not necessarily contemporaneous. 20 μg protein loaded in each lane, except in EGFR blot where 40 μg protein loaded. Tubulin used as loading control

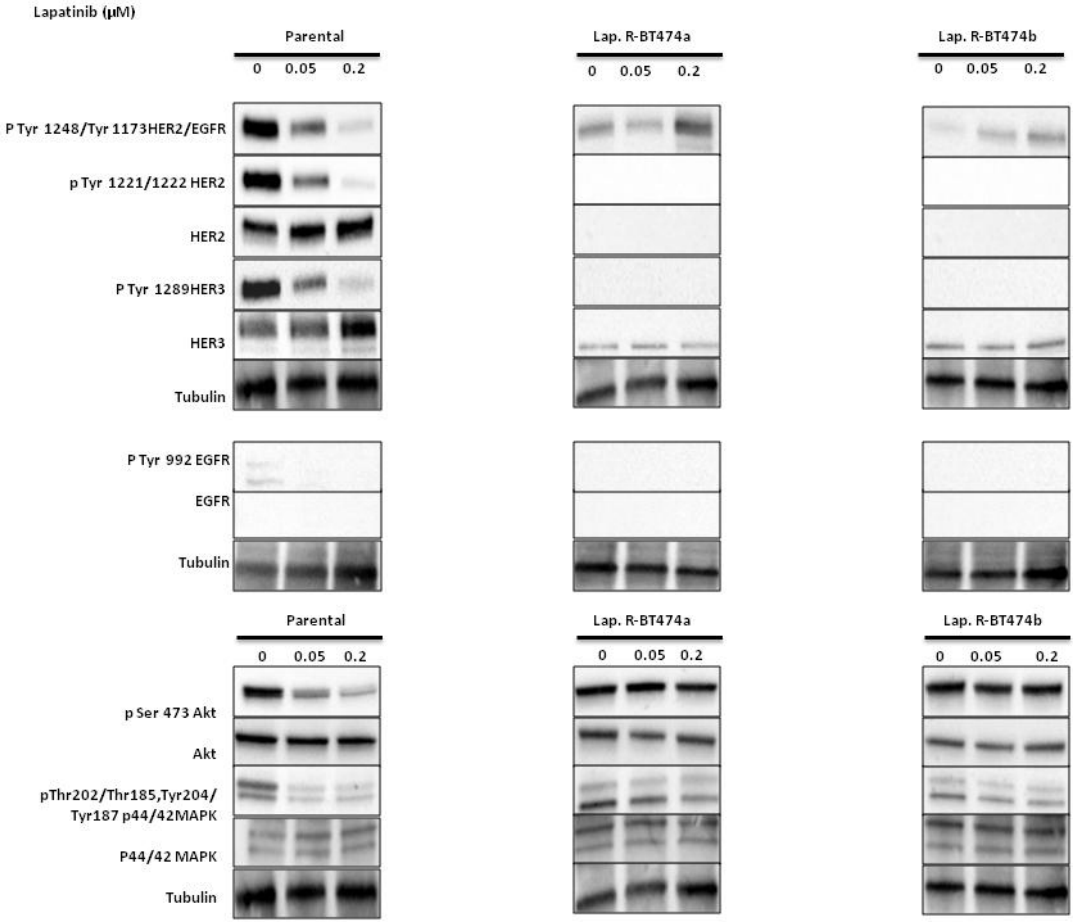

Figure 7.20: Persistent activation of Akt and p44/42 MAPK was observed in lapatinib resistant BT474 cells in the presence of escalating doses of lapatinib. Parental and resistant cell lines were treated overnight with escalating doses of lapatinib before lysate was generated for western blotting. Optimal exposures for each individual cell line displayed and therefore parental and resistant cell line images not necessarily contemporaneous. 20 μg protein loaded in each lane, except in EGFR blot where 40 μg protein loaded. Tubulin used as loading control.

7.10.3 Initial exploration of additional mechanisms of acquired resistance to HER2 targeted TKIs

Mechanisms of acquired resistance to HER2 targeted therapies have been the focus of numerous previously published studies [147] [330]. Using lysate from untreated parental cell lines and their AZD8931 or lapatinib resistant derivatives, we used western blotting to explore whether any of these previously established resistance mechanisms were present in our cell lines. Consistent with our earlier observations that AZD8931 resistant cell lines were cross resistant with lapatinib resistant cell lines and vice versa (Figure 7.9 and 7.15), we observed considerable overlap in the resistance strategies used by AZD8391 and lapatinib resistant cell lines. Resistance to both AZD8931 and lapatinib was associated with loss of PTEN expression (Figure 7.21). Despite a reduction in total Src in all 3 AZD8931 resistant cell lines, we observed an increase in pTyr 416 Src expression suggesting increased Src activity in these cell lines. A similar increase in pTyr 416 Src expression was observed in lapatinib resistant SKBR3 cell lines although total Src expression was unchanged. However, we did not observe any consistent change in Src activity in BT474 derived lapatinib resistant cell lines. Using pTyr 1162 /1163 IGF1R expression, 2 key autophosphorylation sites on IGF1R [331], we measured IGF1R signalling activity. Again, we observed an increase in IGF1R activity in both AZD8931 and lapatinib resistant SKBR3 cells but saw no change in activity in BT474 derived lapatinib resistant cell lines. Phosphorylation of the EphA2 receptor tyrosine kinase receptor by Akt on serine residue 897 has been associated with increased cell migration [332]. We found that pSer 897 EphA2 expression was increased in all resistant cell lines along with total EphA2 which has also been linked to resistance

In summary, we identified multiple signalling changes in all the resistant cell lines. However, further experiments are required in the future to identify which of these changes, if any, were responsible for driving resistance.

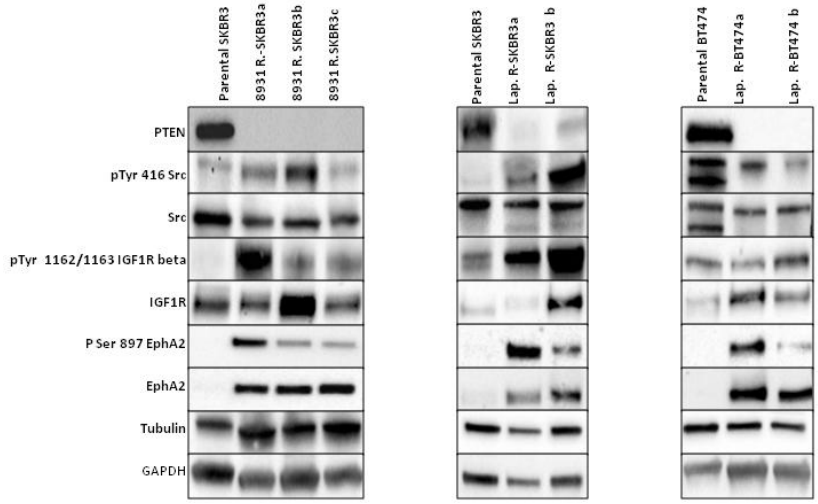

Figure 7.21- Key changes in signalling pathways linked to resistance in AZD8931 and lapatinib resistant cell lines. 20 µg protein loaded in each lane. Tubulin and GAPDH used as loading controls. EphA2 blots in AZD8931 resistant cell line by J. Main.

7.10.4 Confirmation of induction of EMT in resistant cell lines

As previously described, acquisition of both lapatinib and AZD8931 resistance was associated with a distinctive change in phenotype and development of a mesenchymal appearance. We therefore compared expression of EMT markers in parental and resistant cell lines. Both N-cadherin [333] and vimentin [334] expression were upregulated in all resistant cell lines (Figure 7.22), consistent with their mesenchymal appearance (Figures 7.5 and 7.11). Loss of E-cadherin is considered a hallmark of EMT [333] and we observed loss of expression in lapatinib resistant BT474 cells. However, the SKBR3 cell line contains a deletion in CDH1, the E-cadherin encoding gene, and therefore does not express any E-cadherin protein [335]. Although CDH1 mutations are not frequently reported in ductal breast carcinomas, reduced E-cadherin protein expression is common [336]. Therefore, EMT in a low E-cadherin expressing tumour is likely to be a commonly encountered scenario making our lapatinib and AZD8931 resistant cell lines still relevant in the wider clinical context.

Cells which have undergone EMT display an increasingly migratory phenotype [337], [338]. Using AZD8931 resistant cell lines, we conducted random migration studies to further confirm that resistant cells had undergone EMT. 3000 cells were seeded in a 6 well dish and images acquired every 15 minutes overnight. Image J software was used to analyse the images and to calculate the total and the vectorial distance covered by individual cells **(analysis by J. Main)**. The mean accumulated distance was significantly increased in all 3 resistant cell lines ($p<0.001$, One way ANOVA, Figure 7.23). The mean distance travelled by parental SKBR3 cell lines was only 10.89 μm compared to 59.22 μm and 52.60 μm covered by 8931 R-SKBR3b and 8931 R-SKBR3c cell lines respectively. 8931 R-SKBR3a was the most motile of all cell lines with a mean of 73.47 μm travelled, which was significantly greater than the motility of parental SKBR3 and 8931 R-SKBR3b and 8931R-SKBR3c cell lines. Similarly, in terms of the vectorial distance covered, all 3 resistant cell lines demonstrated increasingly motility with 8931 R-SKBR3a being the most motile of all cell lines ($p<0.001$, one way ANOVA). Persistence of movement, defined as vectorial distance/accumulated distance, was not significantly different between any of the cell lines ($p=0.078$, One way ANOVA).

An increase in invasion capacity is also characteristic of mesenchymal cells [337], [338]. 3D invasion studies through matrigel (**performed by J. Main**) demonstrated a non-significant

increase in invasive capacity of the 3 resistant cell lines (p=0.092, One way ANOVA, Figure 7.24). When compared to the invasive capacity of the parental SKBR3 cell line at 60 μm, mean invasive capacity of 8931-RSKBR3a, 8931-RSKBR3b and 8931- RSKBR3c was 152.9%, 165.9% and 240.2% respectively.

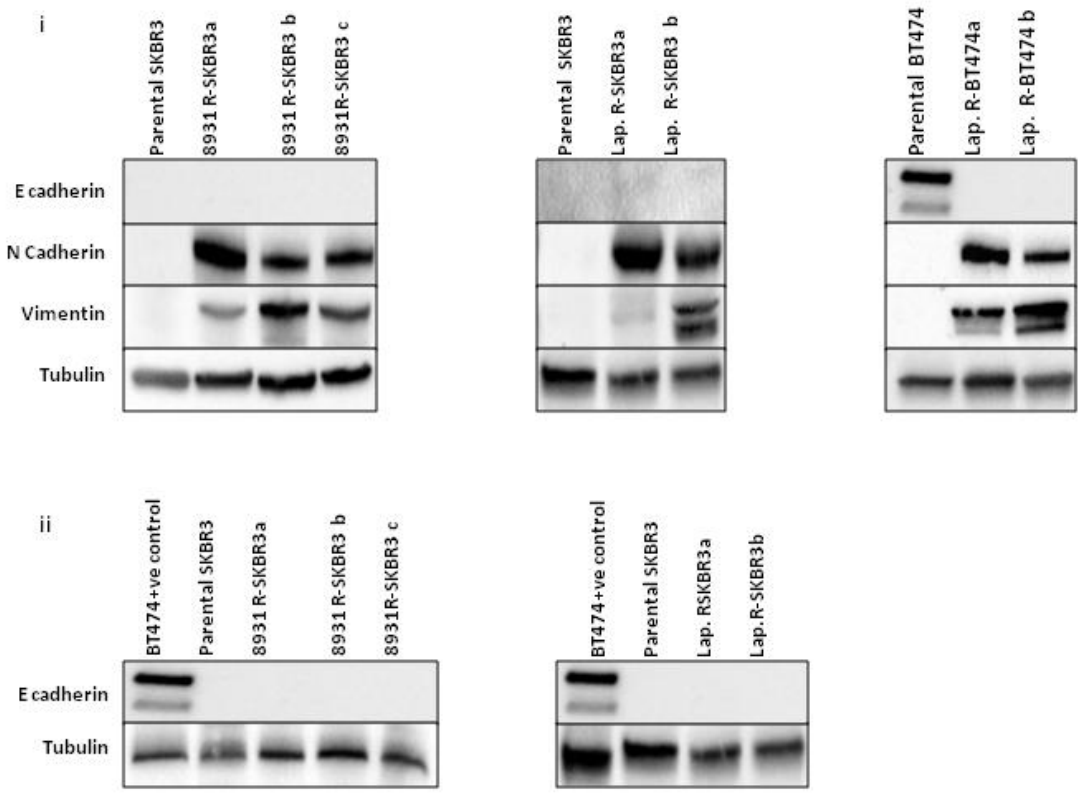

Figure 7.22- AZD8931 and lapatinib resistant cell lines have changes in EMT markers. Ai: Western blots demonstrating loss of epithelial markers in BT474 resistant cell lines and acquisition of mesenchymal markers in SKBR3 and BT474 resistant cell lines. 20 µg protein loaded in each lane. Tubulin used as loading control Aii: western blot confirming absence of E-cadherin expression in all SKBR3 cell lines. BT474 included as a positive control.

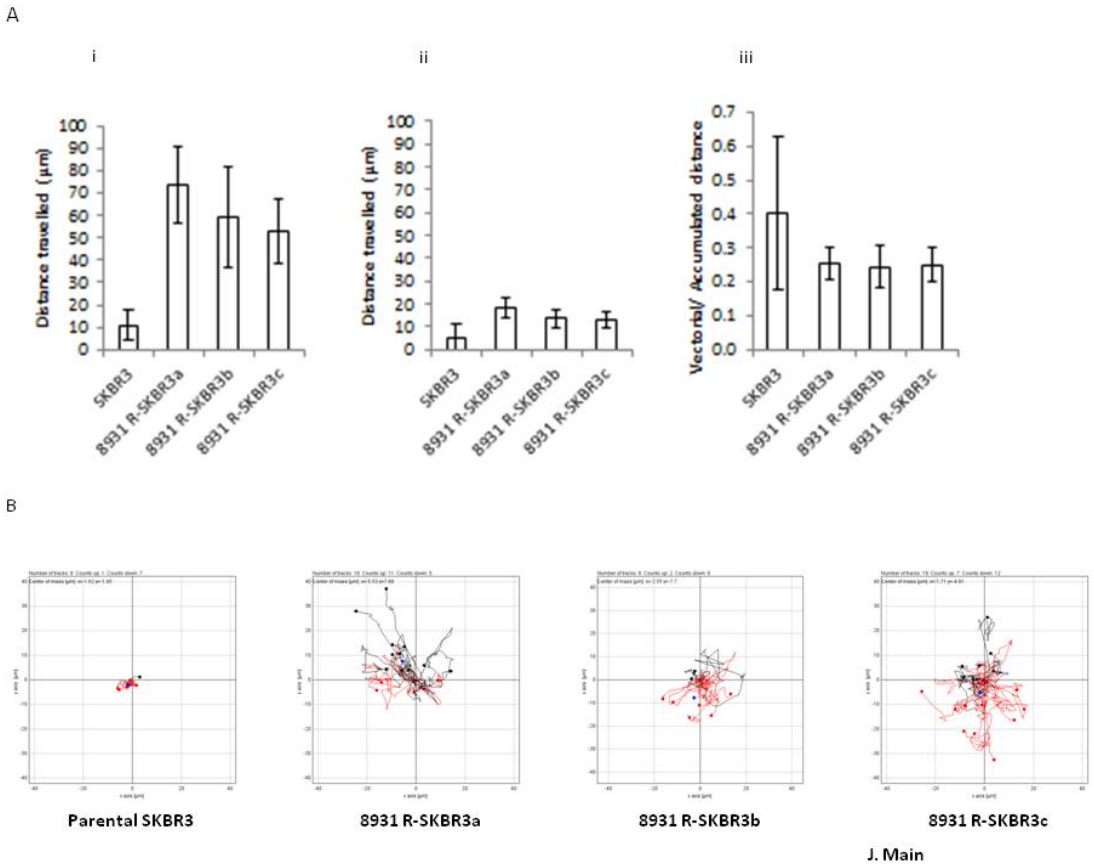

Figure 7.23- 8931 R-SKBR3 cell lines demonstrated an increasingly motile phenotype. A 6 well dish was seeded with 3000 cells in total media and images recorded every 15 minutes overnight using the automated Olympus Scan R-screening station. Experiments performed in triplicate and analysed using Image J. Ai: total cumulative distance travelled was statistically increased in all 3 AZD8931 resistant cell lines compared to the parental cell line ($p<0.001$, one way ANOVA). Aii: Significantly increased vectorial distance travelled by the 3 AZD8931 resistant cell lines ($p<0.001$, one way ANOVA). A iii: No significant difference was observed in persistence (vectorial distance/accumulated distance) between parental and AZD8931 resistant cell lines ($p=0.078$, one way ANOVA). Graphs depict mean value. Error bars represent standard deviation (data analysed and figures prepared by J. Main). B: Representative cell tracks showing distance travelled by individual parental and resistant cells during experiment. The red line depicts migration track of cells which finish below the horizontal line whilst the black line represents migration of track cells which finish above the horizontal line. Blue dot represents median net migration distance of all representative cells.

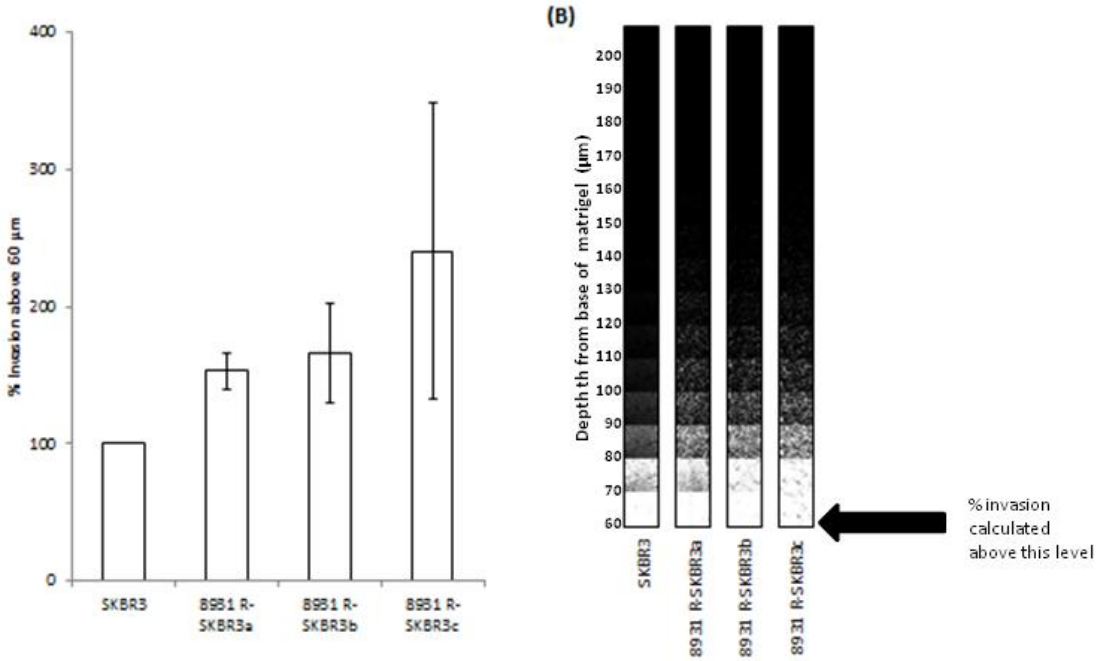

Figure 7.24- 8931 R-SKBR3 cell lines demonstrated non-statistical increase in invasive capacity. A: Invasion of parental and 8931-R SKBR3 cell lines through matrigel-coated invasion chambers over 24 hours, where invasion of parental SKBR3 cell line was defined as 100%. All experiments performed in triplicate. Mean value displayed with error bars representing standard deviation. P=0.092 (one way ANOVA). B: Montage of representative confocal images taken at 10 µm intervals through the 3D matrigel matrix for each cell line. (J. Main).

7.11 RPPA analysis of signalling changes associated with AZD8931 resistance

Numerous studies have already explored mechanisms of acquired resistance to lapatinib. We therefore decided to focus our further studies on mechanisms of acquired resistance to the novel drug AZD8931. RPPA platforms use a candidate driven approach to provide simultaneous quantitative evaluation of changes in multiple intracellular signaling pathways. We performed RPPA analysis on parental and resistant AZD8931 SKBR3 cell lines (**K. Macleod**). All experiments were performed in triplicate. The signal intensity obtained with each antibody reflected both the antibody's affinity for its target protein and the protein's abundance. Therefore, to try and ensure the biological relevance of our results, only data for antibodies in which the median signal in either the parental or resistant cell lines was in excess of 1.5 times the signal of the secondary antibody alone were included in our dataset with the aim of preventing over-analysis of data derived from weak or non-specific signals which were not reflective of true changes in pathway activity. We retrospectively set this threshold after observing that the signal with the pTyr 1248/ Tyr 1173 HER2/EGFR was approximately 1.5 times that of the secondary antibody and having previously demonstrated that this level of phosphorylation with this antibody was readily detectable on western blot, we felt this was a practical strategy to ensure inclusion of only meaningful results. In the following description only values which met this arbitrary threshold have been included and where possible the ratio of phospho:corresponding total protein is presented to give a measure of changes in activity within individual pathways [206]. Where this was not possible, the RFI has been presented, corrected using global normalization technique [282]. The $\log_2$ of all values in the resistant cell lines have been calculated and normalized against the $\log_2$ of the corresponding parental cell line value. Therefore in the following figures (Figures 7.25, 7.26, 7.27 and 7.28), any data series with a positive value on the Y-axis represents increased protein expression in the resistant cell lines compared to the parental cell line. Any data series with a negative value on the Y-axis indicates reduced protein expression in the resistant cell lines (for full set of results see Appendix 4).

Initial inspection of results showed close agreement between the 3 resistant cell lines in expression patterns of individual proteins suggesting common mechanisms of resistance/ were present (Figure 7.25, 7.26, 7.27, 7.28). In terms of individual proteins, we wanted to further explore changes in HER2, HER3 and EGFR expression and activity. Consistent with our western blot data, we saw a dramatic reduction in total HER2 expression in all 3 of the

resistant cell lines using RPPA. The RFIs obtained with antibodies for other HER family signaling proteins were often narrowly in excess of the 1.5 fold secondary antibody threshold (corresponding to an RFI of 103.00, Figure 7.25B). Although we used the same pTyr 1248/1173 HER2/EGFR antibody in both our western blotting and RPPA experiments, we saw no reduction in the expression of this protein using RPPA. Western blotting is still considered to be the gold-standard technique and the discrepancy between our results achieved using this technique and RPPA is likely due to low level of signal achieved with this antibody on this platform. This suggests that in retrospect our 1.5 fold threshold may have been inadequate to exclude non-specific signals and that this antibody was not suitable for use on this platform. Similarly, we saw no difference in expression of either total or the phosphorylated and active subsets of either HER3 between the parental SKBR3 and AZD8931 resistant cell lines and this was most likely because both these antibodies also lacked sensitivity on the RPPA platform. The level of EGFR expression alone was too low to quantify in all cell lines and therefore analysis was restricted to expression of pTyr 1173 EGFR alone. We did not identify any significant difference in pTyr 1173 EGFR expression between resistant and parental cell lines, although again the generated signal was probably too low in all lines to permit reliable interpretation of the data. In summary, due to lack of sensitive antibodies, the RPPA platform was not suitable for exploring changes in expression of HER family signaling receptors in our resistant cell lines.

We looked down stream of the HER family receptors at Akt and p44/42 MAPK signaling. The RFI achieved for both total and the phosphorylated and activated subsets of these proteins was at least 2 fold in excess of our 1.5 fold threshold. We found a significant increase in Akt activity as measured by both pSer473 and pTyr 308 Akt expression (Figure 7.26A). This increase in Akt signaling was likely due, at least in part, to loss of PTEN expression ($p<0.001$, one way ANOVA), which we demonstrated using both RPPA and western blotting (RPPA data not shown). Consistent with our observed increase in Akt activity, we observed an increase in pThr 389 p70 S6 kinase expression ($p<0.001$, one way ANOVA), which as an auto-phosphorylation site acts as a marker of this protein's activity [339]. Similarly, we observed an increase in the phosphorylation of S6 ribosomal protein at 2 separate sites [340], ($p<0.001$, one way ANOVA), which again was consistent with an increase in Akt signaling. Furthermore, we observed a statistically significant reduction in the activity of GSKβ ($p=0.031$, one way ANOVA), again consistent with increased Akt activity. MAPKs are also important downstream readouts of HER family signaling. Intriguingly, on western blot, we identified an increase of similar magnitude in both total p44/42 MAPK and pThr 202/Thr 185, Tyr 204/Tyr 187 p44/42 MAPK. However, using RPPA we found a statistically significant reduction in p44/42 MAPK activity ($p=0.001$, one way ANOVA, Figure 7.26B).

Considering total p44/42 MAPK and pThr 202/Thr 185, Tyr 204/Tyr 187 p44/42 MAPK separately, we found that expression of total protein was unchanged between parental and resistant cell lines. However, unexpectedly, we found a substantial reduction in pThr 202/Thr 185, Tyr 204/Tyr 187 p44/42 MAPK in the resistant cell lines. We also noted a significant increase in activity of the SAPK/JNK MAPK (p= 0.034).

During this analysis, we compared the expression of several proteins which have been previously implicated in resistance to HER2 targeted therapies. Increased Src activity has been identified as a critical player in a number of independent pathways which result in trastuzumab resistance [155]. We observed a statistically significant increase in Src activity in all 3 of our resistant cell lines (p=0.001, one way ANOVA, Figure 7.27A). The receptor tyrosine kinase, MET has also been shown to be upregulated following trastuzumab treatment and to contribute to acquired resistance by HER2 independent activation of the PI3K/Akt pathway [156]. We did not observe any difference in total MET expression between our parental and resistant cell lines, although again the RFIs achieved with this antibody were only just in excess of our 1.5 fold secondary antibody threshold. Unfortunately, expression of pTyr 1234 MET was too low to permit reliable quantification.

Defects in cell cycle regulation and apoptosis have also been linked to resistance to HER2 directed therapies [147]. We observed an increase in CDK2 expression (Figure 7.27B), which plays a key role in promoting passage through the G1/S check point [342]. However, we did not observe any difference in cyclin D1 expression, which has also been implicated in regulating the same checkpoint [343] and we observed a reduction in expression of pSer 216 cdc25c in resistant cell lines (p <0.001, one way ANOVA) consistent with reduced cell cycle progression and specifically entry into mitosis [341]. Counter-intuitively, we observed a statistically significant increase in expression of the pro-apoptotic protein Bid [344] and a reduction in the expression of the inhibitor of apoptosis survivin [345]. No difference in expression of either total Bim or pSer69 Bim, which is responsible for triggering the degradation of this pro-apoptotic molecule [346], were observed. Taken together, these changes suggest that avoidance of apoptosis was not an important mechanism underpinning resistance to AZD8931.

We also used RPPA to explore changes in expression of a number of other signaling pathways. We observed a statistically significant reduction in expression of total Stat3 in all 3

resistant cell lines ($p<0.001$, one way ANOVA, Figure 7.28A). We also observed a reduction in pTyr 783 PLCɣ: PLCɣ expression ($p<0.001$, one way ANOVA, Figure 7.18B), which is a well established target of EGFR [347]. CrkL is phosphorylated by BCR/Abl on tyrosine residue 207 [348] and we observed an increase in pTyr 207 CrkL expression in all 3 resistant cell lines ($p <0.001$, one way ANOVA, Figure 7.18B).

In summary, this data suggests that our resistant cell lines adopted multiple different resistance strategies, including down regulation of HER2, development of HER2 independent mechanisms of activating Akt and defects in cell cycle regulation.

A

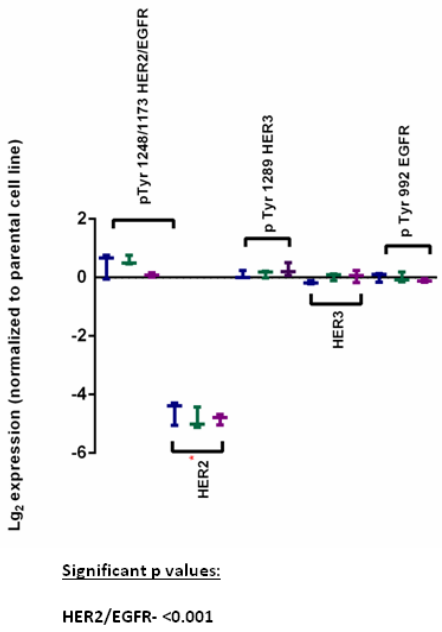

B

	SKBR3	8931R-SKBR3a	8931R-SKBR3b	8931R-SKBR3c
P Tyr 1248/1173 HER2/EGFR	148.25	131.347	125.83	117.64
HER2	4126.66	158.78	137.31	158.74
P Tyr 1289 HER3	199.73	175.03	178.30	194.65
HER3	143.80	111.14	112.21	122.61
pTyr 992 EGFR	108.31	110.49	107.70	99.47

Figure 7.25- A. Changes in expression of total and phosphorylated HER2, HER3 and EGFR associated with AZD8931 resistance. Statistically significant p values denoted by red asterix. Vertical lines demonstrate range between maximum and minimum values. Horizontal bar represents median value (n=3). Blue, green and purple lines represent 8931R-SKBR3a, 8931R-SKBR3b and 8931R-SKBR3c data sets respectively. All p values calculated using one way ANOVA. B. Tabulated RFI values of HER family signaling proteins. All included values met the arbitrary threshold set at 1.5 times the median secondary antibody value, which was equal to an RFI of 103.00.

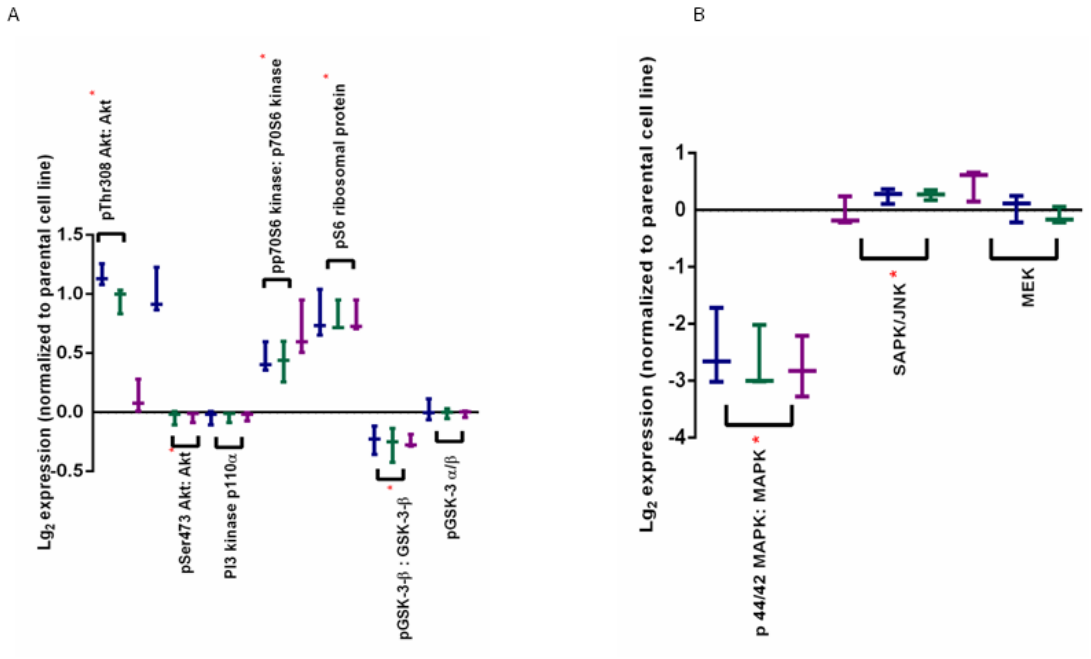

Significant p values:

pThr308 Akt: Akt : <0.001
pSer 473 Akt: Akt: <0.001
PTEN: <0.001
pp70S6 kinase: p70 S6 kinase :<0.001
pS6 ribosomal protein :<0.001
pGSK-3β: 0.031

p44/42 MAPK : MAPK : 0.001
SAPK/JNK: 0.034

Figure 7.26- A. RPPA analysis demonstrated that AZD8931 resistance was associated with an increase in Akt signalling and its downstream signalling pathways. B: A statistically significant reduction in p44/42 MAPK signalling and an increase in SAPK/JNK expression were observed in AZD8931 resistant cell lines. Vertical lines demonstrate range between maximum and minimum values. Horizontal bar represents median value (n=3). Blue, green and purple lines represent 8931R-SKBR3a, 8931R-SKBR3b and 8931R-SKBR3c data sets respectively. Statistically significant p values denoted by red asterix. All p values calculated using one way ANOVA.

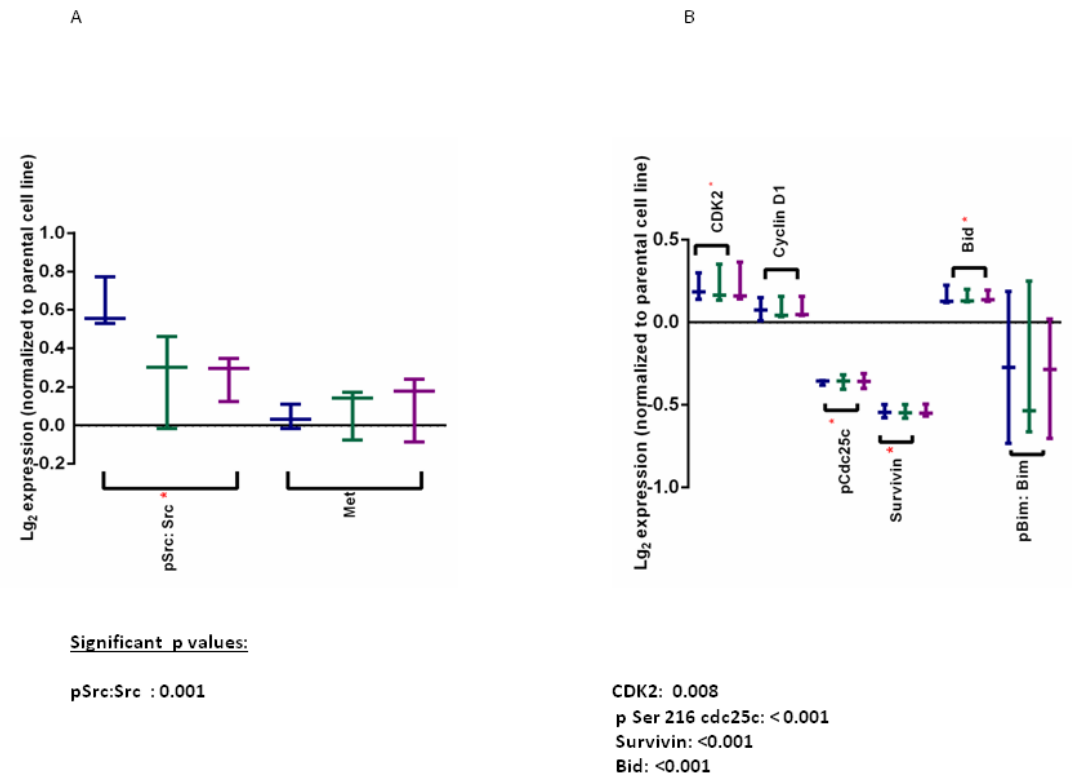

Figure 7.27- A. AZD8931 resistance was associated with a statistically significant increase in Src activity. B: Changes in signalling pathways regulating cell cycle control and apoptosis were observed in AZD8931 resistant cell lines. Vertical lines demonstrate range between maximum and minimum values. Horizontal bar represents median value (n=3). Blue, green and purple lines represent 8931R-SKBR3a, 8931R-SKBR3b and 8931R-SKBR3c data sets respectively. Statistically significant p values denoted by red asterix. All p values calculated using one way ANOVA.

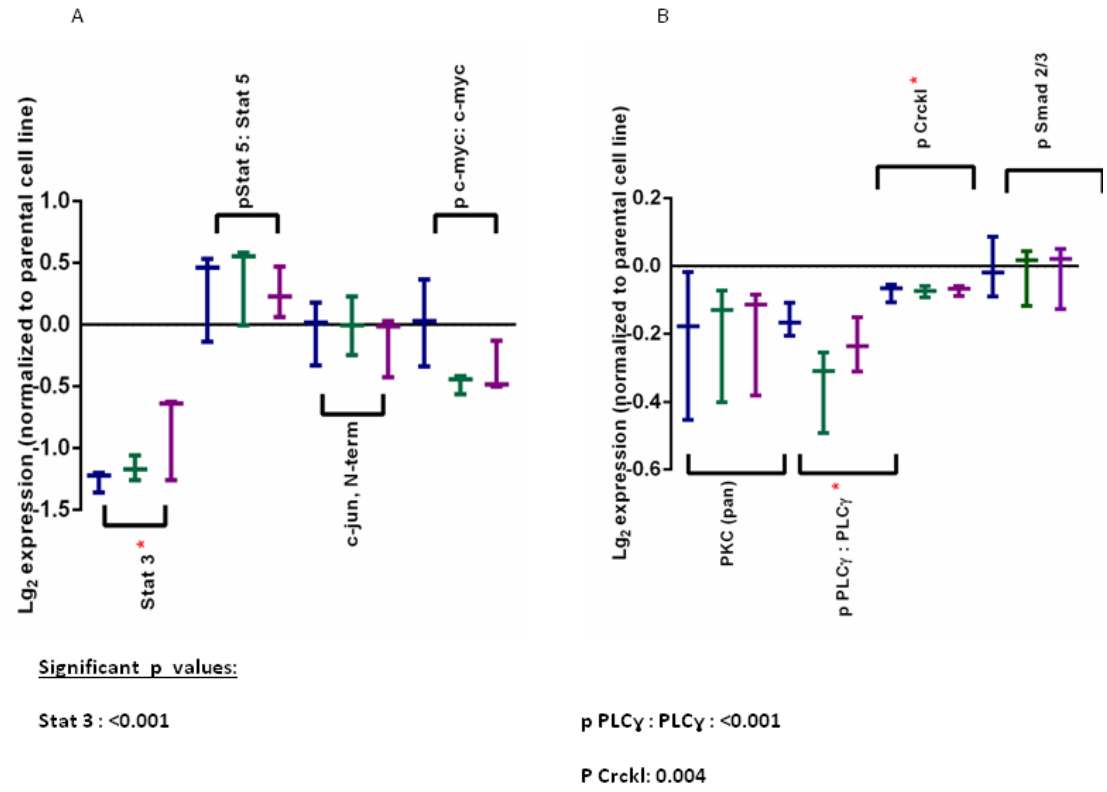

Figure 7.28- A. Development of AZD8931 resistance was associated with a reduction in total Stat3 expression. B: Reduced PLCɣ signalling activity and reduced expression of pCrkl was observed in AZD8931 resistant cell lines. Vertical lines demonstrate range between maximum and minimum values. Horizontal bar represents median value (n=3). Blue, green and purple lines represent 8931R-SKBR3a, 8931R-SKBR3b and 8931R-SKBR3c data sets respectively. Statistically significant p values denoted by red asterix. All p values calculated using one way ANOVA.

7.12 Mass spectrometry analysis of differences in protein expression patterns between parental and AZD 9831 resistant cell lines.

Mass spectrometry can also be used to interrogate signalling network interactions and to identify both specific molecules and broader cellular processes underpinning drug resistance. This approach can incorporate multiplex, non-targeted measurements in a quantitative manner enabling a more global assessment of protein expression in our cell lines. Label free mass spectrometry was therefore performed by one of our collaborators (**Dr. Thierry Le Bihan**) on both parental SKBR3 and 8931R-SKBR3c cells to provide more information on critical cellular processes underpinning the resistant phenotype.

We classified proteins as being significantly differently expressed between the 2 cell lines if the following 2 criteria were met: 1. fold change in expression between the 2 cell lines, as measured by at least 2 peptides, was >2, 2. the calculated pair-wise p value was ≤0.05. In total 533 proteins were significantly differently expressed between the parental and resistant cell lines (Figure 7.29). Expression of 72.8% (n=388) of these proteins was reduced in 8931 R-SKBR3c compared to the parental cell line. Expression of only 27.2% (n=145) proteins was increased in 8931 R-SKBR3c compared to the parental cell line. (For a full list of these proteins see Appendix 5). Western blotting was used to confirm the results of a selection of the differentially expressed proteins in all 3 resistant cell lines (Figure 7.30). As with our initial western blots, close agreement was observed between protein expression in all 3 resistant cell lines again suggesting that resistance in the 3 lines was driven by common mechanisms.

Classification of proteins according to function demonstrated that proteins affecting gene transcription and cytoskeletal structure, adhesion and cell migration were the most commonly altered representing 13.7% and 12.8% of all differentially expressed proteins respectively (Figure 7.30, Figure 7.31). Proteins which were up-regulated in the 8931 R-SKBR3c cell line and were classified within the same functional group did not always have complementary actions, for example caldesmon, which inhibited the motility of gastric cancer cell *in vitro* and was associated with reduced lymph node metastases *in vivo* [349], was up-

regulated in the 8931 R-SKBR3c cell line. Conversely, talin 1, which was also up-regulated in 8931 R-SKBR3c cell lines, enhanced the motility of glioma cells *in vitro* [350]. This lack of complementary actions between proteins in the same functional group was also evident amongst proteins which were down-regulated in the 8931 R-SKBR3c cell line, suggesting changes in complex signalling pathways had rendered some signalling pathways redundant. More detailed systemic analysis is currently underway.

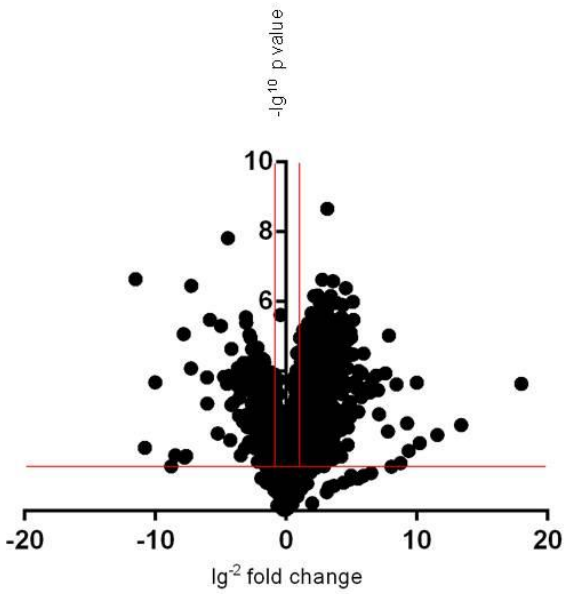

Figure 7.29- Volcano plot demonstrating 533 differentially expressed proteins between parental SKBR3 and 8931R-SKBR3c cell lines. Each data point represents 1 protein. The difference in expression between parental and resistant cell line, expressed as lg^{-2} fold change, is plotted on the x axis. The statistical significance of this difference (calculated using one way ANOVA) is plotted on the y axis. Proteins with a fold change > 1.5 or < 0.6667, measured by at least 2 peptides, and with a p value ≤ 0.05 are considered statistically differently expressed between the 2 cell lines. These proteins are plotted in the upper, outer regions (marked by the red lines) on the above graph. Amongst the differentially expressed proteins, over half had reduced expression in the resistant cell line compared to the parental cell line resulting in the distribution being shifted to the right on the above volcano plot.

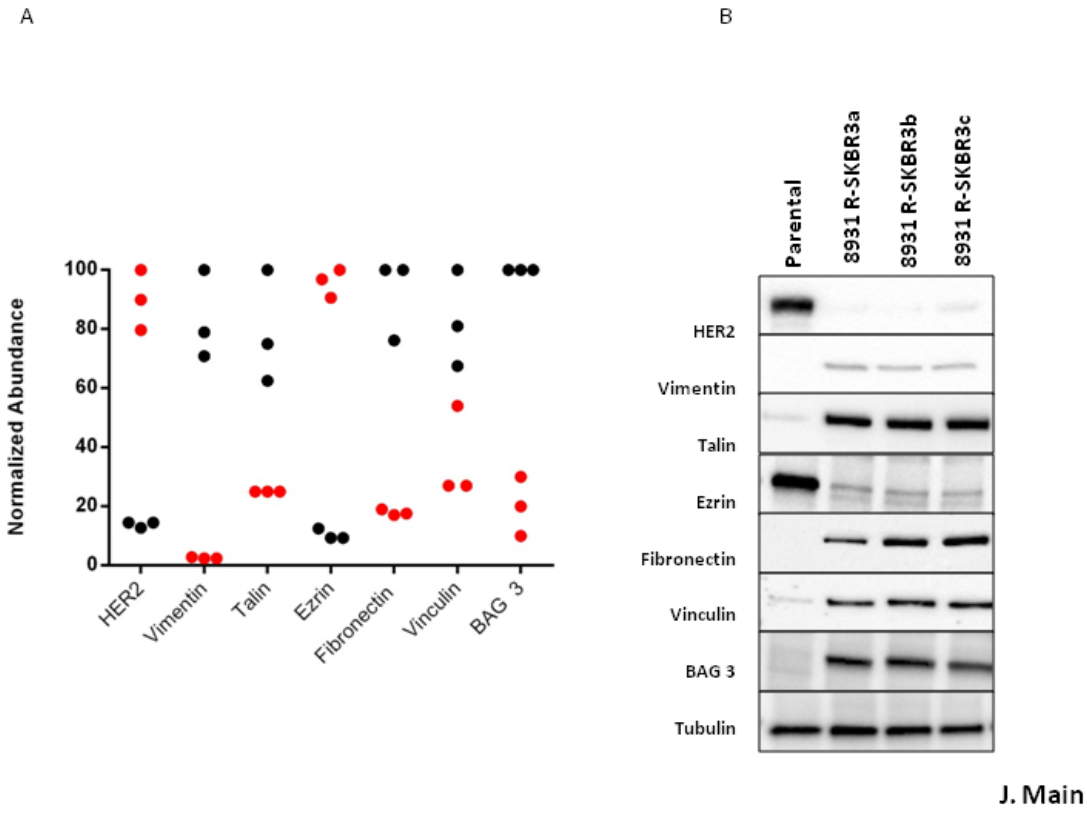

Figure 7.30- Validation of proteomic data by western blot. A: Graphical depiction of selected proteomic data. All experiments performed in triplicate. Red data points represent parental SKBR3 values. Black data points represent 8931-RSKBR3 c values. B: Confirmation of proteomic data by western blot. 20 µg protein loaded in each lane. Tubulin used as a loading control (J. Main). Note consistency of expression of proteins across 3 resistant cell lines on western blot.

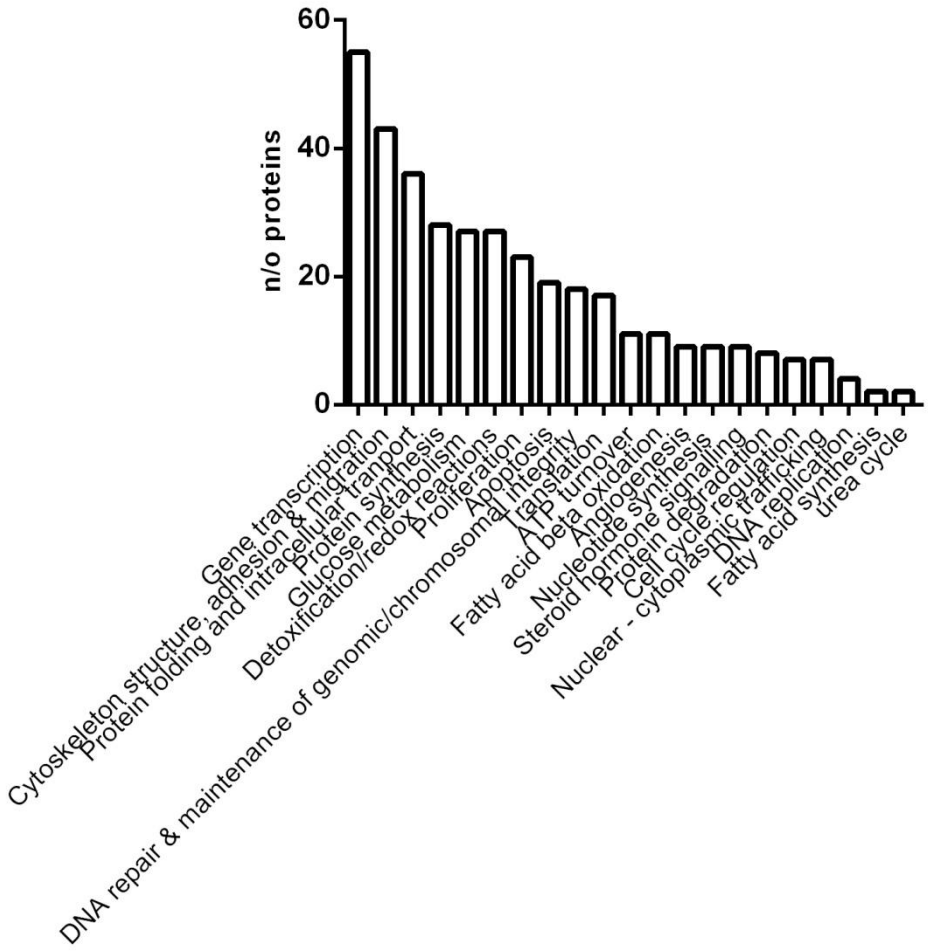

Figure 7.31- Classification of proteins with reduced expression in 8931R-SKBR3c cell line according to function. 87.9% of proteins with significantly reduced expression in the 8931 R-SKBR3c cell line could be classified into the above functions. Proteins which affected gene transcription, cytoskeletal structure, cell adhesion and migration were the most frequently down regulated in the resistant cell line. When proteins had more than 1 function, they have been classified under both functions.

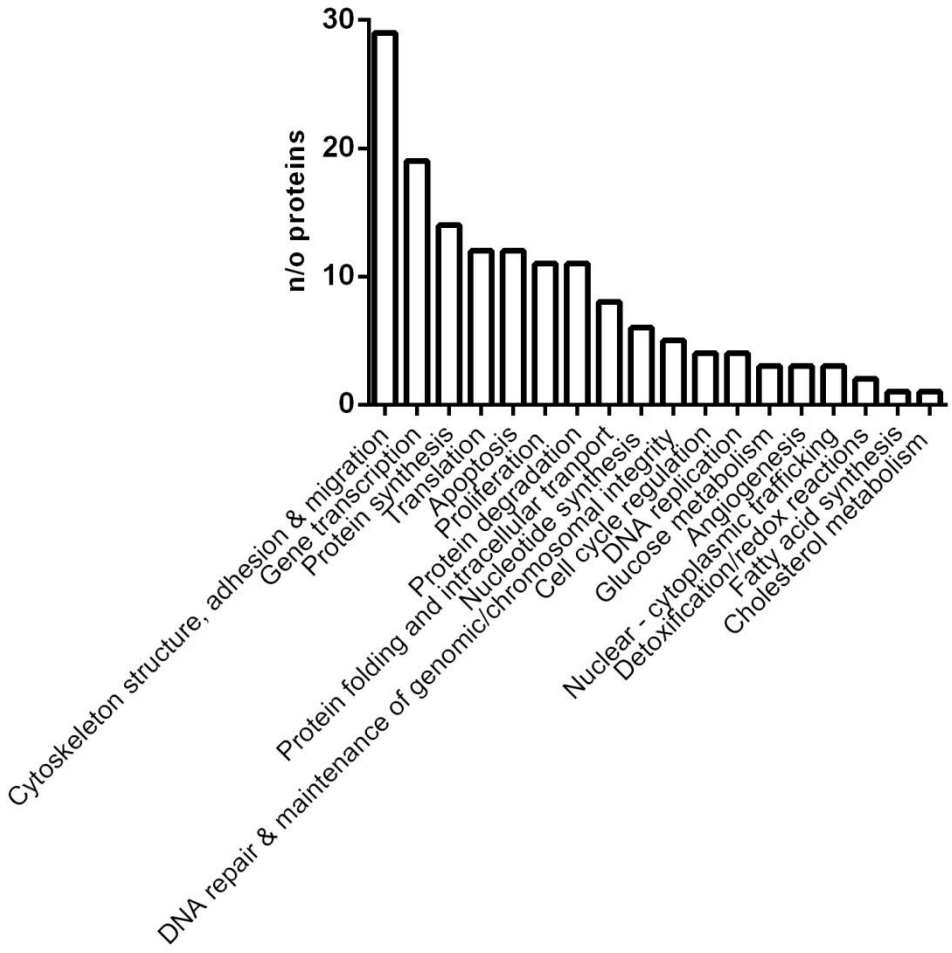

Figure 7.32- Classification of proteins with increased expression in 8931R-SKBR3c cell line according to function. 92.4% of proteins with significantly increased expression in the 8931 R-SKBR3c cell line could be classified into the above functions. Proteins which affect gene transcription, cytoskeletal structure, cell adhesion and migration were the most frequently up-regulated in the resistant cell line. When proteins had more than 1 function, they have been classified under both functions.

7.13 Discussion

In this current series of experiments we aimed to explore mechanisms of acquired resistance to the TKIs lapatinib and AZD8931. We found that previously established MMTV-NIC PTEN$^{+/-}$ cell lines were inherently resistant to both drugs, most likely as a result of the loss of HER2 expression during *in vitro* culture, which we had previously observed with another cell line in this panel (see Chapter 5). We therefore decided to undertake this work in 2 widely used human HER2 positive cell lines; SKBR3 and BT474. Following continuous culture in the presence of escalating doses of lapatinib we generated 2 resistant cell lines from both the BT474 and SKBR3 parental cell lines, which retained their resistance even after drug withdrawal. After prolonged culture of the parental SKBR3 cell line in the absence of drug, we also observed a reduction in its sensitivity to lapatinib. Consistent with our observations that the resistant cell lines had undergone EMT (see below for further discussion), Lesniak described spontaneous induction of EMT in selected untreated SKBR3 cell clones resulting in these cells becoming resistant to trastuzumab [167]. It is therefore likely that in the SKBR3 cell line, lapatinib accelerated the natural selection process favouring the growth of a pre-existent, rapidly proliferative and inherently resistant subpopulation of cells. However, both our BT474 derived lapatinib resistant cell lines also developed a similar phenotype and histomorphology as our SKBR3 resistant cell lines suggesting that at least during *in vitro* culture this is a real mechanism through which cells are able to adapt to culture in the presence of lapatinib and is not only restricted to the SKBR3 cell line. Cells were classified as lapatinib resistant when able to proliferate in the presence of 5 μM of drug, which is its maximum aqueous solubility. We elected to culture cells in this maximum achievable concentration with the aim of amplifying any active resistant strategies to ensure their detection. However, the maximum drug concentration achieved in humans at the recommended dose of 1500 mg daily is between 1 and 2 μg/ml [327], which equates to a concentration of 1.72 to 3.4 μM. Although, we maintained our cells in a drug concentration in excess of this, we observed the characteristic morphological changes in our resistant cell lines when cultured at sub-maximal concentrations and therefore the mechanisms of resistance we have identified are likely to have been active at physiologically relevant concentrations.

To determine whether these changes were specific to lapatinib resistant cells, we also generated 3 SKBR3 cell lines with acquired resistance to the novel equipotent inhibitor of HER2 and EGFR, AZD8931. As we had observed during generation of our lapatinib resistant

cell lines, we also noted a progressive loss of AZD8931 sensitivity following prolonged culture of our parental SKBR3 cell line, suggesting that again continuous drug exposure accelerated the selection of inherently drug resistant cell clones with a mesenchymal phenotype. This is further supported by our data showing that lapatinib resistant cells were cross resistant to AZD8931 and vice versa. Cells were classified as AZD8931 resistant once they were able to proliferate in the presence of 0.670 μM of drug. This concentration falls within the range of plasma concentrations observed at the MTD during the phase 1 trial [326] and therefore the resistance mechanisms identified are potentially clinically relevant.

The BT474 cell line has an activating mutation in the PI3K catalytic domain [328]. PI3K is a positive regulator of Akt activity and activating mutations within its catalytic domain have been linked to trastuzumab and lapatinib resistance in preclinical models [147] [351] [154]. Although clinical data relating to the impact of PI3K mutational status on lapatinib sensitivity is less conclusive [352] [191] [353], it might therefore be predicted that the BT474 cell line would adapt to continuous culture in the presence of drug more readily than the SKBR3 cell line, which does not have such a mutation. However, generating lapatinib resistant BT474 cells was challenging and required a longer period of drug exposure to achieve this than the development of lapatinib resistance in SKBR3 cells. Furthermore, despite prolonged efforts, we were unable to render BT474 cells resistant to AZD8931. Therefore, our inability to generate an AZD8931 resistant BT474 cell line appears to be partially drug and partially cell line related. In terms of drug related causes, AZD8931 robustly inhibits HER2, HER3 and EGFR signalling but although lapatinib potently inhibits HER2 it less potently inhibits both EGFR and HER3 signalling [273]. Therefore, the ability to develop lapatinib resistance in BT474 cells may be due to residual EGFR and HER3 signalling activity, which is not present when cells are treated with AZD8931. There are several possible explanations why as a cell line BT474 cells might be more resilient to resistance generation that the SKBR3 cell line. Firstly, the BT474 cell line appears to be more homogeneous as it does not display the same tendency to spontaneously change phenotype and lose drug sensitivity over time as the SKBR3 cell line. During the development of resistance in the SKBR3 cell line, drug treatment appears to act to speed up a naturally occurring phenomenon and it is therefore unsurprising that the development of lapatinib resistance in BT474 cells is a more lengthy process. Furthermore, the cell doubling time of BT474 cells is much longer than that of SKBR3 cells and this may also contribute to the longer time interval required to generate resistance. Finally, when the effects of PI3 kinase mutations on sensitivity to HER2 directed therapies have been considered in clinical trials, all mutations tend to have been considered as 1 pooled group. However, prospective analysis of samples collected as part of the Neosphere

trial, comparing treatment with single agent trastuzumab versus trastuzumab with pertuzumab, showed that although when considered as a whole, PI3K mutations were not predictive of treatment outcomes, on an individual basis, certain mutations appeared to be associated with worse outcomes [324]. It is therefore feasible that certain PI3 kinase mutations could be protective against the development of resistance.

In summary, through continuous culture in the presence of drug, we have generated a panel of cell lines with acquired resistance to either lapatinib or AZD8931.

7.13.1 Loss of target receptor expression as a mechanism of resistance

Several previous studies have shown that acquisition of resistance to HER2 targeting TKIs is associated with changes in expression of HER family receptors. Our data agrees with that of Lesniak and colleagues, who demonstrated loss of HER2 expression during induction of EMT in SKBR3 cells leading to lapatinib resistance [167]. Importantly our data also demonstrates that this mechanism of resistance is not solely restricted to the SKBR3 cell line but shows that BT474 cells can be rendered resistant to lapatinib through a similar mechanism. However, unlike our results and those of Lesniak, the majority of previously published studies have shown persistent HER2 signalling following the development of HER2 targeted therapy resistance. Loss of HER2 expression has been identified in up to a third of patients with metastatic breast cancer previously treated with trastuzumab ± lapatinib [168] suggesting that our cell lines are clinically relevant models. Furthermore, we have demonstrated that several mechanisms of resistance which were initially identified in cell lines with persistent HER2 signalling, including loss of PTEN, increased IGF1IR expression and enhanced Src activity, were active in our resistant cell lines suggesting that certain signalling pathways are activated following the development of resistance, irrespective of its mechanism. To date clinical approaches to overcoming resistance have predominantly focused on utilizing different strategies to target HER2 signalling yet this overlap between HER2 dependent and HER2 independent resistance strategies may explain why, although frequently initially effective, development of novel methods of targeting HER2 have had limited longer term efficacy with the development of resistance still remaining inevitable.

It is also interesting to note that short and long-term TKI treatment had very different effects on HER family receptor expression. In contrast to the loss of HER2 expression seen following long-term TKI treatment, we observed a dose-dependent increase in total HER2 expression following short-term AZD8931 and lapatinib treatment. This increase in total HER2 has previously been noted following short-term lapatinib treatment [354] and has been attributed to reduced receptor ubiquitination resulting in the accumulation of the inactive receptor at the plasma membrane [355]. Similarly, although long-term TKI treatment resulted in loss of HER3, we observed a tendency towards increased total HER3 expression following short-term treatment with both AZD8391 and lapatinib treatment, which when observed following lapatinib treatment has been attributed at least in part to changes in transcriptional regulation [356]. As predicted, we observed a dose-dependent reduction in both pTyr 1148/1173 HER2/EGFR and pTyr 1221/1222 HER2 expression following short-term TKI treatment but interestingly, we also observed a dose-dependent reduction in HER3 activity following treatment with either drug. AZD8931 is a more potent inhibitor of both HER2 and HER3 phosphorylation with IC_{50} values of 3 nmol/L and 4 nmol/L respectively compared to 9 nmol/L and 13 nmol/l for lapatinib [273]. Furthermore, the duration of this inhibition is likely to be markedly different between the 2 drugs. Through equipotent inhibition of both HER2 and EGFR, AZD8931 results in robust and persistent inhibition of HER3 signalling [273]. However, previously published data has shown that transphosphorylation of HER3 is only transiently inhibited following lower doses of lapatinib with restoration of signaling after 48 hours despite continued drug treatment. The resumption of HER3 signalling occurs due to persistent Akt inhibition, which normally exerts a negative regulatory effect on HER3 expression through a combination of both transcriptional and post-transcriptional mechanisms [356] and ultimately also results in restoration of Akt and p44/42 MAPK activity. Therefore, lapatinib's initial success in suppressing Akt drives an increase in HER3 signalling and subsequently enables an escape from lapatinib's inhibitory effect on cell proliferation.

A major issue we encountered during this series of experiments was our inability to replicate our initial western blotting findings of reduced total and phosphorylated HER2 and HER3 in our AZD8931 resistant cell lines using RPPA. Western blotting remains the gold standard technique for exploring changes in protein expression during tissue culture although its usefulness is limited by its low throughput nature and at best when used to determine the extent of changes in protein expression, it can be described as semi-quantitative. RPPA is an increasingly widespread technique which has been attracting considerable excitement as it offers may benefits including high throughput analysis of multiple samples enabling the precise and simultaneous analysis of expression changes in numerous proteins despite only requiring a small amount of primary material. However, the ability to determine changes in

the expression of any given protein is dependent on both the relative abundance of the individual protein and the affinity and specificity of the antibody being used. Previous studies have shown that RPPA is able to detect proteins expressed in the fentogram/ml range with linearity seen at the sub pictogram/ml range. However, the major limiting factor in detecting many phosphorylated proteins or other post-translationally modified proteins is the availability of highly specific antibodies as unlike in western blotting, RPPA only generates a single signal and it is therefore impossible to distinguish between proteins of different molecular weights [357]. Validation of an individual antibody for use in RPPA involves demonstrating that it produces a single band on western blot; the intensity of which correlates with the signal generated on the RPPA platform. All the antibodies used in these experiments have previously been validated but as this is a costly and time consuming process, efforts have been made within the RPPA community to share this data and thereby accelerate the widespread introduction of RPPA into laboratory practice. Therefore not all of the antibodies have been validated on the platform used in these experiments. The quality of antibodies can also vary over time and therefore although these antibodies have previously been validated this should be repeated. The data from these experiments suggest that at present, with the exception of the total HER2 antibody, the HER family receptor antibodies are not suitable for use on the RPPA platform and that our western blot data should be accepted as the most representative result. Furthermore, this data also illustrates the fact that RPPA should still be considered a screening tool rather than providing definitive data and therefore we should use western blotting to confirm the remainder of our results.

A further issue relating to the use of RPPA is determining an appropriate threshold below which any signal generated is attributed to non-specific antibody binding. This threshold will by definition always be somewhat arbitrary in nature. In these experiments, we used the strength of the signal generated with the pTyr 1248/1173 HER2/EGFR antibody to set this threshold at 1.5 times the signal generated with the secondary antibody alone, having previously demonstrated that we could detect differences in expression of this protein between our parental and resistant cell lines with this antibody by western blotting. In retrospect, this was not the most appropriate criteria to determine such a threshold as the data obtained using RPPA was not validated using western blotting. It would have been more appropriate to set this threshold according to the signal generated using an antibody where our RPPA data was consistent with our western blotting data, such as Akt. Setting such a threshold is a balancing act between minimising the over-interpretation of data artefact and inappropriate rejection of genuine results. The intensity of the signal generated using the Akt antibody was considerably higher than that obtained with the pTyr 1248/1173 HER2/EGFR antibody and therefore adopting this as a threshold would allow a greater

degree of confidence that any novel targets identified using RPPA were likely to represent genuine results. However, it does increase the risk of novel markers of resistance identified using RPPA being falsely rejected as representing data artefact. With greater experience of this technology, determining an appropriate threshold is likely to become more straightforward but at present our experience further serves to highlight the importance of validating data obtained using RPPA by western blotting.

7.13.2 Effects of lapatinib and AZD8931 resistance on Akt and p44/42 MAPK signaling

Although we identified loss of HER family receptor expression in both AZD8931 and lapatinib resistant cell lines, the downstream consequence on Akt and p44/42 MAPK signaling were different depending on the agent used to generate resistance. Using both western blotting and RPPA, we identified an increase in both total and pSer473 Akt expression in all 3 AZD8931 resistant cell lines. Furthermore, using RPPA we showed appropriate changes in several signalling pathways downstream of Akt, including an increase in p70S6 kinase activity, which has previously been identified as a marker of resistance in lapatinib resistant HER2 over-expressing MCF7 cells [160]. Although we identified an increase in p44/42 MAPK activity on western blot, we found a reduction in its activity using RPPA. As discussed above, the validity of results obtained with certain antibodies on the RPPA platform, in this case the pThr202/Thr185, Tyr 204/Tyr 187 p 44/42 MAPK is the most likely explanation for our disconcordant results and therefore we have taken the increase in p44/42 MAPK activity identified on western blot as the most representative result. However, when looking at Akt and p44/42 MAPK expression in our lapatinib resistant cell lines using western blotting we found the activity of both signalling pathways was reduced in all cell lines. The impact of Akt and p44/42 MAPK signalling has been the focus of numerous studies. Several previous studies have causally linked persistent Akt signalling to lapatinib resistance. Yu and colleagues showed that the presence of an activating mutation within PI3K p110α or over-expression of PI3K p110α culminated in increased Akt activity and lapatinib resistance. Furthermore, inhibition of PI3K p110α, but not p110β, inhibited cell proliferation both *in vitro* and *in vivo* [351]. In a separate study, persistent Akt activity in lapatinib resistant cells was overcome using the mTOR inhibitors rapamycin and ridaforolimus and when combined with lapatinib these drugs acted in a synergistic manner to reduce tumour cell proliferation both *in vitro* and *in vivo* [177]. Similarly, when combined with lapatinib, the mTOR1/2 and Akt inhibitor INK-128 inhibited HER2 and HER3 phosphorylation and not only suppressed PI3K/Akt/mTOR activity but also p44/42 MAPK activity resulting in sustained tumour

shrinkage in lapatinib resistant xenografts [178]. Wilson et al found that HGF treatment was able to rescue lapatinib sensitive cell lines from the drug's cytotoxic effects and resulted in the outgrowth of a subset of cells with enhanced MET expression resulting in re-activation of both PI3K/Akt and p44/42 MAPK signaling [157]. However, another study identified RON tyrosine kinase, a member of the MET receptor tyrosine kinase family, as a potential upstream activator of Akt in lapatinib resistance and reported that treatment with the PI3 kinase inhibitor GDC-0941 but not the MEK inhibitor PD0325901 was able to reduce cell proliferation in this model [185]. Whilst in a further study looking at the effects of MEK inhibition alone, Gayle found that failure of lapatinib to suppress p44/42 MAPK activity was associated with inherent resistance to the drug and that combined treatment with lapatinib and the same MEK inhibitor (PD0325901) resulted in a synergistic inhibition of cell growth and induced a G0/1 cell cycle arrest [358]. These studies suggest there is a lack of consensus regarding the contribution of p44/42 MAPK activity to the resistant phenotype and although collectively they appear to implicate persistent Akt activity in lapatinib resistance, it is important to note that several other signaling pathways, independent of both Akt and p44/42 MAPK activity, have been linked to lapatinib resistance. These include increased ER [183] [191] and NF-κβ (due to increased either NIPB [193] or RelA [153] expression) signaling, up-regulated survivin expression and an enhanced glucose deprivation response [166]. It is possible that one of these Akt and p44/42 MAPK independent signaling pathways, or an as of yet unidentified pathway, may be active within our lapatinib resistant lines. Together with the published literature, our data serves to emphasise that even within the relatively restricted parameters of cell line and xenograft assays, numerous different resistance mechanisms are seen within the different models used. Therefore, considering the vast array of different genetic and epigenetic permutations found within human breast cancer, the range of different resistance mechanisms active within the clinical setting is likely to be immense. It is therefore extremely unlikely that a single strategy that will universally overcome clinical resistance will ever be identified and ideally in the future clinical trials will need to focus on testing novel therapeutic approaches within a cohort of patients in whom a predetermined resistance strategy has already been identified.

AZD8931 offers more robust inhibition of HER family receptors than lapatinib [273] and it may therefore seem counter-intuitive that AZD8931 resistant cell lines expressed increased Akt and p44/42 MAPK whilst lapatinib resistant cell lines developed alternative signalling strategies. Previous studies have identified complex cross-coupling between Akt and p44/42 MAPK signalling with inhibition of Akt causing up-regulation of p44/42 MAPK signalling and vice versa [356]. It is therefore feasible that more complete inhibition of HER family signalling in the longer term results in a compensatory increase of both downstream signalling

pathways. Combinational therapy using drugs which target the PI3K/Akt and p44/42 MAPK pathways may therefore be an attractive option in both subsets of patients with AZD8931 and lapatinib resistance. Combined treatment with MEK and PI3K targeting drugs has previously been shown to synergistically inhibit growth of both a KRAS-driven lung cancer model and an N-RAS mutant melanoma model [359]. However, considerable concern has been expressed as to whether these drugs could be used together at therapeutically relevant doses without incurring intolerable toxicities. Three phase 1 trials using combinations of PI3K and MEK inhibitors in advanced solid cancers have already been reported and several more are underway. In 2 of the 3 trials already reported, the combination was well tolerated with preliminary evidence of activity, particularly in low-grade serous ovarian cancer and advanced melanoma, although both of these tumour types have previously been shown to respond to single agent MEK inhibitors [360]. There were no documented responses in HER2 positive breast cancer in these trials, although they are unlikely to recruit such patients as there is currently no scope for continuing HER2 directed therapy within them.

In summary, inhibition of PI3K/Akt and/or p44/42 MAPK pathways appears an attractive option to overcome HER2 TKI resistance in a proportion of cases.

7.13.3 Strategies to identify mechanisms of resistance to HER2 targeted therapies

We used 2 complementary approaches to further explore the mechanisms underpinning resistance in our AZD8931 resistance model; RPPA and mass spectrometry. RPPA is an increasingly widely available target driven technology, which is useful for detecting changes in expression of large groups of proteins connected to pre-specified signaling pathways, the activity of which might be predicted to have changed within the biological system of interest. However, as discussed above, the availability of good quality antibodies, particularly those detecting phosphorylated proteins, limits its ability to detect signaling changes within certain pathways. It is also an inefficient technique for discovering novel therapeutic candidate proteins which might be implicated in the resistant phenotype. We therefore also performed mass spectrometry, which is a non-targeted approach that allows global and quantitative assessment of protein expression and can therefore be used to both identify individual proteins and broader cellular processes involved in the development of resistance. Previous studies have tended to focus on changes in expression of phosphorylated proteins giving a

measure of signaling pathway activity in different models. In this series of experiments, we have focused on changes in total protein level, rather than focusing on post-transcriptional modifications, although analysis of phosphospecific proteomic changes is currently underway.

Using these approaches, we have identified changes in the expression of a number of proteins which have previously been linked to resistance, including loss of HER2 receptor expression [167], up-regulation of p70S6 kinase expression [160] and increased Src activity [155]. Enhanced Src activity in particular appears a promising therapeutic target as it has been identified as a common downstream event in several independent pathways resulting in resistance to HER2 directed therapies [155]. Consistent with previous studies [361] [155], we demonstrated increased Src activity in all 3 AZD8931 resistant cell lines compared to the parental SKBR3 cell line. We also identified a similar increase in Src activity in our lapatinib resistant SKBR3 cell lines, suggesting this is a common mechanism of resistance to HER2 targeting TKIs. Furthermore, looking at our data regarding the *in vivo* efficacy of AZD9831 in the MMTV-NIC model, we observed complete suppression of Src activity in the sensitive MMTV-NIC PTEN $^{FL/+}$ model but not in the less sensitive MMTV-NIC PTEN$^{+/-}$ model (Chapter 4.2.6.2), suggesting the association between Src activity and AZD8931 resistance is not exclusively an *in vitro* phenomenon. Intriguingly, there have been no clinical reports on the efficacy of combining Src inhibitors with either trastuzumab or lapatinib, although the reported activity of single agent dasatinib in HER2 positive breast cancer was disappointing [179].

Contrary to the published data, we observed reduced expression of the inhibitor of apoptosis (IAP) survivin [362] in our AZD8931 resistant cell lines. Previously published studies have shown that the expression of survivin in HER2 positive breast cancer is up-regulated by PI3K [363] [354] and that the anti-tumour effects of lapatinib are closely correlated with the down regulation of survivin [183]. It is therefore feasible that suppression of survivin could protect cells against an important mechanism of HER2 directed therapy cytotoxicity. However, to date no such association between reduced survivin expression and drug resistance has been described in the published literature. Indeed, several previous studies have implicated elevated survivin expression in both primary [165] [192] and acquired [183] [192] resistance to trastuzumab and lapatinib.

We also identified several potential novel markers of AZD8931 resistance, including reduced pTyr 783 PLCɣ: PLCɣ expression. The SH2 domain of PLCɣ is phosphorylated on tyrosine residue 783 by EGFR [364] and therefore expression of pTyr 783 PLCɣ can be used as a biological readout of EGFR activity. This reduction was therefore consistent with the reduction in pTyr 992 EGFR expression initially identified on western blot.

We also observed a statistically significant reduction in STAT3 expression in our AZD8931 resistant cell lines, although this has yet to be confirmed by western blotting. One study demonstrated STAT3 expression in the cytoplasm and nucleus of 69% and 23% of cases of node-negative breast cancer respectively and found that nuclear STAT3 expression was associated with improved survival [365]. However, in a separate study of 571 breast cancer, no association between STAT3 expression and prognosis was documented [366]. Furthermore, no relationship between STAT3 expression and resistance to HER2 targeted therapies has previously been described although prior studies have identified an association between Stat3 expression and HER2 gene amplification [261]. Given the substantial reductions in HER2 expression in our resistant cell lines, it is unsurprising that Stat3 expression was also reduced. Unfortunately, the signal generated with the pTyr 705 Stat3 antibody was too low to determine whether AZD8931 resistance was associated with a change in specific activity of Stat3.

During these experiments numerous potential novel proteins involved in the resistant phenotype, particularly using mass spectrometry, have been identified. In the first instance, these potential hits need validation using western blotting although to date this technique has successfully corroborated our results in all of the proteins tested. Once change in expression has been confirmed, functional studies using either gene silencing techniques, such as siRNA, or forced over-expression will be required to determine which of these changes have actively contributed to the development of the resistant phenotype and which were merely passenger mutations. This dataset may also prove a useful resource in identifying potential markers of resistance to HER2 targeting TKIs. Finally, any successfully identified driver-mutations or putative biomarkers will need to be validated in clinical samples to ensure that they are clinically relevant. Our proteomics data has highlighted a number of possible mechanisms for further study and suggests that future efforts to overcome resistance will need to target multiple different signalling pathways, either by inhibition of multiple molecular targets individually or, if possible, inhibition of targets at critical pathway intersections. One particularly interesting mechanism identified on both western blotting and in our proteomic data set was EMT.

7.13.4 Association of HER2 targeted resistance with EMT

We found that proteins which altered gene transcription or cytoskeletal structure, adhesion and cell migration were the most commonly affected groups of proteins in our proteomic data set. Consistent with our earlier observations that AZD8391 resistance was associated with loss of epithelial characteristics and acquisition of mesenchymal traits, we identified changes in expression of several other proteins which have been previously been established as hallmarkers of EMT, including loss of cytokeratin expression, up-regulation of fibronectin and changes in expression of several genes which regulate the expression of matrix metalloproteinases (MMPs) [367]. The receptor tyrosine kinase Axl has previously been linked to EMT within breast [334] [368] and pancreatic [369] cancers and more recently within non-small cell lung cancer (NSCLC) [370]. A previous study comparing the expression of Axl in matched primary and secondary breast cancers found up-regulation of Axl expression within metastatic tumours and furthermore expression within the primary tumour was an independent risk factor for reduced OS [368]. We have previously shown, using western blotting, that expression of Axl was increased in all 3 of our AZD8931 resistant cell lines [114]. Furthermore, using mass spectrometry we identified an increase in the expression of vimentin and YAP1 in our resistant cell line, both of which have previously been linked to Axl expression. Up-regulation of Axl expression has previously been identified as driving resistance in lapatinib resistant BT474 cells [186]. Further experiments are currently underway to explore whether inhibition of this receptor successfully inhibits growth in our model. Cells which have undergone EMT have been widely reported to be resistant to most conventional anti-cancer therapies, including chemotherapy and radiotherapy and therefore considerable effort has been invested in attempts to develop therapies which specifically target the EMT process [367]. Inhibition of Axl is amongst the most promising of these strategies and it has previously been shown that Axl inhibitors are able to interact synergistically with anti-mitotic drugs to trigger cell death amongst cancer cells which have undergone EMT [371]. Furthermore, it has been suggested that Axl inhibition inhibits the proliferation of NSCLC cells that have undergone EMT and acts to restore sensitivity to the EGFR inhibitor, erlotinib [370], although this has not been replicated in other studies [371]. Forfetinib is a multi-kinase inhibitor, which inhibits MET, VEGFR-2, RON, KIT and Axl, and has already been tested in phase 1 clinical trials. Initial results appeared promising with 74% of patients having a best response of stable disease [372]. However, pharmacodynamic studies did not explore whether significant inhibition of Axl was achieved at the MTD and as one of the most commonly experienced adverse events in this study was hypertension, a

well-established complication of anti-angiogenic drugs, such as VEGFR inhibitors, it is possible that side-effects due to inhibition of other signaling pathways may have prevented dose escalation to a sufficient level to achieve adequate Axl inhibition. Attempts to generate more specific Axl inhibitors are currently underway.

Associations between HER2, EMT and trastuzumab resistance have previously been well documented. HER family signaling is one of the many factors to have been implicated in the induction of EMT [338]. Furthermore, induction of EMT has been linked to acquisition of a stem-cell properties and resistance to trastuzumab [373]. However, the nature of this association remains controversial. Ortega-Cava et al described a continuous requirement for HER2 kinase activity to trigger loss of epithelial cell polarity and lumen formation in a 3D *in vitro* assay. However, consistent with our data, other groups have described concomitant loss of HER2 expression with the induction of EMT in both *in vitro* [330] [167] and *in vivo* models [374], suggesting that proliferation in these transformed mesenchymal cells was independent of HER2 signaling. These results are also consistent with earlier observations that acquired resistance to AZD8931 in some MMTV-NIC PTEN$^{+/-}$ tumours was associated with loss of HER2 expression and development of a mesenchymal appearance (see Chapter 6.5). However, whilst induction of EMT has been associated with resistance to HER2 directed therapies using both *in vitro* and *in vivo* preclinical models, this association has not been validated in clinical studies and so its relevance within the patient population remains uncertain. In fact, controversy still exists as to the relevance of EMT in human tumours as mesenchymal cells within human cancer are rarely more than an isolated phenomenon, although this has been attributed to the potentially transient and reversible nature of EMT [367]. Further controversy also exists about the impact of individual markers of EMT on prognosis; a large meta-analysis of 1107 breast cancer samples reported that tumours with increased gene expression of the EMT markers SNA1, TWIST1 and VIM or reduced expression of CDH1 had a reduced recurrence free survival [375]. However, a second study failed to replicate these findings [376].

7.14 Summary

Resistance to HER2 targeted therapies is a commonly encountered clinical scenario and overcoming this resistance has been the focus of numerous studies. We have generated lapatinib resistant BT474 and SKBR3 cell lines and AZD8931 resistant SKBR3 cell lines through continuous culture of cells in the presence of escalating drug doses. Initial characterization of our cell lines demonstrated that both lapatinib and AZD8931 resistant cell lines displayed common morphological and intracellular signaling changes and were cross-resistant to the opposing TKI. Although functional studies have not yet been performed, resistance appeared to be multi-factorial in nature and was associated with loss of HER receptor expression and induction of EMT. Further proteomic analysis is currently being undertaken.

Chapter 8: Discussion, future studies and conclusions

In this thesis, using the BLG-HER2^{KI} PTEN$^{+/-}$ and MMTV-NIC models of HER2 positive breast cancer, we have demonstrated that GEMMs are powerful tools in which to study mechanisms of tumour response and resistance in the presence of both a functioning immune system and an intact microenvironment. Although identical mutations are responsible for driving tumourigenesis in animals of the same genotype, the random acquisition of secondary mutations generates tumours with variable growth kinetics and therapeutic responses which model more accurately the huge spectrum of tumour behaviour observed within the clinical population. Using the MMTV-NIC model, we have generated tumours with acquired resistance to AZD8931 and shown that different tumours develop resistance via distinct mechanisms, for example loss of HER2 expression was identified in tumours which had undergone EMT whilst HER2 expression and an epithelial phenotype was preserved in another tumour, strongly suggesting that a 'one size fits all solution' for HER2 directed therapy resistance is likely to be unattainable. To better understand these mechanisms of resistance, we generated a panel of AZD8931 resistant cell lines and used a combination of RPPA and mass spectrometry to further interrogate signalling changes within the resistant cell lines. These resistant cell lines lacked the heterogeneity seen within our resistant GEMM tumours with all resistant cell lines having undergone EMT and loss of HER2 expression. However, the consistency of these results with those observed in a subset of our resistant MMTV-NIC tumours suggests that despite their well published limitations, traditional *in vitro* cell line approaches can still make an important contribution to preclinical drug development programmes, as long as the findings can be replicated in more physiologically relevant pre-clinical models. In our experience, resistant cell lines were relatively rapidly generated and provided an almost limitless supply of material for proteomic screening, enabling us to reserve our limited supply of resistant tumour material for analysis of the most potentially interesting hits. For example, several proteins implicated in EMT, initially identified by mass spectrometry, have since been demonstrated to be up-regulated in our resistant cell lines by western blotting and 1 of these proteins, YAP1, has also been shown to be up-regulated in AZD8931 resistant tumours, which had undergone EMT (**M. Canel**). Furthermore, use of publically available gene expression databases indicated that over-expression of several of these EMT associated proteins, such as BAG3, YAP1 and galectin 1, were associated with poor prognosis in HER2 positive breast cancer. Over-

expression of all 3 genes was a better predictor of outcome than any individual gene alone (**A. Sims**) and whilst gene expression data does not necessarily translate into meaningful changes in protein expression, these findings suggest that our dataset could be used to identify a set of EMT markers associated with resistance to HER2 targeted therapies. If such a gene or proteomic signature could be validated within human tumour samples, it could in the future be used to identify a sub-set of patients in whom treatment with HER2 targeted therapies leads to induction of EMT who may benefit from treatments that specifically target cells which have undergone EMT, such as Axl inhibitors.

Major technical advances in preclinical studies have led to the identification of increasing numbers of potential therapeutic targets, enhanced understanding of the mechanisms underpinning tumuorigenesis and ever growing numbers of new molecularly targeted agents. Gratifyingly, some of these advances have already been translated into meaningful improvements in the management of cancer patients. For example, crizotinib, a selective inhibitor of ALK and MET tyrosine kinases, showed high RR in phase 1 trials of heavily pre-treated patients with advanced NSCLC harbouring ALK rearrangements [377] . Impressively, target identification, initiation of a phase 1 trial and enrollment of a phase 3 registration trial was all achieved within 3 years and crizotinib has subsequently been approved by both the Food and Drug Authority (FDA) and European Medicines Authority (EMA). A recent meta-analysis confirmed that crizotinib offers improved outcomes compared to previous standard treatments [378] and marks a significant advance in the management of this group of poor prognostic patients with previously few treatment options. However, for the most part incorporation of knowledge from preclinical studies into clinical practice has been frustratingly slow and arguably early phase oncological trials currently face a period of unprecedented technical, logistical and financial challenges.

Whilst improved preclinical models have furthered our understanding of the role of several key proteins and targets in the pathogenesis of cancer, validating these findings in human tumours remains of critical importance. Several studies have highlighted discrepancies between the role of proteins in mouse models and human tumours, for example resistance to PARP inhibitors has been attributed to up-regulation of drug efflux proteins in a GEMM of BRCA1 deficient tumour, which has not been replicated in their human counterparts [67]. High throughput assays are increasingly used in preclinical studies and to a much more limited extent in clinical trials. More widespread introduction into clinical studies would be a

major undertaking involving training of large numbers of staff and standardization of techniques from initial sample collection and fixation to sample processing and assay calibration. Furthermore, analysis of human samples is likely to be complicated by the additional heterogeneity observed in human tumours compared to their murine counterparts, in part a consequence of the increased frequency of somatic mutations and structural rearrangements observed in human cancers [72]. Within a heterogeneous cell population, the proliferation of different sub-clones is likely to be regulated by a range of independent of driving mutations. Greater understanding of the tumorigenic potential of individual signalling abnormalities is required in order to establish what proportion of cells must display a given abnormality to benefit from a specific targeted agent. Furthermore, when multiple driving mutations are present throughout the tumour, consideration must be given to establishing some sort of hierarchy for selecting the most appropriate targets for inhibition. Given the restrictions of poly-pharmacology, we believe that whilst molecularly targeted agent are likely to play increasingly important roles in the management of human tumours in the future, more broad spectrum cytotoxics will continue to make a fundamental contribution to the management of patients with cancer allowing us to reserve targeted agents for the most tumorigenic mutations and chemoresistant phenotypes. Inclusion of non-epithelial elements in samples for analysis is likely to be a further source of tumour heterogeneity. Whilst micro-dissection may be used to ensure samples consist purely of epithelial cells, it risks over-simplifying the complex functional interactions found in mature tumours, where non-epithelial elements do not simply provide architectural support but modify tumour behaviour and therapeutic response. Should high throughput screening techniques be successfully incorporated into clinical trials, an additional factor to consider will be the need to balance the capacity for increasingly refined tumour molecular characterisation versus the feasibility of accruing sufficient patients to conduct a clinical trial within a realistic time frame. Failure to achieve the correct balance could unintentionally delay progress.

Integral to robust characterisation of advanced cancers prior to entry into clinical studies is the need to perform further biopsies at the time of disease recurrence. The value of repeat biopsies has been well documented by numerous studies showing significant differences in the phenotypes of primary tumours and corresponding metastases. For example in one study 12% of HER2 negative primary tumours gave rise to HER2 positive metastases [379] and in separate studies up to a third of metastases from HER2 positive primary tumours had lost HER2 over-expression [168]. However, the ethics as well as the significant logistical and financial issues entailed in such an undertaking have led to this being a hotly debated issue

within the clinical setting. Clearly, the risk-benefit ratio of performing further biopsies needs to be well balanced on a case by case basis and individual decisions will be influenced by the extent and site of material available. Even if repeat biopsying at the time of disease recurrence is accepted as standard practice, most patients develop multiple metastatic deposits and therefore consideration needs to be given as to which of these heterogeneous lesions should be sampled. As already discussed, this is likely to be dictated to a large extent by the safety of biopsying lesions at certain anatomical locations, for example biopsy of a superficial metastatic nodal deposit is technically more straight forward and safer than biopsy of a liver metastases, although accurate characterisation and optimisation of therapeutic response of the latter is arguably more important as it is likely to have the greatest impact on patient morbidity and mortality.

Due to the ease of access, use of circulating tumour cells (CTCs) and cell free DNA are potentially attractive options to avoid many of the issues involved in repeating tumour biopsies. The presence of CTCs at presentation of metastatic breast cancer has previously been demonstrated to be the strongest predictor of OS when compared to age, HR status, HER2 status and site of metastases [380]. Furthermore, CTCs have been shown to be better at predicting early response to treatment in breast cancer than traditional imaging techniques [381]. However, both CTCs and cell free DNA need to be validated as being representative of metastatic deposits prior to their use for tumour characterisation.

A further factor contributing to the low success rate of novel molecularly targeted agents in clinical trials is the paucity of validated biomarkers. Comparison of trial outcomes for drugs developed alongside a companion biomarker with those lacking such a marker highlights their importance in streamlining drug development; the percentage of drugs with an accompanying biomarker successfully progressing through phase 1, 2 and 3 trials is 90%, 69% and 85% respectively. In contrast, for drugs developed in the absence of such a biomarker only 74%, 47% and 51% successfully progress through phase 1, 2 and 3 clinical trials respectively [382]. Despite these results, 67% of non-orphan drugs in phase 1 clinical trials do not have a companion biomarker [383]. Numerous factors contribute to the challenges faced in developing biomarkers but in particular incomplete understanding of the biology underpinning individual biomarkers is likely to be of critical importance. For example, KRAS mutational status has been successfully introduced to predict benefit from treatment with the EGFR inhibitor cetuximab [384]. However, more recently, it has been demonstrated

that not all KRAS mutations have an equal impact on cetuximab sensitivity, with tumours possessing a mutation in codon 13 displaying similar RR to those seen in wild-type KRAS [385]. Further issues relate to difficulties in standardizing sample collection, sample processing and assay technique as exemplified by the findings that 20% of HER2 assays performed at primary treatment sites as part of 2 large adjuvant breast studies were considered incorrect on central pathological review [386] [387]. Finally, the criteria for any given biomarker may well be tumour type specific, for example different criteria are used to determine HER2 positivity in gastric [388] and breast [389] cancers thereby potentially dramatically increasing the number of biomarkers required.

The time pressures associated with the introduction of ever more sophisticated tumour characterization techniques into clinical trials are also likely to be immense. Whilst in preclinical studies, tumour material is frequently stored and analyzed simultaneously; this is clearly not feasible in clinical trials. Large numbers of samples will need to be processed as part of later phase clinical trials and appropriate time frames for analysis will largely be dictated by pressures to start patients on therapy in a timely fashion as for the majority of patients with advanced malignancies there remains a relatively short, critical window in which patients are fit to consider further treatment.

Finally, the huge financial expenditure associated with such developments means that the cost of clinical trials and drug development programmes only looks set to rise. To recuperate their initial expenses, the pharmaceutical industry will be forced to pass these on to the consumer in terms of escalating drug prices. The inescapable and uncomfortable reality is that in the future only a minority of patients are likely to be able to afford to access such innovative therapies, whether through state or private funded means. Therefore, the differences in treatment outcomes between patients who can and cannot afford such treatments only looks set to widen.

In conclusion:

- GEMMs are a valuable addition to preclinical drug development programmes.
- Src plays an important role in early tumour development and the Src inhibitor dasatinib may be useful in preventing tumour development in high risk individuals.

- Distinct mechanisms lead to resistance to HER2 directed therapies within individual tumours and therefore a ‘one size fits all’ solution to acquired resistance is likely to be unobtainable.
- PTEN loss moderates tumour sensitivity to AZD8931 in the MMTV-NIC model.
- Induction of EMT and loss of HER2 expression may represent an important mechanism of resistance in a subset of tumours, although this requires further clinical validation.

References

1. Stenehjem, D.D., et al., *Response monitoring, tolerability, and effectiveness of imatinib treatment for chronic myeloid leukemia in a retrospective research database.* J Natl Compr Canc Netw, 2014. **12**(8): p. 1113-21.
2. Arteaga, C.L., et al., *Treatment of HER2-positive breast cancer: current status and future perspectives.* Nat Rev Clin Oncol, 2012. **9**(1): p. 16-32.
3. Von Hoff, D.D., *There are no bad anticancer agents, only bad clinical trial designs--twenty-first Richard and Hinda Rosenthal Foundation Award Lecture.* Clin Cancer Res, 1998. **4**(5): p. 1079-86.
4. Kummar, S., et al., *Drug development in oncology: classical cytotoxics and molecularly targeted agents.* Br J Clin Pharmacol, 2006. **62**(1): p. 15-26.
5. Sharpless, N.E. and R.A. Depinho, *The mighty mouse: genetically engineered mouse models in cancer drug development.* Nat Rev Drug Discov, 2006. **5**(9): p. 741-54.
6. Kerbel, R.S., *Human tumor xenografts as predictive preclinical models for anticancer drug activity in humans: better than commonly perceived-but they can be improved.* Cancer Biol Ther, 2003. **2**(4 Suppl 1): p. S134-9.
7. Ivy, S.P., et al., *Approaches to phase 1 clinical trial design focused on safety, efficiency, and selected patient populations: a report from the clinical trial design task force of the national cancer institute investigational drug steering committee.* Clin Cancer Res, 2010. **16**(6): p. 1726-36.
8. Simon, R., *Designs for efficient clinical trials.* Oncology (Williston Park), 1989. **3**(7): p. 43-9; discussion 51-3.
9. Goodwin, R., et al., *Targeted agents: how to select the winners in preclinical and early clinical studies?* Eur J Cancer, 2012. **48**(2): p. 170-8.
10. Seymour, L., et al., *The design of phase II clinical trials testing cancer therapeutics: consensus recommendations from the clinical trial design task force of the national cancer institute investigational drug steering committee.* Clin Cancer Res, 2010. **16**(6): p. 1764-9.
11. Ocana, A., et al., *Phase III trials of targeted anticancer therapies: redesigning the concept.* Clin Cancer Res, 2013. **19**(18): p. 4931-40.
12. Benson, J.D., et al., *Validating cancer drug targets.* Nature, 2006. **441**(7092): p. 451-6.
13. Hoelder, S., P.A. Clarke, and P. Workman, *Discovery of small molecule cancer drugs: successes, challenges and opportunities.* Mol Oncol, 2012. **6**(2): p. 155-76.
14. Hunsberger, S., et al., *Dose escalation trial designs based on a molecularly targeted endpoint.* Stat Med, 2005. **24**(14): p. 2171-81.

15. Parulekar, W.R. and E.A. Eisenhauer, *Phase I trial design for solid tumor studies of targeted, non-cytotoxic agents: theory and practice.* J Natl Cancer Inst, 2004. **96**(13): p. 990-7.
16. Creedon, H. and V.G. Brunton, *Src kinase inhibitors: promising cancer therapeutics?* Crit Rev Oncog, 2012. **17**(2): p. 145-59.
17. Mayer, E.L., et al., *A phase 2 trial of dasatinib in patients with advanced HER2-positive and/or hormone receptor-positive breast cancer.* Clin Cancer Res, 2011. **17**(21): p. 6897-904.
18. Betensky, R.A., D.N. Louis, and J.G. Cairncross, *Influence of unrecognized molecular heterogeneity on randomized clinical trials.* J Clin Oncol, 2002. **20**(10): p. 2495-9.
19. Roberts, T.G., Jr., et al., *Trends in the risks and benefits to patients with cancer participating in phase 1 clinical trials.* JAMA, 2004. **292**(17): p. 2130-40.
20. Decker, S., et al., *The hollow fibre model in cancer drug screening: the NCI experience.* Eur J Cancer, 2004. **40**(6): p. 821-6.
21. Temmink, O.H., et al., *The Hollow Fibre Assay as a model for in vivo pharmacodynamics of fluoropyrimidines in colon cancer cells.* Br J Cancer, 2007. **96**(1): p. 61-6.
22. Voskoglou-Nomikos, T., J.L. Pater, and L. Seymour, *Clinical predictive value of the in vitro cell line, human xenograft, and mouse allograft preclinical cancer models.* Clin Cancer Res, 2003. **9**(11): p. 4227-39.
23. Venditti, J.M., R.A. Wesley, and J. Plowman, *Current NCI preclinical antitumor screening in vivo: results of tumor panel screening, 1976-1982, and future directions.* Adv Pharmacol Chemother, 1984. **20**: p. 1-20.
24. Damia, G. and M. D'Incalci, *Contemporary pre-clinical development of anticancer agents--what are the optimal preclinical models?* Eur J Cancer, 2009. **45**(16): p. 2768-81.
25. Johnson, J.I., et al., *Relationships between drug activity in NCI preclinical in vitro and in vivo models and early clinical trials.* Br J Cancer, 2001. **84**(10): p. 1424-31.
26. Becher, O.J. and E.C. Holland, *Genetically engineered models have advantages over xenografts for preclinical studies.* Cancer Res, 2006. **66**(7): p. 3355-8, discussion 3358-9.
27. DeNardo, D.G. and L.M. Coussens, *Inflammation and breast cancer. Balancing immune response: crosstalk between adaptive and innate immune cells during breast cancer progression.* Breast Cancer Res, 2007. **9**(4): p. 212.
28. Polyak, K. and R. Kalluri, *The role of the microenvironment in mammary gland development and cancer.* Cold Spring Harb Perspect Biol, 2010. **2**(11): p. a003244.
29. Firestone, B., *The challenge of selecting the 'right' in vivo oncology pharmacology model.* Curr Opin Pharmacol, 2010. **10**(4): p. 391-6.
30. Bibby, M.C., *Orthotopic models of cancer for preclinical drug evaluation: advantages and disadvantages.* Eur J Cancer, 2004. **40**(6): p. 852-7.

31. Peterson, J.K. and P.J. Houghton, *Integrating pharmacology and in vivo cancer models in preclinical and clinical drug development.* Eur J Cancer, 2004. **40**(6): p. 837-44.
32. Eisenhauer, E.A., et al., *New response evaluation criteria in solid tumours: revised RECIST guideline (version 1.1).* Eur J Cancer, 2009. **45**(2): p. 228-47.
33. Valoti, G., et al., *Ecteinascidin-743, a new marine natural product with potent antitumor activity on human ovarian carcinoma xenografts.* Clin Cancer Res, 1998. **4**(8): p. 1977-83.
34. Sessa, C., et al., *Trabectedin for women with ovarian carcinoma after treatment with platinum and taxanes fails.* J Clin Oncol, 2005. **23**(9): p. 1867-74.
35. Krasner, C.N., et al., *A Phase II study of trabectedin single agent in patients with recurrent ovarian cancer previously treated with platinum-based regimens.* Br J Cancer, 2007. **97**(12): p. 1618-24.
36. Monk, B.J., et al., *Trabectedin plus pegylated liposomal doxorubicin (PLD) versus PLD in recurrent ovarian cancer: overall survival analysis.* Eur J Cancer, 2012. **48**(15): p. 2361-8.
37. Sarraf, P., et al., *Differentiation and reversal of malignant changes in colon cancer through PPARgamma.* Nat Med, 1998. **4**(9): p. 1046-52.
38. Kulke, M.H., et al., *A phase II study of troglitazone, an activator of the PPARgamma receptor, in patients with chemotherapy-resistant metastatic colorectal cancer.* Cancer J, 2002. **8**(5): p. 395-9.
39. Monami, M., I. Dicembrini, and E. Mannucci, *Thiazolidinediones and cancer: results of a meta-analysis of randomized clinical trials.* Acta Diabetol, 2014. **51**(1): p. 91-101.
40. Barretina, J., et al., *The Cancer Cell Line Encyclopedia enables predictive modelling of anticancer drug sensitivity.* Nature, 2012. **483**(7391): p. 603-7.
41. Tan, M.H., E.D. Holyoke, and M.H. Goldrosen, *Murine colon adenocarcinoma: syngeneic orthotopic transplantation and subsequent hepatic metastases.* J Natl Cancer Inst, 1977. **59**(5): p. 1537-44.
42. Sheth, K.R. and B.M. Clary, *Management of hepatic metastases from colorectal cancer.* Clin Colon Rectal Surg, 2005. **18**(3): p. 215-23.
43. Pasqualini, R. and E. Ruoslahti, *Organ targeting in vivo using phage display peptide libraries.* Nature, 1996. **380**(6572): p. 364-6.
44. Kuo, T.H., et al., *Site-specific chemosensitivity of human small-cell lung carcinoma growing orthotopically compared to subcutaneously in SCID mice: the importance of orthotopic models to obtain relevant drug evaluation data.* Anticancer Res, 1993. **13**(3): p. 627-30.
45. Fichtner, I., et al., *Establishment of patient-derived non-small cell lung cancer xenografts as models for the identification of predictive biomarkers.* Clin Cancer Res, 2008. **14**(20): p. 6456-68.
46. Rubio-Viqueira, B., et al., *An in vivo platform for translational drug development in pancreatic cancer.* Clin Cancer Res, 2006. **12**(15): p. 4652-61.

47. Daniel, V.C., et al., *A primary xenograft model of small-cell lung cancer reveals irreversible changes in gene expression imposed by culture in vitro.* Cancer Res, 2009. **69**(8): p. 3364-73.
48. Garber, K., *From human to mouse and back: 'tumorgraft' models surge in popularity.* J Natl Cancer Inst, 2009. **101**(1): p. 6-8.
49. Boven, E., et al., *Phase II preclinical drug screening in human tumor xenografts: a first European multicenter collaborative study.* Cancer Res, 1992. **52**(21): p. 5940-7.
50. DeRose, Y.S., et al., *Tumor grafts derived from women with breast cancer authentically reflect tumor pathology, growth, metastasis and disease outcomes.* Nat Med, 2011. **17**(11): p. 1514-20.
51. Tentler, J.J., et al., *Identification of predictive markers of response to the MEK1/2 inhibitor selumetinib (AZD6244) in K-ras-mutated colorectal cancer.* Mol Cancer Ther, 2010. **9**(12): p. 3351-62.
52. Fichtner, I., et al., *Anticancer drug response and expression of molecular markers in early-passage xenotransplanted colon carcinomas.* Eur J Cancer, 2004. **40**(2): p. 298-307.
53. Romanelli, A., et al., *Inhibiting aurora kinases reduces tumor growth and suppresses tumor recurrence after chemotherapy in patient-derived triple-negative breast cancer xenografts.* Mol Cancer Ther, 2012. **11**(12): p. 2693-703.
54. Morton, C.L. and P.J. Houghton, *Establishment of human tumor xenografts in immunodeficient mice.* Nat Protoc, 2007. **2**(2): p. 247-50.
55. Tentler, J.J., et al., *Patient-derived tumour xenografts as models for oncology drug development.* Nat Rev Clin Oncol, 2012. **9**(6): p. 338-50.
56. Malaney, P., S.V. Nicosia, and V. Dave, *One mouse, one patient paradigm: New avatars of personalized cancer therapy.* Cancer Lett, 2014. **344**(1): p. 1-12.
57. Fisher, G.H., et al., *Development of a flexible and specific gene delivery system for production of murine tumor models.* Oncogene, 1999. **18**(38): p. 5253-60.
58. Frese, K.K. and D.A. Tuveson, *Maximizing mouse cancer models.* Nat Rev Cancer, 2007. **7**(9): p. 645-58.
59. Jonkers, J. and A. Berns, *Conditional mouse models of sporadic cancer.* Nat Rev Cancer, 2002. **2**(4): p. 251-65.
60. Huijbers, I.J., et al., *Rapid validation of cancer genes in chimeras derived from established genetically engineered mouse models.* Bioessays, 2011. **33**(9): p. 701-10.
61. Singh, M., C.L. Murriel, and L. Johnson, *Genetically engineered mouse models: closing the gap between preclinical data and trial outcomes.* Cancer Res, 2012. **72**(11): p. 2695-700.
62. Hung, K.E., et al., *Comprehensive proteome analysis of an Apc mouse model uncovers proteins associated with intestinal tumorigenesis.* Cancer Prev Res (Phila), 2009. **2**(3): p. 224-33.

63. Chan, A.T., et al., *Cathepsin B expression and survival in colon cancer: implications for molecular detection of neoplasia.* Cancer Epidemiol Biomarkers Prev, 2010. **19**(11): p. 2777-85.
64. De, P., M. Hasmann, and B. Leyland-Jones, *Molecular determinants of trastuzumab efficacy: What is their clinical relevance?* Cancer Treat Rev, 2013. **39**(8): p. 925-34.
65. Wang, Q., et al., *Addition of the Akt inhibitor triciribine overcomes antibody resistance in cells from ErbB2/Neu-positive/PTEN-deficient mammary tumors.* Int J Oncol, 2014. **44**(4): p. 1277-83.
66. Rottenberg, S., et al., *High sensitivity of BRCA1-deficient mammary tumors to the PARP inhibitor AZD2281 alone and in combination with platinum drugs.* Proc Natl Acad Sci U S A, 2008. **105**(44): p. 17079-84.
67. Bouwman, P. and J. Jonkers, *Molecular pathways: how can BRCA-mutated tumors become resistant to PARP inhibitors?* Clin Cancer Res, 2014. **20**(3): p. 540-7.
68. Perl, A.K., et al., *Reduced expression of neural cell adhesion molecule induces metastatic dissemination of pancreatic beta tumor cells.* Nat Med, 1999. **5**(3): p. 286-91.
69. Doornebal, C.W., et al., *A preclinical mouse model of invasive lobular breast cancer metastasis.* Cancer Res, 2013. **73**(1): p. 353-63.
70. Mattison, J., et al., *Novel candidate cancer genes identified by a large-scale cross-species comparative oncogenomics approach.* Cancer Res, 2010. **70**(3): p. 883-95.
71. Rangarajan, A. and R.A. Weinberg, *Opinion: Comparative biology of mouse versus human cells: modelling human cancer in mice.* Nat Rev Cancer, 2003. **3**(12): p. 952-9.
72. Varela, I., et al., *Somatic structural rearrangements in genetically engineered mouse mammary tumors.* Genome Biol, 2010. **11**(10): p. R100.
73. Maser, R.S., et al., *Chromosomally unstable mouse tumours have genomic alterations similar to diverse human cancers.* Nature, 2007. **447**(7147): p. 966-71.
74. Sorlie, T., *Molecular portraits of breast cancer: tumour subtypes as distinct disease entities.* Eur J Cancer, 2004. **40**(18): p. 2667-75.
75. Perou, C.M., et al., *Molecular portraits of human breast tumours.* Nature, 2000. **406**(6797): p. 747-52.
76. Sorlie, T., et al., *Gene expression patterns of breast carcinomas distinguish tumor subclasses with clinical implications.* Proc Natl Acad Sci U S A, 2001. **98**(19): p. 10869-74.
77. Barros, F.F., et al., *Understanding the HER family in breast cancer: interaction with ligands, dimerization and treatments.* Histopathology, 2010. **56**(5): p. 560-72.
78. Hynes, N.E. and H.A. Lane, *ERBB receptors and cancer: the complexity of targeted inhibitors.* Nat Rev Cancer, 2005. **5**(5): p. 341-54.
79. Lee, K.F., et al., *Requirement for neuregulin receptor erbB2 in neural and cardiac development.* Nature, 1995. **378**(6555): p. 394-8.

80. Crone, S.A., et al., *ErbB2 is essential in the prevention of dilated cardiomyopathy.* Nat Med, 2002. **8**(5): p. 459-65.
81. Ozcelik, C., et al., *Conditional mutation of the ErbB2 (HER2) receptor in cardiomyocytes leads to dilated cardiomyopathy.* Proc Natl Acad Sci U S A, 2002. **99**(13): p. 8880-5.
82. Morris, J.K., et al., *Rescue of the cardiac defect in ErbB2 mutant mice reveals essential roles of ErbB2 in peripheral nervous system development.* Neuron, 1999. **23**(2): p. 273-83.
83. Wolff, A.C., et al., *American Society of Clinical Oncology/College of American Pathologists guideline recommendations for human epidermal growth factor receptor 2 testing in breast cancer.* J Clin Oncol, 2007. **25**(1): p. 118-45.
84. Menard, S., et al., *Role of HER2 gene overexpression in breast carcinoma.* J Cell Physiol, 2000. **182**(2): p. 150-62.
85. Konecny, G., et al., *Her-2/neu and urokinase-type plasminogen activator and its inhibitor in breast cancer.* Clin Cancer Res, 2001. **7**(8): p. 2448-57.
86. Slamon, D.J., et al., *Human breast cancer: correlation of relapse and survival with amplification of the HER-2/neu oncogene.* Science, 1987. **235**(4785): p. 177-82.
87. Harris, R.C., E. Chung, and R.J. Coffey, *EGF receptor ligands.* Exp Cell Res, 2003. **284**(1): p. 2-13.
88. Burgess, A.W., et al., *An open-and-shut case? Recent insights into the activation of EGF/ErbB receptors.* Mol Cell, 2003. **12**(3): p. 541-52.
89. Zhang, X., et al., *An allosteric mechanism for activation of the kinase domain of epidermal growth factor receptor.* Cell, 2006. **125**(6): p. 1137-49.
90. Franklin, M.C., et al., *Insights into ErbB signaling from the structure of the ErbB2-pertuzumab complex.* Cancer Cell, 2004. **5**(4): p. 317-28.
91. Cho, H.S., et al., *Structure of the extracellular region of HER2 alone and in complex with the Herceptin Fab.* Nature, 2003. **421**(6924): p. 756-60.
92. Guy, P.M., et al., *Insect cell-expressed p180erbB3 possesses an impaired tyrosine kinase activity.* Proc Natl Acad Sci U S A, 1994. **91**(17): p. 8132-6.
93. Jura, N., et al., *Structural analysis of the catalytically inactive kinase domain of the human EGF receptor 3.* Proc Natl Acad Sci U S A, 2009. **106**(51): p. 21608-13.
94. Yarden, Y., *The EGFR family and its ligands in human cancer. signalling mechanisms and therapeutic opportunities.* Eur J Cancer, 2001. **37 Suppl 4**: p. S3-8.
95. Graus-Porta, D., et al., *ErbB-2, the preferred heterodimerization partner of all ErbB receptors, is a mediator of lateral signaling.* EMBO J, 1997. **16**(7): p. 1647-55.
96. Citri, A., K.B. Skaria, and Y. Yarden, *The deaf and the dumb: the biology of ErbB-2 and ErbB-3.* Exp Cell Res, 2003. **284**(1): p. 54-65.
97. Schulze, W.X., L. Deng, and M. Mann, *Phosphotyrosine interactome of the ErbB-receptor kinase family.* Mol Syst Biol, 2005. **1**: p. 2005 0008.

98. Janes, P.W., et al., *Structural determinants of the interaction between the erbB2 receptor and the Src homology 2 domain of Grb7.* J Biol Chem, 1997. **272**(13): p. 8490-7.
99. Stein, D., et al., *The SH2 domain protein GRB-7 is co-amplified, overexpressed and in a tight complex with HER2 in breast cancer.* EMBO J, 1994. **13**(6): p. 1331-40.
100. Fruman, D.A., R.E. Meyers, and L.C. Cantley, *Phosphoinositide kinases.* Annu Rev Biochem, 1998. **67**: p. 481-507.
101. Yuan, T.L. and L.C. Cantley, *PI3K pathway alterations in cancer: variations on a theme.* Oncogene, 2008. **27**(41): p. 5497-510.
102. Baselga, J., *Targeting the phosphoinositide-3 (PI3) kinase pathway in breast cancer.* Oncologist, 2011. **16 Suppl 1**: p. 12-9.
103. Castellano, E. and J. Downward, *RAS Interaction with PI3K: More Than Just Another Effector Pathway.* Genes Cancer, 2011. **2**(3): p. 261-74.
104. Depowski, P.L., S.I. Rosenthal, and J.S. Ross, *Loss of expression of the PTEN gene protein product is associated with poor outcome in breast cancer.* Mod Pathol, 2001. **14**(7): p. 672-6.
105. Majumder, P.K. and W.R. Sellers, *Akt-regulated pathways in prostate cancer.* Oncogene, 2005. **24**(50): p. 7465-74.
106. Sarbassov, D.D., et al., *Phosphorylation and regulation of Akt/PKB by the rictor-mTOR complex.* Science, 2005. **307**(5712): p. 1098-101.
107. Cantley, L.C., *The phosphoinositide 3-kinase pathway.* Science, 2002. **296**(5573): p. 1655-7.
108. Duronio, V., *The life of a cell: apoptosis regulation by the PI3K/PKB pathway.* Biochem J, 2008. **415**(3): p. 333-44.
109. Li, Y., et al., *Regulation of FOXO3a/beta-catenin/GSK-3beta signaling by 3,3'-diindolylmethane contributes to inhibition of cell proliferation and induction of apoptosis in prostate cancer cells.* J Biol Chem, 2007. **282**(29): p. 21542-50.
110. Li, Y., D. Dowbenko, and L.A. Lasky, *AKT/PKB phosphorylation of p21Cip/WAF1 enhances protein stability of p21Cip/WAF1 and promotes cell survival.* J Biol Chem, 2002. **277**(13): p. 11352-61.
111. Shin, I., et al., *PKB/Akt mediates cell-cycle progression by phosphorylation of p27(Kip1) at threonine 157 and modulation of its cellular localization.* Nat Med, 2002. **8**(10): p. 1145-52.
112. Engelman, J.A., J. Luo, and L.C. Cantley, *The evolution of phosphatidylinositol 3-kinases as regulators of growth and metabolism.* Nat Rev Genet, 2006. **7**(8): p. 606-19.
113. Sarbassov, D.D., et al., *Rictor, a novel binding partner of mTOR, defines a rapamycin-insensitive and raptor-independent pathway that regulates the cytoskeleton.* Curr Biol, 2004. **14**(14): p. 1296-302.
114. Creedon, H., et al., *Exploring mechanisms of acquired resistance to HER2 (human epidermal growth factor receptor 2)-targeted therapies in breast cancer.* Biochem Soc Trans, 2014. **42**(4): p. 822-30.

115. *Effects of radiotherapy and surgery in early breast cancer. An overview of the randomized trials. Early Breast Cancer Trialists' Collaborative Group.* N Engl J Med, 1995. **333**(22): p. 1444-55.
116. Ruiterkamp, J., et al., *Presence of symptoms and timing of surgery do not affect the prognosis of patients with primary metastatic breast cancer.* Eur J Surg Oncol, 2011. **37**(10): p. 883-9.
117. Dominici, L., et al., *Surgery of the primary tumor does not improve survival in stage IV breast cancer.* Breast Cancer Res Treat, 2011. **129**(2): p. 459-65.
118. Association of Breast Surgery at, B., *Surgical guidelines for the management of breast cancer.* Eur J Surg Oncol, 2009. **35 Suppl 1**: p. 1-22.
119. Poortmans, P., *Optimal approach in early breast cancer: Radiation therapy.* European Journal of Cancer Supplements, 2013. **11**(2): p. 27-36.
120. Mauri, D., N. Pavlidis, and J.P. Ioannidis, *Neoadjuvant versus adjuvant systemic treatment in breast cancer: a meta-analysis.* J Natl Cancer Inst, 2005. **97**(3): p. 188-94.
121. Guarneri, V. and P.F. Conte, *The curability of breast cancer and the treatment of advanced disease.* Eur J Nucl Med Mol Imaging, 2004. **31 Suppl 1**: p. S149-61.
122. Early Breast Cancer Trialists' Collaborative, G., *Effects of chemotherapy and hormonal therapy for early breast cancer on recurrence and 15-year survival: an overview of the randomised trials.* Lancet, 2005. **365**(9472): p. 1687-717.
123. Azim, H.A., Jr., et al., *Long-term toxic effects of adjuvant chemotherapy in breast cancer.* Ann Oncol, 2011. **22**(9): p. 1939-47.
124. Nowak, A.K., et al., *Systematic review of taxane-containing versus non-taxane-containing regimens for adjuvant and neoadjuvant treatment of early breast cancer.* Lancet Oncol, 2004. **5**(6): p. 372-80.
125. Chan, S., et al., *Prospective randomized trial of docetaxel versus doxorubicin in patients with metastatic breast cancer.* J Clin Oncol, 1999. **17**(8): p. 2341-54.
126. Holmes, F.A., et al., *Phase II trial of taxol, an active drug in the treatment of metastatic breast cancer.* J Natl Cancer Inst, 1991. **83**(24): p. 1797-805.
127. Blum, J.L., et al., *Multicenter phase II study of capecitabine in paclitaxel-refractory metastatic breast cancer.* J Clin Oncol, 1999. **17**(2): p. 485-93.
128. Jones, S., et al., *Randomized comparison of vinorelbine and melphalan in anthracycline-refractory advanced breast cancer.* J Clin Oncol, 1995. **13**(10): p. 2567-74.
129. Vaz-Luis, I., et al., *Impact of hormone receptor status on patterns of recurrence and clinical outcomes among patients with human epidermal growth factor-2-positive breast cancer in the National Comprehensive Cancer Network: a prospective cohort study.* Breast Cancer Res, 2012. **14**(5): p. R129.
130. Benz, C.C., et al., *Estrogen-dependent, tamoxifen-resistant tumorigenic growth of MCF-7 cells transfected with HER2/neu.* Breast Cancer Res Treat, 1992. **24**(2): p. 85-95.

131. Prat, A. and J. Baselga, *The role of hormonal therapy in the management of hormonal-receptor-positive breast cancer with co-expression of HER2.* Nat Clin Pract Oncol, 2008. **5**(9): p. 531-42.
132. Kaufman, B., et al., *Trastuzumab plus anastrozole versus anastrozole alone for the treatment of postmenopausal women with human epidermal growth factor receptor 2-positive, hormone receptor-positive metastatic breast cancer: results from the randomized phase III TAnDEM study.* J Clin Oncol, 2009. **27**(33): p. 5529-37.
133. Johnston, S., et al., *Lapatinib combined with letrozole versus letrozole and placebo as first-line therapy for postmenopausal hormone receptor-positive metastatic breast cancer.* J Clin Oncol, 2009. **27**(33): p. 5538-46.
134. Romond, E.H., et al., *Trastuzumab plus adjuvant chemotherapy for operable HER2-positive breast cancer.* N Engl J Med, 2005. **353**(16): p. 1673-84.
135. Gianni, L., et al., *Neoadjuvant chemotherapy with trastuzumab followed by adjuvant trastuzumab versus neoadjuvant chemotherapy alone, in patients with HER2-positive locally advanced breast cancer (the NOAH trial): a randomised controlled superiority trial with a parallel HER2-negative cohort.* Lancet, 2010. **375**(9712): p. 377-84.
136. Slamon, D.J., et al., *Use of chemotherapy plus a monoclonal antibody against HER2 for metastatic breast cancer that overexpresses HER2.* N Engl J Med, 2001. **344**(11): p. 783-92.
137. Nielsen, D.L., M. Andersson, and C. Kamby, *HER2-targeted therapy in breast cancer. Monoclonal antibodies and tyrosine kinase inhibitors.* Cancer Treat Rev, 2009. **35**(2): p. 121-36.
138. Geyer, C.E., et al., *Lapatinib plus capecitabine for HER2-positive advanced breast cancer.* N Engl J Med, 2006. **355**(26): p. 2733-43.
139. Baselga, J., et al., *Lapatinib with trastuzumab for HER2-positive early breast cancer (NeoALTTO): a randomised, open-label, multicentre, phase 3 trial.* Lancet, 2012. **379**(9816): p. 633-40.
140. Cameron, D., et al., *A phase III randomized comparison of lapatinib plus capecitabine versus capecitabine alone in women with advanced breast cancer that has progressed on trastuzumab: updated efficacy and biomarker analyses.* Breast Cancer Res Treat, 2008. **112**(3): p. 533-43.
141. Burris, H.A., 3rd, et al., *Phase II study of the antibody drug conjugate trastuzumab-DM1 for the treatment of human epidermal growth factor receptor 2 (HER2)-positive breast cancer after prior HER2-directed therapy.* J Clin Oncol, 2011. **29**(4): p. 398-405.
142. Garrett, J.T., et al., *Dual blockade of HER2 in HER2-overexpressing tumor cells does not completely eliminate HER3 function.* Clin Cancer Res, 2013. **19**(3): p. 610-9.
143. Gradishar, W.J., *Emerging approaches for treating HER2-positive metastatic breast cancer beyond trastuzumab.* Ann Oncol, 2013. **24**(10): p. 2492-500.
144. Baselga J., H.R., Losado M., Vidaurre T., Lluch A.,Petrakova K. , *A phase II randomized placebo-controlled study of AZD 8931, an inhibitor of EGFR, HER2, and HER3 signalling, plus paclitaxel vs. paclitaxel alone in patients*

with low HER2-expressing advanced breast cancer (THYME). . Cancer Research, 2013. **73**(8 (suppl)): p. nr LB-146.
145. Johnston SRD., B.M., Hegg R., Lousoontomsiri W., Grzeda L., Clemmons M., *Phase II Randomized Study of the EGFR, HER2, HER3 Signalling Inhibitor AZD8931in Combination with Anastrozole in Women with Endocrine Naieve Advanced Breast Cancer* J Clin Oncol, 2013. **31 (suppl abst 531)**.
146. Milani, A., et al., *Active immunotherapy in HER2 overexpressing breast cancer: current status and future perspectives.* Ann Oncol, 2013. **24**(7): p. 1740-8.
147. Rexer, B.N. and C.L. Arteaga, *Intrinsic and acquired resistance to HER2-targeted therapies in HER2 gene-amplified breast cancer: mechanisms and clinical implications.* Crit Rev Oncog, 2012. **17**(1): p. 1-16.
148. Niikura, N., et al., *Loss of human epidermal growth factor receptor 2 (HER2) expression in metastatic sites of HER2-overexpressing primary breast tumors.* J Clin Oncol, 2012. **30**(6): p. 593-9.
149. Scaltriti, M., et al., *Expression of p95HER2, a truncated form of the HER2 receptor, and response to anti-HER2 therapies in breast cancer.* J Natl Cancer Inst, 2007. **99**(8): p. 628-38.
150. Bhosle, J., et al., *TREATMENT WITH GEFITINIB OR LAPATINIB INDUCES DRUG RESISTANCE THROUGH DOWNREGULATION OF TOPOISOMERASE IIalpha EXPRESSION.* Mol Cancer Ther, 2013.
151. Wang, Q., et al., *Concomitant targeting of tumor cells and induction of T-cell response synergizes to effectively inhibit trastuzumab-resistant breast cancer.* Cancer Res, 2012. **72**(17): p. 4417-28.
152. Xia, W., et al., *Lapatinib antitumor activity is not dependent upon phosphatase and tensin homologue deleted on chromosome 10 in ErbB2-overexpressing breast cancers.* Cancer Res, 2007. **67**(3): p. 1170-5.
153. Xia, W., et al., *Resistance to ErbB2 tyrosine kinase inhibitors in breast cancer is mediated by calcium-dependent activation of RelA.* Mol Cancer Ther, 2010. **9**(2): p. 292-9.
154. Eichhorn, P.J., et al., *Phosphatidylinositol 3-kinase hyperactivation results in lapatinib resistance that is reversed by the mTOR/phosphatidylinositol 3-kinase inhibitor NVP-BEZ235.* Cancer Res, 2008. **68**(22): p. 9221-30.
155. Zhang, S., et al., *Combating trastuzumab resistance by targeting SRC, a common node downstream of multiple resistance pathways.* Nat Med, 2011. **17**(4): p. 461-9.
156. Shattuck, D.L., et al., *Met receptor contributes to trastuzumab resistance of Her2-overexpressing breast cancer cells.* Cancer Res, 2008. **68**(5): p. 1471-7.
157. Wilson, T.R., et al., *Widespread potential for growth-factor-driven resistance to anticancer kinase inhibitors.* Nature, 2012. **487**(7408): p. 505-9.
158. Zhuang, G., et al., *Elevation of receptor tyrosine kinase EphA2 mediates resistance to trastuzumab therapy.* Cancer Res, 2010. **70**(1): p. 299-308.

159. Rhee, J., et al., *High serum TGF-alpha predicts poor response to lapatinib and capecitabine in HER2-positive breast cancer.* Breast Cancer Res Treat, 2011. **125**(1): p. 107-14.
160. Vazquez-Martin, A., et al., *Low-scale phosphoproteome analyses identify the mTOR effector p70 S6 kinase 1 as a specific biomarker of the dual-HER1/HER2 tyrosine kinase inhibitor lapatinib (Tykerb) in human breast carcinoma cells.* Ann Oncol, 2008. **19**(6): p. 1097-109.
161. Spector, N.L., et al., *Study of the biologic effects of lapatinib, a reversible inhibitor of ErbB1 and ErbB2 tyrosine kinases, on tumor growth and survival pathways in patients with advanced malignancies.* J Clin Oncol, 2005. **23**(11): p. 2502-12.
162. Alcala, M.A., et al., *Luminescence targeting and imaging using a nanoscale generation 3 dendrimer in an in vivo colorectal metastatic rat model.* Nanomedicine, 2011. **7**(3): p. 249-58.
163. Derksen, P.W., et al., *Somatic inactivation of E-cadherin and p53 in mice leads to metastatic lobular mammary carcinoma through induction of anoikis resistance and angiogenesis.* Cancer Cell, 2006. **10**(5): p. 437-49.
164. Chakrabarty, A., et al., *Trastuzumab-resistant cells rely on a HER2-PI3K-FoxO-survivin axis and are sensitive to PI3K inhibitors.* Cancer Res, 2013. **73**(3): p. 1190-200.
165. Oliveras-Ferraros, C., et al., *Inhibitor of Apoptosis (IAP) survivin is indispensable for survival of HER2 gene-amplified breast cancer cells with primary resistance to HER1/2-targeted therapies.* Biochem Biophys Res Commun, 2011. **407**(2): p. 412-9.
166. Komurov, K., et al., *The glucose-deprivation network counteracts lapatinib-induced toxicity in resistant ErbB2-positive breast cancer cells.* Mol Syst Biol, 2012. **8**: p. 596.
167. Lesniak, D., et al., *Spontaneous epithelial-mesenchymal transition and resistance to HER-2-targeted therapies in HER-2-positive luminal breast cancer.* PLoS One, 2013. **8**(8): p. e71987.
168. Foukakis, T., et al., *When to order a biopsy to characterise a metastatic relapse in breast cancer.* Ann Oncol, 2012. **23 Suppl 10**: p. x349-53.
169. Bose, R., et al., *Activating HER2 mutations in HER2 gene amplification negative breast cancer.* Cancer Discov, 2013. **3**(2): p. 224-37.
170. Castiglioni, F., et al., *Role of exon-16-deleted HER2 in breast carcinomas.* Endocr Relat Cancer, 2006. **13**(1): p. 221-32.
171. Chen, A.C., et al., *Upregulation of mucin4 in ER-positive/HER2-overexpressing breast cancer xenografts with acquired resistance to endocrine and HER2-targeted therapies.* Breast Cancer Res Treat, 2012. **134**(2): p. 583-93.
172. Gijsen, M., et al., *HER2 phosphorylation is maintained by a PKB negative feedback loop in response to anti-HER2 herceptin in breast cancer.* PLoS Biol, 2010. **8**(12): p. e1000563.

173. Xia, W., et al., *An heregulin-EGFR-HER3 autocrine signaling axis can mediate acquired lapatinib resistance in HER2+ breast cancer models.* Breast Cancer Res, 2013. **15**(5): p. R85.
174. Lee-Hoeflich, S.T., et al., *A central role for HER3 in HER2-amplified breast cancer: implications for targeted therapy.* Cancer Res, 2008. **68**(14): p. 5878-87.
175. Ritter, C.A., et al., *Human breast cancer cells selected for resistance to trastuzumab in vivo overexpress epidermal growth factor receptor and ErbB ligands and remain dependent on the ErbB receptor network.* Clin Cancer Res, 2007. **13**(16): p. 4909-19.
176. José Baselga, S.V., Jungsil Ro, Jens Huober, Ellie Guardino, Liang Fang, Steven Olsen, Sanne De Haas, Mark Pegram, *Relationship between tumor biomarkers (BM) and efficacy in EMILIA, a phase 3 study of trastuzumab emtansine (T-DM1) in HER2-postitive metastatic breast cancer (MBC) (abstract).* Proceedings of the 104th Annual Meeting of the American Association for Cancer Research; 2013 Apr 6-10; Washington, DC. Philadelphia (PA): AACR; Cancer Res, 2013. **73**(8 suppl): p. LB63.
177. Gayle, S.S., et al., *Pharmacologic inhibition of mTOR improves lapatinib sensitivity in HER2-overexpressing breast cancer cells with primary trastuzumab resistance.* Anticancer Agents Med Chem, 2012. **12**(2): p. 151-62.
178. Garcia-Garcia, C., et al., *Dual mTORC1/2 and HER2 blockade results in antitumor activity in preclinical models of breast cancer resistant to anti-HER2 therapy.* Clin Cancer Res, 2012. **18**(9): p. 2603-12.
179. Mayer, E., et al., *A phase 2 trial of dasatinib in patients with advanced HER2-positive and/or hormone receptor-positive breast cancer.* Clin Cancer Res, 2011.
180. Tandon, M., S.V. Vemula, and S.K. Mittal, *Emerging strategies for EphA2 receptor targeting for cancer therapeutics.* Expert Opin Ther Targets, 2011. **15**(1): p. 31-51.
181. Liang, K., et al., *Recombinant human erythropoietin antagonizes trastuzumab treatment of breast cancer cells via Jak2-mediated Src activation and PTEN inactivation.* Cancer Cell, 2010. **18**(5): p. 423-35.
182. Fox, E.M., et al., *A kinome-wide screen identifies the insulin/IGF-I receptor pathway as a mechanism of escape from hormone dependence in breast cancer.* Cancer Res, 2011. **71**(21): p. 6773-84.
183. Xia, W., et al., *A model of acquired autoresistance to a potent ErbB2 tyrosine kinase inhibitor and a therapeutic strategy to prevent its onset in breast cancer.* Proc Natl Acad Sci U S A, 2006. **103**(20): p. 7795-800.
184. Arteaga, C.L., *HER3 and mutant EGFR meet MET.* Nat Med, 2007. **13**(6): p. 675-7.
185. Wang, Q., et al., *RON confers lapatinib resistance in HER2-positive breast cancer cells.* Cancer Lett, 2013. **340**(1): p. 43-50.
186. Liu, L., et al., *Novel mechanism of lapatinib resistance in HER2-positive breast tumor cells: activation of AXL.* Cancer Res, 2009. **69**(17): p. 6871-8.

187. Gjerdrum, C., et al., *Axl is an essential epithelial-to-mesenchymal transition-induced regulator of breast cancer metastasis and patient survival.* Proc Natl Acad Sci U S A, 2010. **107**(3): p. 1124-9.
188. Salt, M.B., S. Bandyopadhyay, and F. McCormick, *Epithelial-to-Mesenchymal Transition Rewires the Molecular Path to PI3K-Dependent Proliferation.* Cancer Discov, 2014. **4**(2): p. 186-99.
189. Lesniak, D., et al., *Beta1-integrin circumvents the antiproliferative effects of trastuzumab in human epidermal growth factor receptor-2-positive breast cancer.* Cancer Res, 2009. **69**(22): p. 8620-8.
190. Azuma, K., et al., *Switching addictions between HER2 and FGFR2 in HER2-positive breast tumor cells: FGFR2 as a potential target for salvage after lapatinib failure.* Biochem Biophys Res Commun, 2011. **407**(1): p. 219-24.
191. Wang, Y.C., et al., *Different mechanisms for resistance to trastuzumab versus lapatinib in HER2-positive breast cancers--role of estrogen receptor and HER2 reactivation.* Breast Cancer Res, 2011. **13**(6): p. R121.
192. Valabrega, G., et al., *HER2-positive breast cancer cells resistant to trastuzumab and lapatinib lose reliance upon HER2 and are sensitive to the multitargeted kinase inhibitor sorafenib.* Breast Cancer Res Treat, 2011. **130**(1): p. 29-40.
193. Wetterskog, D., et al., *Identification of novel determinants of resistance to lapatinib in ERBB2-amplified cancers.* Oncogene, 2013.
194. Osipo, C., et al., *ErbB-2 inhibition activates Notch-1 and sensitizes breast cancer cells to a gamma-secretase inhibitor.* Oncogene, 2008. **27**(37): p. 5019-32.
195. Aird, K.M., et al., *X-linked inhibitor of apoptosis protein inhibits apoptosis in inflammatory breast cancer cells with acquired resistance to an ErbB1/2 tyrosine kinase inhibitor.* Mol Cancer Ther, 2010. **9**(5): p. 1432-42.
196. Crawford, A. and R. Nahta, *Targeting Bcl-2 in Herceptin-Resistant Breast Cancer Cell Lines.* Curr Pharmacogenomics Person Med, 2011. **9**(3): p. 184-190.
197. Martin, A.P., et al., *Lapatinib resistance in HCT116 cells is mediated by elevated MCL-1 expression and decreased BAK activation and not by ERBB receptor kinase mutation.* Mol Pharmacol, 2008. **74**(3): p. 807-22.
198. Martin, A.P., et al., *Inhibition of MCL-1 enhances lapatinib toxicity and overcomes lapatinib resistance via BAK-dependent autophagy.* Cancer Biol Ther, 2009. **8**(21): p. 2084-96.
199. Faber, A.C., et al., *BIM expression in treatment-naive cancers predicts responsiveness to kinase inhibitors.* Cancer Discov, 2011. **1**(4): p. 352-65.
200. Sheaff, R.J., et al., *Cyclin E-CDK2 is a regulator of p27Kip1.* Genes Dev, 1997. **11**(11): p. 1464-78.
201. Nahta, R., et al., *P27(kip1) down-regulation is associated with trastuzumab resistance in breast cancer cells.* Cancer Res, 2004. **64**(11): p. 3981-6.
202. Scaltriti, M., et al., *Cyclin E amplification/overexpression is a mechanism of trastuzumab resistance in HER2+ breast cancer patients.* Proc Natl Acad Sci U S A, 2011. **108**(9): p. 3761-6.

203. Puig, T., et al., *A novel inhibitor of fatty acid synthase shows activity against HER2+ breast cancer xenografts and is active in anti-HER2 drug-resistant cell lines.* Breast Cancer Res, 2011. **13**(6): p. R131.
204. Musolino, A., et al., *Immunoglobulin G fragment C receptor polymorphisms and clinical efficacy of trastuzumab-based therapy in patients with HER-2/neu-positive metastatic breast cancer.* J Clin Oncol, 2008. **26**(11): p. 1789-96.
205. Gennari, R., et al., *Pilot study of the mechanism of action of preoperative trastuzumab in patients with primary operable breast tumors overexpressing HER2.* Clin Cancer Res, 2004. **10**(17): p. 5650-5.
206. Tibes, R., et al., *Reverse phase protein array: validation of a novel proteomic technology and utility for analysis of primary leukemia specimens and hematopoietic stem cells.* Mol Cancer Ther, 2006. **5**(10): p. 2512-21.
207. Frame, M.C., *Newest findings on the oldest oncogene; how activated src does it.* J Cell Sci, 2004. **117**(Pt 7): p. 989-98.
208. Parsons, S.J. and J.T. Parsons, *Src family kinases, key regulators of signal transduction.* Oncogene, 2004. **23**(48): p. 7906-9.
209. Summy, J.M. and G.E. Gallick, *Src family kinases in tumor progression and metastasis.* Cancer Metastasis Rev, 2003. **22**(4): p. 337-58.
210. Elsberger, B., et al., *Is expression or activation of Src kinase associated with cancer-specific survival in ER-, PR- and HER2-negative breast cancer patients?* Am J Pathol, 2009. **175**(4): p. 1389-97.
211. Kanomata, N., et al., *Clinicopathological significance of Y416Src and Y527Src expression in breast cancer.* J Clin Pathol, 2011. **64**(7): p. 578-86.
212. Shupnik, M.A., *Crosstalk between steroid receptors and the c-Src-receptor tyrosine kinase pathways: implications for cell proliferation.* Oncogene, 2004. **23**(48): p. 7979-89.
213. Chen, S., et al., *Autophagy facilitates the Lapatinib resistance of HER2 positive breast cancer cells.* Med Hypotheses, 2011. **77**(2): p. 206-8.
214. Herynk, M.H., et al., *Cooperative action of tamoxifen and c-Src inhibition in preventing the growth of estrogen receptor-positive human breast cancer cells.* Mol Cancer Ther, 2006. **5**(12): p. 3023-31.
215. Ishizawar, R. and S.J. Parsons, *c-Src and cooperating partners in human cancer.* Cancer Cell, 2004. **6**(3): p. 209-14.
216. Vergara, D., et al., *Lapatinib/Paclitaxel polyelectrolyte nanocapsules for overcoming multidrug resistance in ovarian cancer.* Nanomedicine, 2012. **8**(6): p. 891-9.
217. Lombardo, L.J., et al., *Discovery of N-(2-chloro-6-methyl- phenyl)-2-(6-(4-(2-hydroxyethyl)- piperazin-1-yl)-2-methylpyrimidin-4- ylamino)thiazole-5-carboxamide (BMS-354825), a dual Src/Abl kinase inhibitor with potent antitumor activity in preclinical assays.* J Med Chem, 2004. **47**(27): p. 6658-61.
218. Serrels, A., et al., *Identification of potential biomarkers for measuring inhibition of Src kinase activity in colon cancer cells following treatment with dasatinib.* Mol Cancer Ther, 2006. **5**(12): p. 3014-22.

219. Vultur, A., et al., *SKI-606 (bosutinib), a novel Src kinase inhibitor, suppresses migration and invasion of human breast cancer cells.* Mol Cancer Ther, 2008. **7**(5): p. 1185-94.
220. Morton, J.P., et al., *Dasatinib inhibits the development of metastases in a mouse model of pancreatic ductal adenocarcinoma.* Gastroenterology, 2010. **139**(1): p. 292-303.
221. Trevino, J.G., et al., *Inhibition of SRC expression and activity inhibits tumor progression and metastasis of human pancreatic adenocarcinoma cells in an orthotopic nude mouse model.* Am J Pathol, 2006. **168**(3): p. 962-72.
222. Finn, R.S., et al., *Dasatinib as a Single Agent in Triple-Negative Breast Cancer: Results of an Open-Label Phase 2 Study.* Clin Cancer Res, 2011. **17**(21): p. 6905-6913.
223. Chiu, C.G., et al., *HER-3 overexpression is prognostic of reduced breast cancer survival: a study of 4046 patients.* Ann Surg, 2010. **251**(6): p. 1107-16.
224. Leyland-Jones, B., *Human epidermal growth factor receptor 2-positive breast cancer and central nervous system metastases.* J Clin Oncol, 2009. **27**(31): p. 5278-86.
225. Muller, W.J., et al., *Single-step induction of mammary adenocarcinoma in transgenic mice bearing the activated c-neu oncogene.* Cell, 1988. **54**(1): p. 105-15.
226. Mendrola, J.M., et al., *The single transmembrane domains of ErbB receptors self-associate in cell membranes.* J Biol Chem, 2002. **277**(7): p. 4704-12.
227. Andrechek, E.R., et al., *Gene expression profiling of neu-induced mammary tumors from transgenic mice reveals genetic and morphological similarities to ErbB2-expressing human breast cancers.* Cancer Res, 2003. **63**(16): p. 4920-6.
228. Jensen, J.D., et al., *PIK3CA mutations, PTEN, and pHER2 expression and impact on outcome in HER2-positive early-stage breast cancer patients treated with adjuvant chemotherapy and trastuzumab.* Ann Oncol, 2012. **23**(8): p. 2034-42.
229. Moreno-Aspitia, A., et al., *RC0639: phase II study of paclitaxel, trastuzumab, and lapatinib as adjuvant therapy for early stage HER2-positive breast cancer.* Breast Cancer Res Treat, 2013. **138**(2): p. 427-35.
230. Faratian, D., et al., *Systems biology reveals new strategies for personalizing cancer medicine and confirms the role of PTEN in resistance to trastuzumab.* Cancer Res, 2009. **69**(16): p. 6713-20.
231. Dourdin, N., et al., *Phosphatase and tensin homologue deleted on chromosome 10 deficiency accelerates tumor induction in a mouse model of ErbB-2 mammary tumorigenesis.* Cancer Res, 2008. **68**(7): p. 2122-31.
232. Gallagher, R.C., et al., *Inactivation of Apc perturbs mammary development, but only directly results in acanthoma in the context of Tcf-1 deficiency.* Oncogene, 2002. **21**(42): p. 6446-57.
233. Novak, *z/EG, a double reporter mouse line that expresses enhanced green fluorescent protein upon cre-mediated excision.* genesis, 2000. **28**: p. 9.

234. Pathmanathan, N. and R.L. Balleine, *Ki67 and proliferation in breast cancer.* J Clin Pathol, 2013. **66**(6): p. 512-6.
235. Franke, W.W., et al., *Diversity of cytokeratins. Differentiation specific expression of cytokeratin polypeptides in epithelial cells and tissues.* J Mol Biol, 1981. **153**(4): p. 933-59.
236. Miyoshi, K., et al., *Activation of different Wnt/beta-catenin signaling components in mammary epithelium induces transdifferentiation and the formation of pilar tumors.* Oncogene, 2002. **21**(36): p. 5548-56.
237. Miyoshi, K., et al., *Activation of beta -catenin signaling in differentiated mammary secretory cells induces transdifferentiation into epidermis and squamous metaplasias.* Proc Natl Acad Sci U S A, 2002. **99**(1): p. 219-24.
238. SM, V., *Proliferation Index as a Prognostic Marker in Breast Cancer.* Cancer, 1993. **71**(12).
239. Nicholson, D.W., et al., *Identification and inhibition of the ICE/CED-3 protease necessary for mammalian apoptosis.* Nature, 1995. **376**(6535): p. 37-43.
240. Selbert, S., et al., *Efficient BLG-Cre mediated gene deletion in the mammary gland.* Transgenic Res, 1998. **7**(5): p. 387-96.
241. Wagner, K.U., et al., *Spatial and temporal expression of the Cre gene under the control of the MMTV-LTR in different lines of transgenic mice.* Transgenic Res, 2001. **10**(6): p. 545-53.
242. Webster, M.A., R.D. Cardiff, and W.J. Muller, *Induction of mammary epithelial hyperplasias and mammary tumors in transgenic mice expressing a murine mammary tumor virus/activated c-src fusion gene.* Proc Natl Acad Sci U S A, 1995. **92**(17): p. 7849-53.
243. Marcotte, R., et al., *Mammary epithelial-specific disruption of c-Src impairs cell cycle progression and tumorigenesis.* Proc Natl Acad Sci U S A, 2012. **109**(8): p. 2808-13.
244. Hebbard, L., et al., *Control of mammary tumor differentiation by SKI-606 (bosutinib).* Oncogene, 2011. **30**(3): p. 301-12.
245. Serrels, B., et al., *A novel Src kinase inhibitor reduces tumour formation in a skin carcinogenesis model.* Carcinogenesis, 2009. **30**(2): p. 249-57.
246. Luttrell, D.K., et al., *Involvement of pp60c-src with two major signaling pathways in human breast cancer.* Proc Natl Acad Sci U S A, 1994. **91**(1): p. 83-7.
247. Muthuswamy, S.K. and W.J. Muller, *Direct and specific interaction of c-Src with Neu is involved in signaling by the epidermal growth factor receptor.* Oncogene, 1995. **11**(2): p. 271-9.
248. Muthuswamy, S.K., et al., *Mammary tumors expressing the neu proto-oncogene possess elevated c-Src tyrosine kinase activity.* Mol Cell Biol, 1994. **14**(1): p. 735-43.
249. Belsches-Jablonski, A.P., et al., *Src family kinases and HER2 interactions in human breast cancer cell growth and survival.* Oncogene, 2001. **20**(12): p. 1465-75.

250. Anagnostopoulou, A., et al., *Differential effects of Stat3 inhibition in sparse vs confluent normal and breast cancer cells.* Cancer Lett, 2006. **242**(1): p. 120-32.
251. Marcotte, R., et al., *c-Src associates with ErbB2 through an interaction between catalytic domains and confers enhanced transforming potential.* Mol Cell Biol, 2009. **29**(21): p. 5858-71.
252. Kaminski, R., et al., *Role of SRC kinases in Neu-induced tumorigenesis: challenging the paradigm using Csk homologous kinase transgenic mice.* Cancer Res, 2006. **66**(11): p. 5757-62.
253. Finn, R.S., et al., *Dasatinib, an orally active small molecule inhibitor of both the src and abl kinases, selectively inhibits growth of basal-type/"triple-negative" breast cancer cell lines growing in vitro.* Breast Cancer Res Treat, 2007. **105**(3): p. 319-26.
254. Huang, F., et al., *Identification of candidate molecular markers predicting sensitivity in solid tumors to dasatinib: rationale for patient selection.* Cancer Res, 2007. **67**(5): p. 2226-38.
255. Jallal, H., et al., *A Src/Abl kinase inhibitor, SKI-606, blocks breast cancer invasion, growth, and metastasis in vitro and in vivo.* Cancer Res, 2007. **67**(4): p. 1580-8.
256. Pichot, C.S., et al., *Dasatinib synergizes with doxorubicin to block growth, migration, and invasion of breast cancer cells.* Br J Cancer, 2009. **101**(1): p. 38-47.
257. Canel, M., et al., *Quantitative in vivo imaging of the effects of inhibiting integrin signaling via Src and FAK on cancer cell movement: effects on E-cadherin dynamics.* Cancer Res, 2010. **70**(22): p. 9413-22.
258. Coluccia, A.M., et al., *SKI-606 decreases growth and motility of colorectal cancer cells by preventing pp60(c-Src)-dependent tyrosine phosphorylation of beta-catenin and its nuclear signaling.* Cancer Res, 2006. **66**(4): p. 2279-86.
259. Garcia-Gomez, A., et al., *Dasatinib as a bone-modifying agent: anabolic and anti-resorptive effects.* PLoS One, 2012. **7**(4): p. e34914.
260. Wilson, G.R., et al., *Activated c-SRC in ductal carcinoma in situ correlates with high tumour grade, high proliferation and HER2 positivity.* Br J Cancer, 2006. **95**(10): p. 1410-4.
261. Diaz, N., et al., *Activation of stat3 in primary tumors from high-risk breast cancer patients is associated with elevated levels of activated SRC and survivin expression.* Clin Cancer Res, 2006. **12**(1): p. 20-8.
262. Baltayan, A., et al., *LEA.135 expression: identifies low-risk patients with breast ductal carcinoma in situ.* Anticancer Res, 2002. **22**(5): p. 2933-7.
263. Madan, R., et al., *Focal adhesion proteins as markers of malignant transformation and prognostic indicators in breast carcinoma.* Hum Pathol, 2006. **37**(1): p. 9-15.
264. Aceto, N., et al., *Tyrosine phosphatase SHP2 promotes breast cancer progression and maintains tumor-initiating cells via activation of key*

transcription factors and a positive feedback signaling loop. Nat Med, 2012. **18**(4): p. 529-37.
265. Fisher, B., et al., *Tamoxifen in treatment of intraductal breast cancer: National Surgical Adjuvant Breast and Bowel Project B-24 randomised controlled trial.* Lancet, 1999. **353**(9169): p. 1993-2000.
266. Siegel, P.M., et al., *Elevated expression of activated forms of Neu/ErbB-2 and ErbB-3 are involved in the induction of mammary tumors in transgenic mice: implications for human breast cancer.* EMBO J, 1999. **18**(8): p. 2149-64.
267. Mitra, D., et al., *An oncogenic isoform of HER2 associated with locally disseminated breast cancer and trastuzumab resistance.* Mol Cancer Ther, 2009. **8**(8): p. 2152-62.
268. Murphy, D., *Transgenic animals and the study of cancer.* Methods Mol Biol, 1993. **18**: p. 23-36.
269. Bouchard, L., et al., *Stochastic appearance of mammary tumors in transgenic mice carrying the MMTV/c-neu oncogene.* Cell, 1989. **57**(6): p. 931-6.
270. Ursini-Siegel, J., et al., *ShcA signalling is essential for tumour progression in mouse models of human breast cancer.* EMBO J, 2008. **27**(6): p. 910-20.
271. O'Brien, N.A., et al., *Activated phosphoinositide 3-kinase/AKT signaling confers resistance to trastuzumab but not lapatinib.* Mol Cancer Ther, 2010. **9**(6): p. 1489-502.
272. Schade, B., et al., *PTEN deficiency in a luminal ErbB-2 mouse model results in dramatic acceleration of mammary tumorigenesis and metastasis.* J Biol Chem, 2009. **284**(28): p. 19018-26.
273. Hickinson, D.M., et al., *AZD8931, an equipotent, reversible inhibitor of signaling by epidermal growth factor receptor, ERBB2 (HER2), and ERBB3: a unique agent for simultaneous ERBB receptor blockade in cancer.* Clin Cancer Res, 2010. **16**(4): p. 1159-69.
274. Gajria, D., A. Seidman, and C. Dang, *Adjuvant taxanes: more to the story.* Clin Breast Cancer, 2010. **10 Suppl 2**: p. S41-9.
275. Ghersi, D., N. Wilcken, and R.J. Simes, *A systematic review of taxane-containing regimens for metastatic breast cancer.* Br J Cancer, 2005. **93**(3): p. 293-301.
276. Bhalla, K.N., *Microtubule-targeted anticancer agents and apoptosis.* Oncogene, 2003. **22**(56): p. 9075-86.
277. Moasser, M.M., *Targeting the function of the HER2 oncogene in human cancer therapeutics.* Oncogene, 2007. **26**(46): p. 6577-92.
278. Bledzka, K., et al., *Tyrosine phosphorylation of integrin beta3 regulates kindlin-2 binding and integrin activation.* J Biol Chem, 2010. **285**(40): p. 30370-4.
279. Sergina, N.V., et al., *Escape from HER-family tyrosine kinase inhibitor therapy by the kinase-inactive HER3.* Nature, 2007. **445**(7126): p. 437-41.
280. Menendez, J.A. and R. Lupu, *Transphosphorylation of kinase-dead HER3 and breast cancer progression: a new standpoint or an old concept revisited?* Breast Cancer Res, 2007. **9**(5): p. 111.

281. Gotoh, N., et al., *Epidermal growth factor-receptor mutant lacking the autophosphorylation sites induces phosphorylation of Shc protein and Shc-Grb2/ASH association and retains mitogenic activity.* Proc Natl Acad Sci U S A, 1994. **91**(1): p. 167-71.
282. Guo, H., et al., *An efficient procedure for protein extraction from formalin-fixed, paraffin-embedded tissues for reverse phase protein arrays.* Proteome Sci, 2012. **10**(1): p. 56.
283. Tuominen, V.J., et al., *ImmunoRatio: a publicly available web application for quantitative image analysis of estrogen receptor (ER), progesterone receptor (PR), and Ki-67.* Breast Cancer Res, 2010. **12**(4): p. R56.
284. Izumi, Y., et al., *Tumour biology: herceptin acts as an anti-angiogenic cocktail.* Nature, 2002. **416**(6878): p. 279-80.
285. Zhao, W.B., et al., *Evaluation of PRL-3 expression, and its correlation with angiogenesis and invasion in hepatocellular carcinoma.* Int J Mol Med, 2008. **22**(2): p. 187-92.
286. Andrechek, E.R., et al., *Amplification of the neu/erbB-2 oncogene in a mouse model of mammary tumorigenesis.* Proc Natl Acad Sci U S A, 2000. **97**(7): p. 3444-9.
287. Guy, C.T., et al., *Expression of the neu protooncogene in the mammary epithelium of transgenic mice induces metastatic disease.* Proc Natl Acad Sci U S A, 1992. **89**(22): p. 10578-82.
288. Sauter, G., et al., *Guidelines for human epidermal growth factor receptor 2 testing: biologic and methodologic considerations.* J Clin Oncol, 2009. **27**(8): p. 1323-33.
289. Devaud, C., et al., *Tissues in different anatomical sites can sculpt and vary the tumor microenvironment to affect responses to therapy.* Mol Ther, 2014. **22**(1): p. 18-27.
290. Husemann, Y., et al., *Systemic spread is an early step in breast cancer.* Cancer Cell, 2008. **13**(1): p. 58-68.
291. Eniu, A., F.M. Palmieri, and E.A. Perez, *Weekly administration of docetaxel and paclitaxel in metastatic or advanced breast cancer.* Oncologist, 2005. **10**(9): p. 665-85.
292. Tiezzi, D.G., et al., *HER-2, p53, p21 and hormonal receptors proteins expression as predictive factors of response and prognosis in locally advanced breast cancer treated with neoadjuvant docetaxel plus epirubicin combination.* BMC Cancer, 2007. **7**: p. 36.
293. Pusztai, L., *Markers predicting clinical benefit in breast cancer from microtubule-targeting agents.* Ann Oncol, 2007. **18 Suppl 12**: p. xii15-20.
294. Buzdar, A.U., et al., *Significantly higher pathologic complete remission rate after neoadjuvant therapy with trastuzumab, paclitaxel, and epirubicin chemotherapy: results of a randomized trial in human epidermal growth factor receptor 2-positive operable breast cancer.* J Clin Oncol, 2005. **23**(16): p. 3676-85.

295. Sparreboom, A., et al., *Nonlinear pharmacokinetics of paclitaxel in mice results from the pharmaceutical vehicle Cremophor EL.* Cancer Res, 1996. **56**(9): p. 2112-5.
296. Rottenberg, S. and J. Jonkers, *Modeling therapy resistance in genetically engineered mouse cancer models.* Drug Resist Updat, 2008. **11**(1-2): p. 51-60.
297. Mohsin, S.K., et al., *Neoadjuvant trastuzumab induces apoptosis in primary breast cancers.* J Clin Oncol, 2005. **23**(11): p. 2460-8.
298. Fadok, V.A. and P.M. Henson, *Apoptosis: getting rid of the bodies.* Curr Biol, 1998. **8**(19): p. R693-5.
299. Zhou, F., et al., *Intravital imaging of tumor apoptosis with FRET probes during tumor therapy.* Mol Imaging Biol, 2010. **12**(1): p. 63-70.
300. Liao, P.C. and C.H. Lieu, *Cell cycle specific induction of apoptosis and necrosis by paclitaxel in the leukemic U937 cells.* Life Sci, 2005. **76**(14): p. 1623-39.
301. Mittendorf, E.A., et al., *Loss of HER2 amplification following trastuzumab-based neoadjuvant systemic therapy and survival outcomes.* Clin Cancer Res, 2009. **15**(23): p. 7381-8.
302. Davies, M.A., et al., *Integrated Molecular and Clinical Analysis of AKT Activation in Metastatic Melanoma.* Clin Cancer Res, 2009. **15**(24): p. 7538-7546.
303. Wulfkuhle, J.D., et al., *Multiplexed cell signaling analysis of human breast cancer applications for personalized therapy.* J Proteome Res, 2008. **7**(4): p. 1508-17.
304. Capri, G., et al., *An open-label expanded access study of lapatinib and capecitabine in patients with HER2-overexpressing locally advanced or metastatic breast cancer.* Ann Oncol, 2010. **21**(3): p. 474-80.
305. Stambolic, V., et al., *Negative regulation of PKB/Akt-dependent cell survival by the tumor suppressor PTEN.* Cell, 1998. **95**(1): p. 29-39.
306. Miller, T.W., et al., *Mutations in the phosphatidylinositol 3-kinase pathway: role in tumor progression and therapeutic implications in breast cancer.* Breast Cancer Res, 2011. **13**(6): p. 224.
307. Sundquist M., E.Z., Brudin L., Teijler G., *Trends in Survival in Metastatic Breast Cancer.* EJC, 2010. **8**(3): p. 191 (abstract 453).
308. Rottenberg, S., et al., *Selective induction of chemotherapy resistance of mammary tumors in a conditional mouse model for hereditary breast cancer.* Proc Natl Acad Sci U S A, 2007. **104**(29): p. 12117-22.
309. Zander, S.A., et al., *Sensitivity and acquired resistance of BRCA1;p53-deficient mouse mammary tumors to the topoisomerase I inhibitor topotecan.* Cancer Res, 2010. **70**(4): p. 1700-10.
310. Meryman, H.T., *General principles of freezing and freezing injury in cellular materials.* Ann N Y Acad Sci, 1960. **85**: p. 503-9.
311. Varticovski, L., et al., *Accelerated preclinical testing using transplanted tumors from genetically engineered mouse breast cancer models.* Clin Cancer Res, 2007. **13**(7): p. 2168-77.

312. Dales, J.P., et al., *Overexpression of hypoxia-inducible factor HIF-1alpha predicts early relapse in breast cancer: retrospective study in a series of 745 patients.* Int J Cancer, 2005. **116**(5): p. 734-9.
313. Ward, C., et al., *New strategies for targeting the hypoxic tumour microenvironment in breast cancer.* Cancer Treat Rev, 2013. **39**(2): p. 171-9.
314. Shi, Y., et al., *PTEN at a glance.* J Cell Sci, 2012. **125**(Pt 20): p. 4687-92.
315. Smith HW., H.A., Sanguin-Gendreau V., Zuo D., Muller WJ., *c-Src and PRC2 activity in ErbB2-driven mammary tumorigeneiss and acquired resistance to ErbB2-targeted therapy.* Program and Proceedings of Advances in Breast Cancer Research: genetics, biology and clinical applications, October 3rd-6th, 2013. , 2013.
316. Kim, J.B., *Three-dimensional tissue culture models in cancer biology.* Semin Cancer Biol, 2005. **15**(5): p. 365-77.
317. Nagata, Y., et al., *Peptides derived from a wild-type murine proto-oncogene c-erbB-2/HER2/neu can induce CTL and tumor suppression in syngeneic hosts.* J Immunol, 1997. **159**(3): p. 1336-43.
318. Belizario, J., *Immunodeficient mouse models : an overview.* The open immunology journal, 2009. **2**: p. 79-85.
319. Meric-Bernstam, F., et al., *Concordance of Genomic Alterations Between Primary and Recurrent Breast Cancer.* Mol Cancer Ther, 2014.
320. Cooper, C.L., et al., *Molecular alterations in metaplastic breast carcinoma.* J Clin Pathol, 2013. **66**(6): p. 522-8.
321. Olive, K.P., et al., *Inhibition of Hedgehog signaling enhances delivery of chemotherapy in a mouse model of pancreatic cancer.* Science, 2009. **324**(5933): p. 1457-61.
322. Dua, R., et al., *EGFR over-expression and activation in high HER2, ER negative breast cancer cell line induces trastuzumab resistance.* Breast Cancer Res Treat, 2010. **122**(3): p. 685-97.
323. Blackwell, K.L., et al., *Randomized study of Lapatinib alone or in combination with trastuzumab in women with ErbB2-positive, trastuzumab-refractory metastatic breast cancer.* J Clin Oncol, 2010. **28**(7): p. 1124-30.
324. Gianni, L., et al., *Efficacy and safety of neoadjuvant pertuzumab and trastuzumab in women with locally advanced, inflammatory, or early HER2-positive breast cancer (NeoSphere): a randomised multicentre, open-label, phase 2 trial.* Lancet Oncol, 2011.
325. Baselga, J., et al., *Pertuzumab plus Trastuzumab plus Docetaxel for Metastatic Breast Cancer.* N Engl J Med, 2011.
326. Tjulandin, S., et al., *Phase I, dose-finding study of AZD8931, an inhibitor of EGFR (erbB1), HER2 (erbB2) and HER3 (erbB3) signaling, in patients with advanced solid tumors.* Invest New Drugs, 2013.
327. Burris, H.A., 3rd, et al., *Phase I safety, pharmacokinetics, and clinical activity study of lapatinib (GW572016), a reversible dual inhibitor of epidermal growth factor receptor tyrosine kinases, in heavily pretreated patients with metastatic carcinomas.* J Clin Oncol, 2005. **23**(23): p. 5305-13.

328. Subik, K., et al., *The Expression Patterns of ER, PR, HER2, CK5/6, EGFR, Ki-67 and AR by Immunohistochemical Analysis in Breast Cancer Cell Lines.* Breast Cancer (Auckl), 2010. **4**: p. 35-41.
329. Weigelt, B., P.H. Warne, and J. Downward, *PIK3CA mutation, but not PTEN loss of function, determines the sensitivity of breast cancer cells to mTOR inhibitory drugs.* Oncogene, 2011. **30**(29): p. 3222-33.
330. Bedard, P.L., F. Cardoso, and M.J. Piccart-Gebhart, *Stemming resistance to HER-2 targeted therapy.* J Mammary Gland Biol Neoplasia, 2009. **14**(1): p. 55-66.
331. Li, W. and W.T. Miller, *Role of the activation loop tyrosines in regulation of the insulin-like growth factor I receptor-tyrosine kinase.* J Biol Chem, 2006. **281**(33): p. 23785-91.
332. Miao, H., et al., *EphA2 mediates ligand-dependent inhibition and ligand-independent promotion of cell migration and invasion via a reciprocal regulatory loop with Akt.* Cancer Cell, 2009. **16**(1): p. 9-20.
333. Hazan, R.B., et al., *Cadherin switch in tumor progression.* Ann N Y Acad Sci, 2004. **1014**: p. 155-63.
334. Vuoriluoto, K., et al., *Vimentin regulates EMT induction by Slug and oncogenic H-Ras and migration by governing Axl expression in breast cancer.* Oncogene, 2011. **30**(12): p. 1436-48.
335. Pierceall, W.E., et al., *Frequent alterations in E-cadherin and alpha- and beta-catenin expression in human breast cancer cell lines.* Oncogene, 1995. **11**(7): p. 1319-26.
336. Berx, G. and F. Van Roy, *The E-cadherin/catenin complex: an important gatekeeper in breast cancer tumorigenesis and malignant progression.* Breast Cancer Res, 2001. **3**(5): p. 289-93.
337. Dave, B., et al., *Epithelial-mesenchymal transition, cancer stem cells and treatment resistance.* Breast Cancer Res, 2012. **14**(1): p. 202.
338. Roxanis, I., *Occurrence and significance of epithelial-mesenchymal transition in breast cancer.* J Clin Pathol, 2013. **66**(6): p. 517-21.
339. Weng, Q.P., et al., *Regulation of the p70 S6 kinase by phosphorylation in vivo. Analysis using site-specific anti-phosphopeptide antibodies.* J Biol Chem, 1998. **273**(26): p. 16621-9.
340. Ferrari, S., et al., *Mitogen-activated 70K S6 kinase. Identification of in vitro 40 S ribosomal S6 phosphorylation sites.* J Biol Chem, 1991. **266**(33): p. 22770-5.
341. Bulavin, D.V., et al., *Dual phosphorylation controls Cdc25 phosphatases and mitotic entry.* Nat Cell Biol, 2003. **5**(6): p. 545-51.
342. Morgan, D.O., *Cyclin-dependent kinases: engines, clocks, and microprocessors.* Annu Rev Cell Dev Biol, 1997. **13**: p. 261-91.
343. Lukas, J., J. Bartkova, and J. Bartek, *Convergence of mitogenic signalling cascades from diverse classes of receptors at the cyclin D-cyclin-dependent kinase-pRb-controlled G1 checkpoint.* Mol Cell Biol, 1996. **16**(12): p. 6917-44. Korsmeyer, S.J., et al., *Pro-apoptotic cascade activates BID, which*

oligomerizes BAK or BAX into pores that result in the release of cytochrome c. Cell Death Differ, 2000. **7**(12): p. 1166-73.
345. Reed, J.C. and S.I. Reed, *Survivin' cell-separation anxiety.* Nat Cell Biol, 1999. **1**(8): p. E199-200.
346. Luciano, F., et al., *Phosphorylation of Bim-EL by Erk1/2 on serine 69 promotes its degradation via the proteasome pathway and regulates its proapoptotic function.* Oncogene, 2003. **22**(43): p. 6785-93.
347. Dittmar, T., et al., *Induction of cancer cell migration by epidermal growth factor is initiated by specific phosphorylation of tyrosine 1248 of c-erbB-2 receptor via EGFR.* FASEB J, 2002. **16**(13): p. 1823-5.
348. de Jong, R., et al., *Tyrosine 207 in CRKL is the BCR/ABL phosphorylation site.* Oncogene, 1997. **14**(5): p. 507-13.
349. Hou, Q., et al., *Identification and functional validation of caldesmon as a potential gastric cancer metastasis-associated protein.* J Proteome Res, 2013. **12**(2): p. 980-90.
350. Sen, S., W.P. Ng, and S. Kumar, *Contributions of talin-1 to glioma cell-matrix tensional homeostasis.* J R Soc Interface, 2012. **9**(71): p. 1311-7.
351. Yu, D., et al., *Enhanced PI3K p110alpha signaling confers acquired lapatinib resistance which can be effectively reversed by a p110alpha-selective PI3K inhibitor.* Mol Cancer Ther, 2013.
352. Dave, B., et al., *Loss of phosphatase and tensin homolog or phosphoinositol-3 kinase activation and response to trastuzumab or lapatinib in human epidermal growth factor receptor 2-overexpressing locally advanced breast cancers.* J Clin Oncol, 2011. **29**(2): p. 166-73.
353. José Baselga SV, J.R., Jens Huober, Ellie Guardino, Liang Fang, Steven Olsen, Sanne De Haas, Mark Pegram., *Relationship between tumor biomarkers (BM) and efficacy in EMILIA, a phase 3 study of trastuzumab emtansine (T-DM1) in HER2-postitive metastatic breast cancer (MBC) (abstract).* . Proceedings of the 104th Annual Meeting of the American Association for Cancer Research; 2013 Apr 6-10; Washington, DC Philadelphia (PA): AACR;Cancer Res., 2013(8 suppl).
354. Tanizaki, J., et al., *Roles of BIM induction and survivin downregulation in lapatinib-induced apoptosis in breast cancer cells with HER2 amplification.* Oncogene, 2011. **30**(39): p. 4097-106.
355. Scaltriti, M., et al., *Lapatinib, a HER2 tyrosine kinase inhibitor, induces stabilization and accumulation of HER2 and potentiates trastuzumab-dependent cell cytotoxicity.* Oncogene, 2009. **28**(6): p. 803-14.
356. Amin, D.N., et al., *Resiliency and vulnerability in the HER2-HER3 tumorigenic driver.* Sci Transl Med, 2010. **2**(16): p. 16ra7.
357. Akbani, R., et al., *Realizing the Promise of Reverse Phase Protein Arrays for Clinical, Translational, and Basic Research: A Workshop Report: The RPPA (Reverse Phase Protein Array) Society.* Mol Cell Proteomics, 2014. **13**(7): p. 1625-43.
358. Gayle, S.S., et al., *MEK inhibition increases lapatinib sensitivity via modulation of FOXM1.* Curr Med Chem, 2013. **20**(19): p. 2486-99.

359. Fruman, D.A. and C. Rommel, *PI3K and cancer: lessons, challenges and opportunities.* Nat Rev Drug Discov, 2014. **13**(2): p. 140-56.
360. Britten, C.D., *PI3K and MEK inhibitor combinations: examining the evidence in selected tumor types.* Cancer Chemother Pharmacol, 2013. **71**(6): p. 1395-409.
361. De Luca, A., et al., *Src and CXCR4 are involved in the invasiveness of breast cancer cells with acquired resistance to lapatinib.* Cell Cycle, 2013. **13**(2).
362. Tamm, I., et al., *IAP-family protein survivin inhibits caspase activity and apoptosis induced by Fas (CD95), Bax, caspases, and anticancer drugs.* Cancer Res, 1998. **58**(23): p. 5315-20.
363. Asanuma, H., et al., *Survivin expression is regulated by coexpression of human epidermal growth factor receptor 2 and epidermal growth factor receptor via phosphatidylinositol 3-kinase/AKT signaling pathway in breast cancer cells.* Cancer Res, 2005. **65**(23): p. 11018-25.
364. Emlet, D.R., et al., *Subsets of epidermal growth factor receptors during activation and endocytosis.* J Biol Chem, 1997. **272**(7): p. 4079-86.
365. Dolled-Filhart, M., et al., *Tissue microarray analysis of signal transducers and activators of transcription 3 (Stat3) and phospho-Stat3 (Tyr705) in node-negative breast cancer shows nuclear localization is associated with a better prognosis.* Clin Cancer Res, 2003. **9**(2): p. 594-600.
366. Yamashita, H., et al., *Stat5 expression predicts response to endocrine therapy and improves survival in estrogen receptor-positive breast cancer.* Endocr Relat Cancer, 2006. **13**(3): p. 885-93.
367. Steinestel, K., et al., *Clinical significance of epithelial-mesenchymal transition.* Clin Transl Med, 2014. **3**: p. 17.
368. Gjerdrum, C., et al., *Axl is an essential epithelial-to-mesenchymal transition-induced regulator of breast cancer metastasis and patient survival.* Proceedings of the National Academy of Sciences of the United States of America, 2010. **107**(3): p. 1124-1129.
369. Koorstra, J.B., et al., *The Axl receptor tyrosine kinase confers an adverse prognostic influence in pancreatic cancer and represents a new therapeutic target.* Cancer Biol Ther, 2009. **8**(7): p. 618-26.
370. Byers, L.A., et al., *An epithelial-mesenchymal transition gene signature predicts resistance to EGFR and PI3K inhibitors and identifies Axl as a therapeutic target for overcoming EGFR inhibitor resistance.* Clin Cancer Res, 2013. **19**(1): p. 279-90.
371. Wilson, C., et al., *AXL inhibition sensitizes mesenchymal cancer cells to anti-mitotic drugs.* Cancer Res, 2014.
372. Shapiro, G.I., et al., *A Phase 1 dose-escalation study of the safety and pharmacokinetics of once-daily oral foretinib, a multi-kinase inhibitor, in patients with solid tumors.* Invest New Drugs, 2013. **31**(3): p. 742-50.
373. Oliveras-Ferraros, C., et al., *Epithelial-to-mesenchymal transition (EMT) confers primary resistance to trastuzumab (Herceptin).* Cell Cycle, 2012. **11**(21): p. 4020-32.

374. Moody, S.E., et al., *The transcriptional repressor Snail promotes mammary tumor recurrence.* Cancer Cell, 2005. **8**(3): p. 197-209.
375. Tobin, N.P., et al., *Cyclin D1, Id1 and EMT in breast cancer.* BMC Cancer, 2011. **11**.
376. Lee J, Y.G., Paik S, Chung M. , *Does E-cadherin or N-cadherin or epithelial-mesenchymal transition have a probability of clinical implication of the prognostic marker in invasive ductal carcinoma?* Cancer Res, 2012. **3**: p. Abstract nr P2-10-39.
377. Kwak, E.L., et al., *Anaplastic lymphoma kinase inhibition in non-small-cell lung cancer.* N Engl J Med, 2010. **363**(18): p. 1693-703.
378. Qian, H., et al., *The efficacy and safety of crizotinib in the treatment of anaplastic lymphoma kinase-positive non-small cell lung cancer: a meta-analysis of clinical trials.* BMC Cancer, 2014. **14**: p. 683.
379. Zidan, J., et al., *Comparison of HER-2 overexpression in primary breast cancer and metastatic sites and its effect on biological targeting therapy of metastatic disease.* Br J Cancer, 2005. **93**(5): p. 552-6.
380. Cristofanilli, M., et al., *Circulating tumor cells: a novel prognostic factor for newly diagnosed metastatic breast cancer.* J Clin Oncol, 2005. **23**(7): p. 1420-30.
381. Budd, G.T., et al., *Circulating tumor cells versus imaging--predicting overall survival in metastatic breast cancer.* Clin Cancer Res, 2006. **12**(21): p. 6403-9.
382. Hayashi, K., S. Masuda, and H. Kimura, *Impact of biomarker usage on oncology drug development.* J Clin Pharm Ther, 2013. **38**(1): p. 62-7.
383. Martell, R.E., et al., *Oncology drug development and approval of systemic anticancer therapy by the U.S. Food and Drug Administration.* Oncologist, 2013. **18**(1): p. 104-11.
384. Lievre, A., et al., *KRAS mutation status is predictive of response to cetuximab therapy in colorectal cancer.* Cancer Res, 2006. **66**(8): p. 3992-5.
385. De Roock, W., et al., *Association of KRAS p.G13D mutation with outcome in patients with chemotherapy-refractory metastatic colorectal cancer treated with cetuximab.* JAMA, 2010. **304**(16): p. 1812-20.
386. Paik, S., et al., *Real-world performance of HER2 testing--National Surgical Adjuvant Breast and Bowel Project experience.* J Natl Cancer Inst, 2002. **94**(11): p. 852-4.
387. Roche, P.C., et al., *Concordance between local and central laboratory HER2 testing in the breast intergroup trial N9831.* J Natl Cancer Inst, 2002. **94**(11): p. 855-7.
388. Albarello, L., L. Pecciarini, and C. Doglioni, *HER2 testing in gastric cancer.* Adv Anat Pathol, 2011. **18**(1): p. 53-9.
389. Wolff, A.C., et al., *American Society of Clinical Oncology/College of American Pathologists guideline recommendations for human epidermal growth factor receptor 2 testing in breast cancer.* Arch Pathol Lab Med, 2007. **131**(1): p. 18-43.

Appendix 1- RPPA data Comparison of signalling pathways between vehicle and dasatinib treated BLG-6222 derived tumours.

RPPA analysis was performed on lysate of vehicle and dasatinib treated BLG-6222 derived tumours. Where possible phosphorylated the ratio of phospho : corresponding total protein is presented {Tibes, 2006 #2112}. The relative fluorescence intensity (RFI) for all other antibodies is presented, corrected using global normalization technique {Guo, 2012 #69}. P values calculated using one way ANOVA.

	Median Vehicle (range)	**Median dasatinib (range)**	**P value**
P Tyr 416 Src: Src	0.21 (0.17-0.21)	0.12 (0.12-0.13)	0.07
P Tyr1248/Tyr1173 HER2/EGFR	0.07 (0.06-0.08)	0.05 (0.04-0.05)	0.07
P Tyr 1173 EGFR	0.15 (0.14-0.17)	0.15 (0.15-0.16)	1.0
P Ser380,Thr382,Thr383 PTEN:PTEN	0.39 (0.36-0.42)	0.40 (0.39-0.47)	0.51
P Tyr 308 Akt: Akt	0.27 (0.17-0.41)	0.08 (0.07-0.09)	0.08
P Ser 473 Akt: Akt	0.34 (0.26-0.42)	0.09 (0.08-0.09)	0.07
p44/42 MAPK (ERK1/2) P Thr202/Thr185,Tyr204/Tyr187: p44/42 MAPK	0.15 (0.12-0.18)	0.07 (0.06-0.14)	0.19
P Ser2448 mTOR: mTOR	3.19 (2.23-3.31)	2.69 (2.59-3.15)	0.66

P Ser240,Ser244S6 Ribosomal protein:S6	2.64 (2.42-2.90)	2.20 (2.20-2.84)	0.38
P Ser235,Ser236S6 Ribosomal protein:S6	1.86 (1.86-2.33)	1.71 (1.51-1.90)	0.38
GSK-3-beta	0.57 (0.53-0.67)	0.68 (0.65-0.69)	0.19
P Ser21/Ser9 GSK-3-alpha/beta	0.46 (0.31-0.56)	0.49 (0.29-0.53)	1.0
P Thr 389 p70 S6 kinase	0.30 (0.28-0.30)	0.30 (0.24-0.35)	0.66
P Tyr 783 PLCɣ: PLC ɣ	0.28 (0.23-0.35)	0.17 (0.17-0.21)	0.08
pY397 FAK1:FAK1	0.95 (0.84-1.53)	1.07 (1.02-1.34)	0.66
P Tyr 1162, 1163 IGF1R beta	0.20 (0.14-0.26)	0.18 (0.13-1.22)	1.0
PYStat 5: Stat 5	0.04 (0.04-0.05)	0.03 (0.02-0.03)	0.07
P Tyr 542 SHP2	0.18 (0.17-0.27)	0.13 (0.12-0.15)	0.08

P Thr 172 AMPK alpha: AMPK alpha	1.57 (1.16-2.76)	1.09 (1.04-1.53)	0.19
P Tyr 1054, Tyr 1055 Tyk2	0.09 (0.09-0.11)	0.08 (0.08-0.09)	0.16
P Ty 207 Crkl	0.09 (0.08-0.10)	0.09 (0.07-0.1)	1.0
LKB1	0.10 (0.09-0.13)	0.12 (0.10-0.12)	0.82

Appendix 2- RPPA data Comparison of signalling pathways between MMTV-Nic PTEN $^{FL/+}$ and MMTV-Nic PTEN+/- models

RPPA data confirming reduced expression of PTEN and increased Akt activation in MMTV-Nic PTEN$^{+/-}$ tumours. RPPA analysis was performed on lysate of MMTV-Nic PTEN $^{FL/+}$ (n=4) and MMTV-Nic PTEN$^{+/-}$ (n=3) tumours. Where possible the ratio of phospho : corresponding total protein is presented {Tibes, 2006 #35}. The relative fluorescence intensity (RFI) for all other antibodies is presented, corrected using global normalization technique {Guo, 2012 #34}. P values calculated using Mann-Whitney U test.

	Median MMTV-Nic PTEN $^{FL/+}$ value	**Median MMTV-Nic PTEN$^{+/-}$ value**	**P value**
HER2 (DAKO)	1562.6 (760.34-2954.65)	78.90 (299.85-1097.21)	0.07
HER2 (Cell signaling technology)	204.00 (135.31-411.26)	300.30 (14.64-316.77)	0.93
P Tyr1248/Tyr1173 Her2/EGFR	77.20 (43.77-168.45)	61.70 (26.79-91.97)	0.22
P Tyr 1173 EGFR	41.40 (33.05-56.53)	33.00 (0.0-48.53)	0.24
P Tyr 1289 HER3: HER3	8.97 (6.39-68.29)	10.03 (8.89-17.98)	0.36
PI3 Kinase p110-alpha	163.59 (135.76-211.54)	153.02 (130.12-180.14)	0.35
P Ser380,Thr382,Thr383 PTEN	114.55 (17.77-155.90)	36.80 (0-56.93)	0.02
P Tyr 416 Src: Src	0.24 (0.21-0.27)	0.23 ((0.21-0.26)	0.38
P Tyr 308 Akt: Akt	0.24 (0.15-0.83)	1.02 (0.00-1.32)	0.33

P Ser 473 Akt: Akt	0.20 (0.17-0.25)	1.42 (0.99-21.62)	0.005
P Ser2448 mTOR	149.50 (64.70-182.84)	89.30 (63.25-138.71)	0.12
P Ser2481 mTOR	31.50 (14.68-200.92)	13.30 (0.00-173.54)	0.28
p Ser240,Ser244S6: S6 Ribosomal protein	2.08 (1.36-3.39)	3.01 (0.25-4.72)	0.58
P Ser235,Ser23 S6:S6 Ribosomal protein	2.26 (0.90-2.83)	3.49 (2.36-4.42)	0.11
P Ser9: GSK-3-beta GSK-3-beta	0.19 (0.14-0.29)	0.29 (0.11-0.52)	0.09
P Ser21/Ser9 GSK-3-alpha/beta	107.60 (0.04-0.29)	136.50 (0.11-0.35)	0.72
PThr180,Tyr182 p38 MAPK:p38	0.70 (0.40-0.96)	0.74 (0.61-1.15)	0.35
P Thr202/Thr185,Tyr204/Tyr187 p44/42 MAPK (ERK1/2): p44/42 MAPK	0.60 (0.20-0.61)	0.33 (0.21-0.38)	0.38
P Ser660 (beta-2) PKC (pan)	141.55 (90.06-142.68)	177.81 (172.50-203.24)	0.10

P (R/K)X(S*)(Hyd)(R/k) PKC substrate	470.60 (269.05-487.90)	478.60 (387.13-587.86)	0.22
P Thr638 PKC-alpha	672.20 (627.38-847.17)	898.40 (786.72-1113.90)	0.07
E-Cadherin	434.60 (350.91-673.79)	558.40 (367.77-619.13)	0.41
Beta-actin	31.5 (14.68-103.81)	13.28 (0.83-36.74)	0.17
Beta- tubulin	486.9 (90.15-642.75)	558.6 (473.01-690.66)	0.10

Appendix 3- RPPA data Comparison of signalling pathways between vehicle and AZD 8931 treated tumours in the MMTV-Nic PTEN $^{FL/+}$ and MMTV-Nic PTEN$^{+/-}$ models

RPPA analysis was performed on lysate of vehicle and AZD 8931 treated tumours from both the MMTV-Nic PTEN $^{FL/+}$ and MMTV-Nic PTEN$^{+/-}$ tumours. Where possible phosphorylated the ratio of phospho : corresponding total protein is presented {Tibes, 2006 #35}. The relative fluorescence intensity (RFI) for all other antibodies is presented, corrected using global normalization technique {Guo, 2012 #34}. P values calculated using Mann-Whitney U test.

	MMTV-Nic PTEN $^{FL/+}$			MMTV-Nic PTEN$^{+/-}$		
	Median Vehicle (range)	**Median AZD8931 (range)**	**P value**	**Median Vehicle (range)**	**Median AZD8931 (range)**	**P value**
HER2 (DAKO)	1562.5 (760.00-1954.65)	12241.1 (117.61-1875.54)	0.51	878.9 (299.48-1097.21)	863.3 (668.85-1008.17)	0.95
HER2 (Cell signaling technology)	301.4 (249.70-411.27)	375.5 (358.66-410.74)	0.07	294.1 (14.64-316.77)	364.8 (299.72-478.97)	0.01
P Tyr1248/Tyr1173 HER2/EGFR	47.2 (43.77-182.84)	50.9 (17.57-136.54)	0.30	61.7 (26.79-91.97)	67.5 (0.00-191.31)	0.80

	MMTV-Nic PTEN $^{FL/+}$			MMTV-Nic PTEN$^{+/-}$		
	Median Vehicle (range)	**Median AZD8931 (range)**	**P value**	**Median Vehicle (range)**	**Median AZD8931 (range)**	**P value**
P Tyr 1173 EGFR	41.4 (33.05-56.53)	42.6 (32.95-52.55)	0.89	33.0 (0-48.53)	15.3 (0-66.53)	0.74
P Tyr 1289 HER3: HER3	9.0 (6.39-68.29)	8.3 (6.67-25.96)	0.92	9.5 (8.89-17.99)	7.9 (2.18-12.71)	0.46
PI3 Kinase p110-alpha	163.6 (135.76-221.54)	133.9 (119.57-161.40)	0.05	153.0 (132.32-180.14)	149.6 (0-191.76)	0.91

	MMTV-Nic PTEN $^{FL/+}$			MMTV-Nic PTEN$^{+/-}$		
	Median Vehicle (range)	**Median AZD8931 (range)**	**P value**	**Median Vehicle (range)**	**Median AZD8931 (range)**	**P value**
P Ser380,Thr382,Thr383 PTEN	114.6 (17.77-155.89)	146.2 (109.74-192.52)	0.34	36.8 (0.00-56.93)	69.4 (0.00-230.82)	0.18
P Tyr 416 Src: Src	0.2 (0.21-0.26)	0.1 (0.16-0.21)	0.03	0.2 (0.20-0.26)	0.2 (0.20-0.27)	0.77
P Tyr 308 Akt: Akt	0.2 (0.14-0.83)	0.2 (0.09-0.83)	0.35	1.0 (0.00-1.32)	0.5 (0.21-0.61)	0.33
P Ser 473 Akt: Akt	0.2 (0.17-0.26)	0.1 (0.06-0.15)	0.01	1.4 (0.99-21.6)	0.04 (0.22-0.96)	<0.01

	MMTV-Nic PTEN $^{FL/+}$			MMTV-Nic PTEN$^{+/-}$		
	Median Vehicle (range)	**Median AZD8931 (range)**	**P value**	**Median Vehicle (range)**	**Median AZD8931 (range)**	**P value**
mTOR P Ser2448	147.5 (0.00-182.84)	75.3 (48.35-102.26)	0.18	89.3 (0.00-138.71)	73.0 (0.00-213.08)	0.81
mTOR P Ser2481	99.4 (76.29-200.92)	113.9 (95.66-147.99)	0.46	95.2 (0.00-114.57)	84.9 (61.17-118.42)	1.00
S6 Ribosomal protein p Ser240,Ser244:S6	2.1 (1.37-3.39)	0.1 (0.039-1.73)	0.04	3.5 (2.56-4.72)	1.2 (0.91-1.53)	0.12
S6 Ribosomal protein P Ser235,Ser236:S6	1.7 (0.90-4.17)	0.4 (0.24-0.81)	0.01	3.7 (2.35-4.65)	0.1 (0.63-0.80)	0.01
GSK-3-beta P Ser9: GSK-3-beta	0.2 (0.04-0.29)	0.1 (0.04-0.16)	0.34	0.3 (0.25-0.35)	0.2 (0.16-0.50)	0.30

	MMTV-Nic PTEN $^{FL/+}$			MMTV-Nic PTEN$^{+/-}$		
	Median Vehicle (range)	**Median AZD8931 (range)**	**P value**	**Median Vehicle (range)**	**Median AZD8931 (range)**	**P value**
GSK-3-alpha/beta P Ser21/Ser9	107.6 (42.03-276.20)	56.0 (18.17-96.04)	0.07	159.5 (109.65-169.18)	139.6 (0.00-191.76)	0.20
p38 MAPK PThr180,Tyr182:p38	0.7 (0.40-0.96)	0.5 (0.48-0.59)	0.78	0.7 (0.62-1.15)	0.8 (0.59-1.18)	0.48
p44/42 MAPK (ERK1/2) P Thr202/Thr185,Tyr204/Tyr187: p44/42 MAPK	0.6 (0.21-0.61)	0.1 (0.02-0.15)	0.01	0.3 (0.21-0.38)	0.1 (0.04-0.24)	0.03
Met P Tyr1234	130.5 (88.98-163.35)	97.2 (81.27-113.04)	0.25	1143.4 (120.16-245.55)	1139.3 (0-162.26)	1.00

	MMTV-Nic PTEN $^{FL/+}$			MMTV-Nic PTEN$^{+/-}$		
	Median Vehicle (range)	**Median AZD8931 (range)**	**P value**	**Median Vehicle (range)**	**Median AZD8931 (range)**	**P value**
PKC (pan) P Ser660 (beta-2)	141.6 (90.06-171.65)	117.5 (88.73-185-76)	1.00	177.8 (96.69-203.24)	158.9 (85.62-231.30)	0.60
PKC substrate P (R/K)X(S*)(Hyd)(R/k)	470.6 (269.05-487.90)	380.7 (312.90-476.23)	0.60	478.6 (387.13-587.86)	484.5 (411.51-511.52)	0.75
PKC-alpha P Thr638	672.2 (656.48-800.24)	898.40 (786.72-113.90)	0.07	1053.7 (954.36-1171.43)	1171.20 (1367.44)	0.33
E-Cadherin	439.8 (350.91-673.79)	577.3 (443.70-681.25)	0.16	483.0 (367.77-619.13)	487.8 (336.78-568.44)	1.00
Beta-actin	31.6 (32.87-491.32)	17.1 (20.74-666.41)	0.16	254.9 (0.83-589.99)	64.1 (25.71-552.37)	0.77

	MMTV-Nic PTEN $^{FL/+}$			**MMTV-Nic PTEN$^{+/-}$**		
	Median Vehicle (range)	**Median AZD8931 (range)**	**P value**	**Median Vehicle (range)**	**Median AZD8931 (range)**	**P value**
Beta- tubulin	486.9 (90.15-642.75)	547.2 (411.59-697.58)	0.30	558.6 (473.01-690.66)	510.7 (380.76-806.07)	0.48

Appendix 4: Comparison of signalling pathways between parental SKBR3 and AZD8931 resistant cell lines

RPPA analysis was performed on lysate of untreated parental SKBR3 and AZD8931 resistant cell lines. Where possible phosphorylated the ratio of phospho : corresponding total protein is presented {Tibes, 2006 #35}. The relative fluorescence intensity (RFI) for all other antibodies is presented, corrected using global normalization technique {Guo, 2012 #34}. P values calculated using one way ANOVA.

	Median parental SKBR3 (range)	**Median AZD8931 R-SKBR3a (range)**	**Median AZD8931 R-SKBR3b (range)**	**Median AZD8931 R-SKBR3c (range)**	**P value**
P Tyr1248/Tyr1173 HER2/EGFR: HER2/EGFR	0.04 (0.03-0.04)	0.85* (0.76-1.08)	1.23* (0.95-1.51)	0.83* (0.76-0.91)	<0.001
P Tyr 1173 EGFR	91.51 (88.15-97.88)	106.11 (98.22-107.44)	102.53 (98.22-108.61)	95.66 (92.30-102.52)	0.591
P yr 1289 HER3/EGFR: HER3/EGFR	0.67 (0.65-0.82)	0.60 (0.59-0.60)	0.61 (0.61-0.75)	0.60 (0.58-0.67)	0.190
P Tyr 308 Akt: Akt	0.81* (0.85-0.90)	1.93** (1.80-1.96)	1.70** (1.44-1.84)	0.95* (0.81-1.03)	<0.001
PTEN	157.23 (150.76-164.28)	84.75** (77.78-98.02)	85.38** (82.88-87.38)	85.13** (84.73-85.39)`	<0.001
PI3 kinase p110 alpha	136.54 (134.79-141.96)	133.21 (131.89-137.35)	133.98 (133.59-135.50)	134.84 (134.60-134.94)	0.289
P Ser 473 Akt: Akt	1.11* (0.89-1.13)	2.08** (2.03-2.13)	1.93** (1.80-2.38)	1.06* (0.94-1.06)	<0.001

	Median parental SKBR3 (range)	**Median AZD8931 R-SKBR3a (range)**	**Median AZD8931 R-SKBR3b (range)**	**Median AZD8931 R-SKBR3c (range)**	**P value**
mTOR	0.25 (0.23-0.27)	0.31 (0.30-0.33)	0.32 (0.24-0.33)	0.24 (0.22-0.27)	0.472
P Thr 389 p70 S6 kinase: p70 S6 kinase	1.66 (1.42-1.70)	2.18* (2.15-2.20)	2.16* (1.99-2.31)	2.52** (2.42-2.75)	<0.001
P Ser235,Ser236 S6 Ribosomal protein	459.76 (395.48-468.83)	779.39** (722.84-812.99)	764.99** (756.21-771.22)	763.53** (761.46-765.35)	<0.001
P Ser 9 GSK-3-beta:GSK-3-beta	0.32* (0.29-0.33)	0.26*/** (0.24-0.29)	0.26** (0.25-0.27)	0.26*/** (0.25-0.27)	0.031
P Thr202/Thr185,Tyr204/Tyr187 p44/42 MAPK: p44/42 MAPK	1.92 (1.14-2.41)	0.30* (0.30-0.35)	0.28* (0.24-0.30)	0.25* (0.25-0.27)	0.001
P Ser21/Ser9 GSK-3-alpha/beta	143.57 (142.26-147.67)	147.24 (136.20-155.27)	142.45 (142.35-146.57)	143.26 (143.18-144.06)	0.916

	Median parental SKBR3 (range)	**Median AZD8931 R-SKBR3a (range)**	**Median AZD8931 R-SKBR3b (range)**	**Median AZD8931 R-SKBR3c (range)**	**P value**
SAPK/JNK	110.28* (96.02-115.04)	124.16*/** (123.94-134.15)	124.29*/** (122.06-139.37)	147.27** (127.67-173.89)	0.034
MEK ½	104.72 (84.80-106.20)	113.76 (98.52-126.63)	94.46 (89.70-108.77)	115.18 (92.40-125.96)	0.412
P Tyr 416 Src: Src	0.36 (0.30-0.36)	0.52 (0.52-0.53)*	0.42 (0.35-0.45)*	0.39 (0.29-0.45)*	0.001
MET	97.80 (95.62-102.20)	101.11 (97.77-105.56)	105.50 (92.79-105.50)	110.58 (96.30-112.98)	0.612
CDK2	221.02 (190.85-223.71)	246.43* (234.93-251.20)	245.49* (243.49-247.68)	246.77* (245.98-246.90)	0.008
Cyclin D1	186.58 (185.94-172.32)	191.30 (188.02-195.70)	191.55 (191.29-192.16)	192.10 (192.01-192.31)	0.054

	Median parental SKBR3 (range)	Median AZD8931 R-SKBR3a (range)	Median AZD8931 R-SKBR3b (range)	Median AZD8931 R-SKBR3c (range)	P value
P Ser 216 Cdc25c	135.72 (131.25-139.98)	106.17 (102.87-107.51)	105.28 (105.66-106.12)	105.00 (105.87-106.10)	<0.001
Survivin	319.83 (307.23-323.73)	217.62* (216.96-219.34)	217.75* (216.69-218.80)	218.34* (218.15-218.36)	<0.001
Bid	123.86 (119.04-124.86)	136.35* (134.54-139.04)	136.57* (135.04-136.64)	136.35* (136.27-136.34)	<0.001
P Ser 68 Bim: Bim	0.20 (0.13-0.22)	0.14 (0.14-0.15)	0.14 (0.14-0.15)	0.14 (0.13-0.17)	0.302
PKC (pan)	139.23 (136.66-166.67)	123.09 (121.09-134.98)	127.32 (126.26-129.98)	128.73 (128.07-128.85)	0.067
P Tyr 783 PLCɣ: PLC ɣ	1.07 (1.03-1.09)	0.96* (0.93-0.97)	0.86** (0.78-0.86)	0.92*/** (0.86-0.93)	<0.001

	Median parental SKBR3 (range)	**Median AZD8931 R-SKBR3a (range)**	**Median AZD8931 R-SKBR3b (range)**	**Median AZD8931 R-SKBR3c (range)**	**P value**
P Ty 207 Crkl	90.48 (90..00-91.98)	85.99* (84.03-88.52)	86.28* (85.98-86.43)	86.43* (86.39-86.55)	0.004
P Ser 465/Ser 423, Ser 467/Ser 425 Smad 2/3	141.82 (139.17-157.57)	147.80 (139.94-148.11)	143.52 (143.46-145.28)	144.09 (143.94-144.36)	0.958
P Ser 463/Ser 465 Smad 1/5	89.64 (86.44-95.23)	91.87 (84.05-94.93)	90.46 (88.30-90.57)	89.95 (89.80-90.07)	0.996
Stat 3	670.55 (557.98-672.26)	262.17* (242.80-287.59)	280.45* (267.90-298.87)	361.32* (281.27-431.59)	<0.001
P Tyr 694 Stat 5: Stat 5	1.28 (1.16-1.32)	1.68 (1.20-1.77)	1.74 (1.31-1.88)	1.50 (1.38-1.61)	0.256
C –jun, N- term	112.93 (97.52-131.40)	110.54 (104.61-114.18)	112.54 (110.93-114.31)	97.75 (96.56-115.21)	0.604

	Median parental SKBR3 (range)	**Median AZD8931 R-SKBR3a (range)**	**Median AZD8931 R-SKBR3b (range)**	**Median AZD8931 R-SKBR3c (range)**	**P value**
P Thr 58, Ser 62 c-myc:c-myc	4.49 (4.42-4.56)	4.58 (3.60-5.70)	3.36 (3.02-3.36)	3.22 (3.21-4.08)	0.051

Appendix 5- List of proteins differentially expressed between parental SKBR3 and AZD8931 R-SKBR3c cell lines.

Genes Up-regulated in RSKBR3 c versus parental SKBR3 cell line

- 3-hydroxy-3-methylglutaryl-Coenzyme A synthase 1 (soluble).
- BCL2-associated athanogene 3.
- COP9 constitutive photomorphogenic homolog subunit 2 (Arabidopsis).
- CTP synthase.
- DNA (cytosine-5-)-methyltransferase 1.
- Dan (Hsp40) homolog, subfamily A, member 1- Co-chaperone of Hsp70.
- RAN, member RAS ontogeny family.
- SERPINE1 mRNA binding protein 1.
- SH3-domain GRB2-like endophilin B1.
- Sec61 beta subunit.
- TAR DNA binding protein.
- Triosephosphate isomerase 1.
- UDP-glucose pyrophosphorylase 2.
- Y box binding protein 1.
- Acetyl-Coenzyme A carboxylase alpha.
- Alanyl-tRNA synthetase.
- Annexin A1.
- Basic transcription factor 3.
- Block of proliferation 1.
- Carbamoyl-phosphate synthetase 2, aspartate transcarbamylase, and dihydroorotase.
- Cold shock domain protein A.
- Cytochrome b5 type A (microsomal).
- Cihydropyrimidinase-like 2.
- Eukaryotic translation elongation factor 1 gamma.
- Eukaryotic translation initiation factor 2, subunit 2 beta, 38kDa.
- Eukaryotic translation initiation factor 2, subunit 3 gamma, 52kDa.
- Eukaryotic translation initiation factor 3, subunit A .
- Eukaryotic translation initiation factor 3, subunit D.
- Eukaryotic translation initiation factor 3, subunit E.
- Eukaryotic translation initiation factor 3, subunit F.
- Eukaryotic translation initiation factor 3, subunit L.
- Eukaryotic translation initiation factor 4H.
- Eukaryotic translation initiation factor 5A.
- Fibronectin 1.
- Filamin A, alpha (actin binding protein 280).
- Glutamate dehydrogenase 1.
- Guanine nucleotide binding protein (G protein), alpha inhibiting activity polypeptide 2.
- Heterogeneous nuclear ribonucleoprotein A3.
- Retinoblastoma binding protein 4.
- Methylthioadenosine phosphorylase.
- Minichromosome maintenance complex component 6.
- Myosin, heavy chain 9, non-muscle.
- Neural precursor cell expressed, developmentally down-regulated 4.
- Non-metastatic cells 1, protein (NM23A).
- Non-metastatic cells 2, protein (NM23B).
- Peroxiredoxin 4.
- Phosphogluconate dehydrogenase.

- Phosphoglycerate dehydrogenase.
- Phosphoglycerate mutase 1 (brain).
- Poly(A) binding protein.
- 1 poly-U binding splicing factor 60KDa.
- Polymerase I and transcript release factor.
- Proliferating cell nuclear antigen.
- Proteasome (prosome, macropain) 26S subunit, ATPase, 2.
- Proteasome (prosome, macropain) 26S subunit, ATPase, 3.
- Proteasome (prosome, macropain) 26S subunit, non-ATPase, 4.
- Proteasome (prosome, macropain) 26S subunit, non-ATPase, 6.
- Protein phosphatase 2 (formerly 2A), regulatory subunit A, alpha isoform.
- Ribonucleotide reductase M1One of the 2 subunits comprising RRM1.
- Ribosomal protein L17.
- Ribosomal protein L18.
- Ribosomal protein L19.
- Ribosomal protein L27.
- Ribosomal protein L28.
- Ribosomal protein L35.
- Ribosomal protein L35a.
- Ribosomal protein L3.
- Ribosomal protein L4.
- Ribosomal protein L6.
- Ribosomal protein S14.
- Ribosomal protein S15.
- Ribosomal protein S17.
- Ribosomal protein S9.
- Ribosomal protein, large, P2.
- Sequestosome 1.
- Serine/threonine kinase receptor associated protein (STRAP).
- Seryl-tRNA synthetase.
- Proteasome 26S subunit, ATPase, 4.
- ATP-binding cassette, sub-family E (OABP), member 1.
- Eukaryotic translation initiation factor 4A, isoform 1.
- Similar to heat shock 70kD protein binding protein; suppression of tumorigenicity 13 (colon carcinoma) (Hsp70 interacting protein).
- Spectrin, beta, non-erythrocytic 1.
- Splicing factor 3b, subunit 3, 130kDa.
- Thioredoxin-like 1.
- Ubiquitin-conjugating enzyme E2 variant 1
- Ubiquitin-conjugating enzyme E2K (UBC1 homolog, yeast).
- Valosin-containing protein.
- Actinin alpha 1.
- Annexin A2.
- Chloride intracellular channel 4.
- Gelsolin (amyloidosis, Finnish type).
- Heterogeneous nuclear ribonucleoprotein A/B.
- Microtubule-associated protein, RP/EB family, member 1.
- 14-3-3 protein epsilon.
- Tyrosine 3-monooxygenase/tryptophan 5-monooxygenase activation protein, zeta polypeptide.
- Vinculin.
- EH-domain containing 2.
- H3 histone, family 3B (H3.3B)
- Caldesmon 1.
- Calponin 3, acidic
- Dynactin 1 (p150, glued homolog, Drosophila)
- Fascin homolog 1, actin-bundling protein (Strongylocentrotus purpuratus).
- Heat shock 70kDa protein 4.
- Lamin A/C.
- Structural maintenance of chromosomes 2.

- Talin 1.
- BAI1-associated protein 2.
- Karyopherin (importin) beta 1.
- Septin 11.
- Tubulin, alpha 4a.
- EH-domain containing 1.
- Sec61 beta subunit.
- Clathrin, light chain (Lca).
- Myosin, light chain 6, alkali, smooth muscle and non-muscle.
- ADP-ribosylation factor 5.
- NM_005347; heat shock 70kDa protein.
- Proteasome (prosome, macropain) 26S subunit, ATPase, 4.
- ARP1 actin-related protein 1 homolog A, centractin alpha.
- Angio-associated, migratory cell protein.
- Moesin.
- Vimentin.
- Hypoxanthine phosphoribosyltransferase 1.
- Vesicle amine transport protein 1 homolog.
- UDP-N-acteylglucosamine pyrophosphorylase 1-like 1.
- Yes-associated protein 1, 65kDa.
- Fragile X mental retardation, autosomal homolog 1.
- Fragile X mental retardation, autosomal homolog 2.
- Esterase D/formylglutathione hydrolase.
- Kinectin 1 (kinesin receptor).
- Plectin 1, intermediate filament binding protein 500kDa.
- Family with sequence similarity 49, member B
- Calumenin
- Lectin, galactoside-binding, soluble, 1
- Poly(A) binding protein, cytoplasmic 1
- AHNAK nucleoprotein
- ATP-binding cassette, sub-family F (GCN20), member 2
- CDV3 homolog (mouse)
- COP9 constitutive photomorphogenic homolog subunit 4 (Arabidopsis)
- S100 calcium binding protein A10
- UDP-N-acteylglucosamine pyrophosphorylase 1-like 1-
- WD repeat domain 1
- Annexin A8-like 2
- Cold shock domain containing E1, RNA-binding.
- Guanine nucleotide binding protein (G protein), beta polypeptide 2-like 1.
- Myoferlin.
- Myosin, light chain 12A, regulatory, non-sarcomeric.
- Protein kinase, cAMP-dependent, regulatory, type I, alpha (tissue specific extinguisher 1).
- Tetratricopeptide repeat domain 35.

Genes Down-regulated in RSKBR3 c versus parental SKBR3 cell line

- ATP synthase, H+ transporting, mitochondrial F1 complex, alpha subunit 1.
- ATPase, H+ transporting, lysosomal 50/57kDa, V1 subunit H.
- ATPase, Na+/K+ transporting, alpha 1 polypeptide.
- CD3e molecule, epsilon associated protein.
- DEAD (Asp-Glu-Ala-Asp) box polypeptide 1.
- DEAD (Asp-Glu-Ala-Asp) box polypeptide 17
- DEAD (Asp-Glu-Ala-Asp) box polypeptide 47
- DEAH (Asp-Glu-Ala-His) box polypeptide 9.
- EMG1 nucleolar protein homolog.
- FK506 binding protein 4.
- GNAS complex locus.
- IMP (inosine monophosphate) dehydrogenase 1.

- IMP (inosine monophosphate) dehydrogenase 2.
- MYB binding protein (P160) 1a.
- NAD(P)H dehydrogenase, quinone 1.
- NADH dehydrogenase (ubiquinone) Fe-S protein 1, 75kDa.
- NADH dehydrogenase (ubiquinone) Fe-S protein 3, 30kDa.
- NADH dehydrogenase (ubiquinone) flavoprotein 1, 51kDa.
- NOL1/NOP2/Sun domain family, member 2.
- NOP56 ribonucleoprotein homolog.
- Obg-like ATPase 1.
- PEST proteolytic signal containing nuclear protein.
- PHD finger protein 5A.
- PRP40 pre-mRNA processing factor 40 homolog A.
- Parkinson disease (autosomal recessive, early onset) 7.
- RAB6C, member RAS oncogene family.
- RAB6A, member RAS oncogene family.
- RAD23 homolog B.
- RAN binding protein 2.
- RNA binding motif protein 28.
- SWI/SNF related, matrix associated, actin dependent regulator of chromatin, subfamily a, member 4.
- SWI/SNF related, matrix associated, actin dependent regulator of chromatin, subfamily c, member 2.
- Shwachman-Bodian-Diamond syndrome.
- Sjogren syndrome antigen B (autoantigen La).
- THO complex 4.
- TNF receptor-associated protein 1.

- Treacher Collins-Franceschetti syndrome 1.
- Tu translation elongation factor, mitochondrial.
- X-ray repair complementing defective repair in Chinese hamster cells 5 (double-strand-break rejoining).
- X-ray repair complementing defective repair in Chinese hamster cells 6.
- Acetyl-Coenzyme A acyltransferase 1.
- Acyl-CoA synthetase long-chain family member 3.
- Acyl-Coenzyme A dehydrogenase.
- Adenine phosphoribosyltransferase.
- Adenosine deaminase, RNA-specific.
- Adenosine kinase.
- Adenylate kinase 2.
- Aldehyde dehydrogenase 4 family, member A1.
- Aldehyde dehydrogenase 7 family, member A1.
- Aldo-keto reductase family 1, member A1 (aldehyde reductase).
- Aldolase A, fructose-bisphosphate.
- Aminoacyl tRNA synthetase complex-interacting multifunctional protein 1.
- Argininosuccinate synthetase 1.
- Arginyl aminopeptidase (aminopeptidase B).
- Arginyl-tRNA synthetase.
- asparaginyl-tRNA synthetase.
- Calreticulin.
- Carbamoyl-phosphate synthetase 1.
- Carbonyl reductase 1.
- Carnitine palmitoyltransferase 1A.
- Catechol-O-methyltransferase.
- Catenin (cadherin-associated protein), delta 1
- Cathepsin D.
- Cellular retinoic acid binding protein 2.
- Chaperonin containing TCP1, subunit 2 (beta) .
- Chaperonin containing TCP1, subunit 5 (epsilon).
- Chromodomain helicase DNA binding protein 4.
- Chromosome 1 open reading frame 25.Citrate synthase.

- Cleavage and polyadenylation specific factor 6, 68kDa.
- Coatomer protein complex, subunit alpha.
- Creatine kinase.
  - Creatine kinase, mitochondrial 1A; creatine kinase, mitochondrial 1B.
  - Cullin-associated and neddylation-dissociated 1.
  - Cytidine monophosphate (UMP-CMP) kinase 1, cytosolic.
  - Desmoplakin.
  - Dicarbonyl/L-xylulose reductase.
  - Dihydrolipoamide S-acetyltransferase.
  - Dihydrolipoamide S-succinyltransferase (E2 component of 2-oxo-glutarate complex).
  - Dihydrolipoamide dehydrogenase.
  - Enolase 1, (alpha).
  - Enoyl Coenzyme A hydratase 1.
  - Eukaryotic translation elongation factor 1 beta 2; eukaryotic translation elongation factor 1 beta 2-like
  - Eukaryotic translation elongation factor 1 delta (guanine nucleotide exchange protein).
  - Eukaryotic translation initiation factor 3, subunit C.
  - Eukaryotic translation initiation factor 4 gamma, 1.
  - Eukaryotic translation initiation factor 4A, isoform 3.
  - Eukaryotic translation initiation factor 4E
  - Eukaryotic translation initiation factor 5B.
  - Exosome component 6.
  - Far upstream element (FUSE) binding protein 1.
  - Fatty acid synthase.
  - Fibrillarin.
  - Flap structure-specific endonuclease 1.
  - Fumarate hydratase.
  - Fusion (involved in t(12;16) in malignant liposarcoma).
  - General transcription factor II.
  - Glucose-6-phosphate dehydrogenase.
  - Glutamyl-prolyl-tRNA synthetase.
  - Glyceraldehyde-3-phosphate dehydrogenase-like 6.
  - Glycyl-tRNA synthetase.
  - Glyoxylate reductase/hydroxypyruvate reductase.
  - Guanine monphosphate synthetase.
  - Heat shock 60kDa protein 1 (chaperonin).
  - Heat shock 70kDa protein 1A; heat shock 70kDa protein 1B.
  - Heat shock 70kDa protein 8.
  - Heat shock 70kDa protein 9 (mortalin).
  - Heat shock protein 90kDa alpha (cytosolic), class A member 2; heat shock protein 90kDa alpha (cytosolic), class A member 1.
  - Heterogeneous nuclear ribonucleoprotein A2/B.
  - Heterogeneous nuclear ribonucleoprotein C (C1/C2).
  - Heterogeneous nuclear ribonucleoprotein D (AU-rich element RNA binding protein 1, 37kDa).
  - Heterogeneous nuclear ribonucleoprotein D-like.
  - Heterogeneous nuclear ribonucleoprotein F.
  - Heterogeneous nuclear ribonucleoprotein H1 (H).
  - Heterogeneous nuclear ribonucleoprotein M.
  - Heterogeneous nuclear ribonucleoprotein R.
  - Hexokinase 1.
  - Hexokinase 2.
  - High-mobility group box 1.
  - Hydroxyacyl-Coenzyme A dehydrogenase/3-ketoacyl-Coenzyme A thiolase/enoyl-Coenzyme A hydratase (trifunctional protein), alpha subunit.
  - Hydroxyacyl-Coenzyme A dehydrogenase/3-ketoacyl-Coenzyme A thiolase/enoyl-Coenzyme A hydratase (trifunctional protein), beta subunit.
  - Hydroxysteroid (17-beta) dehydrogenase 10.
  - Inosine triphosphatase.
  - Interleukin enhancer binding factor 2, 45kDa.

- Interleukin enhancer binding factor 3, 90kDa.
- Isocitrate dehydrogenase 2 (NADP+), mitochondrial.
- Isocitrate dehydrogenase 3 (NAD+) alpha.
- Isoleucyl-tRNA synthetase.
- Karyopherin alpha 2 (RAG cohort 1, importin alpha 1)/
- Keratin 7.
- Lactate dehydrogenase A.
- Lactate dehydrogenase B.
- Leucine rich repeat (in FLII) interacting protein 1.
- Leucine rich repeat containing 47.
- Leucine-rich PPR-motif containing.
- Leucyl-tRNA synthetase.
- Lysyl-tRNA synthetase.
- Mago-nashi homolog, proliferation-associated.
- Malate dehydrogenase 2, NAD (mitochondrial).
- Methylcrotonoyl-Coenzyme A carboxylase 1 (alpha).
- Methylcrotonoyl-Coenzyme A carboxylase 2 (beta).
- Microsomal glutathione S-transferase 1.
- Mitochondrial ribosomal protein L49.
- Nicotinamide phosphoribosyltransferase.
- Nucleosome assembly protein 1-like 1.
- Oxidative-stress responsive 1.
- Paraspeckle component 1.
- Peroxiredoxin 1.
- Peroxiredoxin 2.
- Peroxiredoxin 3.
- Peroxiredoxin 6.
- Phosphatidylinositol-3,4,5-trisphosphate-dependent Rac exchange factor 1.
- Phosphofructokinase, muscle.
- Phosphoribosylglycinamide formyltransferase, phosphoribosylglycinamide synthetase, phosphoribosylaminoimidazole synthetase.
- Phosphorylase, glycogen; brain.
- Poly (ADP-ribose) polymerase 1.
- Polynucleotide kinase 3'-phosphatase.
- Polypyrimidine tract binding protein 1.
- Prohibitin 2.
- Prolyl 4-hydroxylase, alpha polypeptide I.
- Prostaglandin E synthase 3 (cytosolic).
- Proteasome (prosome, macropain) 26S subunit, non-ATPase, 12.
- Proteasome (prosome, macropain) activator subunit 1 (PA28 alpha).
- Proteasome (prosome, macropain) activator subunit 2 (PA28 beta).
- Protein disulfide isomerase family A, member 6.
- Protein phosphatase 1G (formerly 2C), magnesium-dependent, gamma isoform.
- Pyridoxal-dependent decarboxylase domain containing 1.
- Pyrophosphatase (inorganic) 1.
- Pyruvate carboxylase.
- Pyruvate dehydrogenase (lipoamide) beta.
- Ribonuclease/angiogenin inhibitor 1.
- Ribophorin II.
- Ribosomal L1 domain containing 1.
- Ribosomal protein L13.
- Ribosomal protein L14.
- Ribosomal protein L15.
- Ribosomal protein L22.
- Ribosomal protein L7.
- Ribosomal protein L9.
- Ribosomal protein S18.
- Ribosomal protein S24.
- Ribosomal protein S25.
- Ribosomal protein S27a.

- Ribosomal protein, large, P1.
- Ribosome binding protein 1 homolog 180kDa.
- Scaffold attachment factor B.
- Sepiapterin reductase.
- Serrate RNA effector molecule homolog (Arabidopsis).
- Signal transducer and activator of transcription 3 (acute-phase response factor).
- Ewing sarcoma breakpoint region 1.
- Pyruvate kinase, muscle..
- RNA binding motif protein, X-linked.
- Small nuclear ribonucleoprotein 200kDa (U5).
- Calcyclin binding protein.
- Chaperonin containing TCP1, subunit 8 (theta).
- Eukaryotic translation initiation factor 4A, isoform 2.
- Heterogeneous nuclear ribonucleoprotein L.
- Protein kinase, DNA-activated, catalytic polypeptide.
- Small nuclear ribonucleoprotein 70kDa (U1).
- Solute carrier family 25 (mitochondrial carrier; dicarboxylate transporter), member 10.
- Solute carrier family 25, member 13 (citrin).
- Solute carrier family 7 (cationic amino acid transporter, y+ system), member 5.
- Sorbitol dehydrogenase.
- Splicing factor proline/glutamine-rich (polypyrimidine tract binding protein associated).
- Splicing factor, arginine/serine-rich 6.
- Staphylococcal nuclease and tudor domain containing 1.
- Succinate dehydrogenase complex, subunit A, flavoprotein (Fp).
- Suppressor of Ty 16 homolog (S. cerevisiae).
- Tankyrase 1 binding protein 1, 182kDa.
- Thioredoxin.
- Thioredoxin domain containing 12.
- Thymidine kinase 1.
- Topoisomerase (DNA) I.
- Topoisomerase (DNA) II alpha.
- Transaldolase 1.
- Transducin (beta)-like 3.
- Translocated promoter region (to activated MET oncogene).
- Trichorhinophalangeal syndrome I.
- Tripartite motif-containing 28.
- Tryptophanyl-tRNA synthetase.
- Tubulin tyrosine ligase-like family, member 12.
- Tubulin tyrosine ligase-like family, member 3.
- Ubiquitin specific peptidase 7.
- Ubiquitin-like modifier activating enzyme 1.
- HER2.
- Within bgcn homolog.
- 2',3'-cyclic nucleotide 3' phosphodiesterase.
- 2,4-dienoyl CoA reductase 1, mitochondrial.
- AHA1, activator of heat shock 90kDa protein ATPase homolog 1 (yeast).
- ATP citrate-lyase.
- ATP synthase, H+ transporting, mitochondrial F1 complex, O subunit.
- ATP synthase, H+ transporting, mitochondrial F1 complex, alpha subunit 1, cardiac muscle.
- APEX nuclease (multifunctional DNA repair enzyme) 1.
- CNDP dipeptidase 2 (metallopeptidase M20 family).
- N-ethylmaleimide-sensitive factor.
- Acetyl-Coenzyme A acetyltransferase 2- 2 acetyl-CoA.
- Aldehyde dehydrogenase 2 family.
- Calpain 2, (m/II) large subunit.
- Calpain, small subunit 1.
- Cathepsin C.
- Copine III.
- Tripeptidyl peptidase II.

- Nitrilase family, member 2.
- Crystallin, zeta (quinone reductase).
- Cytochrome c oxidase subunit Vib polypeptid e 1 (ubiquitous).
- VAMP (vesicle-associated membrane protein)-associated protein B and C.
- Complement component 1, q subcomponent binding protein.
- Keratin 18.
- Keratin 19
- Keratin 8.
- Programmed cell death 6 interacting protein.
- Transportin 1.
- Transferrin receptor (p90, CD71).
- SEC22 vesicle trafficking protein homolog B (S. cerevisiae).
- SEC24 family, member C (S. cerevisiae).
- USO1 homolog, vesicle docking protein (yeast).
- Archain 1.
- Coatomer protein complex, subunit alpha.
- Coatomer protein complex, subunit beta 2 (beta prime).
- Coatomer protein complex, subunit epsilon.
- Hook homolog 1 (Drosophila).
- Vacuolar protein sorting 35 homolog (S. cerevisiae).
- Importin 4.
- Optic atrophy 1 (autosomal dominant).
- Ras homolog gene family, member T2.
- Scinderin.
- Sec1 family domain containing 1.
- Secernin 1.
- Secretory carrier membrane protein 3.
- Signal recognition particle 14kDa (homologous Alu RNA binding protein)
- Signal recognition particle receptor (docking protein).
- Solute carrier family 25 (mitochondrial carrier; adenine nucleotide translocator), member 6.
- Tyrosine 3-monooxygenase/tryptophan 5-monooxygenase activation protein, beta polypeptide.
- Unc-13 homolog D (C. elegans).
- Protein disulfide isomerase family A, member 3.
- Transforming, acidic coiled-coil containing protein 2.
- CAP, adenylate cyclase-associated protein 1 (yeast).
- H2A histone family, member Y.
- LIM domain and actin binding 1.
- RAB5C, member RAS oncogene family.
- USO1 homolog, vesicle docking protein (yeast).
- Apoptotic chromatin condensation inducer 1.
- Capping protein (actin filament) muscle Z-line, alpha 1.
- Capping protein (actin filament) muscle Z-line, beta.
- Coronin, actin binding protein 1A.
- Desterin (Actin depolymerazing factor).
- Emerin.
- Guanine nucleotide binding protein (G protein), alpha inhibiting activity polypeptide 3.
- Histone cluster 1, H1b.
- Histone cluster 1, H2bb.
- Histone cluster 1, H2bi; histone cluster 1, H2bg; histone cluster 1, H2be; histone cluster 1, H2bf; histone cluster 1, H2bc.
- Inverted formin, FH2 and WH2 domain containing.
- Keratin 4.
- Metastasis associated 1 family, member 2.
- Profilin 1.
- Ras-related C3 botulinum toxin substrate 2 (rho family, small GTP binding protein Rac2).
- Regulator of chromosome condensation 1.
- Regulator of chromosome condensation 2.
- ADP-ribosylation factor 4.

- GDP dissociation inhibitor 2**.**
- RAB1B, member RAS oncogene family.
- Myosin 1C.
- Nucleoporin 88kDa.
- Selenium binding protein 1.
- Signal recognition particle 14kDa (homologous Alu RNA binding protein).
- Signal recognition particle receptor (docking protein).
- GTPase activating protein and VPS9 domains 1.
- Mannose-6-phosphate receptor binding protein 1-Mannose 6-phosphate receptors.
- Spectrin, beta, non-erythrocytic 2.
- NDRG family member 3.
- Peroxiredoxin 5.
- Solute carrier family 9 (sodium/hydrogen exchanger), member 3 regulator 1.
- S100 calcium binding protein A16.
- Glutathione S-transferase mu 3 (brain).
- Heat shock 27kDa protein 1.
- Hypoxia up-regulated 1.
- Protein kinase, cAMP-dependent, regulatory, type II, alpha.
- Signal recognition particle 68kDa.
- Tight junction protein 2 (zona occludens 2).
- GTPase activating protein (SH3 domain) binding protein 1.
- Anterior gradient homolog 2 (Xenopus laevis).
- Sideroflexin 1.
- Tumor protein D52.
- Rho GDP dissociation inhibitor (GDI) alpha.
- ATP citrate lyase.
- Cysteine-rich protein 2.
- Family with sequence similarity 62 (C2 domain containing), member A.
- Family with sequence similarity 120A.
- Cortactin.
- ATPase family, AAA domain containing 3A.
- DAZ associated protein 1.
- DEAD (Asp-Glu-Ala-Asp) box polypeptide 21.
- EPS8-like 2.
- IQ motif containing GTPase activating protein 1.
- KIAA0664.
- LPS-responsive vesicle trafficking, beach and anchor containing.
- LUC7-like 2 (S. cerevisiae).
- PDGFA associated protein 1; similar to PDGFA associated protein 1.
- Ran GTPase activating protein 1.
- S100 calcium binding protein A14.
- StAR-related lipid transfer (START) domain containing 10.
- Acetyl-Coenzyme A acetyltransferase 1.
- Basic leucine zipper and W2 domains 2.
- Breast carcinoma amplified sequence 1.
- Calcyphosine.
- Canopy 2 homolog (zebrafish).
- Chromosome 14 open reading frame 166.
- Chromosome 8 open reading frame 55.
- Coiled-coil domain containing 6.
- Coiled-coil-helix-coiled-coil-helix domain containing 2
- Coronin, actin binding protein, 1B.
- Cysteine and glycine-rich protein 1.
- Cytoskeleton-associated protein 4.
- Epiplakin 1.
- Epithelial cell adhesion molecule.
- Family with sequence similarity 62 (C2 domain containing), member B.
- Family with sequence similarity 83, member H.
- Growth factor receptor-bound protein 7:
- Heterogeneous nuclear ribonucleoprotein U-like 2.

Ladinin 1.

- Metastasis associated 1 family, member 3.
- Nucleolin.
- Ornithine aminotransferase (gyrate atrophy).
- Periplakin.
- Plakophilin 3
- Progesterone receptor membrane component 1.
- Protein kinase C substrate.
- Regulation of nuclear pre-mRNA domain containing 1B.
- Ring finger protein 114.
- Stomatin (EPB72)-like 2.
- Stress-induced-phosphoprotein 1.
- Symplekin.
- Testis derived transcript (3 LIM domains).
- Thymopoietin.
- Transketolase.
- Tripartite motif-containing 25.

Appendix 6: Related Publications